Dynamic Covalent Chemistry

Dynamic Covalent Chemistry

Principles, Reactions, and Applications

Edited by

Wei Zhang
Department of Chemistry and Biochemistry
University of Colorado
USA

Yinghua Jin
Department of Chemical and Biological Engineering and
Department of Chemistry and Biochemistry
University of Colorado
USA

WILEY

The right of Wei Zhang and Yinghua Jin to be identified as the authors of this editorial material in this work has been asserted in accordance with law.

For details of our global editorial offices, customer services, and more information about Wiley products visit us at www.wiley.com.

Wiley also publishes its books in a variety of electronic formats and by print-on-demand. Some content that appears in standard print versions of this book may not be available in other formats.

Contents

Preface

In the past two decades, dynamic covalent chemistry (DCvC) has emerged as a powerful synthetic tool in organic synthesis, materials development, drug discovery, and biotechnology. Similar to supramolecular chemistry, DCvC is the chemistry of reversible bond formation under equilibrium control and dynamic in nature. However, unlike supramolecular chemistry, which is based on weak non-covalent intermolecular interactions, DCvC involves reversible yet robust covalent bond formation/cleavage. Therefore, DCvC is molecular chemistry whereas supramolecular chemistry is the chemistry beyond molecules. Nature has practiced supramolecular chemistry for millions years in many biological systems and processes. The arrival of supramolecular chemistry to scientists was formally recognized by the 1987 Nobel Prize in Chemistry to Pedersen, Cram and Lehn. Supramolecular chemistry has revolutionized the bottom-up approach to nanostructured systems with extraordinary properties and amazing applications in biology and materials science. Importing the dynamic feature of supramolecular chemistry into the molecular level, DCvC combines the error-correction capability of supramolecular chemistry and the robustness of covalent bonding. Although relatively young, DCvC has advanced rapidly over the years on the foundation of supramolecular chemistry. This book presents DCvC as a powerful tool for those who are interested in the assembly of molecular architectures, dynamic combinatorial chemistry, and responsive materials. This book is not meant to be a comprehensive compilation of all the examples reported in the literature involving DCvC, but instead provides general guidance, balanced understanding of this field, and inspiration by introducing concepts, principles, methods, and selective examples of exciting applications in diverse research areas, such as synthetic chemistry, biotechnology, and materials science. We put a particular focus on accomplishments made within the past decade.

Chapter 1 provides a general introduction to this field, including the basic concepts of DCvC, its thermodynamically controlled nature, "error checking" and "proof-reading" characters, and important criteria for reversible systems. Descriptions of various reversible covalent reactions that have been explored so far, along with their characteristics, are provided.

Chapter 2 gives a general overview of dynamic combinatorial libraries (DCL), which are freely interconverting mixtures of distinct molecular species (covalently or non-covalently bonded) resulting from dynamic combinatorial chemistry. Theoretical considerations and the adaptability of DCLs under external stimuli, such as template and physical means (solvent, light, temperature, mechanical force, etc.), are presented. Interesting multiphase DCLs and kinetically interrupted non-equilibrium DCLs are

also discussed. The most important accomplishments in DCL (e.g., molecular separation, catalysis, self-replicating, drug discovery, etc.), characterization/analysis approaches, together with challenges and perspectives for the future, are highlighted.

Chapter 3 covers shape-persistent macrocycles prepared through dynamic covalent reactions under thermodynamic control. The design, synthesis, and property study of these cyclic rigid oligomers with non-collapsible backbones and inside cavities are discussed. Homo-sequenced macrocycles prepared through reversible alkyne metathesis, imine metathesis, olefin metathesis, and boronate ester formation, and hetero-sequenced macrocycles formed through orthogonal dynamic covalent reactions are presented. The great potential of shape-persistent macrocycles in various applications, such as host–guest chemistry, organic electronic materials, chemical sensors, and transmembrane mass transportation, are also discussed.

Chapter 4 reviews the research progress on organic molecular cages (OMCs) synthesized via a DCvC approach. Similar to the formation of macrocyclic compounds, molecular cages, also called covalent organic polyhedrons, can be obtained as the predominant species at the equilibrium through thermodynamically controlled cyclooligomerization from suitably designed monomer species. The synthesis of OMCs through various dynamic covalent reactions and strategies of OMC functionalization are discussed. Finally, the interesting applications of OMCs in molecular recognition/separation, catalysis, and template synthesis of nanoparticles are discussed.

Chapter 5 reviews the orthogonal application of more than one type of bonding interaction to construct various well-defined molecular architectures. Orthogonal use of multiple dynamic covalent reactions, dynamic covalent reactions with hydrogen bonding interactions, and dynamic covalent reactions with π–π stacking interactions are presented. This protocol represents a nice addition to the current tool box of DCvC, easily accessing more complex molecular architectures of tunable shapes, sizes and symmetries, in many cases, with the aid of supramolecular interactions.

Chapter 6 introduces the self-sorting concept and describes self-sorting processes involving interchange of components through the formation and breakage of dynamic covalent bonds. Thermodynamically controlled self-sorting in DCLs through multiple operational exchange reactions and kinetically controlled self-sorting under an irreversible chemical or physical stimulus are discussed. These self-sorting processes result from a network of competing recognition processes among a complex mixture of components to form ordered sub-systems, and have shown great potential in forming complex ordered structures and in separation applications.

Chapter 7 reviews the design, synthesis, and study of molecular machines through DCvC. Mechanically interlocked molecular systems are introduced first, followed by discussions on several molecular machine systems, including motors, switches, shuttles, and molecular walkers. Compared to those systems utilizing non-covalent bonding interactions, molecular machines driven by covalent bonding changes offer more distinctive states, implying more functions and controllability. Also, as it is manifested in macrocycle and molecular cage synthesis, the use of orthogonal DCvC enables the fabrication of more sophisticated artificial molecular machines.

Chapters 8 and 9 review the responsive and self-healing polymers, respectively, which are all prepared via DCvC. Dynamic covalent polymers are capable of adapting to their surroundings to exhibit responses including self-healing, conformational changes, and malleability. Such materials have great potential in a broad range of applications, such

as therapeutics, diagnostics, cell and tissue engineering, optoelectronics, sensors, coating, and textiles. The design principles of dynamic covalent polymers, and their response and self-healing mechanisms, are briefly overviewed. Recent advances in the area of stimuli-responsive and self-healing polymers with dynamic characteristics are also discussed.

Chapter 10 reviews emerging applications of DCvC, with a particular focus on nanoscale. The applications of dynamic systems utilizing nanoscale assemblies in biomedical-related fields, as well as in other fields such as organic electronics, gas storage, catalysis, and separations, are discussed. The outlook for potential growth areas of DCvC in nanotechnology is also provided.

Finally, we would like to acknowledge all the contributing authors for their high-quality work. We thank Yuou Zhang for her help with the initial design of the cover art. We sincerely hope this book can provide a comprehensive review of the DCvC field and inspire chemists working on DCvC or supramolecular chemistry as well as those who plan to move into such an exciting and rapidly growing field.

June 2017
Wei Zhang
Yinghua Jin

List of Contributors

Jessica J. Cash
George & Josephine Butler Polymer
Research Laboratory
Center for Macromolecular Science &
Engineering
Department of Chemistry
University of Florida
USA

Rufan Chen
Key Laboratory of Biomedical Polymers
(Ministry of Education)
College of Chemistry and Molecular
Sciences
Wuhan University
China

Huimin Ding
Key Laboratory of Biomedical Polymers
(Ministry of Education)
College of Chemistry and Molecular
Sciences
Wuhan University
China

Megan Dunn
Department of Chemical Engineering
University of Michigan
USA

Joseph C. Furgal
Department of Chemical Engineering
University of Michigan
USA

Chia-Wei Hsu
Department of Chemistry
University of Houston
USA

Keiichi Imato
Department of Organic and Polymeric
Materials
Tokyo Institute of Technology
Japan

Yinghua Jin
Department of Chemistry and
Biochemistry
University of Colorado
USA

Dávid Komáromy
University of Groningen
Centre for Systems Chemistry
Stratingh Institute
The Netherlands

Ken Cham-Fai Leung
Department of Chemistry
Hong Kong Baptist University
Hong Kong

Zhan-Ting Li
Department of Chemistry
Fudan University
China

Yi Liu
The Molecular Foundry
Lawrence Berkeley National Laboratory
USA

Ognjen Š. Miljanić
Department of Chemistry
University of Houston
USA

Soma Mukherjee
George & Josephine Butler Polymer
Research Laboratory
Center for Macromolecular Science &
Engineering
Department of Chemistry
University of Florida
USA

Piotr Nowak
University of Groningen
Centre for Systems Chemistry
Stratingh Institute
The Netherlands

Hideyuki Otsuka
Department of Organic and Polymeric
Materials
Tokyo Institute of Technology
Japan

Sijbren Otto
University of Groningen
Centre for Systems Chemistry
Stratingh Institute
The Netherlands

Olof Ramström
Department of Chemistry
KTH – Royal Institute of Technology
Stockholm
Sweden

Fredrik Schaufelberger
Department of Chemistry
KTH – Royal Institute of Technology
Stockholm
Sweden

Timothy F. Scott
Department of Chemical Engineering,
and Macromolecular Science and
Engineering Program
University of Michigan
USA

Brent S. Sumerlin
George & Josephine Butler Polymer
Research Laboratory
Center for Macromolecular Science &
Engineering
Department of Chemistry
University of Florida
USA

Brian J. J. Timmer
Department of Chemistry
KTH – Royal Institute of Technology
Stockholm
Sweden

Cheng Wang
Key Laboratory of Biomedical Polymers
(Ministry of Education)
College of Chemistry and Molecular Sciences
Wuhan University
China

Tao Wei
Department of Chemical Engineering
University of Michigan
USA

Chao Yu
Department of Chemistry and
Biochemistry
University of Colorado
USA

Dan-Wei Zhang
Department of Chemistry
Fudan University
China

Wei Zhang
Department of Chemistry and
Biochemistry
University of Colorado
USA

1

Principles of Dynamic Covalent Chemistry

Fredrik Schaufelberger, Brian J.J. Timmer, and Olof Ramström

1.1 Introduction

1.1.1 What is Dynamic Covalent Chemistry?

A key feature in supramolecular chemistry is its dynamic nature. The weak non-covalent bonds utilized are labile and reversible, and supramolecular systems spontaneously organize into the thermodynamically most preferred composition. However, the same inherent instability of supramolecular assemblies precludes their use in many applications where a higher degree of robustness is required. Thus, a demand for a set of reactions that combine the dynamic properties of supramolecular chemistry with the stability and robustness of covalent bonds arose. To meet this requirement, *dynamic covalent chemistry* (DCvC*) was developed.[1–3] This chemistry is based on reversible covalent bonds and extends traditional supramolecular chemistry into the molecular domain. The resulting combination gives rise to *constitutional dynamic chemistry* (CDC), a type of chemistry where the molecular constitution of a chemical system may undergo changes over time or in response to stimuli (Figure 1.1).[4] In this context, the generation of mixtures of interconverting constituents can lead to compound collections, representing a sub-field of CDC normally termed *dynamic combinatorial chemistry* (DCC).[2,5]

Dynamic covalent chemistry is not a new concept and its origins can be traced back to the roots of chemistry.[6] Fundamental discoveries in the field were made by, for example, Williamson, Schiff, and Fischer, and the concept of reversible covalent bonds was also discussed by Werner during investigations of metal–ligand coordination. An early application of the concept in template synthesis was reported in the 1920s by Seidel, where macrocyclization of 2-aminobenzaldehyde in the presence of $ZnCl_2$ resulted in an unidentified structure that was later identified as a tetrameric macrocycle (Scheme 1.1).[7,8]

The field of DCvC has, however, evolved rapidly in recent years and today reversible covalent bonds are utilized in a plethora of applications (Figure 1.2).[9,10] DCvC has

---

*To avoid confusion with DCC, and in congruence with Zhang's proposed nomenclature, dynamic covalent chemistry is abbreviated DCvC in this chapter.

ADAPTATION AT SYSTEMS LEVEL

Constitutional
Dynamic Chemistry

Self-organization...
...by design
...by selection

Dynamic
Covalent Chemistry

Dynamic
Non-covalent Chemistry

ADAPTATION AT MOLECULAR LEVEL   ADAPTATION AT SUPRAMOLECULAR LEVEL
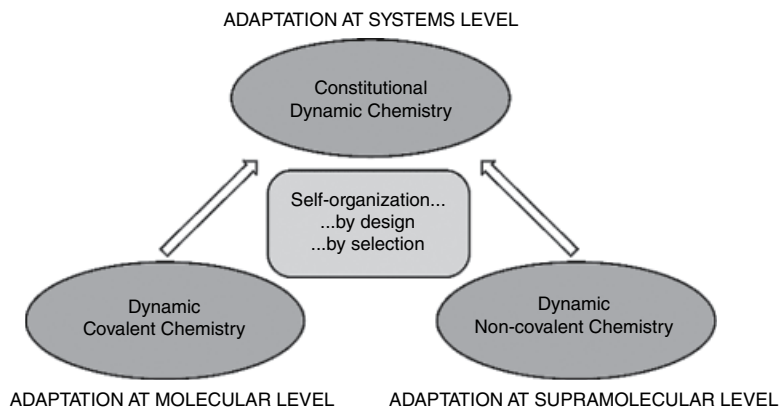
Figure 1.1 Overview of the structural order of dynamic chemistry.

ZnCl$_2$
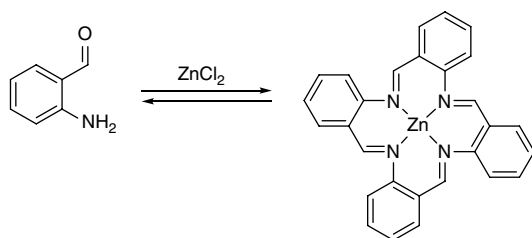
Scheme 1.1 Template-assisted macrocyclization of 2-aminobenzaldehyde under thermodynamic control.

Ligand screening

Complex molecular architectures

Dynamic catalysis and catalyst screening

Dynamic
Covalent Chemistry

Functional systems

Adaptive and responsive materials

Sensing and pattern recognition
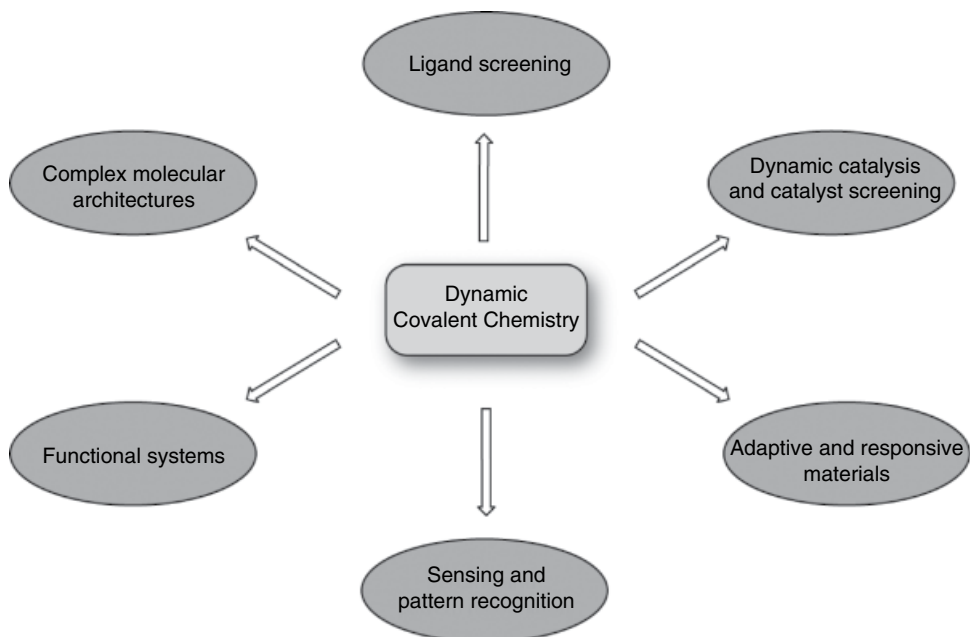
Figure 1.2 Selected applications of dynamic covalent chemistry.

found extensive use in, for example, materials science, nanochemistry, catalysis, surface chemistry, chemical biology, and analytical sensing.[11–16]

In this chapter, the underlying features of dynamic covalent chemistry are described, followed by a short exposé over the toolbox of reversible covalent reactions available today. Furthermore, some of the analytical challenges in DCvC are briefly highlighted.

1.1.2 Importance of Dynamic Covalent Chemistry

Dynamic covalent bonds are ubiquitous in nature, and they are continuously being utilized in biotic settings to provide a wide range of functions. For example, reversible disulfide chemistry controls protein folding and thus the self-assembly of polypeptides into ternary structures, dynamic imines are integral for human vision, reversible thioesters are key players in our metabolic pathways, and dynamic covalent enone chemistry is a reason why red peppers are so pungent.[17]

Furthermore, DCvC provides an entry into the design of complex systems capable of continuous adaptation and evolution. Creating function by design is a central objective in chemistry, and dynamic covalent bonds provide access to systems capable of self-sorting, replication, adaptation towards selection pressures, self-healing, and the construction of highly complex molecular architectures. Some macrocyclic/cage molecules synthesized through DCvC approaches are displayed in Figure 1.3. The Solomon link (left), prism (middle), and nanocapsule (right) all represent structures that would be difficult to access without DCvC.[18–20]

Since dynamic covalent chemistry operates under thermodynamic control, it allows a system of components (building blocks) and/or constituents (products) to settle into its thermodynamically most favorable state. Thus, the information stored in the molecular components of a system can be expressed with high precision and a high degree of "proof-reading", giving access to the optimal molecular architectures for a given setting. In comparison with "static", non-dynamic chemistry, DCvC thus relies on the inherent molecular information in the system. Since any constituent created during a synthesis utilizing reversible covalent bonds is eventually reprocessed, DCvC acts as a sort of error-correction, where non-optimal intermediates are recycled to form the thermodynamically more stable products.

1.1.3 Basic Concepts

Large *dynamic systems* (Figure 1.4) of interconverting molecular entities can be generated using DCvC. These systems undergo continuous exchange towards an equilibrium point through the information contained in either the molecules themselves or their surroundings.

As mentioned, when the intrinsic dynamic nature of CDC is applied to large systems with collections of molecular entities, *dynamic* (DCLs) or *virtual combinatorial libraries* (VCLs) can be created, the latter representing situations where constituents remain unexpressed in the absence of stabilizing entities.[21–23]

A dynamic covalent bond is reversible and can be broken and reformed to eventually reach a thermodynamic equilibrium. Once this has been established, the molecular status quo can be disturbed if the system is perturbed by stimuli. For example, the constitution of dynamic systems can respond to changes in chemical environment (complexing entities, etc.) or physical conditions (temperature, mechanical stress,
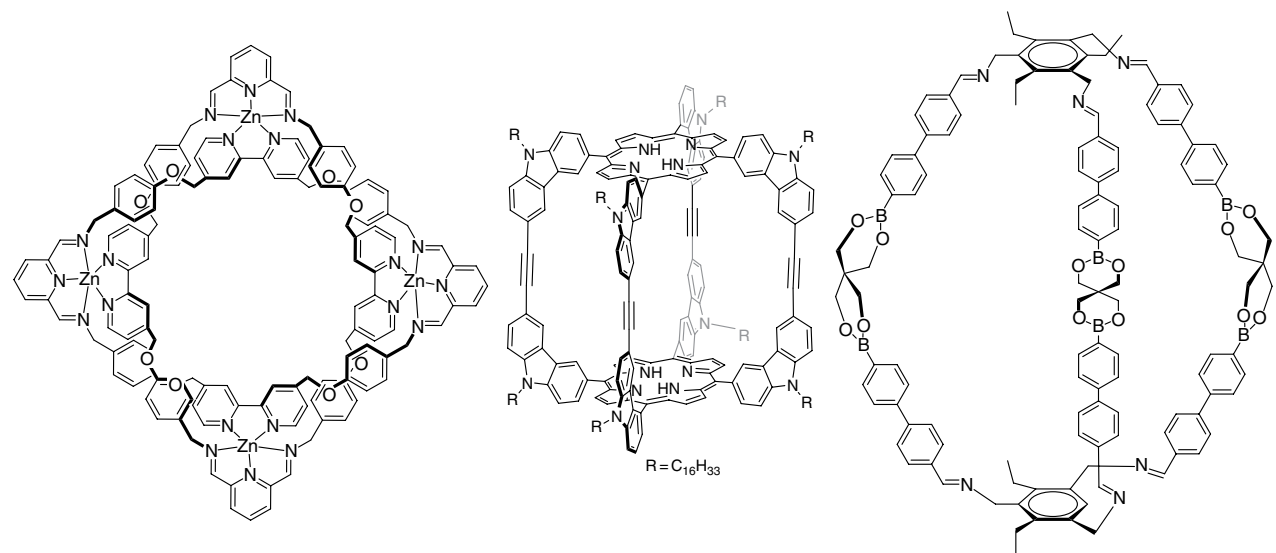
Figure 1.3 Examples of complex macrocyclic/cage structures created through dynamic covalent chemistry.
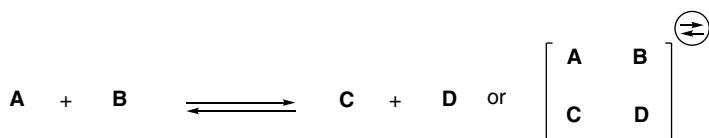
Figure 1.4 Two alternative representations of a dynamic system with the components A, B, C, and D undergoing reversible exchange.
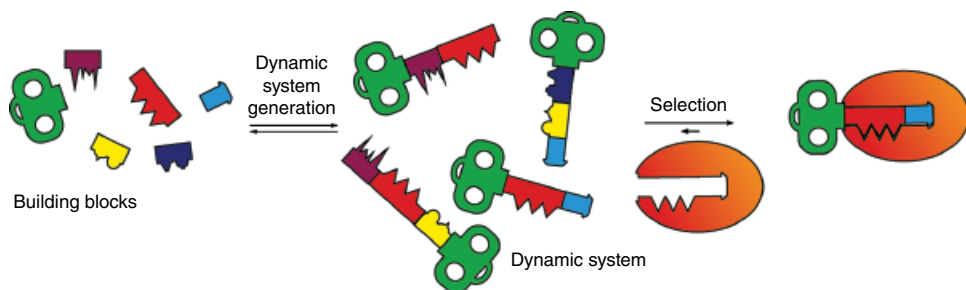
Figure 1.5 Illustration of the basic concept behind selection in dynamic covalent chemistry. The building blocks self-assemble into different "keys", and the key that best fits into the "lock" is amplified at the expense of the other keys.

electric field, irradiation, etc.). This constitutional adaptation leads to the "evolution" of a more favorable thermodynamic system under the new conditions. For example, when a dynamic system is exposed to a target selector (e.g., ligand, receptor) that can selectively interact with one of the many interconverting substituents, the system can be perturbed. The transient stabilization of the best constituent by the target selector will cause re-equilibration of the system, ideally leading to amplification of the "fittest" compound at the expense of all other combinations. The concept can be illustrated through Emil Fischer's lock-and-key metaphor (Figure 1.5). Here, the keys are constructed from different dynamically reacting components, and the addition of a lock stabilizes and amplifies the key that best fits the keyhole. This type of "thermodynamic self-screening" is appealing for drug/ligand discovery applications, as the best binder can be directly identified from a large system by inspection of the component distribution before and after target addition. This circumvents the need for synthesis and purification as well as screening of each individual compound.

1.2 The Dynamic Covalent Bond

1.2.1 Requirements for Dynamic Covalent Bonds

The most important criteria for dynamic covalent bonds are the covalent nature and the bond strengths. For some systems, a lifetime of each bond in the range $1\,\text{ms} < \tau < 1\,\text{min}$ has been proposed to yield connections that are stable and detectable with most analytical methods, yet dynamic enough to allow swift adaptation.[9] This translates into equilibrium times in the order of hours to days for large dynamic systems. The upper limit of the equilibration time for a DCvC application is also related to the degradation

stability of the components and constituents in the system, as equilibrium must be attained before the system starts degrading.

As covalent connections are intrinsically more stable than supramolecular interactions, dynamic covalent bonds are typically much more robust but also slower to exchange than the corresponding supramolecular interactions. Thus, most dynamic covalent bonds require some type of catalysis in order to promote exchange (discussed further in section 1.2.2).

For dynamic covalent bonds, mild reaction conditions are beneficial for preserving the integrity of the bond and to maintain delicate non-covalent interactions of interest in the system. The reactions should also be compatible with the application of interest, and resistance to moisture and oxygen is of general importance. For biological applications, a dynamic covalent bond should exchange readily in water or water/organic solvent mixtures, although only a few bonds obeying such criteria have been discovered. Note that a tradeoff between equilibration rates and stability is often observed, with more reactive dynamic covalent bonds leading to lower system stabilities and more difficult analyses.

1.2.2 Catalysis of Exchange

The majority of the dynamic covalent bonds in use today require catalysis to facilitate equilibration. Although this introduces additional operations and increases the complexity of the systems, it also provides several benefits. Primarily, catalysis allows control of the system's progress towards the thermodynamic equilibrium. Manipulations of the catalyst can, for example, be used to halt equilibration prior to analysis or toggle exchange on or off if such switchability is important for system function (see section 1.2.3). Ideally, a catalyst should only modulate the system exchange rate and not the component distribution, but high catalyst loadings can lead to altered equilibrium positions due to complexation effects.[24] Although the energetics of dynamic systems is governed by many response factors, it is preferred to work with lower catalyst concentrations where the catalyst acts fully "innocent".

The catalyst activity and turnover is of critical importance in DCvC applications. The catalyst needs to remain active over many cycles, and a catalyst that is easily deactivated can lead to a situation where the component distribution remains static as a result of catalyst degradation rather than system equilibration. For this reason, it is often necessary to probe if equilibrium has been reached (see section 1.2.5) when working with dynamic bond exchange reactions that require sensitive catalysts.

A widespread selection of bond exchange catalysts has been developed for DCvC purposes, ranging from buffered acid or base solutions to complex catalysts assembled through multistep syntheses. Progress has also been made in the use of immobilized catalysts, for example with solid-supported enzymes or Grubbs metathesis catalysts.[25,26]

1.2.3 Halting Equilibration

"Freezing" of the equilibration process is commonly desired in order to facilitate analysis of the systems. Dynamic equilibration can, for example, be halted by temperature changes, removal of light input or catalyst, or changes in pH. For some bonds, such as imines or hemithioacetals, irreversible derivatization is required to fully "freeze" the equilibrium. In such a case, the freezing reaction needs to be very rapid in relation to
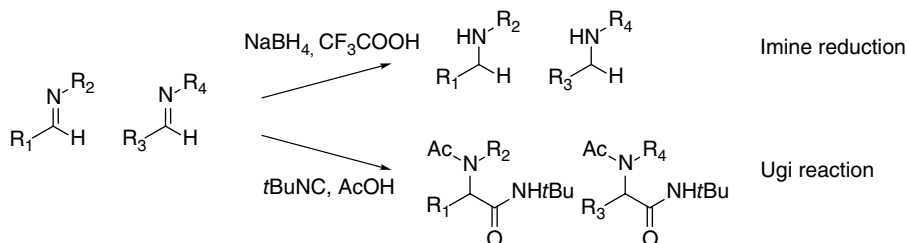
Scheme 1.2 Methods to freeze imine systems by reduction or derivatization to Ugi adducts.

the dynamic exchange reaction, lest the system equilibrates during derivatization. For imine bonds, some ways to freeze an equilibrium without scrambling are highlighted in Scheme 1.2. Reduction of imines to amines with no formation of the scrambling products can be completed with $NaBH_4$ in less than 1 s under certain conditions.[27] Also, other derivation reactions such as the Ugi reaction with isocyanides to create Ugi adducts have been used to halt dynamic equilibration.[28]

1.2.4 Exchange Symmetry

A key feature of dynamic covalent bonds is the bond exchange symmetry. Three main categories of symmetry classes can be discerned: *symmetric*, *unsymmetric*, and *trans-symmetric* bonds (Figure 1.6). Symmetric exchange indicates that both exchange partners undergo interchange through the same functional group, while unsymmetric exchange means that two different types of functional groups build up the dynamic covalent bond. The latter thus leads to directionality of the bond type. Trans-symmetric exchange represents a combination of both exchange modes, where two connected reversible reactions work in concert so that a functional group in an unsymmetric reaction is reversibly transformed into the other.[29]

The exchange symmetry of the bonds has implications for the complexity of dynamic systems. For symmetric connections, there is full symmetry in the exchanging bond, no directionality exists, and the combinations R–R′ and R′–R are mutually commutative. Self-exchange is thus always occurring, as well as oligomerization if multidentate building blocks are used. For unsymmetric exchange, the two functional groups constituting the exchanging reaction are different and self-inert. The advantage is that one can introduce complementary functionalities on each building block. By varying the substituents on one of the functional exchanging groups while keeping the other constant, screening towards cooperativity or optimizing ligand scaffolds becomes more straightforward. On the other hand, it is harder to access all compound combinations within the system
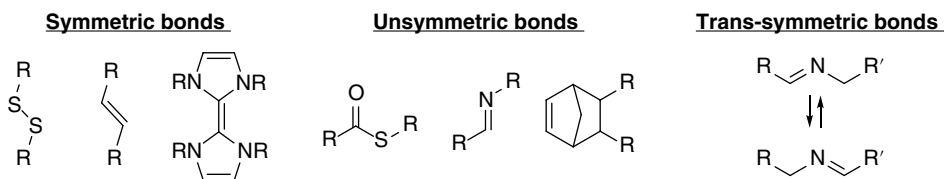
Figure 1.6 Examples of common dynamic covalent bonds within each symmetry class.

with unsymmetrical exchange, limiting the structural diversity. This limitation is, however, overcome with trans-symmetric connections, where the directionality of the linkage can be reversed, resulting in higher complexity.

1.2.5 Methods to Confirm Reversibility

Once a dynamic covalent system has been generated, there is usually a need to confirm that equilibrium is reached. Two methods, both illustrated in Figure 1.7, are commonly employed. The first method is termed *dual entry-point analysis.* Here, a dynamic system is being generated from two different systemic starting compositions while maintaining the overall ratio of the building blocks. Pathway-independence is the defining characteristic of a system at equilibrium. Thus, if the same component distribution is obtained regardless of entry point, it provides evidence that the system is under thermodynamic control. This type of test constitutes the most robust and well-utilized application for testing new dynamic systems and dynamic covalent bonds.

Another useful way to probe equilibration is the *stationary state perturbation* method. Here, an initial dynamic system is generated under the conditions of interest and allowed to evolve until a point is reached where the system composition no longer changes. Thereafter, another exchange partner is added and the system is again allowed to settle into equilibrium. If the new partner has been incorporated into the dynamic system and the initial component distribution has changed, it provides a good indication that the system originally was at equilibrium. For practical purposes, a large excess (typically 5–10 equivalents) of the perturbing compound is usually added so that effects are more clear-cut and easily interpreted. This methodology is advantageous when acquisition of compounds from both "directions" of a dynamic system is difficult (i.e., if one or more of the necessary molecules are commercially unavailable, expensive or difficult to handle).

Finally, it can also be mentioned that a change in the physical properties of the system (i.e., temperature, solvent, concentration, pressure, etc.) commonly produces an equilibrium response, which in specialized applications can be used to test whether a given system is at equilibrium.

Dual entry-point analysis
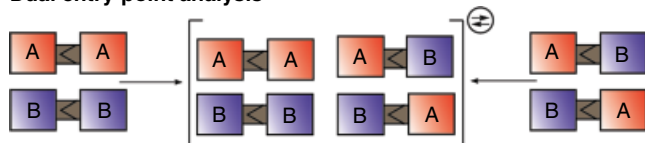
Stationary state perturbation
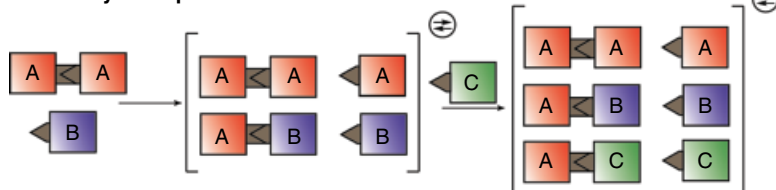
Figure 1.7 Methods to probe if equilibrium has been reached.

1.3 Dynamic Covalent Reactions

The following sections will focus on expanding the theory of dynamic covalent bonds into more concrete examples. These include descriptions of most of the reversible covalent reactions, along with their characteristics.

1.3.1 Dynamic Polar Reactions

A majority of all reversible covalent bonds belong to the class of dynamic polar reactions, which means they pass through charged reactive intermediates during the exchange process. The following reactions are sorted by the main type of bond that is formed or broken during the exchange process.

1.3.1.1 C–N Bonds

The most well-utilized family of bonds in DCvC is C–N bonds. A summary of the available C–N bond exchange reactions can be found in Figures 1.8 to 1.12.

The most prominent example of a reversible C–N bond is the imine, the most extensively used dynamic covalent bond since the inception of DCvC. Dynamic imines have been applied in a remarkable variety of applications, including formation of complex molecular architectures, self-sorting systems, switches and molecular motors.[30] Imines are formed through condensation of the respective aldehyde and amine. Exchange occurs either through a hydrolysis/recondensation pathway or, if water is unavailable, through so-called transimination or imine metathesis mechanisms (Figure 1.8a–c). The exchange mechanisms have been studied in great detail and are discussed in depth in a recent review.[31] Exchange of imines occurs under neutral conditions without additives, but to accelerate the equilibration process one can use Brønsted acid, Lewis acid or nucleophilic catalysis.

Lewis acid activation of imines has been known for decades.[32] The transimination pathway have also been studied in detail by Lehn and coworkers, who discovered that the Lewis acid $Sc(OTf)_3$ is a highly efficient transimination catalyst.[24] It was also demonstrated that the equilibrium composition of the system depends on the basicity of the amine, with the most basic amine forming the most stable imine. Using amines of similar basicity resulted in the highest equilibration rates. Furthermore, it was demonstrated that Lewis acids were more efficient catalysts than Brønsted acids due to a lower degree of deactivation of the nucleophile and catalyst. The last type of imine exchange acceleration is through nucleophilic catalysis with primary amines, shifting the imine exchange reaction to a transimination type mechanism.[33]

C-N exchange with imines
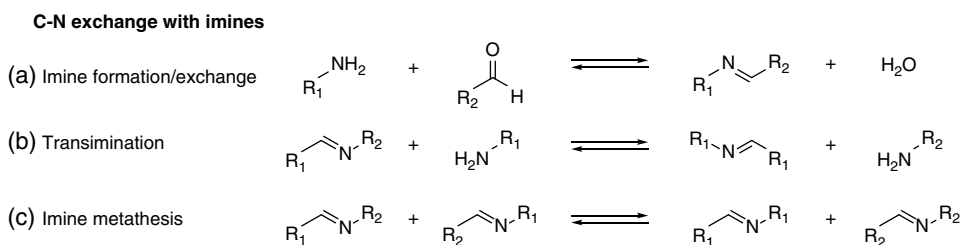
Figure 1.8 C–N bond formation by reversible exchange of imines.

C–N exchange with imine intermediates

(a) Aminal formation

(b) β–amino-enone exchange

(c) Imine rearrangement
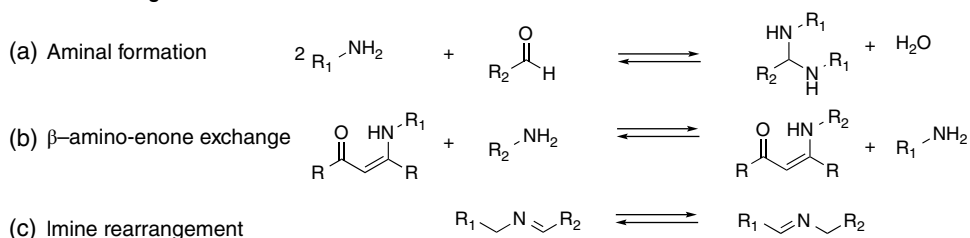
Figure 1.9 Possible exchange intermediates during imine exchange.

Beside the aldehyde and amine components, there are several intermediates involved in imine exchange. Due to their low stability, they can be considered virtual constituents of a system. Labile intermediates like hemi-aminals can only be stabilized through unusual measures, such as complexation inside a synthetic cavitand.[34] An example of reversible hemiaminal and more stable aminal constructs (Figure 1.9a), stabilized by *N*-methyl pyrrolidone, have been demonstrated in dynamic covalent networks formed from diamines and formaldehyde.[35] Due to the reversible nature of this reaction, the polymeric networks formed are recyclable and have self-healing properties, while maintaining high rigidity.

A second type of intermediates from imine formation are β-amino-enones (Figure 1.9b). The presence of the electron-withdrawing keto fragment makes it possible for the molecule to tautomerize to form an imine/iminium ion. This iminium ion undergoes reversible exchange with other amines.[36,37] Similar exchange has also been shown previously with iminium ions as electron-withdrawing facilitator.[38] In both cases, exchange could be achieved in the absence of catalysts and can even be run at near physiological conditions.

Recently, imine rearrangement of α-acidic imines was shown to be fully reversible (Figure 1.9c).[29] In the presence of a quinuclidine catalyst, an "allylic"-type rearrangement takes place. This exchange reaction effectively shifts around carbonyl groups of aldehydes with amine groups of benzylic amines, increasing the dimensions of standard imine systems when coupled to a secondary dynamic reaction such as transimination.

Furthermore, C=N bond exchange reactions aside from normal imines have seen extensive use. The most common alternative C=N exchange reactions are summarized in Figure 1.10, each utilizing N- or O-substituted amines as nucleophiles. Due to the presence of free electron pairs on the adjacent atom to the reactive nitrogen, these molecules have a higher nucleophilic character. This also increases the stability of the formed imine bond, due to the reduced electrophilicity.

Uncharged hydrazones, acylhydrazones and oximes (Figure 1.10a–c) have been studied extensively due to their compatibility with biological systems. However, the enhanced stability leads to slow exchange kinetics. In comparison to imines, acylhydrazones and especially oximes are very stable and require efficient catalysis for exchange to occur. Oximes can be formed using aniline catalyst, which works most effectively at slightly acidic conditions (pH = 4.5) to protonate the intermediate aniline-derived imine (Scheme 1.3).[39,40]

For hydrazones and acylhydrazones, a decrease in stability is observed compared to oximes, making exchange more straightforward. For hydrazone exchange, it has been
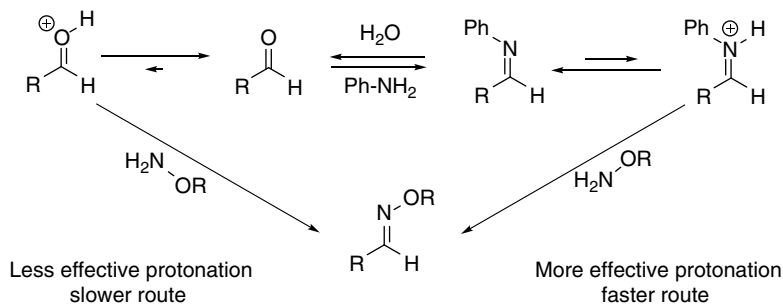
Scheme 1.3 Oxime formation catalyzed by aniline.

shown that strong acid catalysis results in decomposition products, but efficient exchange can be obtained using Lewis acid catalyst with loadings as low as 1%.[41] Due to its resemblance to a peptide bond, the acylhydrazone moiety has sometimes been referred to as a "dynamic peptide" and research has focused on improving the biological compatibility of the exchange process. The dynamic system can easily be frozen by pH modulation and, similar to oximes, exchange can be accelerated using aniline catalysis.[42] This procedure later was made more compatible with biological conditions by making exchange available at pH values as high as 6.[43]

Nitrones are the least studied reversible $C=N$ bonds (Figure 1.10d). Their exchange can be directly facilitated using a combination of nucleophilic and Brønsted acid catalysis.[44] Unlike all the other imine type bonds, the nitrone exchange equilibrium seems to be insensitive to the concentration of acid catalyst utilized.

Besides imine-type exchange, other reversible C–N bonds have been designed. The amide bond (Figure 1.12a) is of high biological importance, and dynamic versions of this connection are thus highly desirable. Efficient exchange of amides could lead to discovery of important applications for dynamic polymers, drug discovery and many other areas. However, the amide bond is chemically robust and requires harsh conditions or specific enzymes to break up. One way to facilitate transamidation is using metal catalysts to activate secondary amides, shown using Fe(III) salts and $Al_2(NMe_2)_6$.[45,46]

Imine exchange with α-effect nucleophiles
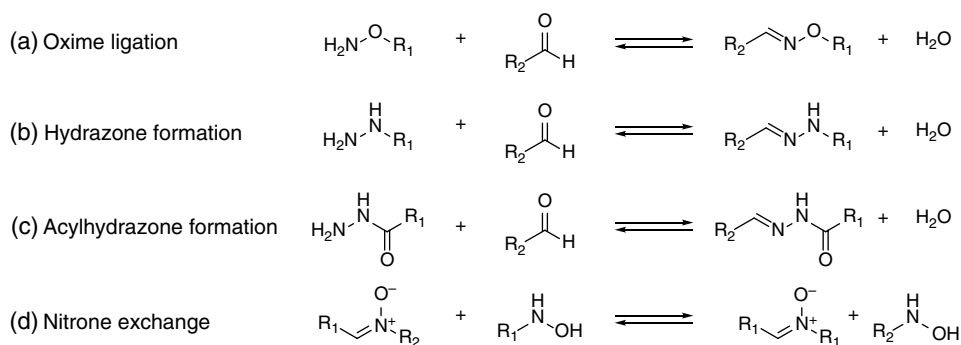
Figure 1.10 Imine-type bonds with different nucleophiles.

However, both of these procedures require elevated temperatures and organic solvents, making them incompatible with biological systems. $Zr(NMe)_4$ has also been used, enabling exchange of tertiary amides in organic solvents under ambient conditions.[47] Exchange of tertiary amides is, however, more straightforward, circumventing deprotonation of the otherwise relatively acidic amide protons. This was also used in a method related to native chemical ligation, where efficient amide exchange in peptides was demonstrated.[48] Introduction of an *N*-(methyl)cysteine residue in the peptide chain shifted the reaction mechanism from intermolecular transamidation to intramolecular amide-thioester exchange (Figure 1.11).

Ureas are structurally related to amides but have been shown to undergo dynamic exchange via the isocyanate (Figure 1.12b).[49] Destabilization of the urea bond by introduction of bulky substituents on the nitrogen facilitated the dissociation/recombination procedure, and the exchange rate and the equilibrium constant could easily be controlled by changing the size of the substituent (Scheme 1.4). Bulkier substituents favored the formation of the isocyanate, while less bulky substituents led to favored urea formation.

The last reversible C–N bond type discussed here is reversible nucleophilic substitution, typically at quaternary nitrogen centra (Figure 1.12c). It has, for example, been shown that paraquat-based macrocycles undergo reversible ring opening and closing under catalysis with iodide ions, allowing efficient access to catenane-type structures.[50,51]

1.3.1.2 C–C Bonds

Formation of carbon–carbon bonds is the core of organic chemistry and reversible polar C–C single bond exchange has thus been studied extensively. A summary of the available reactions can be found in Figures 1.13 to 1.16.

A classical reversible C–C bond formation is the aldol reaction (Figure 1.13a). This reaction has not found much application in DCvC, mainly because of challenges with side reactions and finding suitable catalysts. An example of reversible aldol exchange was, however, carried out under enzyme catalysis with *N*-acetylneuraminic acid aldolase to facilitate exchange between a variety of hexoses and sodium pyruvate.[52] Another example of aldol exchange used a combination of Brønsted base and Lewis acid catalysis, utilizing triazabicyclo[4.4.0]dec-5-ene and Al_2O_3, which resulted in relatively rapid formation of aldol products in both aqueous and apolar aprotic conditions.[53] When extending this catalytic system to a full system, an excess of ketone was necessary to facilitate exchange.

In the nitroaldol- (Henry) reaction, nitroalkanes are used as nucleophiles (Figure 1.13b). In contrast to the aldol reaction, this system readily undergoes dynamic exchange under a variety of conditions.[54] A stereocenter is also formed during the addition step, generating an additional level of structural information that can be selectively interpreted or resolved in a selection step.[55]

Cyanohydrins are highly important compounds in both biochemistry and organic synthesis due to their versatility as synthetic intermediates. Cyanation of aldehydes was found to be readily reversible in the presence of a base catalyst, and the exchange process was biocompatible and rapid (Figure 1.13c). Another dynamic C–C bond formation based on cyanide addition is the Strecker reaction, where a cyanide ion adds to an in situ formed imine, yielding an α-amino nitrile (Figure 1.13d). The dynamic behavior of this three-component reaction has been studied extensively,[56,57] where the cyanation
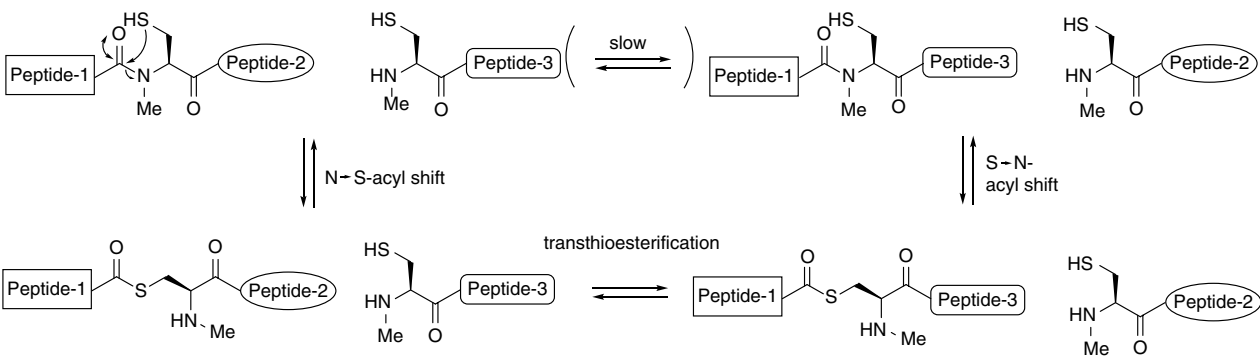
Figure 1.11 Amide exchange proceeding through intramolecular thioester exchange.
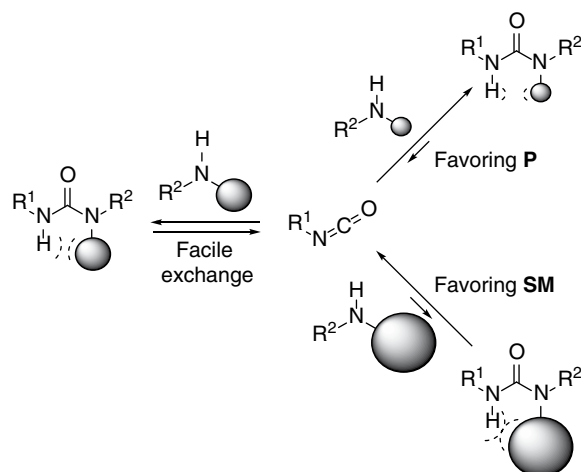
Scheme 1.4 Tuning of equilibrium position in urea–isocyanate equilibrium by changing the steric bulk of substituents.

Other C–N exchange reactions

(a) Transamidation

(b) Urea formation

(c) Nucleophilic substitution
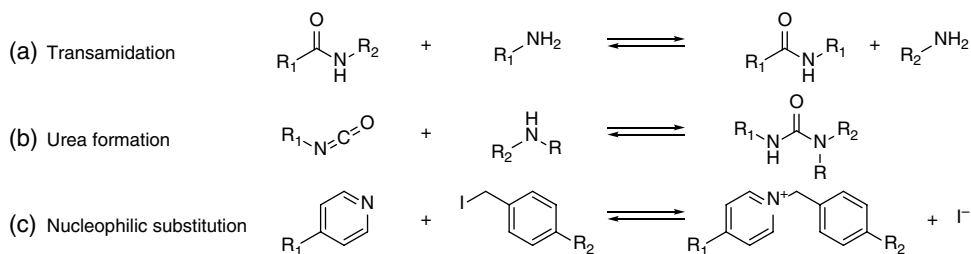
Figure 1.12 Other C–N bond formation reactions.

Carbon nucleophile additions to carbonyls

(a) Aldol reaction

(b) Nitroaldol reaction

(c) Cyanohydrin formation

(d) Strecker reaction

(e) Knoevenagel reaction
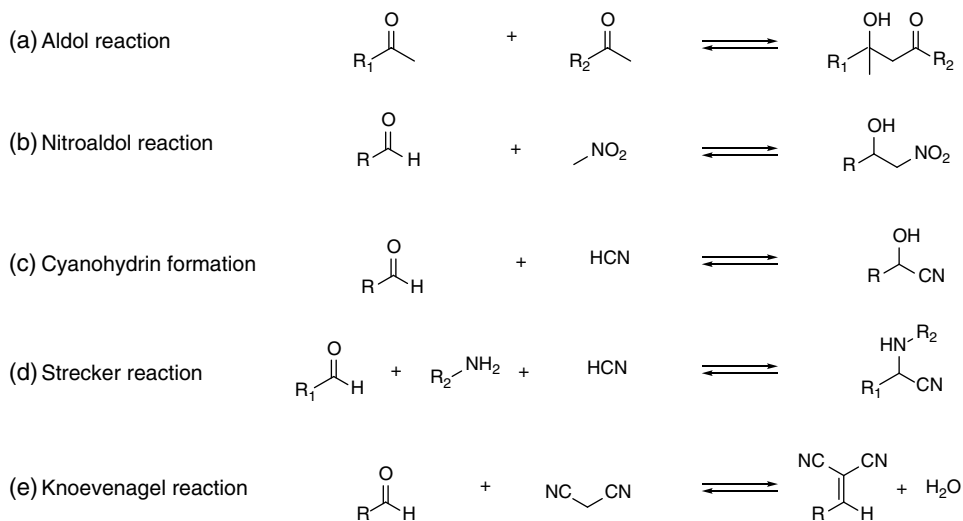
Figure 1.13 C–C bond formation by nucleophilic addition of carbon nucleophiles.

Carbene-based C–C exchange

(a) Carbene dimerization

(b) Carbene isothiocyanate coupling
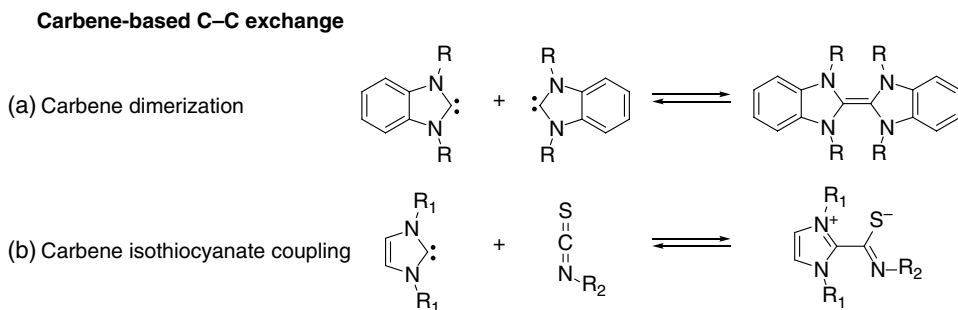
Figure 1.14 C–C bond formation employing carbene building blocks.

was found to be reversibly catalyzed by Lewis acids like zinc halides. Zinc bromide proved especially efficient in the overall, three-component Strecker reaction, catalyzing not only the cyanide exchange, but also the transimination step.

Recently, this type of chemistry has been expanded to include Knoevenagel-type products (Figure 1.13e), which exchange readily in the presence of water under catalysis by secondary amines such as *L*-proline. This type of exchange was also compatible with imine chemistry, leading to connected dynamic systems where several different equilibria operated simultaneously.[58,59]

A second group of C–C bond-forming reactions consists of carbene-based reactions. *N*-heterocyclic carbenes (NHCs) exist as both monomers and dimers (see Figure 1.14a), and the equilibrium position depends on the nature of the heterocyclic ring and the size of the substituents. It has, for example, been demonstrated that a dicarbene structure can form a mixture of polymers and free carbenes, which changes composition in a reversible fashion based on the amount of heat or chain transfer agent applied.[60] Reversible NHC coupling to isothiocyanates was also shown (Figure 1.14b).[61] This reaction favors the formation of the adduct, but at elevated temperatures the NHC is reversibly released.

Reversible C–C bond formations based on electrophilic aromatic substitutions have furthermore been developed (Figure 1.15). It was discovered that when a Lewis acid catalyzed Friedel–Crafts alkylation between a symmetrical bis-nucleophilic and a symmetrical bis-electrophilic species was performed, a macrocycle consisting of an odd number of starting materials was obtained. Since the starting materials are symmetrical, this phenomenon is only explicable if the reaction is reversible.[62] A variety of Lewis acids like $ZnCl_2$, $FeCl_3$, $BF_3 \cdot OEt_2$ and $AlCl_3$ proved capable of facilitating this exchange at room temperature, with $AlCl_3$ being the most efficient. Another electrophilic aromatic substitution found to be reversible is the condensation of formaldehyde with electron-rich aromatic rings (Figure 1.15b). It thus was shown that calix[8]arenes undergo reorganization to calix[4]arenes under strongly basic conditions at elevated temperatures.[63] Similarly, it was also demonstrated that reversibility for this reaction can be attained using elevated temperatures and strongly acidic conditions.[64]

The most useful dynamic covalent C–C bond-forming reaction is probably olefin metathesis (Figure 1.16a). Although principally not polar in nature, this reaction allows for exchange of the substituents on a C=C double bond in the presence of a metal catalyst. Proceeding through sequential [2 + 2] cycloadditions via metallacyclic

Electrophilic aromatic substitutions

(a) Friedel-Crafts alkylation

(b) Electrophilic aromatic substitution
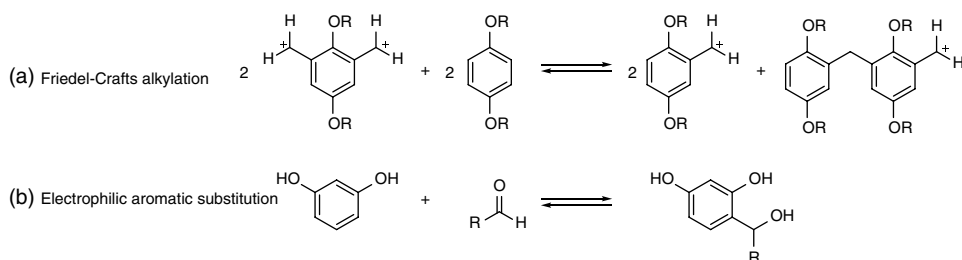
Figure 1.15 C–C bond formations by electrophilic aromatic substitution.

Dynamic organometallic C–C bond formations

(a) Alkene metathesis

(b) Alkyne metathesis
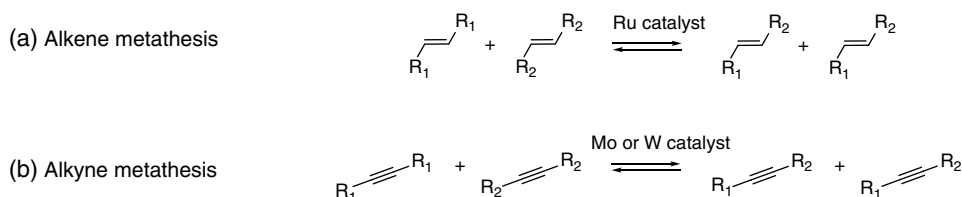
Figure 1.16 C–C bond formations proceeding through organometallic intermediates with transition metal catalysis.

intermediates, the overall reversibility of the reaction is well known. The reaction has been used extensively, for example, in dynamic combinatorial applications, and for the construction of shape-persistent macrocycles under thermodynamic control.[26, 65–68] A wide array of catalysts for the transformation is available, with the Grubbs second-generation catalyst and the Grubbs–Hoveyda catalyst (Figure 1.17) being the most prominent.[69]

Olefin metathesis has advantages such as mild reaction conditions, wide functional group tolerance, commercially available catalysts, fast exchange kinetics, and orthogonal reactivity relative to many other dynamic covalent bonds. Most common functionalities can operate simultaneously with olefin metathesis, although strongly coordinating compounds such as amines, nitriles or phosphines sometimes poison the catalyst. Other pitfalls in dynamic olefin metathesis can be found in the reactivity difference between terminal and internal alkenes, rendering the reactions prone to kinetic traps. Also, the catalyst turnover numbers are sometimes inadequate for long-term DCvC applications, and the presence of both *E*- and *Z*-alkenes complicates analysis. Lastly, the equilibrium is hard to freeze, and even trace amounts of remaining catalyst during purification can promote further metathesis.[70]

Another type of metal-catalyzed dynamic reaction is alkyne metathesis (Figure 1.16b), which initially suffered from stability problems and low turnovers of the catalysts. However, recent development of new classes of Schrock-type Mo(VI) based catalysts has led to significantly decreased moist and air sensitivities (Figure 1.17, bottom), improving the usability for dynamic chemistry.[71,72]

Figure 1.17 Catalysts for dynamic alkene and alkyne metathesis.

Olefin metathesis:

Grubbs
2nd generation

Grubbs-Hoveyda
catalyst
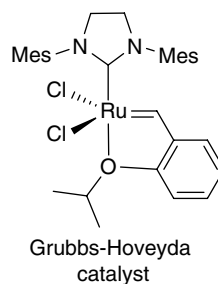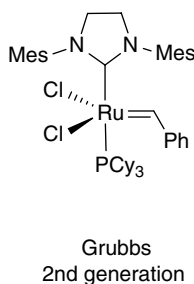
Alkyne metathesis:
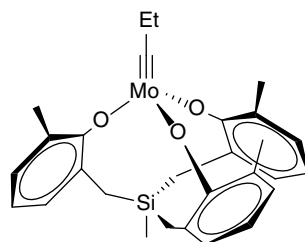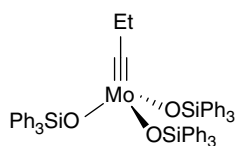
1.3.1.3 C–O Bonds

The dynamic exchange of C–O bonds has been extensively studied, although applications in dynamic systems are rather limited. A summary of the available reactions can be found in Figures 1.18 and 1.19.

The first class of dynamic C–O bonds are based on nucleophilic additions to C=O bonds. One of the most unstable reversible bonds of this type is hemiacetals (Figure 1.18a). Hemiacetals form readily under basic as well as acidic conditions, but can normally not be isolated due to the unfavorable equilibria. In combination with metal-templating, however, observable hemiacetals can be formed.[73]

Oxygen nucleophile addition to carbonyls

(a) Hemiacetal exchange

(b) Acetal exchange

(c) Orthoester exchange

(d) Ester exchange
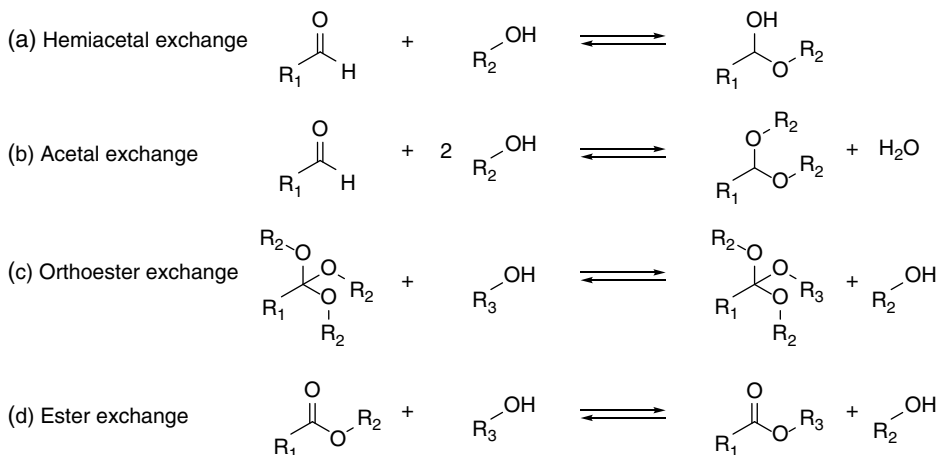
Figure 1.18 C–O bond formation by nucleophilic addition of oxygen nucleophiles to carbonyl groups.

Dynamic organometallic C–O bond formations

(a) Nicholas ether exchange

(b) Transallylesterification
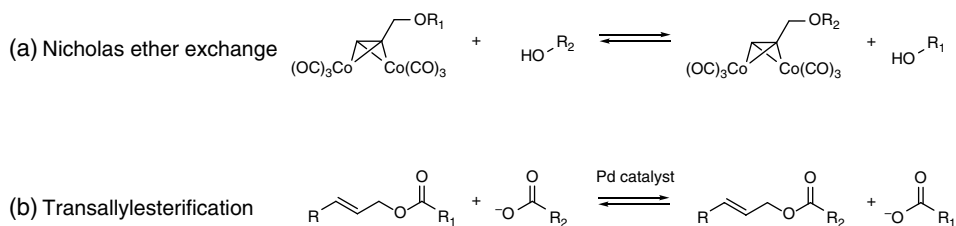
Figure 1.19 C–O bond formations proceeding through organometallic intermediates.

When hemiacetal formation is carried out under acidic conditions, the reaction can proceed further through a dehydration step to form more easily handled acetals (Figure 1.18b).[74,75] The exchange, however, needs to be carried out under dry conditions to avoid hydrolysis of the acetals. Furthermore, alcohol exchange with orthoesters was recently demonstrated.[76,77] Rapid exchange was observed under Brønsted acid catalysis, but, similar to acetal exchange, this reaction is incompatible with aqueous environments, as hydrolysis products dominate the system. However, when considering direct exchange between two distinct orthoesters, the addition of a minimal amount of water aids the reaction by release of alcohols as mediator. This reaction is of significant interest due to the three-dimensional nature, as the tripodal exchange motif is unique in a dynamic chemistry context.

Ester exchange, as shown in Figure 1.18d, is another reaction where the dynamics of C–O bonds are used. In traditional (trans)esterifications, strong acids or bases are commonly utilized as catalysts.[78] However, undesired decomposition of components of the system can occur under harsh conditions, especially during prolonged exchange. Equilibration of esters have also been performed using strong Brønsted bases like NaOt-Bu and DBU, or Lewis acids such as $Ti(OBu)_4$ as catalysts.[79,80] A high excess of base can be necessary to increase the equilibration rates in these cases.

Beside the dynamic C–O bonds that utilize the inherent reactivity of functional groups, some transition metal-catalyzed C–O bond exchange procedures have also been developed (Figure 1.19). For example, another way to utilize alkynes as dynamic linkages aside from alkyne metathesis is to convert them into their corresponding Nicholas ether adducts. These cobalt complexes have recently been demonstrated to be reversible when the ether groups are positioned α to the cobalt carbonyl–alkyne complex (Figure 1.19a).[81] In order for dynamic covalent exchange to proceed rapidly, strong Lewis or Brønsted acids such as $BF_3 \cdot OEt_2$ or TfOH need to be added, with resulting equilibration times in the order of 3–24 h. The original alkynes can also be efficiently regenerated using cerium(IV) ammonium nitrate. Another type of dynamic C–O bond is reversible transallylesterification, utilizing palladium catalysis to scramble allylic esters under thermodynamic control (Figure 1.19b).[82]

1.3.1.4 C–S Bonds

Dynamic C–S bonds have much in common with C–O bonds, as implicated by the related positions of S and O in the periodic table. Sulfur has a more nucleophilic character, however, and is also a better leaving group. Reversible exchange reactions with C–S bonds thus tend to follow similar reaction pathways as with C–O bonds, but

Sulfur nucleophile addition to electrophilic carbon
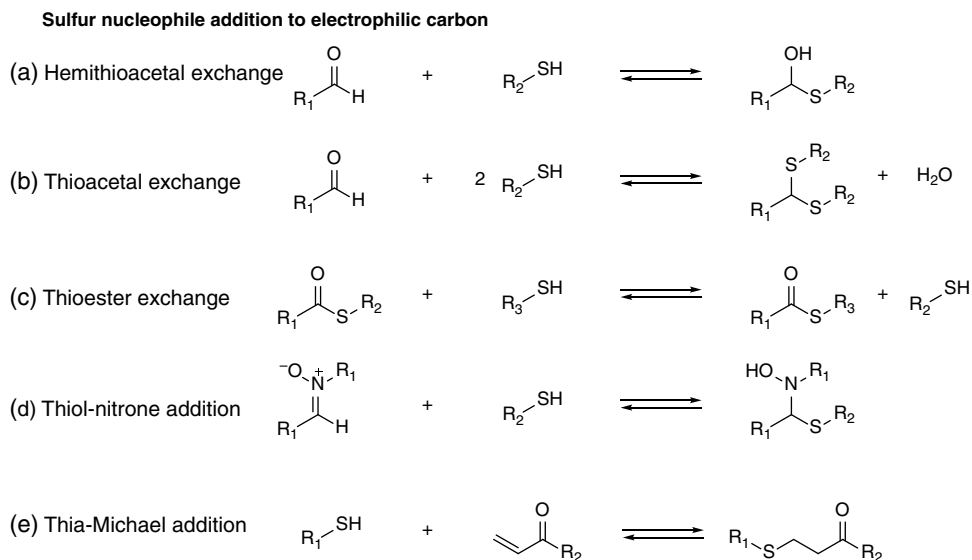
Figure 1.20 C–S bond by addition of sulfur nucleophiles to electrophilic carbon atoms.

characteristics regarding equilibration rates and catalysis are different. A summary of the reactions discussed in this section can be found in Figure 1.20.

Similar to alcohols, thiols can also add to carbonyl groups to generate unstable hemithioacetals (Figure 1.20a).[83,84] When the reaction is conducted with excess thiol and removal of H_2O, stable thioacetals (Figure 1.20b) can be obtained. The dehydration step is crucial and only acidic conditions give satisfactory equilibration rates. Brønsted acids promote thioacetal formation but not the reverse reaction, whereas the Lewis acid $Zn(OTf)_2$ result in swift forward and reverse reactions.[85]

When comparing ester exchange with thioester exchange (Figure 1.20c), the differences are even more striking. Whereas ester exchange requires harsh conditions and is incompatible with aqueous conditions, thioester exchange does not require any catalysis and can be conducted under mild conditions in water.[86,87] Due to the reactivity of thiols towards thioesters, thioester exchange is also compatible with functionalities present in peptides and nucleic acids.[88,89] In addition, it has been shown that introduction of positively charged residues in the molecule can enhance the equilibration rate by possible stabilization of the negative charge building up in the transition state.[90]

Thiols can also add to other carbonyl-type bonds such as nitrones (Figure 1.20d).[91] However, the equilibrium constants are heavily weighted towards starting materials, and the established equilibria are essentially virtual. Nevertheless, the exchange is rapid and biocompatible, and the formed products can be kinetically trapped to drive the equilibrium away from the nitrone side.

Reversible thia-Michael additions (Figure 1.20e) have also been demonstrated. Due to the presence of surface-centered cysteine residues on many proteins, this type of exchange is of great interest for the design of reversible covalent drugs, a rapidly expanding area.[15] For specific systems, the thia-Michael addition has been shown to be reversible on a short timescale under slightly basic conditions (pH = 8), with a fairly equal distribution between the starting materials and the adducts.[92] When shifting to
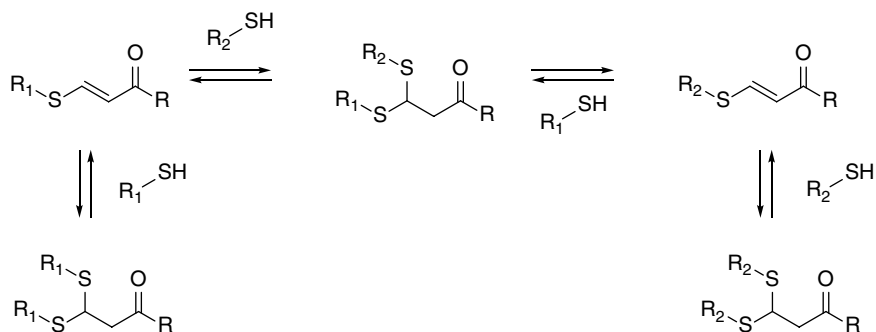
Scheme 1.5 Thioacetal exchange through thia-Michael addition.

acidic conditions, equilibration was halted. Using the more electron-poor enone fragments derived from benzalcyanoacetamides, significantly enhanced equilibration rates were demonstrated.[93] Moreover, it was shown that the equilibrium position could be shifted by substituting the aromatic ring with electron-withdrawing groups, reducing the electron density of the enone fragment.

It has also been shown that thia-Michael systems starting from β-sulfido-substituted enone fragments efficiently exchange thiols to form new β-sulfido-substituted enones and β-dithiane carbonyls.[94] In these specific systems, the thioacetal exchange (Scheme 1.5) could be performed under basic conditions, proceeding through a Michael-type instead of hemiacetal-type mechanism.

1.3.1.5 S–S Bonds and Se–Se Bonds

The second most utilized dynamic covalent connection after imines are the disulfides.[95] Other chalcogenic exchange reactions such as selenide–selenide and sulfur–selenide exchange have also been reported, but as the disulfide exchange reaction is of exceptional importance in DCvC the following section will mainly focus on this reaction.

Disulfide chemistry (Figure 1.21a) plays an important role in many biological processes, such as protein folding, and remains ubiquitous in DCvC since its inception.[96,97] The exchange can be triggered by nucleophilic attack of a thiolate anion on the disulfide bond, creating a new disulfide and regenerating a new thiolate anion. Phosphines have furthermore been shown to catalyze the reaction.[98,99] As the exchange requires a deprotonated thiol, this reaction is dependent on the pH of the mixture and a pH range around 7–9 is usually adequate to achieve fast equilibration. Not only can addition of thiol catalyze the exchange, but the same thermodynamic equilibrium can be obtained when starting from solely disulfides and adding reducing agent to form a catalytic amount of thiols *in situ*. Another common method to generate disulfide systems is to simply mix the corresponding thiols and allow the mixture to oxidize in the presence of air, or by addition of other oxidation agents.[100,101] The exchange can be stopped by either complete oxidation to disulfides or protonating the thiolates by lowering the pH of the mixture. Disulfide exchange can also be performed using thiolate- or transition metal catalysis in organic solvents.[102]

An extension of S–S bond chemistry is found when selenols and diselenides are utilized instead (Figure 1.21b,c). As selenols are more acidic than the corresponding thiols, there will be a comparatively higher concentration of selenolates in the mixture at

Disulfide- and diselenide-type exchange

(a) Disulfide exchange

(b) Selenylsulfide exchange

(c) Diselenide exchange
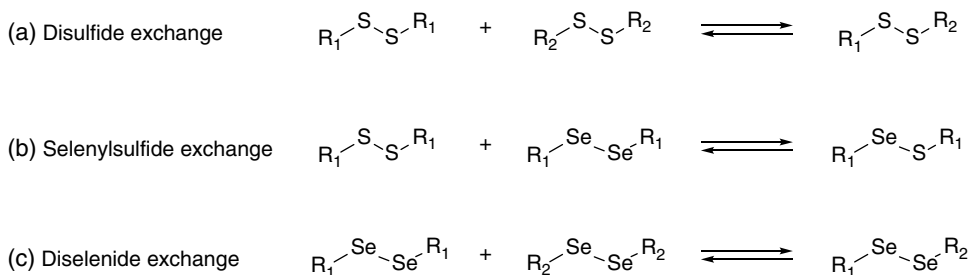
Figure 1.21 Disulfide and diselenide exchange reactions.

neutral pH. It has been shown that diselenide exchange in combination with a thiol initiator remains efficient down to a pH of 5.[103] When combining a diselenide building block with a disulfide building block, scrambling of the components and reorganization of the system towards both homocoupled and heterocoupled products could be observed. Because the sulfur–selenide heteroexchange proved to be faster, a small amount of diselenide can be added to disulfide mixtures to facilitate disulfide exchange. Diselenide exchange has also been demonstrated under visible light catalysis,[104] proceeding in a variety of solvents under mild conditions.

1.3.1.6 B–O Bonds

The last of extensively investigated dynamic polar bonds are the B–O bonds. While B–O bonds can be made with monovalent alcohols, the thermodynamic stability of the formed product is low and isolation and characterization is difficult. For that reason, the main exchange reactions involving B–O bonds generally involve diols, which form more stable products (Figure 1.22a).

Due to the reversible interaction of boronic acids with Lewis bases, these compounds have found applications in molecular recognition, sensing and self-assembly of complex molecular architectures.[105] The first type of reversible B–O bond formation are the boronic esters (Figure 1.22a). As reactants for Suzuki couplings, a lot of attention has gone into the synthesis of boronic esters, which similarly to normal esters are formed through dehydration reactions. To achieve efficient exchange of boronic esters at room

B–O bond exchange

(a) Boronic ester formation

(b) Boronate ester formation
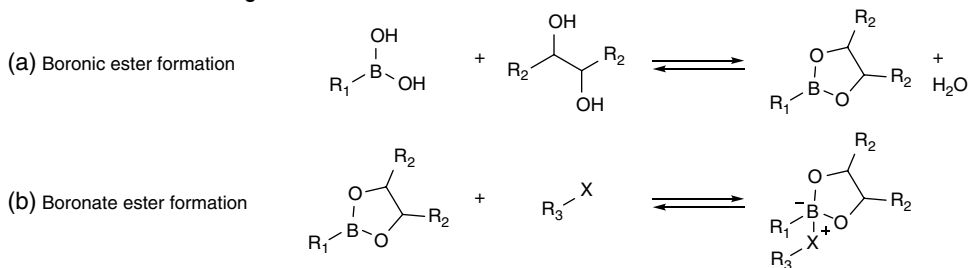
Figure 1.22 B–O bond formation by condensation and addition.

temperature, the presence of a nucleophile like water or alcohols is necessary[34,106] However, the dynamic system is not necessarily restricted to boronic esters, as the boron center still acts as a Lewis acid. Coordination of additional ligands results in formation of boronate esters (Figure 1.22b). Ligands that have been successfully used in this exchange include water, alcohols, phosphonic acids and nitrogen-containing aromatic heterocycles, all of which exchange readily at room temperature.[107–109] To ensure that boronate ester formation is the favored pathway, one can increase the pH of the mixture to higher levels than the pK_a of the present boronic esters.[108]

1.3.1.7 N–X Bonds

Even though a wide range of dynamic polar reactions are available today, there is still much ongoing research towards development of new exchange processes. Some interesting types include Se–N bonds and P–N bonds. Se–N bonds can be formed between selenylhalides and pyridine substituents in the presence of heat or DMAP as a catalyst, and P–N bonds can be formed between azides and phosphines in a reaction that is readily reversible at ambient temperature without addition of a catalyst.[110,111]

1.3.2 Other Dynamic Reaction Types

1.3.2.1 Dynamic Covalent Pericyclic Reactions

Reversible pericyclic reactions have also been pursued, and some examples are summarized in Figure 1.23. The advantage of this class of transformation resides in the self-contained nature of the reaction, meaning all atoms present in the reactants are also incorporated into the products. This property is of high interest for dynamic polymers, as it entails potential self-healing properties to the resulting material without the need for any additives. Furthermore, pericyclic reactions are orthogonal with most other dynamic covalent bonds.

The Diels–Alder reaction is the prototypical pericyclic reaction (Figure 1.23a). Formally classified as a [4 + 2] cycloaddition, the reversibility of this highly useful reaction has been well known for many years.[112] However, since the Diels–Alder reaction can be defined as a net formation of two C–C σ bonds at the expense of two weaker C–C π bonds, it is inherently exothermic and the retro reaction can thus be kinetically disfavored. Usually, either high temperatures or highly tailored dienes and dienophiles are required for swift reversibility. An example of such a system is when electron-poor dienes and electron-rich dienophiles are employed. Then, the HOMO–LUMO energy gap is relatively small, resulting in facile dynamic [4 + 2] exchange even under mild conditions.

Room-temperature dynamic covalent Diels–Alder reactions have been demonstrated.[113] In one example, the dynamic exchange reaction between adducts formed from fulvenes and cyanoethylenes proceeded with very quick equilibration time (<1 minute) at room temperature in CDCl$_3$. Both the exchange specificity and the system stability were very high. In another example, dimethyl-substituted anthracenes were applied as efficient dienes for dynamic covalent [4 + 2] reactions (Scheme 1.6).[114] The exchange rates were slower as compared to the fulvenes, with room temperature equilibration in the order of days to weeks.

Due to higher accessibility and synthetic utility, efforts to understand and utilize the reversibility in the more conventional Diels–Alder reaction between maleimides and

Dynamic pericyclic reactions

(a) Diels-Alder reaction

(b) Ene reaction

(c) [2+1] cycloadditions

X = CHR', O

(d) [4+4] cycloadditions

$h\nu$

(e) Cope rearrangement

+ other isomers
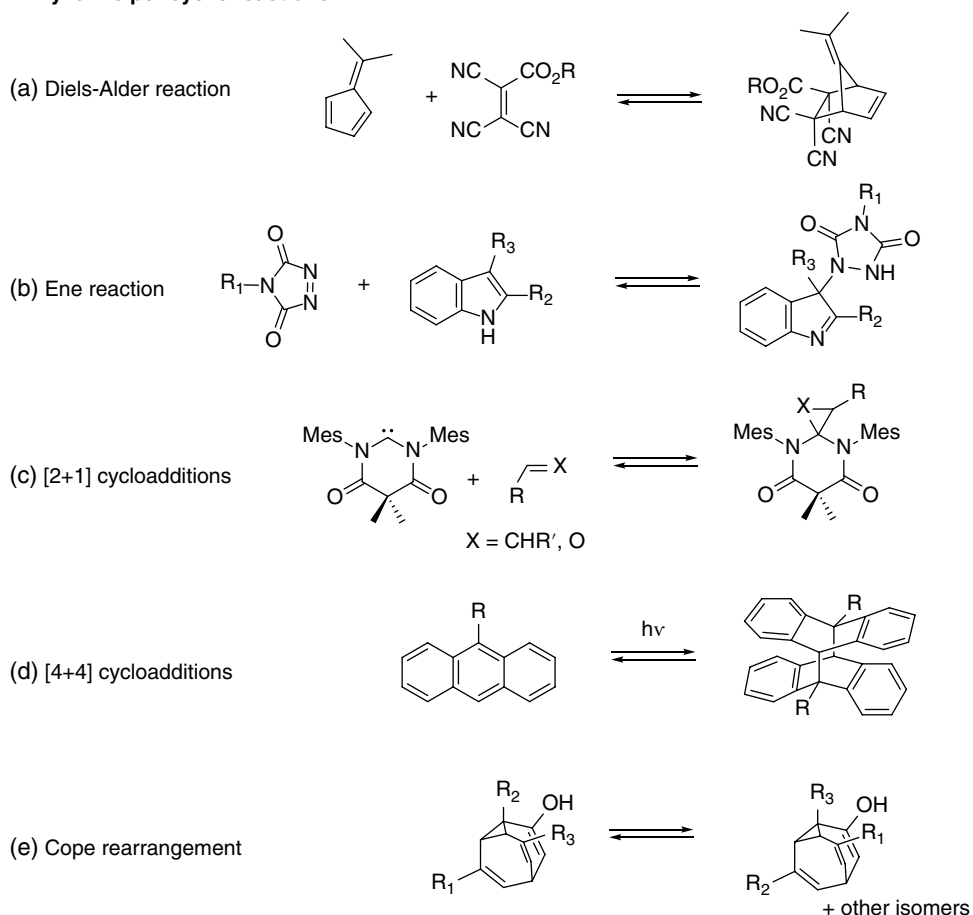
Figure 1.23 Dynamic covalent pericyclic reactions.

$CDCl_3$, r.t.
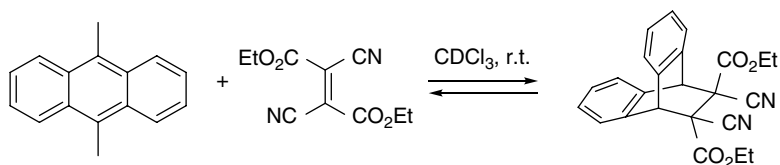
Scheme 1.6 Dynamic covalent Diels–Alder reaction with anthracenes as dienes.

furans have also been made. The practical utility of these systems is diminished by the kinetic barrier for the retro-reaction. Heating for prolonged times at 70–100 °C is normally required for full equilibration. A combined experimental and computational study with the aim of uncovering more facile maleimide-furan cycloadditions was recently reported.[115] It was discovered that the furan substitution dictated the reactivity and reversibility of the system, with changes on the maleimide moiety showing only minor influence in the system activity. With electron-poor furans such as furfural,
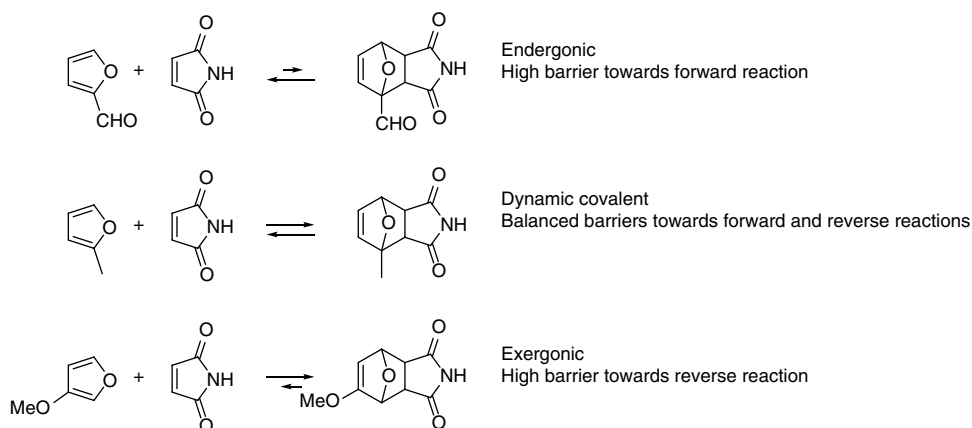
Figure 1.24 The influence of furan substitution pattern on Diels–Alder reversibility.

the Diels–Alder progressed at very low rates, and with electron-rich furans like 3-methoxyfuran the reaction was too exergonic and the reverse reaction thus hindered. An efficient dynamic covalent behavior reaction was only displayed for moderately electron-rich and neutral furans like 2-methylfuran (Figure 1.24).

Recently, the application of 1,2,4-triazoline-3,5-diones (TADs) as coupling partners in dynamic covalent ene reactions with indoles was reported (Figure 1.23b).[116] Establishment of this connection proceeded almost instantly under ambient conditions and the reaction was fully reversible at elevated temperatures (ca. 100 °C). Despite the high reactivity of both coupling partners, exchange selectivity was excellent, providing an example of highly specific exchange operating in the presence of other functionalities.

The dynamic covalent [2 + 1] cycloaddition between stabilized diamidocarbenes and olefins or aldehydes to yield reversible three-membered ring formation has also been demonstrated, as shown in Figure 1.23c.[117] Interestingly, both electron-poor and electron-rich olefins could participate in the reaction. Dynamic exchange between cyclopropane and epoxide derivatives could also be performed with equilibration times around 16 h at 80 °C (Scheme 1.7). A further report has also uncovered the mechanism of the epoxide formation through use of magnetization transfer spectroscopy, revealing that this reaction (unlike the cyclopropanation) essentially proceeds stepwise via an anionic intermediate.[118]
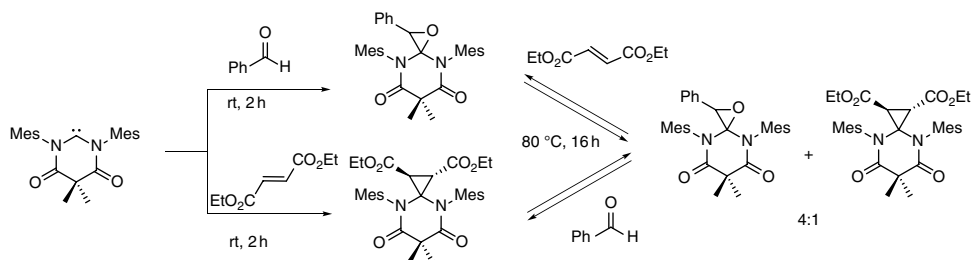
Scheme 1.7 Dynamic [2 + 1] cycloadditions between diamidocarbenes and olefins or aldehydes.

Scheme 1.8 Reversible [4 + 4] photodimerization of anthracene.
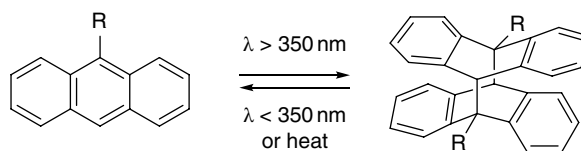
In addition to the thermal cycloadditions presented above, reversible photochemical [4 + 4] cycloaddition of functionalized anthracenes to create dimers (Figure 1.23d) has also been reported.[119] As can be seen from Scheme 1.8, irradiation at wavelengths above 350 nm led to complete dimerization within a few hours, while heating at 60 °C for 20 h or irradiating at shorter wavelengths regenerated the monomers.

While most dynamic covalent pericyclic reactions belong to the cycloaddition subclass, dynamic sigmatropic rearrangements using bullvalone derivatives have also been developed (Figure 1.23e), resulting in fluxional dynamics where the "shape-shifting" molecules can undergo continuous internal rearrangement and interconvert via hundreds of different isomers.[120,121] Early efforts to turn on and off the fluxionality via photocontrol have also been reported.[122]

Overall, dynamic covalent pericyclic reactions represent a growing class of reversible connections with importance for many areas of adaptive chemistry. However, several issues remain unaddressed with current systems, such as the inability to switch on or off exchange to freeze the equilibrium, or finding conditions tolerant of a wider variety of functional groups.

1.3.2.2 Dynamic Covalent Radical Reactions

The final class of dynamic covalent bonds highlighted in this chapter is that of dynamic radical reactions (Figure 1.25).

Dynamic radical reactions

(a) Alkoxyamine exchange

(b) Diarylbibenzofuranone exchange

(c) Trithiocarbonate exchange
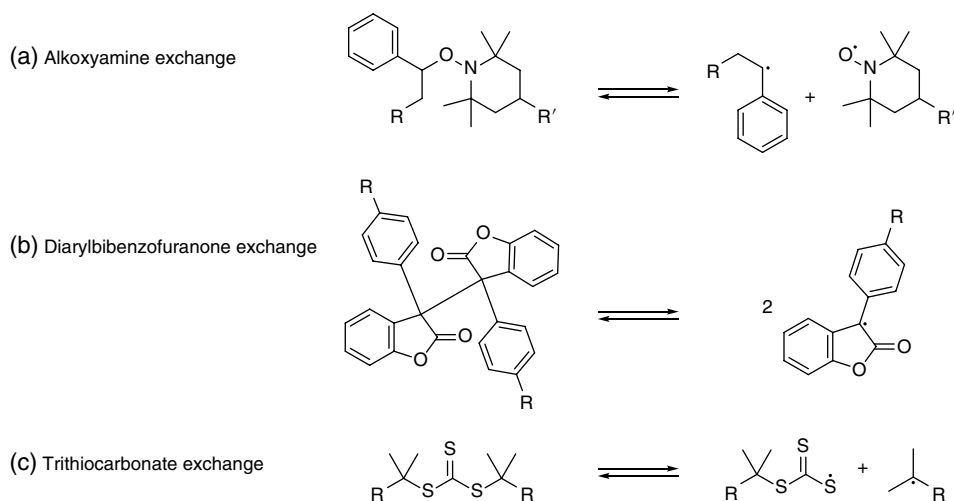
Figure 1.25 Dynamic covalent radical reactions.

A well-explored dynamic covalent radical system is based on the formation of persistent aminoxyl radicals (Figure 1.25a). Apart from its application in radical polymerization, the system has been used to achieve self-healing and reversible cross-linking for a range of different materials.[123] Recently, new types of dynamic radical exchange such as diarylbibenzofuranone exchange (Figure 1.25b) have been demonstrated.[124,125] This functional group is derived from arylbenzofuranone and displays very high air and water tolerance as well as good functional group compatibility. The resulting dynamic polymers displayed autonomous self-healing properties at room temperature without any stimuli. The trithiocarbonate functional group also displays good reversibility at room temperature under UV irradiation (Figure 1.25c).[126] Dynamic covalent polymers based on this scaffold exhibited efficient photoinduced self-healing properties at room temperature in MeCN.

1.4 Conclusions

In a relatively short time, DCvC has evolved from a tool intended for macrocycle synthesis to a highly advanced framework with broad applicability within many areas in contemporary chemistry. Many types of dynamic covalent bonds have been developed, and their properties have been examined in various amounts of detail. Dynamic systems have been utilized in an exceptional range of problems within molecular recognition, lead compound discovery, catalyst design, nanotechnology, materials science, and many other areas. Furthermore, DCvC allows access to highly advanced molecular architectures where the form and shape is dictated by thermodynamics. Subsequent chapters will focus more specifically on the applications of DCvC within these different areas.

References

1 Y. Jin, C. Yu, R. J. Denman, W. Zhang, *Chem. Soc. Rev.* **2013**, *42*, 6634–6654.

2 P. T. Corbett, J. Leclaire, L. Vial, K. R. West, J.-L. Wietor, J. K. M. Sanders, S. Otto, *Chem. Rev.* **2006**, *106*, 3652–3711.

3 S. J. Rowan, S. J. Cantrill, G. R. Cousins, J. K. Sanders, J. F. Stoddart, *Angew. Chem., Int. Ed.* **2002**, *41*, 898–952.

4 M. Barboiu, J.-M. Lehn, *Proc. Nat. Acad. Sci.* **2002**, *99*, 5201–5206.

5 J. Li, P. Nowak, S. Otto, *J. Am. Chem. Soc.* **2013**, *135*, 9222–9239.

6 O. Ramström, *Latv. J. Chem.* **2007**, *4*, 263–269.

7 F. Seidel, *Berichte der deutschen chemischen Gesellschaft (A and B Series)* **1926**, *59*, 1894–1908.

8 G. A. Melson, D. H. Busch, *J. Am. Chem. Soc.* **1965**, *87*, 1706–1710.

9 Y. Zhu, H. Yang, Y. Jin, W. Zhang, *Chem. Mater.* **2013**, *25*, 3718–3723.

10 A. Herrmann, *Chem. Soc. Rev.* **2014**, *43*, 1899–1933.

11 R. J. Wojtecki, M. A. Meador, S. J. Rowan, *Nat. Mater* **2011**, *10*, 14–27.

12 P. Nowak, V. Saggiomo, F. Salehian, M. Colomb-Delsuc, Y. Han, S. Otto, *Angew. Chem., Int. Ed.* **2015**, *54*, 4192–4197.

13 P. Dydio, P.-A. R. Breuil, J. N. H. Reek, *Isr. J. Chem.* **2013**, *53*, 61–74.

14 L. Tauk, A. P. Schröder, G. Decher, N. Giuseppone, *Nat. Chem.* **2009**, *1*, 649–656.

15 I. M. Serafimova, M. A. Pufall, S. Krishnan, K. Duda, M. S. Cohen, R. L. Maglathlin, J. M. McFarland, R. M. Miller, M. Frödin, J. Taunton, *Nat. Chem. Biol.* **2012**, *8*, 471–476.

16 K. Severin, *Analytical Applications of Dynamic Combinatorial Chemistry*, in Dynamic Combinatorial Chemistry (eds J. N. H. Reek, S. Otto), Wiley-VCH, Weinheim, **2010**.

17 L. J. Macpherson, A. E. Dubin, M. J. Evans, F. Marr, P. G. Schultz, B. F. Cravatt, A. Patapoutian, *Nature* **2007**, *445*, 541–545.

18 T. Prakasam, M. Lusi, M. Elhabiri, C. Platas-Iglesias, J.-C. Olsen, Z. Asfari, S. Cianférani-Sanglier, F. Debaene, L. J. Charbonnière, A. Trabolsi, *Angew. Chem., Int. Ed.* **2013**, *52*, 9956–9960.

19 C. Zhang, Q. Wang, H. Long, W. Zhang, *J. Am. Chem. Soc.* **2011**, *133*, 20995–21001.

20 B. Içli, N. Christinat, J. Tönnemann, C. Schüttler, R. Scopelliti, K. Severin, *J. Am. Chem. Soc.* **2009**, *131*, 3154–3155.

21 J. N. H. Reek, S. Otto, Dynamic Combinatorial Chemistry, Wiley-VCH, Weinheim, **2010**.

22 B. L. Miller, Dynamic Combinatorial Chemistry, John Wiley & Soncs, Inc., Hoboken, NJ, **2010**.

23 M. Barboiu, Constitutional Dynamic Chemistry, Springer Verlag, Berlin Heidelberg, **2012**.

24 N. Giuseppone, J.-L. Schmitt, E. Schwartz, J.-M. Lehn, *J. Am. Chem. Soc.* **2005**, *127*, 5528–5539.

25 R. J. Williams, A. M. Smith, R. Collins, N. Hodson, A. K. Das, R. V. Ulijn, *Nat. Nano* **2009**, *4*, 19–24.

26 S.-A. Poulsen, L. F. Bornaghi, *Bioorg. Med. Chem.* **2006**, *14*, 3275–3284.

27 K. Ziach, J. Jurczak, *Org. Lett.* **2008**, *10*, 5159–5162.

28 L. A. Wessjohann, D. G. Rivera, F. León, *Org. Lett.* **2007**, *9*, 4733–4736.

29 F. Schaufelberger, L. Hu, O. Ramström, *Chem. Eur. J.* **2015**, 9776–9783.

30 M. E. Belowich, J. F. Stoddart, *Chem. Soc. Rev.* **2012**, *41*, 2003–2024.

31 M. Ciaccia, S. Di Stefano, *Org. Biomol. Chem.* **2015**, *13*, 646–654.

32 D. L. Leussing, B. E. Leach, *J. Am. Chem. Soc.* **1971**, *93*, 3377–3384.

33 M. Ciaccia, R. Cacciapaglia, P. Mencarelli, L. Mandolini, S. Di Stefano, *Chem. Sci.* **2013**, *4*, 2253–2261.

34 T. Iwasawa, R. J. Hooley, J. Rebek, *Science* **2007**, *317*, 493–496.

35 J. M. García, G. O. Jones, K. Virwani, B. D. McCloskey, D. J. Boday, G. M. ter Huurne, H. W. Horn, D. J. Coady, A. M. Bintaleb, A. M. S. Alabdulrahman, F. Alsewailem, H. A. A. Almegren, J. L. Hedrick, *Science* **2014**, *344*, 732–735.

36 A. Sanchez-Sanchez, D. A. Fulton, J. A. Pomposo, *Chem. Commun.* **2014**, *50*, 1871–1874.

37 H. Jędrzejewska, M. Wierzbicki, P. Cmoch, K. Rissanen, A. Szumna, *Angew. Chem., Int. Ed.* **2014**, *53*, 13760–13764.

38 A. Paul, S. Ladame, *Org. Lett.* **2009**, *11*, 4894–4897.

39 A. Dirksen, T. M. Hackeng, P. E. Dawson, *Angew. Chem., Int. Ed.* **2006**, *45*, 7581–7584.

40 E. H. Cordes, W. P. Jencks, *J. Am. Chem. Soc.* **1962**, *84*, 826–831.

41 N. Giuseppone, J.-L. Schmitt, J.-M. Lehn, *Angew. Chem., Int. Ed.* **2004**, *43*, 4902–4906.

42 A. Dirksen, S. Dirksen, T. M. Hackeng, P. E. Dawson, *J. Am. Chem. Soc.* **2006**, *128*, 15602–15603.

43 V. T. Bhat, A. M. Caniard, T. Luksch, R. Brenk, D. J. Campopiano, M. F. Greaney, *Nat. Chem.* **2010**, *2*, 490–497.

44 S. M. Turega, C. Lorenz, J. W. Sadownik, D. Philp, *Chem. Commun.* **2008**, 4076–4078.

45 S. E. Eldred, D. A. Stone, S. H. Gellman, S. S. Stahl, *J. Am. Chem. Soc.* **2003**, *125*, 3422–3423.

46 L. Becerra-Figueroa, A. Ojeda-Porras, D. Gamba-Sánchez, *J. Org. Chem.* **2014**, *79*, 4544–4552.

47 N. A. Stephenson, J. Zhu, S. H. Gellman, S. S. Stahl, *J. Am. Chem. Soc.* **2009**, *131*, 10003–10008.

48 Y. Ruff, V. Garavini, N. Giuseppone, *J. Am. Chem. Soc.* **2014**, *136*, 6333–6339.

49 H. Ying, Y. Zhang, J. Cheng, *Nat. Commun*. **2014**, 5, doi: 10.1038/ncomms4218.

50 O. Š. Miljanić, J. F. Stoddart, *Proc. Nat. Acad.Sci.* **2007**, *104*, 12966–12970.

51 J.-M. Lehn, S. Kulchat, *Chem. Asian J.* **2015**, *10*, 2484–2496.

52 R. J. Lins, S. L. Flitsch, N. J. Turner, E. Irving, S. A. Brown, *Angew. Chem., Int. Ed.* **2002**, *41*, 3405–3407.

53 A. Martinez-Castaneda, H. Rodriguez-Solla, C. Concellon, V. del Amo, *Org. Biomol. Chem.* **2012**, *10*, 1976–1981.

54 P. Vongvilai, M. Angelin, R. Larsson, O. Ramström, *Angew. Chem., Int. Ed.* **2007**, *46*, 948–950.

55 P. Vongvilai, R. Larsson, O. Ramström, *Adv. Synth. Catal.* **2008**, *350*, 448–452.

56 P. Vongvilai, O. Ramström, *J. Am. Chem. Soc.* **2009**, *131*, 14419–14425.

57 M. Sakulsombat, P. Vongvilai, O. Ramstrom, *Chem. Eur. J.* **2014**, *20*, 11322–11325.

58 N. Wilhelms, S. Kulchat, J.-M. Lehn, *Helv. Chim. Acta* **2012**, *95*, 2635–2651.

59 S. Kulchat, K. Meguellati, J.-M. Lehn, *Helv. Chim. Acta* **2014**, *97*, 1219–1236.

60 J. W. Kamplain, C. W. Bielawski, *Chem. Commun.* *2006*, 1727–1729.

61 B. C. Norris, D. G. Sheppard, G. Henkelman, C. W. Bielawski, *J. Org. Chem.* **2011**, *76*, 301–304.

62 M. Holler, N. Allenbach, J. Sonet, J.-F. Nierengarten, *Chem. Commun.* **2012**, *48*, 2576–2578.

63 C. D. Gutsche, D. E. Johnston, D. R. Stewart, *J. Org. Chem.* **1999**, *64*, 3747–3750.

64 H. Kudo, K. Shigematsu, K. Mitani, T. Nishikubo, N. C. Kasuga, H. Uekusa, Y. Ohashi, *Macromolecules* **2008**, *41*, 2030–2036.

65 C. A. Denard, H. Huang, M. J. Bartlett, L. Lu, Y. Tan, H. Zhao, J. F. Hartwig, *Angew. Chem., Int. Ed.* **2014**, *53*, 465–469.

66 L. Hunter, G. C. Condie, M. M. Harding, *Tetrahedron Lett.* **2010**, *51*, 5064–5067.

67 Y. Jin, A. Zhang, Y. Huang, W. Zhang, *Chem. Commun.* **2010**, *46*, 8258–8260.

68 C. Zhang, C. Yu, H. Long, R. J. Denman, Y. Jin, W. Zhang, *Chem. Eur. J.* **2015**, *21*, 16935–16940.

69 G. C. Vougioukalakis, R. H. Grubbs, *Chem. Rev.* **2010**, *110*, 1746–1787.

70 D. A. Leigh, R. G. Pritchard, A. J. Stephens, *Nat. Chem.* **2014**, *6*, 978–982.

71 J. Heppekausen, R. Stade, R. Goddard, A. Fürstner, *J. Am. Chem. Soc.* **2010**, *132*, 11045–11057.

72 K. Jyothish, W. Zhang, *Angew. Chem., Int. Ed.* **2011**, *50*, 8478–8480.

73 D. Drahoňovský, J.-M. Lehn, *J. Org. Chem.* **2009**, *74*, 8428–8432.

74 R. Cacciapaglia, S. Di Stefano, L. Mandolini, *J. Am. Chem. Soc.* **2005**, *127*, 13666–13671.

75 B. Fuchs, A. Nelson, A. Star, J. F. Stoddart, S. Vidal, *Angew. Chem., Int. Ed.* **2003**, *42*, 4220–4224.

76 R.-C. Brachvogel, M. von Delius, *Chem. Sci.* **2015**, *6*, 1399–1403.

77 R.-C. Brachvogel, F. Hampel, M. von Delius, *Nat. Commun.* **2015**, *6*, doi:10.1038/ncomms8129.

78 S. J. Rowan, P. A. Brady, J. K. M. Sanders, *Angew. Chem., Int. Ed.* **1996**, *35*, 2143–2145.

79 Q. Ji, O. Š. Miljanić, *J. Org. Chem.* **2013**, *78*, 12710–12716.

80 Y.-H. Ahn, Y.-T. Chang, *Chem. Eur. J.* **2004**, *10*, 3543–3547.

81 N. Kihara, K. Kidoba, *Org. Lett.* **2009**, *11*, 1313–1316.

82 G. Kaiser, J. K. M. Sanders, *Chem. Commun*. **2000**, 1763–1764.

83 M. Sakulsombat, Y. Zhang, O. Ramström, *Chem. Eur. J.* **2012**, *18*, 6129–6132.

84 R. Caraballo, H. Dong, J. P. Ribeiro, J. Jiménez-Barbero, O. Ramström, *Angew. Chem., Int. Ed.* **2010**, *49*, 589–593.

85 L. R. Sutton, W. A. Donaubauer, F. Hampel, A. Hirsch, *Chem. Commun*. **2004**, 1758–1759.

86 R. Larsson, Z. C. Pei, O. Ramstrom, *Angew. Chem., Int. Ed.* **2004**, *43*, 3716–3718.

87 R. Larsson, O. Ramstrom, *Eur. J. Org. Chem*. **2005**, 285–291.

88 Y. Ura, J. M. Beierle, L. J. Leman, L. E. Orgel, M. R. Ghadiri, *Science* **2009**, *325*, 73–77.

89 M. G. Woll, S. H. Gellman, *J. Am. Chem. Soc.* **2004**, *126*, 11172–11174.

90 S. Ghosh, L. A. Ingerman, A. G. Frye, S. J. Lee, M. R. Gagné, M. L. Waters, *Org. Lett.* **2010**, *12*, 1860–1863.

91 L. Hu, Y. Zhang, O. Ramstrom, *Org. Biomolec. Chem.* **2014**, *12*, 3572–3575.

92 B. Shi, M. F. Greaney, *Chem. Commun*. **2005**, 886–888.

93 Y. Zhong, Y. Xu, E. V. Anslyn, *Eur. J. Org. Chem.* **2013**, *2013*, 5017–5021.

94 G. Joshi, E. V. Anslyn, *Org. Lett.* **2012**, *14*, 4714–4717.

95 R. Caraballo, Dynamic Sulfur Chemistry: Screening, Evaluation and Catalysis, KTH Royal Institute of Technology (Stockholm), **2010**.

96 O. Ramström, J.-M. Lehn, *Chembiochem.* **2000**, *1*, 41–48.

97 H. Hioki, W. C. Still, *J. Org. Chem.* **1998**, *63*, 904–905.

98 R. Caraballo, M. Rahm, P. Vongvilai, T. Brinck, O. Ramstrom, *Chem. Commun*. **2008**, 6603–6605.

99 R. Caraballo, M. Sakulsombat, O. Ramstrom, *Chem. Commun.* **2010**, *46*, 8469–8471.

100 S. Otto, R. L. E. Furlan, J. K. M. Sanders, *J. Am. Chem. Soc.* **2000**, *122*, 12063–12064.

101 Z. Pei, R. Larsson, T. Aastrup, H. Anderson, J.-M. Lehn, O. Ramström, *Biosens. Bioelectron.* **2006**, *22*, 42–48.

102 M. Arisawa, M. Yamaguchi, *J. Am. Chem. Soc.* **2003**, *125*, 6624–6625.

103 B. Rasmussen, A. Sorensen, H. Gotfredsen, M. Pittelkow, *Chem. Commun.* **2014**, *50*, 3716–3718.

104 S. Ji, W. Cao, Y. Yu, H. Xu, *Angew. Chem., Int. Ed.* **2014**, *53*, 6781–6785.

105 S. D. Bull, M. G. Davidson, J. M. H. van den Elsen, J. S. Fossey, A. T. A. Jenkins, Y.-B. Jiang, Y. Kubo, F. Marken, K. Sakurai, J. Zhao, T. D. James, *Acc. Chem. Res.* **2013**, *46*, 312–326.

106 J. J. Cash, T. Kubo, A. P. Bapat, B. S. Sumerlin, *Macromolecules* **2015**, *48*, 2098–2106.

107 N. Luisier, K. Schenk, K. Severin, *Chem, Commun*, **2014**, *50*, 10233–10236.

108 M. Demetriades, I. K. H. Leung, R. Chowdhury, M. C. Chan, M. A. McDonough, K. K. Yeoh, Y.-M. Tian, T. D. W. Claridge, P. J. Ratcliffe, E. C. Y. Woon, C. J. Schofield, *Angew. Chem., Int. Ed.* **2012**, *51*, 6672–6675.

109 J. Tönnemann, R. Scopelliti, K. O. Zhurov, L. Menin, S. Dehnen, K. Severin, *Chem. Eur. J.* **2012**, *18*, 9939–9945.

110 Y. Yi, H. Xu, L. Wang, W. Cao, X. Zhang, *Chem. Eur. J.* **2013**, *19*, 9506–9510.

111 M. Alajarin, J. Berna, C. Lopez-Leonardo, J. W. Steed, *Chem. Commun*. **2008**, 2337–2339.

112 O. Diels, K. Alder, *Berichte der deutschen chemischen Gesellschaft (A and B Series)* **1929**, *62*, 2337–2372.

113 P. J. Boul, P. Reutenauer, J.-M. Lehn, *Org. Lett.* **2005**, *7*, 15–18.

114 P. Reutenauer, P. J. Boul, J.-M. Lehn, *Eur. J. Org. Chem.* **2009**, *2009*, 1691–1697.

115 R. C. Boutelle, B. H. Northrop, *J. Org. Chem.* **2011**, *76*, 7994–8002.

116 S. Billiet, K. De Bruycker, F. Driessen, H. Goossens, V. Van Speybroeck, J. M. Winne, F. E. Du Prez, *Nat. Chem.* **2014**, *6*, 815–821.

117 J. P. Moerdyk, C. W. Bielawski, *Nat. Chem.* **2012**, *4*, 275–280.

118 D. T. Chase, J. P. Moerdyk, C. W. Bielawski, *Org. Lett.* **2012**, *14*, 5510–5513.

119 J.-F. Xu, Y.-Z. Chen, L.-Z. Wu, C.-H. Tung, Q.-Z. Yang, *Org. Lett.* **2013**, *15*, 6148–6151.

120 A. R. Lippert, J. Kaeobamrung, J. W. Bode, *J. Am. Chem. Soc.* **2006**, *128*, 14738–14739.

121 O. Ramström, J.-M. Lehn, *Nat. Rev. Drug Discov.* **2002**, *1*, 26–36.

122 A. R. Lippert, A. Naganawa, V. L. Keleshian, J. W. Bode, *J. Am. Chem. Soc.* **2010**, *132*, 15790–15799.

123 T. Maeda, H. Otsuka, A. Takahara, *Prog. Polym. Sci.* **2009**, *34*, 581–604.

124 K. Imato, T. Ohishi, M. Nishihara, A. Takahara, H. Otsuka, *J. Am. Chem. Soc.* **2014**, *136*, 11839–11845.

125 K. Imato, M. Nishihara, T. Kanehara, Y. Amamoto, A. Takahara, H. Otsuka, *Angew. Chem., Int. Ed.* **2012**, *51*, 1138–1142.

126 Y. Amamoto, J. Kamada, H. Otsuka, A. Takahara, K. Matyjaszewski, *Angew. Chem., Int. Ed.* **2011**, *50*, 1660–1663.

2

Dynamic Combinatorial Libraries

Dávid Komáromy, Piotr Nowak, and Sijbren Otto

2.1 Introduction

Dynamic combinatorial libraries (DCL) are products of dynamic combinatorial chemistry (in this chapter abbreviated as DCC). They are mixtures of distinct (supra)molecular species (library members), which can interconvert from one to another. Diversity in DCLs is usually generated by reversible formation of library members from building blocks, exchange between the library members, and isomerization reactions. DCLs are adaptive: a physical or chemical stimulus can modify the Gibbs energy landscape of a DCL, changing its composition. In our review in 2006[1] we defined DCC as "combinatorial chemistry under thermodynamic control". Since then, the field has ventured into many fascinating avenues, often discarding the need for thermodynamic control. What all the applications of DCC still have in common is their adaptive diversity generated with specific, reversible interactions[2]. Several great reviews, perspectives, and books[3–27] have been published in recent years. We aim here to provide a general overview of the field and highlight its most important accomplishments, together with challenges and perspectives for the future.

2.1.1 A Short History of DCLs

Chemists have known about the concept of thermodynamic equilibrium since van't Hoff and how to influence it thanks to the work of Le Chatelier and Braun. The idea to use molecular templates to control chemical reactivity is as old as Emil Fischer's "lock and key" enzyme model[28] and further permeated the chemical community after the discovery of DNA structure [29–31]. The first work showing how to use a template effect to drive the equilibrium in the desired direction was published in 1962 by Busch[32], 5 years before Pedersen's synthesis of crown ethers[33].

After Busch's initial forays into the templated synthesis of imine macrocycles, it took another three decades to properly establish the field as we know it today (Figure 2.1). The work of Goodwin and Lynn[34], followed by the groups of Hamilton[35], Harding[36], and Venton[37], exploited some of the principles of DCC. The terms "dynamic combinatorial library", "dynamic combinatorial chemistry", and "virtual combinatorial library" were first used by Sanders *et al.* in the context of macrolactonization[38,39]
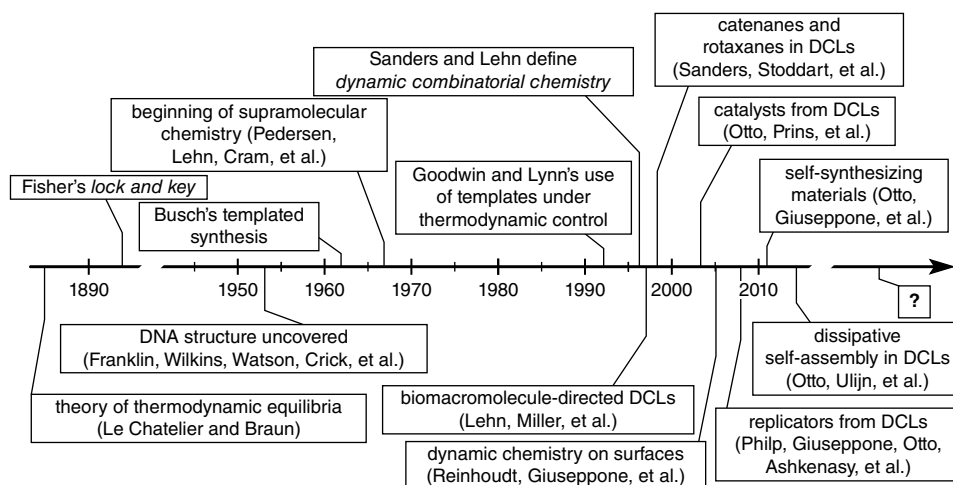
Figure 2.1 A brief timeline of dynamic combinatorial chemistry and the underlying concepts.

and Lehn *et al.* in the context of helicates[40,41] and protein-directed DCC[42]. In 1997, Miller *et al.* showed DCLs templated by DNA[43], while Sasaki *et al.* applied DCC to create lectin ligands[44]. A similar approach was proposed by Eliseev and Nelen[45], who separated the equilibration step (photochemical isomerization) and selection (affinity column).

In subsequent years DCC operating according to the principles outlined by its pioneers expanded dramatically by creating not only more receptors for small molecules and ions or ligands for biomacromolecules, but also catalysts[46], catenanes[47], and rotaxanes[48] (Section 2.2). This would not have been possible without the multiple new dynamic covalent chemistries described in Chapter 1. Removing the traditional distinction between templates and library members led to systems, with library members stabilizing themselves by folding[49] (Sections 2.2.6) or creating (poly)cyclic structures and cages thanks to the strong chelate cooperativity of multiple dynamic bonds (Chapters 3 and 4). Template effects were utilized not only to find good complementary binders, but also to sense analytes[50], and interpret[51] and process chemical information[52] (Section 2.5.1).

Subsequent developments led to self-replicating systems, where library members not only associate together, but also dissociate to give two species capable of further propagating the chain reaction[53] (Section 2.2.4). Replicators self-assembling into larger structures found application in materials science, as they are effectively self-synthesizing materials (see Section 2.5.2).

Of course replication processes are not a property of an equilibrium mixture; instead, their nature is determined by kinetics. In the context of DCC, they describe either how the system reaches its thermodynamic minimum or how an equilibrating mixture responds to an irreversible reaction. Indeed, control over kinetic barriers in complex equilibrating systems provided the possibility of imposing directionality on motionally dynamic systems[54], which are otherwise fully stochastic[55].

A creative combination of kinetically controlled transformations with DCLs was applied by Miljanic's group to self-sorting driven by phase changes[56]. Performing DCC

in multiphase systems allowed Sanders and Lüning to optimize library members not only to bind molecular entities, but also to transfer them between phases[57,58] (see Section 2.4).

Inclusion of dendrimers[59], nanoparticles[60,61], and surface immobilized building blocks[62] has established DCC as a promising player within in the field of nanotechnology (see also Chapter 10).

It is clear that the last two decades have witnessed an explosive evolution of diversity of DCLs. How is it possible that it ignited only a century after the theoretical framework had been planted? Marcellin Berthelot once famously stated, "chemistry creates its own subject"[63]. Even more so, until the advent of modern spectroscopic techniques, chemical analysis was largely reliant on synthesis. Peter Galison argued[64] that tools are no less important than paradigm shifts[65] to drive scientific progress[66]. Indeed, Section 2.7 shows that without modern analytical techniques and modelling, the spark of complexity oriented chemistry would not have been ignited.

2.1.2 Terminology

Bertrand Russell, in his lectures delivered in 1918, commented in his work on the foundations of mathematics that "everything is vague to a degree you do not realize till you have tried to make it precise"[67]. The same problem seems to appear when looking at the field full of similar terms and acronyms that emerged recently: DCC (dynamic combinatorial chemistry), DCvC (or sometimes DCC, dynamic covalent chemistry), CDC (constitutional dynamic chemistry), VCL (virtual combinatorial library), DCL (dynamic combinatorial library). Although this diversity in terminology might seem redundant and confusing at first glance, we will show that they all denote different aspects of diversity-oriented approaches.

Figure 2.2 shows overlaps between different chemistries. DCC is a subset of combinatorial chemistry where diversity is generated either by dynamic covalent or/ and supramolecular means.
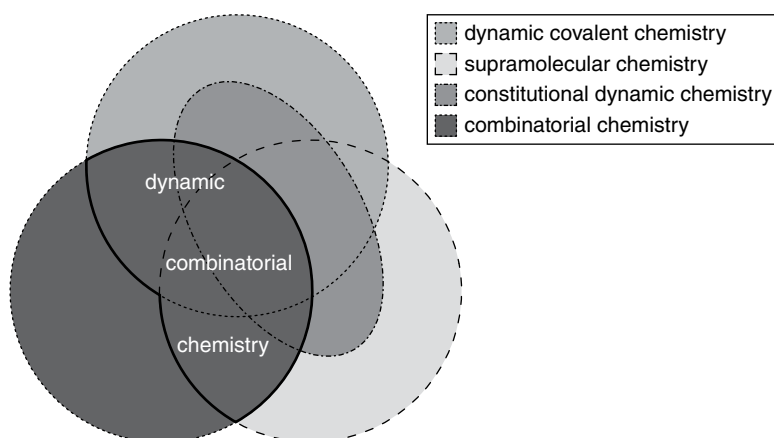
Figure 2.2 An Euler diagram showing overlaps between combinatorial chemistry, dynamic covalent chemistry, supramolecular chemistry, and constitutional dynamic chemistry. The area at the intersection of combinatorial chemistry with supramolecular and dynamic covalent chemistry denotes dynamic combinatorial chemistry. The sizes of the ellipses are arbitrary.

The overlap between supramolecular and covalent chemistries is intentional for two reasons. First, both "covalent" and "non-covalent" bonds share exactly the same underlying principles (Feynman and Ehrenfest forces)[68], making the distinction between them rather arbitrary. Second, within the framework of DCC, they are coupled with each other by feedback loops. Non-covalent interactions between the library members and templates, between different library members, and within a single library member affect the covalent equilibria and *vice versa.*

Constitutional dynamic chemistry, defined by Lehn[14,69], requires the components of the system to change their constitution (connectivity) by breaking and forming bonds in a reversible manner. Thus, it excludes equilibria which deal with stereoisomerism or conformational changes.

Figure 2.2 suggests that not all systems based on dynamic reactions can be classified as DCLs. Systems governed by a single equilibrium (e.g. $A + B \rightleftarrows C + D$) are not combinatorial. On the other hand, there are multiple systems which exhibit very complex equilibria, but the components are too labile to be called library members, for example protonation equilibria for a protein (covalent) or solvation of a solute (supramolecular). Thus, DCLs require coupled equilibria to link library members with definable and identifiable structures (covalent or supramolecular). Of course, the boundaries are rather fluid as some reactions can lead to undefinable aggregates or well-defined species depending on the conditions applied.

A very rare case involves dynamic transformations which stem not from a thermodynamic equilibrium where two or more components are connected with a single transformation satisfying the principle of microscopic reversibility, but rather two irreversible processes where one creates library members and the other destroys them. In such dissipative systems, continuous delivery of chemical energy is required to constantly replenish the population of the library members (see Section 2.6)[70].

Another gray area contains multicomponent dynamic systems which, due to strong chelate cooperativity, lead to formation of only one measurable library member (e.g., varous self-assembled cages[71]). The efficient formation of single species necessarily involves formation of multiple intermediates, which are disfavored with respect to the free building blocks and the products if the cooperative effect is positive[72]. Such intermediates are termed "virtual", because at least theoretically they can exist, but are not necessarily measurable[42,73,74]. In those cases the term DCL is much more appropriate in systems which are addressable, that is, when the structure of cooperative self-assembly depends on the applied physicochemical conditions.

To summarize, DCLs are built of one or more building blocks which give rise to multiple library members connected with multiple addressable equilibria. The type of transformations involved (covalent, non-covalent, or even conformational) does not matter as long as the library members are clearly distinguishable from each other.

2.1.3 Theoretical Considerations

Equilibrium reactions have been mostly avoided within the paradigm of static chemistry as they nearly always lead to mixtures rather than pure compounds. However, the aim of DCC is diversity. The Le Chatelier–Brown principle ensures that the diversity of a
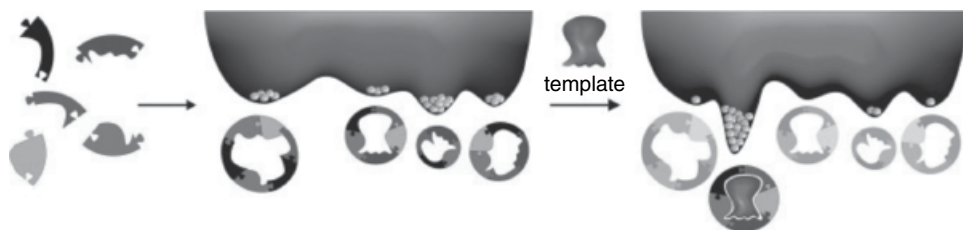
Figure 2.3 A schematic representation of a template-directed DCL. Multiple building blocks react with each other to form an equilibrating mixture of library members. Addition of a template that binds strongly to one of the library members shifts the composition of the DCL towards the formation of the template-library member complex.

DCL adapts to changes in the environment. In the DCC context, the environment of a library is everything that is not the library but can still affect its composition by shifting the equilibria within the DCL (physical conditions, template molecules, solvent, etc.). The boundaries between the DCLs and their environment are not always clear. For instance, addition of a template molecule which is able to bind one of the library members effectively creates yet another library member (Figure 2.3). The binding event withdraws the free library member from the system, causing re-equilibration to regenerate some of the free library member. In many cases it is difficult to directly quantify the distribution of a library member between its bound and unbound states. For simplicity, both are usually treated as the same library member.

The most important aspect of DCLs is their adaptability. For each library member A in a library which evolves from the reference state x to a new state y under external influence:

$$\mathrm{DCL}_x \underline{\mathit{perturbation}} \, \mathrm{DCL}_y, \tag{2.1}$$

we can quantify adaptability using amplification factors (AF), which are defined as the ratio of the total concentration of that particular library member in a perturbed library to the corresponding concentration in the initial DCL:

$$AF = \frac{\left[\mathrm{A}\right]_{\mathrm{total},y}}{\left[\mathrm{A}\right]_{\mathrm{total},x}} \tag{2.2}$$

For DCLs where a library member A is affected by a template molecule T we have equilibria $i\mathrm{A} + j\mathrm{T} \leftrightarrows \mathrm{A}_i\mathrm{T}_j$, where $i = \{1, 2, ..., n\}$ and $j = \{1, 2, ..., m\}$. Cases where i and j are larger than 1 correspond to the formation of aggregates of different sizes. Thus Equation 2.2 becomes:

$$AF = \frac{\sum\limits_{i=1}^{n}\sum\limits_{j=0}^{m} i\left[\mathrm{A}_i\mathrm{T}_j\right]_y}{\left[\mathrm{A}\right]_x} \tag{2.3}$$

In the simplest case when $i = j = 1$ (1:1 binding between the library member A and template T) the numerator in equation 2.3 becomes a sum of the concentrations of the free library member A and the complex AT:

$$AF = \frac{[A]_y + [AT]_y}{[A]_x} \tag{2.4}$$

Some analytical techniques (e.g., HPLC) normally cannot distinguish between different complexes/aggregation states for a given library member, only providing signal proportional to its total concentration. While this simplifies calculation of the amplification factors, it also enshrouds the mechanisms behind the library response.

For comparisons between different library members, normalized amplification factors (AF_n) are more indicative than traditional amplification factors as they take into account the maximal theoretical increase in the concentration of any library member[75,76]. They are defined by Equation 2.5:

$$AF_n = \frac{[A]_{total,y} - [A]_{total,x}}{[A]_{max} - [A]_{total,x}}, \tag{2.5}$$

where $[A_{max}]$ is the maximum possible concentration of A in a DCL allowed by the composition of the DCL and the stoichiometry of A.

Due to the presence of several interconnected chemical equilibria, the calculation of the binding affinities and other equilibrium constants from easily measurable AF or AF_n values is far from trivial. In the worst case scenario, a significant amplification can be experienced by library members which do not exhibit any affinity to the target[77,78]. Thus, in a series of papers, we[79–86] and Severin[77,87,88] explored the correlation between amplification and binding. Moreover, we examined the impact of library size on the probability of exploring the ideal receptors for a given template. Two softwares were elaborated for these purposes: *DCLSim,* (which enabled the calculation of the library member distribution from initial concentrations, stoichiometries, and equilibrium constants[79]) and *DCLFit*[83] (which enabled the calculation of equilibrium constants from a given library member distribution). With these two tools, large data sets could be obtained and analysed *in silico,* providing interesting insights into the theory of DCLs. The main results are summarized here in order to serve as guidelines for those who intend to explore new binders from DCLs by amplification studies:

- The formation of small, but weaker binders may be preferred over that of large, but strong ones[88], which can produce false positives in templating studies. The reason is that the overall entropic penalty is usually very high in the latter case due to the restriction of translational and rotational freedom, and it is often not compensated by the gain resulting from guest binding. Furthermore, at a fixed number of building blocks, more molecules of small binders can be produced than big ones, which results in an overall lower ΔG.
- This unwanted bias is even more pronounced at high template concentrations, because the amount of accessible template does not restrict the system from forming the smaller but weaker members[77,81]. More detailed calculations show[80]

Figure 2.4 (a) The mean deviation of the correlation between binding affinity and amplification in DCLs, as a function of template and total building block concentration. (b) The probability of the most strongly binding host in a DCL being the most amplified compound in DCLs, as a function of template and total building block concentration.

(a)

(b)
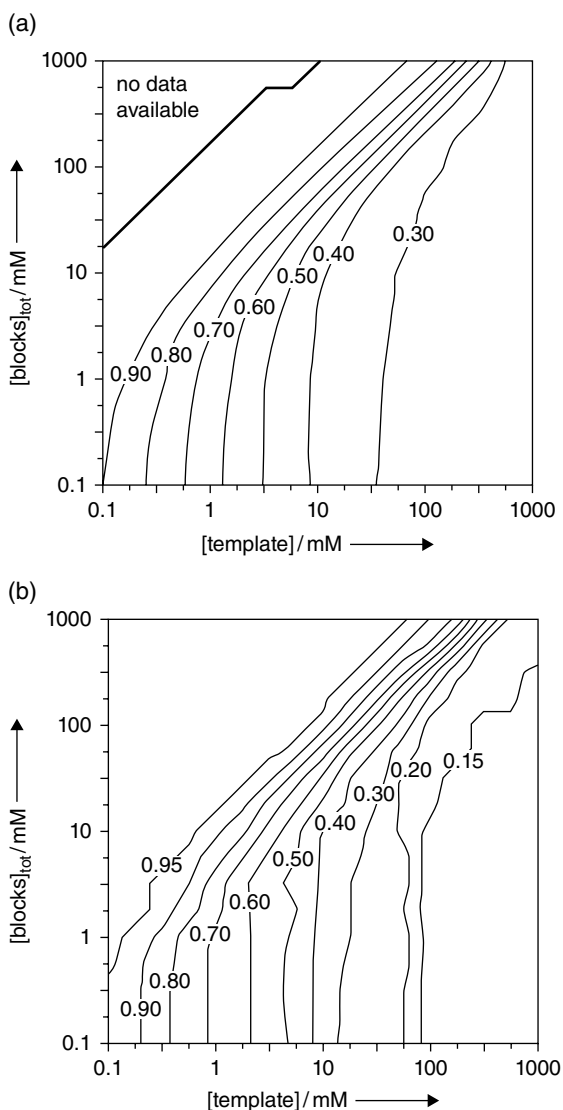
that using ca. 0.1 equivalents of template even in libraries with a large number of members results in a good ($R^2 = 0.90$) correlation between amplification and binding (see Figure 2.4a). Under these conditions there is a probability of 0.95 that the most amplified member is the best binder (see Figure 2.4b). In contrast, at higher template concentrations, the correlation and the corresponding probablities rapidly break down.

- In DCLs generated from more than one building block, the formation of heteromeric guests is preferred over that of homomeric ones, due to simple probability reasons[77,81], which may again furnish false positives regarding amplification. In contrast, this bias is not observed if a heteromeric DCL member is amplified[87].

- Amplification depends not only on the template-to-building block ratio, but also on the relative concentrations of building blocks. Thus, if a good binder, with a building block composition that matches that of the library, competes with a better binder, whose building block composition is very different from that of the library, the amplification of the best binder can be negligible[80]. On the other hand, if a specific member is found to be amplified even to a small extent, it could serve as a good starting point to generate a biased library (containing only the relevant building blocks in the appropriate ratio) and to re-evaluate binding[89,90].

- From Equation 2.5 it can be clearly deduced that AF_n values are large either if the concentration of the corresponding members is high in the final DCL or if it is low in the initial one. That is, if one attempts to obtain high amplification factors, it is recommended to use building blocks which, in the absence of the template, form library members only to a negligible extent. In other words, virtual combinatorial libraries are highly privileged in initial binding studies[77].

- Whereas on careful selection of experimental conditions a good correlation between amplification factor and binding affinity (among potential hosts) for a given guest can be established, there is much less satisfactory correlation for a given host (among potential guests). This results from the fact that each guest has its unique order of preference among the various library members[84].

- *In silico* simulation and analysis of DCLs enables the study of the effect of library size on the probability of finding the best binder. In principle, the more diverse a library is, the higher the possibility of finding good binder for a given guest[79]. Although the relative amount of the best binder decreases strongly with increasing library size, the statistically expected binding affinity of the best binder increases even more rapidly, so that the concentration of best binder remains above the detection threshold. Similarly, in a given parameter space (template and building block concentration), the region where any amplification can be detected, increases with increasing library size[86].

- Supramolecular interactions (aggregation) between the library members themselves can be regarded as binding events competing with the host–guest binding to be studied. Simulations show that the determination of aggregation constants is possible but requires careful selection of the building block concentration range, that is, a regime where the extents of formation of the library members (from the building blocks) and the formation of aggregates (from the library members) are comparable[85]. Furthermore, aggregation of the best binder can result in diminished amplification factors (false negative) and can even yield false positives if the worst binder in the same system does not undergo aggregation[91].

- As mentioned above, amplification of a homomeric DCL member could trigger the amplification of other members devoid of the corresponding building block. This trend can be generalized, that is, if the incorporation of one or more building blocks has a considerable cost in free energy, then amplification proceeds along patterns (Figure 2.5a,b). First, the non-penalized members are amplified, followed by those which contain more and more from unfavoured building blocks. This behavior can be exploited to form signalling cascades. For example, if in a library composed of building blocks **A**–**E**, two members **AB** and **CD** are amplified by templates **T1** and **T2**, respectively, the remaining **E** building blocks will form library member **EE**, which is thus co-amplified (agonist behavior, upregulation[78]) (Figure 2.5c). In a more complex
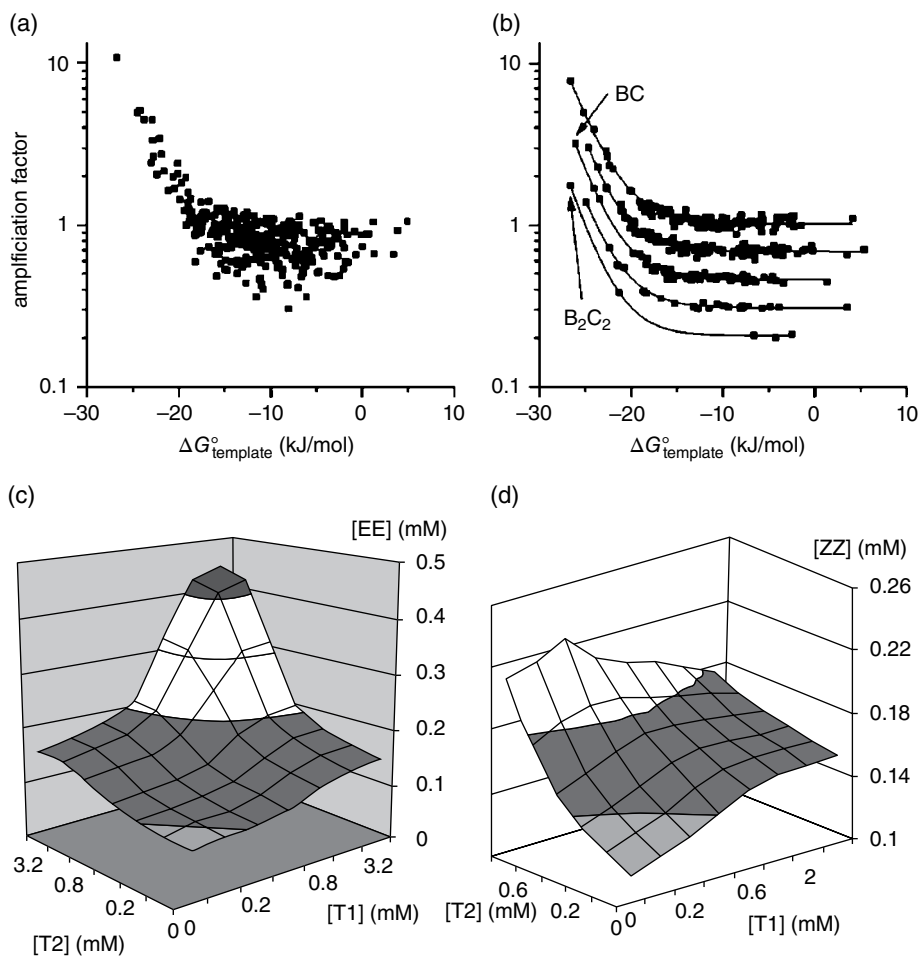
Figure 2.5 Dependence of the amplification factor on binding free energy in a DCL with (a) randomly distributed binding affinities and (b) binding affinities where the incorporation of building blocks **B** and **C** is penalized. (c) Upregulation of library member **EE** in a DCL from building blocks **A**–**E**, where templates T_1 and T_2 amplify members **AB** and **CD**, respectively. (d) Template concentration-dependent up- and downregulation of library member **ZZ** in a DCL from building blocks **W**–**Z**, where templates T_1 and T_2 amplify members **WW** and **WXY**.

scenario, the library is constructed from building blocks **W**–**Z**, with **WW** and **WXY** amplified by **T1** and **T2**, respectively. **T2** causes upregulation of **ZZ,** whereas subsequent addition of **T1** liberates building blocks **X** and **Y**, which in turn can form heteromeric members with **ZZ** (antagonist behavior, downregulation) (Figure 2.5d).

To conclude: good binders for a given template can be explored with a high probability of finding a hit in large, diverse libraries, with a low template-to-building block ratio and low building block concentration (to prevent aggregation). In this case, even small amplifications can indicate good binding, so the templation experiment should be

repeated in a biased library containing only the building blocks present in the amplified member(s) and at low template concentration, to increase the probability that the best binder is the one that is most strongly amplified.

2.2 Template-controlled DCLs

Template-controlled DCLs are powerful tools for finding the best receptor of a given target from a large set of chemical species. Given that the system is at equilibrium, that is, there is continuous exchange between the library members, a given template ideally shifts the equilibrium in favor of the library member which is its best binder, at the expense of other members. In other words, the template selects and constructs its own receptor.

To ensure that the observed amplification is solely the consequence of guest-induced re-equilibration, one should check that the untemplated DCL is under thermodynamic control. This is the case if the same library member distribution can be reached from different initial mixtures containing the same overall number of building blocks[92]. Notably, even chemical reactions which are considered nondynamic (i.e., possess a high activation barrier)[93,94] can be rendered dynamic with a suitable catalyst[95]. Moreover, as mentioned above, if one aims at high amplification factors, the concentration of the possible good binders in the initial library should be kept low. This can be achieved by applying a strong competing agent in excess, for example monothiol reducing agents for disulfide libraries[96].

Different modes of templating, such as molding and casting, may be distinguished. In the former, building blocks arrange themselves around a guest, which is usually a small ion (see Sections 2.2.1.1 and 2.2.1.2) or molecule (see Sections 2.2.1.3 and 2.2.1.4), whereas in the latter the DCL members are the guests of a macromolecular host (see Section 2.2.2)[42]. Recently, simultaneous casting and molding, resulting in allosteric binding of a DCL member, has been reported[97]. Furthermore, the template can be a mimic of the transition state of a given reaction as well (see Section 2.2.3). The distinction between casting and molding only applies if external templates are used. If one of the members is stabilized by intermolecular interactions with a copy of itself, autocatalytic formation of this member can be observed (see Section 2.2.4), whereas, if it is stabilized in an intramolecular manner, interlocked (see Section 2.2.5) or folded (see Section 2.2.6) members can be amplified.

2.2.1 Receptors for Small Molecules and Ions

2.2.1.1 Inorganic Cations

Inorganic cations were amongst the first[39,98] guests used in the quest for artificial receptors from DCLs. Over recent years, several different types of templates have been explored for alkali metals[99–105] alkali earths[106–109], and transition metals[74,92,110–114], giving rise to monocyclic[102,106,107,115], bicyclic[104,108], grid-like[74,110], helical[74,111,116,117], or cage-like[118–121] assemblies.

The Lüning group used imine chemistry to explore the templating capability of alkali metals and alkali earths. Utilizing pyridine-2,6-dicarbaldehyde and oligo(ethyleneoxide)-linked di- or triamines they found that Mg^{2+}, Ca^{2+}, and Ba^{2+} selectively template one or
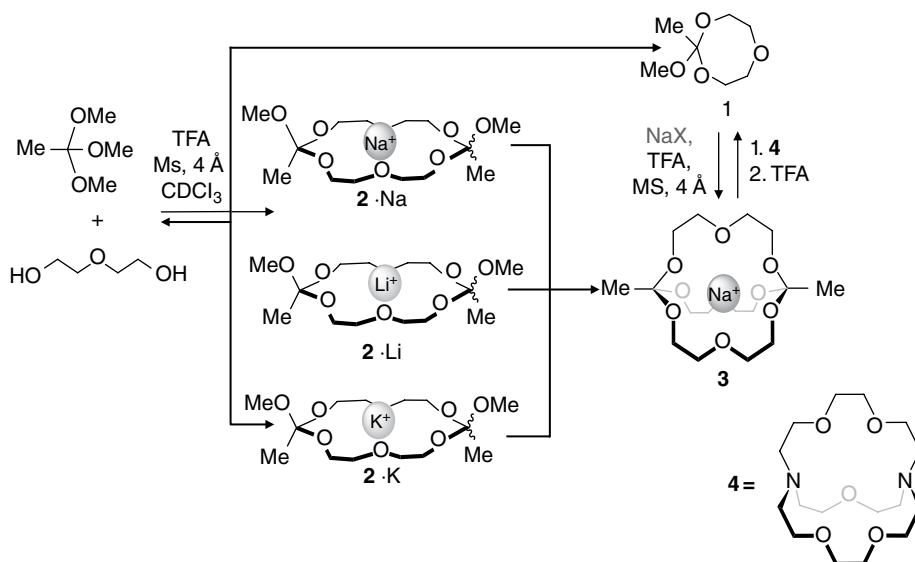
Figure 2.6 A dynamic orthoester library and the resulting dynamic orthoester cryptate. Diethylene glycol and trimethyl orthoformate forms oligo(ethyleneoxide) macrocycles **1** and **2** in the absence and presence of alkali metal ions, respectively. In the latter cases, the DCL transforms to a dynamic orthoester cryptate **3** · Na. The complex decomposes by competitive cation binding with cryptate **4** and subsequent hydrolysis of free **3** cryptate but can be reformed on addition of excess Na+.

other macrocycle from a DCL of linear, cyclic, or cage-like oligoimines[106,108]. The use of acyl hydrazones with an enlarged aromatic or aliphatic core instead of amines led to the discovery of receptors for Sr^{2+}[109] and Ba^{2+}[122].

A more remarkable dynamic system has been reported very recently by von Delius *et al.*[123]. Dynamic orthoester chemistry[124] was used to generate different cyclic oligo(ethyleneoxides) from two cheap bulk chemicals, methyl orthoformate and diethylene glycol, in the presence of a catalytic amount of TFA (Figure 2.6). The cyclic [1 + 1] adduct **1** was the dominant library member in the absence of any metal, while the [2 + 2] macrocycle **2** prevailed if Li+, K+, or Na+ was added. However, applying Na+ as a template, accompanied by removal of water (with molecular sieves), resulted in a [3 + 2] orthoester cryptate **3** · Na. The binding constant was found to be $10^6 \, M^{-1}$ by competitive NMR titration with 15-crown-5. In the absence of acid, **3** · Na is unprecedentedly stable against hydrolysis. However, it remains dynamic: on addition of a competitive chelating agent **4**, Na+ can be removed and the metastable free **3** hydrolyzes to give **1**. Even more remarkably, **3** · Na could be isolated and characterized by single-crystal X-ray diffraction. The example shows that DCC, combined with cation-guided self-assembly, can give rise to remarkably complex and stable architectures.

Transition-metal-templated DCLs have been reported as well. In an early example[92], Ag+ ions were reported to selectively amplify a small macrocycle from a simple aromatic acetal DCL due to cation–π interactions. Transition metal templates can, however, induce far more intricate architectural transformations. For example, aldehyde **5** and diamine **6** form a library consisting of (**5** · **6**)$_n$ linear polymers and the **5**$_2$**6**$_2$ macrocycle (see Scheme 2.1)[125]. On subsequent addition of Cd^{2+} ions as templates, the DCL
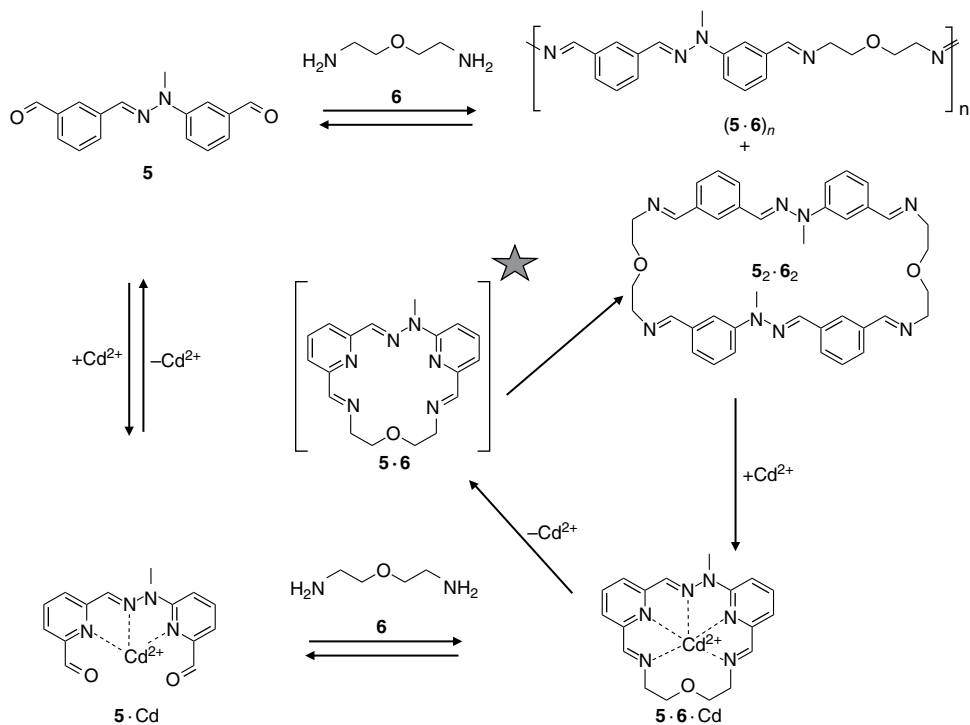
Scheme 2.1 Generating unstable intermediates via cation-templated DCC. **5** and **6** form an imine DCL, which converges to **5·6·Cd** upon addition of Cd^{2+}. Demetalation of **5·6·Cd** proceeds through an out-of equilibrium state **5·6**.

collapses to macrocycle **5·6·Cd**. This state can also be achieved via another pathway (reverse order of reagent addition), with the shape-switched[114,115,126] metal complex **5·Cd** as an intermediate. In contrast to this fully reversible cycle, demetalation of **5·6·Cd** results not directly in the original DCL, but proceeds through a strained, unstable macrocycle **5·6**, which is detectable for several hours in solution. Thus, metal-templated DCC enables access to out-of-equilibrium states, which are not accessible directly from the thermodynamically stable states of the system in the absence of the template.

Metal templation can result in even more intriguing structural switching in DCLs[111]. On mixing the helical tetrahydrazone **7** and the bishydrazine **8** in the presence of a Lewis acid ($Sc(OTf)_3$), a DCL of more than 25 interconverting aromatic oligohydrazones was generated. On addition of Zn^{2+} ions, the DCL, collapsed to a simple 2×2 grid-like coordination complex **9**, with the tetrahedrally coordinated cations located in the nodes of the grid, surrounded by two pyrimidyl, one pyridyl, and one hydrazone nitrogen atom (Scheme 2.2).

In the context of cation-templated DCLs, subcomponent self-assembly should be mentioned as a valuable two-level method to construct diverse metallosupramolecular structures from simple DCL members and transition metals[127]. At the first level, oligoaldehyde and amine building blocks (subcomponents) form a DCL of imines. The aldehyde subcomponents usually feature a 1-formylpyridine structural motif. This enables the formation of imines with nitrogen atoms in 1,4 positions in an
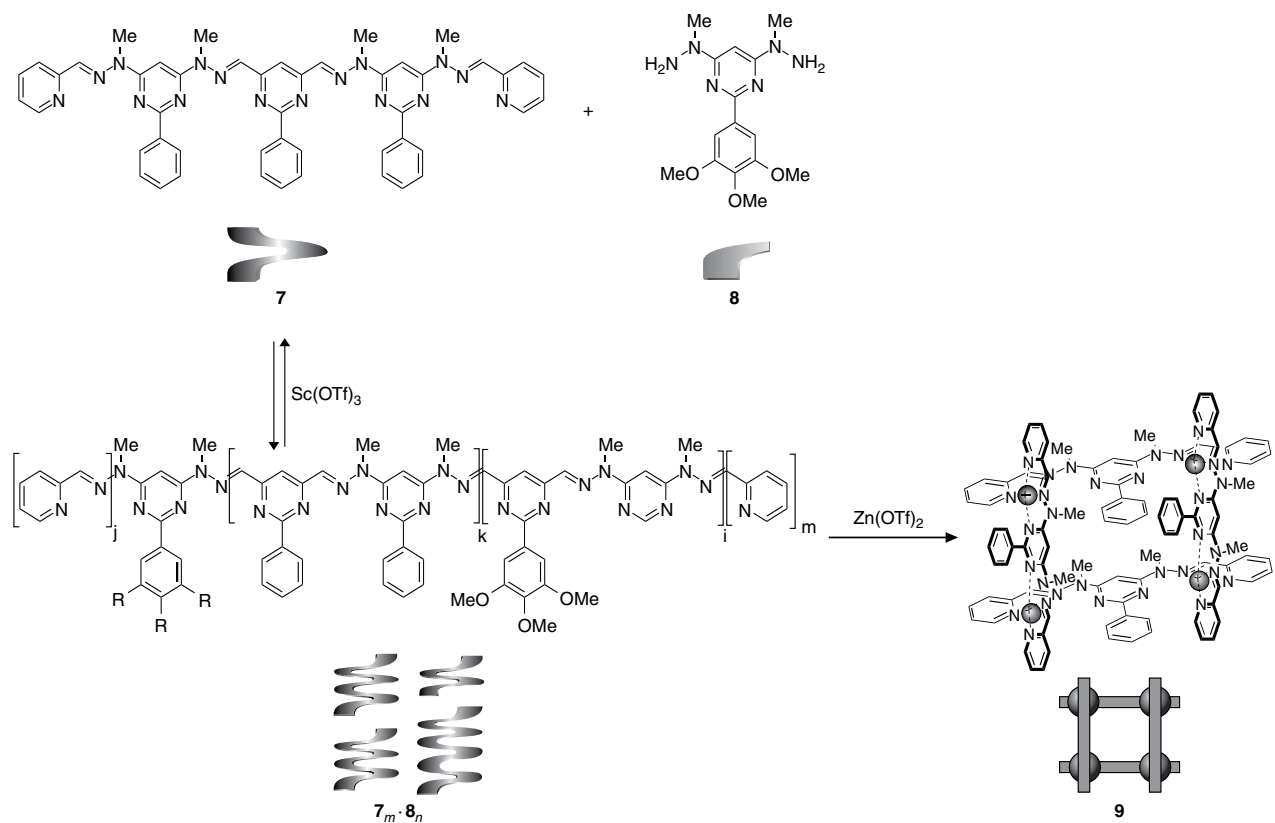
Scheme 2.2 Cation-mediated collapse of a helical hydrazone DCL to the single grid-shaped metal complex **9**.

anti-s-cis-anti conformation, ideal for metal chelation. At the second level, two or three of the corresponding DCL members can form a tetra-or octahedral chelate around the metal cation, which thus serve as vertices in the so-constructed polygonal[109], interwoven[74], or polyhedral[127] architectures. The so-formed metallo-supramolecular species usually possess a hydrophobic cavity of appreciable size, which leads to remarkable host–guest properties and thus enables the control of architectural changes on template addition (see Section 2.2.1.2).

2.2.1.2 Inorganic Anions

Anionic templates have been explored to a somewhat lesser extent in DCC than cations[128,129]. Nevertheless, a decent number of various linear[130] macrocyclic[76,131–137], and three-dimensional[42,119] architectures resulting from the interaction of anions and DCLs have been studied.

Recently, Riddell *et al.*[119] undertook a systematic study on the templating effect of various transition metal cations (Fe^{2+}, Ni^{2+}, Co^{2+}, Zn^{2+}) and organic as well as inorganic anions (ClO_4^-, OTf^-, NTf_2^-, BF_4^-, NO_3^-) on a DCL formed from 6,6′-diformyl-3,3′-bipyridine and *p*-toluidine (Scheme 2.3). The original library consisted of <dout> coordinated unsaturated metal complexes of diimine **10**. However, it gave rise to a large variety of distinct architectures on the addition of the aforementioned ionic templates. For example, Co^{2+} ions in combination with PF_6^- ions provided the
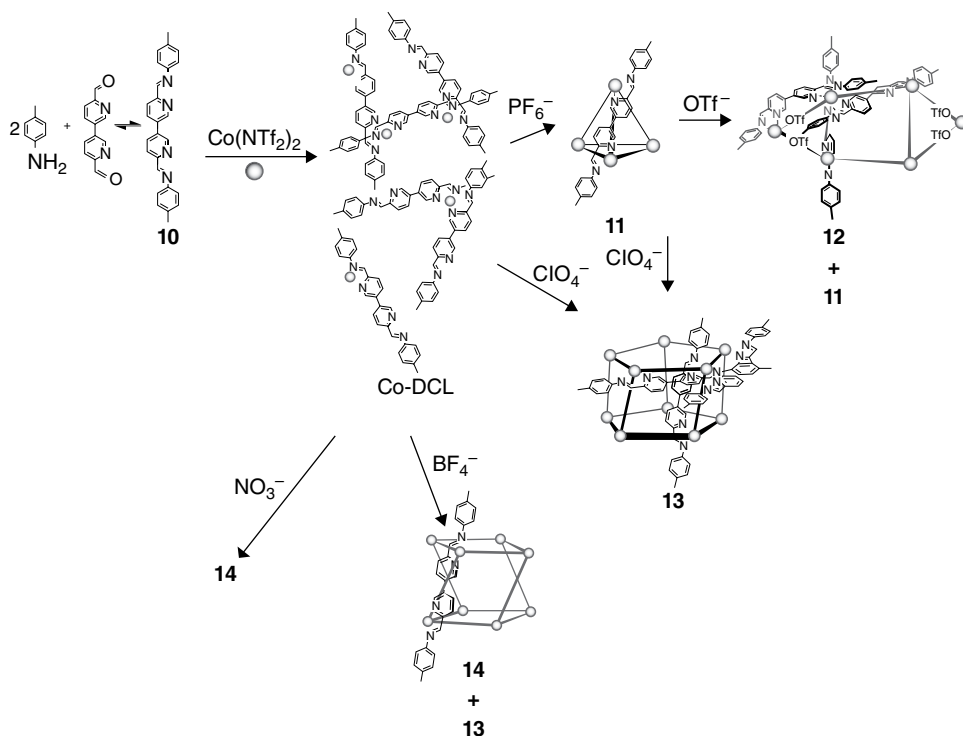
Scheme 2.3 A DCL constructed from 6,6′-diformyl-3,3′-bipyridine and *p*-toluidine can be templated with various transition metals and anions to provide diverse metallosupramolecular architectures.

tetrahedral complex **11**, which itself is stimuli-responsive, transforming in the presence of OTf$^-$ and ClO_4^- into the D_2-symmetric polyhedron **12** and pentagonal prismatic **13**, respectively. Templation with BF_4^- results in a mixture of **13** and the tetragonal prismatic cage **14**, whereas on interaction with NO_3^- only **14** emerges. Remarkably, the preference for the different cages depends on the cation as well: whereas the BF_4^- templated DCL with Co^{2+} gives **13** and **14**, Ni^{2+} produces the analogues of **11** and **12**, while Fe^{2+} provides pure **11**.

Encouraged by these results, the studies were extended to a system where Cd^{2+} served as a cationic template[141]. This system has been proven to be similarly diverse, giving rise to simple helical, tetrahedral, tetragonal prismatic, pentagonal, and hexagonal prismatic architectures. Additionally, the system can be switched in diverse ways between the various states, that is, by cation exchange (Fe^{2+} vs. Cd^{2+}), primary (ClO_4^-, AsF_6^-) and secondary (F^-, Cl^-, Br^-, HF_2^-) anion templation, as well as concentration change. More recently, similar template effects were reported for metallate guests[143].

Whereas the recognition of various anions can proceed smoothly and with high affinity in organic solvents, anion recognition in water still remains a challenge. Kubik *et al.*[131,133,138] used a bowl-shaped cyclopeptide appended with a thiol group, to generate a DCL of dimeric capsules. On addition of various inorganic anions, the anionic guest templates its best receptor, which led to the isolation and characterization (Isothermal Titration Calorimetry (ITC), X-ray diffraction) of a receptor binding sulfate ions with low micromolar affinity[131]. Further optimization of the linker[133], as well as introduction of a second thiol group into the cyclopeptide[138], resulted in an even more compact dimeric capsule capable of binding sulfate ions in an aqueous environment with nanomolar affinity.

2.2.1.3 Biologically Relevant Small Molecules

DCC was originally conceived with the goal of constructing suitable receptors for biologically relevant targets,thus providing a better insight into the non-covalent binding processes ongoing in living systems. From this standpoint it is easily understandable that ever since the beginnings of DCC, the quest for receptors for biologically relevant molecules such as nucleotides[144–146], small peptides[147–151], carbohydrates[152–154], and neurotransmitters[75,155–157], has been the focus of research.

Waters *et al.* developed receptors for methylated arginine and lysine residues via disulfide-based DCC[148–151]. These non-ribosomal amino acid residues are produced on post-translational modification processes, whose disregulation can contribute to serious diseases such as leukemia or lymphoma. The recognition relies mainly on cation–π interactions between the protonated amino acid side chains and the aromatic binding pockets of the proteins. Their approach[149] utilized a DCL of two aromatic dithiols and Arg-containing small peptides as templates. The amplified receptor showed binding affinities comparable with that of the Tudor domain proteins (which are responsible for this specific recognition process). In a related attempt, the same group developed disulfide macrocycle receptors for peptides with differently methylated lysines in the sequence, by systematic redesign of the dithiol building blocks[150,151].

In recent years, Gagné *et al.* conducted intensive research on the recognition of nucleotides by hydrazone DCLs prepared from amino-acid-derived hydrazone-acetal (protected aldehyde) building blocks. In the earlier studies, a single building block was applied as racemate. The enantiopure nucleotide templates were found to desymmetrize the originally racemic DCL[144,145]. In a more recent example[146], two different,
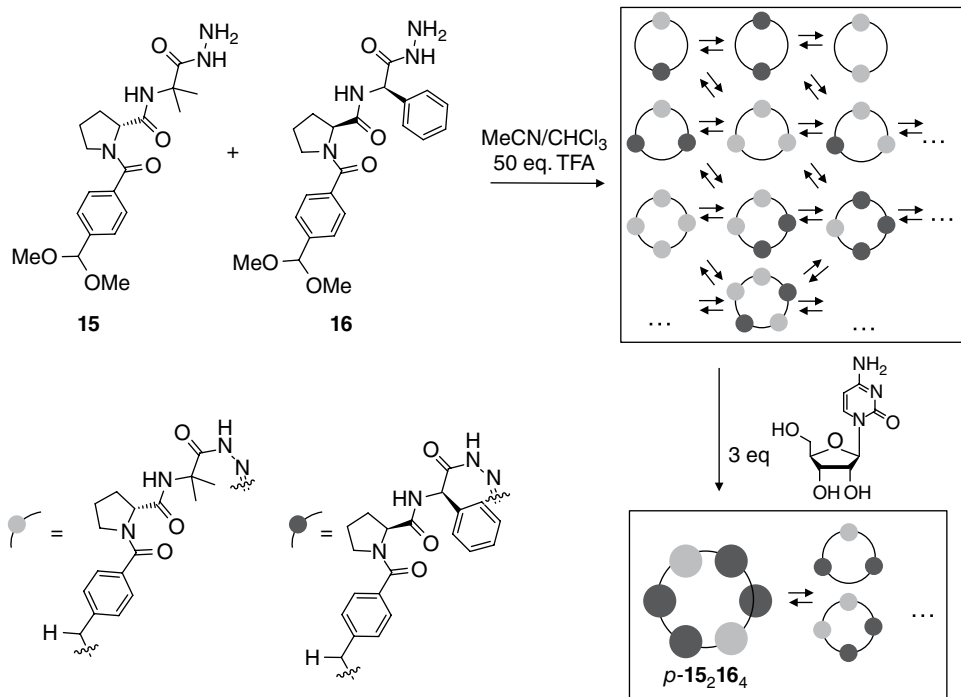
Scheme 2.4 Two amino acid based bifunctional hydrazone-acetal building blocks **15** and **16** form a diverse library of dimers up to octamers. On addition of cytidine the para-**15**$_2$**16**$_4$ hexamer, which was undetectable in the untemplated library, was amplified.

but enantiopure building blocks (**15** and **16**) were implemented (see Scheme 2.4). The DCL contained hydrazones up to octamers[146], while templation with (–)cytidine resulted in selective amplification of one of the mixed **15**$_2$**16**$_4$ hexamers. This is a perfect example of a virtual combinatorial library (see Section 2.1), as none of the hexamers were detectable in the untemplated DCL. Combined NMR and tandem MS experiments were carried out to assign the structure of the amplified species as the *para* isomer. Due to the large number of the equilibria governing the library, DCLFit (see Section 2.1.3) was used to estimate the free binding energy between the amplified hexamer and (–)cytidine, which was calculated to be –21 kJ/mol.

The aforementioned DCLs are less versatile in the sense that they are specifically designed for the recognition of one or two templates. Our group recently reported on a library which was capable of interacting with a handful of organic substrates[75]. The DCL was prepared from two simple dithiol building blocks **17** and **18**, which furnished 34 macrocyclic and catenated species upon oxidation. The library was then tested as a possible platform for templation among a wide structural variety of 30 organic amines and ammonium salts, most of which possess significant biological activity. The template-responsiveness of the system is unique in the sense that almost all of the templates amplify one or more of the DCL members. The most remarkable normalized amplification factors (see Section 2.1.3) are shown by spermine (0.79 for **17**$_4$), cadaverine (0.52 for **17**$_3$**18**), tyramine (0.92 for the **17**$_2$**18**$_2$ isomers), dobutamine (0.38 for **18**$_3$**17**)

and 1-adamantylamine (0.79 for the isomeric DCL membes 18_4) (see Scheme 2.5a, left to right). Remarkably, few templates amplify more than one isomeric set of library members. Several binding constants were determined, mostly with DCLFit (see Section 2.1.3), giving values of up to $9.8 \times 10^4 \, M^{-1}$ (between tyramine and $17_2 18_2$). This example shows the versatility of DCC as a high-throughput method for finding receptors for diverse biologically relevant molecules from a restricted number of building blocks.

Jurczak *et al.*[76] discovered a similarly flexible platform for the recognition of various anions of diverse form and shape (see Scheme 2.5b). The library is based on dithiol **19**, which forms oligomeric macrocycles (19_n, $n = 2$–6) on oxidation. Whereas several small organic anions such as benzoate or squarate were found to template 19_2 with AF_n values up to 0.68, it has proved to be challenging to find appropriate templates for the larger library members. Nevertheless, extended oligocarboxylates were found to amplify 19_3, 19_4, 19_5 and 19_6 with AF_n values of 0.58, 0.65, 0.26 and 0.14, respectively. Remarkably, each larger oligocarboxylate template selectively amplified the library member constructed from the corresponding number of monomers via hydrogen bonding with the amide protons. The relatively large AF_n values, together with selective amplification, are unique for such large macrocyclic guests constructed from a DCL.

2.2.1.4 Miscellaneous Organic Molecules

Besides biologically relevant molecules, several others are pursued as interesting templates (guests), such as fullerenes[158–164], simple aromatic[165,166] and polyaromatic hydrocarbons[167], multivalent N-donor ligands[168–171], or even very small guests such as CO_2[172]. From this diverse collection of divergent approaches, we will focus on fullerenes, and describe two different approaches to illustrate their ability to interact with various DCLs.

Interestingly, exploration of fullerene receptors has gained remarkable interest in recent years, mainly due to the electron-acceptor properties of these carbon allotropes, which render them suitable for the construction of molecular electronic devices. Controlled and reversible complexation is a convenient means of solubilizing and thus processing fullerenes, which are highly insoluble in common organic solvents. However, their curved and apolar surface renders the construction of suitable receptors rather challenging[173]. DCC can alleviate this problem by furnishing a single aromatic binding unit with functional groups suitable for DCC, thus eliminating the often laborious synthetic procedure of covalently linking them together.

Two different approaches are presented here. In a recent work by Stefankiewicz *et al.* a series of naphtalenediimide (NDI) – amino acid conjugates were synthesized. In $CDCl_3$ these formed a hydrogen-bonded DCL consisting of helical nanotubes of various sizes[174], which accomodated C_{60} in their inner channel[175]. On the other hand, addition of C_{70} triggered a remarkable structural change, furnishing hexameric nanocapsules[176]. On competition of the two guests, the C_{70}-hexamer complexes formed preferentially for entropic reasons. Addition of an increasing amount of base to the mixed library resulted in stepwise disassembly of the DCL, due to the disruption of hydrogen bonds[163]. C_{70} was released first (as the hexameric capsule requires more hydrogen bonds per receptor moiety than the nanotubes), followed by the release of C_{60} and monomeric, deprotonated library members. The pH switching turned out to be fully reversible.
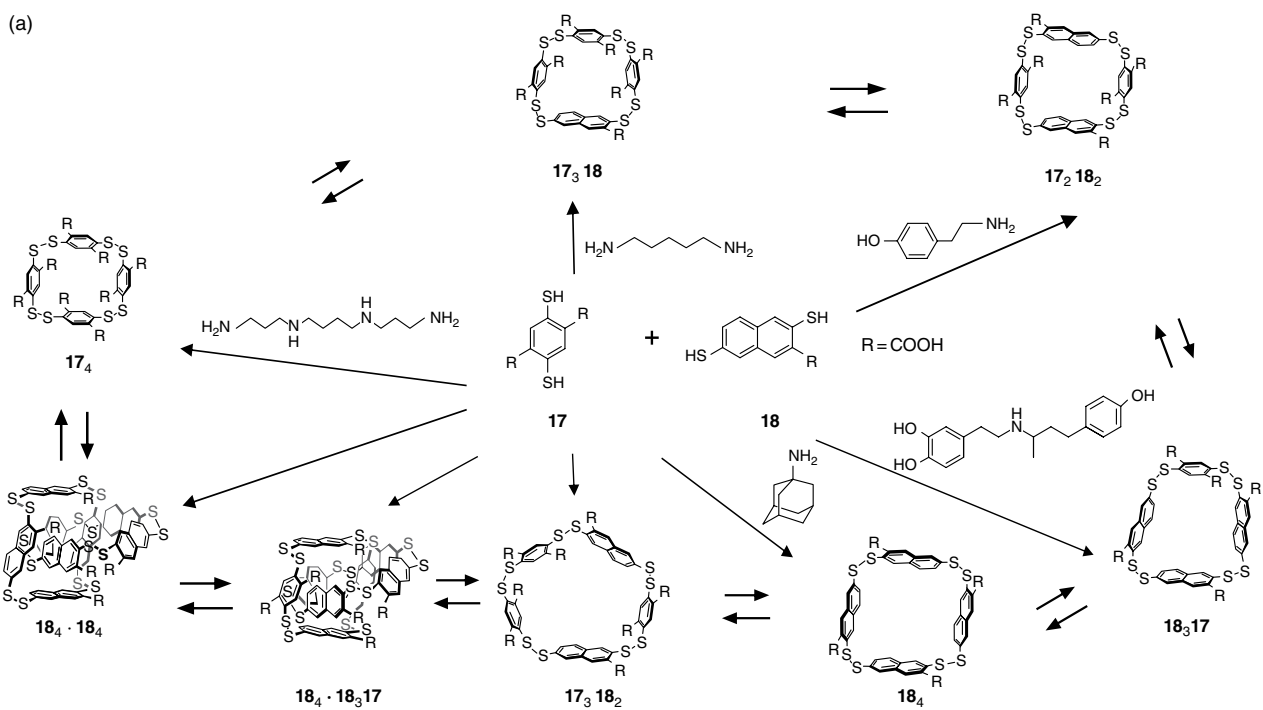
Scheme 2.5 Two "dial-a-receptor" DCLs. (a) Aromatic dithiols **17** and **18** form a DCL of macrocyclic and catenated species (R = COOH). The displayed organic amines, most of which are of biological importance, amplify diverse macrocycles from the DCL. (b) Picolinic acid-based dithiol **19** forms a DCL of macrocycles up to hexamers. These can serve as guests for various organic oligoanions.

(b)

19₂

19₃

19

19₄

19₅

19₆
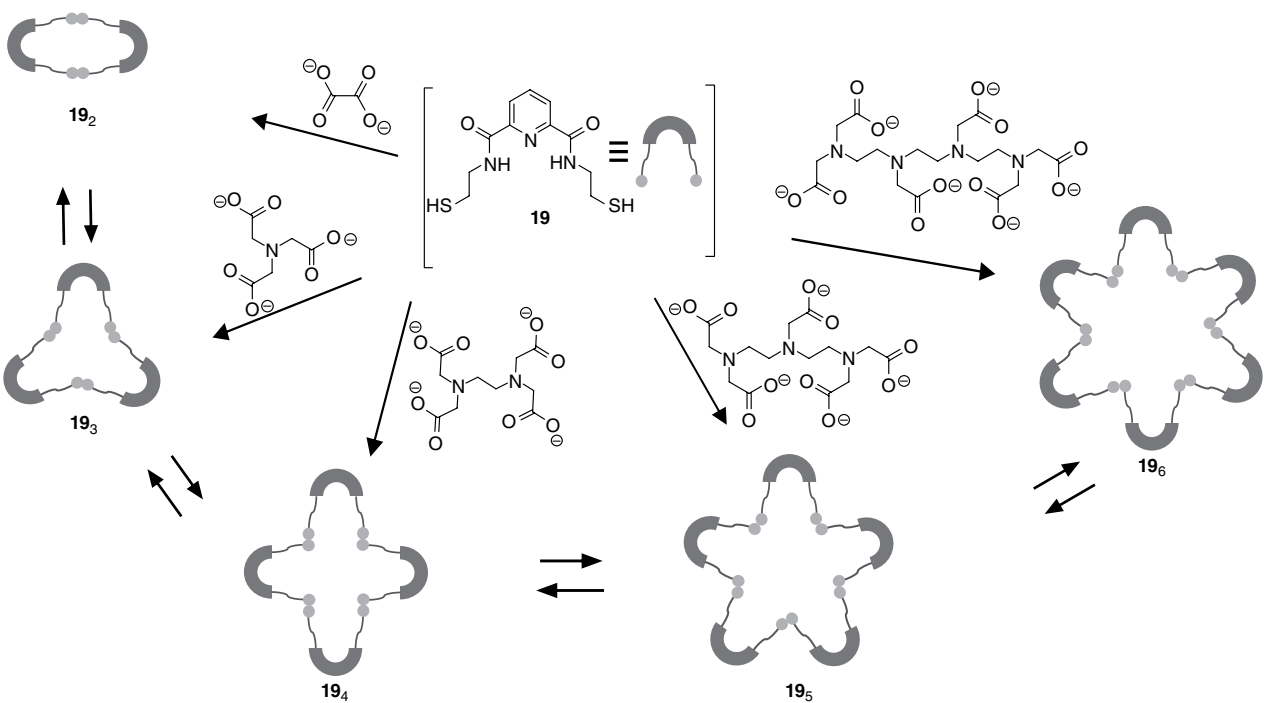
Scheme 2.5 (Continued)

These studies show that receptors for fullerenes with remarkably different topologies can indeed be produced via DCC from easily accessible organic monomers and can reconfigure on further chemical stimuli.

In the previous examples, library members formed by covalent linkage of two or more building blocks. Bode *et al.*[154,160,161,177] envisaged a completely different approach for fabricating receptors from a DCL by providing DCLs in which library members are mutually interconvertible constitutional isomers. For this purpose, they exploited the chemistry of bullvalenes. Unsubstituted [1.1.1]-bullvalene ($C_{10}H_{10}$) can undergo a series of Cope-rearrangements, producing an ensemble of more than 10^6 energetically equivalent and thus indistinguishable constitutional isomers. The DCLs were constructed by de-symmetrizing bullvalene with appropriate substitutents, furnishing energetically different, yet still dynamic, isomers. Moreover, the substituents were able to serve as hosts for specific templates, thus a set of isomers can be amplified on template addition. Furthermore, the receptor design allowed the freezing of dynamic rearrangements to trap the set of amplified receptors. For this purpose, a dynamic bullvalene derivative **20** was prepared (Figure 2.7), which was equipped with two porphyrin moieties, providing the recognition site for fullerene guests. Another key feature of the molecule was a photocleavable nitroveratryl-oxycarbonate (NVOC) moiety, resulting from the enolization and subsequent trapping of an intermediate bullvalone. The receptor itself was
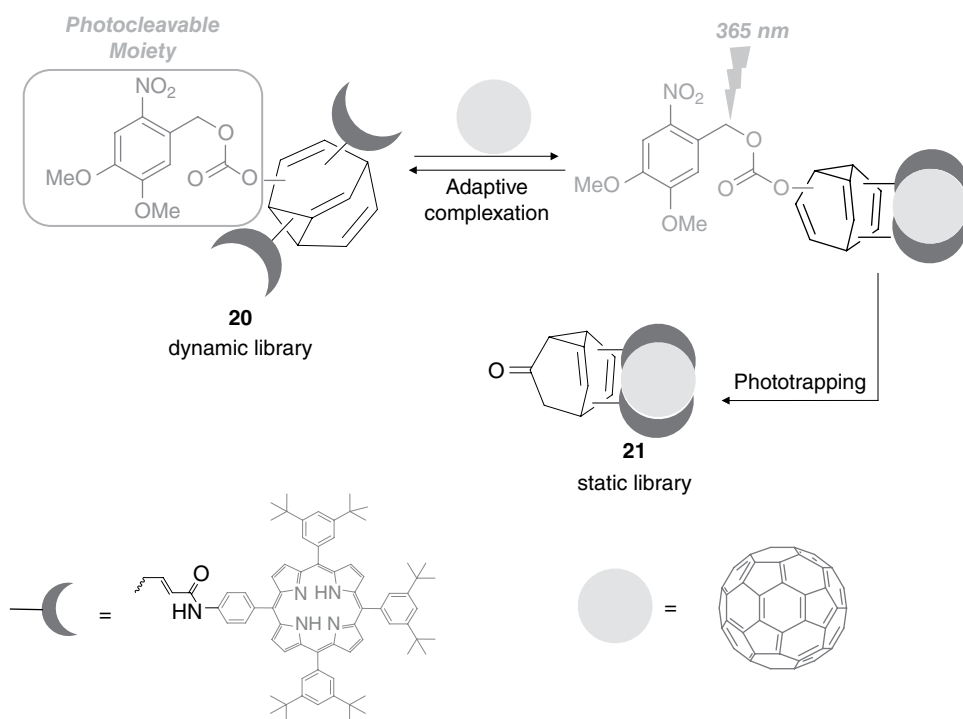
Figure 2.7 A dynamic library of interconverting isomers of **20** (containing a photocleavable NVOC moiety) is able to form host–guest complexes with C_{60}. Library members whose structure is more suitable for guest binding are amplified. On photocleavage of the NVOC group, a static library of compound **21** is formed, containing mainly the derivatives of good binders.

fluxional, being present as a more than 1.8×10^6-membered DCL of isomers. On addition of C_{60}, a characteristic change in the ^{13}C NMR spectrum and a marked shift in the UV-visible spectrum were observed, indicating that the library distribution was shifted. Subsequent irradiation with UV light at 365 nm resulted in the cleavage of the NVOC moiety, resulting in a static library of isomeric bullvalones **21**. Although the separation of the isomers could not be achieved even in a static library, the average binding constant of the dynamic and static libraries were determined by NMR and UV titrations to provide binding constants of $3 \times 10^3 M^{-1}$ and $7 \times 10^3 M^{-1}$, respectively.

2.2.2 Ligands for Biomolecules

As mentioned earlier (see Section 2.2.1.3), one prominent goal of template-controlled DCC has been to develop receptors of biologically active small molecules. DCC is already regarded as a promising means of designing ligands for biomolecules (enzyme inhibitors and nucleic acid binders) and consequently a promising starting point for drug design. Beginning with the seminal papers of Lehn[42] and Miller[43], diverse proteins, as well as RNA and DNA fragments have been targeted. The subject has recently been summarized in two review articles[27,178].

2.2.2.1 Protein Inhibitors

Some general features of protein-directed DCLs should be mentioned. First, at least one of the building blocks usually contains a structural element that is an already known good binder. This building block (supporting ligand) can thus serve as a starting point for DCC binding studies (site-directed ligand discovery, see[179–182]). If two or more binding pockets are targeted simultaneously, an extended tethering strategy is used: the building block occupying the first pocket is covalently bound to the protein, but contains a free functional group capable of engaging in dynamic covalent bond formation, for which the other building blocks compete to bind into the neighboring pocket[183,184]. Second, the dynamic chemistry used for ligand discovery should be selected carefully so that it is fast enough and the target protein is sufficiently stable under the conditions of the DCC used. Third, in order to ensure that the order of ligand amplification corresponds to their binding capability to the target, building blocks of similar reactivity and stability have to be used[27]. Last but not least, although even low nanomolar affinity binders can be obtained via DCC, normally the amplified members are not stable enough for direct medicinal chemistry applications[27] so these should be covalently modified to replace the dynamic moiety with non-dynamic bonds[185,186].

From the analytical point of view, a number of special aspects, arising mainly from the large number of experiments and the complex chemical structure of the targets, have to be mentioned. When mass spectrometry is the main analytical tool (see Section 2.7.2), DCL members of distinct mass should be present. NOESY-related NMR methods based on water or ligand signal relaxation are often used as they require a substoichiometric amount of the often scarce protein target[182,187]. However, neither MS nor NMR enable high throughput screening. In contrast, application of a fluorescent probe bound either covalently[188] or non-covalently[189] to the target could greatly enhance the detection sensitivity and analysis time. One should note that despite the existence of high-throughput methods, libraries are usually divided into sublibraries[190,191], thus reducing the number of experiments. Another tool for decreasing analysis time is the dynamic

deconvolution method. In this procedure, an assay (based usually on fluorescence) is used to assess binding strength to a specific target. The fluorescent signal arising from the initial DCL is compared to libraries from which a specific building block (one compound at a time) is removed. A drastic drop in the fluorescence response indicates which building block is responsible for binding[192,193].

The first example of protein-directed DCC[42] involved site-directed imine chemistry to enable the discovery of a sulfonamide-containing inhibitor of carbonic anhydrase II (CAII). Since then, the site-directed method has become the prominent method of DCC-based drug discovery. A recent example[181] is shown on Scheme 2.6. In this work, boronic acid-diol DCC was applied for the first time to target an oxygenase, prolyl hydroxylase domain isoform2 (PHD2). As site-directing or support ligand, the boronic acid **22a** was used, which is based on N-oxalylglycine (**22b**), a well-known chelator of the Fe^{2+} ion in the active site of PHD2. The aromatic diols **23a–f** were used and binding was followed by non-denaturing ESI-HRMS and NMR-based water relaxation experiments. The results showed that the adducts with **23e–f** were the best binders. These boronic esters were further modified on the pyridine ring as well as in the connector moiety (dynamic to non-dynamic) to finally give ligand **24** with an IC_{50} value of 0.013 μM. The binding was confirmed by single crystal X-ray analysis of Mn^{2+}-modified PHD2, complexed with **24**, showing the naphthalene moiety occupying the substrate binding site.

Greaney's group studied ligand discovery for gluthathione (GSH) S-transferase (GST) enzymes using thiol-enone conjugate addition as dynamic covalent reaction. Ethacrynic acid (EA), an enone itself, or GSH served as support ligand, whereas the other component of the dynamic reaction was modified. This approach led to the parallel discovery of inhibitors for two binding sites of the SjGST enzyme[194]. Later on, the same target was probed with dynamic hydrazone chemistry. This approach required the use of aniline as catalyst, which enabled fast equilibration even at the nearly neutral conditions that are required for the enzyme to remain stable. Their results furnished inhibitors with an IC_{50} value of 22 μM, which were further decreased to 5.25 μM by covalently attaching GSH to the aldehyde building block[95]. The GSH-modified aldehyde was used in the next step of binder optimization with bivalent acyl hydrazones, resulting in the discovery of an inhibitor for the structurally related enzyme mGSTM1-1 with an IC_{50} value of 60 nM[195].

Whereas site-directed ligand discovery is often combined with dynamic combinatorial methods, true *de novo* structure-based design (in which the screening is initiated without a known hit compound) is rather rare. One novel example is described in the work of Hirsch *et al.*[182], who combined amino acid-derived acylhydrazones with simple aromatic aldehydes leading to a DCL to target the aspartic protease endothiapepsin. Initial guesses about the prospective structure of a good binder were gained from molecular modeling. The two best binders had IC_{50} values of 6 and 7 μM, respectively. Similarly to the case mentioned above, cocrystals of the hydrazone hits and the target protein could be obtained and the resulting X-ray structures were in agreement with those predicted by modeling.

A completely different approach was envisaged by Fulton's group, who used polymer-scaffolded DCLs (PS-DCL)[196,197] to target proteins. This method is illustrated in Scheme 2.7. An aldehyde-containing block copolymer **25** was prepared, which was reacted with hydrazones featuring positively charged (**26**) or neutral (**27, 28**) side chains.

23a

23b

23c

23d

22a

23e

23f

22b

24
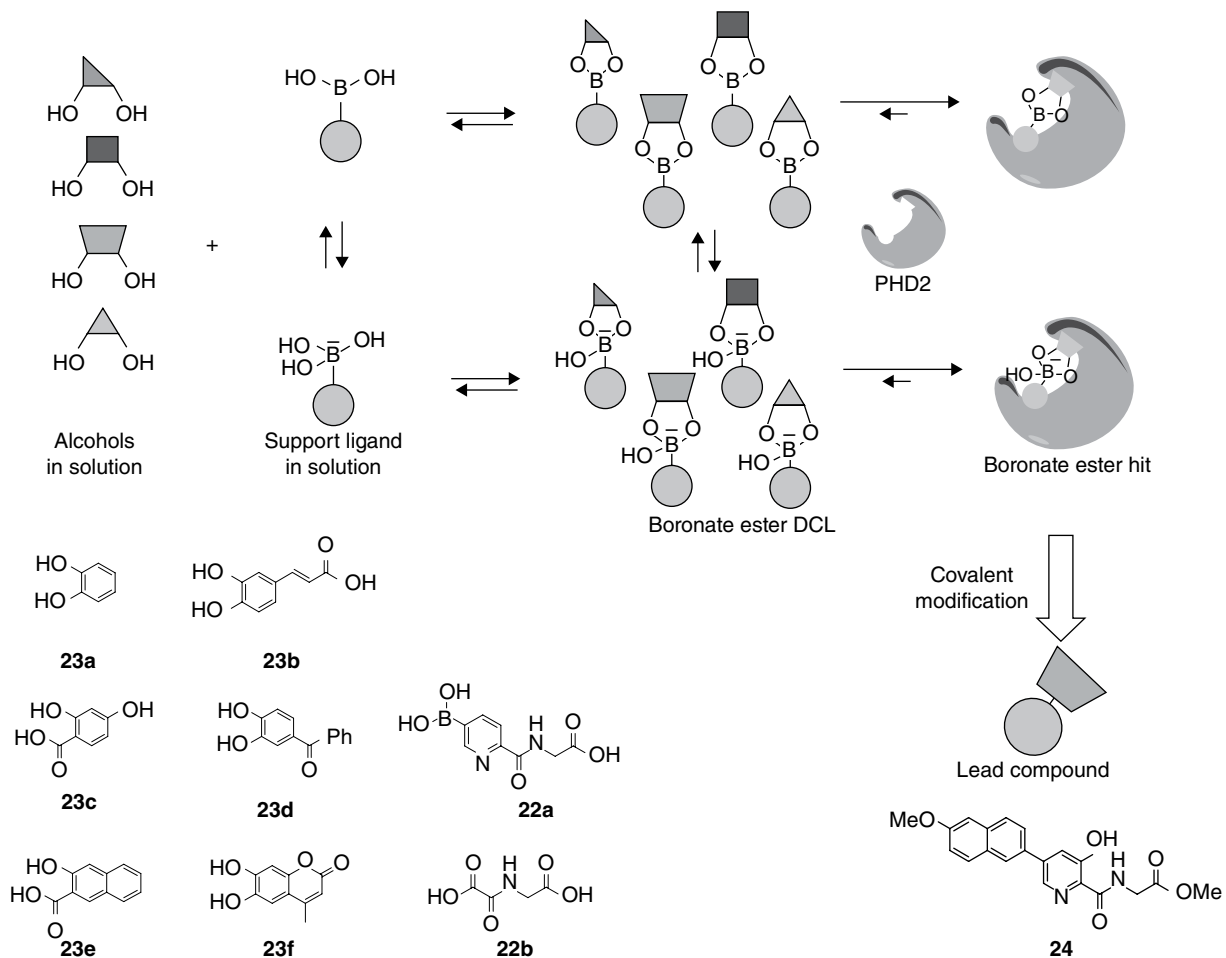
Scheme 2.6 Discovery of potential inhibitors of the oxygenase PHD2 from a boronic-acid based DCL.
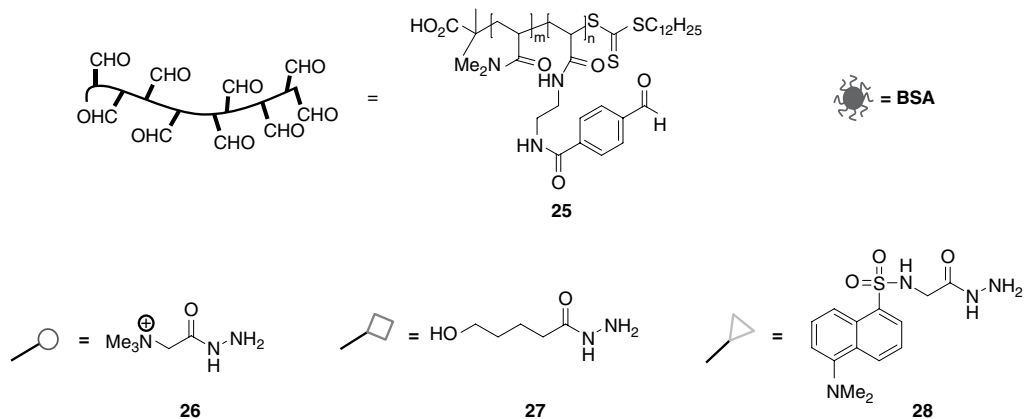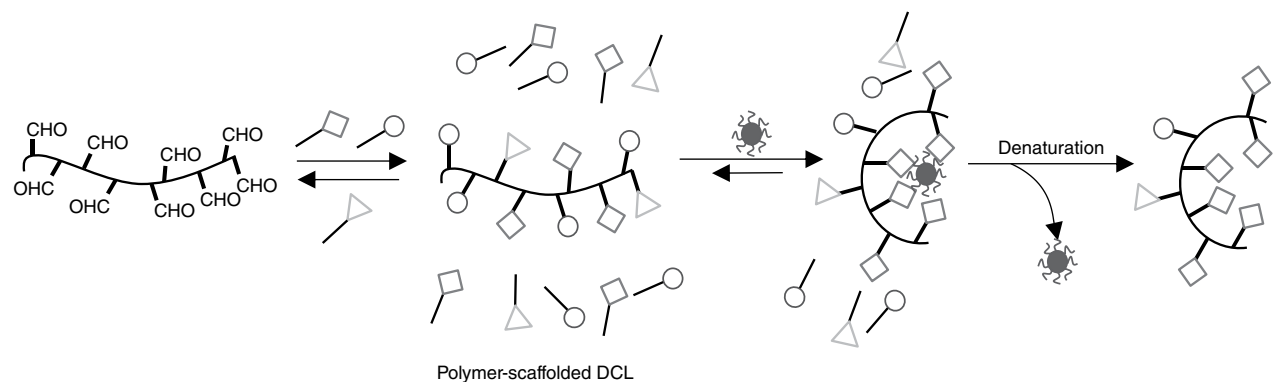
Scheme 2.7 Development of a BSA (bovine serum albumine) binding functionalized polymer based on a polymer-scaffolded hydrazide DCL.

Hydrazone formation was quantitatively followed by ^{1}H NMR. First, static libraries were prepared with a given ratio of various hydrazones. The functionalized polymers were separated and their binding affinity to negatively (polystyrene sulfonate) or positively (bovine serum albumine, BSA) charged macromolecular templates was determined. As expected, targets with a specific charge on their surface amplified PS-DCL members carrying the opposite charge. Next, all hydrazones were added in parallel in the presence of the corresponding solid-supported template. The amplified fraction was separated by preparative Gel Permeation Chromatography (GPC) and the binding constant (with the template) was determined. This resulted in improvement of the binding constants by approximately one order of magnitude compared to the static libraries, giving K_d values of 1.3×10^6 M^{-1}[197]. Later, the same method was applied using a similar aldehyde-functionalized polymer and carbohydrate-functionalized hydrazides to template lectins[198]. In the amplified polymers the arrangement of the side chains cannot be controlled, that is, the elaboration of sequence-specific binders has not yet been achieved. Nevertheless, this approach illustrates that DCC, combined with multivalent interactions, is capable of providing good binders for biological targets, even without knowing their exact structure.

Lectins, that is, proteins binding to cell membranes by carbohydrate complexation, were also targeted by other DCLs. Ramström and Lehn[192] combined monosaccharide-appended aldehydes and simple aliphatic oligohydrazones to generate a DCL with the lectin concanavaline A as a target. Their investigations showed that mannose-containing DCL members were the most effective binders. Later on, de Mendoza *et al.*[199] targeted the same lectin, applying a Fe^{2+}-scaffolded DCL based on monosaccharide-decorated 2,2′-bipyridine building blocks. Dynamic deconvolution again showed the priority of all-mannose-containing DCL members.

In the examples above, the protein target, although being catalytically active, did not modify the molecular structure of the bound DCL members. However, coupling of an enzyme-catalyzed irreversible reaction to the reversible binding process would result in the gradual removal of the most strongly binding member from the DCL and thus shifting of the equilibrium. In their catalytic self-screening method[200], Ramström *et al.* targeted a cholinesterase by reacting different thioesters with thiocholine in the presence of the enzyme, which binds the choline fragment and subsequently hydrolyzes the thioester bond. Thus, by monitoring the conversion of different thioester substrates, their relative order of binding strength could be assessed. Later on, these investigations were extended to a dynamic system of acetylthiocholine (ATCh) and symmetric bis-thioesters in the presence of acetylcholinesterase (AChE)[201]. The same concepts were applied in a nitroaldol DCL with lipase PS-C I as a target, which performed an enantioselective acylation (dynamic combinatorial resolution) on the most strongly binding member[202]. The same enzyme was capable of selecting the three best binders from a two-level 24-membered DCL, based on the Strecker reaction.[203]

2.2.2.2 Nucleic Acids

In the context of template-directed synthesis, nucleic acids possess a privileged position as they are involved in storage and expression of genetic information. Thus, the design of suitable targets for nucleic acid structures is crucial in the control of biochemical processes, yet it has remained a challenging task for two reasons. First, sequence-specificity is hard to achieve in the light of the low number of different nucleotide

building blocks (compared to amino acids). Second, nucleic acids can form diverse secondary structures, such as duplexes, triplexes, quadruplexes, hairpins and loops, which require structurally unique and mostly unexplored binding motifs[178].

The first DCLs for the recognition of DNA[43] and RNA[204] were based on salicylaldimine complexes of various transition metals, in which recognition was promoted by complexation of multivalent aromatic DCL members to the nucleic acid. Although binders with micromolar binding affinity were revealed, the inherent hydrolytic instability of the imines hampered further development. Traditional solution-phase dithiol[96] and acylhydrazone DCC was utilized to find binders for various duplex DNA structures. In the latter case, polymeric binders with low micromolar affinity were obtained, which, in contrast to traditional polyimine binders, could preserve their binding properties even at high salt concentrations[205]. Recently, duplex DNA templates have been used to decorate aldehyde-functionalized gold nanoparticles with DNA-binding amines via imine DCC in aqueous medium[60]. Attachment to the nanoparticle surface occurred in a selective manner, that is, only in the presence of the template, due to multivalency of both nanoparticles and DNA that overcomes the intrinsic instability of imine bonds in water (see Section 2.4.4.2 and Figure 2.18). Similarly, DNA-template-mediated component selection was reported in the functionalization of a cyclopeptide-based oligoaldehyde scaffold via hydrazone DCC[206].

As mentioned earlier, fine-tuning of the ligands has to be achieved to obtain sequence-selective complexation, which is much more likely when applying larger DCL (see Section 2.1.3). Using a resin-based technique (see Section 2.4) Miller *et al.* screened a DCL of quinoline-appended short peptides which form a disulfide DCL with 11,325 members, selectively targeting the stem-loop RNA sequence responsible for the expression of proteins which are vital for the proliferation of the HIV virus[207] and the (CUG) repeat RNA, targeting myotonic dystrophy[208].

In certain guanine-rich sequences quadruple DNA strands (DNA-quadruplexes) can form, for example via templation with K+ ions. These interesting structural units have been targeted with DCC as well. It is not surprising that, due to the large number of
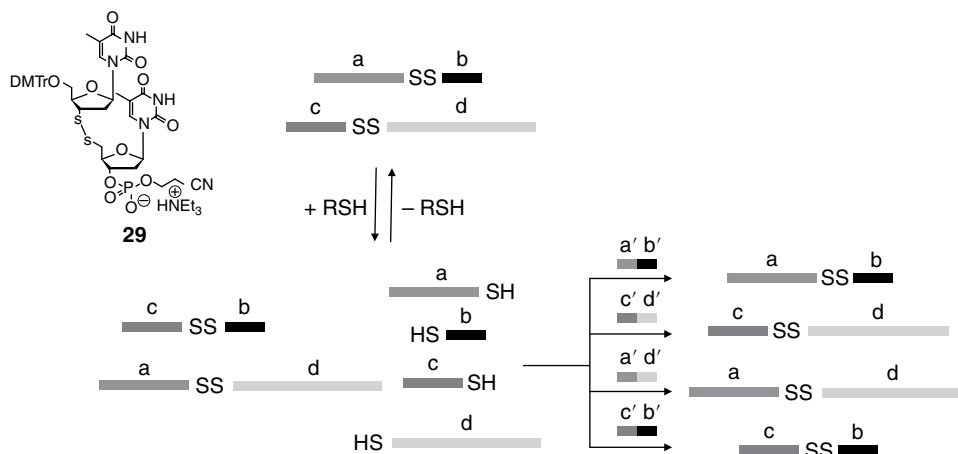
Figure 2.8 A disulfide DCL composed of oligonucleotide strands containing the dynamic dinucleotide **29**.

negative charges in the quadruplex regions, ligands carrying multiple positive charges or electron-deficient aromatic moieties turn out to be the best binders. Following this guideline, it was possible to select and identify micromolar[209,210] or even high nanomolar[211] binders, mainly from disulfide DCLs.

In these examples, even the ones applying diverse and complex DCLs, the DNA remained a static target. In a recent contribution, Gothelf *et al.* showed that the DNA backbone itself can be rendered dynamic (*Angew. Chem. Int. Ed.* 2014, 53, 14415–14418). For this purpose they used the dithymidine dinucleoside **29**, in which a disulfide group replaces the static phosphate unit connecting the deoxysugar moieties (Figure 2.8). This analogue was subsequently incorporated into two oligonucleotide strands, *aSSb* and *cSSd.* An excess of reducing agent rendered this binary mixture a dynamic library of four mono-thiols (*aSH, bSH, cSH, dSH*) and the mixed disulfides. On addition of the complementary strands *a′b′, c′d′, a′d′* and *c′d′* as templates, the corresponding longer oligonucleotides *aSSb, cSSd, aSSd* and *cSSd* are amplified, while the leftover members remain unrecombined (see Figure 2.8). The disulfide linkage could be read by polymerases so that amplification and sequencing of dynamic DNA strands was possible, although a high mutation rate was observed in the sequence surrounding the disulfide modification.

2.2.3 Catalysis

In the previously described examples, DCL members are templated and amplified by receptors or ligands which correspond to a local or global minimum on the corresponding potential energy surface (PES). However, DCL members are likewise capable of serving as hosts for species which correspond to a saddle point (i.e., a transition state, TS) on the PES[46]. Stabilization of a transition state via encapsulation by a DCL member can decrease the activation energy (E_a) of the corresponding reaction. In other words, DCLs can be used as dynamic catalyst systems as well.

One challenging aspect of this type of catalyst screening is that the real TS cannot serve as a template, therefore, a transition state analogue (TSA) has to be used to mimic the TS. This compound should be stable under the conditions of study but should contain structural elements that are suspected to be responsible for binding of the real transition state. The TSA can be designed to be structurally analogous (or identical) to the substrate or to the product or none of them, depending on the structure of the PES[212,213]. A catalytically active DCL member should have a higher binding affinity to the TSA (or rather to the TS, to be exact) than to the substrate (to provide a substantial decrease of the E_a), but it should have a low binding affinity to the product (in order to prevent inhibition of the catalyst).

In a recent example[214], a systems approach to catalysis was presented based on these principles (Scheme 2.8). The ammonium salt **30** can undergo an aza-Cope rearrangement to provide the iminium salt **31**, which further hydrolyzes to aldehyde **32** and dimethylamine. A TSA (**33**) was designed to mimic the structure of the cyclic transition state of the reaction. Dithiol **18** forms tetrameric macrocycles and octameric catenanes in aqueous solution (the lack of a symmetry axis in the building block leads to the production of several isomeric tetramers and catenanes). The formation of interlocked species can be rationalized by the fact that the system tends to minimize the exposure of the large hydrophobic surfaces to water. On addition of the substrate **31**, a sudden increase in the amount of tetramers at the expense of the catenanes was observed,

(a)

30   **31**   **32**   **33**

(b)

18

catenanes
(resting state)

tetramers
(catalyst)
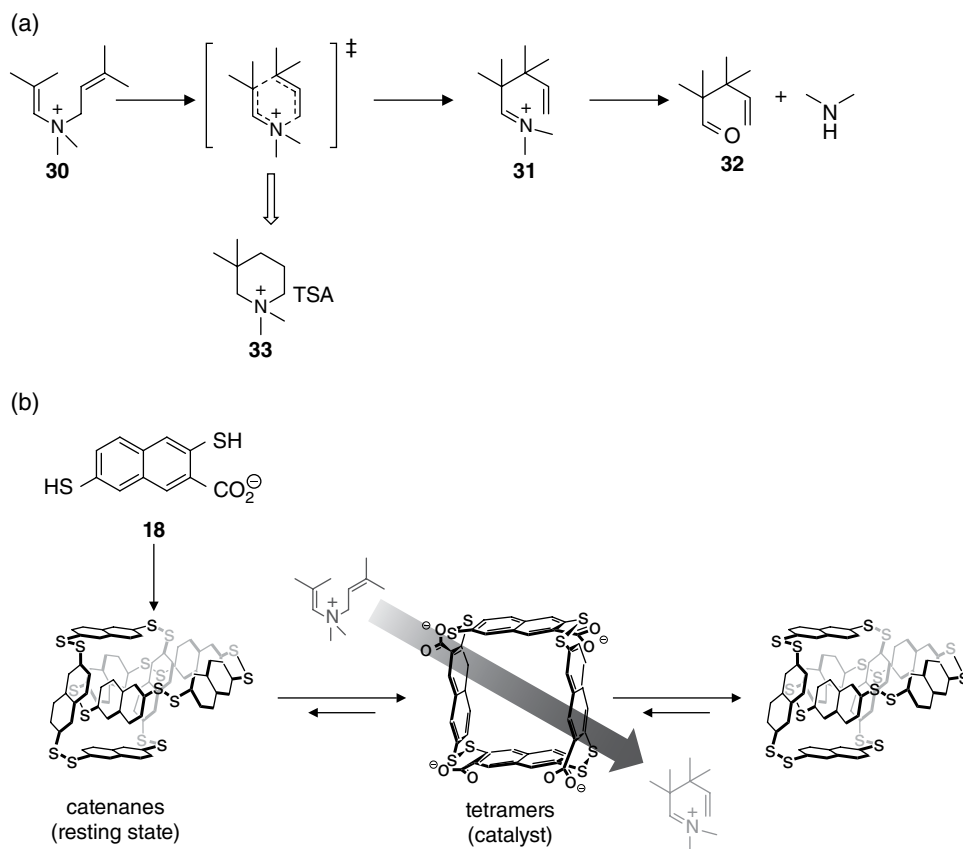
Scheme 2.8 On-demand catalysis from a dynamic combinatorial network. (a) An aza-Cope rearrangement of **30** to **31** with its transition state and TSA **33**. (b) DCL consisting of catenanes from **18** and a small amount of tetramers. Exposure of the system to substrate **30** or the TSA delivers tetramers, which catalyze the rearrangement and convert back to catenanes as the substrate is consumed.

simultaneously with the appearance of **32**. These findings show that the tetramers catalyze the rearrangement. On full consumption of **31**, the library composition reverts to the original one, but on further additions of the substrate, the library remains catalytically active. Kinetic measurements show a ca. six-fold increase of the reaction rate at 50 °C compared to the non-catalyzed reaction. Thus, although the rate enhancement is modest, these results show that DCLs consisting mainly of catalytically inactive species, can provide a catalyst on demand.

2.2.4 Self/Cross-templating and Replicators

Up to now only DCLs controlled by external templates have been discussed. However, several DCLs are reported where one member is capable of either stabilizing itself or binding the building blocks which it is formed from via supramolecular interactions. The first case where a DCL member stabilizes itself is termed self-selection, and is of thermodynamic origin[215,216]. The second case, where a DCL member can lower the

kinetic barrier of its own formation similarly to autocatalysis, is termed self-replication. In this scenario (see Figure 2.9), the template brings the corresponding building blocks into close proximity so that covalent bond formation is more likely to happen. This results in a catalytically inactive dimer of the template. The crucial step to achieve exponential self-replication (i.e., a replication step which is first order in the replicator) is the disassembly of this species to provide two replicator moieties[217]. In order to prove that the emergence of a specific product is not of thermodynamic in origin, seeding experiments are carried out, that is, a small amount of the replicator (seed) is added to a DCL containing non-replicating members (food). Instantaneously triggered exponential growth of the seed indicates that it is autocatalytically active, thus acts as a self-replicator. Notably, initially dynamic self-replicators can become kinetically trapped via the formation of an irreversible covalent bond[218], aggregation[219] or phase separation[220].

Philp and co-workers were among the first who showed that DCC can be coupled to self-replicatory behavior[53]. They utilized a mixed DCL of imines and nitrones competing for the same aldehyde building blocks. The library was treated with a maleimide derivative which underwent an irreversible [3 + 2] cycloaddition with the nitrones. One stereoisomer of the cycloadduct was capable of templating its own formation via complementary hydrogen bonding, similar to that found in DNA base pairs. The replication process caused the aldehyde equipped with the hydrogen bonding unit to become sequestered in the form of the maleimide-nitrone cycloadduct while the unfunctionalized aldehyde and the amines remained in the exchange pool. Later on, another variant of this system was constructed which was based on two interconnected self-replicatory subsystems, the product of each being capable of templating the members of the other subsystem[218]. Simultaneously, Giuseppone et al. used a similar system, based exclusively on imine DCC and hydrogen bonding, as the basis for self-recognition[221].

A fully synthetic exponential replicator[219,222,223], reported by our group, was based on a pentapeptide-appended dithiol **34**, which contains alternating hydrophobic and hydrophilic amino-acid residues. Such peptides are widely known to form β-sheets in an aqueous environment. On oxidation, a mixture of interconverting trimeric, tetrameric and hexameric disulfide macrocycles are formed, with the smaller species being the main products for entropic reasons. This composition is maintained in the absence of mechanical agitation (Figure 2.9). On shaking the solution, however, the hexamers take over and become the dominant product of the library. Transmission Electron Microscopy (TEM) experiments showed that the hexamers form fiber-like stacks, stabilized by hydrogen-bonding between the peptide chains. Agitation is crucial for replication, as during this step the number of fiber ends which are catalytically active, is redoubled (see Section 2.3.4).

Further mechanical investigations[223] revealed that the self-replication is exponential due to an elongation-breakage mechanism. TEM studies showed that during the seeding process the average length of fiber ends remains constant, which is consistent with a mechanism of continuous elongation (growing) and breakage of the fibers. Computational studies proved that, without the breakage step, the process would not be exponential. Importantly, stacking results from multivalent interactions, which dictates a critical macrocycle size suitable for replication. Macrocycles that are too small do not provide enough intermolecular binding energy for stacking, while macrocycles that are too large are entropically unfavoured. The critical macrocycle size, in turn, is dictated by the hydrophilicity of the peptide chain: more hydrophilic peptide chains contribute less intermolecular binding energy per monomer, which requires larger macrocycles to
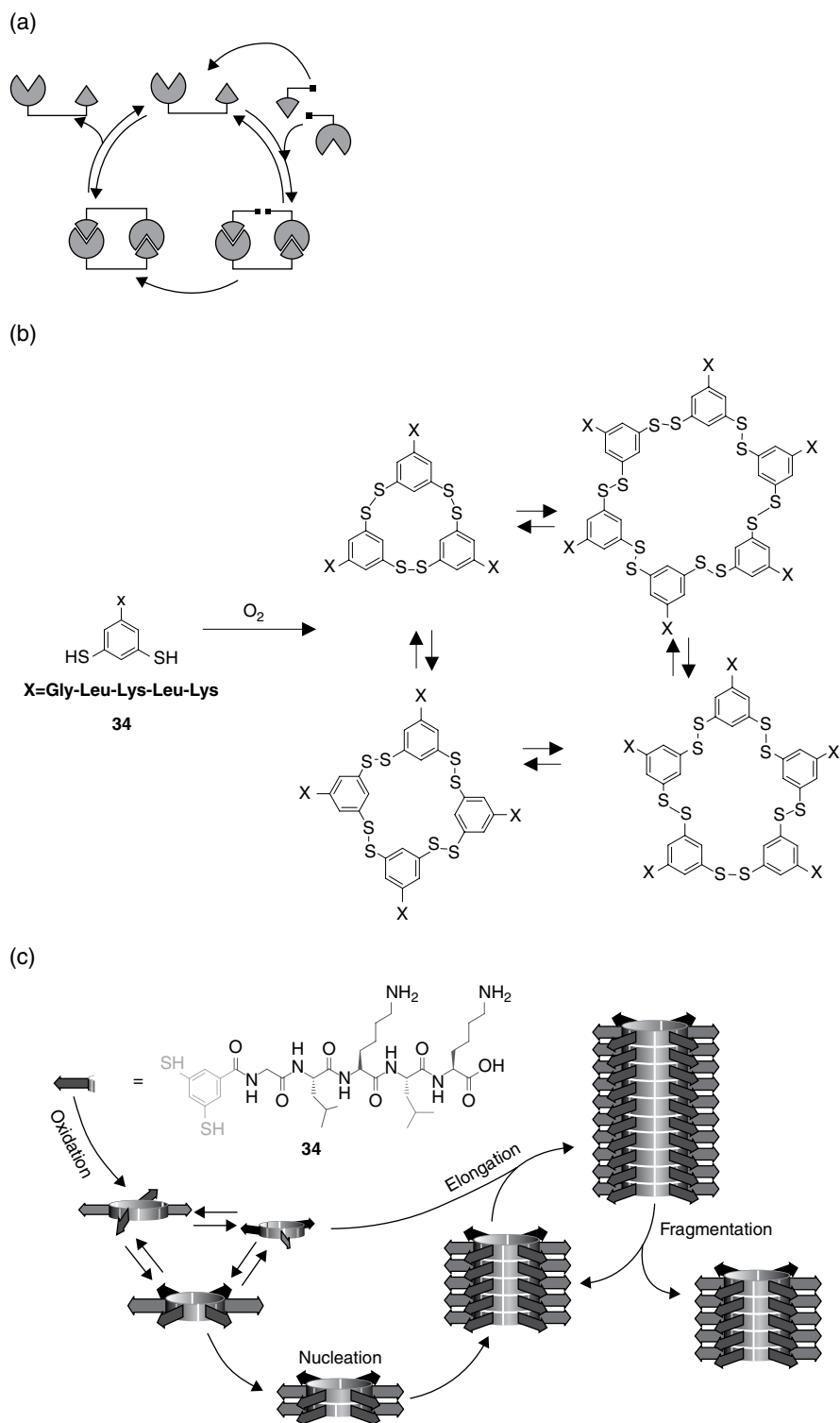
Figure 2.9 Self-replication in a DCL of peptide-functionalized disulfide macrocycles. (a) General scheme of a self-replicating entity. (b) The peptide-functionalized dithiol **34** forms an equilibrium disulfide DCL of various macrocycle sizes. (c) In equilibrium, **34** forms a mixture consisting of trimers, tetramers and hexamers. The latter is capable of forming stacks which are elongated to build fibers. On mechanical agitation fibers undergo breakage, doubling the number of catalytic fiber ends in each cycle, resulting in exponential replication of the hexamer.

provide stable stacks[222]. Research in this field was extended to study the effect of the environment on the replication process[224] (see Section 2.3.1), as well as to control the dimensions and the chemical composition of self-assembling materials[225] (see Section 2.5.2).

The self-templating ability of replicators can be based on various secondary interactions and the aggregates of the replicators can possess various morphologies. For example, Giuseppone[220] and van Esch[226] utilized hydrophobic aldehydes and hydrophilic amines in aqueous solution which formed a DCL of amphiphilic imines. On reaching a critical concentration, the imines self-assembled into various nanoscale assemblies (nanorods or micelles), which formed a separate mesophase, thereby shifting the imine equilibrium to the product side. Importantly, after growing to a critical size, the aggregates undergo division, causing exponential growth of the assemblies.

Ashkenasy and coworkers used a different aggregation type, (trimeric) coiled-coil formation of helical peptides, to induce self-replication[227–230]. The peptides were assembled from an electrophilic (E) and a nucleophilic (N) building block by native chemical ligation[94] in the presence of excess 2-mercaptoethane sulfonate (RSH) to maintain the dynamic nature of the process. In a recent work[231], a DCL of competing self-replicators was studied, constructed from different peptide mutants. Minor changes in the amino-acid structure can drastically modify the stability of the coiled-coil and thus the ability of the corresponding peptide to self-replicate. The peptide sequence of the electrophilic (**35, 36, 37**) and nucleophilic (**38, 38a**) building blocks and that of the resulting peptide replicators **39, 40, 41, 39a, 40a, 41a**, as well as an external template **42** are shown in Figure 2.10. The topology of the system is shown in Figure 2.10. Simple calculations predicted the trimer coiled-coil stability to be **39** > **41** > **40** > **39a** > **41a** > **40a**. This matched the experimental results, based on the reaction profile of a dynamic system (Figure 2.10), which show that **39** (and to a lesser extent **41**) display pronounced growth at the expense of the competitors. It was, however, shown that the preference of replicators can be modified by external stimuli. First, inorganic anions could mask the protonated lysine side chains of **40**, which would otherwise destabilize the coiled-coil due to charge repulsion. Thus, addition of an excess of $NaClO_4$ renders **40** the kinetically favoured product. Nevertheless, in the later stages of replication it is overtaken by **39** and **41,** which form intrinsically more stable coiled-coils (Figure 2.10). Second, the addition of another coiled-coil forming peptide **42** renders the formation of **41** favoured by external templation (Figure 2.10). This example shows that careful design of the building block structure can produce a system of competing replicators, which can further be tuned by modifying the chemical and/or physicochemical conditions of replication.

2.2.5 Interlocked Structures from DCLs

Templates, which themselves are part of a DCL, in addition to self-replicating networks can give rise to interlocked structures, such as catenanes, rotaxanes and knots, which are often impossible to access via non-templated synthesis (although externally templated synthesis of interlocked structures is also reported[155]). This approach is based on the reversibility of the dynamic covalent bonds used, and thus the error-correcting propensity of the system, which renders it capable of furnishing non-trivial structures, provided these correspond to a thermodynamic minimum. Notably, mechanically

Figure 2.10 A DCL of competing peptide self-replicators based on coiled-coil formation. (a) Peptide sequence of the building blocks and the replicators.

(b) The topology of replication. Electrophilic (**35–37**) and nucleophilic (**38** and **38a**) building blocks react to form peptides **39–41** and **39a–41a**. These can form homo-or heteromeric coiled-coil trimers, which themselves serve as template for the monomer formation from the building blocks. The kinetic profiles of replicator concentrations of systems starting from 150 μM building block concentration are shown in the presence of (c) excess RSH (d) 1 M NaClO$_4$ and (e) 45 μM **42** (which templates the formation of **41**). (*See insert for colour representation of the figure.*)
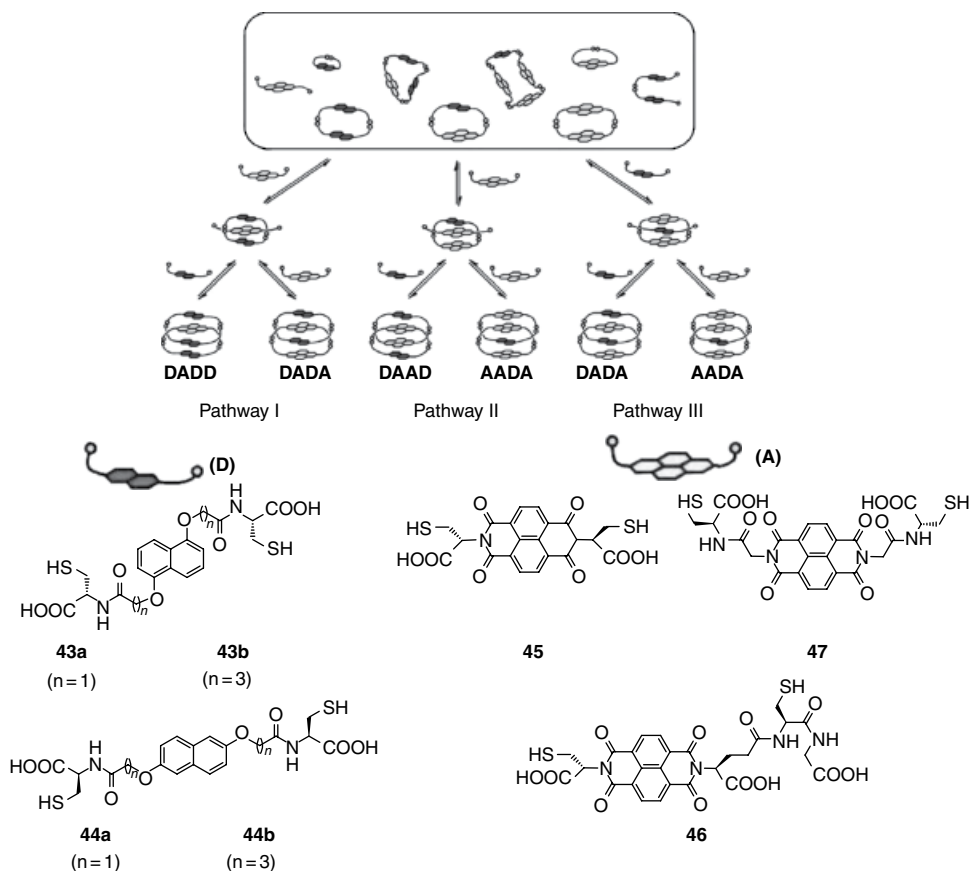
Figure 2.11 Formation pathways leading to different [2]catenane architectures. The key step is the formation of a dimeric macrocycle, templated by the threading of a monomeric dithiol, leading to a pseudorotaxane. The last, non-selective step is the formation of the catenane via the reaction of the intermediate pseudorotaxane with either a donor or an acceptor unit. The used donor (D) (**43a–44b**) and acceptor (A) (**45–47**) dithiols, with various linker sizes, are displayed at the bottom.

bound species tend to be kinetically trapped. Consequently, if several interlocked structures compete for the building blocks, slow equilibration is needed to gain the thermodynamically most favoured species at the end.

Following a report of a [2]catenane based on disulfide chemistry[232,233], Sanders et al. conducted an extensive study of disulfide libraries in water, which delivered various knotted and catenated species. Dithiol building blocks were used, which contained large, flat, hydrophobic surfaces, such as dioxynaphthalenes (DN, **43a–44b**) for the donor (D) and naphthalenediimides (NDI, **45–47**) for the acceptor (A) units (see Figure 2.11). A large number of structurally diverse [2]catenanes[234–236] and [3]catenanes[237,238] were generated, and many of them have been isolated and characterized by extensive multidimensional NMR and tandem MS investigations to reveal their unique structural features[236].

In a detailed study, the parameters ruling the selective formation of different catenane architectures was investigated[239]. Catenane formation proceeds via a general

mechanisms with three key steps: the formation of a dimeric macrocycle, the threading of a monomer unit through the cavity, and finally the ring closure. Three different pathways could be envisaged (see Figure 2.11, upper part). Pathway I is dominant if the donor building block contains a short linker between the ring and the thiol group (thus a tight cavity is formed, in which the A unit can interact with both rings), and bears the substituents in the 2,6-positions (**44a**), thus the formation of the dimeric (instead of the monomeric) disulfide is favoured. Pathway II prevails if the donor building block contains a long linker, as in **43b** and **44b** (preventing the formation of a DD macrocycle due to entropic reasons), but the acceptor contains a short one, as in **45** (so that if an AA macrocycle is formed, no threading is possible due to the tight cavity); thus, both factors render the formation of a DA macrocycle favourable. Finally, pathway III plays the main role if, as in the case of pathway II, the donor building block contains a long linker but the acceptor building block is equipped with a modestly long one, as in **47** (so that the AA macrocycle is tight enough to form a strong complex with the D unit, but the DA macrocycle is loose enough so that its formation is entropically disfavoured). In case of longer acceptor units, such as **46**, products arising from competing pathways are observed. This detailed study shows the power of DCC to gain access to diverse structures from similar building blocks under the same conditions.

Another realm of DCC which often leads to interlocked structures is metal-templated subcomponent self-assembly. Starting with the seminal paper of Stoddart[240], several knot-like[241–244] and catenated[245] species were reported utilizing this strategy. Leigh *et al.* have recently reported the self-assembly of two remarkably different metallosupramolecular knotted architectures from a simple diamine **48**, the highly similar dialdehyde building blocks **49** and **50**, and Fe^{2+} ions. Diamines and dialdehydes form a complex imine library, but, heating the mixtures at 60 °C for one day results in the formation of Solomon link **51** in the case of aldehyde **49**[243], and pentafoil knot **52** in the case of aldehyde **50**[242], despite the small structural difference between the two ligands (see Figure 2.12a). After thus creating *interlocked species from a DCL,* the authors tried to generate a *DCL from interlocked species*[244,246]. The mixture of **48−50** gave, on heating with a stoichiometric amount of $FeCl_2$, a library of pentafoil knots, as proven by NMR and ESI-MS. In sharp contrast, when reacting the two knotted species **51** and **52** with each other under the same conditions, no mixed knots were detected (Figure 2.12b), presumably due to the high kinetic barrier associated with the disruption of mechanical bonds in the assemblies.

2.2.6 Folding

Whereas building blocks containing one hydrophobic unit each can result in a library of interlocked species, as seen above, those featuring more than one hydrophobic moiety often furnish folded structures. In two recent examples[247,248], the Sanders group studied DCLs of different, cysteine-based dithiols **53** and **54** with two and three NDI units, respectively. On oxidation these building blocks furnished DCLs of cyclic and folded species. With building block **53** (Scheme 2.9a), the library provided a mixture of Solomon link **55** and figure eight knot **56**, isolated in 60 and 18% yields, respectively. Interestingly, if a mixture of DD- and LL-cysteine derived building blocks was used, the figure eight knot formed exclusively as a single diastereomer. In the second case (Scheme 2.9b), the trefoil knot **57** emerged exclusively, and could be isolated in a
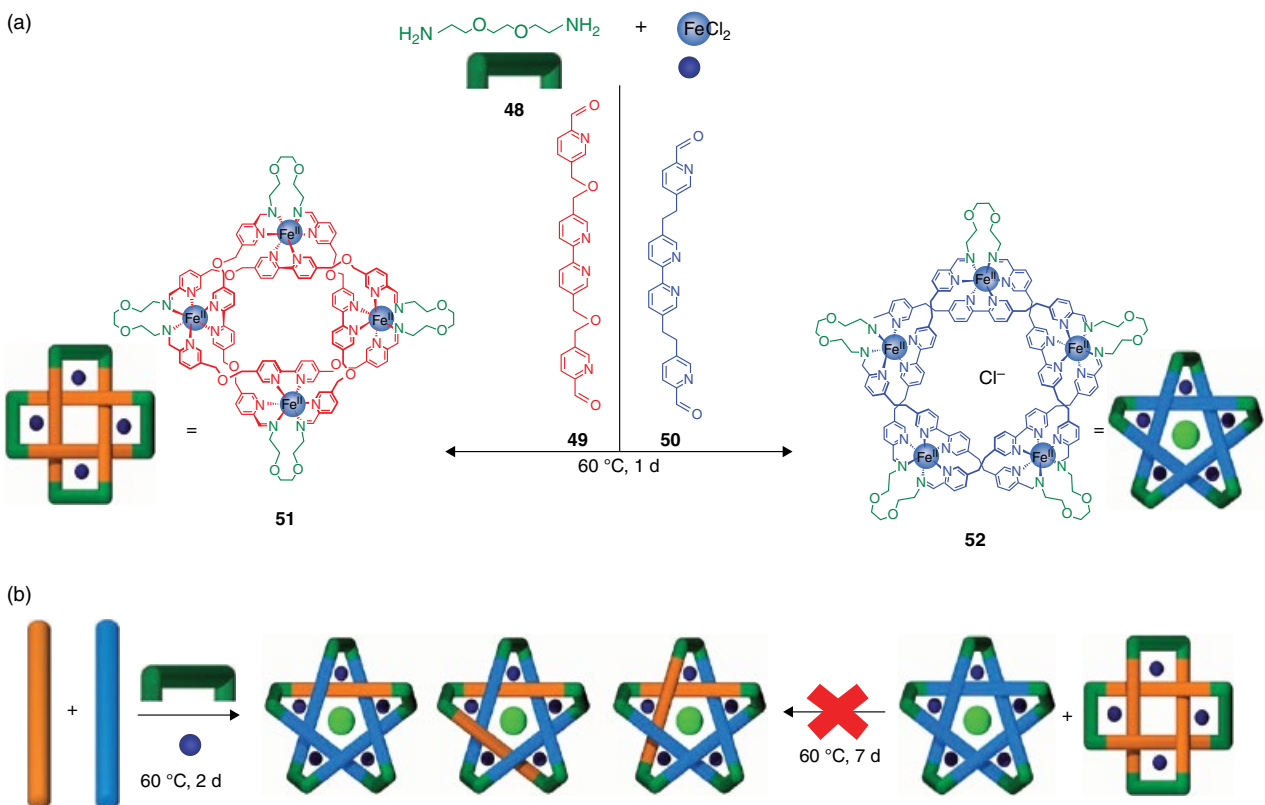
Figure 2.12 (a) The reaction of FeCl₂ and diamine **48** with dialdehyde **49** or **50** gives rise to the Solomon link **51** (left) or the pentafoil knot **52** (right), respectively. (b) Mixing the four subcomponents gives rise to a library of mixed pentafoil knots, while the two knotted species do not undergo subcomponent exchange. (*See insert for colour representation of the figure.*)

(a)

53

pH = 8 | O₂

55
(60%)

+

56
(18%)
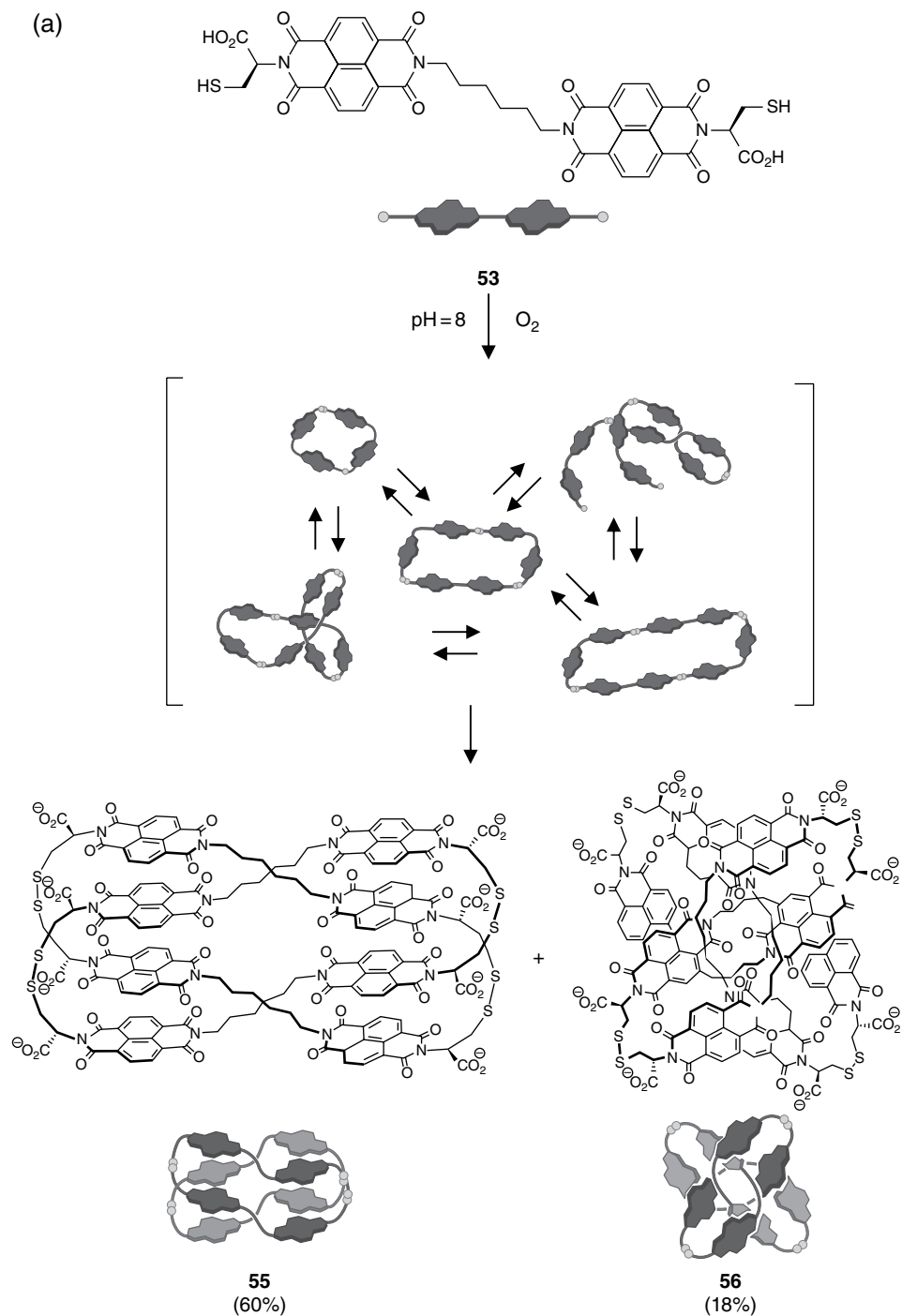
Scheme 2.9 (a) On oxidation with air in slightly basic aqueous solution, the bis-NDI dithiol **53** gives a ca. 3:1 mixture of a Solomon link **55** and a figure eight knot **56**, whereas (b) on the same conditions, the tris-NDI dithiol **54** gives a trefoil knot **57** in near quantitative isolated yield.

(b)

R = COOH

54

pH = 8 | 1M NaNO₃,O₂

57
(94%)
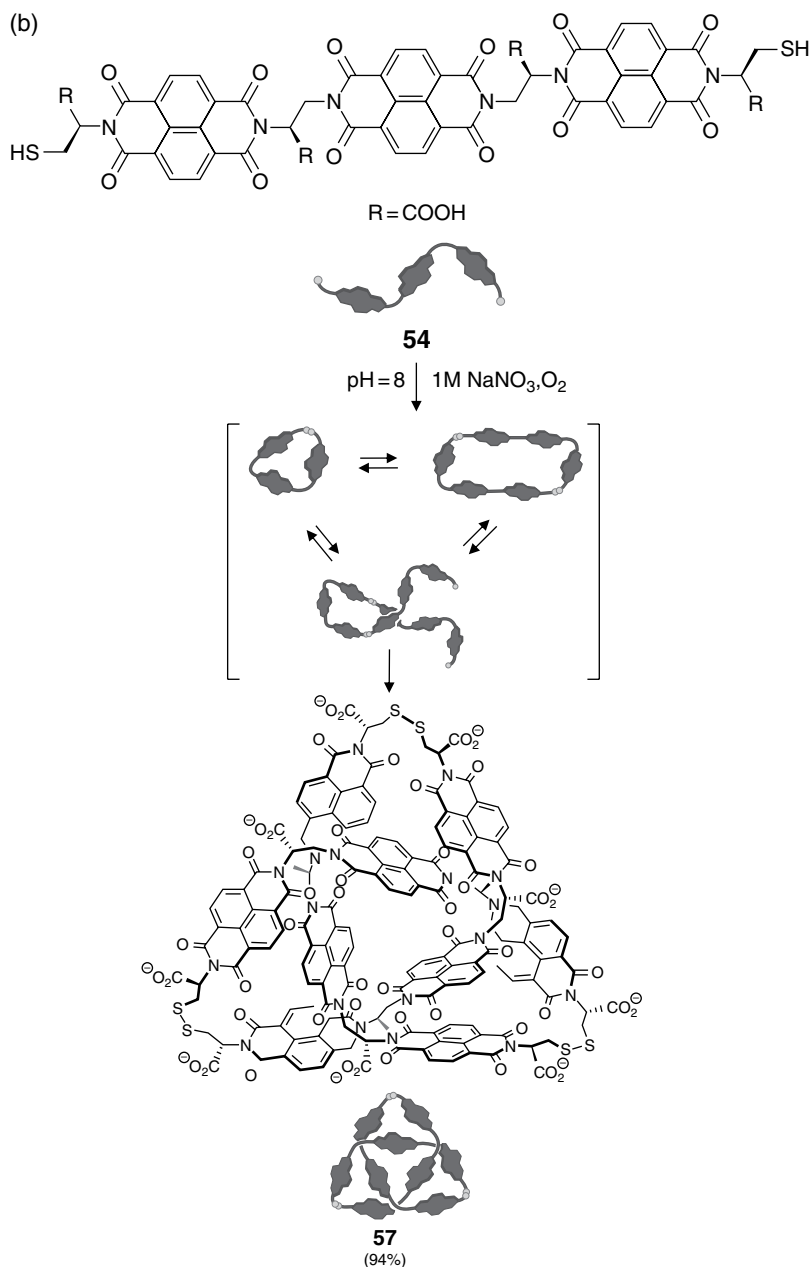
Scheme 2.9 (Continued)

remarkably high yield of 94%. Importantly, this high yield could only be achieved when a high ionic strength was maintained to enhance the hydrophobic interactions. It has to be noted that the assignment of these structures is far from trivial and requires multidimensional NMR techniques such as COSY and ROESY (to prove the spatial proximity

of the protons in different regions of the molecule), as well as tandem MS experiments (to distinguish catenated and folded/cyclid architectures) and CD spectroscopy.

Imine and hydrazone DCLs were likewise reported to provide folded structures of aromatic oligomers. Moore *et al.* performed pioneering work in this field with their studies on the folding properties of dynamic *m*-phenylene ethynylene oligomers[249]. Different small oligomeric building blocks were appended with amine and aldehyde end groups, respectively and were allowed to equilibrate under acidic conditions in polar (MeCN) and apolar (CHCl$_3$) solvents. Above a critical size of the resulting imine oligomers, their formation constants were found to increase rapidly in MeCN, while practically no change of the thermodynamic parameters was observed in CHCl$_3$. These findings are consistent with folding-induced amplification, that is, above the critical size the resulting library members can fold into helical structures, stabilizing themselves. The process is driven by the solvophobic effect, in line with the pronounced difference regarding solvent polarity: the stacking of aromatic rings is energetically much more favorable in a polar than in an apolar solvent. Later, the same principle was used to synthesize guest-selective imine foldamers[250] and large polymers[251].

In another example[252], a DCL was generated from oligo(ethyleneoxide)-based amine (**58** and **59**) and aldehyde (**60** and **61**) building blocks. Amine **59** contains an electron donor DN moiety, while aldehyde **61** has an NDI ring as the central aromatic unit. The four building blocks formed a library of dynamically exchanging polymers (dynamers). Addition of Na$^+$ ions resulted in the folding of oligoethylene units, as these wrapped around the cations in a crown ether-like fashion. The folded species were selectively stabilized in dynamer strands containing alternating **59** and **61** units (**59–61**), as in this case the electron-poor NDI and the electron-rich DN units could come into close proximity with each other, resulting in the selective amplification of this DCL member (Scheme 2.10). The example shows the multifaceted responsiveness of the system, as folding-mediated amplification is triggered by an external stimulus.

2.3 Controlling DCLs by Physical Means

Although the most widespread approaches to influence the product distribution in DCLs utilize intermolecular interactions (with template molecules or between the DCL members themselves), physical (or physicochemical) stimuli can also exert control over dynamic systems. Importantly, the line between physical and chemical effects is not always clear-cut. For example, the effect of increasing the ionic strength of dynamic systems can be attributed to specific interactions between ions and library members (chemical) or to the overall effect of the change in the dielectric constant (physical). In contrast, other physical effects can target complex systems in a highly specific manner, for example light can effectuate the capture or disruption of specific covalent or non-covalent bonds. However, the effect of physical changes on DCLs is not studied as systematically as that of various chemical templates. In this regard, several subfields are fragmentary (such as studies about the effect of electric fields on DCLs, see[253,254]) or non-existent (such as those about the effect of pressure change).
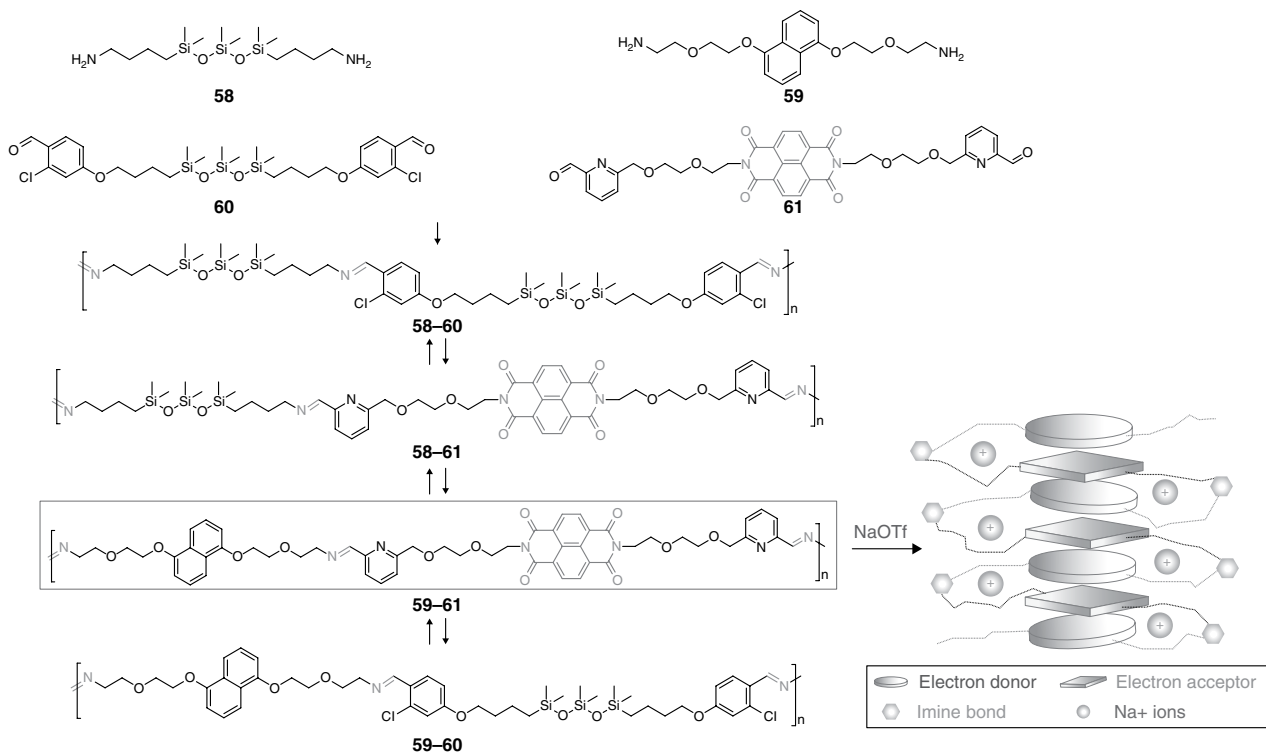
Scheme 2.10 Amines **58** and **59** react with aldehydes **60** and **61** to form a library of dynamers. (The polymer strands contain all four building blocks, but for clarity they are indicated as consisting of only one aldehyde and one hydrazone each.) The dynamers **59** and **61** can be selectively amplified upon Na$^+$-ion mediated folding, which is further reinforced by the stacking of electron-donor DN (**59**) and electron-acceptor NDI (**61**) units.

2.3.1 Solvent Environment

Most often, DCLs are prepared in solution (note that several DCLs are known to distribute between phases; see Section 2.4). Changing the solvent environment is likely to exert an influence over the behavior of these dynamic systems. Addition of co-solvents and/or salts modifies a handful of physical parameters of the medium, such as its density, viscosity, dielectric constant, etc.

On increasing the ionic strength of the environment, the most important trend is that DCL members undergo conformational and constitutional changes to minimize their solvent-accessible apolar surface. Alfonso *et al.* have recently published two papers pointing out these effects. In a DCL generated from symmetric dithiols with Glu, Gln, and Ser side chains in water/DMSO, increasing the salt concentration resulted in the amplification of the Glu-only oligomers at the expense of the mixed ones. The reason is that the repulsive interaction between the negatively charged Glu groups is shielded at high salt concentrations[255]. Extended DCLs with positively charged (Lys-containing) building blocks showed that the increase in ionic strength amplifies library members with similar charges at the expense of oppositely charged ones, due to the better electrostatic shielding effect of the former[256].

Changes in ionic strength can, however, lead to more drastic effects, for example the emergence of completely new species via induced folding, for instance the formation of already discussed catenanes[239] or knots[247]. Solvent effects were shown to play an important role in the behavior of dynamic polymers as well: in a polymer DCL generated from cucurbituril-based oligothiol building blocks[257], nanosheet- or nanosphere-like structures were formed, which could reversibly interconvert depending on the solvent polarity[258]. Similar solvent-dependent architectural changes were found in a polymeric hydrazone DCL[259].

Solvent modulation can also lead to remarkable changes in the thermodynamic or kinetic parameters of the DCLs. In a system generated by the oxidation of pentapeptide-functionalized aromatic dithiol **62** in water, several disulfide oligomers formed, among which the cyclic octamer was shown to be a replicator (see Section 2.2.4). The large macrocycle size is due to the weak secondary interactions holding together the stacked macrocycles. Addition of trifluoroethanol (TFE), a solvent known for reinforcing interpeptide hydrogen bonds by shielding them from competing water molecules, dramatically changes the replication behavior[224]. By changing the TFE content from 13% to 17%, the octamer almost vanishes and the hexamer emerges as a self-replicator (see Figure 2.13). Even more remarkably, cross-seeding experiments (i.e., addition of a small amount of replicator to a replicator-deficient DCL) show that in each environment the identity of the replicator is dictated solely by the solvent composition and not the identity of the seed.

2.3.2 Light

Modulation of DCLs by light is another means of structurally modifying DCL members and thus controling the behavior of the system. UV irradiation at specific wavelengths can lead to the isomerization around (imine, hydrazone) or the disruption of (disulfide, diselenide) dynamic covalent bonds. Noticeably, and in contrast to other physical means, with light one can selectively target one specific type of bond. On a more basic level, bonds, which are primarily static, can be rendered dynamic by UV light, and
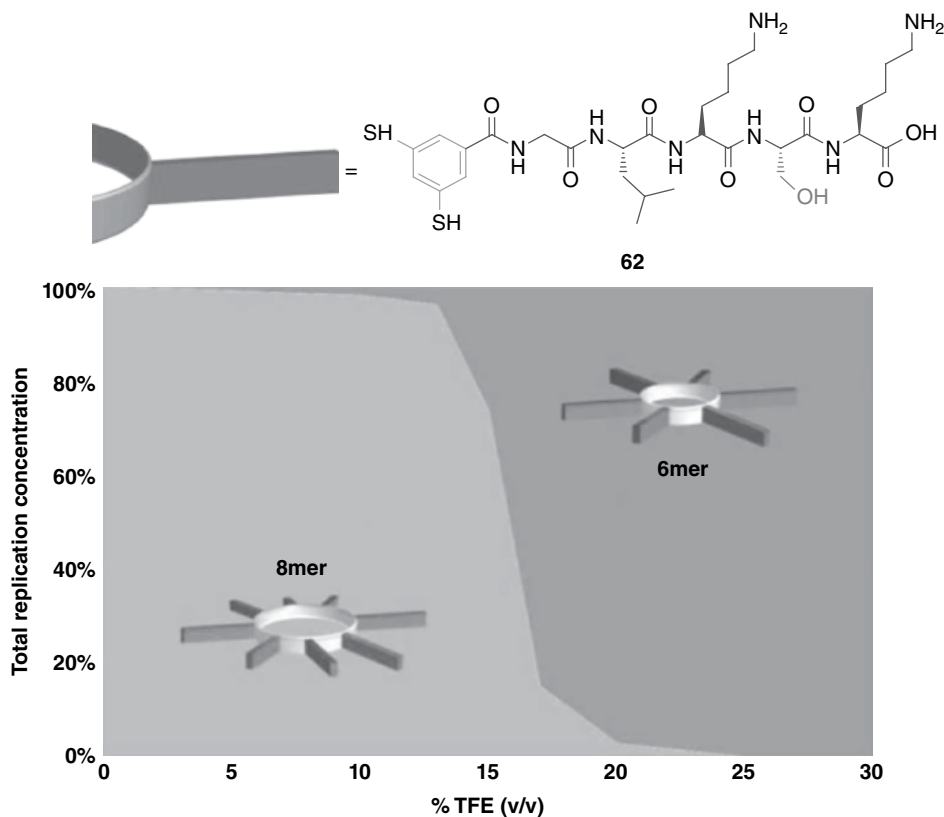
Figure 2.13 The dithiol **62** forms cyclic octameric disulfide replicators in water, but on increasing the concentration of trifluoroethanol (TFE), a sharp decrease in the amount of the octamer is observed, concomitant with the emergence of the hexameric replicator.

could thus serve as a basis for new dynamic covalent chemistries. Examples here are sulfoxide[260] or Se–Se[261] bonds (the latter can be made dynamic even with visible light via a radical mechanism).

Cis-trans isomerization of double bonds by visible light can lead to remarkable configurational changes, which, in turn, might affect the guest binding properties of a dynamic system. Thus, Waters *et al.*[262] studied a hydrazone DCL constructed from building blocks with an azobenzene moiety. At equilibrium, the library members feature exclusively *trans* N = N bonds. Irradiation with UV light at 360 nm leads to the formation of *cis* N = N bonds containing macrocycles, able to complex a polyproline guest, which did not interact with the *all-E* library members. More often, the dynamic bond itself is controlled by light. Lehn *et al.* published a series of papers[263–267] in which the selective modulation of small hydrazide and hydrazone DCLs with visible light was described. Hydrazones and hydrazides of picolinaldehyde were found to undergo reversible isomerization around the C = N bonds on irradiation with UV light at 365 nm, becoming able to bind protons and metal ions, respectively, via chelation by nitrogen atoms. Careful design of the building blocks rendered the amplification of different library members by irradiation (photoselection) or addition of transition

metals (metalloselection) possible. Based on this principle, DCLs capable of phase separation ([266], see Section 2.4 in detail) and guest release[264] were designed. Finally, in a recent example, our group[268] described the covalent capture of self-stacked macrocyclic disulfide replicator fibers by irradiating them with UV light at 365 nm. UV light caused the homolytic cleavage of intramolecular disulfide bonds, followed by the recombination of the radicals to link the macrocycles intermolecularly. This was evidenced by the formation of a strong gel from the initial aqueous solution, pointing toward materials science applications. These examples highlight that photoirradiation can effect significant changes in the architecture of DCLs, at both the molecular and the supramolecular levels.

2.3.3 Temperature

As kinetic and thermodynamic constants of chemical reactions depend on temperature, it is not surprising that complex coupled systems such as DCLs can undergo quantitative changes by varying the temperature (i.e., adjusting the kinetic energy of library members) in a subtle manner. In an early example, Giuseppone and Lehn[78] reported non-linear behaviour of component concentration as a function of temperature in a simple 2×2 imine DCL. Recently, Vantomme and Lehn[264] reported thermally induced Z–E isomerization of a dynamic hydrazone system, thereby switching its complexation ability.

However, only a few examples are reported where temperature modulation entailed qualitative changes in DCLs. For example, a library of hydrazone dynamers (dynamic polymers) was recently reported[269], which assembled in aqueous solution from carbazole-based dialdehyde, and aromatic dihydrazone building blocks, both appended with oligo(ethylene glycol) side chains, and aggregated to form fibers. Heating the solution to 65 °C increased the average molecular weight as well as the fiber length by one order of magnitude. This structural change proved to be fully reversible on cooling the solution. The seemingly counter intuitive behaviour was attributed to the side chains. These form hydrogen bonds with the solvent at room temperature, but, upon heating the entropically unfavourable hydrogen bonds are disrupted and the large hydrophobic surface of the chains becomes exposed to water. This leads to aggregation (microphase separation) of the chains, which, in turn, results in high local concentration of the shorter dynamer strands, thus facilitating chain growth.

2.3.4 Mechanical Force

Similarly to light, the impact of mechanical forces on DCLs can be regarded as a source of energy orthogonal to that provided by chemical means. Indeed, the supply of mechanical energy can assist chemical systems in overcoming kinetic barriers. For example, the disulfide replicator system[219], discussed in detail in Section 2.2.4 (Figure 2.9), gives rise to replicators of different macrocycle size, depending on the way mechanical energy is exerted onto the system: cyclic hexamers form on shaking, while heptameric replicators arise when the system is stirred. The behavior was rationalized as follows: due to the larger number of secondary interactions at the fiber ends, heptamer fibers grow faster than those composed of hexamers, but, for the same reason, heptamer fibers are more difficult to break. The shear stress exerted by stirring is approximately one order of magnitude higher than in the case of shaking. Under

stirring, heptamer and hexamer fibers fragment with comparable efficiency, so that fibers that grow most efficiently (i.e., those made from heptamers) prevail. In contrast, shaking causes more extensive fragmentation of the hexamer fibers than the stronger heptamer fibers, leading to an increased number of hexamer fiber ends, causing the hexamer fibers to grow fastest.

In a different approach, Belenguer *et al.* studied the effect of grinding on the composition of a DCL[270]. Two symmetric disulfides **63** and **64** were mixed in the presence of a catalytic amount of base, either via liquid-assisted grinding (LAG) or in solution phase (MeCN). Interestingly, the first approach provided exclusively the mixed disulfide **65**, whereas the second approach gave **63**, **64**, and **65** in a statistical 1:1:2 ratio. The two systems were interconvertible, that is, dissolving pure **65** in MeCN gave the statistical mixture, whereas evaporation of the solvent, followed by LAG converted this mixture back to **65** (see Figure 2.14). The difference is of thermodynamic origin. The homodimers are of comparable stability in solution, while in the solid phase the heterodimers are favoured due to better stabilization arising from crystal packing. The relatively high kinetic barrier between homodimers and the heterodimer in the solid phase can be effectively overcome by the mechanical energy supplied by grinding.

Further studies[271] revealed that **65** exists in the solid phase in the form of two polymorphs, one of which is stable under LAG conditions but metastable under neat grinding and *vice versa.* Detailed kinetic investigations showed that the different polymorphs of **65** can act as seeds (see Section 2.2.4) in the exchange process. However, the mode of action is different for the different polymorphs under given mechanochemical conditions: if the metastable polymorph of **65** is applied as a seed, it is first transformed to the stable one through a path that involves the transient appearance of **63** and **64**, whereas no such transformation is needed when applying the stable polymorph. This example shows that the subtle interplay between solid state energetics, the environment, and mechanochemical activation can produce dynamic combinatorial systems with markedly different compositions.

2.4 Multiphase DCLs

In Section 2.3.1 we saw how DCLs can be affected by changing the solvent or its ionic strength. Even more interesting phenomena can be observed when mass transfer between multiple phases is enabled. Regardless of the type of phases involved, multiphase libraries can be under thermodynamic or kinetic control, depending on the reversibility of the phase transfer of library members and the dynamics of the bonds used. The DCLs can also carry cargo between multiple phases or even enable control over phase separation.

2.4.1 Multiple Liquid Phases

Usually, DCLs are studied in a single liquid phase. Depending on the application and the solubility of building blocks it can be an aqueous, an organic, or a mixed medium. Unfortunately, restricting a DCL to one phase imposes significant limitations on the system, particularly in the case of low solubility of some building blocks or library members. By adding an additional, immiscible liquid phase it is possible to access library
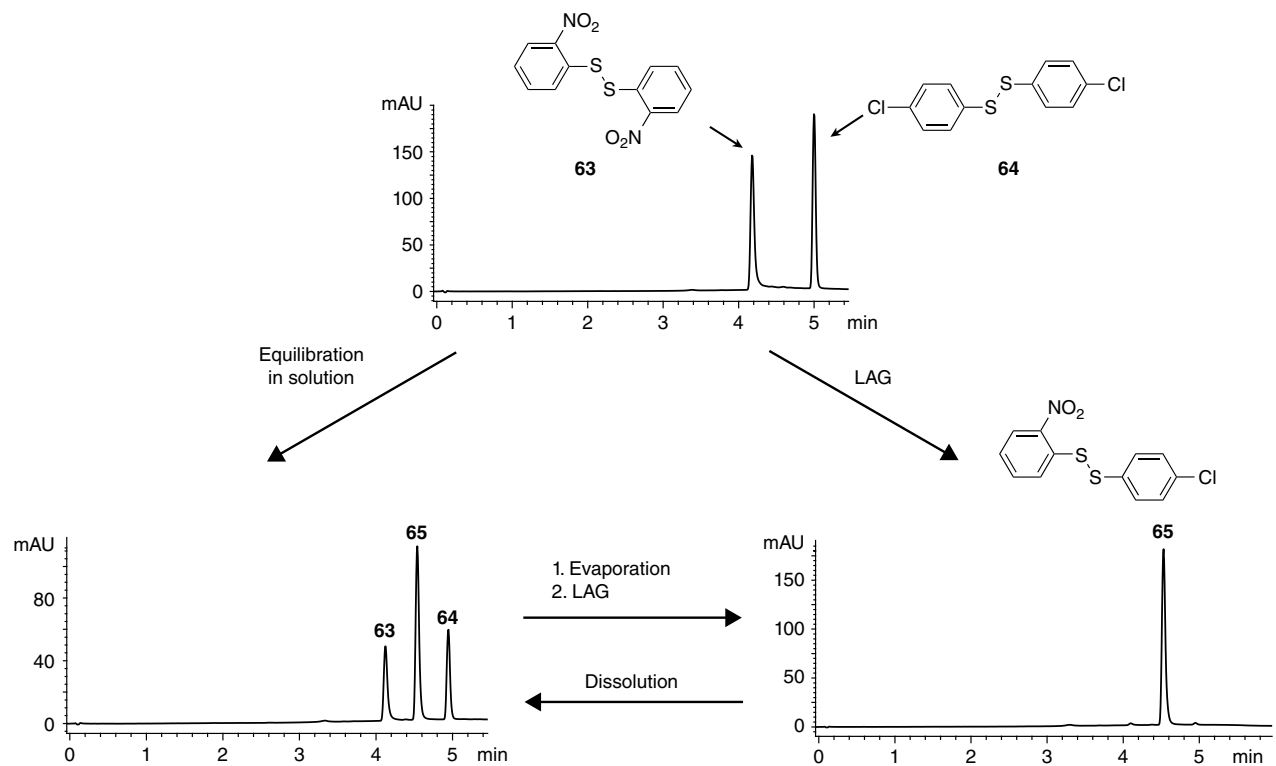
Figure 2.14 Chromatograms of DCLs formed by mixing disulfides **63** and **64** in MeCN solution (left) and on liquid-assisted grinding (LAG) (right).

members composed of building blocks with different solubility characteristics, significantly increasing the diversity of the libraries. The first example was shown by Sanders *et al.,* who performed a DCL experiment using water-soluble and chloroform-soluble thiols[272]. The biphasic system, initially containing the building blocks only in their preferred phases, gave large amounts of mixed disulfides impossible to prepare in a single-phase DCL. More recently, Rotello *et al.* used a similar approach to create self-assembled antimicrobial capsules[273]. A biphasic system contained amine functionalized silica nanoparticles in the aqueous phase and cinnamaldehyde in the peppermint oil phase. After emulsification, cinnamaldehyde reacted with the amine groups on one side of the nanoparticles, while the other remained hydrophilic. The resulting Pickering emulsion contained peppermint oil inside capsules composed of amphiphilic Janus nanoparticles. Such capsules were then successfully used to eradicate biofilms on release of their payload.

In Section 2.3.1 we saw that changing solvent properties significantly affects the composition of libraries. Lehn's group combined this characteristic with reversible phase separation to achieve another possibility of controling DCLs[274]. A mixture of lipophilic and hydrophilic aldehydes and amines was dissolved in an acetonitrile/water medium. By changing the conditions (e.g., by cooling, adding salts, diethyl ether), an initially homogenous mixture could be rendered biphasic. Importantly, subsequent phase recombination was also possible by heating, fractional evaporation, or addition of LiClO$_4$. When the system was homogenous the library had roughly statistical composition, whereas on phase separation the library underwent self-sorting: the acetonitrile phase contained mostly lipophilic imines while the hydrophilic imines dominated the aqueous phase. The same group subsequently combined this system with another dynamic process: *E–Z* photoisomerization of a hydrazone switch, leading to photo-induced phase separation (Figure 2.15)[266]. The hydrazone **66-*E*** strongly binds Ca^{2+} but on photoisomerization to **66-*Z*** most calcium cations are released into the solution, causing phase separation. The reverse reaction is possible by decreasing the pH of the solution. An alternative is provided by the use of analogous acylhydrazones, which can convert to the *E* isomer thermally within 48 hours at 40 °C, thus leading to a spontaneous phase reunification.

2.4.2 Transport

A DCL screened in a multiphase system can reveal not only strong binders but also their ability to transport cargo from one phase into/across another. Building on their research on phase-transfer libraries[272], Sanders used a library of disulfides to discover an unexpected spermine transporter[57]. The DCL was formed from one dithiol **67** and two monothiols **68** and **69** in a water-chloroform system (Figure 2.16). Usually, such libraries generate a mixture of macrocycles and linear dimers to maximize their entropy. In this case, addition of spermine to the aqueous phase led to a two-fold amplification of an entropically disfavoured linear trimer in the organic phase. This trimer formed a 2:1 complex with the template, efficiently transporting it between two aqueous phases through the organic phase. A conceptually similar system was independently discovered by Saggiomo and Lüning, where CaCl$_2$ was capable of amplifying its own receptor in a DCL of imines[58]. The macrocyclic host was able to transport the salt from the aqueous source phase to the receiver phase through a bulk dichloromethane membrane.
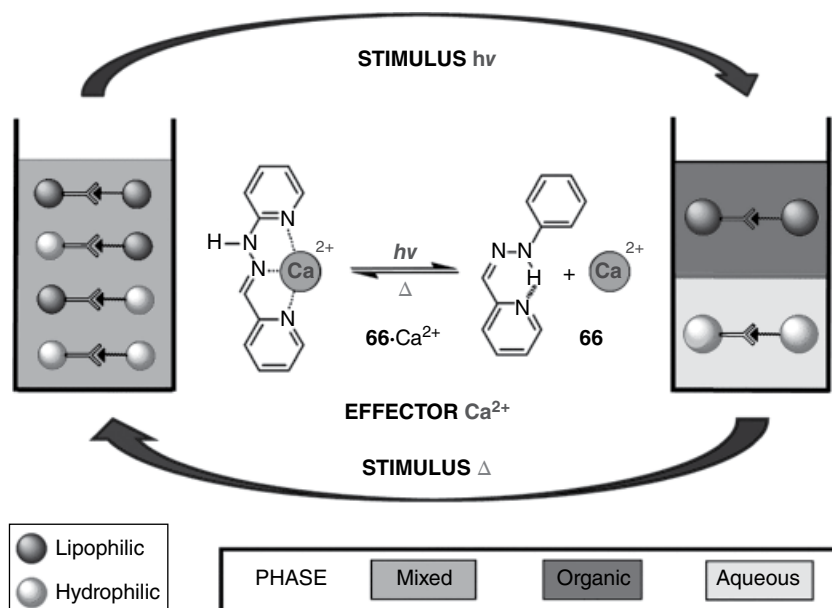
Figure 2.15 A DCL of imines formed from a mixture of lipophilic (dark gray spheres) and hydrophilic (light gray spheres) aldehydes and amines. The system contains a photoswitchable Ca^{2+} receptor **66**, allowing for a photochemically induced phase splitting. The DCL gives roughly a statistical mixture in a homogenous solution and undergoes self-sorting on photochemical dehomogenization.

Subsequently, the Lüning group investigated the system's ion transport capabilities using a supported liquid membrane and liposomes[275].

An extensive body of research on transport through lipid bilayers and cellular uptake using DCC was reported by Matile and colleagues. Dynamic hydrazone-based amphililes were able to bind to nucleic acids using their positively charged heads, while the lipophilic tails facilitated passage of the DNA-amphiphile complex through a lipid membrane[276,277]. The dynamic nature of the amphiphiles allowed them to screen hundreds of of different amphiphiles with different heads, tails, and varying stoichiometries. Finally, the work led to the discovery of siRNA transfection agents[278]. Hydrazone-mediated siRNA delivery resulted in gene knockdown in HeLa cells and human primary fibroblasts, exceeding the efficiency of the commercial Lipofectamine reagent by a factor of two, emphasizing the value of dynamic libraries for screening for function.

A dynamic covalent bond can also be formed between the cargo and the transporter to form a permeable molecule. Gale *et al.* used hemiaminal/imine chemistry between amino acids and electron-poor aldehydes together with a squaramide anion receptor to synergistically transport amino acids through lipid membranes[279].

Multiple systems for cellular delivery have been generated using disulfide exchange/polymerization. Positively charged strained cyclic disulfides can polymerize into cell-permeable poly(disulfide)s when exposed to thiol initiators[280]. Five-membered disulfides are preferred substrates for polymerization due to conformational strain, facilitating ring opening[281]. Reductive depolymerization of such disulfides after their uptake renders them less toxic in comparison to their nondynamic analogues[282].

For a more detailed overview of dynamic covalent systems in cellular uptake see the recent review by Matile *et al.*[283].
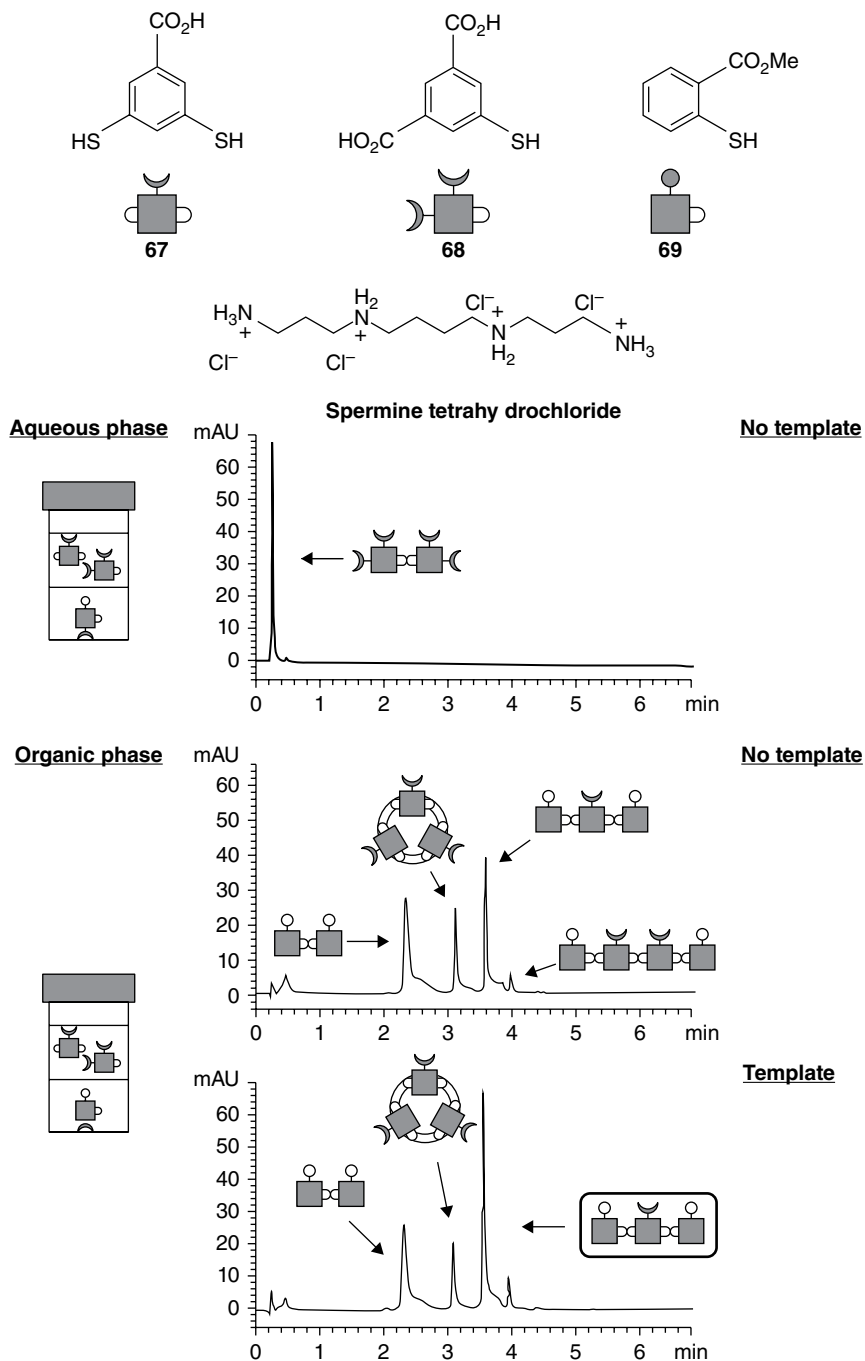
Figure 2.16 A DCL of disulfides formed by oxidation of thiols **67–69** allows for the formation of library members comprising water-soluble **67** and chloroform-soluble **69**. Addition of spermine amplifies the mixed linear species **69, 67** and **69,** which can transport spermine into and through the organic phase.

2.4.3 Amphiphiles

Apart from being distributed over two or more phases, members of DCLs can create mesophases on their own. This is especially true if the library can form amphiphilic species, which then can assemble into, for example, micelles or vesicles. Pioneering work in the area has been performed by the groups of Giuseppone[220,284–286], van Esch[226,287,288], and Zhang[289–292]. In most cases, the amphiphiles are imines formed from amines and functionalized benzaldehydes, where one of the components constitutes the hydrophilic part and the other is hydrophobic (for a review discussing "supra-amphiphiles", formed by supramolecular self-assembly, see[293]). As imines are generally unstable in aqueous solutions, formation of the amphiphiles is highly cooperative due to stabilization of the imine bond within the hydrophobic mesophase of the aggregate[226]. Such stabilization drives imines out of the solution into the aggregates, which subsequently may split, closing the self-replication cycle (see also Section 2.2.4)[220]. Because amines are involved in acid-base equilibria, the mesophases are generally unstable under acidic conditions. This property can be used to reversibly switch between assembled imines in basic pH and dissociated aldehydes and amines in acidic pH[226]. Differences in the *pKa* of amines in a DCL can be used to change the composition of the assemblies[284,285] or even trigger a core-shell inversion of the resulting micelles[286] (Figure 2.17). Cooperative effects stemming from stabilization of imines by their neighbors in the mesophase can shift the pH where the aggregates start forming well below the *pKa* of the amines. This is especially pronounced for polymeric amines, which on reaction with hydrophobic aldehydes form toothbrush-type amphiphiles, aggregating at Ph = 7.4, well below the *pKa* of the parent polylysine (around 9.0)[289].

The shape, flexibility, and size of the building blocks involved are important parameters influencing the critical micelle concentration (CMC) of the imines[226,291,292]. These factors can also influence the morphology of the resulting mesophases. Apart from the most common spherical micelles, it is also possible to obtain rod-like micelles[288]
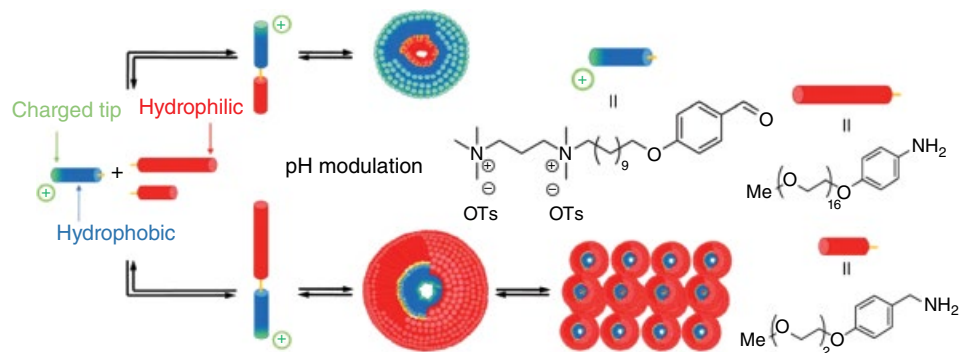
Figure 2.17 A DCL of charged hydrophobic aldehydes and hydrophilic amines can be controlled with pH. At high pH, imines with short hydrophilic tails are formed, assembling into spherical aggregates. Upon increase of pH, imines with long hydrophilic tails are selected, changing the shape of the amphiphiles and causing core-shell inversion of the micelles. The inverted micelles may, depending on their surface interactions, aggregate into larger mesophases. (*See insert for colour representation of the figure.*)

and even vesicles[287]. Using an extensive array of scattering techniques (see also Section 2.7.6), Giuseppone, Buhler, and colleagues characterized a complex dynamic library switching between all three types of mesophases on pH modulation[285].

2.4.4 Surface-liquid Interfaces

The adaptive character of DCLs can be utilized not only for the formation of well-defined species in solution but also to bring new, responsive properties to various kinds of surfaces, affecting interactions with the surrounding solvent and other solutes. In simpler cases, a solid phase can be coupled to a solution-based DCL to simplify analysis and purification of library members and mitigate solubility issues.

2.4.4.1 Resins

The latter principle was applied by Miller *et al.* as a solution to the analytical problems experienced in large libraries[294]. By attaching one building block per library to indexed beads and using a fluorescently tagged template, they were able to significantly simplify the screening process. Their subsequent studies on resin-based DCLs expanded to 11,325 potential components resulted in the discovery of sequence-selective RNA binders for targeting myotonic dystrophy[208] and HIV[207] (see also Section 2.2.2). The group also applied resin-bound bifunctional building blocks for studies on orthogonally addressable disulfide and hydrazone chemistries[295]. The opposite approach was investigated by our group to study the behavior of a DCL in which the target was bound to the solid support[233]. Attachment of the template to the resin prevented aggregation of the library members, thereby allowing the binding constant between the host and a resin-bound guest to be estimated. Subsequent studies showed that a proper choice of the resin results in negligible interference with the solution-based recognition phenomena, allowing for a one-pot amplification and isolation of receptors from large DCLs[296]. Similarly, Prins *et al.* found that hydrazide capture by an aldehyde-functionalized resin with a neighboring phosphonate target shows similar preferences to the selection process in solution[297].

2.4.4.2 Nanoparticles

Thermodynamically controlled functionalization of the surfaces of nanoparticles was first studied by Rotello *et al.*[298] by taking advantage of the mobility of thiolate ligands stabilizing gold nanoparticles (AuNP), first discovered by the Murray group[299]. By exposing chloroform-soluble mixed-monolayer nanoparticles containing thiolate ligands with two different recognition sites to a target molecule, the monolayer reorganized to yield a ditopic receptor for the flavin template. Subsequent work using similar methodology focused on a tetra-aspartate peptide as a template for water-soluble AuNPs containing alkyl and ammonium ligands[300]. Addition of the nanoparticles to the peptide led to a gradual increase in the helicity of the peptide, indicating a slow rearrangement of the ammonium ligands for optimal binding with the negatively charged peptide. Bishop *et al.* used ligand exchange to create Janus-like amphiphilic nanoparticles[301]. Initially, AuNPs functionalized with either hydrophobic or hydrophilic ligands were present in one of the phases of a toluene-water system. Addition of the other ligand led to partial exchange yielding nanoparticles focused at the phase interface. Two subsequent studies from the same group showed that AuNPs stabilized

by a mixture of hydrophobic and negatively charged thiolates can be templated by lipid bilayers[302,303] or by other nanoparticles followed by their self-assembly[304]. Interesting developments in ligand exchange involve ligand exchange activated by photoswitchable[305] and photocaged[306] thiols.

An alternative strategy, which has recently been reported by our group[60,307] and that of Kay[61], is based on bond formation and exchange within the ligand on the nanoparticles instead of exchanging the entire ligand. We used water-soluble mixed-monolayer AuNPs with cationic (**70**) and aldehyde (**71**) ligands for target-directed surface functionalization (Figure 2.18)[60]. In the presence of a DNA template, cooperative effects stabilized the imines on the nanoparticles only if the amine building blocks had affinity to DNA. Because of the inherent instability of imines in water, functionalization occurred only in the vicinity of the template, leaving its molecular imprint on the nanoparticle surface. Studies with different DNA templates revealed that even in simple libraries, imine selection depended not only on the DNA composition, but also on its sequence. Conversely, hydrazone-functionalized nanoparticles remained stable even in the absence of the DNA template[307]. Della Sala and Kay, while examining hydrazone exchange on AuNPs, found that it was possible to tune the solvophilicity of the nanoparticles by their treatment with different aldehydes[61]. DCC on gold nanoparticles was also investigated using ionic binding to positively charged AuNPs and complexation with Hg^{2+} and Au^{+}[308].

It is also possible to perform DCC directly on the vesicular bilayer interface. In our laboratory we used thioester exchange with thioesters anchored to the phosphatidylcholine bilayer and a water-soluble thiol[309]. Interestingly, the DCLs showed a pronounced preference for linear species, defying the entropic effect favoring macrocyclic species in bulk solution. Disulfide exchange confined to cell surfaces was studied the Matile group[281] in the context of cellular uptake.

2.4.4.3 Flat Surfaces

Analysis of DCLs on flat surfaces requires dramatically different techniques than for libraries in bulk solution. As the reactions are confined to the substrate–solution interface, NMR or chromatographic techniques are impossible or, in the best case scenario, difficult to use. On the other hand, techniques usually not applicable to systems in solution can successfully provide crucial information on surface-confined DCLs. The most widely used methods include scanning probe (AFM, STM, etc.; see Section 2.7.5), optical, and electron microscopies, XPS, contact angle, and electrochemical measurements. It is therefore not surprising that it has taken more than a decade for DCC to expand to flat surfaces. The first work in the field focused on reversible imine formation on aldehyde-terminated gold substrates[62]. Imine patterns were formed by microcontact printing and erased with acidic hydrolysis. A subsequent study showed that multivalent amine-terminated dendrimers responded with directional movement along the gradient to maximize the number of imine bonds[310].

DCvC can not only use existing concentration gradients on surfaces but also create new ones in a combinatorial fashion. Giuseppone *et al.* investigated the influence of immersion of aldehyde-terminated surfaces into solutions of variable pH to control attachment of amines with different *pKa* values[311]. This method proved to be very general for making gradients of multiple dyes, molecules of different hydrophobicity, or even proteins.
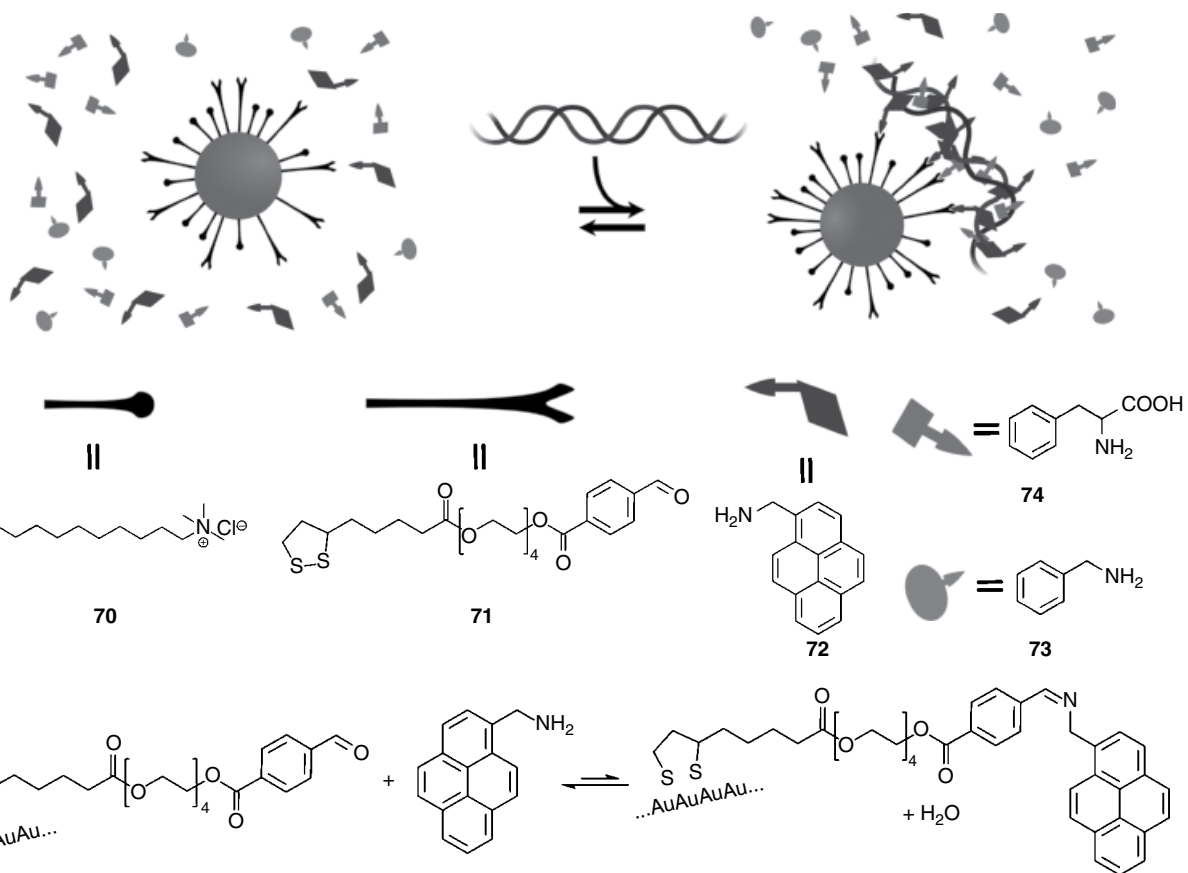
Figure 2.18 The dynamically functionalizable nanoparticles were covered with ligand **70** for water solubility and ligand **71** for imine formation with amines **72–74**. The nanoparticles can be functionalized only in the presence of a DNA template which stabilizes weak imine bonds. Amine **73**, which does not interact strongly with the template, does not participate in surface functionalization.

To create gradients not parallel but perpendicular to a solid substrate, Matile *et al.* developed self-organizing surface-initiated polymerization (SOSIP)[312]. First, an initiator is deposited onto the substrate (e.g., indium-tin oxide, ITO), followed by activation to generate thiols. The surface-confined thiols initiate polymerization of disulfides (ideally derivatives of asparagusic acid[313]). Crucial for the success of the technique was significantly lower critical propagation concentration on the surface than in the solution, likely due to the efficient templating capabilities of the surface-preorganized stacks. The technique allows gradients of NDI derivatives to be created with a perpendicular orientation with respect to the surface for transporting electrons and holes in opposite directions in photovoltaic devices. Subsequent research focused on surface-templated polymerization of multiple different monomers[314] and templated stack exchange (using orthogonal hydrazone exchange) within already polymerized systems[315,316]. Recently, the group has added the third independent dynamic covalent bond to the system : the boronic ester (Figure 2.19)[317,318]. Remarkably, the chemistries do not interfere with each other: first, disulfides are polymerized under basic conditions, the second stack is coaligned using acid-catalyzed hydrazone exchange, whereas the final incorporation of catechols and diols occurs under neutral conditions. With this approach it was possible to incorporate various natural pigments (e.g., riboflavin) to boost the generated photocurrents.

Apart from making dynamic covalent bonds with the substrate, DCLs can equilibrate in a surrounding solution, prior to physisorption to the surface. This approach has been validated by the groups of Samorì and Lehn, who discovered that selection in a library of imines is driven by the decrease in enthalpy from the interaction with the substrate coupled with entropic loss on adsorption, paving the way to a new scheme for controlling the equilibria in DCLs[319].

A solid surface can confine a DCL to its direct vicinity if the dynamic covalent reaction requires a catalyst to operate and the catalyst is attached to the surface. The van Esch group used this approach to trigger gelation only where the acid catalyst had been patterned using microcontact printing[320]. The trihydrazone hydrogelator (reported previously by the same group[321]) is formed from soluble aldehydes and trihydrazides only next to the catalyst, thereby ensuring uniform growth of the fibers from the surface, as depicted in Figure 2.20.

2.4.5 Kinetically Controlled Phase Transfer

Most of the multiphase DCLs described above are governed by the relative thermodynamic stabilities of the library members in different phases, aggregation states, etc. As we show in this section, interesting and useful behavior can be extracted from DCLs if dynamic equilibria can be coupled with an irreversible removal of one of the components[23] to another phase. Usually, phenomena such as crystallization/precipitation or evaporation of some library members are considered problematic because they perturb the equilibria according to the Le Chatelier–Brown principle. Such events can, however, become a blessing in disguise, leading to self-sorting of the library members, increasing yields and simplifying purifications. The first example came from Lehn *et al.* and involved an equilibrating mixture of double-helical, triangular, and grid complexes[322]. Out of these three structures, the helicate was stabilized in the solid state, driving the library to form only that component on crystallization. The same principle was used by
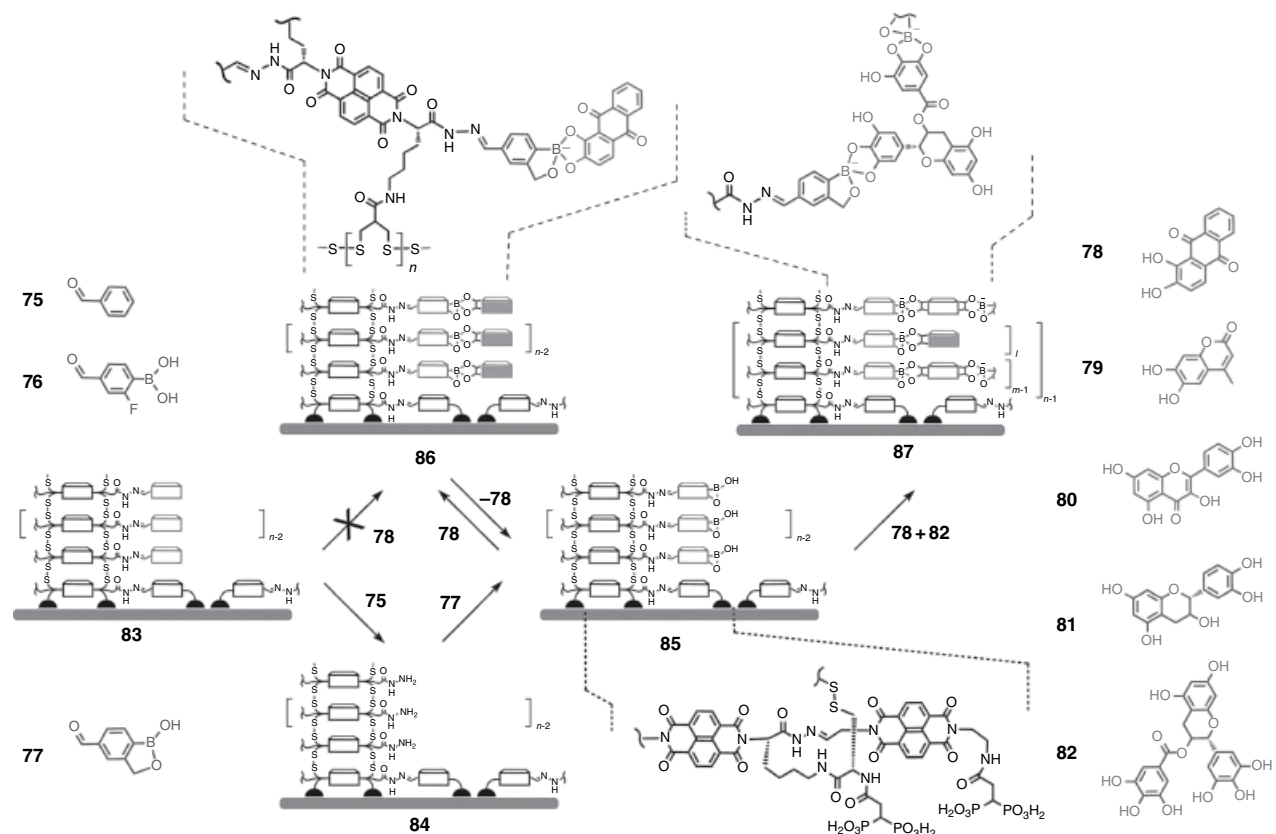
Figure 2.19 Triply-dynamic orthogonal surface functionalization. First, disulfide polymerization creates stacks perpendicular to the surface (**83**). Hydrazone exchange can proceed without disturbing the disulfides to replace aldehyde **75** with bifunctional building block **77**. Resulting stacks **85** can be then functionalized with catechols **78–82** to yield well-defined indium tin oxide-bound architectures **86** and **87**.
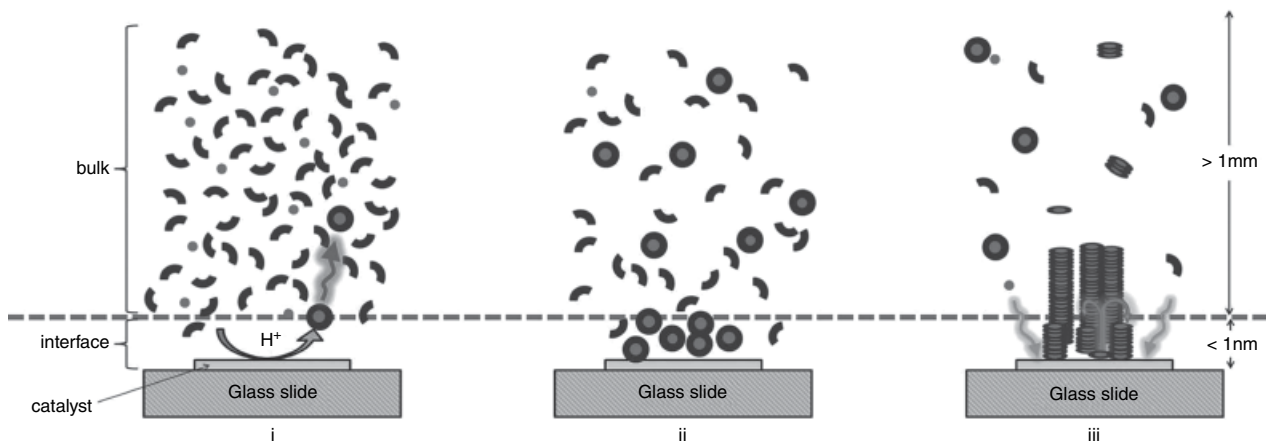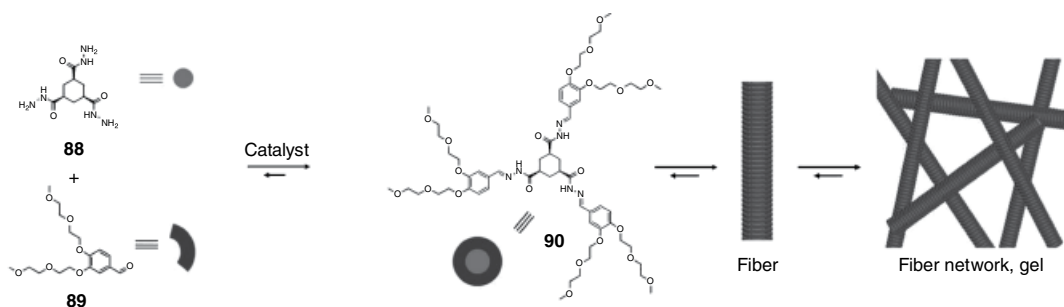
Figure 2.20 A catalyst patterned on a glass slide catalyzes the formation of trihydrazone **90** from trihydrazide **88** and monoaldehyde **89**. The resulting hydrogelator fibers are oriented perpendicular to the surface and exhibit uniform growth due to a higher proton concentration next close to the surface.
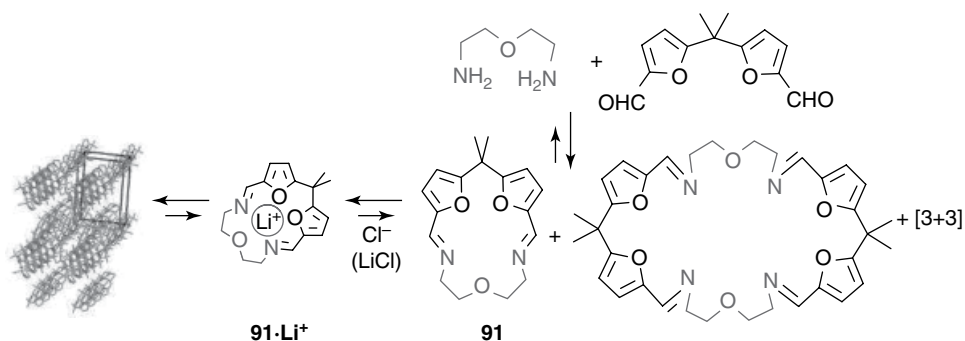
Scheme 2.11 An imine DCL comprising macrocycles of various sizes. Imine **91**, after binding Li^{+}, crystallizes in a chiral space group, driving the equilibrium toward the formation of solid **91** LiCl. Most experiments show spontaneous formation of enantiomeric excess in the solid sample.

Nitschke and colleagues, who showed that a dynamic library of helicates generated from three subcomponents (racemic amine, achiral dialdehyde, and Cu(I)) formed a mixture of all six diastereoisomers in solution, which, on crystallization, self-sorted to yield a single pair of enantiomers[323]. Subsequent research generalized the concept of crystallization-driven DCC to imine exchange in rotaxane formation[246], nitroaldol reaction[324–326], boronic ester formation and exchange[327–329], and other metal-coordination systems[330–333].

Mirror symmetry breaking in crystallization-driven DCLs was recently discovered by Ziach and Jurczak[334,335]. A library of macrocyclic imines in acetonitrile slowly extracted Li^{+} from its solid chloride salt, leading to precipitation of the Li^{+} complex of macrocycle **91** (Scheme 2.11). The Li[+]-**91** crystallized in a chiral space group. Surprisingly, the resulting samples (as evidenced by circular dichroism measurement of the crystals) were deracemized in most experiments. These results bear resemblance to autocatalytic chiral symmetry breaking on crystallization of $NaClO_3$[336] and attrition-induced deracemization of crystals[337,338]. In this case, however, the symmetry breaking was unaffected by agitation of the library.

In a series of papers Miljanic *et al.* took advantage of self-sorting in complex DCLs to obtain multiple library members with high purity by removing them in succession, making the most of their physicochemical differences. This concept has been proven first by distilling five imines one by one from a library of 25 components[56]. Removal of vapors above the library shifts the equilibrium in favor of the most volatile component. After its removal the next lowest boiling library member in the remaining mixture may be distilled in a similar manner. The methodology was later extended to distillation dynamic ester libraries[339] and succesive precipitation of imines based on their solubility.

More recently Hsu and Miljanic applied their technique to adsorption-driven self-sorting on silica gel under flow conditions[340]. They created a library of 16 different members using four aldehydes and four amines of different polarities. As the mixture is applied on a silica gel column and the eluent flow is started, the least polar imine is eluted first, causing re-equilibration of the remaining mixture (Scheme 2.12). After depleting the library from the constituent building blocks, the eluotropic strength is increased, causing elution of the least polar imine possible to form in the remaining DCL and so forth.
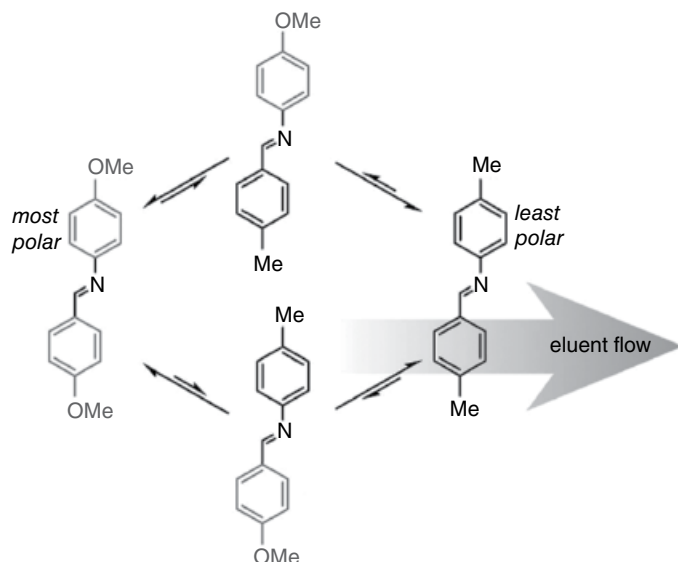
Scheme 2.12 Equilibrium between more and less polar imines adsorbed to silica gel can be influenced by applying eluent flow. Weakly bound non-polar imines will be eluted, whereas the more polar will remain stationary, allowing the library to self-sort.

Slow equilibration of DCLs on evaporation of library members was used by Lehn and Herrmann to control the release of bioactive volatiles such as odorants. They discovered that hydrazones can be turned into profragrances, slowly producing aldehyde and ketone-based scents[341–343] (see Section 2.7.1 for details on headspace analysis). These are especially useful if the odorants are volatile on their own. The rate of fragrance release depends not only on their vapor pressure, but also on the rate of hydrolysis of respective acylhydrazones, which can be controlled by pH. Additionally, hydrazides can be equipped with groups promoting adhesion to fabrics, without affecting the released scents. If protofragrances can reequilibrate while releasing odorants, they can be used to set up a time-dependent scent spectrum. Aminal scent libraries equilibrate fast and therefore are much more suitable for that purpose than acylhydrazone libraries[344]. External control of scent release is possible if some of the dynamic profragrances can be entrapped within a liquid crystalline film[254]. When an electric field is applied to such mixture, imines which cannot form the liquid crystal are expelled, affecting the library equilibrium and therefore releasing the volatile carbonyl compounds.

2.5 Other Applications of DCLs

2.5.1 Information Acquisition and Processing

The responsive nature of DCLs renders them useful in recognizing, transferring, processing, and signaling chemical and physical signals; the abilities termed jointly by Jean-Marie Lehn as *semiochemistry*[345]. Apart from the more traditional approach of modifying receptors amplified in DCLs with reporting units (e.g., dyes), it is also

possible to use the whole DCL as a sensor, utilizing changes in multiple coupled equilibria induced by the analyte[50]. Such an approach was used, for example, to sense Zn^{2+} in libraries of dynamic imine polymers[346,347] and, using linear discriminant analysis, to sense and identify di- and tripeptides in DCLs of dye complexes with Cu^{2+} and Ni^{2+}[348,349]. A dynamic combinatorial sensor based on non-covalent self-assembly of two amphiphilic dyes into micelles was successful for sensing aminoglycosides[350]. In all these cases, sensing DCLs were prepared from multiple components and analyzed by UV-Vis absorption or fluorescence. A creative alternative was provided by Bode *et al.,* who used ^{13}C-labelled bullvalenes substituted with recognition units (see Figure 2.21)[154,351]. The bullvalene core undergoes a rapid Cope rearrangement, which changes the positions of the carbon atoms within the bullvalene, generating a DCL of shapeshifting receptors. The equilibrium population with a characteristic ^{13}C NMR signal can be therefore affected by the addition of an analyte which changes the equilibrium distribution of bullvalene isomers and the resulting spectrum. This allowed for a single -experiment NMR identification of fullerenes with porphyrin-based recognition groups[351] and polyols with boronic acids[154]. In the latter case, each polyol gave a characteristic spectrum, which was then simplified by binning and transformed into a one-dimensional barcode for each analyte.

Multicomponent sensing ensembles, while not necessarily being DCLs on their own, can become such on addition of analytes which exist in equilibrium with their receptor complexes. This tactic has been thoroughly studied by Anslyn *et al.* who used boronate ester exchange coupled with indicator displacement for sensing diols[352], hemiaminal formation and Zn(II) complexation for sensing chirality of alcohols[353,354], and imine formation followed by formation of octahedral Fe(II) complexes for *ee* determination of chiral amines[355]. An even more sophisticated approach was employed by Matile for identification of hydrophobic aldehyde and ketone analytes using cationic hydrazides and DNA polyanions[356]. As the reaction between the analytes and hydrazides led to the formation of vesicle-penetrating complexes with DNA, those complexes were able to pass lipid bilayers (Figure 2.22). After entering into the vesicles, they were able release dyes and their quenchers into the bulk medium, leading to a fluorescent response. By combining experiments from a sensing array comprising different hydrazides, principal component analysis (PCA) could distinguish between different analytes. Therefore, the system became an elegant chemical sensor, capable of identifying odorants in commercial perfumes.

DCLs can not only identify analytes but also uncover information on binding between molecules, their bioactivity, and structures of the targets, providing useful information in the early stages of drug discovery[22,26,27] (see also Section 2.2.2). Useful information on multivalent binding can also be provided by fragment-based drug discovery and DNA-encoded chemical libraries (DECL). Zhang *et al.* have recently successfully interfaced the latter with DCLs, harvesting the benefits of both approaches[357]. In encoded self-assembling chemical libraries, screened fragments are attached to DNA ends equipped with constant hybridization domains and variable encoding domains, allowing hits to be identified by washing away non-binding molecules, followed by DNA amplification and sequencing[358]. Because the hybridization domains are long, the duplexes are static and the number of binding dimers is statistically determined (Figure 2.23, top). In dynamic DECLs, the hybridization domain is shorter, resulting in a lower melting temperature and therefore a possibility of
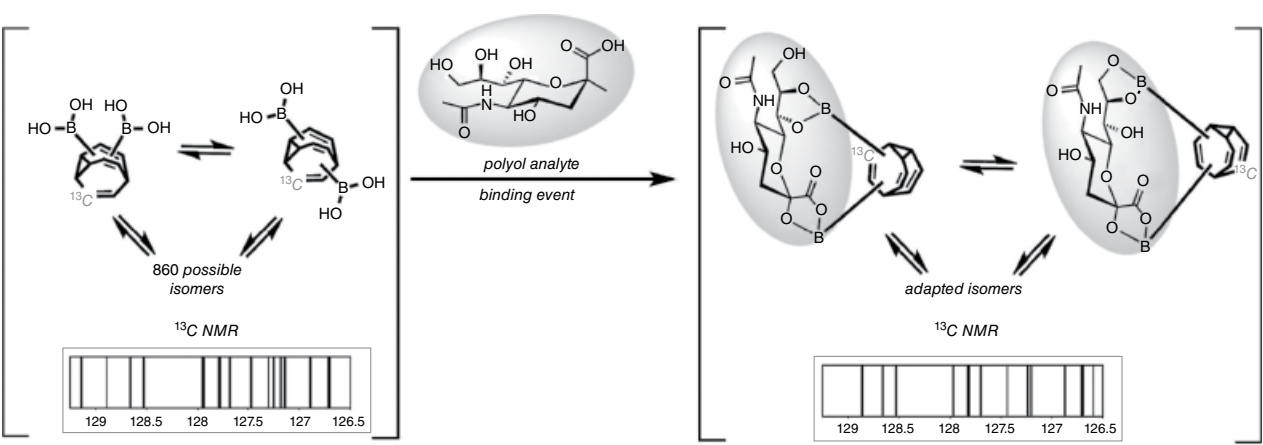
Figure 2.21 A dynamic library of ^{13}C-labelled substituted bullvalenes gives a characteristic ^{13}C NMR spectrum which can be simplified into the corresponding barcode. Addition of an analyte capable of binding to the recognition groups results in a different bullvalene population, yielding a barcode specific for the analyte.
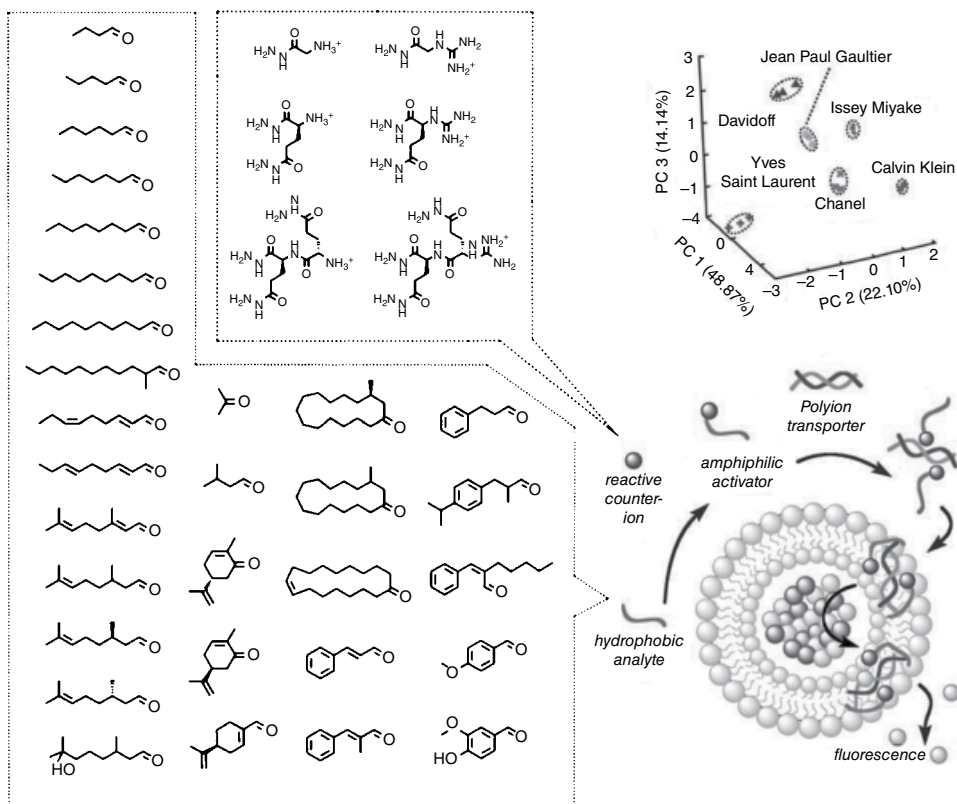
Figure 2.22 A vesicle-based chemical nose. Aldehyde and ketone odorants form a DCL with positively charged hydrazides, which can pass a lipid bilayer on DNA binding. After crossing the membrane, the complex can shuttle fluorophores and quenchers into the bulk medium, generating a fluorescent response. The fluorescent output from the sensor array can be evaluated with principal component analysis, allowing for, for example, identification of commercial perfumes.

re-equilibriating the library to maximize the number of duplexes binding to the target (Figure 2.23, bottom). The dynamic approach increases the signal-to-noise ratio by amplifying the best binders.

Supramolecular interactions are a direct consequence of the structures of the molecules involved. Because the amplification of library members in DCLs results from their interactions with the target, dynamic libraries possess an innate ability to respond to the molecular structure of the template. This property was used to classify a large group of amines and ammonium ions based on their molecular similarity[51] and more recently to determine effective molarities for the formation of imine macrocycles[359].

To make the semiochemical picture of dynamic combinatorial systems more complete, Lehn *et al.* succeeded in making systems capable of information storage by combining three states of dynamic control (photoisomerization, hydrazone exchange, and metal coordination)[263], while Huc, Nitschke, and colleagues developed a library of self-assembling components undergoing programmed cascading transformations resembling signal processing cascades in living organisms[52].
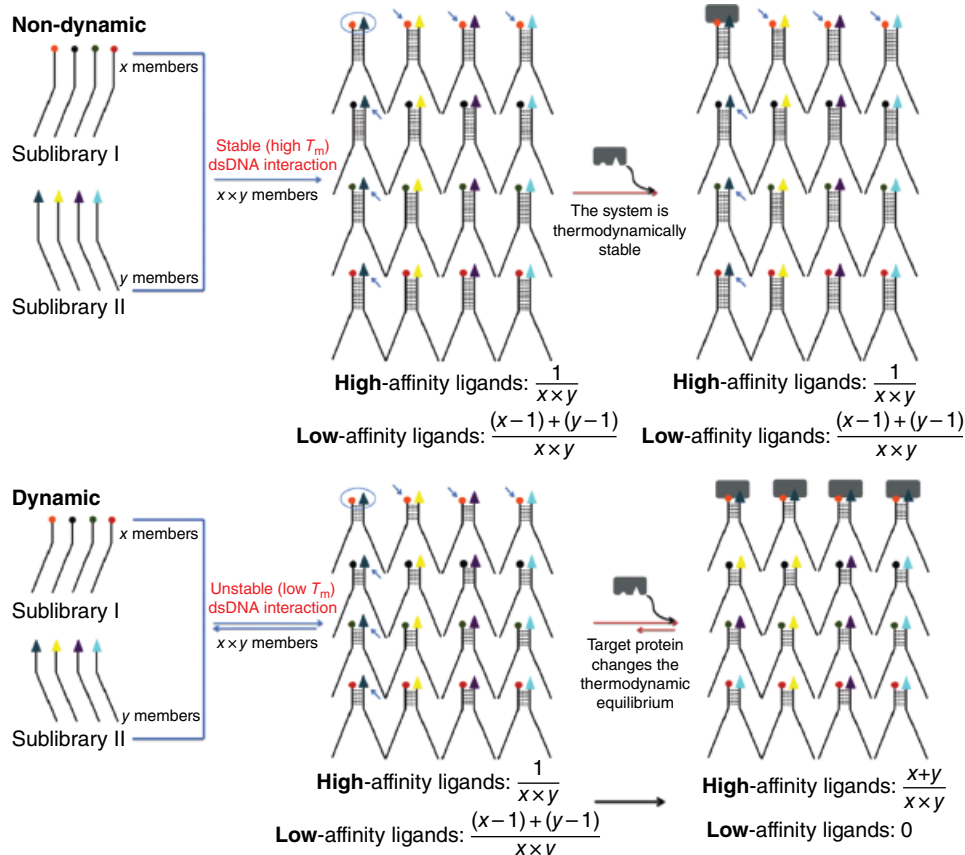
Figure 2.23 A comparison of a static DNA encoded chemical library (top) with a dynamic one (bottom). The dynamic library has shorter DNA complementary domains, allowing for amplification of the best binding dimers by the target protein. (*See insert for colour representation of the figure.*)

2.5.2 Self-synthesizing Materials

Self-assembly provides enormous opportunities to create materials with atomic precision, in large quantities, providing error-correction mechanisms – characteristics prohibitively difficult to achieve with top-down approaches to fabrication[360]. Dynamic combinatorial systems allow supramolecular ordering of molecules to be combined with their molecular synthesis[361]. Where these two levels of organization are coupled with positive feedback loops, they provide a gateway to materials which effectively synthesize themselves[10,219,362]. Self-synthesis is therefore a direct result of self- and cross-replication of molecules, their spatial ordering, or both. Because replicating systems necessarily transfer chemical information to their progeny, they bring some of the unique characteristics of living systems to materials science[362].

As we exemplified in Section 2.2.4, self-replication coupled to a DCL can be controlled by either kinetic or thermodynamic factors. The latter were used by Ulijn *et al.* to create an enzyme-assisted dynamic peptide library in which some Fmoc-functionalized peptides were capable of self-assembly, forming hydrogels[363]. Whereas

endoprotease-catalyzed peptide formation is generally disfavored in an aqueous environment, self-assembly into fibrous structures is sufficient to shift the equilibrium towards those peptides which form thermodynamically stable hydrogels. Because amide formation and hydrolysis can only happen in the presence of the enzyme, formation of the hydrogels could be spatially controlled by localizing the enzyme on a surface. Similarly, hydrogel confinement was achieved in acid-catalyzed hydrazone formation (see[320,321] and Figure 2.20). Introduction of cysteine residues to the system allowed for orthogonalization of self-assembly pathways[364]. Stabilization of weak covalent bonds by self-assembly into fibers was also useful for creating imine-based conjugated polymers in water[365].

In contrast to thermodynamically controlled materials, where only one product can be formed, kinetically controlled libraries allow the desired material to be chosen by exerting control over the assembly pathway. An example of such material was provided by our laboratory, where we created a mechanosensitive replicator with fiber morphology[219] (for a detailed description see Figure 2.9). Agitation conditions determine whether oxidation of dithiol **34** leads to formation of fibers comprising stacked hexamer or heptamer. Although the fibers are too weak to form a hydrogel, their irradiation with UV light leads to scrambling of the disulfide bonds within the fibers, strengthening them, thus creating a hydrogel without any change in the morphology of the fibers[268] (see Section 2.3.2). Interestingly, in the absence of agitation, the system tends to persist in a metastable state with only non-assembling trimers and tetramers present. Therefore, short fibers can be used to seed such mixtures, leading to transformation of small macrocycles into hexamers and uniform growth of the fibers from their ends (Figure 2.24)[225]. The mechanism is analogous to living polymerization, therefore the dispersity of the remaining fibers remains low on their elongation. If the seeds have slightly different peptide sequences to the metastable "food" macrocycles, block-copolymer fibers can be formed.

Recently, our laboratory developed a method of triggering self-synthesis using an external chemical trigger[366]. The system is characterized by a high barrier for the nucleation of the self-replicating nanosheets. The barrier can be crossed if a template molecule is added to the DCL of the non-assembling species, amplifying the assembling library member. This system does not show any spontaneous, untriggered nucleation and does not require the use of a replicator seed to control the formation of the material.

2.6   Non-equilibrium DCLs

The great majority of the libraries described in this chapter are under thermodynamic control, and only a minority are under kinetic control. The latter systems offer a greater degree of control, as their states are pathway-dependent, allowing the final state of the library to be chosen by changing not only the relative minima of the free energy landscape but also the transition states. Control can be exerted by the use of, for example, (auto)catalysts, orthogonal and lockable covalent chemistries, or molecular switches. The last two are conceptually equivalent in the context of molecular machines (see[367,368] and Chapter 7) as they can both result in a controllable switching between two states, changing the free-energy landscape. Because of the possibility of extracting work from
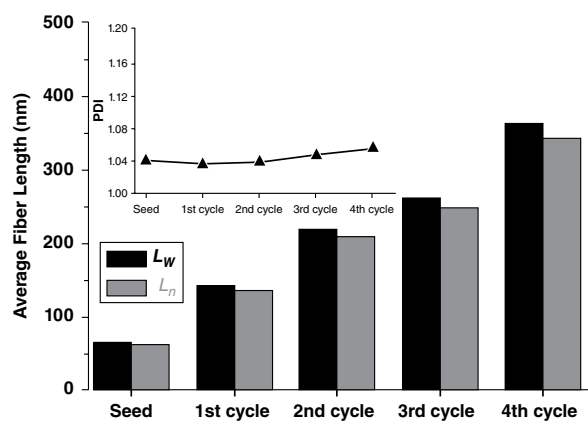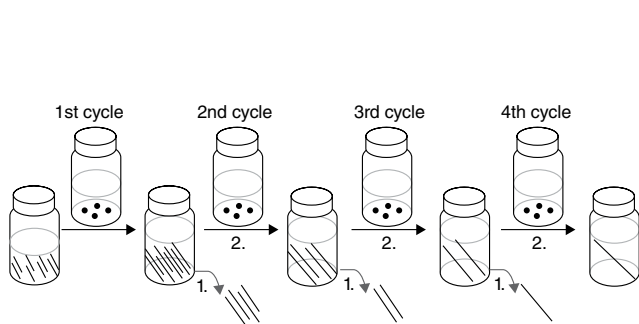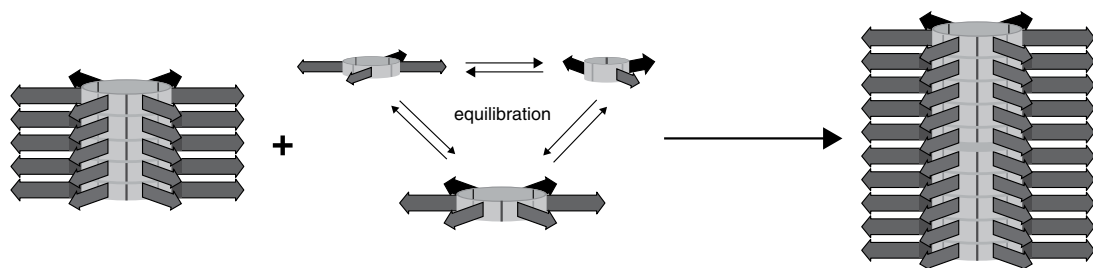
Figure 2.24 When a seed of a fibrous self-replicator is added to a DCL of its food components, the fibers are elongated. The seeded growth process can be repeated multiple times to obtain fibers of the desired length. The polydispersity of the fibers remains low, even after several growth cycles.

such systems, they have been used to direct the motion of molecular walkers along a track[54,369,370]. If the control over the energy landscape is removed, movement is necessarily stochastic and the distribution of walkers along their tracks is thermodynamically controlled[55,371]. In contrast, non-directional movement does not require external intervention; there is no need to adjust the pH or irradiate the system. Recently, Kovaříček and Lehn created an autonomous and directional walker by installing kinetic traps at both ends of a non-symmetric track (Figure 2.25)[372]. The non-directional control can be coupled with thermodynamic traps at the end of the track. Aldehyde **92** walks stochastically in the middle part of the polyamine track, but is stabilized at the left terminus under basic conditions and at the right terminus under acidic conditions. Therefore the walker eventually finds its destination at the given end, while the direction can be switched by pH adjustment.

Even though thermodynamic and kinetic control allows us to direct dynamic systems towards the desired structural outcome by modifying the Gibbs energy landscape, once a (local) minimum is reached, such systems remain static. Despite enormous progress over recent, our self-assembled systems still appear bleak when compared with the exquisitely dynamic and adaptive creations of Nature. Although living systems sometimes rely on kinetically trapped materials (think about bench-stable wooden furniture), most molecular and supramolecular entities created by cells exist only transiently. The cellular assemblies and biomolecules are constantly being synthesized and degraded, for instance the median half-life of a protein in a mammalian cell is around two days[373]. Therefore, cells usually create their components only where and when they are needed, reusing the constituents for other purposes later. Continuous recycling requires constant energy input to preserve the structure and function, making the systems *dissipative.* Creating synthetic dissipative self-assembled systems is challenging because the self-assembly process has to be coupled with irreversible consumption of energy, driving the energy of the components uphill[70,374]. Such actions can be accomplished using physical energy input like irradiation, which switches molecules to their metastable state[375], or applying an electric potential to form a chemical gradient[376]. The use of a chemical fuel to create a dissipative system is also possible, provided that the assembly is able to loose its energy along a pathway different to fuel consumption; otherwise the system would end up in thermodynamic equilibrium. This requirement leads us to a type of dynamic bond which does not rely on the microscopic reversibility principle but is instead coupled with an irreversible transformation of fuel (F) into waste (W):

$$F + A \rightarrow B \rightarrow A + W \qquad (2.6)$$

An example of such a system was first provided by van Esch *et al.,* who used methyl iodide (F) to form methyl esters (B) from carboxylic acids (A) in water under basic conditions. The methyl esters could then assemble into fibers, but because the esters hydrolyze spontaneously back into carboxylic acids (A) and methanol (W), the fibers disassemble shortly after the fuel is consumed[377]. DCLs can be also made dissipative by simply using multiple different substrates able to consume the fuel. Based on their previous results on dynamic fiber instability[378], the Ulijn group recently showed a system using aspartame **94** as a fuel and a mixture of competing amino acids to form a library of tripeptides **95**, which could then assemble into fibers (Scheme 2.13)[379]. Because the tripeptides are hydrolyzed back to the initial amino acid and dipeptide **96**, the fibers degrade spontaneously, but can be reconstituted several times if more
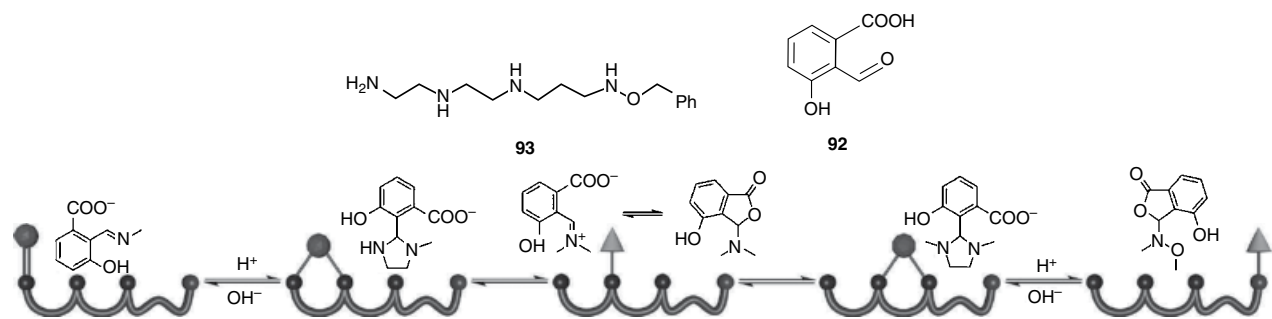
Figure 2.25 A polyamine track **93** and a walker molecule **92**. The walker is attached to the track with an imine bond and moves by addition/elimination of the amines. The movement is stochastic, but the termini act as pH-controlled thermodynamic traps, allowing the walker to be directed to either of the two ends.
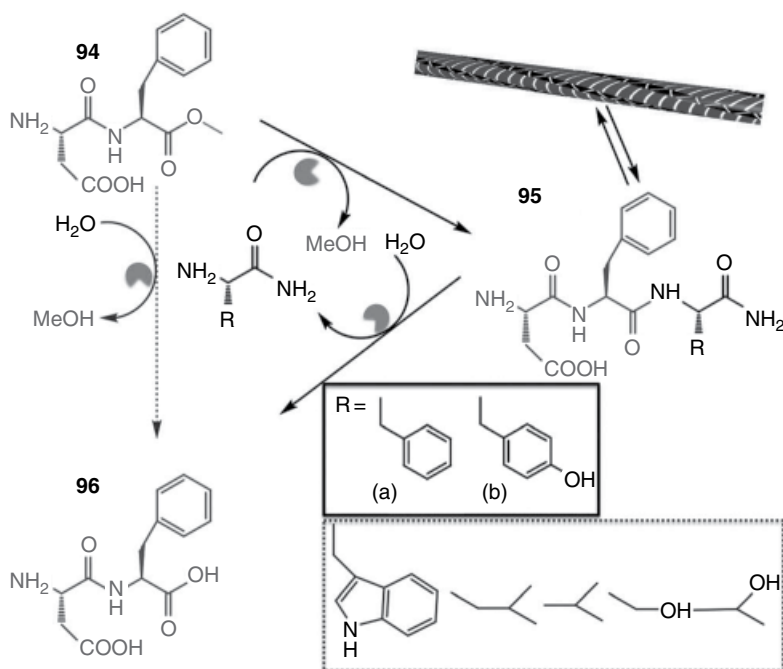
Scheme 2.13 A dissipative DCL consisting of aspartame **94** as a fuel and different amino acids. The enzyme (α-chymotrypsin) converts them into tripeptides **95** and subsequently hydrolyzes them back to the original amino acid and compound **96**. The tripeptides can self-assemble but the structures are transient; they will persist only if the fuel is present in the system.

aspartame fuel is added. Interestingly, in the presence of the fuel, the DCLs were dominated by the kinetically controlled product instead of the thermodynamic one.

As these two examples show, chemically fueled dissipative systems can be built using irreversible reactions. In principle, it should also be possible to employ reversible reactions to create dissipative DCLs, but that would require additional irreversible transformations connecting the library members. An alternative approach was demonstrated by our group by coupling a thermodynamically controlled disulfide library of **18** with unstable template **30**, amplifying some library members (Scheme 2.8)[214]. Because the template gradually undergoes an irreversible transformation to form non-interfering products, the amplified tetramers disappear (i.e., re-equilibrate into thermodynamically more stable library members) together with it. Therefore, the template can be considered a fuel which enables formation of the transient tetrameric macrocycles. In fact, the tetramere catalyze the first step of the transformation of the template to non-binding products, thereby actively working towards their own demise.

2.7 Analysis of DCLs

DCLs are complex mixtures, representing a considerable analytical challenge for several reasons. First, the high number of components requires techniques which ideally give only one analytical signature (signal) per component. More often, hyphenated

techniques are applied in order to extract multidimensional data from a single analysis[380]. Second, continuous and fast exchange of the building blocks necessitates a short analysis time when kinetic parameters have to be determined. Note that exchange should not occur while the sample is being subjected to analysis, which usually requires that exchange should be stopped prior to analysis by suitable change in the physical or chemical properties of the environment. Third, DCLs are often prepared in buffered media or contain additives or catalysts, which represent a considerable matrix effect. Finally, dynamic behavior often needs to be monitored at multiple levels, including the molecular, the supramolecular, or even the nanoscale, each of which requires different analytical tools. In the following, a short overview of the most important methods for DCL analysis is given.

2.7.1 Liquid and Gas Chromatography

Liquid chromatography (LC) and gas chromatography (GC) are the most frequently used analytical methods for the qualitative and quantitative study of complex mixtures, including DCLs. This is because in these techniques each component gives rise to only one signal (in contrast to most spectroscopic methods). As nowadays ultra-high performance LC systems are capable of resolving samples of several tens of components in an analysis time of 10–15 minutes, these methods seem to be the most straightforward analytical tools in the context of DCC analysis. However, several aspects have to be kept in mind. LC and GC do not provide any structural information about the library members, so that additional coupled techniques, most often LC/GC-MS, are required to identify the resolved library members. In the case of aggregate formation, methods have to be employed that disrupt the aggregates[233] to render the analysis quantitative. Moreover, as LC techniques are usually coupled with UV-vis detection, quantitative results can only be obtained if the corresponding extinction coefficients are known. In the most simple cases, where the extinction coefficients of the building blocks are additive, the coefficient for a library member can be computed if its building block composition is known. However, the additivity of the extinction coefficients always has to be proven[75].

As mentioned above, dynamic systems often have to be "frozen" before analysis, that is, the dynamic processes must be rendered slow enough so that no composition change occurs during analysis time. This is usually done by decreasing or increasing the pH[380]. However, some chemical processes, for example imine exchange, remain dynamic in the aqueous medium used for LC analysis[381], regardless of the pH, so that chemical modifications, such as borohydride reduction for imines[102] or more delicate derivatization methods[382], are required. However, specific types of DCLs still remain unsuitable for LC methods. For example, a large number of metallosupramolecular systems are too labile to withstand chromatography.

Nevertheless, this problem can be circumvented in specific cases. Case *et al.*[383,384] investigated protein folding by synthesizing 36 peptides, each equipped with a 2,2′-bipyridyl moiety at the N-terminus, and combined these with a substoichiometric amount of Fe^{2+} ions to get a metallosupramolecular DCL of more than 8000 trimeric peptide–Fe^{II} complexes. Some of these library members were expected to undergo folding-driven amplification, resulting from secondary interactions between the peptide residues. However, due to the large number of DCL members and the presence of metal

ions, direct analysis would have been cumbersome. Thus, after equilibration, the unreacted peptides were separated with size exclusion chromatography (SEC) from the metal complexes. The latter were isolated, demetalated, and the resulting, biased peptide mixture was subjected to the same procedure. After five iteration steps, five peptides were selected from the original set of building blocks. Further MS and CD experiments were necessary to narrow the possible set of library members and to select the most stable homo-and heterotrimers. This example shows that LC combined with other separation techniques renders feasible the analysis of otherwise unsuitable DCLs.

SEC is often used in the analysis of polymeric DCLs. For example, Fulton *et al.* proved the dynamic nature of PS-DCLs (see Section 2.2.2.1) of two differently functionalized hydrazone polymers by monitoring the decrease in the SEC peaks of the components and the simultaneous emergence of a new peak[385]. More interestingly, the same analytical tool was used to monitor the reversible single chain-to-nanoparticle transformation in an imine PS-DCL[386,387].

The use of GC for analysis of DCLs is relatively uncommon and is exclusively applied in the headspace analysis of libraries that are capable of bind and release volatile compounds[254,343] (see Section 2.4.5).

2.7.2 Mass Spectrometry

Mass spectrometry is usually used in DCL analysis coupled in line with LC, to identify and quantify the separated library members. In contrast, direct MS is often regarded as a poor tool for quantification, for several reasons. First, the ionization efficiencies of different library members are typically not equal and hard to quantify. Thus, the composition detected in the gas phase usually poorly reflects the composition of a DCL in solution. Second, in-source fragmentation of a larger oligomer might produce species with the same composition as a smaller one, again furnishing biased results[388]. Nevertheless, it has been shown that the quantification of DCL composition and amplification effects is possible solely by MS, provided the structures of the library members are similar enough[389,390]. However, some MS methods are especially suitable for the analysis of DCLs that comprise too many members to be resolved with (U)HPLC methods. Fourier transform ion cyclotron resonance (FTICR) is especially suited for this purpose due to its extremely highly mass resolution (up to $R = 10^6$) and the theoretically infinite number of isolation/fragmentation cycles in the tandem MS (MS^n) mode. For example, DCLs with more than 100 members were successfully analyzed with species whose mass differed only by a few tenths of a Dalton[380]. FTICR enables the determination of protein-ligand stoichiometry in enzyme -templated DCLs[391] or the detection of unstable intermediates whose presence indicates the pathways of DCL formation[392].

In a recent publication[393], Schalley *et al.* provided an interesting example, showing that structural analysis of complex DCLs of interlocked species is possible by FTICR-MS (Figure 2.26). The NDI-based diamine building block **97** and 2-formylpyridyne react to give bisimine **98** (L), which, in the presence of Fe^{2+} ions (M), generates a metallosupramolecular tetrahedron (M_4L_6) by subcomponent self-assembly (see Section 2.2.1.1). As the metal–ligand bonds are continuously broken and reformed, the electron-deficient vertices thread through the cavity of the electron-rich dinaphto-crown ether molecules **99** (C). The process ends up with a statistical distribution of three-dimensional polycatenanes $M_4L_6C_n$ (Figure 2.26a). Fragmentation of the parent
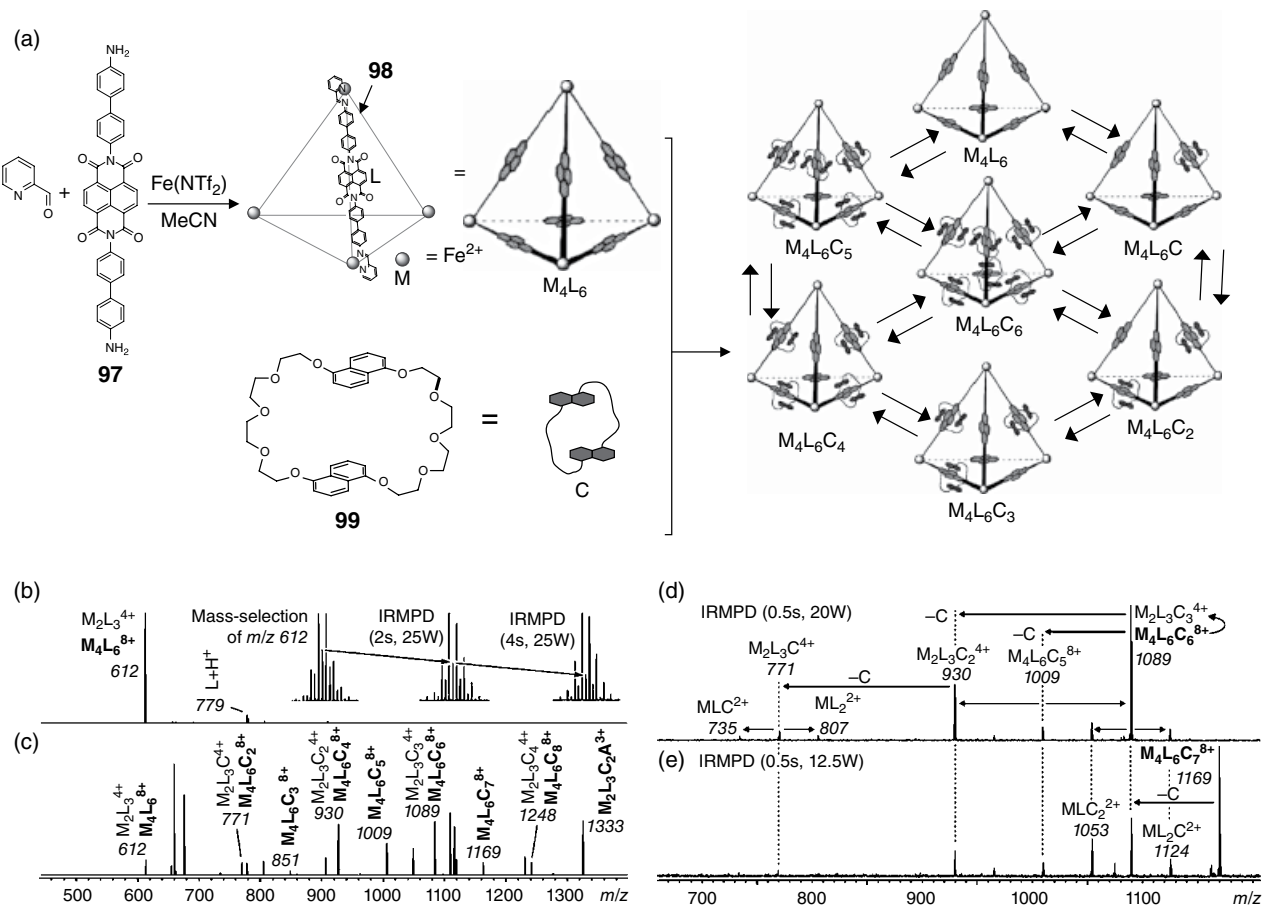
Figure 2.26 (a) Synthesis of tetrahedral cage M_4L_6 from subcomponents and generation of a DCL of $M_4L_6C_n$ polycatenanes. (b) ESI-FTICR-MS spectrum of M_4L_6. The inset shows the increasing number of M_2L_3 fragments on IRMPD (infrared multiphoton dissociation) fragmentation. (c) ESI-FTICR-MS spectrum of a mixture of M_4L_6 and an excess of crown ether **99** (C), showing the presence of $M_4L_6C_n$ polycatenanes ($n = 1–8$). (d) IRMPD of $M_4L_6C_6^{8+}$ shows simultaneous fragmentation to $M_2L_3C_n$ species, indicating that the crown ethers are mechanically bound. (e) IRMPD of $M_4L_6C_6^{8+}$ showing similar fragments to that of $M_4L_6C_6^{8+}$, indicating non-specific binding of the seventh crown ether moiety.

cage by infrared multiphoton dissociation (IRMPD) experiments resulted in two equivalent fragments M_2L_3 due to charge repulsion (Figure 2.26b). FTICR-MS analysis of the DCL revealed the presence of all expected intermediate library members $M_4L_6C_n$ ($n = 1$–6). It would have been challenging to obtain this proof either with NMR (as the signals arising from different members are likely to overlap), or with LC (as the cages are labile to survive chromatography).

Theoretically, the maximal number of coordinating C moieties is six, but assemblies with larger number of crowns were also observed (Figure 2.26c). FTICR-MS was utilized in order to distinguish between mechanical bonding and non-specific aggregation. IRMPD of $M_4L_6C_6^{8+}$ with increasing irradiation energies showed that fragmentation of the cage due to charge repulsion occurs at lower energy than dethreading, indicating that all crown ethers are indeed mechanically bound (Figure 2.26d). In sharp contrast, for $M_4L_6C_7^{8+}$, dissociation of a crown ether moiety occurs first (Figure 2.26d), and the resulting species fragments exactly in the same way as $M_4L_6C_6^{8+}$, indicating non-specific binding of the excess crown ether. This example shows that MS methods can provide valuable insights into the structural properties of otherwise virtually indistinguishable DCL members. In even more challenging cases of metallosupramolecular DCLs, where energetically distinct conformers of the same library members are formed, mass spectroscopy coupled to ion mobility spectrometry (IMS) can provide full resolution. In this technique, ions are separated simultaneously by mass, charge, and collision cross-section in the gas phase, so that differently folded isomers of the same species can be distinguished[394,395].

2.7.3 NMR Spectroscopy

In contrast to LC methods, in NMR, most of the substances give rise to multiple sets of signals, which renders NMR at first sight unsuitable for the study of DCLs. However, in contrast to other methods, NMR enables selective monitoring of the chemical environment change in a given segment of a molecule. In other words although 1D NMR techniques are usually not helpful in the characterization of complex DCLs (a few counterexamples are nevertheless known[92,197,396,397]), they can provide useful information for templated DCLs. Multidimensional experiments, in turn, provide much higher resolution, so that selective monitoring and even quantification of binding becomes possible.

^{13}C-NMR, in combination with isotopic enrichment, was reported to allow for the rapid quantification of DCLs. Prins *et al.* prepared a library of aldehydes, amines and hydrazides with the former building blocks enriched in ^{13}C on the aldehyde carbon[398]. In the $2 \times 2 \times 4$-membered DCL, all components, including the *E/Z* isomers of the hydrazones, could be distinguished. Moreover, the library composition, and consequently the relative thermodynamic stabilities, could be assessed.

In protein-templated DCC, more complex 1D ^{1}H NMR techniques are applied to quantify binding (see Section 2.2.2.1). In a recent example[182], saturation transfer difference (STD)-NMR was used to identify good binders of endothiapepsin from a hydrazone DCL. This technique[399] relies on the observation that selective irradiation of the protons of the target protein leads to saturation transfer to the bound ligand protons as well (similarly to NOESY). On dissociation, saturation is preserved in the unbound state and is detected. Thus, the difference between the spectrum thus obtained

and that without selective saturation provides signals corresponding exclusively to the specific protons of the bound ligands. The same technique was used to identify galactosidase inhibitors from a virtual DCL of hemithioacetals[400]. In a related technique, WaterLOGSY(Water–Ligand Observed via Gradient SpectroscopY), the bulk water protons are saturated and this saturation is again transferred to the ligands either directly or via the water–protein–ligand pathway. Again, a difference spectrum is recorded to determine which library members bind effectively to the target[401]. This technique was used by Ciulli *et al.* to find *Mycobacterium tuberculosis* pantothenate synthase binders from a disulfide library using 5′-deoxy-5′-thioadenosine as a support ligand[180].

Multidimensional methods are more frequently used in DCL analysis. An alternative approach for the above -mentioned ^{13}C enrichment is the use of ^{1}H–^{3}C HSQC, which enabled the resolution of hydrazone protons which were indistinguishable by simple ^{1}H NMR and rendered possible the quick measurement of the kinetic and thermodynamic parameters of an eight-membered DCL[402]. Exchange Spectroscopy (EXSY) spectroscopy has recently been used by Lehn *et al.*[55] to analyze an imine-based dynamic covalent system composed of oligoamines and monoaldehydes. The latter can move nondirectionally on the track represented by the diamine by intramolecular imine exchange via an aminal intermediate (detailed description in Section 2.6). In order to determine the rate of the intramolecular motion, the imine–imine as well as the imine–aminal exchange rates had to be measured, This was enabled only by EXSY as the aminal proton was not detectable in the simple ^{1}H spectrum.

Concerning the speciation of library members of remarkably different size, a system of helical oligohydrazone strands (already mentioned in Section 2.2.1.1)[111] was studied by DOSY-NMR. Although the library consisted of ca. 30 members, only five different levels of diffusion rates (and thus hydrodynamic radii) could be detected. This achievement is nevertheless remarkable, as, compared to HPLC, which previously had been capable of separating nearby all library members, variable temperatureDOSY showed that the size and thus the conformation of the helices change with temperature[403].

2.7.4 Optical Spectroscopy

As already mentioned, UV-vis spectroscopy is applied in nearly every analysis of DCLs with LC methods (see Section 2.7.1). In contrast, direct analysis of dynamic libraries with optical spectroscopy is rare. Prins *et al.* have shown[404] that a simple hydrazone DCL composed of **100**, **101**, **102**, and **103** can be indirectly screened by the addition of *trans*-cinnamaldehyde **104**, which reacts with **101** to give the fluorescent derivative **105**, while no fluorescent product results from the reaction with other members (Scheme 2.14). Consequently, the method is suitable for studying DCLs formed between furane-2-carbohydrazide and other hydrazones as well. Following the concentration of this particular member can thus provide kinetic and thermodynamic information about the DCL.

Related optical spectroscopy techniques are often used in the context of DCL analysis. Lehn *et al.* followed the folding of donor–acceptor–containing dynamers by monitoring the UV signal arising from stacking of the donor–acceptor units[252]. Fluorescence spectroscopy has been more often used to study the formation of secondary structures in DCLs, such as folded fluorene-based imine dynamers[347]
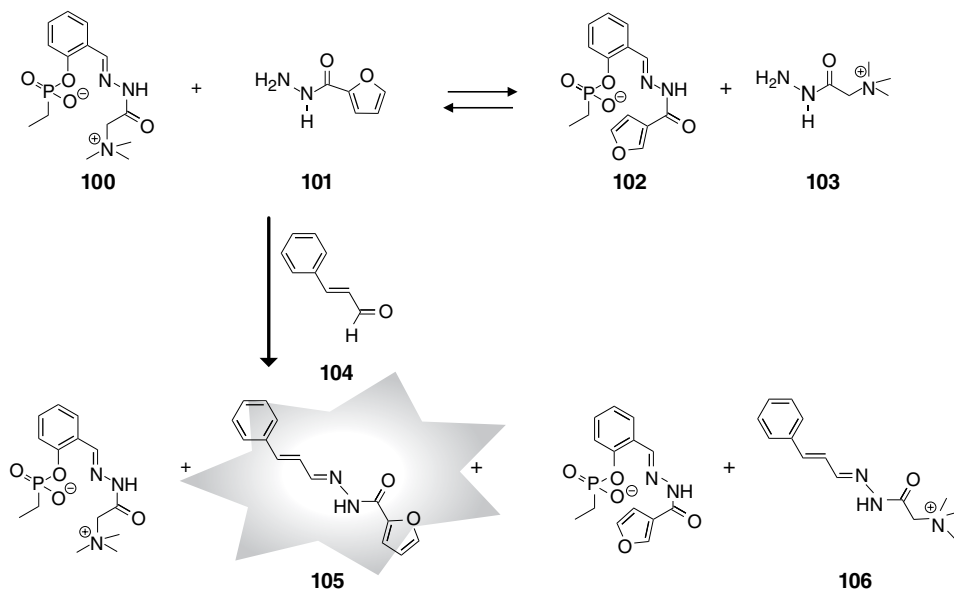
Scheme 2.14 Indirect fluorescent detection of a specific DCL member by selective derivatization.

or disulfide-based amyloid-like fibers[219,222], often combined with various biochemical assays for example for DNA binding[205]. Circular dichroism (CD) spectroscopy was implemented to prove the formation of chiral knot-like structures from disulfide libraries[247,248]. Waters *et al.* used laser polarimetry coupled to HPLC to measure template-induced deracemization of specific members in an originally racemic DCL[145]. These examples show that, although optical spectroscopies cannot provide full characterization for dynamic combinatorial systems, their implementation is indispensable in deciphering particular properties at the system level.

2.7.5 Microscopy Techniques

As DCLs recently have been observed to form large (nanoscale to microscale) objects, microscopy techniques such as transmission electron microscopy (TEM), atomic force microscopy (AFM), and scanning tunneling microscopy (STM) have emerged as valuable tools in uncovering higher levels of self-assembly. For example, TEM was used to identify the assemblies of self-replicating macrocycles[219,222] or self-replicating peptides[227] as fibers with a hydrogen bond-supported β-sheet structure. Recently, TEM has emerged as the main analytical tool for studying the effect of mechanical shear stress on the length distribution of self-assembled fibers emerging from DCLs[223,225]. Samori and Giuseppone applied STM to monitor the on-surface formation of 2D nanopatterns formed form metal–ligand-[405] or imine-[319] based DCLs. The libraries formed were manipulated *in situ* on the surface, proving that more apolar building blocks are adsorbed more strongly and thus replace less apolar ones from on-surface DCLs. The same group used AFM and fluorescence microscopy to monitor the pH-dependent functionalization of aldehyde-coated surfaces with different amine chromophores via imine DCC in order to create spatial and temporal gradients of

dynamic self-assembled monolayers on surfaces[311] (see Section 2.4.4.3). Ulijn *et al.* utilized TEM and AFM to monitor the irreversible formation of gel-forming fibers from a dipeptide DCL rendered dynamic by the enzyme thermolysin. Gelation turned out to dictate the preferential formation of short aromatic dipeptides at the expense of others[93].

Microscopy techniques are especially suitable when the building blocks themselves are macromolecules. For instance, Sumerlin *et al.* synthesized polystyrene-maleic anhydride block copolymers and functionalized these with multiple thiol groups[406]. On oxidation, the polymeric building blocks formed star-like assemblies with polystyrene arms attached to a core held together by multiple disulfide bonds. TEM has been proven to be an easy tool to monitor morphology changes. Interestingly, if larger objects form from DCLs, their morphology and transformation can even be followed by optical microscopy, as in[407] where the guest-steered transformation of disulfide-based giant vesicles was monitored. These few examples already show the wide applicability of microscopy techniques in DCL analysis from the nanometer to the mid-micrometer scale.

2.7.6   Diffraction and Scattering Techniques

In general, diffraction techniques are conceived to detect repeating structural elements in aggregated phases (solid, but also mesophases) of molecular or supramolecular entities. The observability of analysable diffraction patterns thus heavily relies on the chemical uniformity and ordered structure of the material under study. This might sound a non-typical case for DCLs as these are far from being chemically uniform and are most often dissolved in one or two phases. Yet, Jhoti and co-workers probed a hydrazone DCL for optimizing ligands of the enzyme cycline -dependent kinase 2 (see Section 2.2.2.1) by soaking single crystals of the target in the solution and thus directly analyzing the binding capability with X-ray diffraction[408]. Belenguer and Sanders[271] analyzed a solid-phase disulfide library with powder X-ray diffraction to distinguish two polymorphs of a DCL member. These possessed different stability under different mechanochemical conditions (see Section 2.3.4), which deeply influenced their seeding capability (see Section 2.2.4).

Moving to mesophases, several studies are reported where libraries are capable of forming dynamic micellar structures. Structural information of these entities could be gained by small angle X-ray or neutron scattering (SAXS, SANS). These techniques can provide information on various length scales, that is, on that of the assembly–solvent interface, on that of the assembly size, and on that of interactions between assemblies as well. Buhler and Giuseppone studied DCLs of hydrophilic (PEG-based) amines and hydrophobic aldehydes to form imines, self-assembling into micellar, vesicular or rod-like structures[220,284]. The shape of the assemblies was determined by SANS, which enabled distinguishing between the core (which, being constructed from the same aldehyde building block, was constant in all DCLs under study) and the corona (whose size changed as a function of the chain length of the amines used). Later, the same technique was applied to study a system generated from the same hydrophilic amines and a charged, yet hydrophobic, aldehyde[286] (see Section 2.4.3). SANS measurement showed that for amines with short PEG units, the charged hydrophobic aldehyde-containing chains form the corona of the micelles. Yet beyond a certain PEG length, the micelles underwent inversion, that is, the positively charged chains became located in the core

of the assemblies. This finding was clearly visible from a peak in the intermediate q region for the shorter PEG-containing assemblies, corresponding to the repulsion force between charged micelles. Likewise, the pH-dependence of micelle inversion was also assessed with SANS.

Finally, dynamic light scattering (DLS) is also a suitable method in DCC, especially in the case where libraries are constructed of polymeric building blocks. For example, DLS was used to follow the interconversion between unimeric and crosslinked, star-like polymer chains arising from boronic acid functionalized polymers on the addition of polyol crosslinkers[409]. Thus, together with the previously mentioned microscopies (see Section 2.7.5), these analytical techniques turn out to be multifaceted tools in studying the behavior of DCLs on the nano- and mesoscale.

2.7.7 Calculations

Due to the complex nature of DCLs, there is often no straightforward means to extract thermodynamic and kinetic constants from the data provided by the analytical tools listed above. Regarding binding constants, these can be determined by isolating the corresponding DCL member and carrying out ITC or NMR titrations with the corresponding host molecules. However, isolation is often a tedious process accompanied by low yields. Moreover, this procedure does not provide equilibrium constants of the interconversion of the DCL members. These hurdles can be overcome with DCLFit software[83] (see Section 2.1.3), which has been tested on a number of experimental and simulated DCLs. The results show that the fitting procedure reproduces the experimental (or, in case of simulated libraries, the initially given) values of the binding affinities for strongly binding guests. For weaker binders, the match between fitted and "experimental" values is poorer due to the decreased probability of their concentration being higher than the detection limit.

Moreover, DCLFit enables the equilibrium constants of reactions which are impossible to obtain otherwise to be quantified. For example, there is no direct means known to measure the equilibrium constants of catenanes from the parent macrocycles, as the opening of the latter would require extremely high thermal activation energy. Recently, DCLFit was applied to a library containing heteromeric [2]- and [3]catenanes generated from azobenzene-based disulfide macrocycles and cyclodextrins, enabling the quantitative assessment of catenane formation from the parent macrocyclic species[410]. This sole example shows that DCLs in some cases are advantageous, not only in providing models to even more complex systems, but also to explore the properties of simpler ones, which are not accessible otherwise.

2.8 Conclusions and Outlook

Rapid developments over the last two decades have established DCC as a reliable approach for spontaneous generation of complex responsive chemical systems. With improvements in analytical techniques and clever experimental design, it is now possible to identify strong binders for biomacromolecules and hosts for small molecules in DCLs containing thousands of library members (Section 2.2). However, these advances have not yet resulted in any commercialized drug, probably because of

the biggest strength of DCC – dynamic bonds, which are problematic as part of a drug. A possible solution to this problem can be provided by dynamic covalent reactions, which require catalysis and therefore can be activated when screening against their targets, but remain static otherwise. Such reactions include hydrazone exchange and (somewhat underappreciated in the DCC context) alkene/alkyne metathesis. New reversible dynamic reactions yielding stable products under physiological conditions would greatly improve the prospects of DCLs in lead discovery. Merging of the DCL approach with other established techniques, like DNA-encoded chemical libraries, can improve the chances of detecting promising fragment combinations and lead compounds[357,411].

DCLs have proved very useful in many other fields, including chemical analysis, topological chemistry, and self-replication (Sections 2.5.1, 2.2.5, and 2.2.4, respectively), benefiting from their innate addressable complexity. Possibly the most fascinating behavior can be expected where DCC interfaces with other pillars of systems chemistry – nanotechnology, replicators, and out-of-equilibrium systems. We have already witnessed the first steps of dynamic covalent walkers, where the dynamicity of covalent bonds can be coupled with light or pH switching to achieve directional movement (Section 2.6). It would be interesting to see if redox control can be utilized in a similar manner or if these dynamic systems can use chemical fuel for translational motion, mimicking biological motor proteins.

Similar to Darwinian evolution, DCLs can evolve to yield optimized species. However, DCLs are mostly thermodynamically driven and evolve on orders of magnitude shorter timescales and not in the Darwinian sense. The relatively rapid responsiveness makes DCC a promising method for efficient search over large chemical spaces to yield, for example, protein mimetics with desired biological properties when templated with biomacromolecules. Functionalizable polymer and nanoparticle scaffolds provided the first successful examples of such multivalent binders (Sections 2.2.2 and 2.4.4.2). Further progress will require fine-tuning of scaffolds and recognition units to match the target biomacromolecules. Similarly to challenges faced by DCC-based drug discovery, work on switchable dynamic covalent chemistries will greatly enhance the applicability of such dynamically prepared nanoconstructs. The newly developed reversible native chemical ligation[94] might even lead to DCLs of true proteins, possibly unravelling the mysteries of folding thermodynamics and kinetics.

Self-synthesizing materials can benefit from the amplification of tiny amounts of initial seed information, propagating throughout the whole library to yield well-defined materials (Section 2.5.2). We can imagine that, depending on the particular needs in a given time and space, such DCLs can provide materials of markedly different properties. However, such molecular programming will definitely need replicators navigating through very complex potential energy landscapes, requiring well-designed kinetic parameters of different covalent and non-covalent reactions, and the ability to influence energy barriers with chemical triggers interacting with some library components. Far-from-equilibrium control over replicating dynamic combinatorial systems poses an even bigger challenge (Sections 2.2.1 and 2.6). As we can learn from living systems, which are dissipative, replicating, and combinatorial in nature, the rewards should more than compensate the difficulties. The properties of such systems will be possible to tune using not kinetic or thermodynamic control but Darwinian selection and survival of the fittest materials (with the highest dynamic kinetic stability[412,413]).

Another feature common to life as we know it, but largely underrepresented in research on DCLs, is compartmentalization. Although we know how to use dynamic systems in phase-to-phase transport or even make compartments out of library members (Sections 2.4.2 and 2.4.3), we are still very far from creating spatially separated systems capable of communication and directional transport. Yet, the myriad coupled biochemical processes in organisms proceed in separated compartments, that is, within membrane boundaries, in order to avoid unnecessary interference or to convert gradients across membranes into work. Similarly, compartmentalization of DCLs is highly desirable for constructing hierarchically organized responsive dynamic ensembles, and might help in separating unnecessary byproducts from the rest of the system.

The demands on the analytical hardware and software will likely grow as well. Faster, more sensitive, and more powerful chromatographic methods and (mass) spectrometers (often coupled with each other) will become crucial as the complexity of our library members and their complexes increases (Section 2.7). Likewise, (hierarchical) self-assembly in DCLs will call for a better focus on various microscopic techniques, that enable structural characterization across multiple length scales.

Dynamic combinatorial systems very often do not work as expected, frequently leading to exciting discoveries by inquisitive and perceptive researchers. However, we cannot rely only on serendipity to propel the field forward. Whereas thermodynamically controlled systems are easy to model and design using existing software packages (Section 2.7.7), systems under kinetic control linked to multiple coupled equilibria are much more demanding. The resulting multidimensional parameter spaces are difficult to screen experimentally, requiring careful kinetic studies coupled with complex simulations to yield desired systems behavior[414]. It may be interesting to automate all aspects of DCL experiments, including mixing building blocks, monitoring libraries, analyzing their behavior, and even coupling the resulting output with the design of subsequent DCLs with computer-controlled feedback loops to screen for possible emergent phenomena[415]. We might even imagine a situation where a responsive chemical system becomes a part of the computer algorithm itself!

We hope that the first two decades of DCLs have been as entertaining for you as they were for us. We are waiting eagerly to see what kinds of new, fascinating systems can fill in the "question mark" box in Figure 2.1 and we hope to see your work there.

References

1 P. T. Corbett, J. Leclaire, L. Vial, K. R. West, J. L. Wietor, J. K. M. Sanders, S. Otto, *Chem. Rev.* **2006**, *106* (9), 3652–3711.

2 J. M. Lehn, *Angew. Chem. Int. Ed.* **2015**, *54* (11), 3276–3289.

3 B. L. Miller (ed.), *Dynamic Combinatorial Chemistry in Drug Discovery, Bioorganic Chemistry, and Materials Science*, John Wiley & Sons, Inc., Hoboken, NJ, **2010**.

4 J. N. H. Reek, S. Otto (eds), *Dynamic Combinatorial Chemistry*, Wiley-VCH Verlag GmbH & Co. KGaA, Weinheim, Germany, **2010**.

5 J. W. Sadownik, R. V. Ulijn, *Curr. Opin. Biotechnol.* **2010**, *21* (4), 401–411.

6 G. Gasparini, M. Dal Molin, L. J. Prins, *Eur. J. Org. Chem.* **2010** (13), 2429–2440.

7 F. B. L. Cougnon, J. K. M. Sanders, *Acc. Chem. Res.* **2012**, *45* (12), 2211–2221.

8 M. E. Belowich, J. F. Stoddart, *Chem. Soc. Rev.* **2012**, *41* (6), 2003–2024.

9 E. Moulin, N. Giuseppone, *Top. Curr. Chem.*, **2012**, *322*, 87–105.

10 E. Moulin, G. Cormos, N. Giuseppone, *Chem. Soc. Rev.* **2012**, *41* (3), 1031–1049.

11 A. Herrmann, *Chem. Eur. J.* **2012**, *18* (28), 8568–8577.

12 B. L. Miller, *Top. Curr. Chem.* **2012**, *322*, 107–137.

13 M. Barboiu, *Top. Curr. Chem.* **2012**, *322*, 33–53.

14 J. M. Lehn, *Top. Curr. Chem.* **2012**, *322*, 1–32.

15 S. Otto, *Acc. Chem. Res.* **2012**, *45*, 2200–2210.

16 J. Li, P. Nowak, S. Otto, *J. Am. Chem. Soc.* **2013**, *135* (25), 9222–9239.

17 S. Fischmann, U. Lüning, *Isr. J. Chem.* **2013**, *53* (1–2), 87–96.

18 A. W. Jackson, D. A. Fulton, *Polym. Chem.* **2013**, *4* (1), 31–45.

19 J. M. Lehn, *Angew. Chem. Int. Ed.* **2013**, *52* (10), 2836–2850.

20 P. Dydio, R. J. Detz, J. N. H. Reek, *J. Am. Chem. Soc.* **2013**, *135* (29), 10 817–10 828.

21 S. P. Black, J. K. M. Sanders, A. R. Stefankiewicz, *Chem. Soc. Rev.* **2014**, *43* (6), 1861–1872.

22 A. Herrmann, *Chem. Soc. Rev.* **2014**, *43* (6), 1899–1933.

23 Q. Ji, R. C. Lirag, O. Š. Miljanić, *Chem. Soc. Rev.* **2014**, *43* (6), 1873–1884.

24 M. C. Misuraca, E. Moulin, Y. Ruff, N. Giuseppone, *New J. Chem.* **2014**, *38* (8), 3336–3349.

25 C. S. Mahon, D. A. Fulton, *Nat. Chem.* **2014**, *6* (8), 665–672.

26 S. Ulrich, P. Dumy, *Chem. Commun.* **2014**, *50* (44), 5810–5825.

27 M. Mondal, A. K. H. Hirsch, *Chem. Soc. Rev.* **2015**, *44*, 2455–2488.

28 E. Fischer, *Ber. Dtsch. Chem. Ges.* **1894**, *27* (3), 2985–2993.

29 J. D. Watson, F. H. C. Crick, *Nature*, **1953**, *171* (4356), 737–738.

30 M. H. F. Wilkins, A. R. Stokes, H. R. Wilson, *Nature*, **1953**, *171* (4356), 738–740.

31 R. E. Franklin, R. G. Gosling, *Nature* **1953**, *171* (4356), 740–741.

32 M. C. Thompson, D. H. Busch, *J. Am. Chem. Soc.* **1962**, *84* (9), 1762–1763.

33 C. J. Pedersen, *J. Am. Chem. Soc.* **1967**, *89* (10), 2495–2496.

34 J. T. Goodwin, D. G. Lynn, *J. Am. Chem. Soc.* **1992**, *114* (23), 9197–9198.

35 M. S. Goodman, V. Jubian, B. Linton, A. D. Hamilton, *J. Am. Chem. Soc.* **1995**, *117* (46), 11 610–11 611.

36 A. Bilyk, M. M. Harding, *J. Chem. Soc. Chem. Commun.* **1995**, *3* (16), 1697–1698.

37 P. G. Swann, R. A. Casanova, A. Desai, M. M. Frauenhoff, M. Urbancic, U. Slomczynska, A. J. Hopfinger, G. C. Le Breton, D. L. Venton, *Biopolymers* **1996**, *40* (6), 617–625.

38 P. A. Brady, R. P. Bonar-Law, S. J. Rowan, C. J. Suckling, J. K. M. Sanders, *Chem. Commun.* **1996** (3), 319–320.

39 P. A. Brady, J. K. M. Sanders, *J. Chem. Soc., Perkin Trans.* **1997**, *1* (21), 3237–3254.

40 B. Hasenknopf, J. M. Lehn, B. O. Kneisel, G. Baum, D. Fenske, *Angew. Chem. Int. Ed.* **1996**, *35* (16), 1838–1840.

41 B. Hasenknopf, J. M. Lehn, N. Boumediene, A. Dupont-Gervais, A. Van Dorsselaer, B. Kneisel, D. Fenske, *J. Am. Chem. Soc.* **1997**, *119* (45), 10 956–10 962.

42 I. Huc, J. M. Lehn, *Proc. Natl. Acad. Sci. USA* **1997**, *94* (6), 2106–2110.

43 B. Klekota, M. H. Hammond, B. L. Miller, *Tetrahedron Lett.* **1997**, *38* (50), 8639–8642.

44 S. Sakai, Y. Shigemasa, T. Sasaki, *Tetrahedron Lett.* **1997**, *38* (47), 8145–8148.

45 A. V. Eliseev, M. I. Nelen, *J. Am. Chem. Soc.* **1997**, *119* (5), 1147–1148.

46 B. Brisig, J. K. M. Sanders, S. Otto, *Angew. Chem. Int. Ed.* **2003**, *42* (11), 1270–1273.

47 A. C. Try, M. M. Harding, D. G. Hamilton, J. K. M. Sanders, *Chem. Commun.* **1998** (6), 723–724.

48 S. J. Cantrill, S. J. Rowan, J. F. Stoddart, *Org. Lett.* **1999**, *1* (9), 1363–1366.

49 M. Royo, M. A. Contreras, E. Giralt, F. Albericio, M. Pons, *J. Am. Chem. Soc.* **1998**, *120* (27), 6639–6650.

50 S. Otto and K. Severin, *Top. Curr. Chem.* **2007**, *277*, 267–288.

51 V. Saggiomo, Y. R. Hristova, R. F. Ludlow, S. Otto, J. Syst. *Chem.* **2013**, *4* (1), 2.

52 V. E. Campbell, de Hatten, X., N. Delsuc, B. Kauffmann, I. Huc, J. R. Nitschke, *Nat. Chem.* **2010**, *2* (8), 684–687.

53 J. W. Sadownik, D. Philp, *Angew. Chem. Int. Ed.* **2008**, *47* (51), 9965–9970.

54 M. von Delius, E. M. Geertsema, D. A. Leigh, *Nat. Chem.* **2010**, *2* (2), 96–101.

55 P. Kovaříček, J. M. Lehn, *J. Am. Chem. Soc.* **2012**, *134* (22), 9446–9455.

56 K. Osowska, O. Š. Miljanić, *Angew. Chem. Int. Ed.* **2011**, *50* (36), 8345–8349.

57 R. Pérez-Fernández, M. Pittelkow, A. M. Belenguer, L. A. Lane, C. V. Robinson, J. K. M. Sanders, *Chem. Commun.* **2009** (25), 3708–3710.

58 V. Saggiomo, U. Lüning, *Chem. Commun.* **2009** (25), 3711–3713.

59 K. C. F. Leung, F. Aricó, S. J. Cantrill, J. F. Stoddart, *Macromolecules* **2007**, *40* (11), 3951–3959.

60 P. Nowak, V. Saggiomo, F. Salehian, M. Colomb-Delsuc, Y. Han, S. Otto, *Angew. Chem. Int. Ed.* **2015**, *54*, 4192–4197.

61 F. della Sala, E. R. Kay, *Angew. Chem. Int. Ed.* **2015**, *54* (14), 4187–4191.

62 D. I. Rozkiewicz, B. J. Ravoo, D. N. Reinhoudt, *Langmuir* **2005**, *21* (14), 6337–6343.

63 M. Berthelot, *Chimie organique fondée sur la synthèse*, vol. 2, Mallet-Bachelier, Brussels, Belgium, **1860**.

64 P. L. Galison, *Image and Logic: A Material Culture of Microphysics*, University of Chicago Press, Chicago, IL, **1997**.

65 T. Kuhn, *The Structure of Scientific Revolutions*, vol. II, University of Chicago Press, Chicago, IL, **1962**.

66 F. J. Dyson, *Science* **2012**, *338* (6113), 1426–1427.

67 B. Russell, *The Philosophy of Logical Atomism*, Routledge Classics, Taylor & Francis, London, UK, **2009**.

68 J. Hernández-Trujillo, F. Cortés-Guzmán, D. C. Fang, R. F. W. Bader, *Faraday Discuss.* **2007**, *135*, 79–95.

69 J. M. Lehn, *Chem. Soc. Rev.* **2007**, *36* (2), 151–160.

70 E. Mattia, S. Otto, *Nat. Nanotechnol.* **2015**, *10* (2), 111–119.

71 M. M. J. Smulders, I. A. Riddell, C. Browne, J. R. Nitschke, *Chem. Soc. Rev.* **2013**, *42* (4), 1728–1754.

72 C. A. Hunter, H. L. Anderson, *Angew. Chem. Int. Ed.* **2009**, *48* (41), 7488–7499.

73 J. M. Lehn, *Chem. Eur. J.* **1999**, *5* (9), 2455–2463.

74 J. R. Nitschke, J. M. Lehn, *Proc. Natl. Acad. Sci. USA* **2003**, *100* (21), 11 970–11 974.

75 S. Hamieh, V. Saggiomo, P. Nowak, E. Mattia, R. F. Ludlow, S. Otto, *Angew. Chem. Int. Ed.* **2013**, *52* (47), 12 368–12 372.

76 F. Ulatowski, A. Sadowska-Kuziola, J. Jurczak, *J. Org. Chem.* **2014**, *79* (20), 9762–9770.

77 K. Severin, *Chem. Eur. J.* **2004**, *10* (10), 2565–2580.

78 N. Giuseppone, J. M. Lehn, *Chem. Eur. J.* **2006**, *12* (6), 1715–1722.

79 P. T. Corbett, S. Otto, J. K. M. Sanders, *Org. Lett.* **2004**, *6* (11), 1825–1827.

80 P. T. Corbett, S. Otto, J. K. M. Sanders, *Chem. Eur. J.* **2004**, *10* (13), 3139–3143.

81 P. T. Corbett, J. K. M. Sanders, S. Otto, *J. Am. Chem. Soc.* **2005**, *127* (26), 9390–9392.

82 P. Corbett, J. Sanders, S. Otto, *Angew. Chem. Int. Ed.* **2007**, *46* (46), 8858–8861.

83 R. F. Ludlow, J. Liu, H. Li, S. L. Roberts, J. K. M. Sanders, S. Otto, *Angew. Chem. Int. Ed.* **2007**, *46* (30), 5762–5764.

84 P. Corbett, J. Sanders, S. Otto, *Chem. Eur. J.* **2008**, *14* (7), 2153–2166.

85 R. A. R. Hunt, R. F. Ludlow, S. Otto, *Org. Lett.* **2009**, *11* (22), 5110–5113.

86 R. F. Ludlow, S. Otto, *J. Am. Chem. Soc.* **2010**, *132* (17), 5984–5986.

87 Z. Grote, R. Scopelliti, K. Severin, *Angew. Chem. Int. Ed.* **2003**, *42* (32), 3821–3825.

88 I. Saur, K. Severin, *Chem. Commun.* **2005** (11), 1471–1473.

89 S. Otto, R. L. E. Furlan, J. K. M. Sanders, *Science* **2002**, *297* (5581), 590–593.

90 R. F. Ludlow, S. Otto, *J. Am. Chem. Soc.* **2008**, *130* (37), 12 218–12 219.

91 A. G. Orrillo, R. L. E. Furlan, *J. Org. Chem.* **2010**, *75* (1), 211–214.

92 R. Cacciapaglia, S. Di Stefano, L. Mandolini, *J. Am. Chem. Soc.* **2005**, *127* (39), 13 666–13 671.

93 S. K. M. Nalluri, R. V. Ulijn, *Chem. Sci.* **2013**, *4* (9), 3699–3705.

94 Y. Ruff, V. Garavini, N. Giuseppone, *J. Am. Chem. Soc.* **2014**, *136* (17), 6333–6339.

95 V. T. Bhat, A. M. Caniard, T. Luksch, R. Brenk, D. J. Campopiano, M. F. Greaney, *Nat. Chem.* **2010**, *2* (6), 490–497.

96 S. Ladame, A. M. Whitney, S. Balasubramanian, *Angew. Chem. Int. Ed.* **2005**, *44* (35), 5736–5739.

97 J. Li, P. Nowak, S. Otto, *Angew. Chem. Int. Ed.* **2015**, *54* (3), 833–837.

98 R. L. Furlan, Y. F. Ng, G. R. Cousins, J. E. Redman, J. K. Sanders, *Tetrahedron* **2002**, *58* (4), 771–778.

99 R. L. E. Furlan, Y. F. Ng, S. Otto, J. K. M. Sanders, *J. Am. Chem. Soc.* **2001**, *123* (36), 8876–8877.

100 B. Fuchs, A. Nelson, A. Star, J. F. Stoddart, S. Vidal, *Angew. Chem. Int. Ed.* **2003**, *42* (35), 4220–4224.

101 S. L. Roberts, R. L. E. Furlan, S. Otto, J. K. M. Sanders, *Org. Biomol. Chem.* **2003**, *1* (9), 1625–1633.

102 K. Ziach and J. Jurczak, *Org. Lett.* **2008**, *10* (22), 5159–5162.

103 D. Berkovich-Berger, N. G. Lemcoff, S. Abramson, M. Grabarnik, S. Weinman, B. Fuchs, *Chem. Eur. J.* **2010**, *16* (21), 6365–6373.

104 A. M. Escalante, A. G. Orrillo, I. Cabezudo, R. L. E. Furlan, *Org. Lett.* **2012**, *14* (23), 5816–5819.

105 K. Ziach, A. Kulesza, J. Jurczak, *Org. Biomol. Chem.* **2014**, *12* (23), 3827–3830.

106 O. Storm, U. Lüning, *Chem. Eur. J.* **2002**, *8* (4), 793–798.

107 V. Saggiomo, U. Lüning, *Eur. J. Org. Chem.* **2008** (25), 4329–4333.

108 F. Schleef, U. Lüning, *Eur. J. Org. Chem.* **2011** (11), 2062–2065.

109 J. M. Klein, V. Saggiomo, L. Reck, U. Lüning, J. K. M. Sanders, *Org. Biomol. Chem.* **2012**, *10* (1), 60–66.

110 J. R. Nitschke, M. Hutin, G. Bernardinelli, *Angew. Chem. Int. Ed.* **2004**, *43* (48), 6724–6727.

111 N. Giuseppone, J. L. Schmitt, J. M. Lehn, *Angew. Chem. Int. Ed.* **2004**, *43* (37), 4902–4906.

112 A. González-Alvarez, I. Alfonso, V. Gotor, *Chem. Commun.* **2006** (21), 2224–2226.

113 D. Schultz, J. R. Nitschke, *Angew. Chem. Int. Ed.* **2006**, *45* (15), 2453–2456.

114 S. Ulrich, J. M. Lehn, *J. Am. Chem. Soc.* **2009**, *131* (15), 5546–5559.

115 S. Ulrich, J. M. Lehn, *Angew. Chem. Int. Ed.* **2008**, *47* (12), 2240–2243.

116 M. Hutin, G. Bernardinelli, J. R. Nitschke, *Proc. Natl. Acad. Sci. USA* **2006**, *103* (47), 17 655–17 660.

117 M. Hutin, R. Frantz, J. R. Nitschke, *Chem. Eur. J.* **2006**, *12* (15), 4077–4082.

118 K. C. Sham, S. M. Yiu, H. L. Kwong, *Inorg. Chem.* **2013**, *52* (10), 5648–5650.

119 I. A. Riddell, Y. R. Hristova, J. K. Clegg, C. S. Wood, B. Breiner, J. R. Nitschke, *J. Am. Chem. Soc.* **2013**, *135* (7), 2723–2733.

120 S. Zarra, D. M. Wood, D. A. Roberts, J. R. Nitschke, *Chem. Soc. Rev.* **2014**, *44* (2), 419–432.

121 A. J. McConnell, C. S. Wood, P. P. Neelakandan, J. R. Nitschke, *Chem. Rev.* **2015**, *115*, 7729–7793.

122 J. M. Klein, V. Saggiomo, L. Reck, M. McPartlin, G. D. Pantoş, U. Lüning, J. K. M. Sanders, *Chem. Commun.* **2011**, *47* (12), 3371–3373.

123 R. C. Brachvogel, F. Hampel, M. von Delius, *Nat. Commun.* **2015**, *6*, 7129.

124 R. C. Brachvogel, M. von Delius, *Chem. Sci.* **2015**, *6* (2), 1399–1403.

125 L. Ratjen, G. Vantomme, J. M. Lehn, *Chem. Eur. J.* **2015**, *21* (28), 10 070–10 081.

126 S. Ulrich, J. M. Lehn, *Chem. Eur. J.* **2009**, *15* (23), 5640–5645.

127 T. K. Ronson, S. Zarra, S. P. Black, J. R. Nitschke, *Chem. Commun.* **2013**, *49* (25), 2476–2490.

128 R. Vilar (ed.), *Recognition of Anions, Structure and Bonding*, vol. 129, Springer, Berlin, Heidelberg, **2008**.

129 R. Custelcean, *Top. Curr. Chem.* **2012**, *322*, 193–216.

130 S. R. Beeren, J. K. M. Sanders, *J. Am. Chem. Soc.* **2011**, *133* (11), 3804–3807.

131 S. Otto, S. Kubik, *J. Am. Chem. Soc.* **2003**, *125* (26), 7804–7805.

132 M. Bru, I. Alfonso, M. I. Burguete, S. V. Luis, *Angew. Chem. Int. Ed.* **2006**, *45* (37), 6155–6159.

133 Z. Rodriguez-Docampo, S. I. Pascu, S. Kubik, S. Otto, *J. Am. Chem. Soc.* **2006**, *128* (34), 11 206–11 210.

134 C. Olivier, Z. Grote, E. Solari, R. Scopelliti, K. Severin, *Chem. Commun.* **2007** (39), 4000–4002.

135 S. M. Turega, C. Lorenz, J. W. Sadownik, D. Philp, *Chem. Commun.* **2008** (34), 4076–4078.

136 S. R. Beeren, J. K. M. Sanders, *Chem. Sci.* **2011**, *2* (8), 1560–1567.

137 M. Bru, I. Alfonso, M. Bolte, M. I. Burguete, S. V. Luis, *Chem. Commun.* **2011**, *47* (1), 283–285.

138 Z. Rodriguez-Docampo, E. Eugenieva-Ilieva, C. Reyheller, A. M. Belenguer, S. Kubik, S. Otto, *Chem. Commun.* **2011**, *47* (35), 9798–9800.

139 Y. R. Hristova, M. M. J. Smulders, J. K. Clegg, B. Breiner, J. R. Nitschke, *Chem. Sci.* **2011**, *2* (4), 638–641.

140 I. A. Riddell, M. M. J. Smulders, J. K. Clegg, Y. R. Hristova, B. Breiner, J. D. Thoburn, J. R. Nitschke, *Nat. Chem.* **2012**, *4* (9), 751–756.

141 I. A. Riddell, T. K. Ronson, J. K. Clegg, C. S. Wood, R. A. Bilbeisi, J. R. Nitschke, *J. Am. Chem. Soc.* **2014**, *136* (26), 9491–9498.

142 S. Ma, M. M. J. Smulders, Y. R. Hristova, J. K. Clegg, T. K. Ronson, S. Zarra, J. R. Nitschke, *J. Am. Chem. Soc.* **2013**, *135* (15), 5678–5684.

143 I. A. Riddell, T. K. Ronson, J. R. Nitschke, *Chem. Sci.* **2015**, *6* (6), 3533–3537.

144 S. M. Voshell, S. J. Lee, M. R. Gagné, *J. Am. Chem. Soc.* **2006**, *128* (38), 12 422–12 423.

145 M. K. Chung, C. M. Hebling, J. W. Jorgenson, K. Severin, S. J. Lee, M. R. Gagné, *J. Am. Chem. Soc.* **2008**, *130* (35), 11 819–11 827.

146 M. K. Chung, K. Severin, S. J. Lee, M. L. Waters, M. R. Gagné, *Chem. Sci.* **2011**, *2* (4), 744–747.

147 H. Hioki, W. C. Still, *J. Org. Chem.* **1998**, *63* (4), 904–905.

148 L. A. Ingerman, M. E. Cuellar, M. L. Waters, *Chem. Commun.* **2010**, *46* (11), 1839–1841.

149 L. I. James, J. E. Beaver, N. W. Rice, M. L. Waters, *J. Am. Chem. Soc.* **2013**, *135* (17), 6450–6455.

150 N. K. Pinkin, M. L. Waters, *Org. Biomol. Chem.* **2014**, *12* (36), 7059–7067.

151 J. E. Beaver, B. C. Peacor, J. V. Bain, L. James, M. L. Waters, *Org. Biomol. Chem.* **2015**, *13* (11), 3220–3226.

152 M. Rauschenberg, S. Bomke, U. Karst, B. J. Ravoo, *Angew. Chem. Int. Ed.* **2010**, *49* (40), 7340–7345.

153 M. Nakamura, M. Tsutsumi, Y. Ishikawa, H. Umemiya, T. Hasegawa, K. Izawa, H. Abe, Y. Togashi, T. Kinone, S. Sekiguchi, M. Igumi, K. Ide, T. Hasegawa, *Tetrahedron* **2013**, *69* (14), 3019–3026.

154 J. F. Teichert, D. Mazunin, J. W. Bode, *J. Am. Chem. Soc.* **2013**, *135* (30), 11 314–11 321.

155 R. T. S. Lam, A. Belenguer, S. L. Roberts, C. Naumann, T. Jarrosson, S. Otto, J. K. M. Sanders, *Science* **2005**, *308* (5722), 667–669.

156 L. Vial, R. F. Ludlow, J. Leclaire, R. Pérez-Fernandez, S. Otto, *J. Am. Chem. Soc.* **2006**, *128* (31), 10 253–10 257.

157 S. Hamieh, R. F. Ludlow, O. Perraud, K. R. West, E. Mattia, S. Otto, *Org. Lett.* **2012**, *14* (21), 5404–5407.

158 A. L. Kieran, S. I. Pascu, T. Jarrosson, J. K. M. Sanders, *Chem. Commun.* **2005** (10), 1276–1278.

159 T. Haino, H. Mitsuhashi, Y. Ishizu, Y. Fukazawa, *Tetrahedron Lett.* **2006**, *47* (45), 7915–7918.

160 A. R. Lippert, V. L. Keleshian, J. W. Bode, *Org. Biomol. Chem.* **2009**, *7* (8), 1529–1532.

161 A. R. Lippert, A. Naganawa, V. L. Keleshian, J. W. Bode, *J. Am. Chem. Soc.* **2010**, *132* (44), 15 790–15 799.

162 E. Tamanini, G. D. Pantoş, J. K. M. Sanders, *Chem. Eur. J.* **2010**, *16* (1), 81–84.

163 A. R. Stefankiewicz, E. Tamanini, G. D. Pantoş, J. K. M. Sanders, *Angew. Chem. Int. Ed.* **2011**, *50* (25), 5725–5728.

164 D. M. Wood, W. Meng, T. K. Ronson, A. R. Stefankiewicz, J. K. M. Sanders, J. R. Nitschke, *Angew. Chem. Int. Ed.* **2015**, *54* (13), 3988–3992.

165 H. Y. Au-Yeung, P. Pengo, G. D. Pantoş, S. Otto, J. K. M. Sanders, *Chem. Commun.* **2009** (4), 419–421.

166 H. Y. Au-Yeung, F. B. L. Cougnon, S. Otto, G. D. Pantoş, J. K. M. Sanders, *Chem. Sci.* **2010**, *1* (5), 567–574.

167 T. K. Ronson, A. B. League, L. Gagliardi, C. J. Cramer, J. R. Nitschke, *J. Am. Chem. Soc.* **2014**, *136* (44), 15 615–15 624.

168 E. Stulz, S. M. Scott, A. D. Bond, S. J. Teat, J. K. M. Sanders, *Chem. Eur. J.* **2003**, *9* (24), 6039–6048.

169 P. C. M. van Gerven, J. A. A. W. Elemans, J. W. Gerritsen, S. Speller, R. J. M. Nolte, A. E. Rowan, *Chem. Commun.* **2005** (28), 3535–3537.

170 A. L. Kieran, S. I. Pascu, T. Jarrosson, M. J. Gunter, J. K. M. Sanders, *Chem. Commun.* **2005** (14), 1842–1844.

171 M. Rancan, J. Tessarolo, M. Casarin, P. L. Zanonato, S. Quici, L. Armelao, *Inorg. Chem.* **2014**, *53* (14), 7276–7287.

172 J. Leclaire, G. Husson, N. Devaux, V. Delorme, L. Charles, F. Ziarelli, P. Desbois, A. Chaumonnot, M. Jacquin, F. Fotiadu, G. Buono, *J. Am. Chem. Soc.* **2010**, *132* (10), 3582–3593.

173 D. Canevet, E. M. Pérez, N. Martín, *Angew. Chem. Int. Ed.* **2011**, *50* (40), 9248–9259.

174 G. D. Pantoş, P. Pengo, J. K. M. Sanders, *Angew. Chem. Int. Ed.* **2007**, *46* (1–2), 194–197.

175 G. D. Pantoş, J. L. Wietor, J. K. M. Sanders, *Angew. Chem. Int. Ed.* **2007**, *46* (13), 2238–2240.

176 J. L. Wietor, G. D. Pantoş, J. K. M. Sanders, *Angew. Chem. Int. Ed.* **2008**, *47* (14), 2689–2692.

177 A. R. Lippert, J. Kaeobamrung, J. W. Bode, *J. Am. Chem. Soc.* **2006**, *128* (46), 14 738–14 739.

178 C. R. S. Durai, M. M. Harding, *Aust. J. Chem.* **2011**, *64* (6), 671–680.

179 B. M. R. Liénard, R. Hüting, P. Lassaux, M. Galleni, J. M. Frère, C. J. Schofield, *J. Med. Chem.* **2008**, *51* (3), 684–688.

180 D. E. Scott, G. J. Dawes, M. Ando, C. Abell, A. Ciulli, *ChemBioChem* **2009**, *10* (17), 2772–2779.

181 M. Demetriades, I. K. H. Leung, R. Chowdhury, M. C. Chan, M. A. McDonough, K. K. Yeoh, Y. M. Tian, T. D. W. Claridge, P. J. Ratcliffe, E. C. Y. Woon, C. J. Schofield, *Angew. Chem. Int. Ed.* **2012**, *51* (27), 6672–6675.

182 M. Mondal, N. Radeva, H. Köster, A. Park, C. Potamitis, M. Zervou, G. Klebe, A. K. H. Hirsch, *Angew. Chem. Int. Ed.* **2014**, *53* (12), 3259–3263.

183 D. A. Erlanson, J. W. Lam, C. Wiesmann, T. N. Luong, R. L. Simmons, W. L. DeLano, I. C. Choong, M. T. Burdett, W. M. Flanagan, D. Lee, E. M. Gordon, T. O'Brien, *Nat. Biotechnol.* **2003**, *21* (3), 308–314.

184 M. T. Cancilla, M. M. He, N. Viswanathan, R. L. Simmons, M. Taylor, A. D. Fung, K. Cao, D. A. Erlanson, *Bioorg. Med. Chem. Lett.* **2008**, *18* (14), 3978–3981.

185 R. Caraballo, M. Sakulsombat, O. Ramström, *ChemBioChem* **2010**, *11* (11), 1600–1606.

186 M. Sindelar, T. A. Lutz, M. Petrera, K. T. Wanner, *J. Med. Chem.* **2013**, *56* (3), 1323–1340.

187 I. K. H. Leung, M. Demetriades, A. P. Hardy, C. Lejeune, T. J. Smart, A. Szöllössi, A. Kawamura, C. J. Schofield, T. D. W. Claridge, *J. Med. Chem.* **2013**, *56* (2), 547–555.

188 Y. L. Jiang, D. J. Krosky, L. Seiple, J. T. Stivers, *J. Am. Chem. Soc.* **2005**, *127* (49), 17 412–17 420.

189 M. F. Schmidt, A. Isidro-Llobet, M. Lisurek, A. El-Dahshan, J. Tan, R. Hilgenfeld, J. Rademann, *Angew. Chem. Int. Ed.* **2008**, *47* (17), 3275–3278.

190 D. J. Maly, I. C. Choong, J. A. Ellman, *Proc. Natl. Acad. Sci. USA* **2000**, *97* (6), 2419–2424.

191 M. Hochgürtel, H. Kroth, D. Piecha, M. W. Hofmann, C. Nicolau, S. Krause, O. Schaaf, G. Sonnenmoser, A. V. Eliseev, *Proc. Natl. Acad. Sci. USA* **2002**, *99* (6), 3382–3387.

192 O. Ramström, S. Lohmann, T. Bunyapaiboonsri, J. M. Lehn, *Chem. Eur. J.* **2004**, *10* (7), 1711–1715.

193 M. Sindelar, K. T. Wanner, *ChemMedChem* **2012**, *7* (9), 1678–1690.

194 B. Shi, R. Stevenson, D. J. Campopiano, M. F. Greaney, *J. Am. Chem. Soc.* **2006**, *128* (26), 8459–8467.

195 A. J. Clipson, V. T. Bhat, I. McNae, A. M. Caniard, D. J. Campopiano, M. F. Greaney, *Chem. Eur. J.* **2012**, *18* (34), 10 562–10 570.

196 C. S. Mahon, A. W. Jackson, B. S. Murray, D. A. Fulton, *Chem. Commun.* **2011**, *47* (25), 7209–7211.

197 C. S. Mahon, A. W. Jackson, B. S. Murray, D. A. Fulton, *Polym. Chem.* **2013**, *4* (2), 368–377.

198 C. S. Mahon, M. A. Fascione, C. Sakonsinsiri, T. E. McAllister, W. B. Turnbull, D. A. Fulton, *Org. Biomol. Chem.* **2015**, *13* (9), 2756–2761.

199 P. Reeh, J. de Mendoza, *Chem. Eur. J.* **2013**, *19* (17), 5259–5262.

200 R. Larsson, Z. Pei, O. Ramström, *Angew. Chem. Int. Ed.* **2004**, *43* (28), 3716–3718.

201 Y. Zhang, M. Angelin, R. Larsson, A. Albers, A. Simons, O. Ramström, *Chem. Commun.* **2010**, *46* (44), 8457–8459.

202 P. Vongvilai, M. Angelin, R. Larsson, O. Ramström, *Angew. Chem. Int. Ed.* **2007**, *46* (6), 948–950.

203 P. Vongvilai, O. Ramström, *J. Am. Chem. Soc.* **2009**, *131* (40), 14 419–14 425.

204 C. Karan, B. L. Miller, *J. Am. Chem. Soc.* **2001**, *123* (30), 7455–7456.

205 C. Bouillon, D. Paolantoni, J. C. Rote, Y. Bessin, L. W. Peterson, P. Dumy, S. Ulrich, *Chem. Eur. J.* **2014**, *20* (45), 14 705–14 714.

206 E. Bartolami, Y. Bessin, V. Gervais, P. Dumy, S. Ulrich, *Angew. Chem. Int. Ed.* **2015**, *54* (35), 10 183–10 187.

207 B. R. McNaughton, P. C. Gareiss, B. L. Miller, *J. Am. Chem. Soc.* **2007**, *129* (37), 11 306–11 307.

208 P. C. Gareiss, K. Sobczak, B. R. McNaughton, P. B. Palde, C. A. Thornton, B. L. Miller, *J. Am. Chem. Soc.* **2008**, *130* (48), 16 254–16 261.

209 A. M. Whitney, S. Ladame, S. Balasubramanian, *Angew. Chem. Int. Ed.* **2004**, *43* (9), 1143–1146.

210 A. Bugaut, K. Jantos, J. L. Wietor, R. Rodriguez, J. K. M. Sanders, S. Balasubramanian, *Angew. Chem. Int. Ed.* **2008**, *47* (14), 2677–2680.

211 M. C. Nielsen, T. Ulven, *Chem. Eur. J.* **2008**, *14* (31), 9487–9490.

212 G. Gasparini, L. J. Prins, P. Scrimin, *Angew. Chem. Int. Ed.* **2008**, *47* (13), 2475–2479.

213 G. Gasparini, M. Dal Molin, S. Corrà, P. Galzerano, P. Scrimin, L. J. Prins, *Isr. J. Chem.* **2013**, *53* (1–2), 122–126.

214 H. Fanlo-Virgós, A. N. R. Alba, S. Hamieh, M. Colomb-Delsuc, S. Otto, *Angew. Chem. Int. Ed.* **2014**, *53* (42), 11 346–11 350.

215 J. Solà, M. Lafuente, J. Atcher, I. Alfonso, *Chem. Commun.* **2014**, *50* (35), 4564–4566.

216 H. Jędrzejewska, M. Wierzbicki, P. Cmoch, K. Rissanen, A. Szumna, *Angew. Chem. Int. Ed.* **2014**, *53* (50), 13 760–13 764.

217 V. del Amo, D. Philp, *Chem. Eur. J.* **2010**, *16* (45), 13 304–13 318.

218 V. del Amo, A. M. Z. Slawin, D. Philp, *Org. Lett.* **2008**, *10* (20), 4589–4592.

219 J. M. A. Carnall, C. A. Waudby, A. M. Belenguer, M. C. A. Stuart, J. J. P. Peyralans, S. Otto, *Science* **2010**, *327* (5972), 1502–1506.

220 R. Nguyen, L. Allouche, E. Buhler, N. Giuseppone, *Angew. Chem. Int. Ed.* **2009**, *48* (6), 1093–1096.

221 S. Xu, N. Giuseppone, *J. Am. Chem. Soc.* **2008**, *130* (6), 1826–1827.

222 M. Malakoutikhah, J. J. P. Peyralans, M. Colomb-Delsuc, H. Fanlo-Virgós, M. C. A. Stuart, S. Otto, *J. Am. Chem. Soc.* **2013**, *135* (49), 18 406–18 417.

223 M. Colomb-Delsuc, E. Mattia, J. W. Sadownik, S. Otto, *Nat. Commun.* **2015**, *6*, 7427.

224 G. Leonetti, S. Otto, *J. Am. Chem. Soc.* **2015**, *137* (5), 2067–2072.

225 A. Pal, M. Malakoutikhah, G. Leonetti, M. Tezcan, M. Colomb-Delsuc, V. D. Nguyen, J. van der Gucht, S. Otto, *Angew. Chem. Int. Ed.* **2015**, *54* (27), 7852–7856.

226 C. B. Minkenberg, L. Florusse, R. Eelkema, G. J. M. Koper, J. H. van Esch, *J. Am. Chem. Soc.* **2009**, *131* (32), 11 274–11 275.

227 B. Rubinov, N. Wagner, H. Rapaport, G. Ashkenasy, *Angew. Chem. Int. Ed.* **2009**, *48* (36), 6683–6686.

228 Z. Dadon, M. Samiappan, E. Y. Safranchik, G. Ashkenasy, *Chem. Eur. J.* **2010**, *16* (40), 12 096–12 099.

229 Z. Dadon, M. Samiappan, N. Wagner, G. Ashkenasy, *Chem. Commun.* **2012**, *48* (10), 1419–1421.

230 Z. Dadon, M. Samiappan, A. Shahar, R. Zarivach, G. Ashkenasy, *Angew. Chem. Int. Ed.* **2013**, *52* (38), 9944–9947.

231 Z. Dadon, N. Wagner, S. Alasibi, M. Samiappan, R. Mukherjee, G. Ashkenasy, *Chem. Eur. J.* **2015**, *21* (2), 648–654.

232 W. Wang, L. Wang, B. J. Palmer, G. J. Exarhos, A. D. Q. Li, *J. Am. Chem. Soc.* **2006**, *128* (34), 11 150–11 159.

233 K. R. West, R. F. Ludlow, P. T. Corbett, P. Besenius, F. M. Mansfeld, P. A. G. Cormack, D. C. Sherrington, J. M. Goodman, M. C. A. Stuart, S. Otto, *J. Am. Chem. Soc.* **2008**, *130* (33), 10 834–10 835.

234 H. Y. Au-Yeung, G. D. Pantos, J. K. M. Sanders, *Proc. Natl. Acad. Sci. USA* **2009**, *106* (26), 10 466–10 470.

235 H. Y. Au-Yeung, G. D. Pantoş, J. K. M. Sanders, *J. Am. Chem. Soc.* **2009**, *131* (44), 16 030–16 032.

236 H. Y. Au-Yeung, G. D. Pantoş, J. K. M. Sanders, *Angew. Chem. Int. Ed.* **2010**, *49* (31), 5331–5334.

237 F. B. L. Cougnon, N. A. Jenkins, G. D. Pantoş, J. K. M. Sanders, *Angew. Chem. Int. Ed.* **2012**, *51* (6), 1443–1447.

238 F. B. L. Cougnon, N. Ponnuswamy, N. A. Jenkins, G. D. Pantoş, J. K. M. Sanders, *J. Am. Chem. Soc.* **2012**, *134* (46), 19 129–19 135.

239 F. B. L. Cougnon, H. Y. Au-Yeung, G. D. Pantoş, J. K. M. Sanders, *J. Am. Chem. Soc.* **2011**, *133* (9), 3198–3207.

240 K. S. Chichak, S. J. Cantrill, A. R. Pease, S. H. Chiu, G. W. V. Cave, J. L. Atwood, J. F. Stoddart, *Science* **2004**, *304* (5675), 1308–1312.

241 C. D. Pentecost, K. S. Chichak, A. J. Peters, G. W. V. Cave, S. J. Cantrill, J. F. Stoddart, *Angew. Chem. Int. Ed.* **2007**, *46* (1–2), 218–222.

242 J. F. Ayme, J. E. Beves, D. A. Leigh, R. T. McBurney, K. Rissanen, D. Schultz, *Nat. Chem.* **2012**, *4* (1), 15–20.

243 J. E. Beves, C. J. Campbell, D. A. Leigh, R. G. Pritchard, *Angew. Chem. Int. Ed.* **2013**, *52* (25), 6464–6467.

244 J. F. Ayme, J. E. Beves, C. J. Campbell, D. A. Leigh, *Angew. Chem. Int. Ed.* **2014**, *53* (30), 7823–7827.

245 C. Browne, T. K. Ronson, J. R. Nitschke, *Angew. Chem. Int. Ed.* **2014**, *53* (40), 10 701–10 705.

246 P. C. Haussmann, S. I. Khan, J. F. Stoddart, *J. Org. Chem.* **2007**, *72* (18), 6708–6713.

247 N. Ponnuswamy, F. B. L. Cougnon, J. M. Clough, G. D. Pantoş, J. K. M. Sanders, *Science* **2012**, *338* (6108), 783–785.

248 N. Ponnuswamy, F. B. L. Cougnon, G. D. Pantoş, J. K. M. Sanders, *J. Am. Chem. Soc.* **2014**, *136* (23), 8243–8251.

249 K. Oh, K. S. Jeong, J. S. Moore, *Nature* **2001**, *414* (6866), 889–893.

250 T. Nishinaga, A. Tanatani, K. Oh, J. S. Moore, *J. Am. Chem. Soc.* **2002**, *124* (21), 5934–5935.

251 D. Zhao, J. S. Moore, *J. Am. Chem. Soc.* **2002**, *124* (34), 9996–9997.

252 S. Fujii, J. M. *Angew. Chem. Int. Ed.* **2009**, *48* (41), 7635–7638.

253 N. Giuseppone, J. M. Lehn, *Angew. Chem. Int. Ed.* **2006**, *45* (28), 4619–4624.

254 A. Herrmann, N. Giuseppone, J. M. Lehn, *Chem. Eur. J.* **2009**, *15* (1), 117–124.

255 J. Atcher, A. Moure, I. Alfonso, *Chem. Commun.* **2013**, *49* (5), 487–489.

256 J. Atcher, A. Moure, J. Bujons, I. Alfonso, *Chem. Eur. J.* **2015**, *21* (11), 6869–6878.

257 K. Baek, G. Yun, Y. Kim, D. Kim, R. Hota, I. Hwang, D. Xu, Y. H. Ko, G. H. Gu, J. H. Suh, C. G. Park, B. J. Sung, K. Kim, *J. Am. Chem. Soc.* **2013**, *135* (17), 6523–6528.

258 J. Kim, K. Baek, D. Shetty, N. Selvapalam, G. Yun, N. H. Kim, Y. H. Ko, K. M. Park, I. Hwang, K. Kim, *Angew. Chem. Int. Ed.* **2015**, *54* (9), 2693–2697.

259 J. F. Folmer-Andersen, J. M. Lehn, *Angew. Chem. Int. Ed.* **2009**, *48* (41), 7664–7667.

260 S. Di Stefano, M. Mazzonna, E. Bodo, L. Mandolini, O. Lanzalunga, *Org. Lett.* **2011**, *13* (1), 142–145.

261 S. Ji, W. Cao, Y. Yu, H. Xu, *Angew. Chem. Int. Ed.* **2014**, *53* (26), 6781–6785.

262 L. A. Ingerman, M. L. Waters, *J. Org. Chem.* **2009**, *74* (1), 111–117.

263 M. N. Chaur, D. Collado, J. M. Lehn, *Chem. Eur. J.* **2011**, *17* (1), 248–258.

264 G. Vantomme, J. M. Lehn, *Angew. Chem. Int. Ed.* **2013**, *52* (14), 3940–3943.

265 G. Vantomme, S. Jiang, J. M. Lehn, *J. Am. Chem. Soc.* **2014**, *136* (26), 9509–9518.

266 G. Vantomme, N. Hafezi, J. M. Lehn, *Chem. Sci.* **2014**, *5* (4), 1475–1483.

267 L. Ratjen, J. M. Lehn, *RSC Adv.* **2014**, *4* (92), 50 554–50 557.

268 J. Li, J. M. A. Carnall, M. C. A. Stuart, S. Otto, *Angew. Chem. Int. Ed.* **2011**, *50* (36), 8384–8386.

269 J. F. Folmer-Andersen, J. M. Lehn, *J. Am. Chem. Soc.* **2011**, *133* (28), 10 966–10 973.

270 A. M. Belenguer, T. Friščić, G. M. Day, J. K. M. Sanders, *Chem. Sci.* **2011**, *2* (4), 696–700.

271 A. M. Belenguer, G. I. Lampronti, D. J. Wales, J. K. M. Sanders, *J. Am. Chem. Soc.* **2014**, *136* (46), 16 156–16 166.

272 R. Pérez-Fernández, M. Pittelkow, A. M. Belenguer, J. K. M. Sanders, *Chem. Commun.* **2008** (15), 1738–1740.

273 B. Duncan, X. Li, R. F. Landis, S. T. Kim, A. Gupta, L. S. Wang, R. Ramanathan, R. Tang, J. A. Boerth, V. M. Rotello, *ACS Nano* **2015**, *9* (11), 7775–7782.

274 N. Hafezi, J. M. Lehn, *J. Am. Chem. Soc.* **2012**, *134* (30), 12 861–12 868.

275 V. Saggiomo, C. Goeschen, R. Herges, R. Quesada, U. Lüning, *Eur. J. Org. Chem.* **2010** (12), 2337–2343.

276 J. Montenegro, A. Fin, S. Matile, *Org. Biomol. Chem.* **2011**, 9 (8), 2641–2647.

277 J. Montenegro, E. K. Bang, N. Sakai, S. Matile, *Chem. Eur. J.* **2012**, *18* (33), 10 436–10 443.

278 C. Gehin, J. Montenegro, E. K. Bang, A. Cajaraville, S. Takayama, H. Hirose, S. Futaki, S. Matile, H. Riezman, *J. Am. Chem. Soc.* **2013**, *135* (25), 9295–9298.

279 X. Wu, N. Busschaert, N. J. Wells, Y. B. Jiang, P. A. Gale, *J. Am. Chem. Soc.* **2015**, *137* (4), 1476–1484.

280 G. Gasparini, E. K. Bang, G. Molinard, D. V. Tulumello, S. Ward, S. O. Kelley, A. Roux, N. Sakai, S. Matile, *J. Am. Chem. Soc.* **2014**, *136* (16), 6069–6074.

281 G. Gasparini, G. Sargsyan, E. K. Bang, N. Sakai, S. Matile, *Angew. Chem. Int. Ed.* **2015**, *54* (25), 7328–7331.

282 E. K. Bang, G. Gasparini, G. Molinard, A. Roux, N. Sakai, S. Matile, *J. Am. Chem. Soc.* **2013**, *135* (6), 2088–2091.

283 G. Gasparini, E. K. Bang, J. Montenegro, S. Matile, *Chem. Commun.* **2015**, *51* (52), 10 389–10 402.

284 R. Nguyen, E. Buhler, N. Giuseppone, *Macromolecules* **2009**, *42* (16), 5913–5915.

285 N. Jouault, R. Nguyen, M. Rawiso, N. Giuseppone, E. Buhler, *Soft Matter* **2011**, *7* (10), 4787–4800.

286 R. Nguyen, N. Jouault, S. Zanirati, M. Rawiso, L. Allouche, G. Fuks, E. Buhler, N. Giuseppone, *Soft Matter* **2014**, *10* (22), 3926–3937.

287 C. B. Minkenberg, F. Li, P. van Rijn, L. Florusse, J. Boekhoven, M. C. A. Stuart, G. J. M. Koper, R. Eelkema, J. H. van Esch, *Angew. Chem. Int. Ed.* **2011**, *50* (15), 3421–3424.

288 C. B. Minkenberg, B. Homan, J. Boekhoven, B. Norder, G. J. M. Koper, R. Eelkema, J. H. van Esch, *Langmuir* **2012**, *28* (38), 13 570–13 576.

289 C. Wang, G. Wang, Z. Wang, X. Zhang, *Chem. Eur. J.* **2011**, *17* (12), 3322–3325.

290 G. Wang, C. Wang, Z. Wang, X. Zhang, *Langmuir* **2011**, *27* (20), 12 375–12 380.

291 G. Wang, C. Wang, Z. Wang, X. Zhang, *Langmuir* **2012**, *28* (41), 14 567–14 572.

292 G. Wang, G. Wu, Z. Wang, X. Zhang, *Langmuir* **2014**, *30* (6), 1531–1535.

293 Y. Kang, K. Liu, X. Zhang, *Langmuir* **2014**, *30* (21), 5989–6001.

294 B. R. McNaughton, B. L. Miller, *Org. Lett.* **2006**, *8* (9), 1803–1806.

295 A. V. Gromova, J. M. Ciszewski, B. L. Miller, *Chem. Commun.* **2012**, *48* (15), 2131–2133.

296 P. Besenius, P. A. G. Cormack, R. F. Ludlow, S. Otto, D. C. Sherrington, *Org. Biomol. Chem.* **2010**, *8* (10), 2414–2418.

297 G. Gasparini, F. Rastrelli, L. J. Prins, *Org. Biomol. Chem.* **2013**, *11* (38), 6580–6587.

298 A. K. Boal, V. M. Rotello, *J. Am. Chem. Soc.* **2000**, *122* (4), 734–735.

299 M. J. Hostetler, S. J. Green, J. J. Stokes, R. W. Murray, *J. Am. Chem. Soc.* **1996**, *118* (17), 4212–4213.

300 A. Verma, H. Nakade, J. M. Simard, V. M. Rotello, *J. Am. Chem. Soc.* **2004**, *126* (35), 10 806–10 807.

301 D. M. Andala, S. H. R. Shin, H. Y. Lee, K. J. M. Bishop, *ACS Nano* **2012**, *6* (2), 1044–1050.

302 H. Y. Lee, S. H. R. Shin, L. L. Abezgauz, S. A. Lewis, A. M. Chirsan, D. D. Danino, K. J. M. Bishop, *J. Am. Chem. Soc.* **2013**, *135* (16), 5950–5953.

303 S. H. R. Shin, H. Y. Lee, K. J. M. Bishop, *Angew. Chem. Int. Ed.* **2015**, *54* (37), 10 816–10 820.

304 H. Y. Lee, S. H. R. Shin, A. M. Drews, A. M. Chirsan, S. A. Lewis, K. J. M. Bishop, *ACS Nano* **2014**, *8* (10), 9979–9987.

305 R. Klajn, K. J. M. Bishop, B. A. Grzybowski, *Proc. Natl. Acad. Sci. USA* **2007**, *104* (25), 10 305–10 309.

306 C. Franceschini, P. Scrimin, L. J. Prins, *Langmuir* **2014**, *30* (46), 13 831–13 836.

307 Y. Han, P. Nowak, M. Colomb-Delsuc, M. Pernia Leal, S. Otto, *Langmuir* **2015**, *31*, 12658–12663.

308 S. Maiti, L. J. Prins, *Chem. Commun.* **2015**, *51* (26), 5714–5716.

309 F. M. Mansfeld, H. Y. Au-Yeung, J. K. M. Sanders, S. Otto, *J. Syst. Chem.* **2010**, *1* (1), 12.

310 T. Chang, D. I. Rozkiewicz, B. J. Ravoo, E. W. Meijer, D. N. Reinhoudt, *Nano Lett.* **2007**, *7* (4), 978–980.

311 L. Tauk, A. P. Schröder, G. Decher, N. Giuseppone, *Nat. Chem.* **2009**, *1* (8), 649–656.

312 N. Sakai, M. Lista, O. Kel, S. I. Sakurai, D. Emery, J. Mareda, E. Vauthey, S. Matile, *J. Am. Chem. Soc.* **2011**, *133* (39), 15 224–15 227.

313 A. Carmine, Y. Domoto, N. Sakai, S. Matile, *Chem. Eur. J.* **2013**, *19* (35), 11558–11563.

314 E. Orentas, M. Lista, N. T. Lin, N. Sakai, S. Matile, *Nat. Chem.* **2012**, *4* (9), 746–750.

315 N. Sakai, S. Matile, *J. Am. Chem. Soc.* **2011**, *133* (46), 18 542–18 545.

316 M. Lista, E. Orentas, J. Areephong, P. Charbonnaz, A. Wilson, Y. Zhao, A. Bolag, G. Sforazzini, R. Turdean, H. Hayashi, Y. Domoto, A. Sobczuk, N. Sakai, S. Matile, *Org. Biomol. Chem.* **2013**, *11* (11), 1754–1765.

317 K. D. Zhang, S. Matile, *Angew. Chem. Int. Ed.* **2015**, *54* (31), 8980–8983.

318 K. D. Zhang, N. Sakai, S. Matile, *Org. Biomol. Chem.* **2015**, *13* (32), 8687–8694.

319 A. Ciesielski, M. El Garah, S. Haar, P. Kovaříček, J. M. Lehn, P. Samorì, *Nat. Chem.* **2014**, *6* (11), 1017–1023.

320 A. G. L. Olive, N. H. Abdullah, I. Ziemecka, E. Mendes, R. Eelkema, J. H. van Esch, *Angew. Chem. Int. Ed.* **2014**, *53* (16), 4132–4136.

321 J. Boekhoven, J. M. Poolman, C. Maity, F. Li, L. van der Mee, C. B. Minkenberg, E. Mendes, J. H. van Esch, R. Eelkema, *Nat. Chem.* **2013**, *5* (5), 433–437.

322 P. N. W. Baxter, J. M. Lehn, K. Rissanen, *Chem. Commun.* **1997** (14), 1323–1324.

323 M. Hutin, C. J. Cramer, L. Gagliardi, A. R. M. Shahi, G. Bernardinelli, R. Cerny, J. R. Nitschke, *J. Am. Chem. Soc.* **2007**, *129* (28), 8774–8780.

324 M. Angelin, A. Fischer, O. Ramström, *J. Org. Chem.* **2008**, *73* (9), 3593–3595.

325 M. Angelin, M. Rahm, A. Fischer, T. Brinck, O. Ramström, *J. Org. Chem.* **2010**, *75* (17), 5882–5887.

326 M. Angelin, P. Vongvilai, A. Fischer, O. Ramström, *Eur. J. Org. Chem.* **2010** (33), 6315–6318.

327 N. Iwasawa, H. Takahagi, *J. Am. Chem. Soc.* **2007**, *129* (25), 7754–7755.

328 H. Takahagi, N. Iwasawa, *Chem. Eur. J.* **2010**, *16* (46), 13 680–13 688.

329 S. Ito, K. Ono, N. Iwasawa, *J. Am. Chem. Soc.* **2012**, *134* (34), 13 962–13 965.

330 M. Barboiu, F. Dumitru, Y. M. Legrand, E. Petit, A. van der Lee, *Chem. Commun.* **2009** (16), 2192–2194.

331 F. Dumitru, Y. M. Legrand, E. Petit, A. van der Lee, M. Barboiu, *Dalton Trans.* **2012**, *41* (38), 11 860–11 865.

332 M. Rancan, J. Tessarolo, P. L. Zanonato, R. Seraglia, S. Quici, L. Armelao, *Dalton Trans.* **2013**, *42* (21), 7534–7538.

333 I. Kocsis, D. Dumitrescu, Y. M. Legrand, A. van der Lee, I. Grosu, M. Barboiu, *Chem. Commun.* **2014**, *50* (20), 2621–2623.

334 K. Ziach, J. Jurczak, *Chem. Commun.* **2015**, *51* (20), 4306–4309.

335 K. Ziach, J. Jurczak, *Cryst. Growth Des.* **2015**, *15*, 4372–4376.

336 D. K. Kondepudi, R. J. Kaufman, N. Singh, *Science* **1990**, *250* (4983), 975–976.

337 C. Viedma, *Phys. Rev. Lett.* **2005**, *94* (6), 065 504.

338 W. L. Noorduin, E. Vlieg, R. M. Kellogg, B. Kaptein, *Angew. Chem. Int. Ed.* **2009**, *48* (51), 9600–9606.

339 Q. Ji, O. Š. Miljanić, *J. Org. Chem*. **2013**, *78* (24), 12 710–12 716.

340 C. W. Hsu, O. Š. Miljanić, *Angew. Chem. Int. Ed.* **2015**, *54* (7), 2219–2222.

341 B. Levrand, Y. Ruff, J. M. Lehn, A. Herrmann, *Chem. Commun.* **2006** (28), 2965–2967.

342 B. Levrand, W. Fieber, J. M. Lehn, A. Herrmann, *Helv. Chim. Acta* **2007**, *90* (12), 2281–2314.

343 B. Buchs, W. Fieber, F. Vigouroux-Elie, N. Sreenivasachary, J. M. Lehn, A. Herrmann, *Org. Biomol. Chem.* **2011**, *9* (8), 2906–2919.

344 G. Godin, B. Levrand, A. Trachsel, J. M. Lehn, A. Herrmann, *Chem. Commun.* **2010**, *46* (18), 3125–3127.

345 J. M. Lehn, *Angew. Chem. Int. Ed.* **1990**, *29* (11), 1304–1319.

346 N. Giuseppone, J. M. Lehn, *J. Am. Chem. Soc.* **2004**, *126* (37), 11 448–11 449.

347 N. Giuseppone, G. Fuks, J. M. Lehn, *Chem. Eur. J.* **2006**, *12* (6), 1723–1735.

348 A. Buryak, K. Severin, *Angew. Chem. Int. Ed.* **2005**, *44* (48), 7935–7938.

349 A. Buryak, K. Severin, *J. Comb. Chem.* **2006**, *8* (4), 540–543.

350 Z. Köstereli, R. Scopelliti, K. Severin, *Chem. Sci.* **2014**, *5* (6), 2456–2460.

351 K. K. Larson, M. He, J. F. Teichert, A. Naganawa, J. W. Bode, *Chem. Sci.* **2012**, *3* (6), 1825–1828.

352 S. L. Wiskur, P. N. Floriano, E. V. Anslyn, J. T. McDevitt, *Angew. Chem. Int. Ed.* **2003**, *42* (18), 2070–2072.

353 L. You, J. S. Berman, E. V. Anslyn, *Nat. Chem.* **2011**, *3* (12), 943–948.

354 L. You, S. R. Long, V. M. Lynch, E. V. Anslyn, *Chem. Eur. J.* **2011**, *17* (39), 11 017–11 023.

355 J. M. Dragna, G. Pescitelli, L. Tran, V. M. Lynch, E. V. Anslyn, L. Di Bari, *J. Am. Chem. Soc.* **2012**, *134* (9), 4398–4407.

356 T. Takeuchi, J. Montenegro, A. Hennig, S. Matile, *Chem. Sci.* **2011**, *2* (2), 303–307.

357 F. V. Reddavide, W. Lin, S. Lehnert, Y. Zhang, *Angew. Chem. Int. Ed.* **2015**, *54*, 7924–7928.

358 R. M. Franzini, D. Neri, J. Scheuermann, *Acc. Chem. Res.* **2014**, *47* (4), 1247–1255.

359 M. Ciaccia, I. Tosi, L. Baldini, R. Cacciapaglia, L. Mandolini, S. Di Stefano, C. A. Hunter, *Chem. Sci.* **2015**, *6* (1), 144–151.

360 G. M. Whitesides, B. A. Grzybowski, *Science* **2002**, *295* (5564), 2418–2421.

361 Y. Zhang, M. Barboiu, *Chem. Rev.* **2016**, *116* (3), 809–834.

362 N. Giuseppone, *Acc. Chem. Res.* **2012**, *45* (12), 2178–2188.

363 R. J. Williams, A. M. Smith, R. Collins, N. Hodson, A. K. Das, R. V. Ulijn, *Nat. Nanotechnol.* **2009**, *4* (1), 19–24.

364 J. W. Sadownik, R. V. Ulijn, *Chem. Commun.* **2010**, *46* (20), 3481–3483.

365 D. Janeliunas, P. van Rijn, J. Boekhoven, C. B. Minkenberg, J. H. van Esch, R. Eelkema, *Angew. Chem. Int. Ed.* **2013**, *52* (7), 1998–2001.

366 P. Nowak, M. Colomb-Delsuc, S. Otto, J. Li, *J. Am. Chem. Soc.* **2015**, *137*, 10 965–10 969.

367 W. R. Browne, B. L. Feringa, *Nat. Nanotechnol.* **2006**, *1* (1), 25–35.

368 A. Coskun, M. Banaszak, R. D. Astumian, J. F. Stoddart, B. A. Grzybowski, *Chem. Soc. Rev.* **2012**, *41* (1), 19–30.

369 M. von Delius, E. M. Geertsema, D. A. Leigh, D. T. D. Tang, M. V. Delius, *J. Am. Chem. Soc.* **2010**, *132* (45), 16 134–16 145.

370 M. J. Barrell, A. G. A. Campañ, M. von Delius, E. M. Geertsema, D. A. Leigh, *Angew. Chem. Int. Ed.* **2011**, *50* (1), 285–290.

371 A. G. Campaña, A. Carlone, K. Chen, D. T. F. Dryden, D. A. Leigh, U. Lewandowska, K. M. Mullen, *Angew. Chem. Int. Ed.* **2012**, *51* (22), 5480–5483.

372 P. Kovaříček, J. M. Lehn, *Chem. Eur. J.* **2015**, *21* (26), 9380–9384.

373 B. Schwanhäusser, D. Busse, N. Li, G. Dittmar, J. Schuchhardt, J. Wolf, W. Chen, M. Selbach, *Nature* **2011**, *473* (7347), 337–342.

374 M. Fialkowski, K. J. M. Bishop, R. Klajn, S. K. Smoukov, C. J. Campbell, B. A. Grzybowski, *J. Phys. Chem. B* **2006**, *110* (6), 2482–2496.

375 R. Klajn, P. J. Wesson, K. J. M. Bishop, B. A. Grzybowski, *Angew. Chem. Int. Ed.* **2009**, *48* (38), 7035–7039.

376 S. O. Krabbenborg, J. Veerbeek, J. Huskens, *Chem. Eur. J.* **2015**, *21* (27), 9638–9644.

377 J. Boekhoven, A. M. Brizard, K. N. K. Kowlgi, G. J. M. Koper, R. Eelkema, J. H. van Esch, *Angew. Chem. Int. Ed.* **2010**, *49* (28), 4825–4828.

378 S. Debnath, S. Roy, R. V. Ulijn, *J. Am. Chem. Soc.* **2013**, *135* (45), 16 789–16 792.

379 C. G. Pappas, I. R. Sasselli, R. V. Ulijn, *Angew. Chem. Int. Ed.* **2015**, *54* (28), 8119–8123.

380 S. Otto, R. L. E. Furlan, J. K. M. Sanders, *J. Am. Chem. Soc.* **2000**, *122* (48), 12 063–12 064.

381 S. Zameo, B. Vauzeilles, J. M. Beau, *Eur. J. Org. Chem.* **2006** (24), 5441–5444.

382 L. A. Wessjohann, D. G. Rivera, F. León, *Org. Lett.* **2007**, *9* (23), 4733–4736.

383 L. Roy, M. A. Case, *J. Am. Chem. Soc.* **2010**, *132* (26), 8894–8896.

384 L. Roy, M. A. Case, *J. Phys. Chem. B* **2011**, *115* (10), 2454–2464.

385 D. A. Fulton, *Org. Lett.* **2008**, *10* (15), 3291–3294.

386 B. S. Murray, D. A. Fulton, *Macromolecules* **2011**, *44* (18), 7242–7252.

387 A. Sanchez-Sanchez, D. A. Fulton, J. A. Pomposo, *Chem. Commun.* **2014**, *50* (15), 1871–1874.

388 H. Schiltz, M. K. Chung, S. J. Lee, M. R. Gagné, *Org. Biomol. Chem.* **2008**, *6* (19), 3597–3600.

389 B. Brusilowskij, E. V. Dzyuba, R. W. Troff, C. A. Schalley, *Chem. Commun.* **2011**, *47* (6), 1830–1832.

390 H. I. A. Phillips, A. V. Chernikov, N. C. Fletcher, A. E. Ashcroft, J. R. Ault, M. H. Filby, A. J. Wilson, *Chem. Eur. J.* **2012**, *18* (43), 13 733–13 742.

391 S. A. Poulsen, P. J. Gates, G. R. Cousins, J. K. Sanders, *Rapid Commun. Mass Spectrom.* **2000**, *14* (1), 44–48.

392 H. F. Nour, T. Islam, M. Fernández-Lahore, N. Kuhnert, *Rapid Commun. Mass Spectrom.* **2012**, *26* (24), 2865–2876.

393 S. P. Black, A. R. Stefankiewicz, M. M. J. Smulders, D. Sattler, C. A. Schalley, J. R. Nitschke, J. K. M. Sanders, *Angew. Chem. Int. Ed.* **2013**, *52* (22), 5749–5752.

394 X. Li, Y. T. Chan, M. Casiano-Maldonado, J. Yu, G. A. Carri, G. R. Newkome, C. Wesdemiotis, *Anal. Chem.* **2011**, *83* (17), 6667–6674.

395 X. Li, Y. T. Chan, G. R. Newkome, C. Wesdemiotis, *Anal. Chem.* **2011**, *83* (4), 1284–1290.

396 R. Cacciapagliaa, S. Di Stefanoa, L. Mandolinia, *J. Phys. Org. Chem.* **2008**, *21* (7–8), 688–693.

397 J. A. Berrocal, R. Cacciapaglia, S. D. Stefano, *Org. Biomol. Chem.* **2011**, *9* (23), 8190–8194.

398 M. Dal Molin, G. Gasparini, P. Scrimin, F. Rastrelli, L. J. Prins, *Chem. Commun.* **2011**, *47* (46), 12 476–12 478.

399 B. Meyer, T. Peters, *Angew. Chem. Int. Ed.* **2003**, *42* (8), 864–890.

400 R. Caraballo, H. Dong, J. P. Ribeiro, J. Jiménez-Barbero, O. Ramström, *Angew. Chem. Int. Ed.* **2010**, *49* (3), 589–593.

401 C. Dalvit, G. Fogliatto, A. Stewart, M. Veronesi, B. Stockman, *J. Biomol. NMR* **2001**, *21* (4), 349–359.

402 G. Gasparini, B. Vitorge, P. Scrimin, D. Jeannerat, L. J. Prins, *Chem. Commun*. **2008** (26), 3034–3036.

403 N. Giuseppone, J. L. Schmitt, L. Allouche, J. M. Lehn, *Angew. Chem. Int. Ed.* **2008**, *47* (12), 2235–2239.

404 G. Gasparini, F. Bettin, P. Scrimin, L. Prins, *Angew. Chem. Int. Ed.* **2009**, *48* (25), 4546–4550.

405 A. Ciesielski, S. Lena, S. Masiero, G. P. Spada, P. Samorì, *Angew. Chem. Int. Ed.* **2010**, *49* (11), 1963–1966.

406 A. P. Bapat, J. G. Ray, D. A. Savin, B. S. Sumerlin, *Macromolecules* **2013**, *46* (6), 2188–2198.

407 F. M. Mansfeld, G. Feng, S. Otto, *Org. Biomol. Chem.* **2009**, *7* (20), 4289–4295.

408 M. S. Congreve, D. J. Davis, L. Devine, C. Granata, M. O'Reilly, P. G. Wyatt, H. Jhoti, *Angew. Chem. Int. Ed.* **2003**, *42* (37), 4479–4482.

409 A. P. Bapat, D. Roy, J. G. Ray, D. A. Savin, B. S. Sumerlin, *J. Am. Chem. Soc*. **2011**, *133* (49), 19 832–19 838.

410 J. Li, P. Nowak, H. Fanlo-Virgós, S. Otto, *Chem. Sci.* **2014**, *5* (12), 4968–4974.

411 G. Li, W. Zheng, Z. Chen, Y. Zhou, Y. Liu, J. Yang, Y. Huang, X. Li, *Chem. Sci.* **2015**, *6* (12), 7097–7104.

412 A. Pross, *J. Syst. Chem.* **2011**, *2* (1), 1.

413 R. Pascal, A. Pross, J. D. Sutherland, *Open Biol*. **2013**, *3* (11), 130 156.

414 H. W. H. van Roekel, B. J. H. M. Rosier, L. H. H. Meijer, P. A. J. Hilbers, A. J. Markvoort, W. T. S. Huck, T. F. A. de Greef, *Chem. Soc. Rev.* **2015**, *44* (21), 7465–7483.

415 J. M. P. Gutierrez, T. Hinkley, J. W. Taylor, K. Yanev, L. Cronin, *Nat. Commun.* **2014**, *5*, 5571.

3

Shape-persistent Macrocycles through Dynamic Covalent Reactions

Chao Yu, Yinghua Jin, and Wei Zhang

3.1 Introduction and Importance of Shape-persistent Macrocycles

Shape-persistent macrocycles are defined as cyclic oligomeric analogues of rigid polymers with a non-collapsible backbone and an inside cavity in the size range from slightly less than 1 nm up to several nanometers.[1] Compared to polymers, shape-persistent macrocycles are notable for their reproducibility, monodispersity, homogeneity, and potentially high solid state order.[2] Furthermore, they can be constructed in a systematic way with an array of diverse building blocks and thus their solubility, functionality, and stability can be easily controlled. The shape persistency brings minimal conformational heterogeneity and thus many interesting properties have evolved (see details below).[1,3–9]

This chapter focuses on shape-persistent macrocycles prepared via dynamic covalent reactions and their applications. Macrocycles that are assembled through metal ligand coordination or irreversible covalent reactions, and rather flexible rings with methylenes in the backbones will not be covered. This excludes (i) the impressive work on metallacycles by Fujita[10] and Stang,[11] (ii) rigid macrocycles prepared through irreversible covalent reactions (such as cross-coupling, the McMurry reaction, azide-alkyne cycloaddition, and amide formation) by Anderson,[12–14] De Feyter,[15–18] Flood,[19,20] Gong,[21–23] Haley,[24–27] Höger,[1,7,28] Iyoda,[29–32] Li,[33] Schlüter,[4] Tobe,[34,35] Toyota,[36,37] Youngs,[38] Zeng,[39] and many other researchers (comprehensive reviews on allene-containing macrocycles,[9,40,41] azo-containing macrocycles,[42,43] ethynyl–ethylene-containing macrocycles,[44–46] paraphenylene–acetylenes,[47] and paraphenylenes[48–50] have been published and interested readers can refer to cited references), and (iii) flexible rings prepared through disulfide exchange[51] by Otto and Sanders.[52,53]

Shape-persistent macrocycles have shown many interesting applications in host–guest chemistry, organic electronic materials, chemical sensors, transmembrane mass transportation, and also as nanoscale building blocks for materials. Multiple comprehensive reviews on these topics have been published.[4,5,7,9,54] Due to the massive number of literature reports, only a few representative examples are presented here, just to give readers a brief idea of the great potential of shape-persistent macrocycles in various chemistry and materials disciplines.

3.2 Thermodynamic Approach vs. Kinetic Approach

Strategies toward the construction of shape-persistent macrocycles could be divided into two categories: the kinetic approach through irreversible reactions and the thermodynamic approach through reversible reactions.[1,8,55]

The kinetic approach takes advantage of numerous irreversible reactions with high efficiency and conversion. Commonly used irreversible reactions include homo-coupling reactions (e.g., Glaser coupling),[56] cross-coupling reactions (e.g., Stephens–Castro coupling),[57] olefination reactions (e.g., the McMurry reaction),[58] and amide formation.[59] Typically, stepwise formation of oligomers followed by intramolecular ring closure of difunctionalized oligomers provides target macrocyclic products.[60,61] Although the yields of individual steps are high, the overall yield of the multistep approach is quite low. In addition, high-dilution or pseudo-dilution conditions are required to ensure the preferred intramolecular ring closure rather than intermolecular oligomerization/polymerization. One-step cyclo-oligomerization was also attempted to prepare the hexameric phenyleneethynylene macrocycle through Stephens–Castro coupling. However, only 4.6% yield was obtained.[62] The fundamental problem of using coupling reactions in a one-step cyclo-oligomerization approach is the irreversible nature of the bond formations. Statistical distribution of various linear and cyclic oligomers/polymers is inevitable since the undesired bond formation cannot be corrected.[8,63] Alternatively, template-assisted cyclization of multiple fragments could produce high yielding macrocycles. However, this approach requires an additional step to remove templates, which in some cases could be problematic.[64]

In recent years, the thermodynamic approach has emerged as a powerful alternative to produce macrocycles from simple monomers in one step in high yields. The use of dynamic covalent chemistry,[65–68] where the reactions are reversible, enables the self-correction feature and conversion of kinetic products to the thermodynamically most stable product at equilibrium. Furthermore, pathway-independent product distribution provides an intriguing choice of starting materials, for example polymers/oligomers, that produce a macrocycle as the predominant species.[69]

In order to achieve high yields of the target macrocycle through dynamic covalent reactions, special attention has to be paid to a few issues: (i) the angle of building blocks has to closely match that of the desired macrocyclic product to minimize angle strain, (ii) during the course of the reaction, starting materials and intermediates should be soluble in the reaction solvent to prevent precipitation of intermediates which cannot further participate in equilibrium process and exist as kinetic traps, (iii) fast reaction kinetics is preferred to reach the equilibrium in a reasonable time frame and catalysts are often used to speed up equilibrium, (iv) removal of by-products from the system (e.g., removal of water in imine condensation or removal of ethylene in olefin metathesis) to drive the equilibrium towards products (Le Châtelier's principle) is often essential, and (v) optimized reaction temperature and concentration are important to the product distribution, which directly influences the reaction kinetics.

Although the thermodynamic approach through dynamic covalent reactions provides easy access to variety of macrocycles, it is usually limited to the preparation of homo-sequenced macrocycles from symmetric monomers. Hetero-sequenced macrocycles have mainly been prepared through stepwise introduction of different monomers to

form oligomers followed by final cyclization. In addition, since only the thermodynamically most stable product will be produced dominantly at equilibrium, other macrocycles, such as strained ones, cannot be constructed in a thermodynamically controlled process unless the equilibration is interrupted before the equilibrium.

3.3 Macrocycles through Alkyne Metathesis

Ethynylene-linked macrocycles have been interesting synthetic targets due to their rigid conjugated backbone structures, self-aggregation behaviors, and easy modulation of interior and exterior functionalities. Staab's pioneering work on ethynylene-linked shape-persistent macrocycles was reported in 1960s,[62,70] but it attracted no special attention until interesting reports by Youngs,[38,71] Moore,[61,72] Höger,[1,60,73] Oda,[74–76] Vollhardt,[77] Tobe,[78,79] and Haley[25,80] were published in the 1990s. As mentioned in the previous section, these examples all rely on irreversible reactions such as Stephens–Castro coupling, Glaser coupling, and the McMurry reaction. With the development of highly active alkyne metathesis catalysts,[81–83] utilization of reversible alkyne metathesis to construct shape-persistent macrocycles has become a viable approach and received increasing attention. The yields of macrocycles are directly influenced by the choice of alkyne metathesis catalysts. Highly active alkyne metathesis catalysts are preferred to ensure fast interconversion of reaction intermediates and reach equilibrium within 1–2 days. The most common alkyne metathesis catalysts include the Mortreux–Mori–Bunz catalyst (**1**),[84,85] Schrock's catalyst (**2**) [$(Me_3CO)_3WCCMe$],[86] Moore and Zhang's catalysts derived from precursor **3**, $EtCMo[NAr(tBu)]_3$,[82,87] and Fürstner's catalyst derived from precursor **4**, [$PhCMo(OSiPh_3)_3(phen)$].[88] A large variety of aryleneethynylene macrocycles have been prepared through alkyne metathesis either from small organic molecules or large polymers (Figure 3.1).

3.3.1 Monomer-to-Macrocycle Strategy

3.3.1.1 Homo-sequenced Symmetrical Macrocycles
Alkyne metathesis is generally a non-directional and self-exchange reaction, for example monomers self-react to form dimers or oligomers. For simplification, therefore, symmetrical di-acetylene functionalized monomers are typically used to form homo-sequenced symmetrical macrocycles through alkyne metathesis. Since alkyne
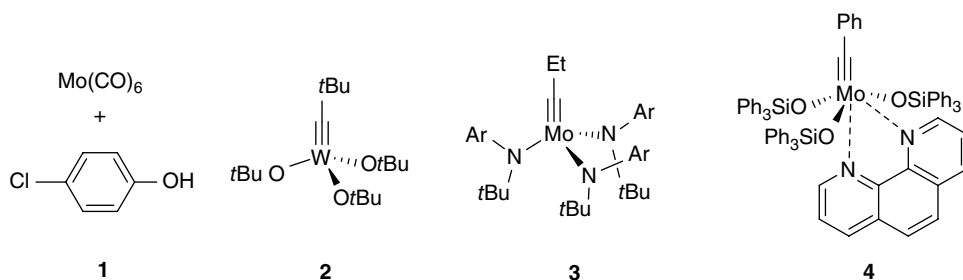
Figure 3.1 Structures of alkyne metathesis catalysts (**1** and **2**) and catalyst precursors (**3** and **4**).

metathesis is a reversible equilibrium process, the removal of one product is usually required to drive the equilibrium to the formation of the macrocyclic product. Propynyl-substituted compounds, which produce 2-butyne through alkyne metathesis with another exchange partner, have been the most commonly used substrates. If 2-butyne remains in the system and undergoes constant exchange with another alkyne partner, the theoretical conversion is close to ~50%, assuming that alkyne metathesis is a nearly energy equal process. Therefore, removal of 2-butyne is necessary in most cases to achieve high conversion of monomers and high yielding of macrocyclic product. Two strategies have been developed to remove 2-butyne from the system: (i) liberating 2-butyne form the system through vacuum application or heating, and (ii) scavenging with molecular sieves.

An alternative approach to shift the equilibrium toward product formation is removal of one product through precipitation. In this case, benzoyldiphenyl-substituted alkynes are used as substrates, producing bis(benzoyldiphenyl)acetylene with poor solubility as a precipitate. All three approaches have been frequently practiced to prepare macrocycles.

The first report on the preparation of ethynylene-linked shape-persistent macrocycles via dynamic covalent reaction was reported by Bunz *et al.* in 2000 (Scheme 3.1).[89] *In situ* generated catalyst (**1**), which was obtained from Mo(CO)$_6$ (5 mol%) and 4-chlorophenol (or 4-trifluoromethylphenol) in 1,2-dichlorobenzene, was used.[90] The reaction mixtures were heated under a light stream of nitrogen (to facilitate removal of butyne by-product) to 150 °C for 16 hours, providing a mixture of oligomers and polymers, from which cyclohexamers **5a**, **5b**, and **5d** were isolated in 0.5–6% yield.[84] Although high temperature was required and low yield was obtained, this early work was quite encouraging. Single crystal X-ray packing of **5a** revealed infinite elliptical channels formed through van der Waals interactions. Additionally, the alkyne group of macrocycle **5a** is able to coordinate with a [Os$_3$(CO)$_{10}$] cluster, which causes significant distortion and reduction of the planarity of the macrocycle.

5a (6%): R$_1$ = tC$_4$H$_9$, R$_2$ = H
5b (1.2%): R$_1$ = nC$_6$H$_{13}$, R$_2$ = H
5c: (yield was not reported)
5d (0.5%): R$_1$ = tC$_4$H$_9$, R$_2$ = CH$_3$
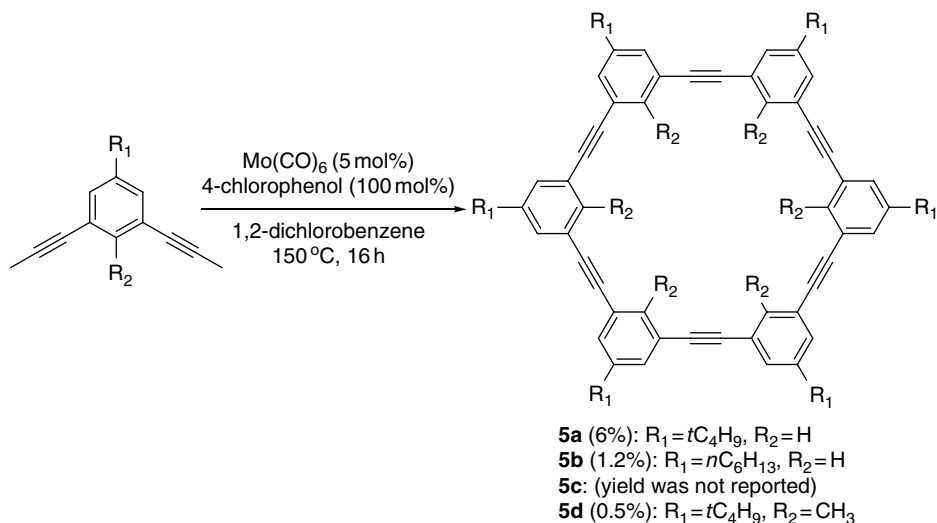
Scheme 3.1 Synthesis of macrocycles **5a–d**.
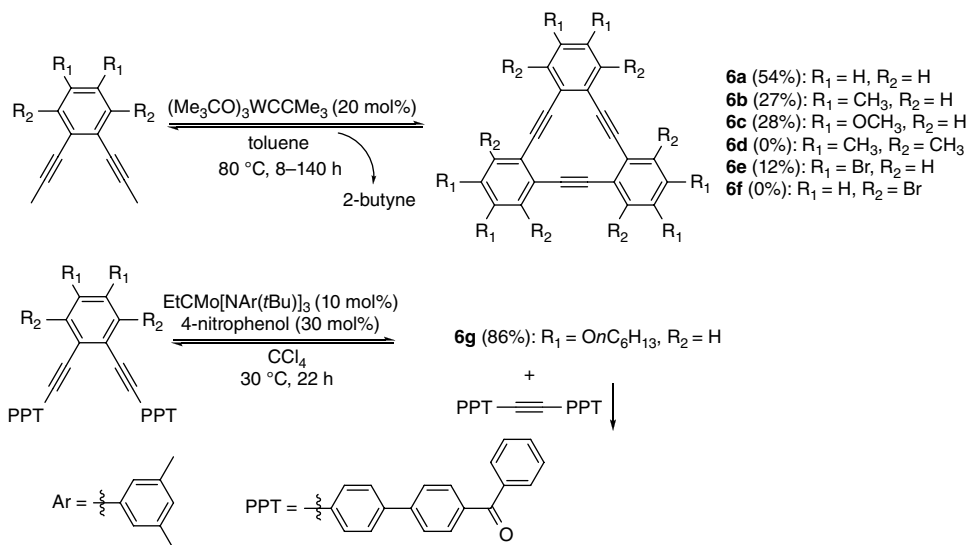
Scheme 3.2 Synthesis of macrocycles **6a–g**.

Interestingly, Vollhardt and co-workers were unable to use the same *in situ* generated catalyst system as Bunz to prepare macrocycle **6a** under similar conditions.[91] Instead, high loading of Schrock's catalyst,[86] [(Me$_3$CO)$_3$WCCMe$_3$] (20 mol%), was used and macrocycles **6a–6c**, and **6e** were obtained in 12–54% yield (80 °C, toluene, 8–140 h, Scheme 3.2). However, doubly ortho-substituted macrocycles **6d** and **6f** were not obtained, presumably due to steric hindrance.

The development of a highly active molybdenum(VI) catalyst by Moore and co-workers[92] has been a breakthrough in the one-step synthesis of macrocycles through alkyne metathesis. For the first time, a single macrocycle was obtained as a major species in one-step cyclo-oligomerization through alkyne metathesis. For example, a triangular-shaped macrocycle **6 g** was prepared in 86% yield through a precipitation-driven alkyne metathesis approach (Scheme 3.2).[93] This yield is markedly higher (6–40 times) than the yield of the same macrocycle obtained through irreversible reactions by Orita (2%)[94] and De Feyter (14%).[95] The catalyst was prepared by mixing molybdenum(VI)-alkylidyne catalyst precursor **3** with 3 equivalents of 4-nitrophenol. The metathesis reaction was conducted under much milder conditions (30 °C for 22 h) compared to the previously mentioned approach using Schrock's catalyst or Bunz's *in situ* generated catalyst system. The discovery by Moore and co-workers thus increased the feasibility of preparation of shape-persistent macrocycles through alkyne metathesis and facilitated the exploration of applications of shape-persistent macrocycles in various research areas.

Using the same catalyst system,[92] Moore and co-workers have also synthesized hexameric phenylene–ethynylene shape-persistent macrocycles through a vacuum-driven alkyne metathesis approach.[96] The metathesis reaction was conducted at 30 °C for 22 h under reduced pressure (vacuum was applied to facilitate removal of 2-butyne), and macrocycles (**5a** and **5e–g**) were obtained in decent yields on a small scale (15–33 mg, 61–76% yield, Scheme 3.3). Both electron-rich and electron-deficient monomers yielded
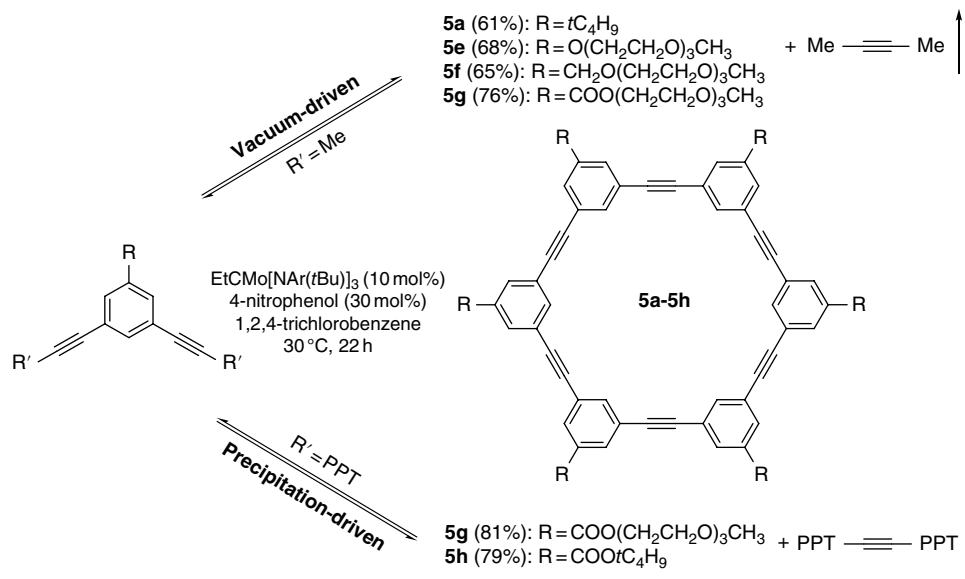
Scheme 3.3 Synthesis of macrocycles **5a** and **5e-g** through vacuum- or precipitation-driven alkyne metathesis.

the desired macrocycles in good yields. Small amounts of cyclic pentamer and heptamer were also obtained, which were separated from the major product **5** through column chromatography. It was found that this vacuum-driven approach was only suitable for milligram scale production of macrocycles. Several attempts to increase the scale of the reactions resulted in poor yields (<10% for **5g**), low conversions, and considerable amounts of oligomeric products, presumably due to catalyst decomposition by air introduced into the reaction vessel. Also, in gram scale synthesis, 2-butyne by-product probably cannot be removed quickly enough, leading to the consumption of the catalyst by polymerization.[97]

To more effectively drive the reaction toward product formation, Moore and co-workers developed a precipitation-driven method in which bis(benzoyldiphenyl) acetylene by-product (PPT–≡–PPT) with poor solubility can be efficiently removed through precipitation. Under otherwise the same conditions, macrocycles **5g** and **5h** were successfully obtained in high yields (81% and 79%, respectively) (Scheme 3.3).[96] Multigram scale synthesis of **5g** was accomplished using this precipitate-driven method in excellent yield (5.68 g, 77%), which represents the first successful large-scale preparation of hexakisphenylene–ethynylene macrocycles. The properties of these macrocycles and their applications in nanofiber formation[98,99] and nanofiltration membrane research[100,101] have been studied subsequently.

Following Moore's impressive work, various square-shaped tetrameric carbazole-based macrocycles (**7**) were prepared through a precipitation-driven alkyne metathesis approach using various catalysts systems. Since high yielding of arylene ethynylene macrocycles is only guaranteed with the high activity of an alkyne metathesis catalyst, macrocycle **7** was often prepared to showcase the catalytic activity of a catalyst. A variety of catalyst systems generated *in situ* from EtCMo[NAr(*t*Bu)]$_3$ (precursor **3**) and a
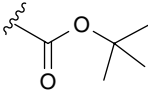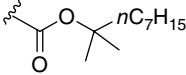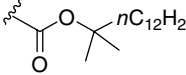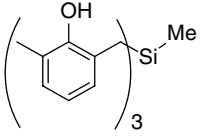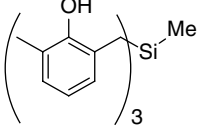
ligand were used to prepare macrocycle **7** under precipitation-driven conditions (Table 3.1).[102,103] Macrocycles **7** with various substituents were obtained in high yields, which are significantly higher than those obtained using the conventional cross-coupling method (e.g., 14.3%, R = $nC_{14}H_{29}$).[104,105] It has been reported that the presence of long alkyl chains is important to provide good solubility of reaction intermediates during the course of macrocycle formation. Low yields (<5%) were reported when short chains were attached to the monomers (Table 3.1, entries 4 and 5)[106] while a similar monomer with long alkyl chain provided the desired macrocycle in good yield (81%, Table 3.1, entry 6).[107] It was also found that the chain length of the substituted groups directly affects the solid-state packing of macrocycles. For example, the packing of macrocycle **7** with *n*-alkyl chains up to nine carbons (e.g., R = nC_9H_{19} or nC_6H_{13}) is dominated by face-on aromatic π–π interactions, whereas macrocycle **7** with longer alkylchains (R = $nC_{11}H_{23}$ or $nC_{10}H_{21}$) exhibits a novel alternating alkyl/aryl packing motif due to the dominating van der Waals interactions between the alkyl chains and aromatic parts of the macrocycles.[103]

Recently, instead of using the vacuum-driven method to remove the 2-butyne by-product, Fürstner and co-workers discovered that 5 Å molecular sieves could act as a 2-butyne scavenger, which largely eased the handling of the alkyne metathesis of propynyl-based substrates.[108] Adding 5 Å molecular sieves to the alkyne metathesis reaction can efficiently remove 2-butyne from the solution, providing the targeted macrocycle in excellent yield. Both catalyst systems prepared from precursor EtCMo[NAr(*t*Bu)]$_3$ (**3**) or [PhCMo(OSiPh$_3$)$_3$(phen)] (**4**) were reported active in the presence of 5 Å molecular sieves, providing macrocycle **6** in excellent yields (Table 3.1, entries 8 and 9). Multigram scale production of cyclic trimer **6h** (4.31 g, 98%) was accomplished using as little as 0.5 mol% of precursor **3** and tris(2-hydroxybenzyl)silane ligand in the presence of molecular sieves (Scheme 3.4).[109] Under similar conditions but with higher loading of catalysts, macrocycle **8** was also obtained in good yield.[110] After deprotection of *t*-butyldimethylsilyl (TBS) groups, the macrocycles **6h** and **8** were used as planar tritopic building blocks for the synthesis of porous covalent organic frameworks (COFs) through the *macrocycle-to-framework* strategy.[110–113]

Multi-porphyrin-containing macrocycles are synthetically challenging but interesting targets, which offer many attractive features, such as large internal voids with coordination environment and unprecedented electronic properties (e.g., migration of excitation energy and electronic coupling). Zhang and co-workers reported an easy route to cyclic porphyrin dimers[114] or trimers[115] through a one-step alkyne metathesis method, utilizing the catalyst generated *in situ* from precursor **3** and multidentate ligand tris(2-hydroxybenzyl)silane or tris(2-hydroxybenzyl)amine.[116] These porphyrin-containing rigid macrocycles exhibit interesting host–guest binding interactions with fullerenes. Macrocycle **9** (Figure 3.2) forms a 1:1 host–guest complex with C_{60}, C_{70} and C_{84}, with binding constants in toluene, respectively, of $1.3 \times 10^4 \, M^{-1}$, $2.0 \times 10^6 \, M^{-1}$, and $2.2 \times 10^7 \, M^{-1}$. Remarkably high C_{84}/C_{60} binding selectivity (1500/1) was observed, which is largely associated with the rigid nature of ethylene-linked macrocycles. Presumably C_{70} fits perfectly inside the cage cavity, while C_{60} fits more loosely, and C_{84} fits a little bit too tightly.[117] Similarly, trisporphyrin-based macrocycles **10a/b** also selectively bind C_{70} ($6 \times 10^3 \, M^{-1}$) over C_{60} and C_{84} (no binding observed).[115]

Table 3.1 Summary of catalyst and conditions used for the preparation of macrocycle **7**.

Entry	R	R′	Catalyst			T (°C)	Time (h)	Yield (%)
			Precursor	Loading (mol%)	Ligand/activator			
1	nC$_{14}$H$_{29}$	PPT	**3**	10	4-nitrophenol	30	22	84
2	nC$_{10}$H$_{21}$	PPT	**3**	10	Ph$_3$SiOH	30–50	22	75
3	nC$_6$H$_{13}$	PPT	**3**	10	Ph$_3$SiOH	30	22	72
4	(t-Bu ester)	PPT	**3**	10	4-nitrophenol	30	22	<5
5	(ester, nC$_7$H$_{15}$)	PPT	**3**	10	4-nitrophenol	30	22	<5
6	(ester, nC$_{12}$H$_{25}$)	PPT	**3**	10	4-nitrophenol	30	22	81
7	nC$_8$H$_{17}$	PPT	**3**	3	(silanol triol, Si–Me)	20	0.5	93
8	nC$_8$H$_{17}$	Me	**3**	3	(silanol triol, Si–Me)	40	5	>99
9	nC$_{14}$H$_{29}$	Me	**4**	5	MnCl$_2$	80	n/a	81
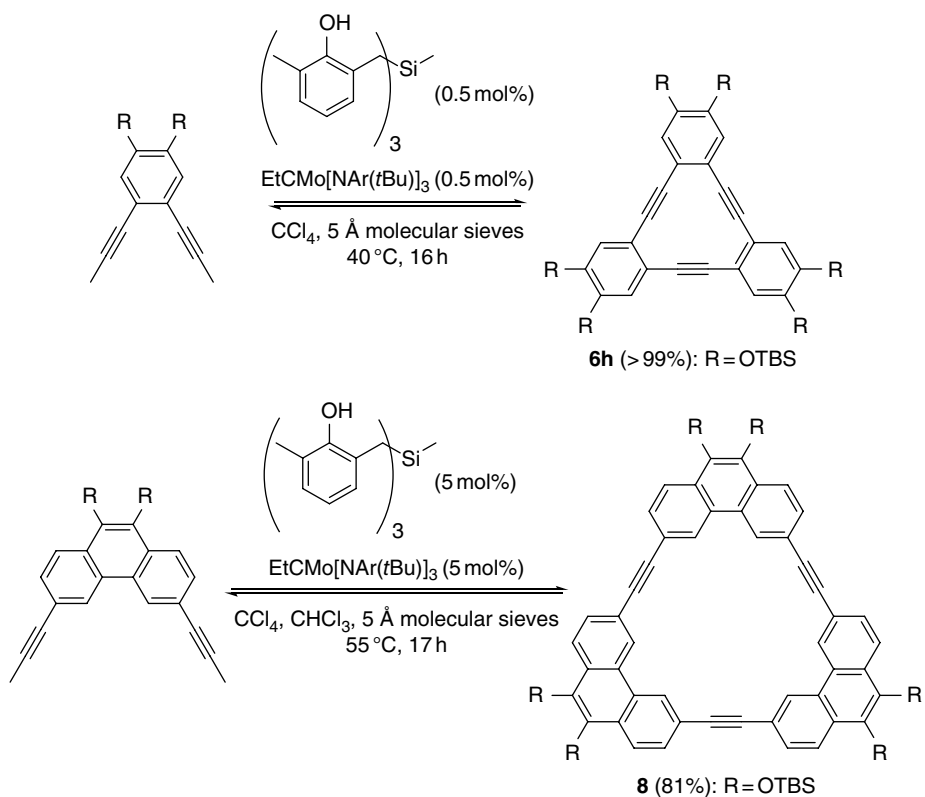
Scheme 3.4 Synthesis of macrocycles **6h** and **8**.

9 (60%): $R_1 = nC_{16}H_{33}$, $R_2 = tC_4H_9$

10a (80%): R = Br
10b (82%): R = $nC_{14}H_{29}$
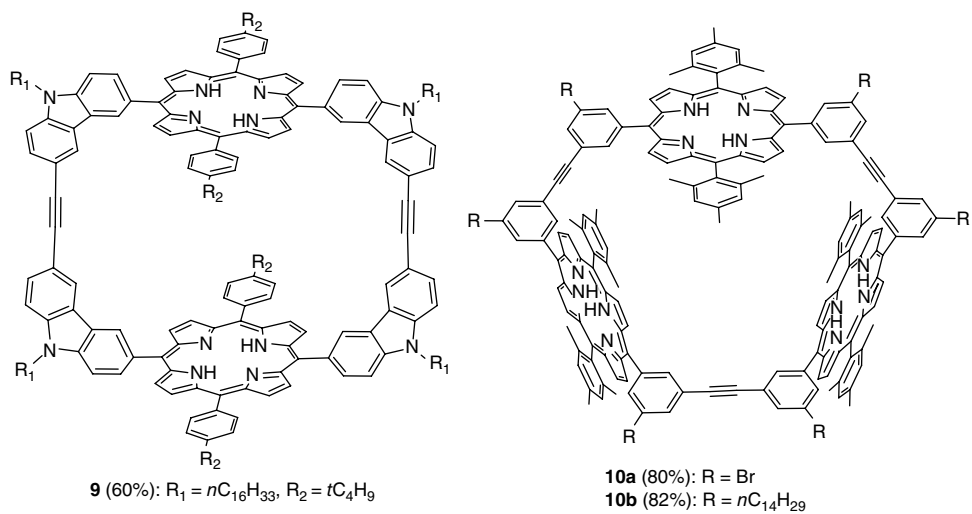
Figure 3.2 The structures of macrocycles **9** and **10**.

3.3.1.2 Hetero-sequenced Macrocycles

As previously mentioned, alkyne metathesis is a self-exchange reaction. Unsymmetrical monomers can therefore produce multiple macrocyclic products. Tew and co-workers have reported an alkyne metathesis reaction of unsymmetrical monomers (Scheme 3.5).[118] Not surprisingly, a 1:3 mixture of two isomers, which were inseparable using HPLC, was obtained in 77% total yield. Such a mixture was able to self-assemble in a chloroform/water system into vesicles (~460 nm diameter), which appear to be identical to those using pure regioisomer[119] prepared through irreversible intramolecular coupling under high dilution conditions.[120]
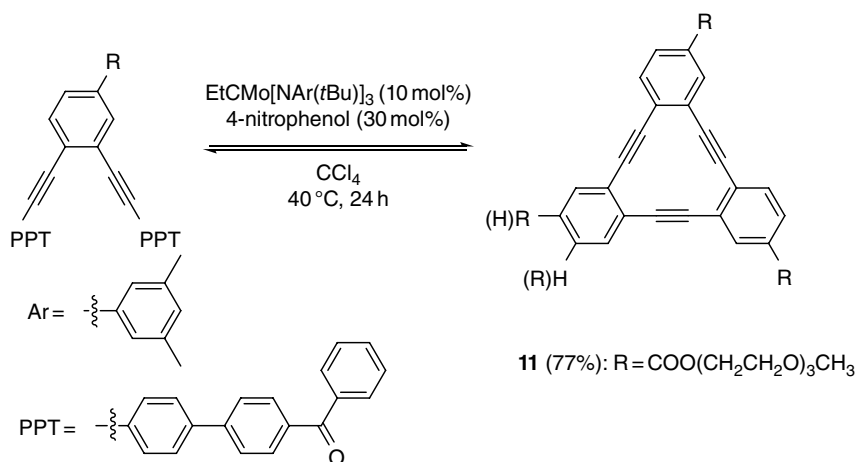
Scheme 3.5 Synthesis of an isomeric mixture of macrocycle **11**.

Hetero-sequenced macrocycles have also been prepared through cross metathesis reactions of two different monomers, albeit in very low yield. For example, macrocycles **12a** and **13a** were obtained in 19% and 6% yields, respectively.[91] Macrocycle **13a** was first synthesized by Haley and co-workers through a stepwise coupling approach with comparable overall yield of 4.4% (Scheme 3.6).[121] The attempted synthesis of macrocycle **14** through alkyne metathesis was not successful. Hexaethynylbenzene proved to be highly sensitive to both heat and oxygen, and also inert to alkyne metathesis, even with a simple substrate, for example propynylbenzene.

Alternatively, hetero-sequenced macrocycles have been prepared through a directed alkyne metathesis approach in significantly higher yields. As shown in Scheme 3.7, Haley and co-workers successfully prepared macrobicyclic compound **13** from a preorganized monomer using high loading of catalysts prepared from [(Me$_3$CO)$_3$WCCMe] or EtCMo[NAr(*t*Bu)]$_3$.[122] Increasing yields and ease of separation were observed with increasing solubility of monomers: **13b** (46%) to **13c** (87%) and **13d** (91%). The overall yields of macrocycles through this route were all ca. 20%, much higher than those of previously reported irreversible/reversible routes (<1%).[122] Construction of a larger derivative **15** through the same approach was also successful, but with much reduced yields (19–31%). Several attempts to synthesize **16** failed. Monomers, oligomers, or intermediates with three of the four [12]cyclyne subunits cyclized were obtained.[122]
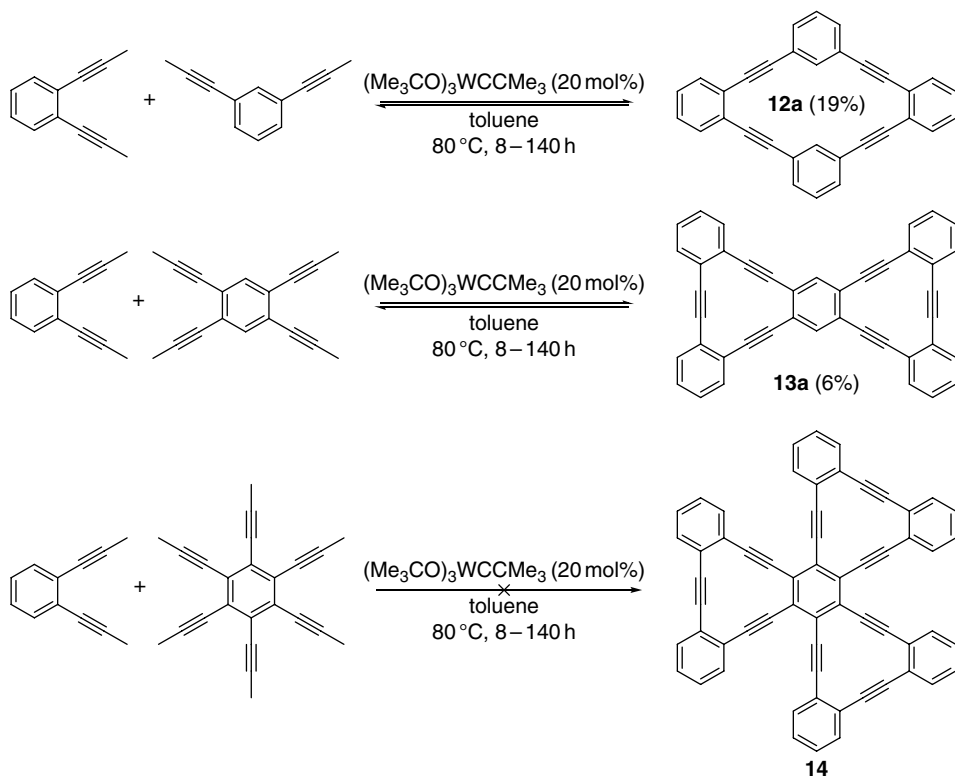
Scheme 3.6 Synthesis of hetero-sequenced macrocycles from two monomers.

These graphyne substructures composed of fused tribenzo[12]cyclyne subunits represent interesting model systems to study the properties of graphyne, a theoretical carbon allotrope composed of sp- and sp^2-hybridized carbon atoms.

Very recently, Tobe and co-workers successfully prepared larger graphyne fragments through a directed alkyne metathesis approach,[123] using a molybdenum(VI) nitride catalyst bearing a triphenylsilyloxy ligand developed by Fürstner *et al.*[88] Macrocycles **17a** and **17b** were prepared in 17–56% yield (Scheme 3.8), while the yield for using irreversible cyclization to prepare their graphdiyne analogue was 1%.[124] The lower yield of **17a** compared to that of **17b** is probably due to the low solubility of monomers and possible intermediates (<0.1 mg/mL in CH_2Cl_2). With extended π-conjugation, **17a** exhibits a remarkable bathochromic shift of the absorption cut-off in the one-photon absorption spectrum compared to those of previously reported graphyne fragments. **17b** showed columnar rectangular mesophases and a moderate charge-carrier mobility (0.12 cm^{2}V^{-1} s^{-1}). These results indicate such graphyne fragments could be good candidates for organic semiconductors.

The directed multi-fold alkyne metathesis approach is a powerful tool to prepare hetero-sequenced macrocyclic systems such as graphyne fragments. The drawback could be the stepwise preparation of preorganized monomers with multiple alkyne groups. The poor solubility of such monomers is also a significant concern.[125]

condition 1

(Me$_3$CO)$_3$WCCMe$_3$ (50 mol%)

toluene
80 °C, 24 h

condition 2

EtCMo[NAr(*t*Bu)]$_3$ (29−67 mol%)
silanol-POSS (171−400 mol%)

1,2,4-trichlorobenzene
75 °C, 0.5−14 h

Ar =

13b (46%): condition 1, R$_1$=*n*C$_4$H$_9$, R$_2$=H
13c (87%): condition 2, R$_1$=*n*C$_{14}$H$_{29}$, R$_2$=H
13d (91%): condition 2, R$_1$=*n*C$_{10}$H$_{21}$, R$_2$=*n*C$_{10}$H$_{21}$

condition 1

(Me$_3$CO)$_3$WCCMe$_3$ (100 mol%)

toluene
80 °C, 24 h
19%

condition 2

EtCMo[NAr(*t*Bu)]$_3$ (40 mol%)
silanol-POSS (250 mol%)

1,2,4-trichlorobenzene
75 °C, 3 h
31%

Ar =

15: R$_1$=*n*C$_{14}$H$_{29}$, R$_2$=*n*C$_{10}$H$_{21}$

condition 1

(Me$_3$CO)$_3$WCCMe$_3$ (100 mol%)

toluene
80 °C, 4 h

condition 2

EtCMo[NAr(*t*Bu)]$_3$ (40 mol%)
silanol-POSS (250 mol%)

1,2,4-trichlorobenzene
75 °C, 3 h

Ar =

16: R=*n*C$_{14}$H$_{29}$

Scheme 3.7 Synthesis of hetero-sequenced macrocycles through a directed alkyne metathesis approach.

Reagents and conditions over reaction arrow:

[NMo(OSiPh$_3$)$_3$(py)] (70 mol%)
silanol-POSS (250 mol%)

1,2,4-trichlorobenzene
150 °C, 24 h

py = pyridine

R$_2$ = CH$_3$, or nC$_2$H$_5$

+ R$_2$ —≡— R$_2$

17a (19%): R$_1$ = tC$_4$H$_9$, R$_2$ = CH$_3$

17b (56%): R$_1$ = [ester group] nC$_8$H$_{17}$, R$_2$ = nC$_2$H$_5$
nC$_6$H$_{13}$
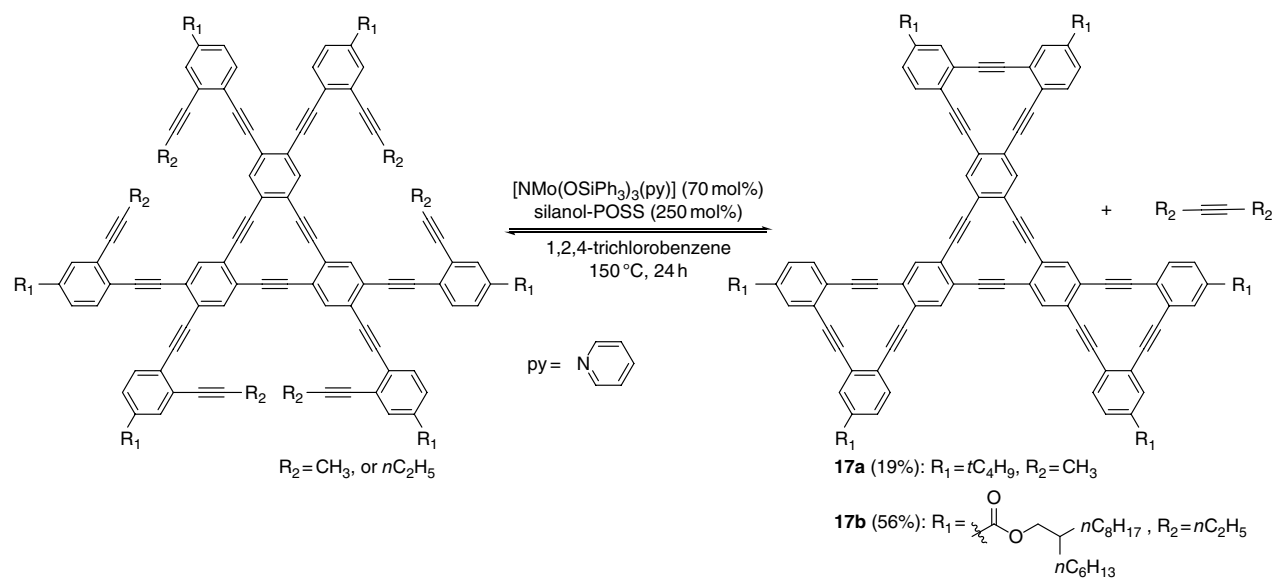
Scheme 3.8 Synthesis of macrocycles **17a** and **17b**.

3.3.2 Mechanism Study of the Cyclooligomerization Process

Cyclooligomerization through dynamic alkyne metathesis is a thermodynamically controlled process in which the system reaches energy minima at the equilibrium. Figure 3.3 shows the cyclo-oligomerization energy landscape. In the early stage of the reaction, various linear or cyclic oligomers form, which gradually transform to the most thermodynamically favored species at the equilibrium. Cyclic hexamer is most thermodynamically favored when 1,3-disubstituted benzenes are used as the monomers. Other cyclic oligomers, for example cyclic pentamers or cyclic heptamers, are enthalpically less favored due to the angle strain. Although entropy prefers the smallest macrocycle (e.g., cyclic trimer), the enthalpic gain of making a less strained macrocycle outweighs the entropic cost, especially for shape-persistent macrocycles. The choice of monomers is therefore critical for the formation of targeted macrocycles. The geometrical features encoded into building blocks (e.g., the angle and directionality of the functional groups) largely determine the product distribution at equilibrium.

A series of experiments were conducted in order to illustrate the underlying principle for the selective generation of certain macrocycles by alkyne metathesis and to demonstrate that the reaction is indeed thermodynamically controlled. First, the alkyne metathesis reaction to form cyclic hexamer **5 g** under precipitation-driven conditions (Scheme 3.3) was monitored by GPC and matrix-assisted laser desorption/ionization mass spectrometry (MALDI MS), which showed open-chain oligomers and larger macrocycles formed in the early stage of the reaction and were eventually converted to cyclic hexamer and a small amount of cyclic pentamer at equilibrium (Figure 3.4).[97] Second, pathway-independent product distribution was observed by subjection of a
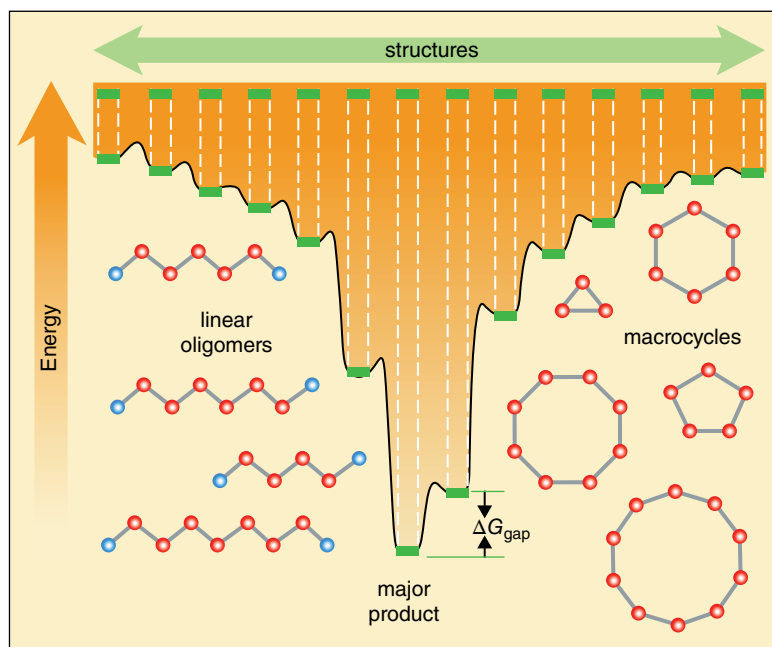
Figure 3.3 The cyclooligomerization energy landscape.
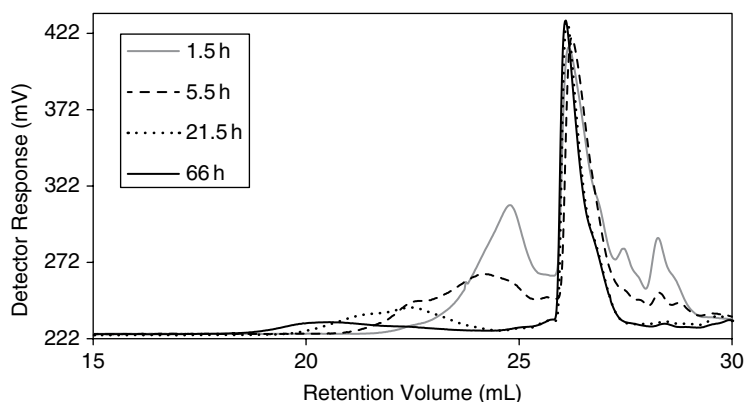
Figure 3.4 Time course of the formation of **5 g** as monitored by gel permeation chromatography (GPC) (tetrahydrofuran, 20 °C).

pre-synthesized phenylene–ethynylene polymer to alkyne metathesis reaction and **5 g** was the major product formed at the equilibrium, supporting the idea that cyclo-oligomerization is under thermodynamic control.[97] Third, a scrambling experiment between **5a** and **5 g** provided a series of scrambled hexameric macrocyclic products with different combinations of -COO(CH$_2$CH$_2$O)$_3$CH$_3$ and $-t$C$_4$H$_9$ substituted groups, showing that these macrocycles are not kinetically trapped and their formation is reversible.[97] Similarly, when **6 g** (m/z 900) and **5I** (m/z 1800) (2:1, n/n) were subjected to alkyne metathesis, a tetrameric macrocycle **12b** (m/z 1200) was observed, which again suggests that these macrocycles are able to undergo re-equilibration to reach the thermodynamic minima of the system (Scheme 3.9).[93] Lastly, calculations of the thermodynamic stabilities of shape-persistent macrocycles provided further theoretical support to the observed product distribution at equilibrium.[97]

3.3.3 Polymer-to-Macrocycle Strategy

As mentioned previously, cyclo-oligomerization through dynamic alkyne metathesis is under thermodynamic control and is pathway independent. This unique feature of thermodynamically controlled systems results in an interesting alternative for starting materials. Instead of starting from small organic monomers, Moore and co-workers developed a depolymerization strategy to prepare macrocycles starting from polymers/oligomers.[126] Using homopolymers **18a** and **18b** (**18a** Mn = 8.5 kDa, PDI = 1.7; **18b** Mn = 6.4 kDa, PDI = 1.8) obtained from cross-coupling reactions as starting materials, the macrocycles **7a** and **7b** were obtained in good yield under alkyne metathesis conditions (Scheme 3.10).[69,127]

When copolymers **19** (Mn = 6.7 kDa, PDI = 1.8) were used as the starting material a mixture of six macrocycles with randomly distributed substituents (R$_1$, R$_2$) were obtained. Silica gel chromatography allowed for the isolation of four pure macrocycles with different polarities. This represents an interesting strategy to prepare a combinatorial library of macrocycles with various substitution patterns.[69] Later, depolymerization – macrocyclization was also applied to the synthesis of directional macrocycles with ester functional groups or amide functional groups through incorporating

6g: R = O*n*C₆H₁₃

5l: R = O*n*C₆H₁₃

EtCMo[NAr(*t*Bu)]₃ (10 mol%)
4-nitrophenol (30 mol%)

CCl₄
30 °C, 22 h

Ar =

12b: R = O*n*C₆H₁₃
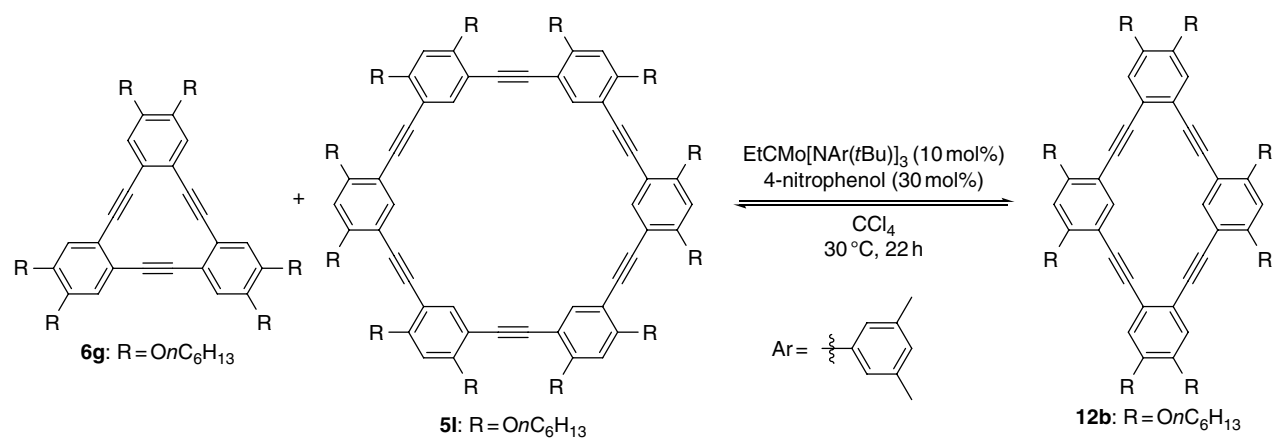
Scheme 3.9 Scrambling experiment of **6 g** and **5l**.
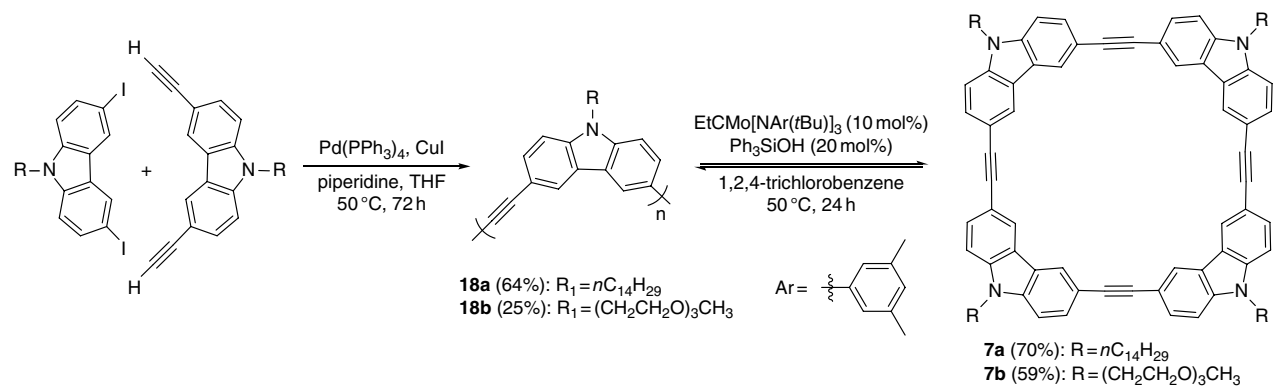
Scheme 3.10 Depolymerization of **18a/b** to synthesize macrocycles **7a/b**.

19: R$_1$ = nC$_{10}$H$_{21}$, R$_2$ = (CH$_2$CH$_2$O)$_3$CH$_3$
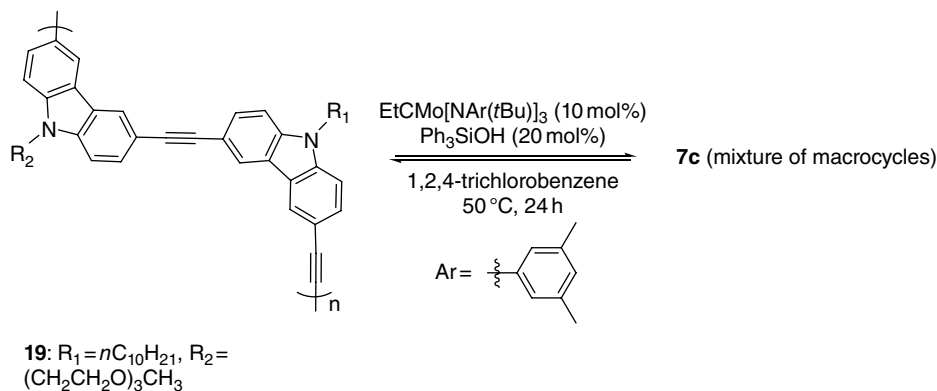
Scheme 3.11 Depolymerization of **19** to a combinatorial library of macrocycle **7**.

direction-defining ester or amide linkages in the polymer backbone.[128–130] The polymer-to-macrocycle strategy prevents the risk of pseudo-poisoning of catalysts by small alkyne by products (e.g. 2-butyne) and is atom economic, with no leaving group by-product during metathesis, especially when compared to a precipitate-driven method from monomers.

3.4 Macrocycles through Imine Metathesis

Dynamic imine formation/exchange is one of the most commonly used dynamic covalent reactions,[131] and the preparation of macrocycles through imine chemistry is no exception.[132] Most of the shape-persistent macrocycles prepared through dynamic imine chemistry contain (N$_2$O$_2$) units (salphen units, salphen = *N*,*N*′-bis(salicylidene) phenylenediamine). These rigid macrocycles feature salen-type (salen = *N*,*N*′-bis(salicylidene)ethylenediamine) coordination environments and crown-ether like interiors, and thus show interesting properties and exceptional supramolecular applications, including host–guest chemistry, ion-induced tubular assembly, chemical sensor, templated inorganic synthesis, metallocavitand, and liquid crystal. These works have been pioneered by Nabeshima[133–135] and MacLachlan.[136,137] Multiple reviews on this topic have been published and provide more comprehensive information for interested readers.[133–144]

3.4.1 Salphen-containing Macrocycles

3.4.1.1 Synthesis

The first Schiff-base shape-persistent 30-membered macrocyclic hexaimine (**20a**) was synthesized by Nabeshima *et al.* in 2001 through condensation of 2,3-dihydroxyterephthalaldehyde and benzene-1,2-diamine (4×10^{-2} M) in acetonitrile at room temperature for 2 weeks.[145] The macrocycle compound **20a** gradually precipitated out of the solution in high yield (91%) (Scheme 3.12). Reactions under lower concentrations (2.5–4.0×10^{-3} M) at room temperature for 1 month led to a decreased yield (19%). X-ray crystallography analysis of macrocycle **20a** showed the existence of a strong intramolecular hydrogen-bond network. X-ray crystallography analysis of a hydrate,

Condition 1:
MeCN, rt, 2 weeks

Condition 2:
CHCl$_3$/MeCN (1:1)
90 °C, 2 h
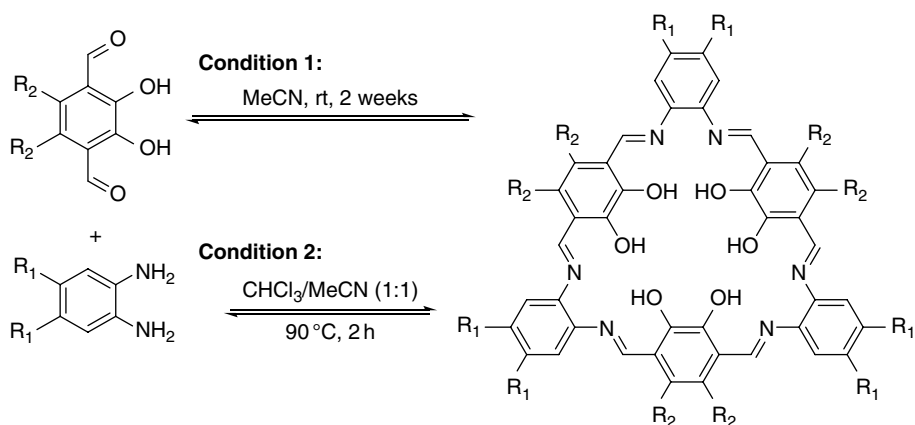
20a (91%): condition 1, R$_1$ = H, R$_2$ = H
20b (n/a): condition 2, R$_1$ = OCH$_3$, R$_2$ = H
20c (77%): condition 2, R$_1$ = OC$_2$H$_5$, R$_2$ = H
20d (68%): condition 2, R$_1$ = OnC$_3$H$_7$, R$_2$ = H
20e (78%): condition 2, R$_1$ = OnC$_4$H$_9$, R$_2$ = H
20f (63%): condition 2, R$_1$ = OnC$_5$H$_{11}$, R$_2$ = H
20g (84%): condition 2, R$_1$ = OneoC$_5$H$_{11}$, R$_2$ = H
20h (75%): condition 2, R$_1$ = OnC$_6$H$_{13}$, R$_2$ = H
20i (70%): condition 2, R$_1$ = OnC$_7$H$_{15}$, R$_2$ = H
20j (87%): condition 2, R$_1$ = OnC$_8$H$_{17}$, R$_2$ = H
20k (59%): condition 2, R$_1$ = OnC$_{10}$H$_{21}$, R$_2$ = H
20l (34%): condition 2, R$_1$ = OnC$_{12}$H$_{25}$, R$_2$ = H
20m (36%): condition 2, R$_1$ = OnC$_{14}$H$_{29}$, R$_2$ = H
20n (18%): condition 2, R$_1$ = OnC$_{16}$H$_{33}$, R$_2$ = H
20o (87%): condition 2, R$_1$ = OC$_2$H$_5$, R$_2$ = CH$_3$
20p (77%): condition 2, R$_1$ = OnC$_5$H$_{11}$, R$_2$ = CH$_3$
20q (24%): condition 2, R$_1$ = H, R$_2$ = nC$_4$H$_9$
20r (28%): condition 2, R$_1$ = OCH$_3$, R$_2$ = nC$_6$H$_{13}$
20s (51%): condition 2, R$_1$ = OnC$_6$H$_{13}$, R$_2$ =
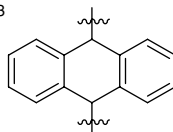
Scheme 3.12 Synthesis of macrocycles **20a–s**.

20a H$_2$O·MeCN, revealed that the inside cavity of this macrocycle was able to bind a water molecule. The formation of intramolecular hydrogen bonds is likely critical for the selective formation of macrocycle **20a**, stabilizing the favorable conformation of the transition state and/or intermediates in the cyclization. The low solubility is another driving force for the selective formation of such macrocycle. Thus, this is also a kinetically trapped product.

Various salphen-containing macrocycles (**34–42**) have been prepared from bifunctional precursors, benzene-1,2-diamine (**32**) and bis(salicylaldehyde) derivatives (**21–31**) (Figures 3.5 and 3.6). [3 + 3] Schiff base macrocycles of various size and substituents incorporating three N$_2$O$_2$ salphen-type binding sites have commonly been studied due to their relative synthetic simplicity.[146–150] More complex [4 + 4] or [6 + 6] Schiff base macrocycles (e.g., **40**[151] and **41**[152]) are relatively rare. Although the yields of macrocycles are
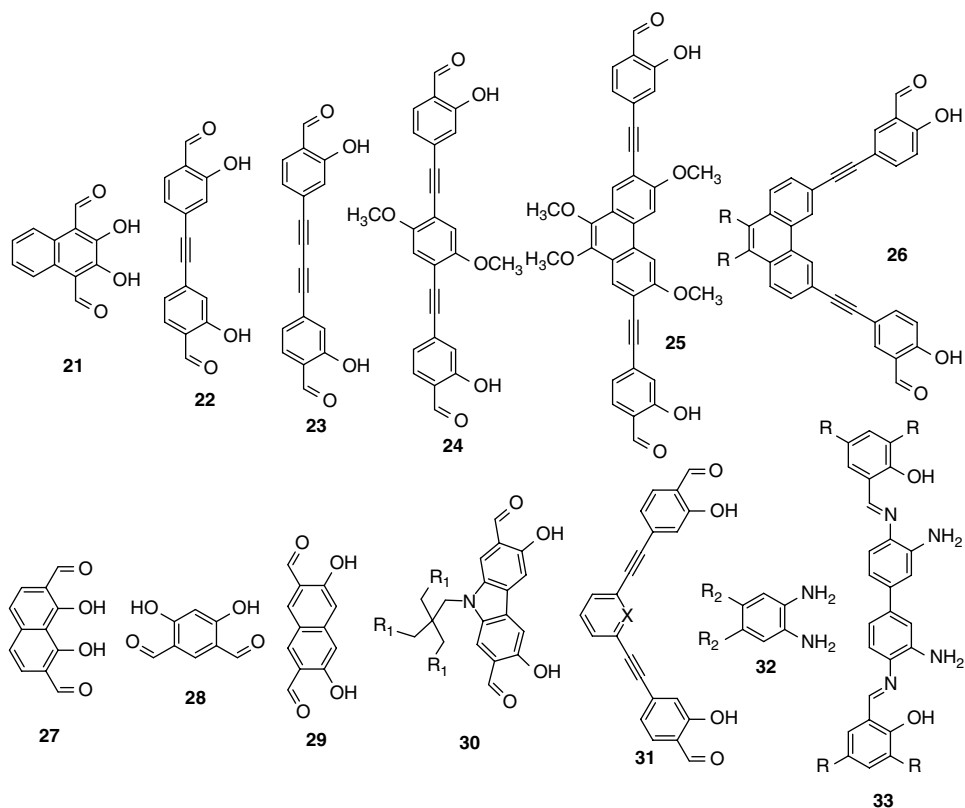
Figure 3.5 Building blocks used in the synthesis of salphen-containing macrocycles.

sensitive to the substituents on the monomers, in many cases they were obtained as predominant species in good yields (up to 88%) in CHCl$_3$/MeCN co-solvent.

In addition to highly symmetrical macrocycles, isomeric macrocycles with inequivalent imine bonds and unsymmetrical salphen-like [N$_2$O$_2$] moieties have been obtained using the differential exchange rates of aldimines and ketimines by MacLachlan and co-workers.[153] As shown in Scheme 3.13, macrocycle **46** was synthesized through a cascade of ketimine condensation followed by aldimine condensation. Through a similar approach, macrocycles **49** and **50** were also synthesized.[153,154] Asymmetric macrocycle **48** with cone conformations similar to calixarene were also synthesized through a stepwise method.[155]

3.4.1.2 Coordination with Metal Ions

These salphen-containing macrocycles have been extensively studied for their complexation with various transition-metal ions. Although tautomerization of hydroxy-imine groups to keto-enamines have been reported for naphthalene-based macrocycle **51** (Scheme 3.14),[156] most other macrocycles are present as enol-imine tautomers. The presence of multiple hydroxyl and imine groups in the cavity of macrocycles enables binding with metal ions to form metal complexes by acting like either crown ethers or planar [N$_2$O$_2$] ligands. For example, macrocycle **20h** can bind small alkali cations such
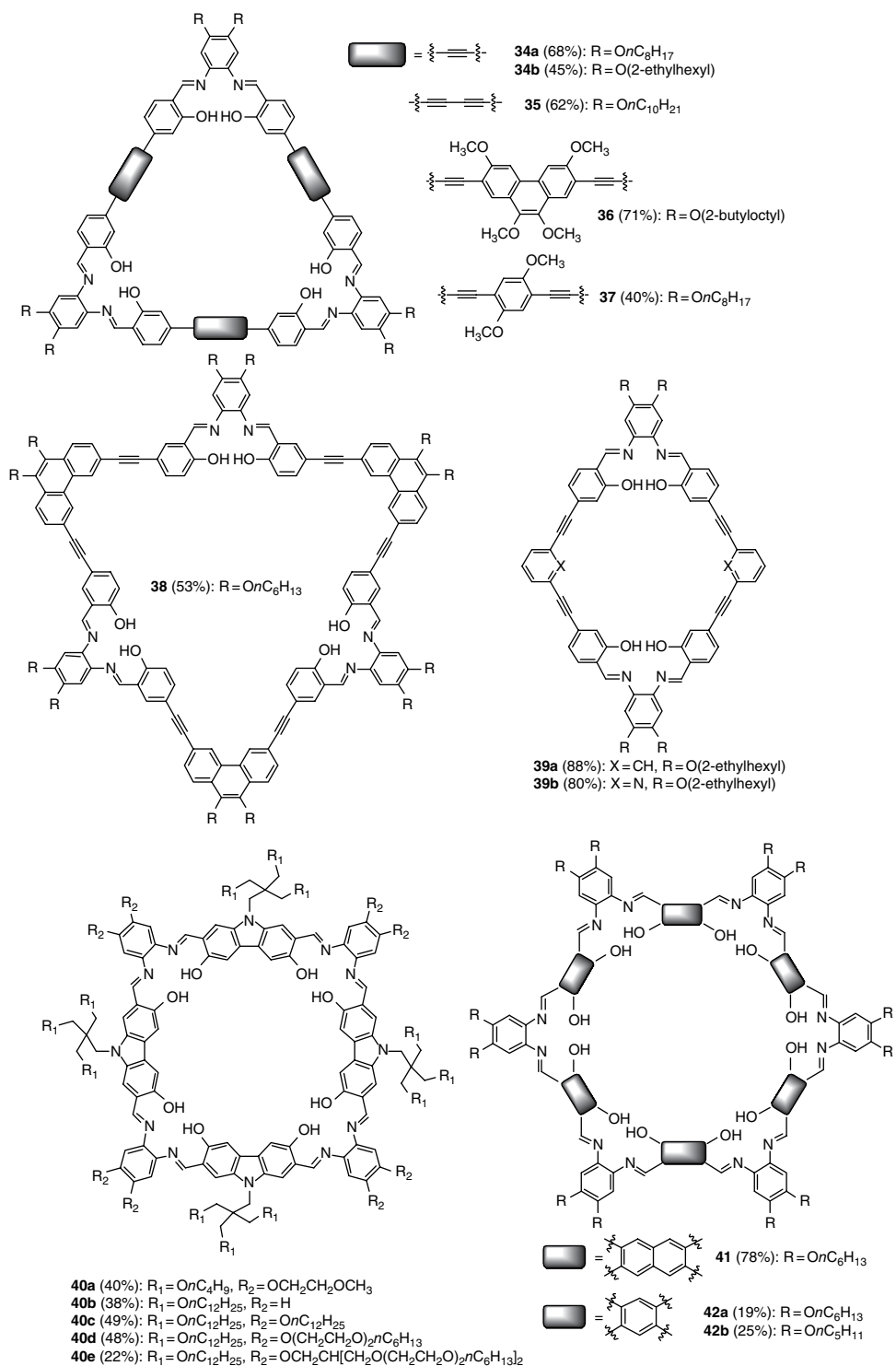
Figure 3.6 Salphen-containing macrocycles.
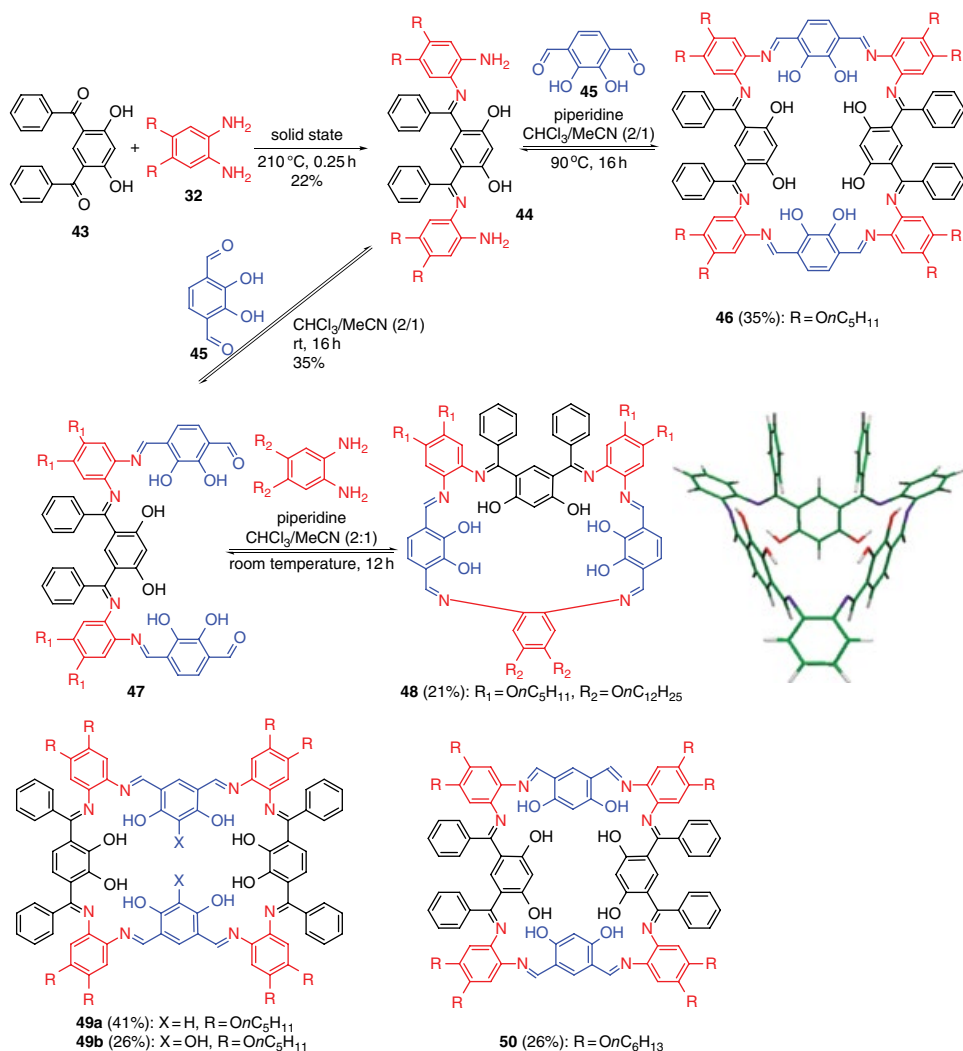
Scheme 3.13 Reversible–irreversible aldimine–ketimine condensation approach towards the synthesis of macrocycles with unsymmetrical salphen pockets.

as Na^+, K^+, and NH_4^+ through coordination to the central hexa(hydroxy) interior rather than in the N_2O_2 pockets, suggesting the crown-ether like interior of **20**.

Interestingly, when transition metal ions are added, metal cluster compounds containing up to seven transition metal cations can be obtained through binding to $[N_2O_2]$ coordination sites.[157,158] For example, the reaction of an excess of $Zn(OAc)_2$ with macrocycles **20c**, **20f**, **20g**, and **20h** gave bowl-shaped heptanuclear Zn complexes featuring Zn in tetrahedral, octahedral, and square-pyramidal geometries,[149,159] with accessible coordination sites on zinc ions inside the bowl (Figure 3.7). Heptazinc metallocavitands could dimerize in a face-to-face fashion in aromatic solvents. It was suggested that up to three metallocavitands bind one C_{60}. However, quantitative information about such
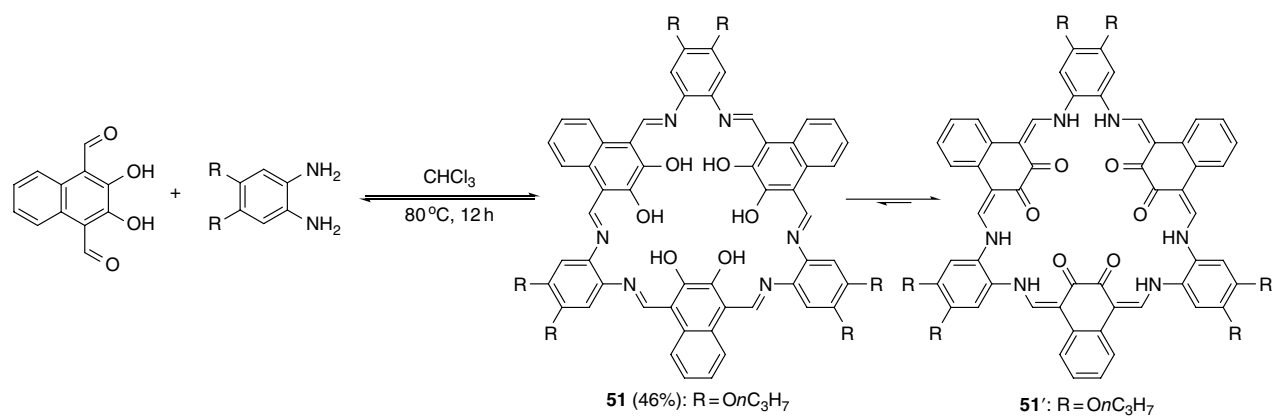
Scheme 3.14 Tautomerization of macrocycle **51**. Keto-enamine tautomers are favored.

(a)

Zn₇-20c: R = nC_2H_5
Zn₇-20f: R = nC_5H_{11}
Zn₇-20g: R = $neoC_5H_{11}$
Zn₇-20h: R = nC_6H_{13}

(b)

(c)
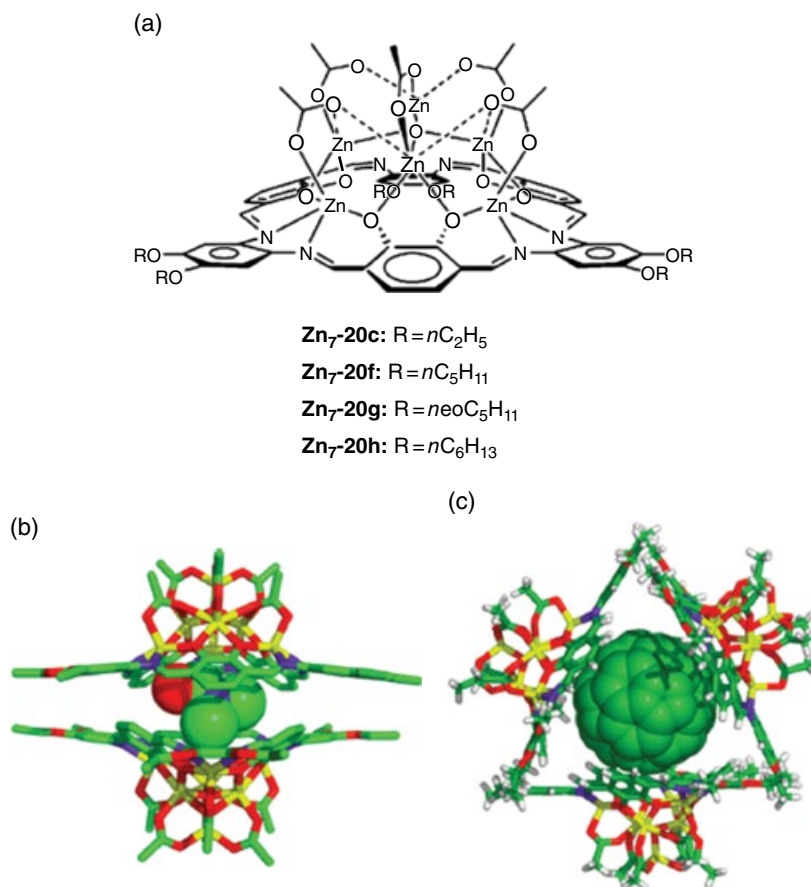
Figure 3.7 The structures of (a) heptazinc metallocavitand, (b) its dimer with encapsulated DMF, and (c) metallocavitand-C_{60} host–guest complex.

a host–guest complex is unavailable.[160] Similarly, heptacadmium cluster metallocavitands with a deeper bowl shape were also obtained through complexation of cadmium ions with macrocycles **20c**, **20 g**, **20 h**, or **20j**. These metallocavitands form interlocking face-to-face capsules in the solid state and dimerize reversibly in DMF or aromatic solvents (benzene, toluene, and *p*-xylene).[161,162] These metal clusters show interesting ligand exchange and guest exchange activities. For example, Nabeshima and co-workers reported the quantitative transformation of homo heptazinc macrocycle **20e** cluster to Zn₃La hetero metal cluster,[157] whose isomer ratio was dependent on the solvent and counter anions.[163]

It appears that often the addition of metal ions to the reaction medium can improve the yield of salphen-containing macrocycles through a template effect.[164] Nabeshima and co-workers reported a high-yielding synthesis of **201** (87%) in the presence of Zn(OAc)₂·2H₂O,[158] which was significantly improved compared to the previously reported 34% by MacLachlan in the absence of metal ions.[148] Similarly, Kleij and co-workers also reported a template effect. Macrocycle **Zn₄-52** was obtained in 88%

Zn$_4$-52 (88%): R = tC$_4$H$_9$

Ni$_2$-53 (46%): M = Ni
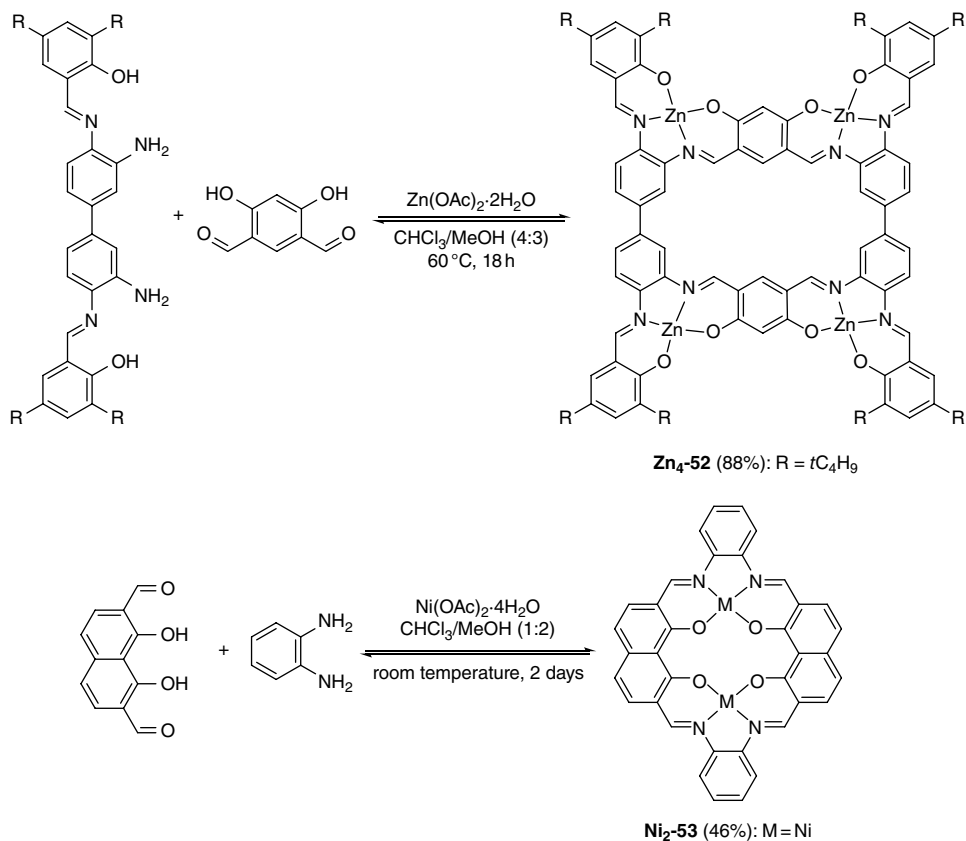
Scheme 3.15 Metal-templated synthesis of macrocycles **Zn$_4$-52** and **Ni$_2$-53**.

yield (Scheme 3.15), while very low conversion was observed without a metal template.[165] Nabeshima and co-workers also found that without a metal ion template preparation of [2 + 2] macrocycle **53** was not efficient,[166] while **Ni$_2$-53** with a highly planar structure was formed predominantly with the addition of Ni(OAc)$_2$. In this case, the unoccupied O$_4$ compartment in the center of the macrocycle was able to bind a third metal ion such as Ni^{2+}, Cu^{2+}, or Zn^{2+}.

It has been revealed that coordination with metals assists the self-aggregation of these salphen-containing macrocycles into tubular structures and further formation of liquid-crystalline phases. The single crystal structure of **20c** revealed a non-planar conformation with strong hydrogen bonding between adjacent hydroxyl groups and imine groups.[148] No liquid crystalline behavior was observed for bare macrocycles **20**, even those with very long alkoxy chains (melting points reduced), likely due to the free rotation of the dihydroxydiiminobenzene rings.[148] However, the addition of alkali metal salts or ammonium salts into a solution of macrocycles with long alkoxy chains (>6) in non-polar solvents (chloroform, toluene, and chlorobenzene) led to the formation of lyotropic liquid crystals.[167] It has been reported that on addition of small cations (e.g., Na$^+$, K$^+$, Rb$^+$, Cs$^+$, NH$_4^+$), **20 h** can aggregate into a tubular structure in which macrocycles are bridged metal ions bound to the central phenolic oxygens.[147] The length and

width of the ion-induced superstructures of **20h** rely on the cation and counter anion of the salts. Macrocycle **20s** with bulky triptycenyl groups cannot form such a tubular structure.[168] The aggregation of these macrocycles is also solvent dependent. For example, tri-zinc metallated larger macrocycles **34a/b** show strong aggregation behavior in non-coordinating solvents such as dichloromethane, whereas the aggregates break up in coordinating solvents (e.g., pyridine, THF, quinuclidine).[169] It is interesting to note that Ni^{2+} or Cu^{2+} metallated macrocycles **34a/b** do not aggregate. Thus, the aggregation is most likely induced by the interactions between Zn^{2+} ions and oxygen atoms from adjacent macrocycles.[169]

Very recently, Tanaka and co-workers reported [4 + 4] macrocycles **40** whose metal complexes display a highly fluid character over a wide range of temperatures.[151] It was found that coordination with metal ions significantly raises the range of the liquid-crystalline temperature of the metallo-macrocycles compared to those of the metal-free macrocycles, likely due to the stiffer and higher planarity of the metallo-macrocycle. Metal-free **40d** and **40e** have phase-transition temperatures to isotropic liquid below decomposition temperatures and **40e** exhibited fluidic liquid crystal phases even below room temperature. **40b** and **40c** even decomposed before their melting points were reached. However, when Ni^{2+} and Cu^{2+} ions were incorporated into **40d** and **40e** to form square-planar metal complexes, these metallocycles were stable without decomposition before melting, and showed highly fluid character over a wide range of temperatures. Liquid-crystalline properties were observed from 340 and 110 °C for **Ni₄-40e** before it solidified via phase transition at 110 °C. It was found that peripheral substituted chains play key role in controlling the temperature range and fluidity of the liquid-crystalline phases.

3.4.2 Other Imine-linked Macrocycles

Other imine-linked macrocycles with conjugated backbone structures have also been of interest of chemists studying the π-stacking interactions leading to their self-aggregation and related applications. Scheme 3.16 shows some examples of imine-linked macrocycles and their synthesis through dynamic imine chemistry. The synthesis is straightforward and the macrocycles are obtained in good yields through condensation of diamines and dialdehydes. These macrocycles show interesting aggregation behaviors in various solvents. Macrocycle **54** aggregates into mostly dimers rather than higher aggregates in acetone,[170] while higher order fibrous aggregates of the macrocycle were observed for **55**[171] and **56**.[172] Macrocycle **55** with twisted biphenyl-2,2′-diimine units forms organogel on ultrasonication of the suspension in dichloromethane for 1 minute and waiting for 0.5 h. Drying of the gel *in vacuo* produced its xerogel, with a fibrous structure (0.1–0.5 μm).

Recently, Moore and co-workers reported synthesis of [*n*]-rung molecular ladders **57a−d** through condensation of oligoamines and oligoaldehydes (Scheme 3.17).[173] As the oligomer length increased, the yield of targeted thermodynamically favored ladder molecules decreased with the increase of higher molecular weight oligomers/polymers. Further evidence from the scrambling experiments revealed that **57a** and (to a lesser extent) **57b** are dynamic and can self-correct, while the other two are kinetically trapped and cannot self-correct to form the desired products in high yield.[174] In other words, the intramolecular reformation of the same undesired bonds is faster than correction of the bonds through dissociation and reformation with another partner.
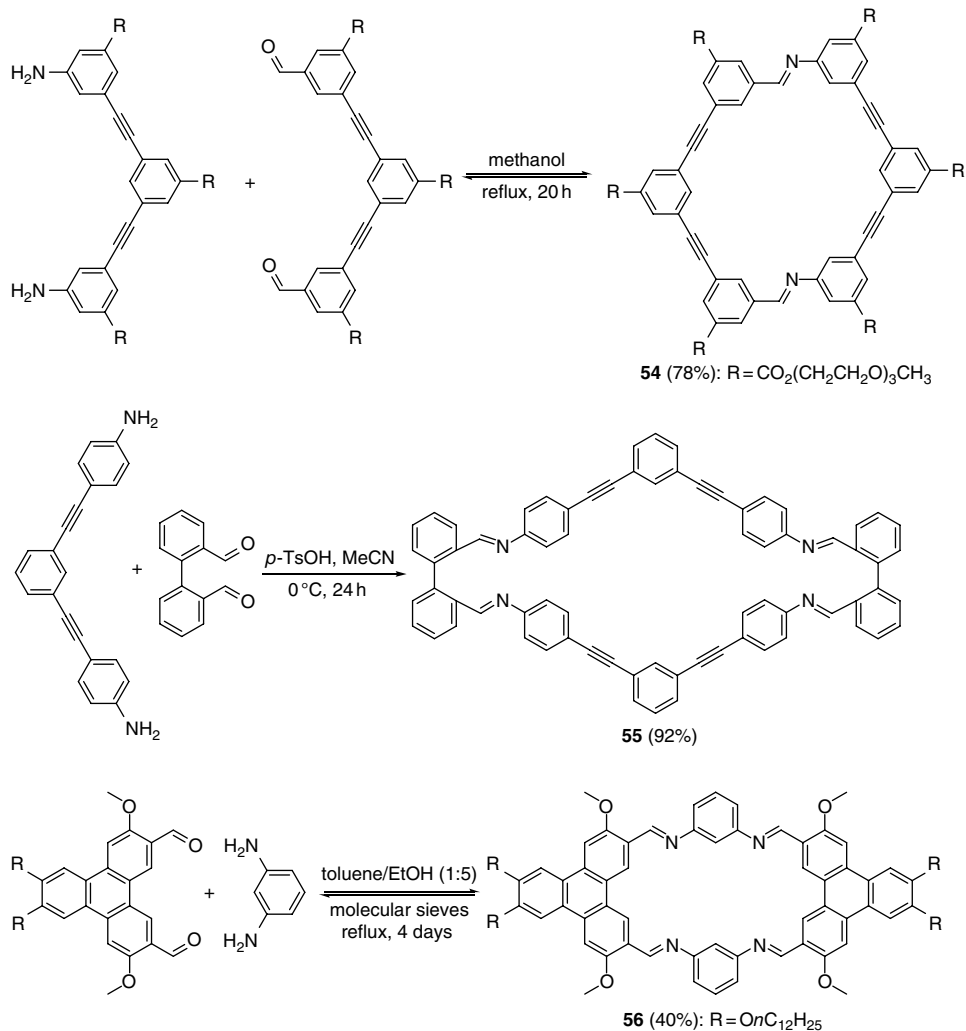
Scheme 3.16 Synthesis of imine-linked macrocycles.

As discussed previously, dynamic covalent chemistry has provided easy access to many symmetric macrocycles. However, asymmetric macrocycles are challenging targets to synthesize using this chemistry. Moore and co-workers have reported an intriguing way to prepare hetero-sequenced macrocycles by taking advantage of the directionality of imine bond formation.[175] The information for the desired sequence was encoded into the monomers by manipulating the patterns of amine or aldehyde functional groups. Three monomers were functionalized with amines or protected aldehydes in such a way that cyclic trimers would be formed as the thermodynamically most stable product. Guided by their imine sequence, self-assembly of three monomers provided an unsymmetric macrocycle as a predominant species. For ease of handling, imine macrocycles were further reduced to amine ones (**58a–c**) (44–58% yields in two steps) (Scheme 3.18). Such a sequence-directed dynamic covalent chemistry approach could be used to prepare more complex polyfunctional molecular architectures.

Step 1:
Sc(OTf)$_3$ (4 mol% per site)

MeCN/CHCl$_3$(1/19)
room temperature, 5 h

Step 2:
NaBH(OAc)$_3$ (10 eq. per site)

room temperature, overnight

57a (71%): $n = 3$, R = O(CH$_2$CH$_2$O)$_3$CH$_3$
57b (62%): $n = 4$, R = O(CH$_2$CH$_2$O)$_3$CH$_3$
57c (17%): $n = 5$, R = O(CH$_2$CH$_2$O)$_3$CH$_3$
57d (10%): $n = 6$, R = O(CH$_2$CH$_2$O)$_3$CH$_3$
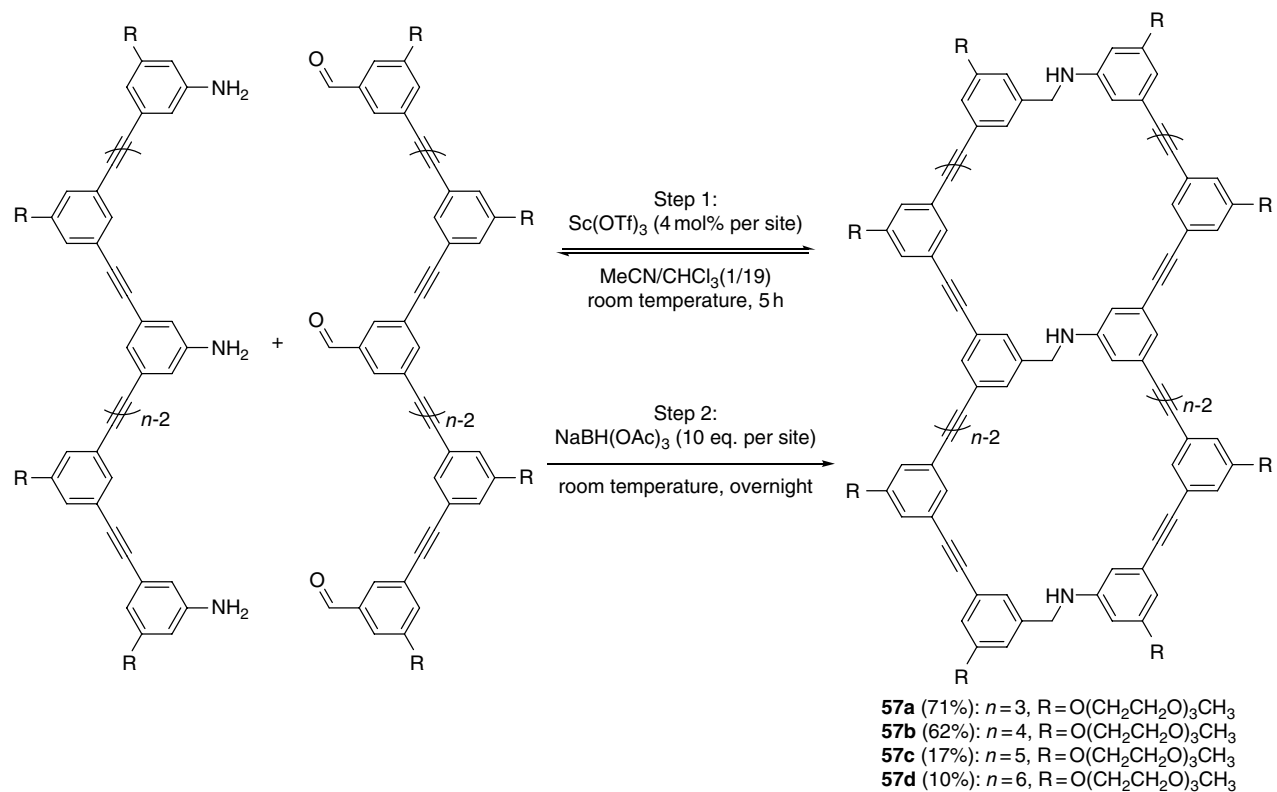
Scheme 3.17 Synthesis of [n]-rung molecular ladders **57a–d**.

(1) Sc(OTf)$_3$
1,2,4-trichlorobenzene
75 °C, 3 h
25 °C, 1 mmHg, 5 h

(2) NaBH(OAc)$_3$
rt, overnight

58a (44%): R$_1$, R$_3$, R$_4$ = O(CH$_2$CH$_2$O)$_3$CH$_3$; R$_2$ = OnC$_{16}$H$_{33}$
58b (56%): R$_1$, R$_2$, R$_3$ = O(CH$_2$CH$_2$O)$_3$CH$_3$; R$_4$ = OnC$_{16}$H$_{33}$
58c (58%): R$_1$, R$_3$ = O(CH$_2$CH$_2$O)$_3$CH$_3$; R$_2$, R$_4$ = OnC$_{16}$H$_{33}$
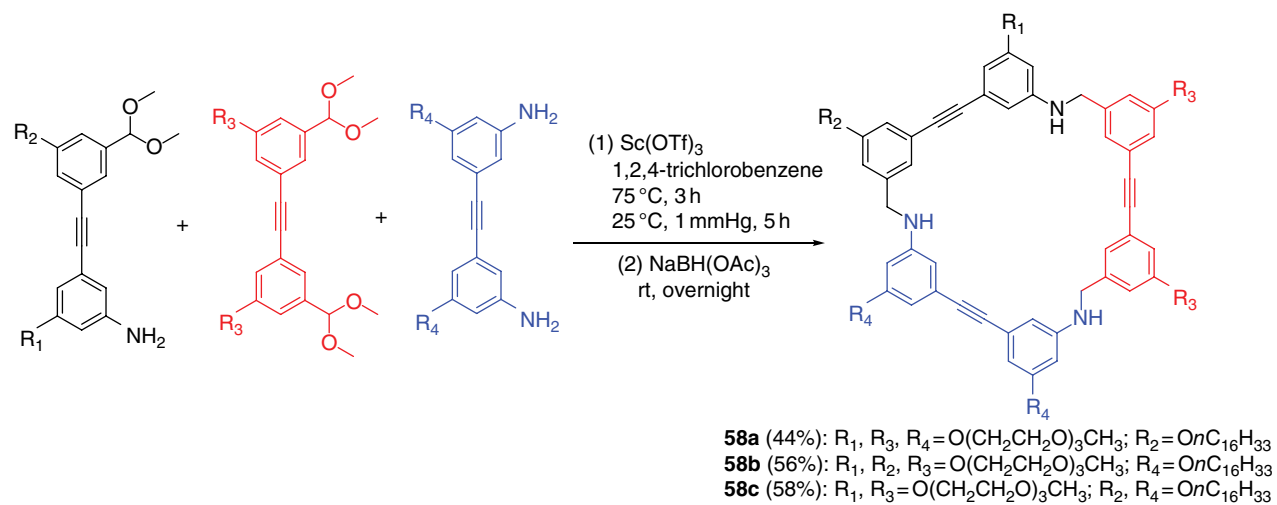
Scheme 3.18 Synthesis of asymmetric macrocycles **58a–c**.

3.5 Macrocycles through Olefin Metathesis

Vinylene groups greatly resemble imine bonds, and both of these can undergo rotational isomerization and thus are more flexible than ethynylene links. Compared to aryleneethynylene macrocycles or imine-linked macrocycles, vinylene-linked macrocycles are rare, presumably due to the synthetic challenges (e.g., control of *E*/*Z* isomer etc.).[32,176] Construction of vinylene-linked macrocycles has mostly relied on irreversible reactions,[58] such as the Ramberg–Bäcklund reaction, the Wittig reaction, the McMurry reaction, aldol condensation, and ring-closing olefin metathesis. Recently, Zhang and co-workers reported preparation of arylenevinylene macrocycles through acyclic diene metathesis macrocyclization (ADMAC) under thermodynamic control.[177,178] Vinylene-linked cyclic hexamers (**59a–h**) and carbazole-based cyclic tetramer **60** with various substituents were obtained in decent yields (45–74%) through simple one-step olefin metathesis[179–181] under the catalysis of Grubbs' second-generation catalyst (Scheme 3.19).[177,178]

It has been reported that ethynylene-linked macrocycles and diyne-linked macrocycles exhibit self-aggregation behavior, and electron-withdrawing groups strongly induce aggregation through π–π stacking while electron-donating groups have negative effect on aggregation.[5,182–185] Interestingly, more flexible arylenevinylene macrocycles generally show stronger aggregation tendency compared to analogous aryleneethynylene macrocycles with the same substituents. Variable concentration NMR experiments on phenylenevinylene cyclic hexamers revealed that they aggregate in chloroform

59a (54%): R = $nC_{10}H_{21}$
59b (65%): R = tC_4H_9
59c (64%): R = $OnC_{10}H_{21}$
59d (74%): R = OnC_4H_9
59e (51%): R = $OCOnC_9H_{19}$
59f (45%): R = $COOnC_{10}H_{21}$
59g (74%): R = $COOnC_4H_9$
59h (47%): R = $COOtC_4H_9$

60 (57%): R = $nC_{10}H_{21}$
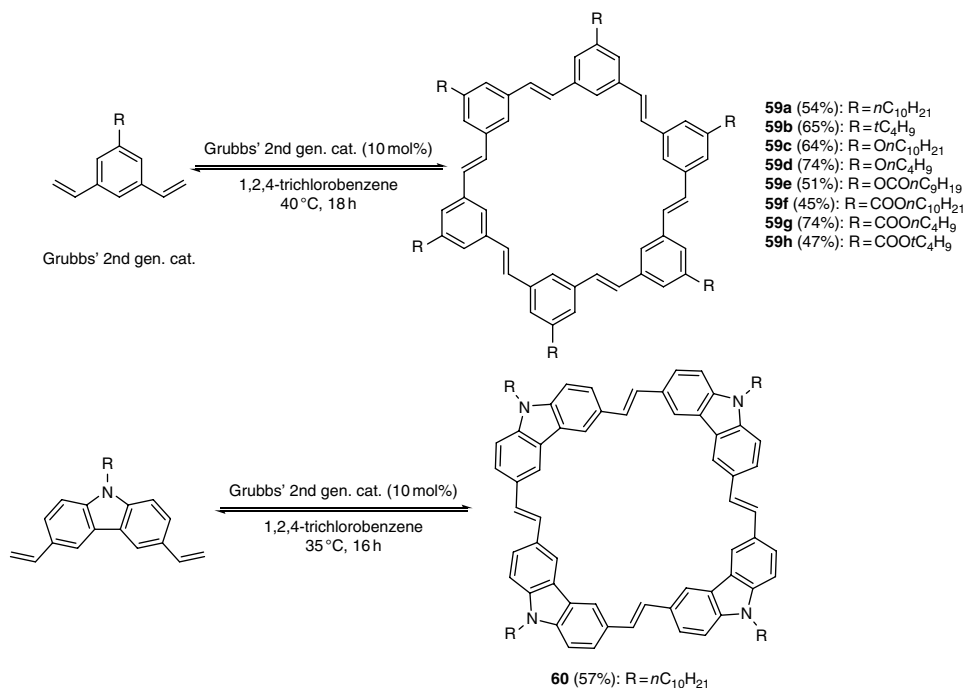
Scheme 3.19 Synthesis of arylenevinylene macrocycles **59a–h** and **60**.

regardless of whether they are substituted with electron-donating (**59c**, **59d**, and **59e**) or electron-withdrawing (**59f**, **59g**, and **59h**) substituents. Thermodynamic study of the aggregation of hexameric phenylenevinylene macrocycles and phenyleneethynylene macrocycles with the same substituents indicates that phenylenevinylene macrocycles gain comparable enthalpy but lose less entropy during the aggregation, which is likely due to their increased conformational freedom. Computer modelling studies have suggested the possible direct through-space electrostatic interaction between the substituents and periphery hydrogen atoms as the additional driving force for the strong aggregation of phenylenevinylene macrocycles. Such aggregation behavior provides experimental evidence to support the direct-interaction model,[186] which argues that direct interactions of the substituent with the neighboring π-system dominate the substituent effects rather than π-polarization.[187]

3.6 Macrocycles through Boronate Ester Formation

The dynamic covalent condensation of boronic acids with diols to form boronate esters has been widely used to prepare COFs,[188–190] capsules,[191,192] and shape-persistent cages.[193,194] Boronate ester formation has also been used to prepare shape-persistent macrocycles.[195] Northrop and co-workers reported efficient synthesis of various boronate ester macrocycles (**66–69**) through simple condensation of bis(catechol) derivatives (**61–64**) and 1,4-benzene diboronic acid (**65**) (Scheme 3.20).[196] Addition of 4 Å molecular sieves assisted full conversion of the starting materials. It was found that incorporation of large solubilizing chains improves the solubility of macrocycles, but reduces the stability of the macrocycles in protic solvents.[197] Comparison of the UV-Vis and fluorescence spectra of **66** and **67** revealed that the electronic properties of these macrocycles can be fine-tuned by changing the conjugation length. Thus, finding the optimal balance of solubility, functionality, and stability is critical to obtaining more complicated analogues.

3.7 Macrocycles through Orthogonal Dynamic Covalent Reactions

Orthogonal dynamic covalent chemistry (ODCC) has attracted great attention since it was first introduced in the early 2000s, and many interesting system have been realized.[55,198] While dynamic covalent approaches utilizing a single type of chemical transformation usually produce highly symmetric homo-sequenced shape-persistent macrocycles, ODCC provides an opportunity to incorporate two or more[199] different functionalities into a discrete molecular structure and enables interesting applications such as molecular machines.

The pioneering work by Severin and Nitschke on the synthesis of hetero-sequenced macrocycles through a combination of imine condensation and boronic acid condensation was reported in 2008 (Scheme 3.21).[200,201] In Severin's synthesis, condensation of 3-formylphenylboronic acid, pentaerythritol, and 1,4-diaminobenzene in a Dean–Stark trap provided macrocycle **70** in 40% yield. Interestingly, Nitschke and co-workers
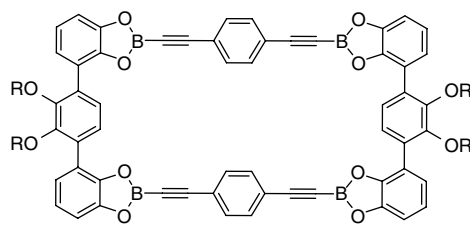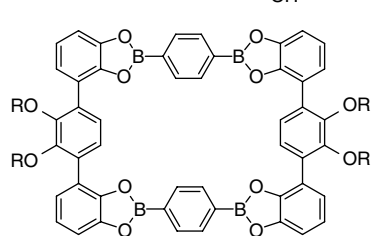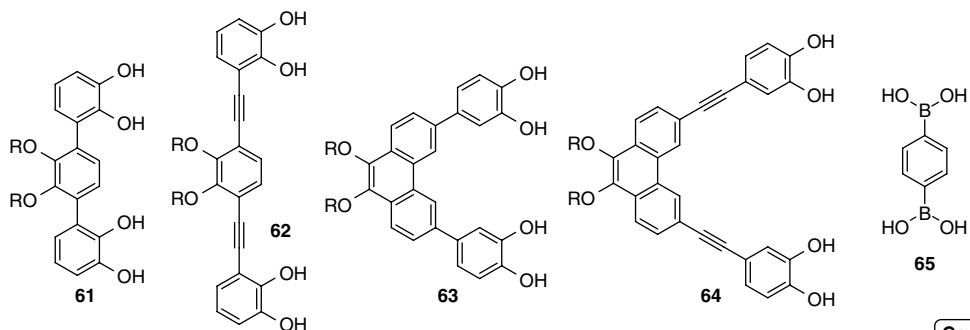
61

62

63

64

HO–B–OH

HO–B–OH

65

66 (94%): condition 1, R = nC$_6$H$_{13}$

67 (> 99%): condition 1, R = nC$_6$H$_{13}$

68a (95%): condition 1, R = nC$_6$H$_{13}$
68b (72%): condition 1, R = (CH$_2$CH$_2$O)$_2$CH$_3$
68c (99%): condition 2, R = CH$_2$(C$_6$H$_2$(OnC$_6$H$_{13}$)$_3$)

69a (97%): condition 1, R = nC$_6$H$_{13}$
69b (82%): condition 1, R = (CH$_2$CH$_2$O)$_2$CH$_3$
69c (82%): condition 2, R = CH$_2$(C$_6$H$_2$(OnC$_6$H$_{13}$)$_3$)
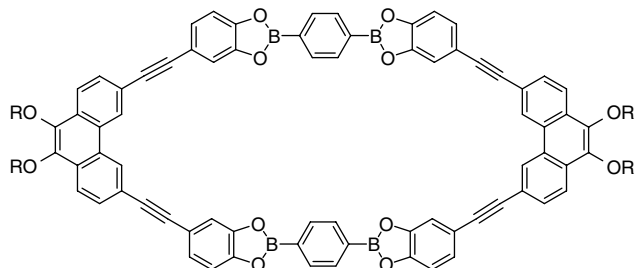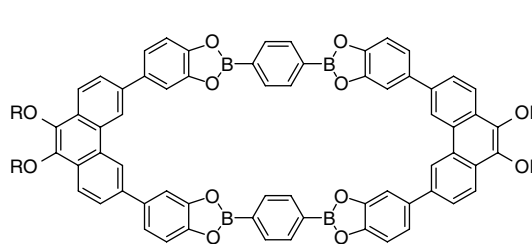
Scheme 3.20 Synthesis of macrocycles (**66–69**) through boronic acid condensation.
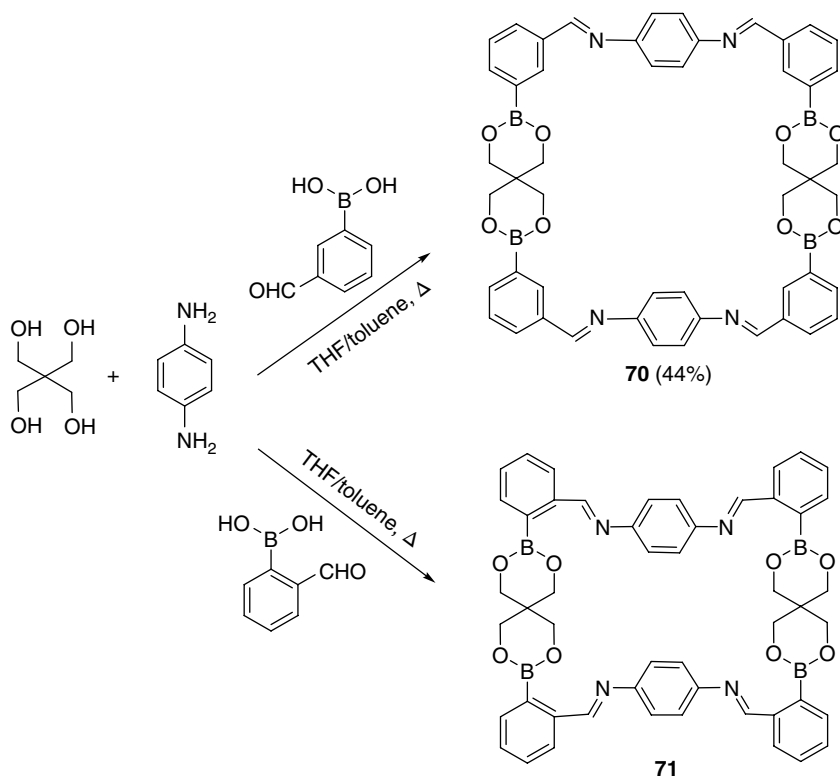
Scheme 3.21 Assembly of three-component macrocycles through imine condensation and boronic acid condensation.

obtained the very similar three-component macrocycle **71** by using 2-formylphenylboronic acid instead of 3-formylphenylboronic acid. This result indicates such macrocycles are likely to be flexible and their formation is not sensitive to building-block geometries. This is in great contrast to shape-persistent aryleneethnylene macrocycles or arylenevinylene macrocycles, whose structures are highly dependent on the angle and directionality of the functional groups attached to building blocks. For example, *ortho*-propynyl substituted phenylenes preferably form cyclic trimer, whereas *meta*-propynyl substituted phenylenes form cyclic hexamer.

In 2013, Zhang and co-workers found that imine metathesis and olefin metathesis could be used in a one-pot cyclization to prepare hetero-sequenced macrocycles.[202,203] Although the simultaneous imine and olefin metathesis was found to be sluggish and provided the target macrocycle in low yield, sequential orthogonal reaction strategies, especially the imine-then-olefin metathesis, was fairly efficient (Scheme 3.22).[202] Imine metathesis catalysed by trifluoroacetic acid (TFA), followed by removal of acid catalyst and water by-product under vacuum, and finally olefin metathesis using Hoveyda–Grubbs' second-generation catalyst, provided a series of hetero-sequenced macrocycles bearing different sizes and shapes (**72–76**) prepared in good yields (64–85%) from various combinations of a small set of building blocks: *ortho*-, *meta*-, and *para*-phenylenes (Scheme 3.22). Three-component assembly of macrocycle **76** was also accomplished.
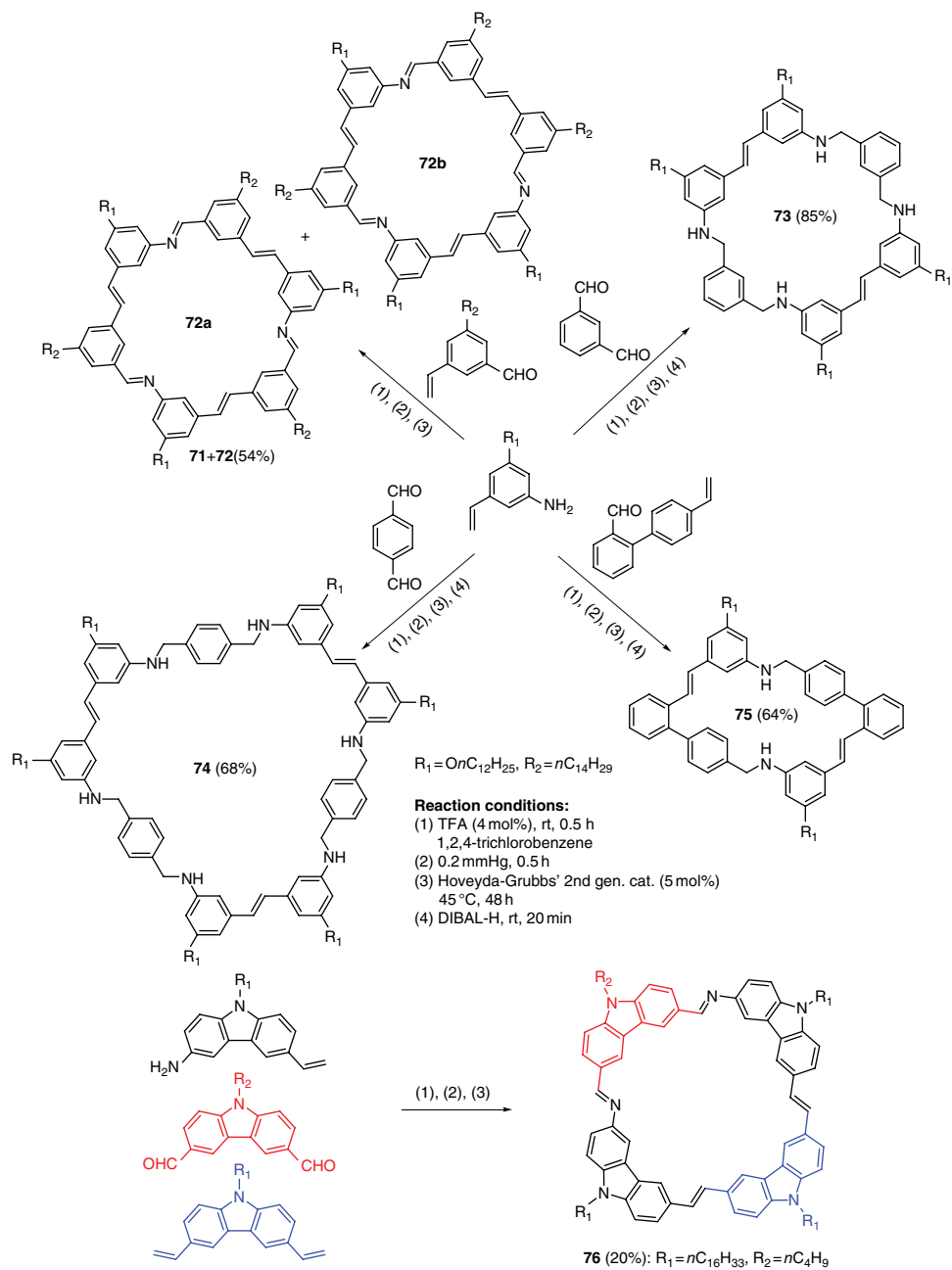
Scheme 3.22 Synthesis of multi-component macrocycles through imine condensation and olefin metathesis.

Although macrocycle **76** appears to be the predominant product in ^{1}H NMR spectra and GPC trace of the crude product mixture, a low isolated yield (20%) was obtained. A small amount of homo-sequenced vinylene-linked macrocycle formed through olefin metathesis was also observed as a side product. Although such sequential ODCC methodology provides facile access to hetero-sequenced shape-persistent macrocycles, a truly orthogonal one-pot dynamic covalent approach is anticipated.

3.8 Conclusions and Outlook

The recent development of dynamic covalent chemistry has opened a new chapter in shape-persistent macrocycles research. The convenient access to multi-gram scale macrocycles through a one-step dynamic covalent approach will greatly facilitate the exploration of their diverse applications in chemistry, materials science, and biology systems. Although it is still very much in infancy, one-step assembly of multi-component and multi-functional macrocycles from simple precursors is not a distant goal.

Various interesting applications have been demonstrated using shape-persistent macrocycles:

1) They are frequently used as building blocks for higher-ordered materials. Self-association[204] of shape-persistent macrocycles through π-stacking and solvophobic interactions[54] could form many advanced organic materials, including liquid crystals,[205] frameworks,[206] gels,[207] and nanofibrils.[208] Interactions between the peripheral substituents could also lead to self-assembled monolayers,[209] cyclindrical brushes,[210] vesicles,[119,211] and porous molecular crystals.[212] Polymerization of the backbone[213] or the substituted groups,[214] or co-polymerization with organic linkers or metal ions/clusters produced two-dimensional polymers,[215,216] COFs,[110,111,113] and metal–organic frameworks (MOFs).[112]

2) The rigid backbone and inside cavity of shape-persistent macrocycles make them perfect hosts for a variety of guests, such as metal ions,[71] anions,[217] small molecules,[218] polycyclic aromatic hydrocarbons,[219] and fullerenes.[117] Such host–guest systems have been used for sensing and molecular electronics, etc.[220–223]

3) Most shape-persistent macrocycles contain conjugated backbone with solely unsaturated bonds and full of aromatic units, for example benzene,[224–226] thiophene,[31,227] pyridine,[228,229] naphthalene,[156,230] bipyridine,[231,232] anthracene,[233,234] phenanthrene,[235–237] phenanthroline,[238,239] carbazole,[104,240] porphyrin,[241–243] and polycyclic aromatic hydrocarbons.[244–246] In addition, their electronic properties can be easily controlled by engineering substituents from electron-donating to electron-withdrawing.[247] Therefore, these macrocycles with cyclic conjugation systems have been ideal model systems for studying the electronic properties of infinitely conjugated systems. Multiple organic electronic devices have been fabricated and their performances have been evaluated (see cited references above).

4) The inside cavity, electronic property, and fluorescence of the macrocycles and the pore/channel in the higher-ordered materials formed by π-stacking or solvophobic interactions enabled sensing towards certain targets, while the rigidity of the macrocycle contributed to the selectivity. Sensors fabricated from shape-persistent macrocycles have been reported with sensing abilities towards metal ions,[248] anions,[249] small molecules,[249] explosives,[2] etc.

5) Owing to their internal cavity and self-aggregation ability to form tubular structures, these macrocycles have also found application as transmembrane mass transporters.[250] Hexameric phenylene–ethynylene macrocycles bearing amide-substituted groups partitioned into the hydrophobic core of lipid bilayers and self-assembled into transmembrane channels, which showed highly selective ion transportation properties and water permeability.

Although a variety of applications have been found for shape-persistent macrocycles, they are mostly explored in laboratory scale and their practical applications have not yet been realized. Previously, laborious synthetic efforts to prepare these macrocycles were the main hurdle for their widespread application. Nowadays, synthetic routes to certain shape-persistent macrocycles have largely been simplified and higher yields can be achieved, which can significantly reduce labor, time, and money costs. Given that shape-persistent macrocycles have already been demonstrated to possess many interesting properties, with a convenient synthetic protocol, the development of novel macrocycles is anticipated (a recent example is the Brønsted pair[251]) and their fantastic properties are waiting to be discovered.[252] Recent advances in dynamic covalent assembly has already shown the power of the thermodynamically controlled approach. However, ongoing efforts also require the development of new dynamic covalent reactions, for example the orthoester exchange reported by von Delius in 2015,[253,254] amide formation/exchange,[255] and diethynylene metathesis,[256] to expand the existing synthetic toolset and get access to novel macrocyclic structures and properties. We hope this review offers useful insight and exciting examples to scientists and encourages more exploration of the possibilities of macrocycles and dynamic covalent reactions.

References

1 S. Höger, *J. Polym. Sci. Part A: Polym. Chem.* **1999**, *37*, 2685–2698.

2 D. E. Gross, L. Zang, J. S. Moore, *Pure Appl. Chem.* **2012**, *84*, 869–878.

3 J. S. Moore, *Acc. Chem. Res.* **1997**, *30*, 402–413.

4 C. Grave, A. D. Schlüter, *Eur. J. Org. Chem.* **2002**, *2002*, 3075–3098.

5 D. Zhao, J. S. Moore, *Chem. Commun.* **2003**, 807–818.

6 Y. Yamaguchi, Z.-i. Yoshida, *Chem. Eur. J.* **2003**, *9*, 5430–5440.

7 S. Höger, *Chem. Eur. J.* **2004**, *10*, 1320–1329.

8 W. Zhang, J. S. Moore, *Angew. Chem., Int. Ed.* **2006**, *45*, 4416–4439.

9 M. Iyoda, J. Yamakawa, M. J. Rahman, *Angew. Chem., Int. Ed.* **2011**, *50*, 10522–10553.

10 M. Fujita, M. Tominaga, A. Hori, B. Therrien, *Acc. Chem. Res.* **2005**, *38*, 369–378.

11 R. Chakrabarty, P. S. Mukherjee, P. J. Stang, *Chem. Rev.* **2011**, *111*, 6810–6918.

12 S. Anderson, H. L. Anderson, J. K. M. Sanders, *Acc. Chem. Res.* **1993**, *26*, 469–475.

13 M. C. O'Sullivan, J. K. Sprafke, D. V. Kondratuk, C. Rinfray, T. D. W. Claridge, A. Saywell, M. O. Blunt, J. N. O'Shea, P. H. Beton, M. Malfois, H. L. Anderson, *Nature* **2011**, *469*, 72–75.

14 M. Pawlicki, L. Latos-Grażyński, *Angew. Chem., Int. Ed.* **2012**, *51*, 11205–11207.

15 S. Furukawa, S. De Feyter, *Topics Curr. Chem.* **2009**, *287*, 87–133.

16 T. Kudernac, S. Lei, J. A. A. W. Elemans, S. De Feyter, *Chem. Soc. Rev.* **2009**, *38*, 402–421.

17 J. A. A. W. Elemans, S. Lei, S. De Feyter, *Angew. Chem., Int. Ed.* **2009**, *48*, 7298–7332.

18 K. S. Mali, J. Adisoejoso, E. Ghijsens, I. De Cat, S. De Feyter, *Acc. Chem. Res.* **2012**, *45*, 1309–1320.

19 Y. Hua, A. H. Flood, *Chem. Soc. Rev.* **2010**, *39*, 1262–1271.

20 K. P. McDonald, Y. Hua, S. Lee, A. H. Flood, *Chem. Commun.* **2012**, *48*, 5065–5075.

21 B. Gong, *Acc. Chem. Res.* **2008**, *41*, 1376–1386.

22 K. Yamato, M. Kline, B. Gong, *Chem. Commun.* **2012**, *48*, 12142–12158.

23 B. Gong, Z. Shao, *Acc. Chem. Res.* **2013**, *46*, 2856–2866.

24 M. M. Haley, *Synlett* **1998**, *1998*, 557–565.

25 M. M. Haley, J. J. Pak, S. C. Brand, *Topics Curr. Chem.* **1999**, *201*, 81–130.

26 J. A. Marsden, G. J. Palmer, M. M. Haley, *Eur. J. Org. Chem.* **2003**, *2003*, 2355–2369.

27 M. M. Haley, *Pure Appl. Chem.* **2008**, *80*, 519–532.

28 S. Höger, *Pure Appl. Chem.* **2010**, *82*, 821–830.

29 M. Iyoda, *Pure Appl. Chem.* **2010**, *82*, 831–841.

30 M. Iyoda, *J. Synth. Org. Chem., Jpn* **2012**, *70*, 1157–1163.

31 M. Iyoda, H. Shimizu, *Chem. Soc. Rev.* **2015**, *44*, 6411–6424.

32 T. Nishiuchi, M. Iyoda, *Chem. Rec.* **2015**, *15*, 329–346.

33 X. Zhao, Z.-T. Li, *Chem. Commun.* **2010**, *46*, 1601–1616.

34 S. Lei, K. Tahara, J. Adisoejoso, T. Balandina, Y. Tobe, S. De Feyter, *Cryst. Eng. Comm.* **2010**, *12*, 3369–3381.

35 K. Tahara, S. Lei, J. Adisoejoso, S. De Feyter, Y. Tobe, *Chem. Commun.* **2010**, *46*, 8507–8525.

36 S. Toyota, *Chem. Lett.* **2011**, *40*, 12–18.

37 S. Toyota, *Pure Appl. Chem.* **2012**, *84*, 917–929.

38 W. J. Youngs, C. A. Tessier, J. D. Bradshaw, *Chem. Rev.* **1999**, *99*, 3153–3180.

39 H. Fu, Y. Liu, H. Zeng, *Chem. Commun.* **2013**, *49*, 4127–4144.

40 F. Diederich, M. Kivala, *Adv. Mater.* **2010**, *22*, 803–812.

41 P. Rivera-Fuentes, F. Diederich, *Angew. Chem., Int. Ed.* **2012**, *51*, 2818–2828.

42 R. Reuter, H. A. Wegner, *Chem. Commun.* **2011**, *47*, 12267–12276.

43 Z. Li, J. Liang, W. Xue, G. Liu, S. H. Liu, J. Yin, *Supramol. Chem.* **2013**, *26*, 54–65.

44 F. Diederich, *Chem. Commun.* **2001**, 219–227.

45 V. Maraval, R. Chauvin, *Chem. Rev.* **2006**, *106*, 5317–5343.

46 R. R. Tykwinski, M. Gholami, S. Eisler, Y. Zhao, F. Melin, L. Echegoyen, *Pure Appl. Chem.* **2008**, *80*, 621.

47 T. Kawase, *Synlett* **2007**, *2007*, 2609–2626.

48 U. H. F. Bunz, S. Menning, N. Martín, *Angew. Chem., Int. Ed.* **2012**, *51*, 7094–7101.

49 S. E. Lewis, *Chem. Soc. Rev.* **2015**, *44*, 2221–2304.

50 E. R. Darzi, R. Jasti, *Chem. Soc. Rev.* **2015**, *44*, 6401–6410.

51 S. P. Black, J. K. M. Sanders, A. R. Stefankiewicz, *Chem. Soc. Rev.* **2014**, *43*, 1861–1872.

52 S. Otto, R. L. E. Furlan, J. K. M. Sanders, *Science* **2002**, *297*, 590–593.

53 J. Li, J. M. A. Carnall, M. C. A. Stuart, S. Otto, *Angew. Chem., Int. Ed.* **2011**, *50*, 8384–8386.

54 M. K. Smith, O. S. Miljanic, *Org. Biomol. Chem.* **2015**, *13*, 7841–7845.

55 S.-L. Huang, G.-X. Jin, H.-K. Luo, T. S. A. Hor, *Chem. Asian J.* **2015**, *10*, 24–42.

56 P. Siemsen, R. C. Livingston, F. Diederich, *Angew. Chem., Int. Ed.* **2000**, *39*, 2632–2657.

57 C. C. C. Johansson Seechurn, M. O. Kitching, T. J. Colacot, V. Snieckus, *Angew. Chem., Int. Ed.* **2012**, *51*, 5062–5085.

58 G. J. Bodwell, P. R. Nandaluru, *Isr. J. Chem.* **2012**, *52*, 105–138.

59 V. R. Pattabiraman, J. W. Bode, *Nature* **2011**, *480*, 471–479.

60 S. Höger, V. Enkelmann, *Angew. Chem., Int. Ed.* **1996**, *34*, 2713–2716.

61 J. S. Moore, J. Zhang, *Angew. Chem., Int. Ed.* **1992**, *31*, 922–924.

62 H. A. Staab, K. Neunhoeffer, *Synthesis* **1974**, *1974*, 424–424.

63 V. Martí-Centelles, M. D. Pandey, M. I. Burguete, S. V. Luis, *Chem. Rev.* **2015**, *115*, 8736–8834.

64 H. L. Anderson, J. K. M. Sanders, *Angew. Chem., Int. Ed.* **1990**, *29*, 1400–1403.

65 J.-M. Lehn, *Chem. Eur. J.* **1999**, *5*, 2455–2463.

66 S. J. Rowan, S. J. Cantrill, G. R. L. Cousins, J. K. M. Sanders, J. F. Stoddart, *Angew. Chem. Int. Ed.* **2002**, *41*, 898–952.

67 P. T. Corbett, J. Leclaire, L. Vial, K. R. West, J.-L. Wietor, J. K. M. Sanders, S. Otto, *Chem. Rev.* **2006**, *106*, 3652–3711.

68 Y. Jin, C. Yu, R. J. Denman, W. Zhang, *Chem. Soc. Rev.* **2013**, *42*, 6634–6654.

69 D. E. Gross, E. Discekici, J. S. Moore, *Chem. Commun.* **2012**, *48*, 4426–4428.

70 H. A. Staab, F. Graf, *Tetrahedron Lett.* **1966**, *7*, 751–757.

71 J. D. Ferrara, C. Tessier-Youngs, W. J. Youngs, *Organometallics* **1987**, *6*, 676–678.

72 J. Zhang, D. J. Pesak, J. L. Ludwick, J. S. Moore, *J. Am. Chem. Soc.* **1994**, *116*, 4227–4239.

73 D. L. Morrison, S. Hoger, *Chem. Commun.* **1996**, 2313–2314.

74 T. Kawase, N. Ueda, H. R. Darabi, M. Oda, *Angew. Chem., Int. Ed.* **1996**, *35*, 1556–1558.

75 T. Kawase, N. Ueda, M. Oda, *Tetrahedron Lett.* **1997**, *38*, 6681–6684.

76 T. Kawase, Y. Hosokawa, H. Kurata, M. Oda, *Chem. Lett.* **1999**, *28*, 745–746.

77 C. Eickmeier, H. Junga, A. J. Matzger, F. Scherhag, M. Shim, K. P. C. Vollhardt, *Angew. Chem., Int. Ed.* **1997**, *36*, 2103–2108.

78 Y. Tobe, N. Utsumi, K. Kawabata, K. Naemura, *Tetrahedron Lett.* **1996**, *37*, 9325–9328.

79 U. H. F. Bunz, Y. Rubin, Y. Tobe, *Chem. Soc. Rev.* **1999**, *28*, 107–119.

80 M. M. Haley, S. C. Brand, J. J. Pak, *Angew. Chem., Int. Ed.* **1997**, *36*, 836–838.

81 A. Furstner, P. W. Davies, *Chem. Commun.* **2005**, 2307–2320.

82 W. Zhang, J. S. Moore, *Adv. Synth. Catal.* **2007**, *349*, 93–120.

83 X. Wu, M. Tamm, *Beilstein J. Org. Chem.* **2011**, *7*, 82–93.

84 U. H. F. Bunz, *Acc. Chem. Res.* **2001**, *34*, 998–1010.

85 A. Mortreux, M. Blanchard, *Chem. Commun.* **1974**, 786–787.

86 R. R. Schrock, *Acc. Chem. Res.* **1986**, *19*, 342–348.

87 K. Jyothish, W. Zhang, *Angew. Chem., Int. Ed.* **2011**, *50*, 8478–8480.

88 M. Bindl, R. Stade, E. K. Heilmann, A. Picot, R. Goddard, A. Fürstner, *J. Am. Chem. Soc.* **2009**, *131*, 9468–9470.

89 P.-H. Ge, W. Fu, W. A. Herrmann, E. Herdtweck, C. Campana, R. D. Adams, U. H. F. Bunz, *Angew. Chem., Int. Ed.* **2000**, *39*, 3607–3610.

90 L. Kloppenburg, D. Jones, U. H. F. Bunz, *Macromolecules* **1999**, *32*, 4194–4203.

91 O. Š. Miljanić, K. P. C. Vollhardt, G. D. Whitener, *Synlett* **2003**, *2003*, 0029–0034.

92 W. Zhang, S. Kraft, J. S. Moore, *J. Am. Chem. Soc.* **2004**, *126*, 329–335.

93 W. Zhang, S. M. Brombosz, J. L. Mendoza, J. S. Moore, *J. Org. Chem.* **2005**, *70*, 10198–10201.

94 F. Xu, L. Peng, K. Shinohara, T. Morita, S. Yoshida, T. Hosoya, A. Orita, J. Otera, *J. Org. Chem.* **2014**, *79*, 11592–11608.

95 T. Balandina, K. Tahara, N. Sändig, M. O. Blunt, J. Adisoejoso, S. Lei, F. Zerbetto, Y. Tobe, S. De Feyter, *ACS Nano* **2012**, *6*, 8381–8389.

96 W. Zhang, J. S. Moore, *J. Am. Chem. Soc.* **2004**, *126*, 12796–12796.

97 W. Zhang, J. S. Moore, *J. Am. Chem. Soc.* **2005**, *127*, 11863–11870.

98 A. Datar, D. E. Gross, K. Balakrishnan, X. Yang, J. S. Moore, L. Zang, *Chem. Commun.* **2012**, *48*, 8904–8906.

99 L. Li, Y. Che, D. E. Gross, H. Huang, J. S. Moore, L. Zang, *ACS Macro Lett.* **2012**, *1*, 1335–1338.

100 Y. Lu, T. Suzuki, W. Zhang, J. S. Moore, B. J. Mariñas, *Chem. Mater.* **2007**, *19*, 3194–3204.

101 T. Suzuki, Y. Lu, W. Zhang, J. S. Moore, B. J. Mariñas, *Environ. Sci. Technol.* **2007**, *41*, 6246–6252.

102 W. Zhang, J. S. Moore, *J. Am. Chem. Soc.* **2004**, *126*, 12796.

103 A. D. Finke, D. E. Gross, A. Han, J. S. Moore, *J. Am. Chem. Soc.* **2011**, *133*, 14063–14070.

104 S. Maruyama, H. Hokari, X.-t. Tao, A. Gunji, T. Wada, H. Sasabe, *Chem. Lett.* **1999**, *28*, 731–732.

105 S. Maruyama, H. Hokari, T. Wada, H. Sasabe, *Synthesis* **2001**, *2001*, 1794–1799.

106 W. Zhang, H. M. Cho, J. S. Moore, *Org. Synth.* **2007**, *84*, 177.

107 T. Naddo, Y. Che, W. Zhang, K. Balakrishnan, X. Yang, M. Yen, J. Zhao, J. S. Moore, L. Zang, *J. Am. Chem. Soc.* **2007**, *129*, 6978–6979.

108 J. Heppekausen, R. Stade, R. Goddard, A. Fürstner, *J. Am. Chem. Soc.* **2010**, *132*, 11045–11057.

109 H. Yang, Z. Liu, W. Zhang, *Adv. Synth. Catal.* **2013**, *355*, 885–890.

110 H. Yang, Y. Du, S. Wan, G. D. Trahan, Y. Jin, W. Zhang, *Chem. Sci.* **2015**, *6*, 4049–4053.

111 X. Feng, Y. Dong, D. Jiang, *Cryst. Eng. Comm.* **2013**, *15*, 1508–1511.

112 T.-H. Chen, I. Popov, Y.-C. Chuang, Y.-S. Chen, O. S. Miljanic, *Chem. Commun.* **2015**, *51*, 6340–6342.

113 L. A. Baldwin, J. W. Crowe, M. D. Shannon, C. P. Jaroniec, P. L. McGrier, *Chem. Mater.* **2015**, *27*, 6169–6172.

114 C. Zhang, H. Long, W. Zhang, *Chem. Commun.* **2012**, *48*, 6172–6174.

115 C. Yu, H. Long, Y. Jin, W. Zhang, *Org. Lett.* **2016**, *18*, 2946–2949.

116 K. Jyothish, W. Zhang, *Angew. Chem. Int. Ed.* **2011**, *50*, 3435–3438.

117 C. Yu, Y. Jin, W. Zhang, *Chem. Rec.* **2015**, *15*, 97–106.

118 J. Jiang, G. N. Tew, *Org. Lett.* **2008**, *10*, 4393–4396.

119 S. H. Seo, J. Y. Chang, G. N. Tew, *Angew. Chem., Int. Ed.* **2006**, *45*, 7526–7530.

120 S. H. Seo, T. V. Jones, H. Seyler, J. O. Peters, T. H. Kim, J. Y. Chang, G. N. Tew, *J. Am. Chem. Soc.* **2006**, *128*, 9264–9265.

121 J. M. Kehoe, J. H. Kiley, J. J. English, C. A. Johnson, R. C. Petersen, M. M. Haley, *Org. Lett.* **2000**, *2*, 969–972.

122 C. A. Johnson, Y. Lu, M. M. Haley, *Org. Lett.* **2007**, *9*, 3725–3728.

123 K. Tahara, Y. Yamamoto, D. E. Gross, H. Kozuma, Y. Arikuma, K. Ohta, Y. Koizumi, Y. Gao, Y. Shimizu, S. Seki, K. Kamada, J. S. Moore, Y. Tobe, *Chem. Eur. J.* **2013**, *19*, 11251–11260.

124 J. A. Marsden, M. M. Haley, *J. Org. Chem.* **2005**, *70*, 10213–10226.

125 Y. Li, L. Xu, H. Liu, Y. Li, *Chem. Soc. Rev.* **2014**, *43*, 2572–2586.

126 B. Trost, *Science* **1991**, *254*, 1471–1477.

127 D. E. Gross, J. S. Moore, *Macromolecules* **2011**, *44*, 3685–3687.

128 S. W. Sisco, J. S. Moore, *J. Am. Chem. Soc.* **2012**, *134*, 9114–9117.

129 S. W. Sisco, J. S. Moore, *Chem. Sci.* **2014**, *5*, 81–85.

130 S. W. Sisco, B. M. Larson, J. S. Moore, *Macromolecules* **2014**, *47*, 3829–3836.

131 M. E. Belowich, J. F. Stoddart, *Chem. Soc. Rev.* **2012**, *41*, 2003–2024.

132 N. E. Borisova, M. D. Reshetova, Y. A. Ustynyuk, *Chem. Rev.* **2007**, *107*, 46–79.

133 S. Akine, T. Nabeshima, *Dalton Trans*. **2009**, 10395–10408.

134 T. Nabeshima, *Bull. Chem. Soc. Jpn* **2010**, *83*, 969–991.

135 T. Nabeshima, M. Yamamura, *Pure Appl. Chem.* **2013**, *85*, 763–776.

136 M. J. MacLachlan, *Pure Appl. Chem.* **2006**, *78*, 873–888.

137 P. D. Frischmann, M. J. MacLachlan, *Comments on Inorg. Chem.* **2008**, *29*, 26–45.

138 S. J. Wezenberg, A. W. Kleij, *Angew. Chem., Int. Ed.* **2008**, *47*, 2354–2364.

139 A. W. Kleij, *Chem. Eur. J.* **2008**, *14*, 10520–10529.

140 H. L. C. Feltham, S. Brooker, *Coord. Chem. Rev.* **2009**, *253*, 1458–1475.

141 C. J. Whiteoak, G. Salassa, A. W. Kleij, *Chem. Soc. Rev.* **2012**, *41*, 622–631.

142 P. A. Vigato, V. Peruzzo, S. Tamburini, *Coord. Chem. Rev.* **2012**, *256*, 953–1114.

143 S. Akine, *J. Incl. Phenom. Macro.* **2012**, *72*, 25–54.

144 R. M. Clarke, T. Storr, *Dalton Trans.* **2014**, *43*, 9380–9391.

145 S. Akine, T. Taniguchi, T. Nabeshima, *Tetrahedron Lett.* **2001**, *42*, 8861–8864.

146 K. E. Shopsowitz, D. Edwards, A. J. Gallant, M. J. MacLachlan, *Tetrahedron* **2009**, *65*, 8113–8119.

147 A. J. Gallant, M. J. MacLachlan, *Angew. Chem., Int. Ed.* **2003**, *42*, 5307–5310.

148 A. J. Gallant, J. K. H. Hui, F. E. Zahariev, Y. A. Wang, M. J. MacLachlan, *J. Org. Chem.* **2005**, *70*, 7936–7946.

149 P. D. Frischmann, A. J. Gallant, J. H. Chong, M. J. MacLachlan, *Inorg. Chem.* **2008**, *47*, 101–112.

150 C. Ma, A. Lo, A. Abdolmaleki, M. J. MacLachlan, *Org. Lett.* **2004**, *6*, 3841–3844.

151 S.-i. Kawano, Y. Ishida, K. Tanaka, *J. Am. Chem. Soc.* **2015**, *137*, 2295–2302.

152 J. K. H. Hui, M. J. MacLachlan, *Chem. Commun.* **2006**, 2480–2482.

153 P. D. Frischmann, J. Jiang, J. K. H. Hui, J. J. Grzybowski, M. J. MacLachlan, *Org. Lett.* **2008**, *10*, 1255–1258.

154 J. Jiang, M. J. MacLachlan, *Chem. Commun.* **2009**, 5695–5697.

155 J. Jiang, M. J. MacLachlan, *Org. Lett.* **2010**, *12*, 1020–1023.

156 A. J. Gallant, M. Yun, M. Sauer, C. S. Yeung, M. J. MacLachlan, *Org. Lett.* **2005**, *7*, 4827–4830.

157 T. Nabeshima, H. Miyazaki, A. Iwasaki, S. Akine, T. Saiki, C. Ikeda, S. Sato, *Chem. Lett.* **2006**, *35*, 1070–1071.

158 T. Nabeshima, H. Miyazaki, A. Iwasaki, S. Akine, T. Saiki, C. Ikeda, *Tetrahedron* **2007**, *63*, 3328–3333.

159 A. J. Gallant, J. H. Chong, M. J. MacLachlan, *Inorg. Chem.* **2006**, *45*, 5248–5250.

160 P. D. Frischmann, S. H. M. Mehr, B. O. Patrick, F. Lelj, M. J. MacLachlan, *Inorg. Chem.* **2012**, *51*, 3443–3453.

161 P. D. Frischmann, M. J. MacLachlan, *Chem. Commun.* **2007**, 4480–4482.

162 P. D. Frischmann, G. A. Facey, P. Y. Ghi, A. J. Gallant, D. L. Bryce, F. Lelj, M. J. MacLachlan, *J. Am. Chem. Soc.* **2010**, *132*, 3893–3908.

163 M. Yamamura, M. Iida, K. Kanazawa, M. Sasaki, T. Nabeshima, *Bull. Chem. Soc. Jpn* **2014**, *87*, 334–340.

164 M. Yamamura, M. Sasaki, M. Kyotani, H. Orita, T. Nabeshima, *Chem. Eur. J.* **2010**, *16*, 10638–10643.

165 G. Salassa, A. M. Castilla, A. W. Kleij, *Dalton Trans.* **2011**, *40*, 5236–5243.

166 S. Akine, Z. Varadi, T. Nabeshima, *Eur. J. Inorg. Chem.* **2013**, *2013*, 5987–5998.

167 J. K. H. Hui, J. Jiang, M. J. MacLachlan, *Can. J. Chem.* **2012**, *90*, 1056–1062.

168 J. K. H. Hui, P. D. Frischmann, C.-H. Tso, C. A. Michal, M. J. MacLachlan, *Chem. Eur. J.* **2010**, *16*, 2453–2460.

169 C. T. L. Ma, M. J. MacLachlan, *Angew. Chem., Int. Ed.* **2005**, *44*, 4178–4182.

170 D. Zhao, J. S. Moore, *J. Org. Chem.* **2002**, *67*, 3548–3554.

171 T. Ide, D. Takeuchi, K. Osakada, *Chem. Commun.* **2012**, *48*, 278–280.

172 T. Dutta, Y. Che, H. Zhong, J. H. Laity, V. Dusevich, J. B. Murowchick, L. Zang, Z. Peng, *RSC Adv.* **2013**, *3*, 6008–6015.

173 C. S. Hartley, E. L. Elliott, J. S. Moore, *J. Am. Chem. Soc.* **2007**, *129*, 4512–4513.

174 E. L. Elliott, C. S. Hartley, J. S. Moore, *Chem. Commun.* **2011**, *47*, 5028–5030.

175 C. S. Hartley, J. S. Moore, *J. Am. Chem. Soc.* **2007**, *129*, 11682–11683.

176 H. Meier, *Synthesis* **2002**, *2002*, 1213–1228.

177 Y. Jin, A. Zhang, Y. Huang, W. Zhang, *Chem. Commun.* **2010**, *46*, 8258–8260.

178 C. Zhang, C. Yu, H. Long, R. J. Denman, Y. Jin, W. Zhang, *Chem. Eur. J.* **2015**, *21*, 16935–16940.

179 Y. Chauvin, *Angew. Chem., Int. Ed.* **2006**, *45*, 3740–3747.

180 R. R. Schrock, *Angew. Chem., Int. Ed.* **2006**, *45*, 3748–3759.

181 R. H. Grubbs, *Angew. Chem., Int. Ed.* **2006**, *45*, 3760–3765.

182 Y. Tobe, N. Utsumi, K. Kawabata, A. Nagano, K. Adachi, S. Araki, M. Sonoda, K. Hirose, K. Naemura, *J. Am. Chem. Soc.* **2002**, *124*, 5350–5364.

183 H. Sugiura, Y. Takahira, M. Yamaguchi, *J. Org. Chem.* **2005**, *70*, 5698–5708.

184 M.-F. Ng, S.-W. Yang, J. Phys. *Chem. B* **2007**, *111*, 13886–13893.

185 L. Shu, M. Muri, R. Krupke, M. Mayor, *Org. Biomol. Chem.* **2009**, *7*, 1081–1092.

186 S. E. Wheeler, *J. Am. Chem. Soc.* **2011**, *133*, 10262–10274.

187 C. A. Hunter, J. K. M. Sanders, *J. Am. Chem. Soc.* **1990**, *112*, 5525–5534.

188 X. Feng, X. Ding, D. Jiang, *Chem. Soc. Rev.* **2012**, *41*, 6010–6022.

189 S.-Y. Ding, W. Wang, *Chem. Soc. Rev.* **2013**, *42*, 548–568.

190 J. W. Colson, W. R. Dichtel, *Nat. Chem.* **2013**, *5*, 453–465.

191 N. Nishimura, K. Kobayashi, *Angew. Chem., Int. Ed.* **2008**, *47*, 6255–6258.

192 S. Klotzbach, T. Scherpf, F. Beuerle, *Chem. Commun.* **2014**, *50*, 12454–12457.

193 G. Zhang, O. Presly, F. White, I. M. Oppel, M. Mastalerz, *Angew. Chem., Int. Ed.* **2014**, *53*, 1516–1520.

194 G. Zhang, O. Presly, F. White, I. M. Oppel, M. Mastalerz, *Angew. Chem., Int. Ed.* **2014**, *53*, 5126–5130.

195 N. Christinat, R. Scopelliti, K. Severin, *Chem. Commun.* **2004**, 1158–1159.

196 M. K. Smith, N. E. Powers-Riggs, B. H. Northrop, *Chem. Commun.* **2013**, *49*, 6167–6169.

197 M. K. Smith, A. R. Goldberg, B. H. Northrop, *Eur. J. Org. Chem.* **2015**, *2015*, 2928–2941.

198 A. Wilson, G. Gasparini, S. Matile, *Chem. Soc. Rev.* **2014**, *43*, 1948–1962.

199 K.-D. Zhang, S. Matile, *Angew. Chem., Int. Ed.* **2015**, *54*, 8980–8983.

200 M. Hutin, G. Bernardinelli, J. R. Nitschke, *Chem. Eur. J.* **2008**, *14*, 4585–4593.

201 N. Christinat, R. Scopelliti, K. Severin, *Angew. Chem., Int. Ed.* **2008**, *47*, 1848–1852.

202 K. D. Okochi, Y. Jin, W. Zhang, *Chem. Commun.* **2013**, *49*, 4418–4420.

203 K. D. Okochi, G. S. Han, I. M. Aldridge, Y. Liu, W. Zhang, *Org. Lett.* **2013**, *15*, 4296–4299.

204 J. Zhang, J. S. Moore, *J. Am. Chem. Soc.* **1992**, *114*, 9701–9702.

205 T. Wöhrle, I. Wurzbach, J. Kirres, A. Kostidou, N. Kapernaum, J. Litterscheidt, J. C. Haenle, P. Staffeld, A. Baro, F. Giesselmann, S. Laschat, *Chem. Rev.* **2016**, *116*, 1139–1241.

206 D. Venkataraman, S. Lee, J. Zhang, J. S. Moore, *Nature* **1994**, *371*, 591–593.

207 C.-H. Lin, J. Tour, *J. Org. Chem.* **2002**, *67*, 7761–7768.

208 L. Zang, Y. Che, J. S. Moore, *Acc. Chem. Res.* **2008**, *41*, 1596–1608.

209 S. Höger, K. Bonrad, A. Mourran, U. Beginn, M. Möller, *J. Am. Chem. Soc.* **2001**, *123*, 5651–5659.

210 S. Rosselli, A.-D. Ramminger, T. Wagner, B. Silier, S. Wiegand, W. Häußler, G. Lieser, V. Scheumann, S. Höger, *Angew. Chem., Int. Ed.* **2001**, *40*, 3137–3141.

211 J.-K. Kim, E. Lee, M.-C. Kim, E. Sim, M. Lee, *J. Am. Chem. Soc.* **2009**, *131*, 17768–17770.

212 I. Hisaki, S. Nakagawa, N. Tohnai, M. Miyata, *Angew. Chem., Int. Ed.* **2015**, *54*, 3008–3012.

213 S. Rondeau-Gagne, J.-F. Morin, *Chem. Soc. Rev.* **2014**, *43*, 85–98.

214 T. Kaneko, T. Horie, S. Matsumoto, M. Teraguchi, T. Aoki, *Macromol. Chem. Phys.* **2009**, *210*, 22–36.

215 P. Kissel, R. Erni, W. B. Schweizer, M. D. Rossell, B. T. King, T. Bauer, S. Götzinger, A. D. Schlüter, J. Sakamoto, *Nat. Chem.* **2012**, *4*, 287–291.

216 M. Li, A. D. Schlüter, J. Sakamoto, *J. Am. Chem. Soc.* **2012**, *134*, 11721–11725.

217 S. Lee, C.-H. Chen, A. H. Flood, *Nat. Chem.* **2013**, *5*, 704–710.

218 H. L. Anderson, J. K. M. Sanders, *Chem. Commun*. **1989**, 1714–1715.

219 B. Schmaltz, A. Rouhanipour, H. J. Räder, W. Pisula, K. Müllen, *Angew. Chem., Int. Ed.* **2009**, *48*, 720–724.

220 D. Canevet, E. M. Pérez, N. Martín, *Angew. Chem., Int. Ed.* **2011**, *50*, 9248–9259.

221 M. Matache, E. Bogdan, N. D. Hădade, *Chem. Eur. J.* **2014**, *20*, 2106–2131.

222 X. Ma, Y. Zhao, *Chem. Rev.* **2015**, *115*, 7794–7839.

223 D.-H. Qu, Q.-C. Wang, Q.-W. Zhang, X. Ma, H. Tian, *Chem. Rev.* **2015**, *115*, 7543–7588.

224 A. Sarkar, J. J. Pak, G. W. Rayfield, M. M. Haley, *J. Mater. Chem.* **2001**, *11*, 2943–2945.

225 O. S. Pyun, W. Yang, M.-Y. Jeong, S. H. Lee, K. M. Kang, S.-J. Jeon, B. R. Cho, *Tetrahedron Lett.* **2003**, *44*, 5179–5182.

226 B. Traber, T. Oeser, R. Gleiter, *Eur. J. Org. Chem.* **2005**, *2005*, 1283–1292.

227 M. Mayor, C. Didschies, *Angew. Chem., Int. Ed.* **2003**, *42*, 3176–3179.

228 Y. Yamaguchi, S. Kobayashi, S. Miyamura, Y. Okamoto, T. Wakamiya, Y. Matsubara, Z.-i. Yoshida, *Angew. Chem., Int. Ed.* **2004**, *43*, 366–369.

229 H. Abe, K. Ohtani, D. Suzuki, Y. Chida, Y. Shimada, S. Matsumoto, M. Inouye, *Org. Lett.* **2014**, *16*, 828–831.

230 T. Nishinaga, H. Nakayama, N. Nodera, K. Komatsu, *Tetrahedron Lett.* **1998**, *39*, 7139–7142.

231 P. N. W. Baxter, *J. Org. Chem.* **2001**, *66*, 4170–4179.

232 M. Venturi, F. Marchioni, V. Balzani, Dorina M. Opris, O. Henze, A. D. Schlüter, *Eur. J. Org. Chem.* **2003**, *2003*, 4227–4233.

233 S. Chen, Q. Yan, T. Li, D. Zhao, *Org. Lett.* **2010**, *12*, 4784–4787.

234 M. Yoshizawa, J. K. Klosterman, *Chem. Soc. Rev.* **2014**, *43*, 1885–1898.

235 H. Meier, M. Fetten, C. Schnorpfeil, *Eur. J. Org. Chem.* **2001**, *2001*, 779–786.

236 T. Li, K. Yue, Q. Yan, H. Huang, H. Wu, N. Zhu, D. Zhao, *Soft Matter* **2012**, *8*, 2405–2415.

237 S.-i. Kato, N. Takahashi, H. Tanaka, A. Kobayashi, T. Yoshihara, S. Tobita, T. Yamanobe, H. Uehara, Y. Nakamura, *Chem. Eur. J.* **2013**, *19*, 12138–12151.

238 M. Schmittel, H. Ammon, *Synlett* **1999**, *6*, 750–752.

239 M. G. Schwab, M. Takase, A. Mavrinsky, W. Pisula, X. Feng, J. A. Gámez, W. Thiel, K. S. Mali, S. de Feyter, K. Müllen, *Chem. Eur. J.* **2015**, *21*, 8426–8434.

240 Y.-S. Guan, Y. Qin, Y. Sun, C. Wang, W. Xu, D. Zhu, *Chem. Commun.* **2015**, *51*, 12182–12184.

241 J. Li, A. Ambroise, S. I. Yang, J. R. Diers, J. Seth, C. R. Wack, D. F. Bocian, D. Holten, J. S. Lindsey, *J. Am. Chem. Soc.* **1999**, *121*, 8927–8940.

242 O. Mongin, A. Schuwey, M.-A. Vallot, A. Gossauer, *Tetrahedron Lett.* **1999**, *40*, 8347–8350.

243 D. V. Kondratuk, M. A. PerdigãoLuís, M. S. EsmailAyad, J. N. O'Shea, P. H. Beton, H. L. Anderson, *Nat. Chem.* **2015**, *7*, 317–322.

244 K. Nakamura, H. Okubo, M. Yamaguchi, *Org. Lett.* **2001**, *3*, 1097–1099.

245 S. Ham, J. Yang, F. Schlosser, F. Würthner, D. Kim, *J. Phys. Chem. Lett.* **2014**, *5*, 2830–2835.

246 P. G. Ghasemabadi, T. Yao, G. J. Bodwell, *Chem. Soc. Rev.* **2015**, *44*, 6494–6518.

247 K. Tahara, T. Fujita, M. Sonoda, M. Shiro, Y. Tobe, *J. Am. Chem. Soc.* **2008**, *130*, 14339–14345.

248 P. N. W. Baxter, *Chem. Eur. J.* **2002**, *8*, 5250–5264.

249 C. N. Carroll, J. J. Naleway, M. M. Haley, D. W. Johnson, *Chem. Soc. Rev.* **2010**, *39*, 3875–3888.

250 X. Zhou, G. Liu, K. Yamato, Y. Shen, R. Cheng, X. Wei, W. Bai, Y. Gao, H. Li, Y. Liu, F. Liu, D. M. Czajkowsky, J. Wang, M. J. Dabney, Z. Cai, J. Hu, F. V. Bright, L. He, X. C. Zeng, Z. Shao, B. Gong, *Nat. Commun.* **2012**, *3*, 949.

251 A. B. Vliegenthart, F. A. L. Welling, M. Roemelt, R. J. M. Klein Gebbink, M. Otte, *Org. Lett.* **2015**, *17*, 4172–4175.

252 K. Landskron, *Chem. Eur. J.* **2015**, *21*, 14258–14267.

253 R.-C. Brachvogel, M. von Delius, *Chem. Sci.* **2015**, *6*, 1399–1403.

254 R.-C. Brachvogel, F. Hampel, M. von Delius, *Nat. Commun.* **2015**, *6*, 7129.

255 N. A. Stephenson, J. Zhu, S. H. Gellman, S. S. Stahl, *J. Am. Chem. Soc.* **2009**, *131*, 10003–10008.

256 S. Lysenko, J. Volbeda, P. G. Jones, M. Tamm, *Angew. Chem., Int. Ed.* **2012**, *51*, 6757–6761.

4

Organic Cages through Dynamic Covalent Reactions

Huimin Ding, Rufan Chen, and Cheng Wang

4.1 Introduction

The design and synthesis of molecular cage compounds with permanent cavities has gained intensive attention over the past few decades, mainly due to their important role in supramolecular chemistry as host molecules.[1–3] Based on the connection mode, molecular cage compounds can be classified into two types: supramolecular cages and covalent organic molecular cages (OMCs). The former are usually constructed with high yield through self-assembly of simple precursors via non-covalent interactions,[4,5] such as metal–ligand coordination[6–8] and hydrogen bonding.[9] A large number of polyhedral coordination cages formed by articulating organic spacers with appropriate metal centers have been reported, which have shown interesting applications in host–guest chemistry, for example the stabilization of highly reactive intermediates.[10,11] Thanks to the efforts of many groups, the construction of supramolecular cages has been relatively well established.

In contrast to supramolecular cages, covalent OMCs have been less well investigated, even though the concept of OMCs has been known for almost 50 years.[12–15] The great challenge has been their synthesis. Initially, OMCs were synthesized via irreversible bond formation in stepwise fashion. The most challenging step to efficiently construct OMCs is the final cyclization step. In order to favor intramolecular cyclization to form OMCs over intermolecular reaction forming acyclic oligomers, high-dilution or pseudo high-dilution conditions are required, which limits large scale production of OMCs. Although the yields of individual steps might be high, the overall yields are usually quite low.[16–19] For instance, trinacrene can be synthesized from hexabromobenzene and furan in four steps, but the overall yield is only <0.01%.[20] As an alternative approach, dynamic covalent chemistry (DCvC)[21–24] has shown its potential in the construction of OMCs from simple precursors with high yield. In recent years, by using various dynamic covalent reactions, a series of OMCs have been successfully synthesized on a large scale, which has facilitated their interesting applications in various areas,[25–28] such as porous materials.

In this chapter we will summarize the research progress on OMCs synthesized via the DCvC approach. First, we will highlight the synthesis of OMCs using various dynamic covalent reactions. After that, strategies of functionalization of OMCs will be

mentioned. Finally, we will discuss the interesting applications of these OMCs. We will exclude those OMCs prepared through irreversible bond formation, although the yields in some cases are still reasonable.

4.2 Synthesis of Organic Molecular Cages

The most critical characteristic of DCvC is that the chemical reactions used are reversible and under thermodynamic control,[21–24] therefore the bond formation can possess elements of "error checking" or "proof-reading", leading to the most thermodynamically stable species at equilibrium. For the construction of OMCs, this trait is very useful and powerful if building blocks are designed in such a way that the target OMCs are thermodynamically the most favored species (minimal angle strain and building units). In this section, we will summarize the synthesis of OMCs via various dynamic covalent reactions (Table 4.1), such as imine reaction, boronic acid condensation, and alkene/alkyne metathesis.

Table 4.1 Dynamic covalent reactions used for construction of OMCs.

Reaction type	Chemical reactions
Imine condensation reaction	$R_1-CHO + R_2\text{-}NH_2 \xrightarrow{-H_2O} R_1-CH=N-R_2$
Hydrazone condensation	$R_1-CHO + R_2-C(=O)NHNH_2 \xrightarrow{-H_2O} R_1-CH=N-NH-C(=O)R_2$
Boronic ester condensation	$R_1-B(OH)_2 + R_2(OH)_2 \xrightarrow{-H_2O} R_1-B(O_2)R_2$
Boronic acid condensation	$R-B(OH)_2 \xrightarrow{-H_2O}$ boroxine (R–B with O–B(R) ring)
Alkyne metathesis	$R_1-C\equiv C-R' + R_2-C\equiv C-R'' \longrightarrow R_1-C\equiv C-R_2 + R'-C\equiv C-R''$
Alkene metathesis	$R_1-CH=CH-R' + R_2-CH=CH-R'' \longrightarrow R_1-CH=CH-R_2 + R'-CH=CH-R''$
Disulfide exchange	$R_1-S-S-R' + R_2-S-S-R'' \longrightarrow R_1-S-S-R_2 + R'-S-S-R''$
Orthogonal reactions	$R_1(OH)_2 + (HO)_2B-R_2-CHO + R_3-NH_2 \xrightarrow{-H_2O} R_1(O_2)B-R_2-CH=N-R_3$
	$CH_2=CH-R_1'-NH_2 + R_2-CHO \xrightarrow[-C_2H_4]{-H_2O} R_2-CH=N-R_1-CH=N-R_2$

4.2.1 OMCs Synthesized through Imine Reaction

One of the most studied reactions in DCvC is the reversible condensation between amines and aldehydes, which involves the loss of H_2O to form imine bonds.[29,30] Since Cram reported the synthesis of a large hemicarcerand by condensation of aldehyde-functional resorcinarenes and 1,3-diaminobenzene in 1991, imine reaction has emerged as a powerful synthetic tool in the construction of OMCs.[31] Following this pioneering work, various [2+3], [4+6], [8+12], and [4+4] OMCs (the numbers denote how many amine and aldehyde monomers are connected in OMCs) have been prepared through condensation of multi-topic amines with aldehydes. For example, Warmuth and co-workers utilized imine chemistry to synthesize cavitand-based OMCs. Starting from 1,3,5-tris-(*p*-aminophenyl)benzene (**1**) and tetraformyl-substituted cavitand (**2**), they were able to construct a giant rhombicuboctahedron (**C1**, Scheme 4.1) by [6+8] condensation, whose structure was confirmed by NMR spectroscopy and mass spectrometry analyses.[32] From the DOSY NMR spectroscopy, the solvodynamic diameter of **C1** was estimated to be 3.9 nm, which is in good agreement with the molecular mechanics force field (MM3) optimized space-filling model.

The Cooper group has contributed a series of [4+6] OMCs via imine condensation reaction of trialdehydes and diamines. In 2009, they reported the synthesis of three OMCs (**C2**–**C4**, Scheme 4.2) through the [4+6] condensation of 1,3,5-triformylbenzene (**3**) with 1,2-ethylenediamine (**4**), 1,2-propylenediamine (**5**), and (*R*,*R*)-1,2-diaminocyclohexane (**6**), respectively.[33] Very impressively, the products were isolated directly as a crystalline solid after leaving the reaction mixture without stirring for ~60 h. As characterized by single-crystal X-ray diffraction, these OMCs have tetrahedral symmetry and each of them has four approximately triangular windows and six vertices consisting of aliphatic amino groups. Later on, the same group found that if the condensation reactions were performed in the presence of trifluoroacetic acid (TFA), triply interlocked OMCs were assembled in one step without adding any template.[34] For example, starting from precursors **3** and **4**, catenated [4+6] OMC (**C5**, Scheme 4.3) was formed with 60% overall yield. It is assumed that the π–π interaction plays an important role in the assembly of these interlocked OMCs, as confirmed by the crystal structures.

Cooper and co-workers reported an interesting effect of alkanediamine chain length on the final structure of OMCs. They reported odd–even effects in synthesizing several imine-based OMCs (Scheme 4.4): diamines with an even number of carbon atoms formed [4+6] OMCs (**C2** and C**7**), while those with odd numbers of carbon atoms formed [2+3] OMCs (**C6** and C**8**).[35] Through a computational study, they also predicted the thermodynamically preferred OMCs and the lowest energy conformer. By using this method, they predicted the formation of [4+4] OMCs with unique "tetrapod" structures, which were later experimentally confirmed through the condensation of tris(2-aminoethyl)amine and tris(4-formylphenyl)amine.[36] Although they are obtained in solution as crystals, such [4+4] OMCs are prone to decomposition and cannot be isolated as dry solid.

Much larger [4+6] OMCs have been obtained via condensation of larger trialdehydes and various cyclic diamines. For example, condensation of tris(4-formylphenyl) amine (**7**) and (*R*,*R*)-1,2-cyclopentanediamine (**8**) provided **C9** (Scheme 4.5).[37] Similarly, Wang and co-workers prepared [4+6] OMC (C**10**, Scheme 4.6) by condensation of 1,3,5-tris-(4-formylphenyl)triazine (**9**) and **6**.[38] The crystal structure analysis showed

6 ×

1

+

8 ×

2

−24H₂O

R = pentyl

C1 (60–70%)
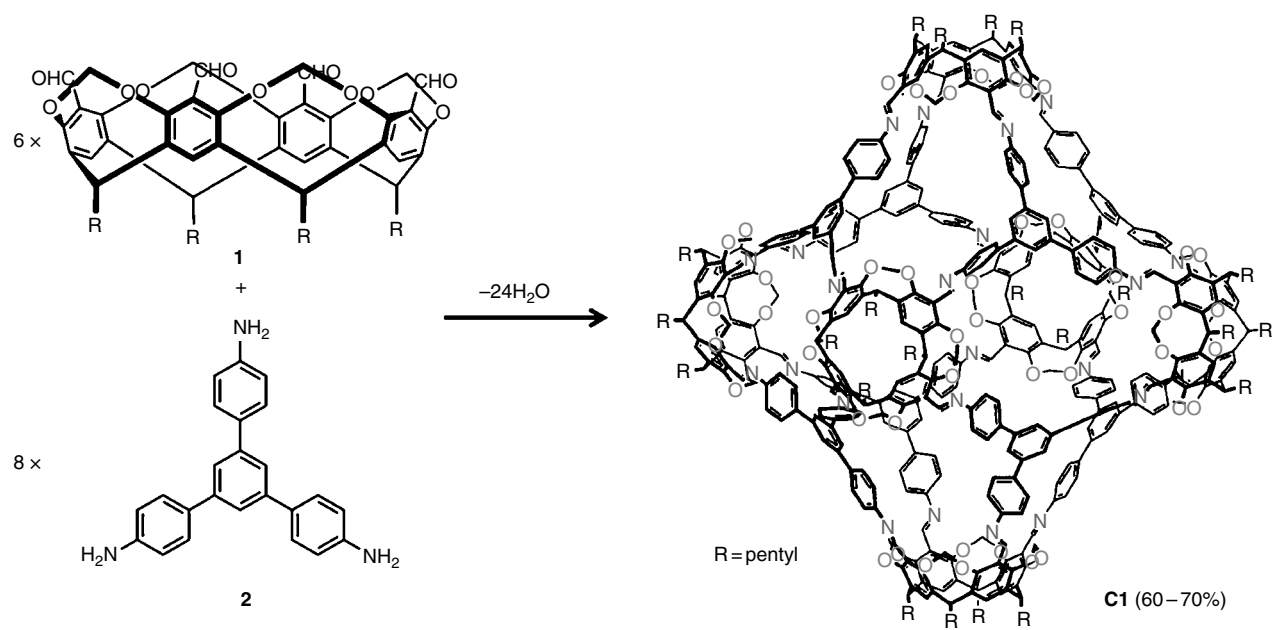
Scheme 4.1 Synthesis of rhombicuboctahedron **C1**.

$4 \times$ ○
$+$
$6 \times$ —

$-12H_2O$

○ ≡ (CHO, OHC, CHO benzene) **3**	III, H₂N-CH₂CH₂-NH₂ **4**, H₂N-CH(CH₂NH₂)-CH₂NH₂ **5**, cyclohexane-1,2-diamine **6**

C2 (35%) **C3** (37%) **C4** (83%)
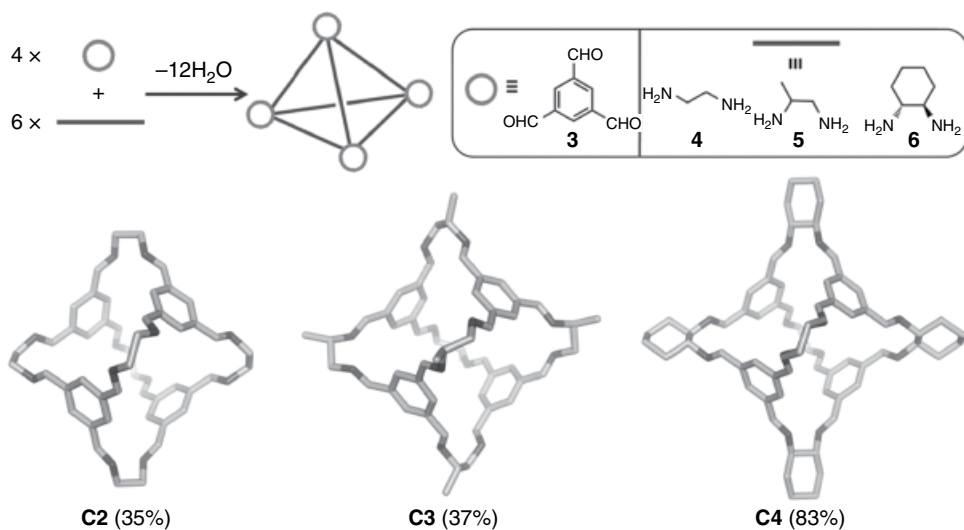
Scheme 4.2 Synthesis of tetrahedral cages **C2–C4.** The crystal structures of **C2–C4** are shown.

$8 \times$

CHO
OHC   CHO
3

$+$

$12 \times$

NH₂
NH₂
4

TFA
$-24H_2O$

C5 (~60%)
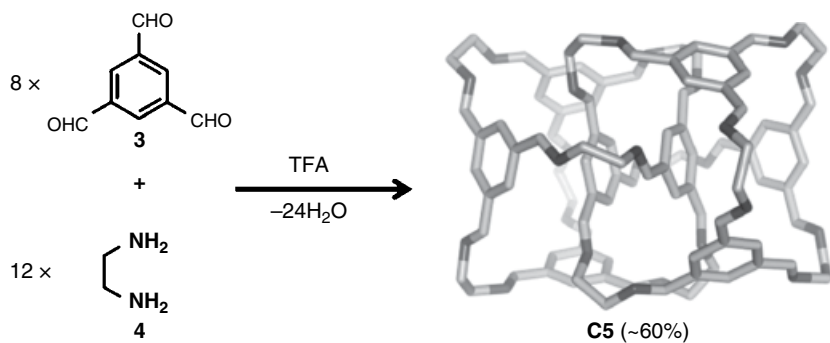
Scheme 4.3 Synthesis of catenated **C5**. The crystal structure of **C5** is shown.

CHO
OHC   CHO
3

$+$

H₂N-(CH₂)ₙ-NH₂
$n = 2, 3, 4, 5$

$n = 3$ **C6** (24%)
$n = 5$ **C8** (100%)
$n = 2$ **C2** (35%)
$n = 4$ **C7** (27%)
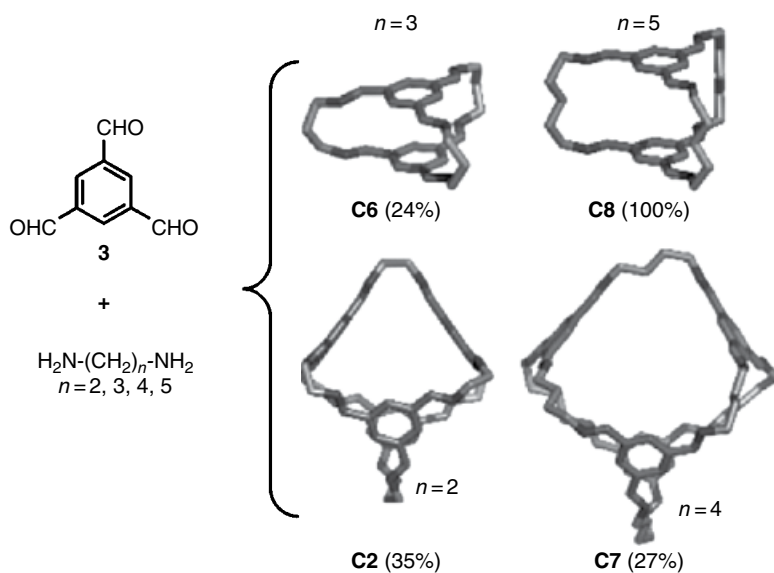
Scheme 4.4 Synthesis of imine-based **C2, C6, C7** and **C8** with odd–even effects.
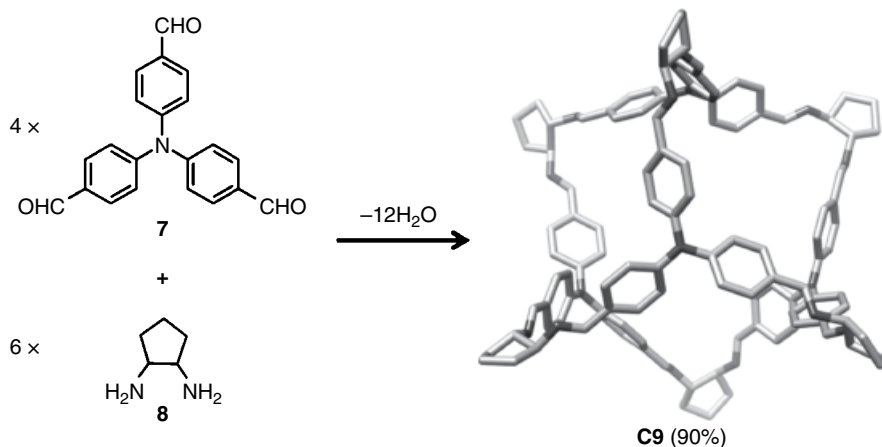
Scheme 4.5 Synthesis of **C9**. The crystal structure of **C9** is shown.
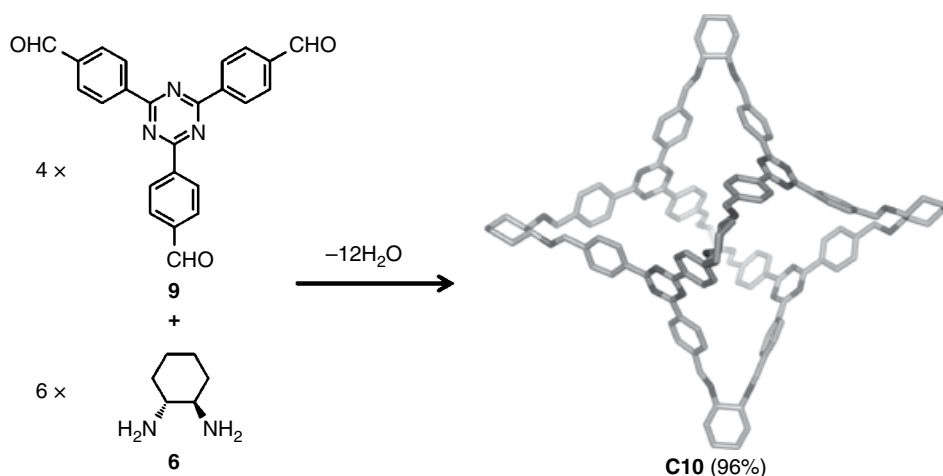
Scheme 4.6 Synthesis of **C10**. The crystal structure of **C10** is shown.

that **C10** has a tetrahedral symmetry with an external distance of 3.0 nm and a large cavity of ~2070 Å^3. Interestingly, when triamine **7** and diamine **6** were condensed, the even larger [8 + 12] OMC (**C11**, Scheme 4.7) was obtained through the formation of 24 imine bonds.[39] From the crystal structure, **C11** has an outer diameter of 2.9 nm. A large [8 + 12] OMC (**C12**, Scheme 4.8) was also prepared by Skowronek and co-workers through the reaction of 1,3,5-triaminocyclohexane (**10**) and 4-*tert*-butyl-2,6-diformylphenol (**11**).[40] According to the crystal structure analysis, **C12** features a large intrinsic cavity and has an outer diameter of 3.0 nm.

It should be noted that the OMCs containing flexible aliphatic diamine monomers were mostly collected as precipitates (precipitation-driven) from the reaction solution. Precipitation of OMCs greatly facilitates the synthesis and isolation of these interesting compounds. However, precipitation is considered as irreversible kinetic trapping due to
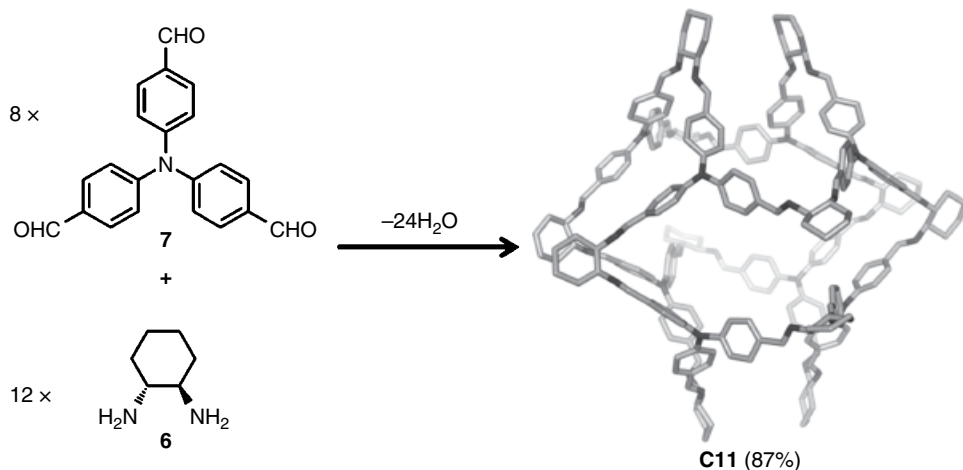
Scheme 4.7 Synthesis of C11. The crystal structure of C11 is shown.

the slower exchange kinetics between components in solution and precipitates. Since precipitates cannot freely exchange with other library components in the dynamic system, the reversible reaction involves precipitation of the products should be considered to be a kinetically interrupted dynamic system. Flexible aliphatic diamine linkers would likely form flexible OMCs, whose formation depends much less on enthalpy. Therefore, the possibility that preferred formation of entropically less favored larger cages [4+6] over [2+3] or [8+12] over [4+6] is precipitation-driven cannot be ruled out.

Mukherjee and co-workers also reported the precipitation-induced synthesis of OMCs through imine chemistry and demonstrated an interesting self-sorting process in a multicomponent system.[41] Condensation of 2 equivalents of triamine and 3 equivalents of dialdehyde in solution induced the precipitation of OMCs C13−C16, which were collected as pure products through filtration. Interestingly, although two different
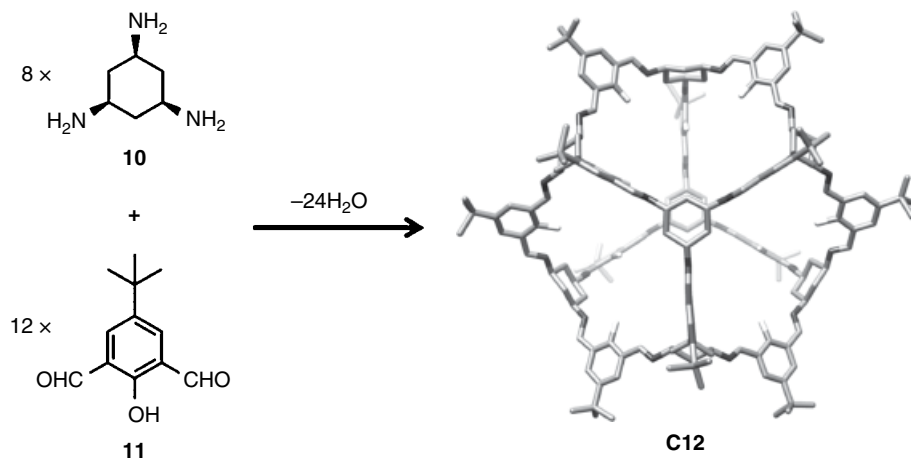
Scheme 4.8 Synthesis of C12. The crystal structure C12 shown.
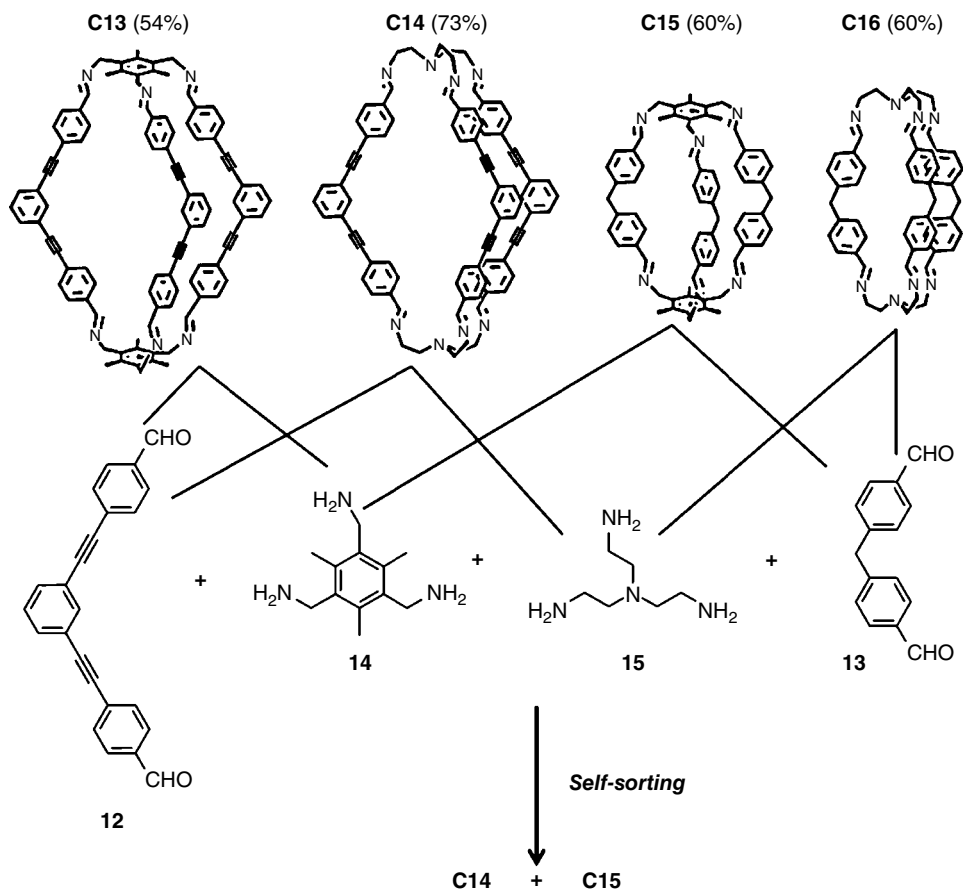
Scheme 4.9 Syntheses of **C13–C16** and the self-sorting behavior in the formation of **C14** and **C15**.

dialdehydes (**12** and **13**) and two different triamines (**14** and **15**) were mixed together to react, only two specific OMCs (C**14** and C**15**, Scheme 4.9) were precipitated from the solution. They also found a non-self-sorted cage could be transformed to either one of the self-sorted OMCs by allowing it to react with the appropriate triamine or dialde-hyde. In this kinetically interrupted dynamic system (i.e., products precipitate as kinetic traps), the driving force for the preferred formation of two OMCs over other possibili-ties in a multi-component system is especially complicated, which is hard to explain with the available kinetic and thermodynamic parameters obtained on the individual component's behavior in the absence of competitors.

To selectively form target OMCs over others from flexible aliphatic building blocks, a template-directed approach is also commonly used. For example, Wang and co-work-ers prepared several porphyrin-based OMCs via one-pot template-directed imine condensation.[42,43] Starting from zinc(II) *meso*-tetra(*m*-formylphenyl)porphyrin (**16**) and by selectively choosing the templating linker and diamine length, porphyrin-based OMCs (**C17–C19**, Scheme 4.10) bearing different sizes were obtained with quantita-tive conversion.
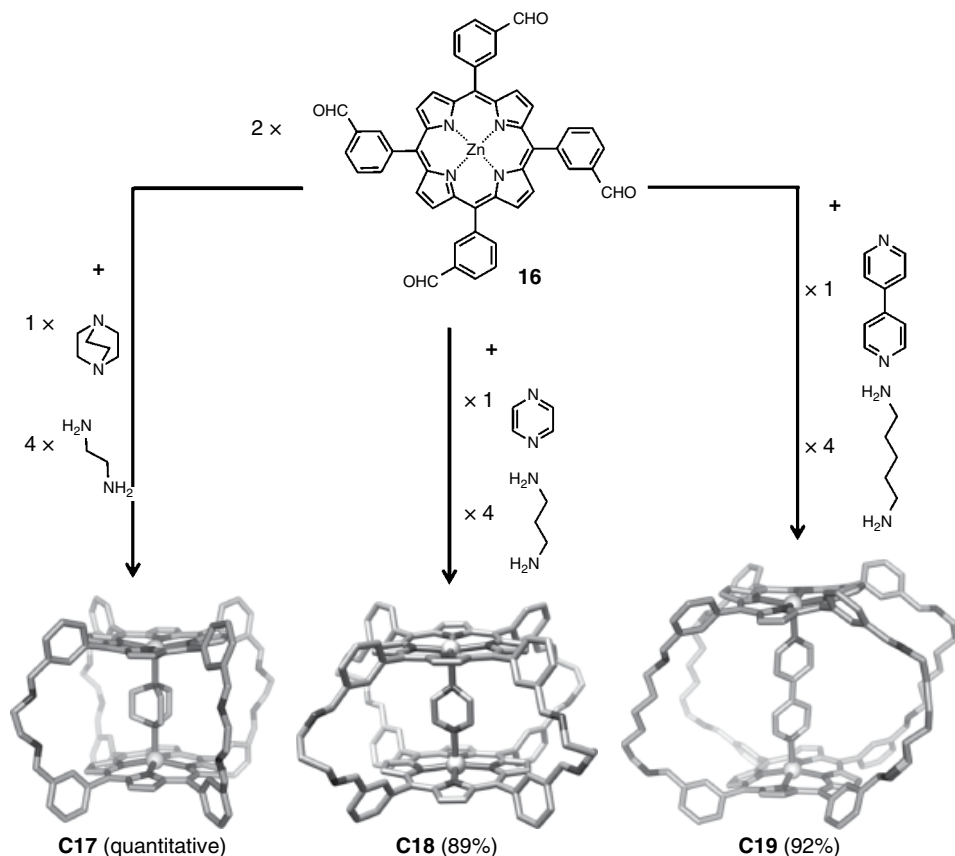
Scheme 4.10 Template synthesis of the porphyrin-based **C17–C19**. The crystal structures of **C17–C19** are shown.

Recently, Kimoon and co-workers also reported the synthesis of porphyrin-based OMCs (**C20** and **C21**, Scheme 4.11) through rational design of monomers in the absence of any template.[44] By combination of three-connected triangular (**15** or **18**) and four-connected square-shaped (**17**) building units, **C20** or **C21** bearing a cavity as large as 1.95 nm was formed. It is interesting to note that **C20**, consisting of rigid aromatic-rich aldehydes/amines, is obtained in the solution phase in almost quantitative yield, whereas **C21**, consisting of flexible aliphatic triamine **15**, was obtained as precipitates.

Rigid imine-based OMCs consisting of aromatic amines and aromatic aldehydes have also been studied by a couple of groups. In 2008, the Mastalerz group reported the synthesis of an *endo*-functionalized [4 + 6] OMC (**C22**, Scheme 4.12) by condensation of trisaminotriptycenes (**19**) and salicyldialdehydes (**11**).[45] According to the minimized structural model, **C22** displays a tetrahedral symmetry with the hydroxyl groups pointing inside the cage interior, which was further verified through a single X-ray diffraction. An *exo*-functionalized [4 + 6] OMC was formed when 4,6-diformyl-2-methylresorcinol was used in place of **11**.[46] In addition, they investigated the influence of molecular
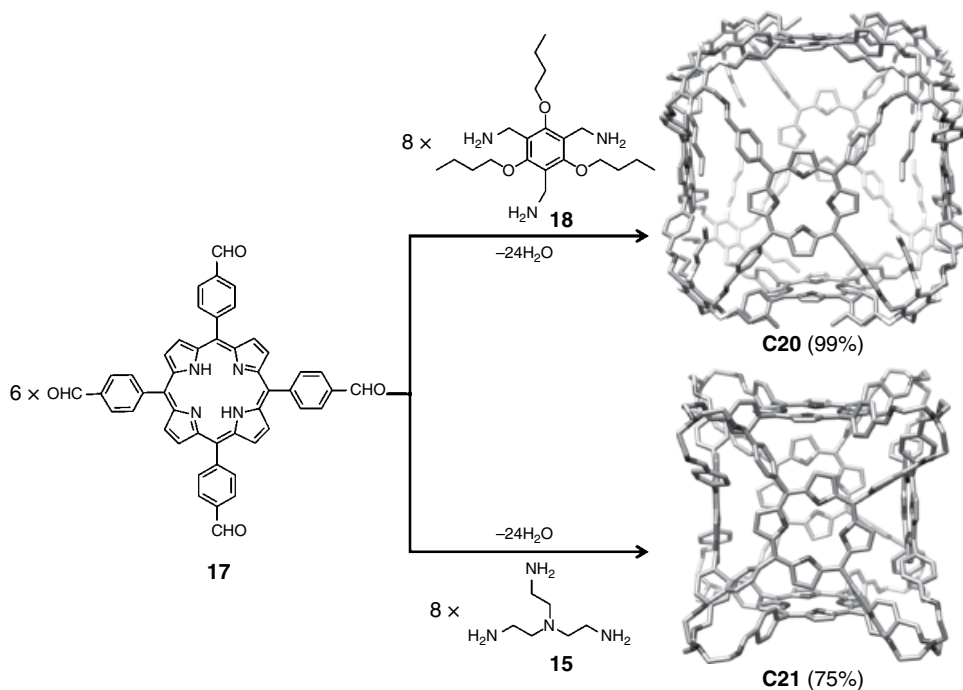
Scheme 4.11 Synthesis of covalent porphyrin boxes **C20** and **C21**. The crystal structures of **C20** and **C21** are shown.
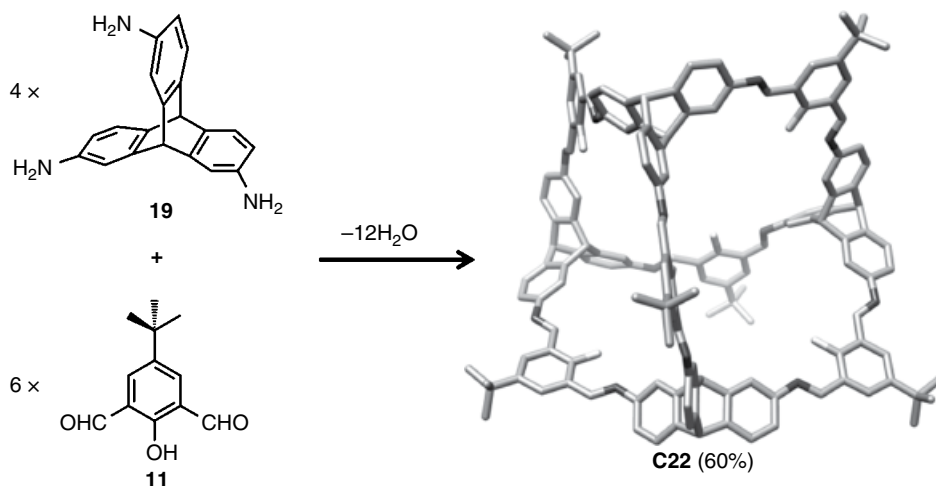
Scheme 4.12 Synthesis of **C22**. The crystal structure of **C22** is shown.

rigidity of the precursors on the formation of OMCs.[47] Starting from **19** and bis(salicylaldehyde) (**20** or **21**), two *exo*-functionalized [2 + 3] OMCs (**C23** and **C24**, Scheme 4.13) were obtained. However, the yield of **C24** is much lower than that of **C23**, indicating that a predefined geometry of reacting functional groups is beneficial for cage formation.
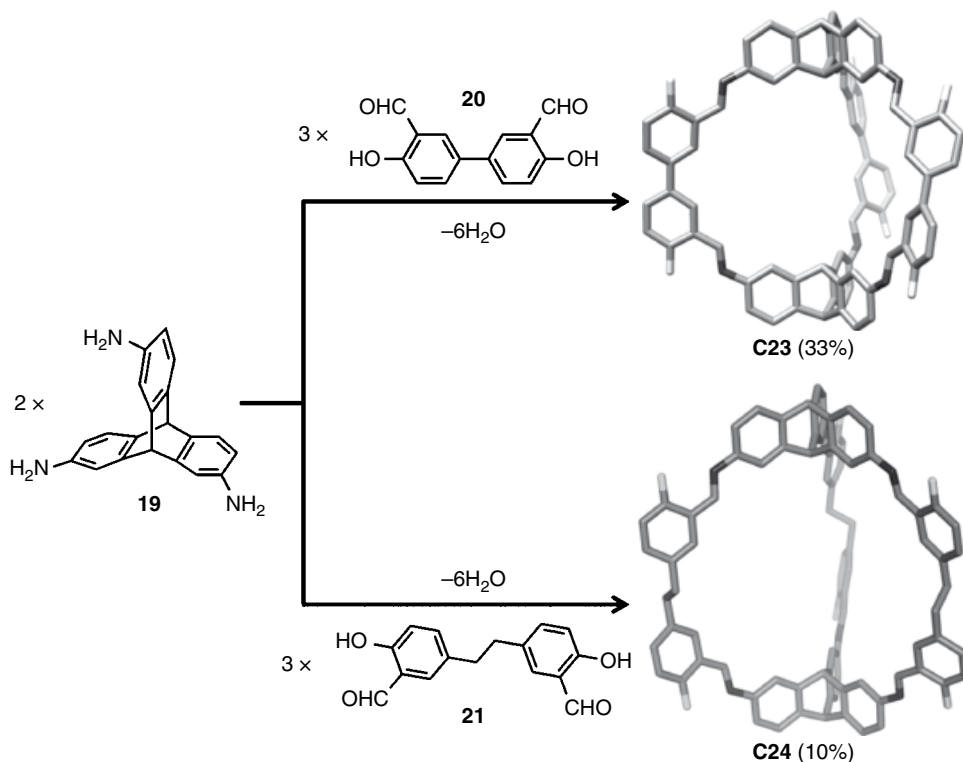
Scheme 4.13 Synthesis of **C23** and **C24**. The crystal structures of **C23** and **C24** are shown.

Zhang and co-workers also reported synthesis of a series of [2+3] OMCs using rigid aromatic building blocks in solution phase through imine chemistry. As shown in Scheme 4.14, the condensation of triamine **22** with dialdehyde **23** provided **C25** in good yield. In contrast to the formation of many OMCs consisting of aliphatic amines (e.g., **C2–C7**), the reaction mixture stayed as a clear solution throughout the reaction, which indicates that all reaction intermediates were able to equilibrate with each other. It was observed that oligomers/polymers formed at the beginning of the reaction, which was followed by their gradual transformation to a cage product. The isolation of **C25** in high yield after imine reduction indicates that **C25** is indeed thermodyanmically the most stable species. Zhang and co-workers also studied buidling block design principles. Unlike aformentioned flexible building blocks, the orientation of aldehyde and amino groups in these purely aromatic rigid building blocks are found to be critical for the successful formation of OMCs. "Misalignment" of amine and aldehyde functional groups results in significant angle strain and prohibits the formation of OMCs. For example, no cage product was observed when planar triamine **22** was reacted with dial- dehyde **24**, whereas cage **C26** was formed in high yield when dialdehyde **24** was reacted with triangular triamine **25** (Scheme 4.15). Therefore, the formation of OMCs from rigid building blocks is highly sensitive to the geometry of building blocks and the orientation of the functional groups, which determine the enthalpic parameter of this thermodynamically controlled process. Since the hydrolytic stability of imine bonds is the concern, the Zhang group reduced the imine bonds to amines *in situ* and isolated
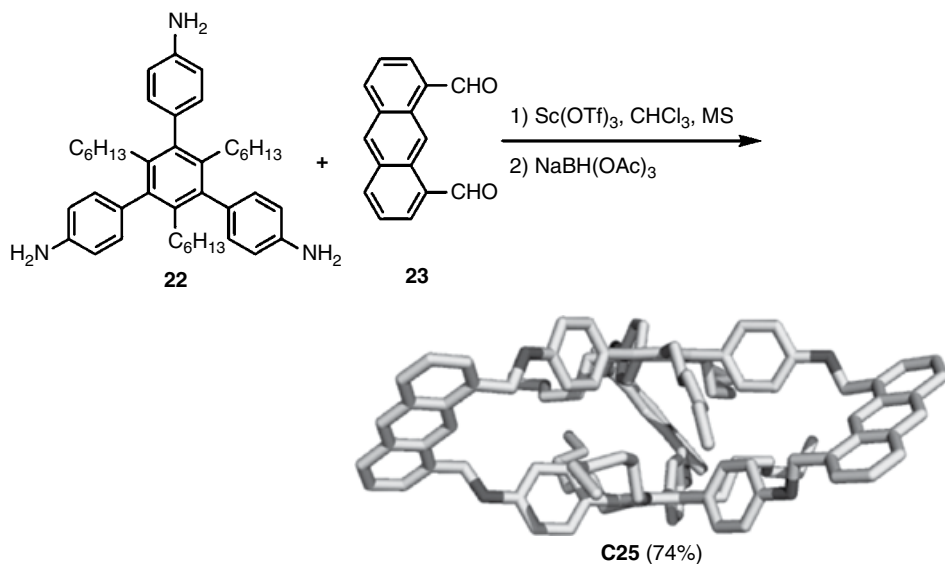
Scheme 4.14 Synthesis of cage **C25**. The crystal structure of **C25** is shown.
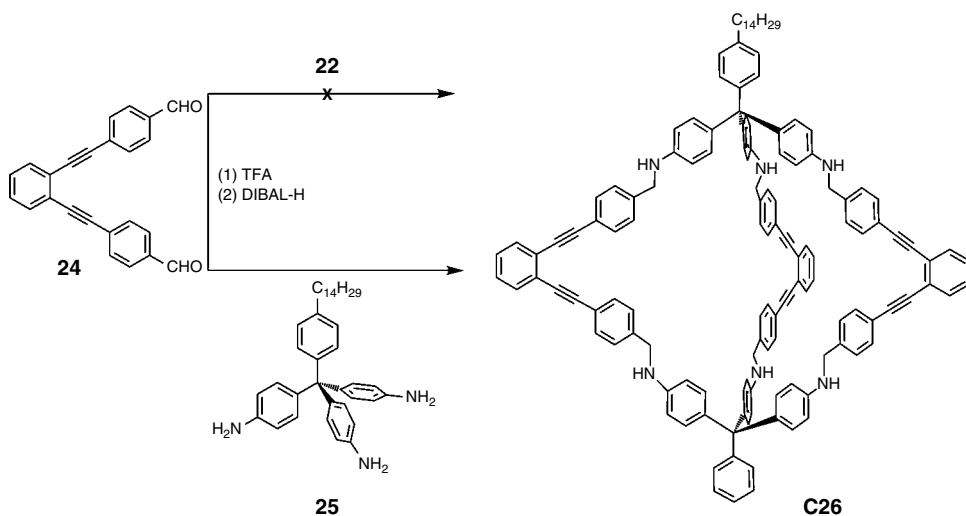
Scheme 4.15 The formation of OMCs from different building blocks.

OMCs through column chromatogarphy after reduction. Although Cooper and co-workers reported that crystals of **C4** are stable in boiling water for at least 4h, the stability of many other imine-linked OMCs is largely unexplored.

4.2.2 OMCs Synthesized through Boronic Acid Condensation

As a well-known dynamic covalent reaction, the condensation of boronic acids with diols to give boronate esters has been widely utilized to construct OMCs. For example,
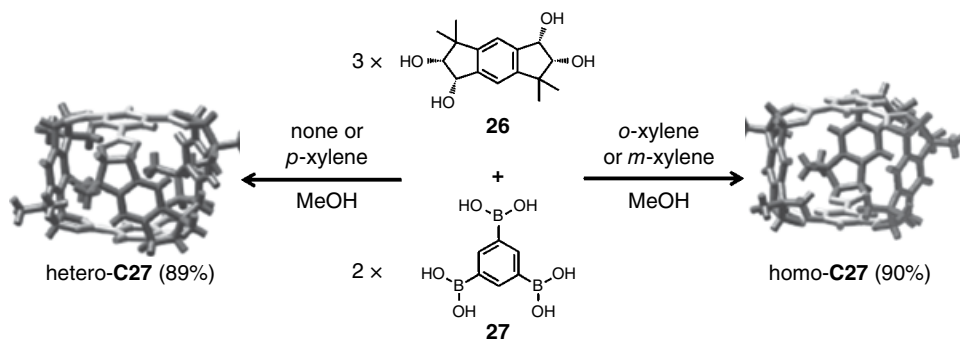
Scheme 4.16 Solvent effect on the formation of hetero-**C27** and homo-**C27**.

Iwasawa and co-workers reported the guest-induced synthesis of two diastereomeric OMCs (**C27**, Scheme 4.16) from 1,3,5-benzenetriboronic acid (**27**) and racemic tetraol (**26**).[48] A highly symmetric [2 + 3] OMC (homo-**C27**) was synthesized in the presence of *p*-xylene, whereas a diaseromeric [2 + 3] hetero OMC (hetero-**C27**) was produced in the presence of *o*-xylene or *m*-xylene. In another example, Kubo and co-workers reported a heterodimeric OMC through [1 + 1] condensation of cyclotricatechylene and a boronic acid-appended hexahomotrioxacalix[3]arene.[49] This condensation reaction cannot happen at room temperature in a protic solution, but the OMC could be formed quantitatively after the addition of Et$_4$NAcO, probably due to the template effect of the cation through cation–π interactions.

Mastalerz and co-workers reported a very large OMC (**C28**, Scheme 4.17) synthesized by a 48-fold condensation of eight molecules of **27** and 12 triptycene tetrol (**28**).[50] Single crystals suitable for crystallography were obtained by slow diffusion of *n*-hexane into a saturated solution of **C28** in chloroform. The crystal structure shows that **C28** has a cavity with a minimum inner diameter of 2.6 nm and a maximum inner diameter of 3.1 nm. Later on, using an isostructurally similar triptycene-based precursor (**29**), they synthesized another OMC (**C29**, Scheme 4.17).[51] They also succeeded in obtaining single crystals suitable for X-ray analysis by vapor diffusion of *n*-hexane into a saturated solution of **C29** in chloroform. Interestingly, an interlocked structure consisting of two quadruply interlocked **C29** structures was found in the solid state, which has an ellipsoid shape with dimensions of 4.6–4.7 nm in length and 4.0 nm in width. This catenation phenomenon is unexpected, as ^{1}H NMR analysis of the solution confirmed the presence of **C29**. The catenane is formed exclusively during the crystallization and is transformed into the non-catenated **C29** as soon as it is redissolved in solvent, indicating catenane is not the thermodynamically favored species. This is another example of precipitation-induced formation of thermodynamically less-favored species (similar enthalpy but entropy loss) from a dynamic system.

Beuerle and co-workers also reported several OMCs synthesized via boronate ester condensation. In 2014, they reported the synthesis of two [8 + 12] OMCs (**C30** and **C31**, Scheme 4.18) through condensation of catechol-functionalized tribenzotriquinacenes (**30**) and phenylene diboronic acids derivatives (**31** and **32**).[52] **C30** was obtained as insoluble microcrystalline material directly from the solution, but as the precursor **32** has additional solubilizing groups (two butyl chains), the solubility of **C31** is enhanced.
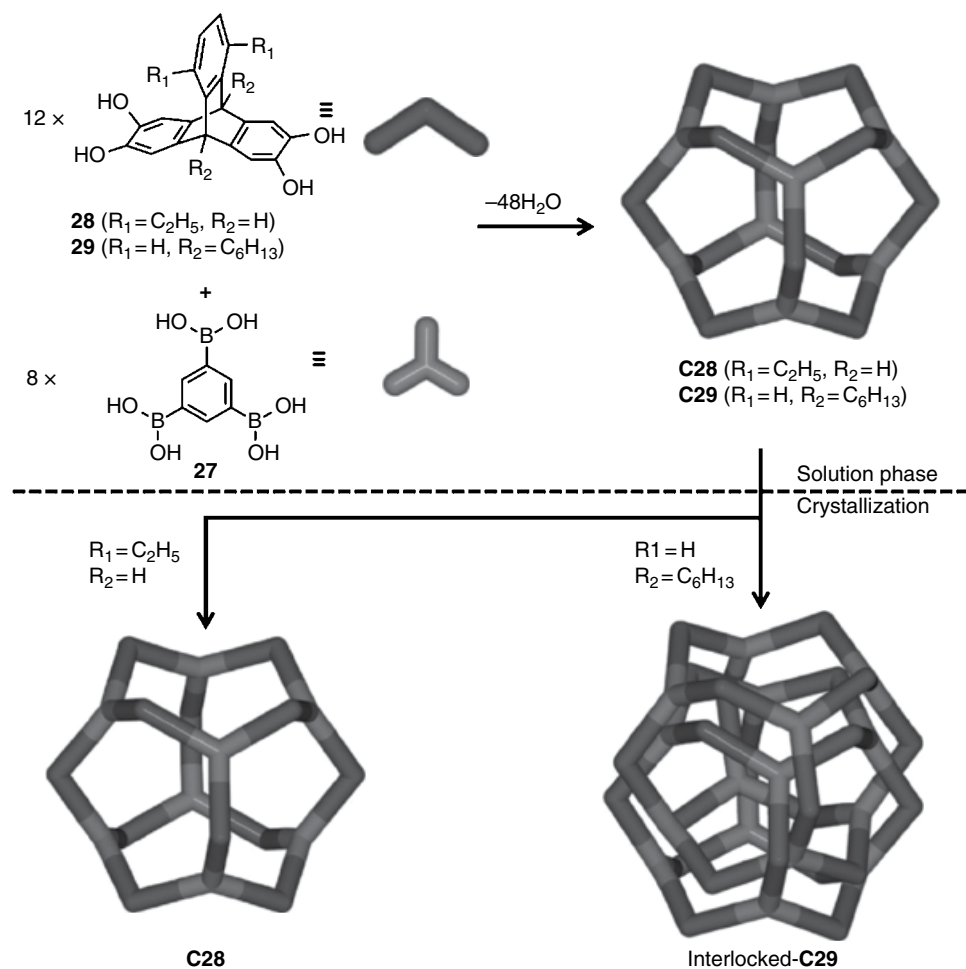
Scheme 4.17 Synthesis of **C28** and interlocked **C29**.

From the calculations, both OMCs have cubic symmetry O_h. Moreover, **C31** exhibits a diagonal corner-to-corner distance of 3.2 nm, which is consistent with that calculated from DOSY NMR spectra. Later on, by condensation **30** and diboronic acids with varying angles between the two reactive sites (**33** and **34**), they were able to synthesize another two OMCs (**C32** and **C33**, Scheme 4.19) with bipyramidal and tetrahedral geometry, respectively.[53] They also investigated the self-sorting of ternary mixtures containing two competitive boronic acids, which revealed either narcissistic or social self-sorting behavior. For example, a ternary mixture of **30/33/34** or **30/31/33** underwent narcissistic self-sorting to form individual binary cages exclusively, whereas a mixture of **30/32/34** in 2:1:2 ratio yielded a three-component cage with lower symmetry through social self-sorting.

In addition, the self-condensation of boronic acid to form boroxine has been utilized to synthesize OMCs. Recently, Iwasawa reported the self-assembly of a series of boroxine-based OMCs by simple dehydration of rationally designed diboronic acids with
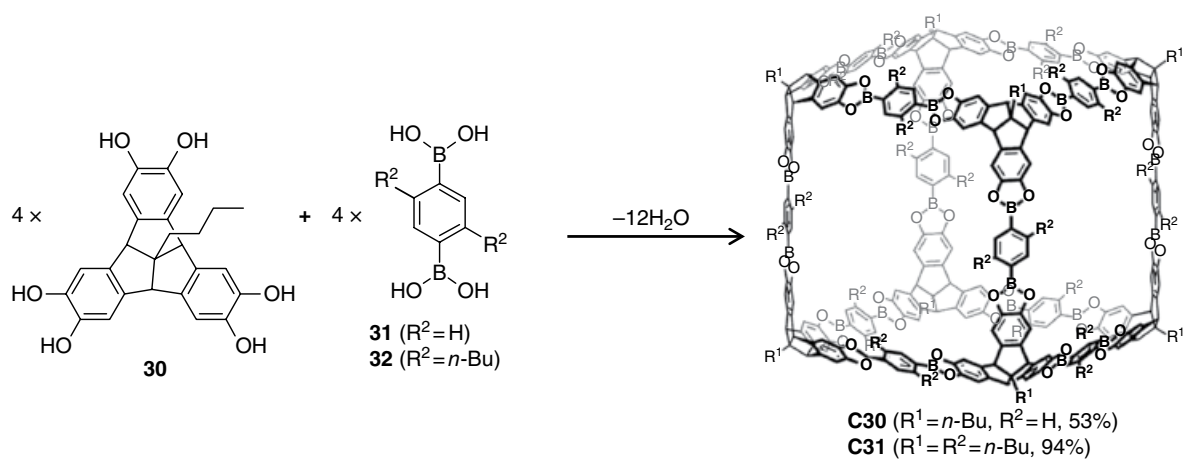
Scheme 4.18 Synthesis of **C30** and **C31**. The computational models of **C30** and **C31** are shown.

4 × **30** + 4 × **31** (R^2=H) **32** (R^2=n-Bu) $\xrightarrow{-12H_2O}$

C30 (R^1=n-Bu, R^2=H, 53%)
C31 (R^1=R^2=n-Bu, 94%)
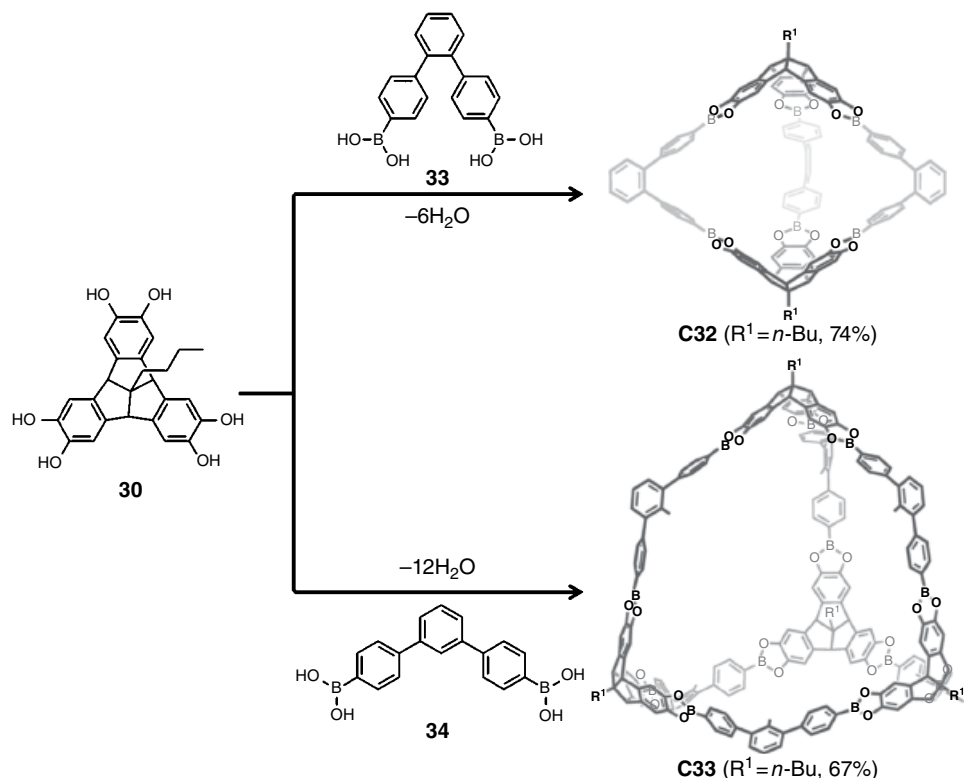
Scheme 4.19 Synthesis of **C32** and **C33**. The computational models of **C32** and **C33** are shown.

different angles between two C–B bonds.[54] For example, starting from 3,6-disubstituted carbazole derivative (**35**) with angle of 84°, an octahedral OMC (**C34**, Scheme 4.20) was quantitatively formed on heating at 60 °C in the presence of 4 Å molecular sieves. They successfully obtained single crystals through slow vapor diffusion of *n*-hexane into a 4-bromoanisole solution of **C34**. The X-ray crystal structure analysis confirmed the expected octahedral structure with a distance between the diagonal nitrogens of 2.8 nm.

4.2.3 OMCs Synthesized through Alkene/Alkyne Metathesis

Alkene metathesis is an organic reaction that entails the redistribution of fragments of alkenes by the scission and regeneration of carbon–carbon double bonds. Alkyne metathesis is similar to alkene metathesis, but deals with redistribution of carbon-carbon triple bonds instead of carbon-carbon double bond. Alkene/alkyne metathesis has played an important role in organic synthesis. The reversible nature of alkene/alkyne metathesis has made it an effective synthetic strategy for OMCs construction. Compared to those formed through imine or B–O linages, the ethylene/ethynylene-linked OMCs exhibit much higher stability, which would allow a wider foreground of applications. In this section, we will introduce the synthesis of OMCs via alkene and alkyne metathesis.

Konishi and co-workers reported template-directed synthesis of a novel OMC (**C35**, Scheme 4.21) through olefin metathesis starting from zinc *meso*-tetraarylporphyrin with four terminal-olefin functionalities (**36**).[55] Pyridine-functionalized Au_{55} was used
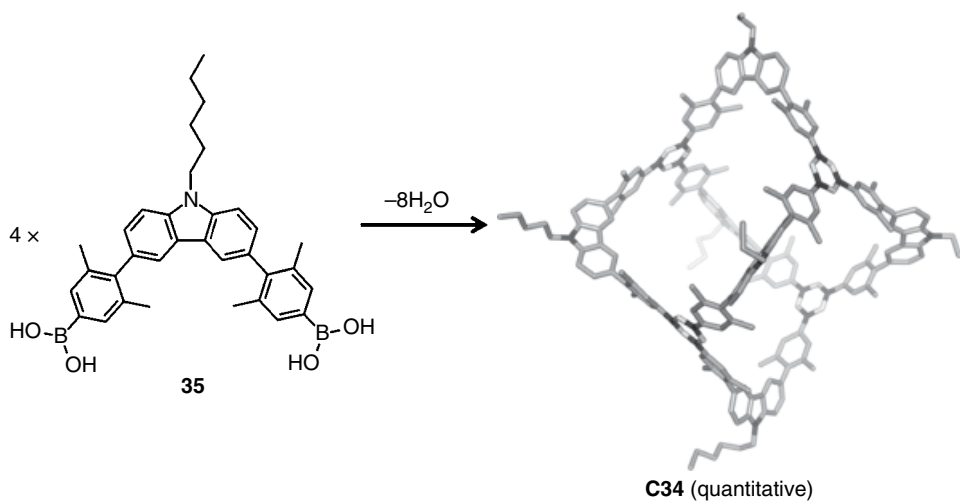
Scheme 4.20 Synthesis of **C34**. The single-crystal X-ray structure of **C34** is shown.
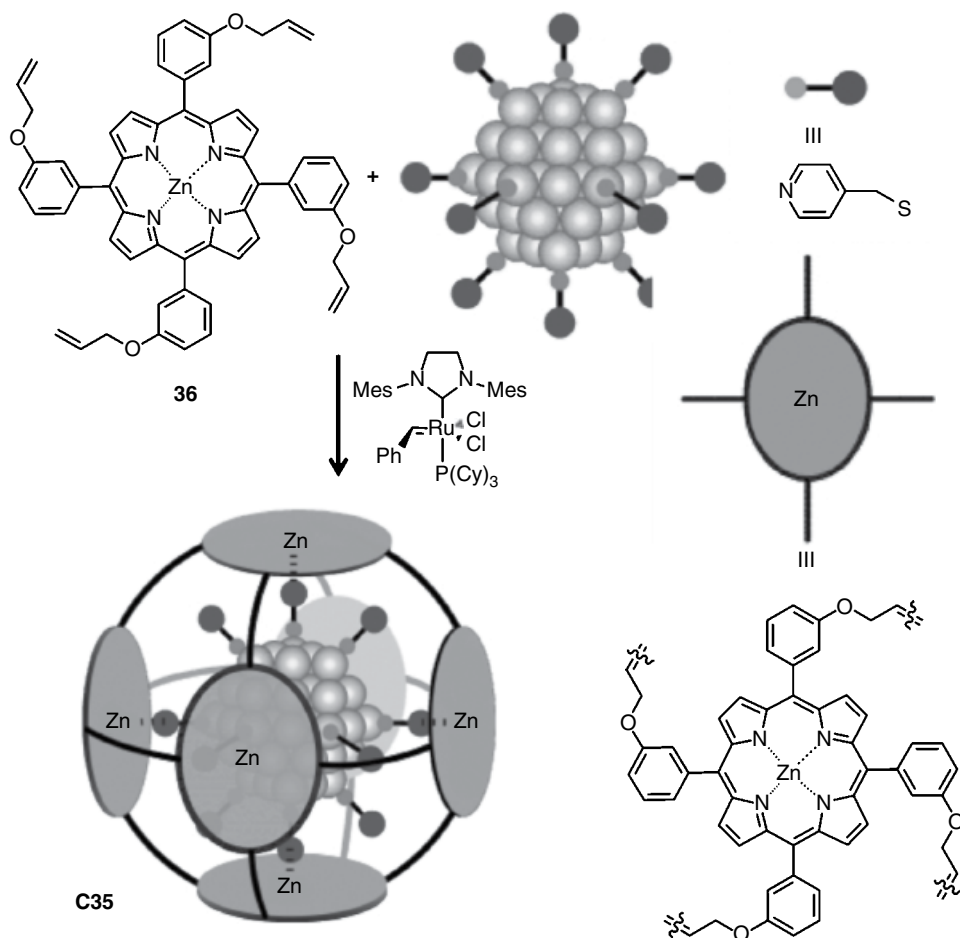
Scheme 4.21 Synthesis of the porphyrin-based **C35** via templated alkene metathesis.

as the template, which can bind porphyrin units through N–Zn interactions. Intermolecular alkene metathesis formed **C35**, consisting of six zinc porphyrins with Au$_{55}$ confined inside, as confirmed by the MALDI TOF-MS spectrum.

Recently, Heitz and co-workers also presented a large and flexible porphyrin-based OMC (**C36**, Scheme 4.22) synthesized through a template-directed alkene metathesis approach.[56] In the presence of 1,4-diazabicyclo[2.2.2]octane (DABCO) as a template, **C36** was formed through one-step ring-closing olefin metathesis of a porphyrin derivative bearing four alkene groups (**37**). The crystal structure of **C36** reveals a highly symmetric structure, in which the DABCO is complexed in between the porphyrinic units through regular N–Zn bonds. Moreover, when subjected to acidic conditions, the template could be removed. Later on, using the same strategy, Li and co-workers described the fabrication of a suite of flexible porphyrin-based OMCs and nanorings.[57] Similar to the previous example, the tetraalkene-derived zinc porphyrin monomers were preorganized in the presence of various multidentate ligands, and further one-step alkene metathesis provided porphyrin-based OMCs and nanorings.

Similar to alkene metathesis, alkyne metathesis has also been practiced in the synthesis of OMCs. The Zhang group has pioneered using this reaction to construct OMCs. In 2011, they reported the first example of successfully synthesizing a three-dimensional rectangular prismatic OMC (**C37**, Scheme 4.23) through alkyne metathesis without using a template.[58] From a readily accessible porphyrin-based precursor (**38**), **C37** could be obtained in one step with reasonable yield. Later on, using the same reaction, they reported the construction of two highly stable interlocked OMCs (**C38** and **C39**, Scheme 4.24) from simple triyne building blocks (**39** and **40**).[59] It is noteworthy that the formation of interlocked **C38** and **C39** is thermodynamically favored in solution, which represents the first example of the thermodynamically controlled solution-phase synthesis of interlocked OMCs. More recently, they systematically investigated the effect of the size and geometry of the building blocks on the formation of aryleneethynylene OMCs.[60] From their results, the dimensions of building components and kinetic competitions play critical roles in determining the topology of the assembled structure.
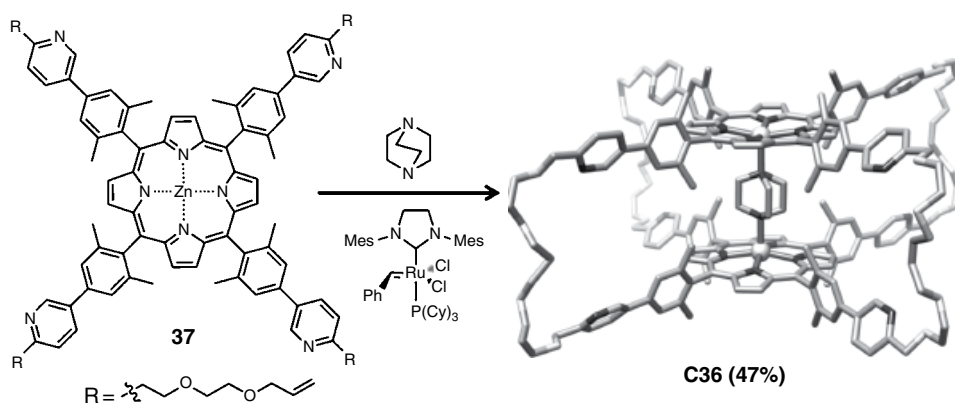
Scheme 4.22 Synthesis of **C36** via DABCO-templated alkene metathesis.

38 (R = C$_{16}$H$_{33}$)

PPT =

C37 (56%)
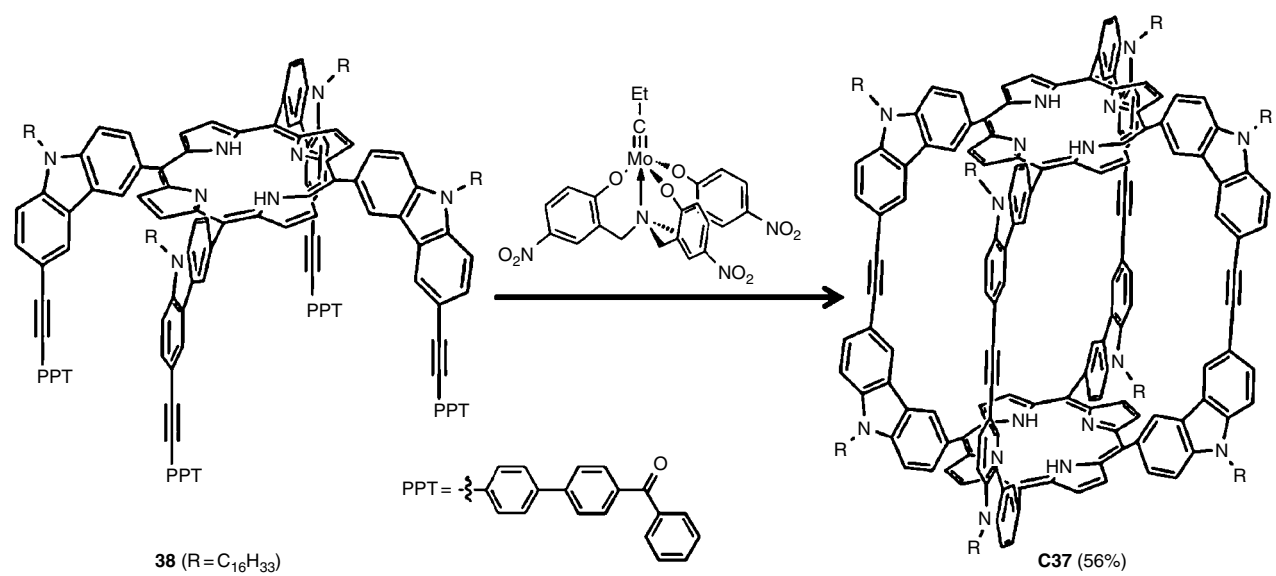
Scheme 4.23 Synthesis of **C37** through alkyne metathesis.
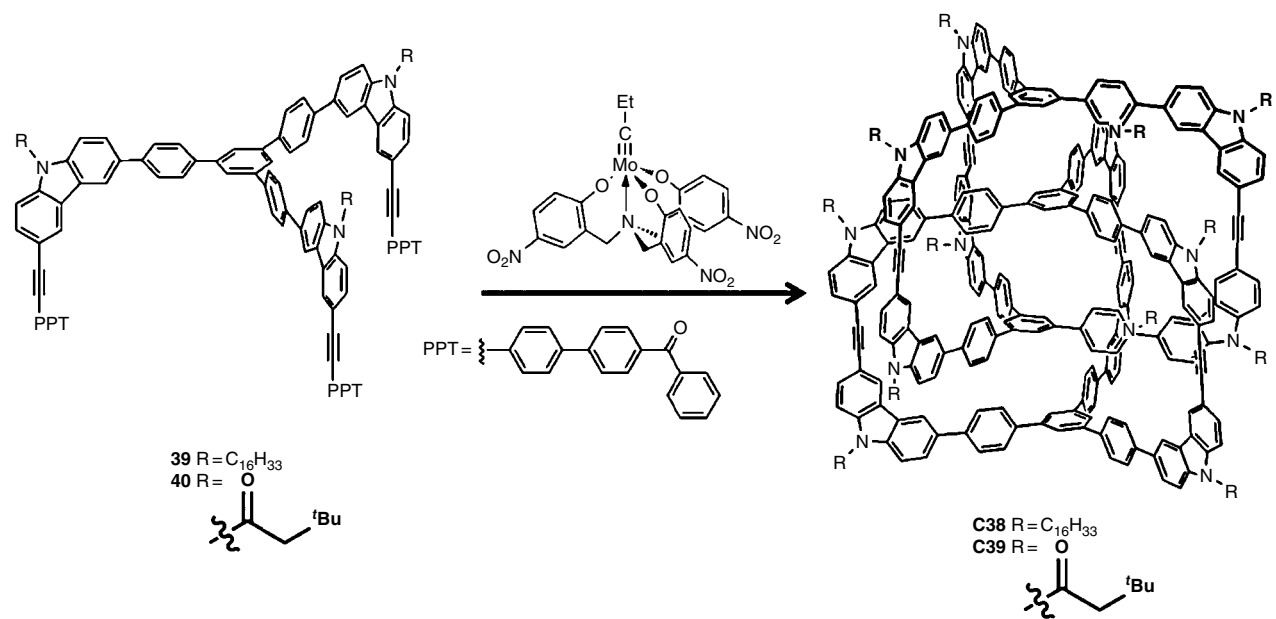
Scheme 4.24 Synthesis of **C38** and **C39** through alkyne metathesis.
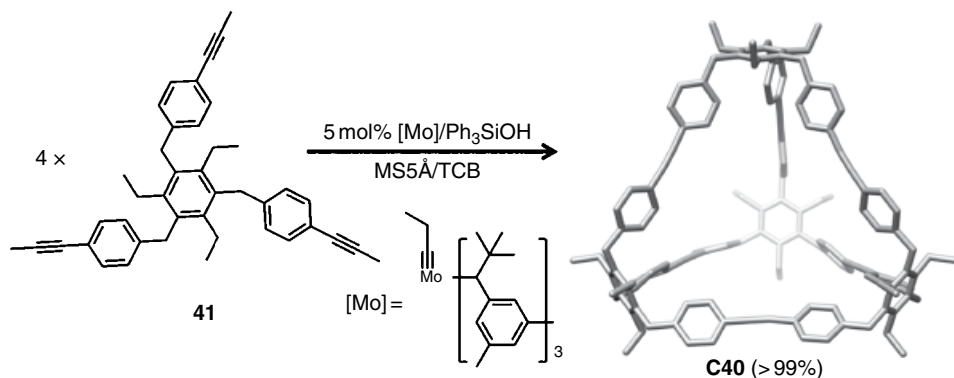
Scheme 4.25 Synthesis of tetrahedral **C40** through alkyne metathesis. The crystal structure of **C40** is shown.

The Zhang group also attempted to synthesize tetrahedral-shaped OMCs via alkyne metathesis starting from tritopic precursors.[61] However, these precursors rapidly formed tetramers with D_{2h} symmetry under the alkyne metathesis condition. Later, tetrahedral OMCs were successfully synthesized by Moore and co-workers via alkyne metathesis from two rationally designed trialkoxy-based precursors.[62] Starting from precursor **41**, tetrahedral-shaper **C40** was obtained in near-quantitative yields (>99%) (Scheme 4.25). They hypothesized that the desired product becomes kinetically trapped under the reaction conditions, which was further proved by dynamic scrambling experiments: the tetrahedral OMCs no longer exchange their vertices once they are formed, therefore kinetically trapped products may facilitate high yields of complex products from dynamic covalent synthesis.

4.2.4 OMCs Synthesized through Other Reactions

In contrast to the OMCs mentioned above, OMCs constructed through other linkages (e.g., disulfide bond and hydrazine bond) have also been reported. Herein, we will briefly introduce the synthesis of OMCs via these reactions.

The dynamically reversible formation of disulfide bonds, which plays a significant role in biological processes, can be used to synthesize OMCs. In 2009, Horing and co-workers presented the synthesis of tri(disulfide) OMC (**C41**, Scheme 4.26) by oxidation of **42**.[63] It is noteworthy that crystals of **C41** were found as precipitates when the oxidation was conducted in DMF solution. Additionally, the nucleophilic substitution reaction of **43** and **44** also yielded **C41**. Sanders and co-workers also reported the discovery of several OMCs assembled from simple tri- and dithiol building blocks.[64] By using a template-driven synthetic approach, a series of water-soluble disulfide-linked OMCs were generated on templation by positively charged polyamine guests of appropriate shape and length. They found that the templates played a crucial role in the efficient and selective synthesis of OMCs.

The condensation of hydrazine and aldehyde organic building blocks to give hydrazone derivatives has also been used to construct OMCs. However, only one such example has been reported up to now. Very recently, Sessler and co-workers reported the synthesis of an interlocked OMC (**C42**, Scheme 4.27) with hydrazone
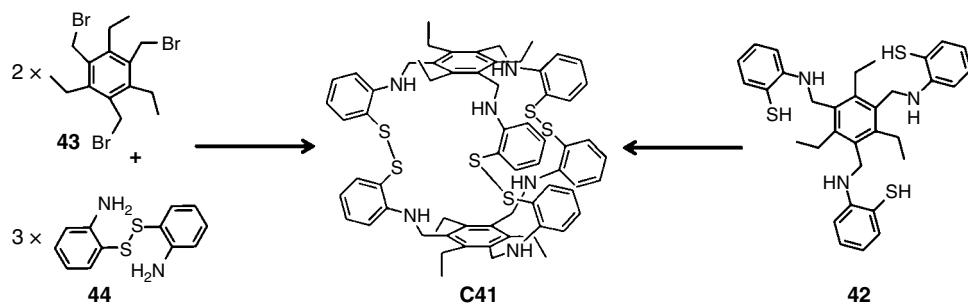
Scheme 4.26 Synthesis of **C41**.

linkage in an acidic aqueous medium. Heating the reaction mixture of **45** and **46** at 70 °C for 8 h provided **C42**.[65] By slow vapor diffusion of Me_2CO into the reaction mixture in D_2O, single crystals of **C42** were obtained. From a side view of the crystal structure, π–π donor–acceptor interactions between the phenyl and triazine subunits were observed, as inferred from an average separation distance of 3.5 Å. Interestingly, **C42** was found to undergo decomposition after adding DMSO to the aqueous solution, presumably as a result of suppressed hydrophobic interactions. However, it can be regenerated via the removal of DMSO and addition of water, indicating that **C42** is not the thermodynamically favored product in the presence of organic solvents.

OMCs have also been synthesized through orthogonal dynamic covalent reactions. Through the combination of both dynamic imine and boronic ester condensation, several OMCs have been synthesized via a one-pot fashion. For example, Nitschke and co-workers successfully synthesized an OMC (**C43**, Scheme 4.28) from cyclotri-catechylene (**47**), *m*-xylylenediamine (**48**), and 2-formylphenylboronic acid (**49**) in DMF.[66] Severin and co-workers reported an OMC (**C44**, Scheme 4.29) synthesized from trisamine (**50**), pentaerythritol (**51**), and 4-formylphenylboronic acid (**52**).[67] By using the elongated building block 4-(4-formylphenyl)phenylboronic acid (**53**), a large OMC (**C45**, Scheme 4.29) was also obtained. Interestingly, when the formation of **C44** and **C45** was performed by ball-milling procedure, the reaction yield was improved significantly compared to the solution-based method they tested (94% vs. 24% in the case of **C44**, and 71% vs. <40% in the case of **C45**).

By combining imine metathesis and olefin metathesis, Zhang and co-workers reported an OMC (**C46**) assembled from six vinylaminocarbazole (**54**) and two trial-dehyde (**55**, Scheme 4.30).[68] In a typical reaction, the reaction mixture was stirred for a while under the catalysis of TFA and left under vacuum before the addition of olefin metathesis catalysts. By passing the crude product through a short plug of silica gel using chloroform as the eluent, **C46** was obtained in 51% yield. Zhang and co-workers also examined the construction of **C46** in a true one-pot, orthogonal fashion, by adding both acid and olefin metathesis catalysts at the same time. However, increased formation of side products was observed along with some **C46**, indicating operating dynamic imine and olefin metathesis simultaneously to achieve complex molecular architectures might be feasible but still need further refinement.

2 ×

+

2 ×

−6H₂O

45

46

C42 (quantitative)
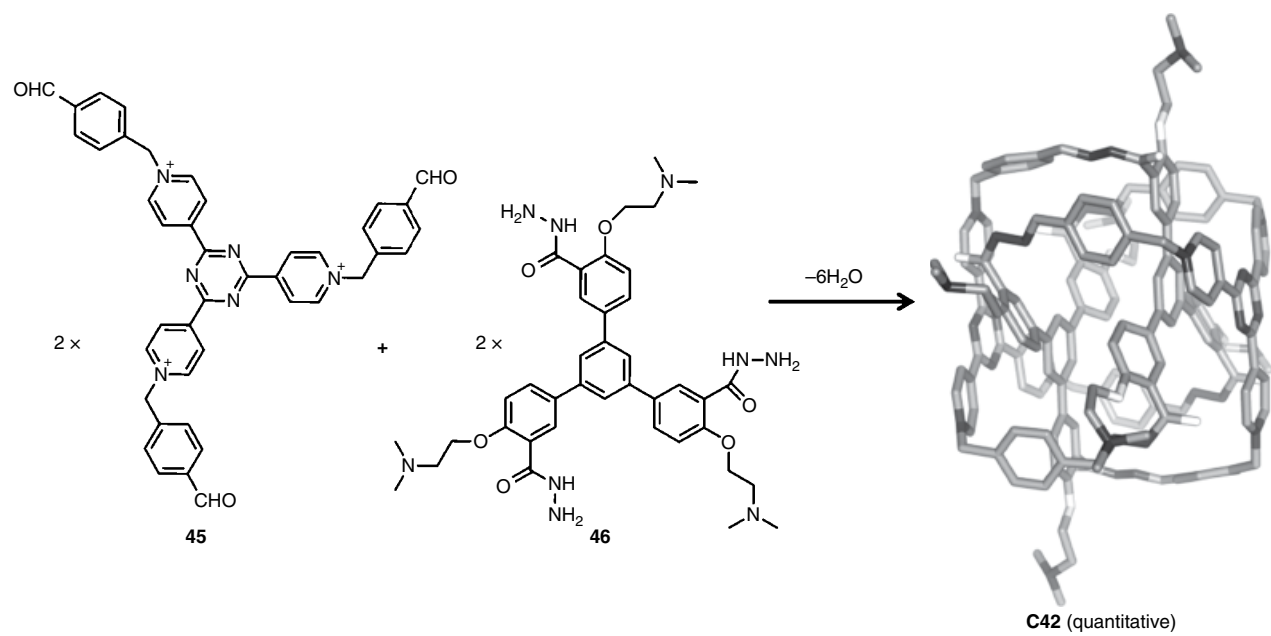
Scheme 4.27 Synthesis of a catenaned cage **C42.** The crystal structure of **C42** is shown.
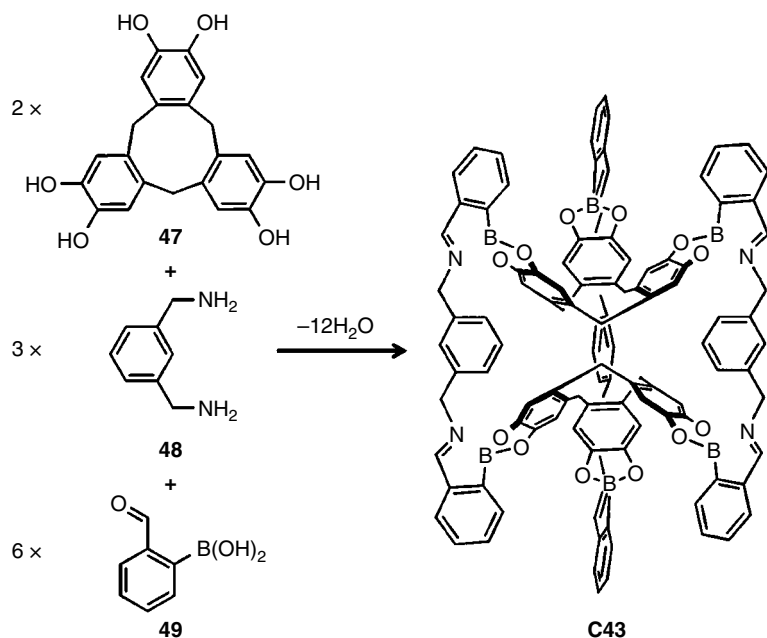
Scheme 4.28 Synthesis of **C43** through iminoboronate condensation.

4.3 Functionalization of Organic Molecular Cages

The functionalization of OMCs has gained increasing attention, as it can enhance possible functions associated within the cavities of OMCs. Starting from precursors with functional groups, OMCs with desired properties can be synthesized directly. For example, electron-deficient cage **C10** suitable as a host for electron-rich molecules can be obtained from electron-deficient triazine-based precursor.[38] However, it is often challenging to incorporate such functional groups directly into OMCs. Alternative approaches therefore have been developed to functionalize OMCs, mainly post-synthesis and "mix and match" approaches. In this section, we will focus on the functionalization of OMCs via these two methods.

Post-synthesis strategy has been widely used to construct functional materials, since it can covalently attach functional moieties into the main molecular skeleton after the scaffold is formed. The functionalization of OMCs through the post-synthetic method has been less explored. Until now, only a few reactions have been successfully used to modify OMCs. For example, Mastalerz and co-workers presented the post-synthetic modification of OMC (**C22**, Scheme 4.31) by Williamson etherification,[69] aiming to "fine-tune" the pore structure of the resulting material in the solid state. Initially, they tried to synthesize the targeted OMCs from functional precursors directly, but all attempts were far from satisfactory. On the contrary, functionalization of cage interior was successfully accomplished through alkylation of the phenolic hydroxyl groups.
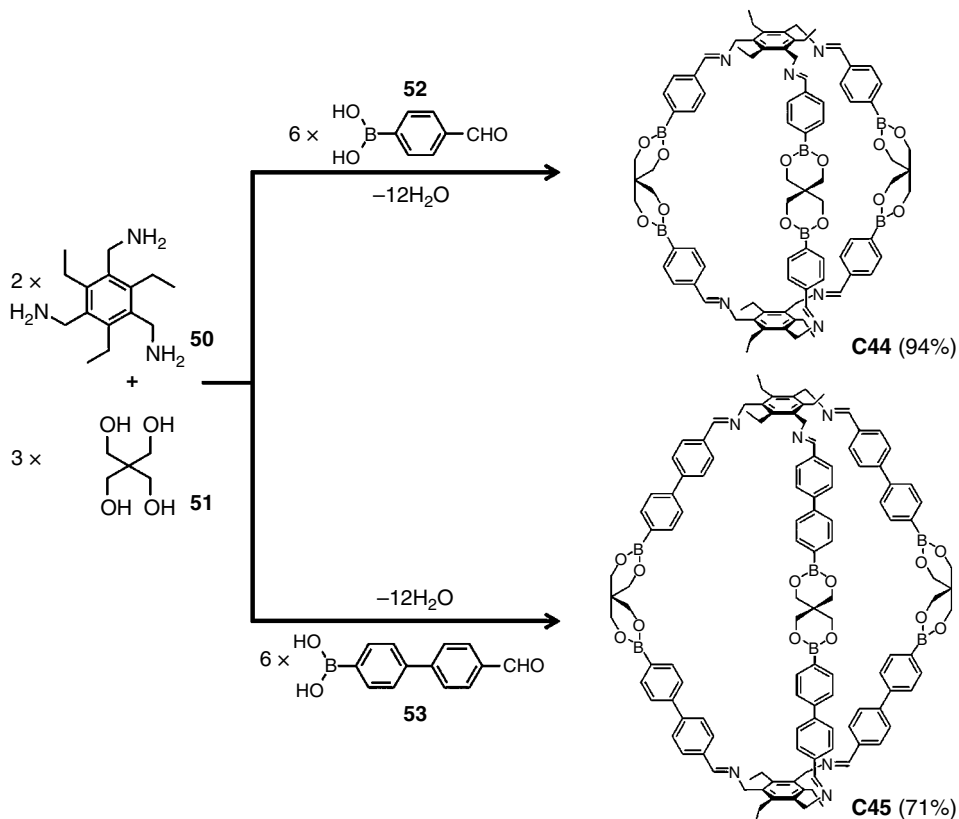
Scheme 4.29 Synthesis of **C44** and **C45** through iminoboronate condensation.

Another promising reaction that has been utilized to functionalize OMC is imine reduction. Due to the reversible nature of the imine bond, imine-linked OMCs usually suffer problems of chemical instability, thus limiting their wider applications. In order to avoid this, a general approach is to reduce the imine linkages to secondary amines through treatment with reducing agents. A series of amine-based OMCs have been successfully prepared by reduction of imine-based OMCs. For example, Zhang and co-workers reported several amine-based OMCs (**C25**, **C47**–**C49**, Scheme 4.32) in good yields by imine condensation of triamines and dialdehydes followed by reduction.[70] These amine-based OMCs overcome some of the drawbacks of their precursors, for example sensitive to acidic conditions and water.

These amine-based OMCs can be further modified via post-synthetic strategy to provide interesting properties. For example, Cooper and co-workers reported the post-synthetic "tying" of an amine-linked OMC (**C50**, Scheme 4.33),[71] which was synthesized in high yield by reduction of **C4** with NaBH$_4$. They found dissolution of **C50** in acetone produced prism-shaped single crystals after ∼30 min, which was later confirmed by several characterizations to be a new OMC **C51**, featuring one of the six diamine

6 ×

54

2 ×

55

C46 (51%)
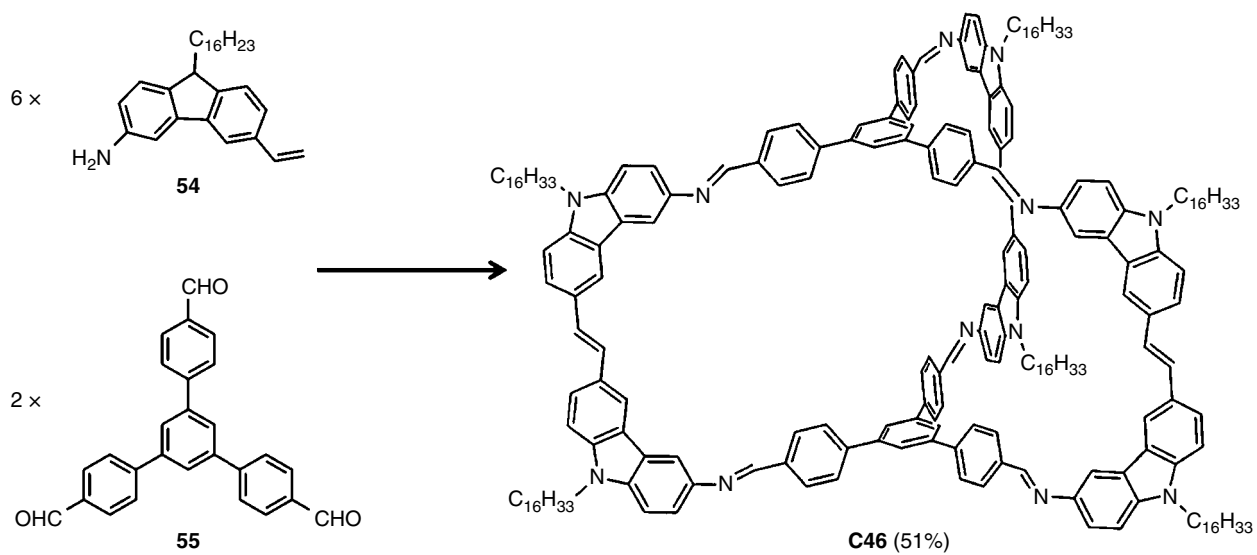
Scheme 4.30 Synthesis of **C46** through dynamic imine reaction and olefin metathesis.
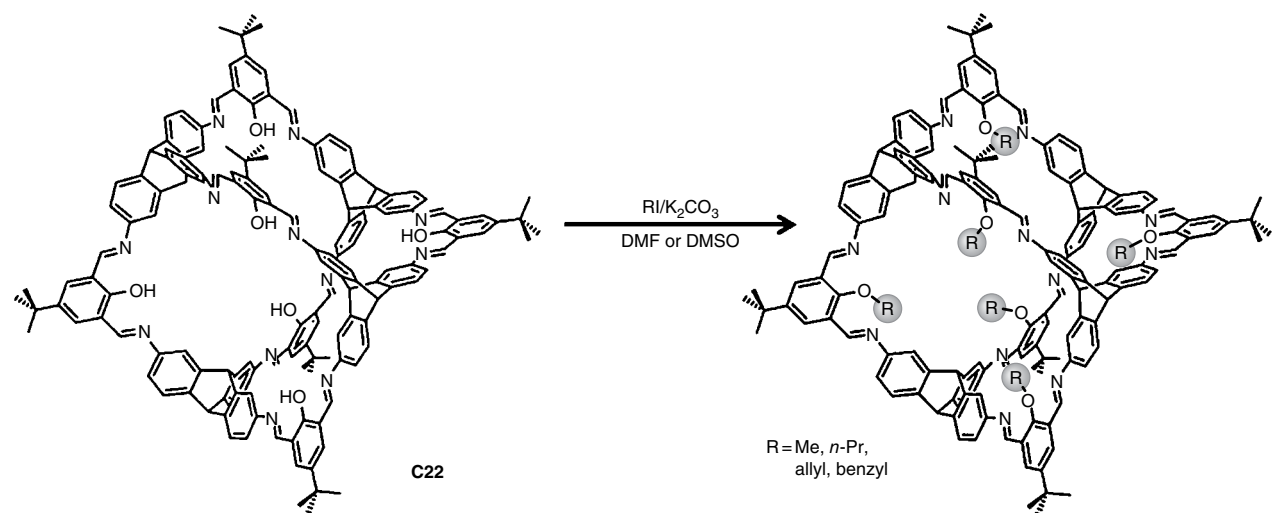
Scheme 4.31 Post-synthetic modification of **C22**.
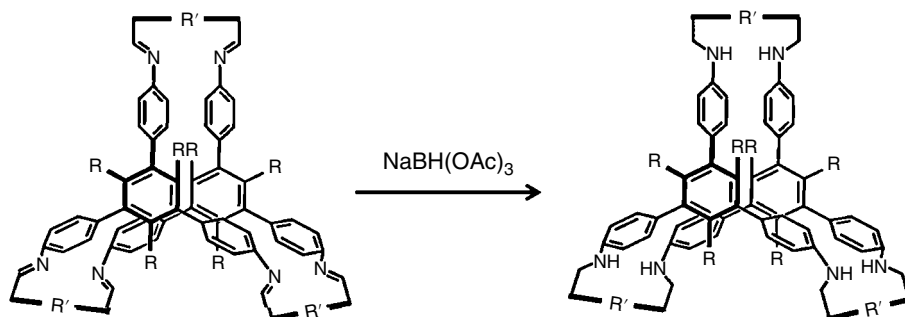
Scheme 4.32 Synthesis of **C25** and **C47–C49** through reduction of imine-linked cages by NaBH(OAc)$_3$ or DIBAL-H.

vertices tied with acetone. Subsequently, by mixing **C50** with formaldehyde at 70 °C in methanol, another OMC (**C52**) with all six diamine groups tied with formaldehyde (aminal formation) was obtained. Interestingly, **C52** showed excellent stability in either acidic or basic solution. Through one-step amidation, cage **C50** was also successfully converted to dodecaamide cage.[72]

Mukherjee and co-workers reported another post-synthetic modification of an amine-based OMC (**C53**, Scheme 4.34) through one-pot, copper(I)-catalysed multi-component A^3-coupling of amine groups, formaldehyde, and terminal alkyne.[73] By employing this reaction, OMCs with phenyl-, xylyl-, and naphthyl-acetylene moieties appended to each amine have been successfully synthesized.

The second strategy used to functionalize OMCs is "mix and match". This concept is quite straightforward and very efficient, as functional OMCs can be constructed by either chemical or physical mixing. By using a dynamic imine–imine interchange reaction, Cooper and co-workers reported a chemical approach for desymmetrizing OMCs (Scheme 4.35).[74] Starting from **3** and a mixture of **4** and **6** with different ratios, various OMCs with a range of structures were synthesized via imine reaction. Interestingly, a number of different molecular pores could be combined in a single solid. They also reported a modular assembly concept to produce functional OMCs, through
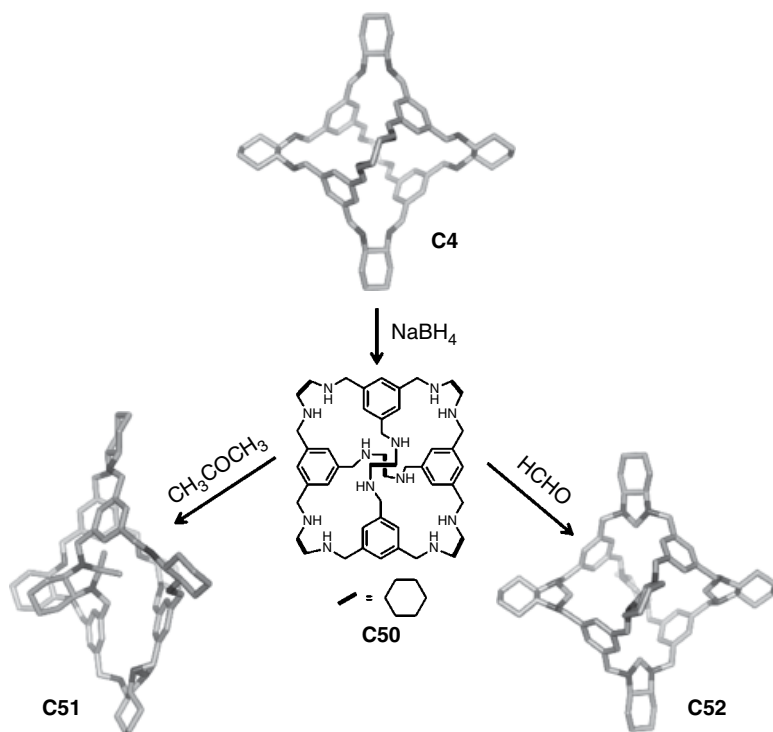
Scheme 4.33 Synthesis of "tied" porous cages **C51** and **C52**. The crystal structures of **C51** and **C52** are shown.
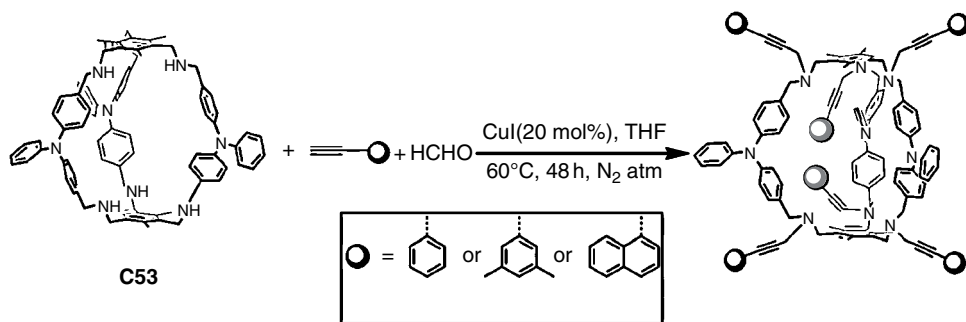
Scheme 4.34 Post-synthetic exterior decoration of **C53** by copper(I)-catalysed A^3-coupling.

co-crystallization of different OMCs into one crystal network. In a typical experiment, physical mixing of two or more solutions of prefabricated OMCs produced a new crystalline polymorph. More importantly, the structures of the resulting polymorph could be predicted using a Monte Carlo simulation method, thus opening up many possibilities of computation-aided design of new materials.
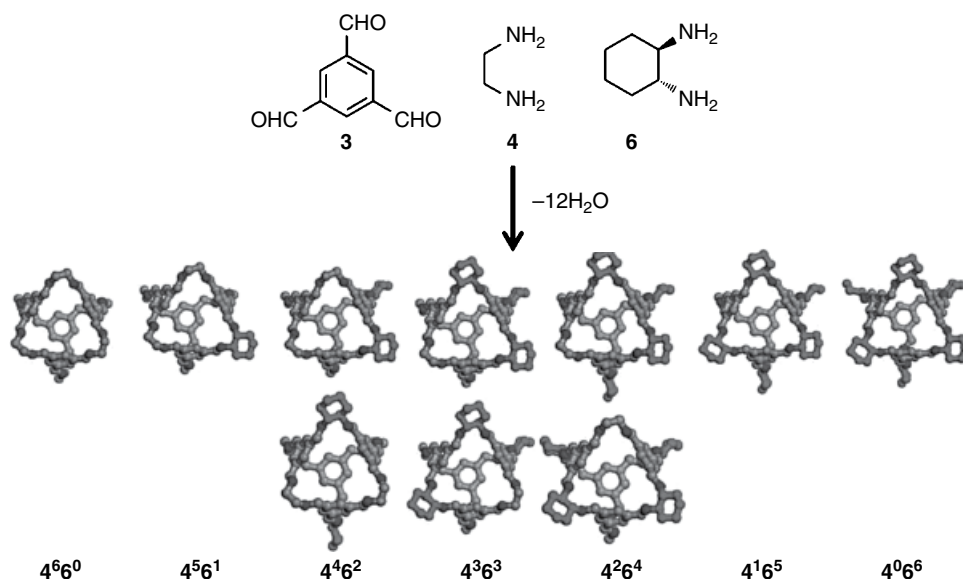
Scheme 4.35 The synthesis of OMCs with a range of structures by using a "mix and match" strategy.

4.4 Applications of Organic Molecular Cages

By using DCvC approach, a diversity of OMCs have been synthesized from simple precursors on a large scale and their applications in different areas have been widely investigated. In this section, we will summarize the application of OMC-based materials synthesized via a DCvC strategy.

4.4.1 Molecular Recognition

As molecular container compounds, OMCs have shown promising application in supramolecular chemistry. The well-defined cavity of OMCs makes them ideal hosts for various guest molecules ranging from ions to molecules. For example, the above-mentioned **C1** can host tetraalkylammonium salts in toluen.[32] Owing to a better fit within the cavity, (n-octyl)$_4$NBr is more strongly bound in **C1** than (n-heptyl)$_4$NBr. Delgado and co-workers reported that a hexaamine OMC (**C54**, Scheme 4.36) synthesized by reduction of an imine-based OMC, exhibited selective recognition of di-negative anions over mono-negative ones at pH values below 5.[75] They successfully obtained the X-ray crystal structure of sulfate cryptate, which shows that sulfate anion is encapsulated in the cavity of **C54** and is sited between the two 2,4,6-triethylbenzene caps. Recently, Nitschke reported two water-soluble amine-based OMCs, with the larger one able to host aromatic polyanions in aqueous media with great affinity.[76]

OMCs can also host molecules of a certain size and shape, for example fullerenes. The rigid **C37**, which has a cavity with a height of 11.9 Å and a diameter of 18.3 Å according to the theoretical calculation, can serve as an excellent receptor for fullerenes by donor–acceptor interaction (Scheme 4.37).[58] It forms 1:1 complexes with C_{60} and C_{70} in toluene and shows high selectivity (>1000) in binding C_{70} over C_{60}. Moreover, the association and dissociation of fullerene–**C37** complexes can be reversibly tuned when
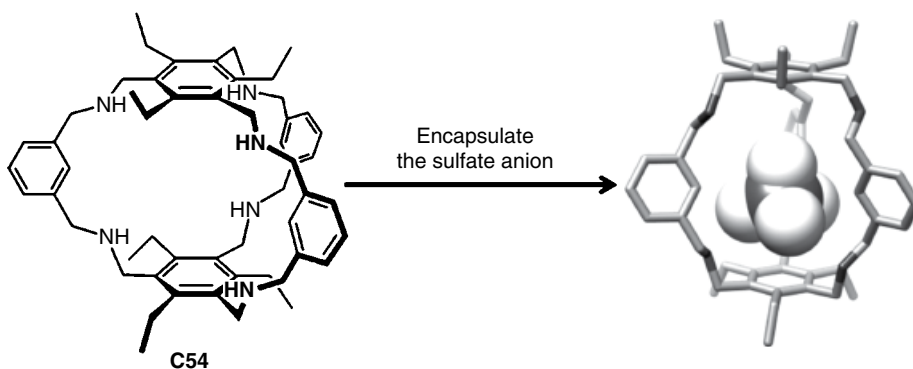
Scheme 4.36 The encapsulation of sulfate cryptate by **C54**. The crystal structure of the complex is shown.
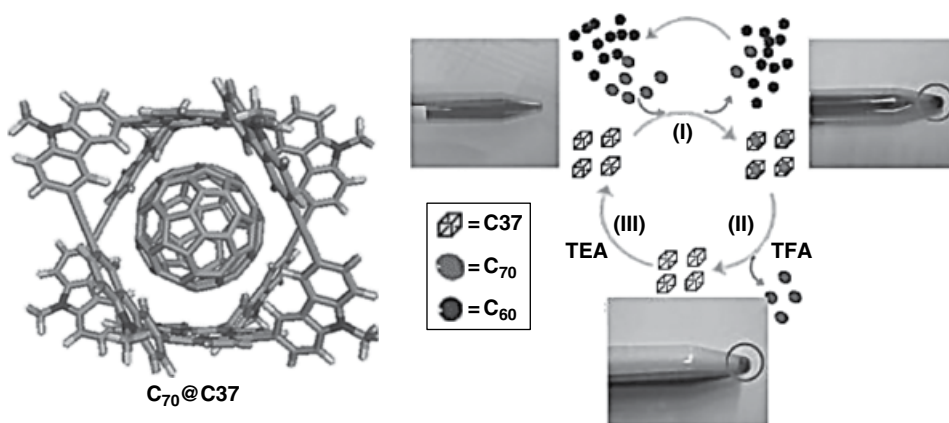
Scheme 4.37 The schematic presentation of the C_{70} isolation process. The energy-minimized structure of **C_{70}@C37** is shown.

treated with acid and base, which enables the isolation of C_{70} from a C_{60}-enriched fullerene mixture through the "selective complexation – decomplexation" strategy. Later on, by simply mixing a 1,2-dichlorobenzene solution of **C_{60}@C37** and a single-walled carbon nanotube, they obtained a novel donor–acceptor nanohybrid through π–π interaction that can be used for light-harvesting.[77]

Recently, Kobayashi and co-workers reported a series of OMCs with different cavity sizes constructed through boronic ester condensation of cavitand tetraboronic acid with various bis(catechol) Linkers.[78] Each OMC has a different size depending on the linker used and shows particular guest encapsulation selectivity. They also demonstrated that a chiral OMC consisting of a chiral bis(catechol) linker can express diastereomeric encapsulation selectivity with respect to a prochiral biphenyl guest.

Quartz crystal microbalances (QCMs) are sensitive gravimetric analysis tools that can be used to determine the affinity of molecules to a surface functionalized with recognition sites. Depositing OMCs as a thin film onto a QCM may generate highly sensitive detectors for various analytes. Mastalerz and Waldvogel successfully modified QCMs with OMCs (e.g. **C22**) or model compounds using electrospray techniques.[79]

These modified QCMs are highly sensitive to aromatic solvent vapors. A clear "cage effect" was observed when compared to model compounds: a higher affinity for larger aromatics was observed with increased cage cavity size. Later on, Mastalerz and Waldvogel modified QCMs with a series of amine-based OMCs, which were able to selectively detect the drug γ-butyrolactone (GBL). They proposed that the hydrogen bonding interactions between GBL and the endo-functionalized groups in OMC play an important role in guest tracing.

4.4.2 Molecular Flask

Like supramolecular cages, OMCs with hollow structures have been used as molecular flasks that protect guests from the outer environment. For example, Warmuth and co-workers reported a water-soluble OMC that is able to stabilize the highly strained and reactive Bredt olefin protoadamantene.[80] They reported that the encapsulated proto-adamantene is stable for days at room temperature in DMSO–d_6/CD$_3$CN due to pro-tection from the bulk solvent by the OMC. Also, under such conditions imine bonds are found to be stable, thus preventing cage decomposition and release of the guest. However, in D$_2$O, the protoadamantene has a lifetime of only a few minutes due to the hydrolysis of imine bonds, which leads to decomposition of the OMC and release of the guest. These results clearly demonstrate that OMCs can be used to stabilize thermally unstable molecules or fragile reactive species under certain conditions.

The spatially confined cavity of OMCs has also provided a unique place to perform reactions in a controlled manner. For example, Zhang and co-workers reported a novel strategy for the controlled synthesis of gold nanoparticles (AuNPs) through NP nuclea-tion and growth inside the cavity of an OMC (**C55**, Scheme 4.38) that was functional-ized with interior thioether groups.[81] By using the two-phase liquid–liquid approach, they successfully synthesized AuNPs with a narrow size distribution (1.9 ± 0.4 nm).

Xu and co-workers reported the utilization of **C4** as a support for immobilizing Rhodium (Rh) NPs of ultrasmall size (∼1.1 nm) (Scheme 4.39).[82] Since **C4** provides an ideal platform for homogenizing the catalysis in solution, the catalytic performance of the obtained **C4**-supported RhNPs was tested. The study showed that such a complex exhibits significantly enhanced catalytic activity toward various liquid-phase catalytic reactions, such as methanolysis of ammonia borane, due to the well-dispersed catalytic sites in solution. More recently, Mukherjee and co-workers also demonstrated that
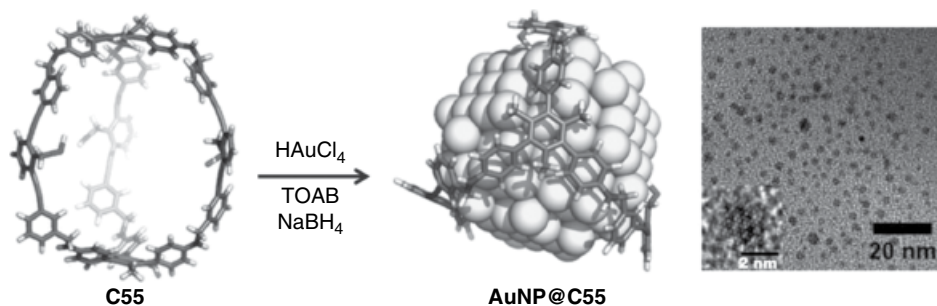
Scheme 4.38 Template synthesis of AuNPs within **C55**. A transmission electron microscopy (TEM) image of such AuNPs is also shown.
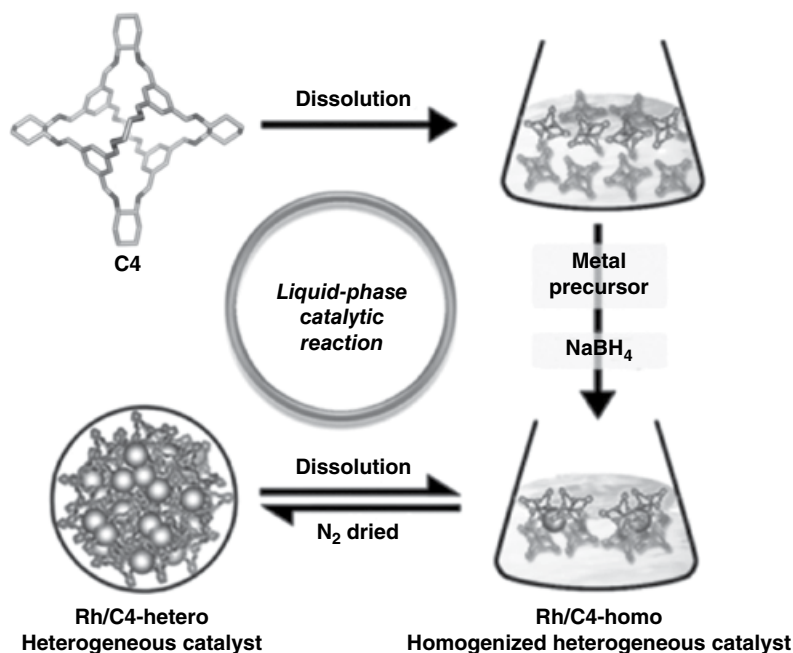
Scheme 4.39 Preparation of homogenized heterogeneous catalyst and its heterogeneous counterpart.

amine-based OMCs foster the size-controlled synthesis of PdNPs. Such heterogeneous encapsulated PdNPs catalysts have shown superior catalytic performance over some well-known palladium catalysts in the cyanation of aryl halides under heterogeneous and additive-free conditions.[83]

The polymerization reactions within OMCs have also been investigated. Uemura and co-workers reported the first example of radical polymerization of vinyl monomers in **C4** with extrinsic porosity (Scheme 4.40).[84] Interestingly, the polymerization reaction strongly depends on the dynamic and responsive packing structure of **C4**. It has been shown that **C4** is highly selective on the polarity of substrates, which is useful to prevent the incorporation of unfavorable monomers into the polymeric products.

4.4.3 Porous Solid

Being composed of lightweight elements, OMC-based porous materials have been touted as potential candidates for gas storage. In 2009, Cooper and co-workers demonstrated for the first time that OMCs can assemble into crystalline microporous materials with permanent porosity,[33] as a consequence of both the internal voids in the OMCs and the inefficient molecular packing in the solid state. Building on this seminal work, the construction of OMC-based porous materials has gained intensive attention and great progress has been made over the past few years. Brunauer–Emmett–Teller (BET) surface areas approaching $4000\,\mathrm{m^2\,g^{-1}}$ have been reported, which is comparable to many other porous materials. The other great advantage of OMC-based porous materials is the tenability of porosity by changing the polymorphism of OMCs. In this section, we will mainly discuss the applications of these porous materials.
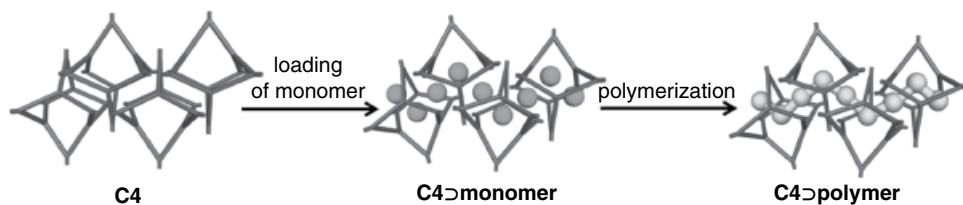
Scheme 4.40 Polymerization of monomers in **C4**.
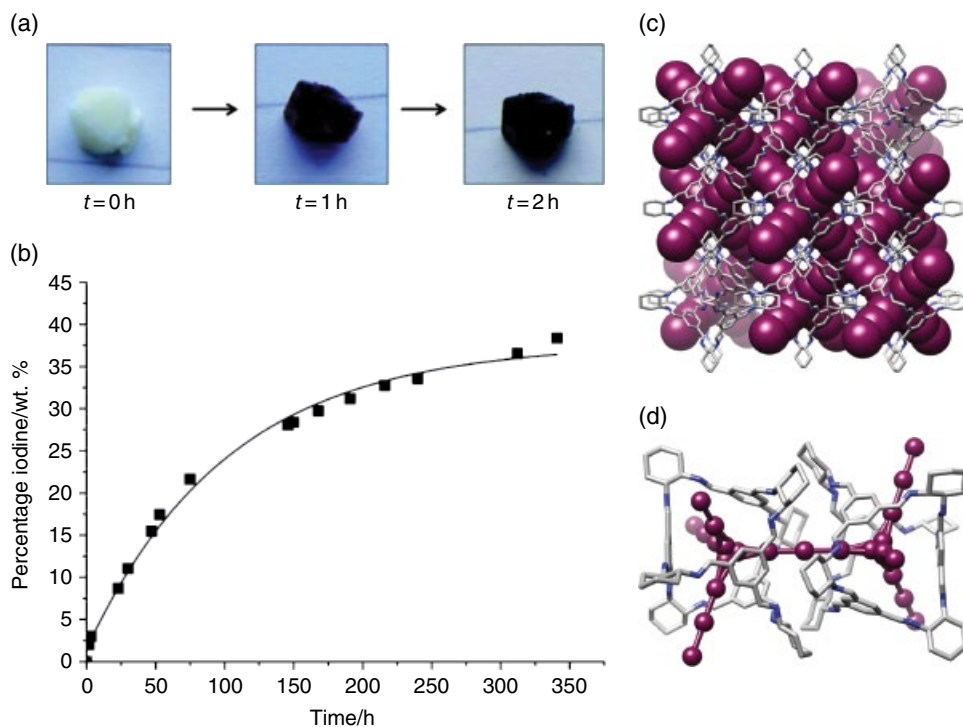
Figure 4.1 (a) The color change when a single crystal of **C4** was exposed to iodine vapor. (b) Gravimetric uptake of iodine as a function of time. (c) Packing diagram for **I@C4**. (d) One possible conformation of I_5^- species in neighboring cage molecules. (*See insert for colour representation of the figure.*)

Cooper and co-workers showed that OMCs (**C2–C4**) could be desolvated to generate porous materials that adsorb nitrogen, hydrogen, methane, and carbon dioxide.[33] They also studied the water absorption behavior of **C4**, and showed that **C4** is stable to moisture and can reversibly adsorb up to 20.1 wt% water in the crystalline state.[85] Moreover, they found that **C4** can adsorb iodine in the solid state (Figure 4.1).[86] According to the X-ray crystal structure, iodine atoms exist as V-shaped I_5^- species in and between the **C4**. On doping through vapor sublimation, the conductivity of **C4** has been significantly enhanced in the case of I_5^-. Besides, the toxic and volatile OsO_4 can also be trapped in **C4**.

Apart from gas adsorption, the gas separation performance of OMC-based porous materials has also been widely investigated. For example, Zhang and co-workers studied

the selective gas uptake behavior of **C25**, which showed extraordinarily high ideal selectivity (73:1, v:v) for the adsorption of CO_2 over N_2 under ambient temperature and pressure.[87] Mastalerz and co-workers demonstrated that **C22** is able to take up 9.4 wt% CO_2 and 0.94 wt% methane, which corresponds to a CO_2/CH_4 selectivity of 10:1 (10:1, w:w).[88] Cooper and co-workers also investigated the gas separation behavior of desymmetrizing OMCs.[74] By varying the ratio of reagents in the scrambling reaction, OMCs with a distribution of structures could be obtained, thus allowing control of the selective absorption of H_2 over N_2.

The separation of rare gases in the air is a significant challenge due to their identical shape and similar kinetic diameters. Cooper and co-workers showed that OMC assemblies are excellent candidates for separating rare gases, such as krypton and xenon.[88] They demonstrated that **C4** exhibits unprecedented separation performance in the solid state owing to its internal cavity, which is precisely the right size to accommodate a single xenon or radon atom. The benchmark value for the selective separation of xenon over krypton (selectivity of 20.4 for Xe/Kr) at real-world concentrations was reported. They also examined a series of OMCs for selective adsorption of sulfur hexafluoride (SF_6), a much more potent greenhouse gas than CO_2.[89] Among various OMCs, **C4** shows the highest SF_6/N_2 selectivity at ambient temperature and pressure, which translates to real separations in a gas breakthrough column. The simulation results show that this high selectivity is likely a result of the flexibility of the **C4** molecular crystal, which allows SF_6 to diffuse by cooperative effects.

Cooper and co-workers demonstrated molecular shape sorting by using **C4**. Solid-state separation of aromatic molecules such as mesitylene and xylenes and its isomers was reported.[90] From the solid–vapor sorption experiments, linear 4-ethyltoluene can be adsorbed by **C4** crystals, whereas mesitylene vapor was rejected completely due to the difference of the guest shape. **C4** crystals show different sorption characteristics for isomers of xylenes and ethyltoluenes, favoring *para* isomers followed by *meta* isomers and *ortho* isomers least. Cooper and co-workers also tested the dynamic separation of mesitylene from 4-ethyltoluene in a continuous-flow setup using a chromatography column packed with **C4** crystals. From the breakthrough plot, mesitylene elutes as soon as it is pumped into the absorbent bed, while 4-ethyltoluene is retained by the cage sorbent.

Unlike other extended network materials that are constructed from covalent or metal-ligand coordination bonds, OMC-based porous materials are soluble in common solvents, which can allow solution processing for interesting applications. For example, OMCs can be deposited inside a standard-format capillary column as a chromatographic stationary phase.[91] Using the simple and commercially scalable static method, Cooper and co-workers successfully prepared a column coated with **C4** for gas chromatography (GC) separation using a homogeneous, molecular solution of the organic cage.[92] The resulting column was found to separate a variety of mixtures, including linear alkanes and chiral alcohols or amines, through molecular sieving. Subsequently, Yuan and co-workers also prepared a column using **C4** diluted with a polysiloxane as a stationary phase for high-resolution GC with excellent enantioselectivity (Figure 4.2).[93] In their experiment, a large number of optical isomers were resolved without derivatization, including chiral alcohols, esters, and organic acids.

OMCs can also be incorporated into porous supports or casted onto membranes toward composite materials. Cooper and co-workers reported the solution-based deposition of **C4** into predominantly macroporous inorganic beads[94] to enhance the surface
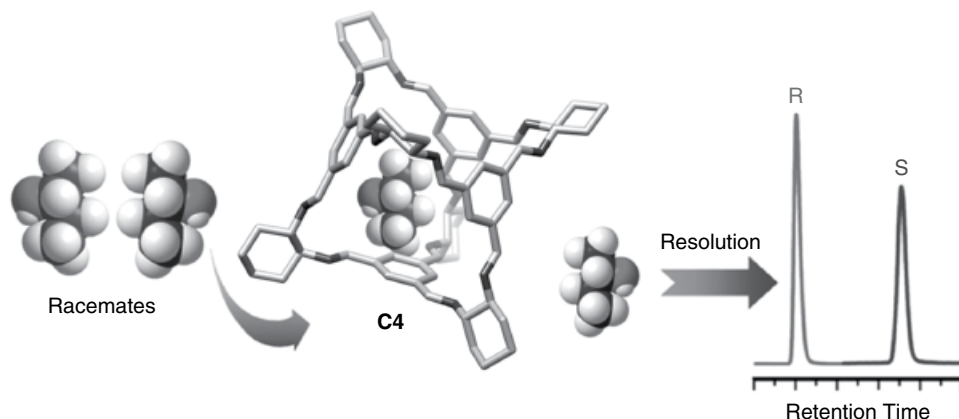
Figure 4.2 Selective separation of racements using **C4**.
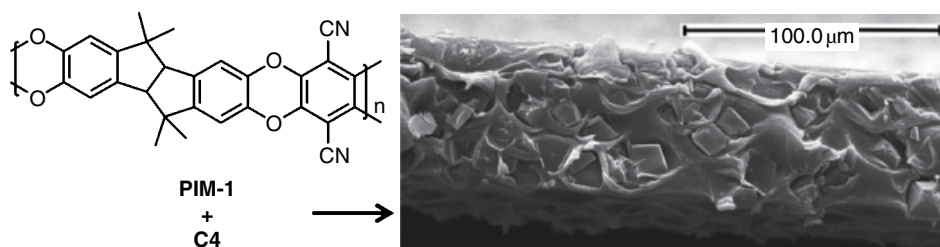
Scheme 4.41 The preparation of nanoporous organic polymer from PIM-1 and **C4**, and its SEM image.

area and microporosity of macroporous inorganic supports. Budd and co-workers later reported a mixed-matrix membrane in which the dispersed phase is generated by *in situ* crystallization of OMCs from a single homogeneous solution (Scheme 4.41).[95] The incorporation of **C4** within a microporous polymer (PIM-1) can substantially enhance permeability while retaining good selectivity and providing better resistance towards physical ageing. Cooper and Sivaniah demonstrated the solution processing of several OMCs into thin films with tunable structure and porosity via a simple, reproducible, and easily controlled spinning coating process.[96] The resulting thin films show potential for application in molecular sensing and selective separations.

4.4.4 Porous Liquid

Recently, engineering permanent microporosity in the liquid state has emerged as an interesting novel concept. Porous liquids, or liquids with permanent porosity, could combine the properties of microporous solids mentioned above with the rapid mass transfer, fluidity, and fast kinetics of liquids.[97] In 2012, the James group reported that attachment of alkyl tails to the outside of OMCs can dramatically decrease the melting points of OMCs from >300 °C to as low as 50 °C. However, these materials are non-porous in their glassy/liquid states.[98] Later on, by changing the size of the terminal chains, Po'polo and co-workers reported more OMCs with melting points ranging from 156 to 40 °C.[99] Unfortunately, these materials are still non-porous in the liquid state due to the
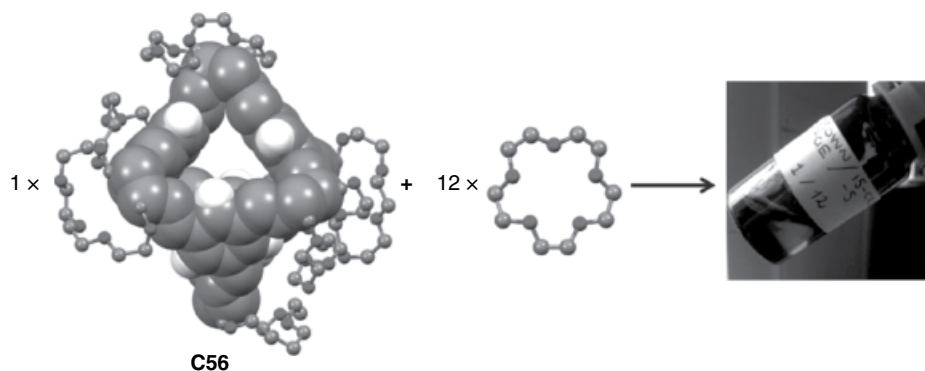
Scheme 4.42 The soluble **C56** with the 15-crown-5 solvent provides porous liquid which flows at room temperature.

invading alkyl chains in the cage. James and co-workers successfully achieved permanently porous liquids using a simple trick: attaching looped chains instead of linear chains to efficiently avoid interpenetration.[100] They synthesized an OMC (**C56**, Scheme 4.42), which has a melting point higher than 180 °C and is not a porous liquid by itself. However, a porous liquid was successfully created by combining OMC with a solvent named 15-crown-5, which is too big to enter the cage's cavities. In addition, they reported an alternative approach to create porous liquids by making scrambled OMCs form a mixture of diamines (**3**, **4**, and **6**, Scheme 4.35). Using hexachloropropene as the solvent, a liquid with similar porosity but lower viscosity compared to that of the material generated from **C56** and 15-crown-5, was obtained. For both gas-filled liquids, when a solvent small enough to enter the cages' cavities was added, bubbles were immediately observed in the liquid due to the displacement of the gas by the solvent (Figure 4.3).
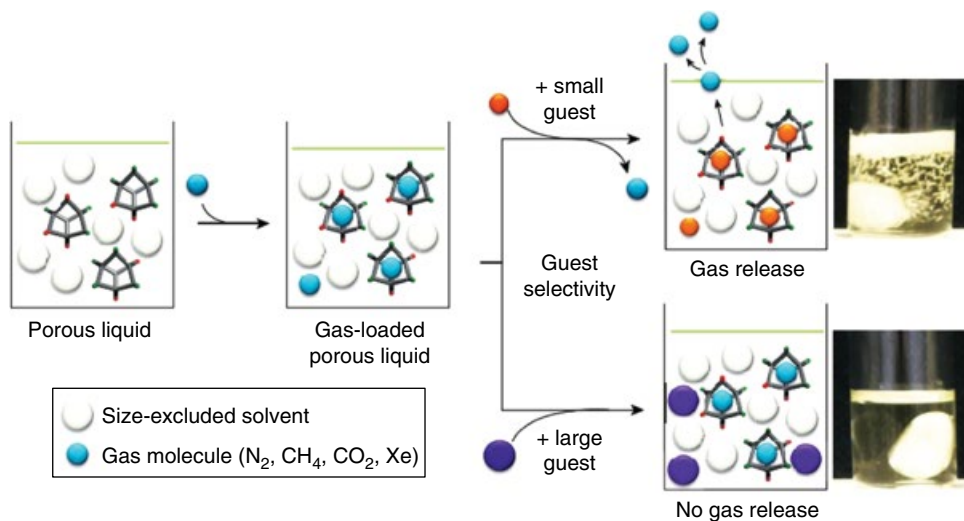
Figure 4.3 The gas-release behavior of porous liquids. (*See insert for colour representation of the figure.*)

4.5 Conclusion and Perspective

In summary, significant progress has been made in the field of OMCs over the past few years. Thanks to the DCvC strategy, a range of OMCs has been successfully synthesized from simple precursors on a large scale, which allows researchers to further study their applications in different areas. However, in comparison with coordination cages, OMCs are still less frequently investigated. Further expansion of this fascinating area is anticipated and the following issues deserve more attention:

1) OMCs with higher hydrolytic stability are desired for prolonged use. The stability of OMCs needs to be further investigated.
2) OMCs with low symmetry are intriguing, but their synthesis via the DCvC approach remains a great challenge.
3) As the crystal structure of OMC can give us valuable information on material design, more theories on crystal engineering or predicting the crystal structure of OMCs should be explored.
4) The use of OMCs as the porous liquids opens a new exciting frontier to porous materials research, but their surface areas and overall gas uptake abilities are much lower than those of the porous solids reported so far. These investigations will enrich the scope of OMCs and provide new applications.

References

1 W. Cullen, M. C. Misuraca, C. A. Hunter, N. H. Williams, M. D. Ward, *Nat. Chem.* **2016**, *8*, 231–236.

2 T. Friscic, *Chem. Soc. Rev.* **2012**, *41*, 3493–3510.

3 M. Yoshizawa, J. K. Klosterman, M. Fujita, *Angew. Chem., Int. Ed.* **2009**, *48*, 3418–3438.

4 S. J. Dalgarno, N. P. Power, J. L. Atwood, *Coord. Chem. Rev.* **2008**, *252*, 825–841.

5 T. Brotin, L. Guy, A. Martinez, J. P. Dutasta, *Differentiation of Enantiomers Ii* **2013**, *341*, 177–230.

6 Z. Laughrey, B. C. Gibb, *Chem. Soc. Rev.* **2011**, *40*, 363–386.

7 R. Chakrabarty, P. S. Mukherjee, P. J. Stang, *Chem. Rev.* **2011**, *111*, 6810–6918.

8 M. Tominaga, K. Suzuki, M. Kawano, T. Kusukawa, T. Ozeki, S. Sakamoto, K. Yamaguchi, M. Fujita, *Angew. Chem., Int. Ed.* **2004**, *43*, 5621–5625.

9 K. S. Iyer, M. Norret, S. J. Dalgarno, J. L. Atwood, C. L. Raston, *Angew. Chem., Int. Ed.* **2008**, *47*, 6362–6366.

10 A. Galan, P. Ballester, *Chem. Soc. Rev.* **2016**, *45*, 1720–1737.

11 P. Mal, B. Breiner, K. Rissanen, J. R. Nitschke, *Science* **2009**, *324*, 1697–1699.

12 M. Mastalerz, *Angew. Chem., Int. Ed.* **2010**, *49*, 5042–5053.

13 J. R. Holst, A. Trewin, A. I. Cooper, *Nat. Chem.* **2010**, *2*, 915–920.

14 M. Xiong, H. M. Ding, B. J. Li, T. L. Zhou, C. Wang, *Curr. Org. Chem.* **2014**, *18*, 1965–1972.

15 J. D. Evans, C. J. Sumby, C. J. Doonan, *Chem. Lett.* **2015**, *44*, 582–588.

16 A. Avellaneda, P. Valente, A. Burgun, J. D. Evans, A. W. Markwell-Heys, D. Rankine, D. J. Nielsen, M. R. Hill, C. J. Sumby, C. J. Doonan, *Angew. Chem., Int. Ed.* **2013**, *52*, 3746–3749.

17 J. H. Zhang, Y. J. Li, W. L. Yang, S. W. Lai, C. J. Zhou, H. B. Liu, C. M. Che, Y. L. Li, *Chem. Commun.* **2012**, *48*, 3602–3604.

18 M. M. Naseer, D. X. Wang, L. A. Zhao, Z. T. Huang, M. X. Wang, *J. Org. Chem.* **2011**, *76*, 1804–1813.

19 T. J. Ryan, G. Lecollinet, T. Velasco, A. P. Davis, *Proc. Natl. Acad. Sci. USA* **2002**, *99*, 4863–4866.

20 P. R. Ashton, U. Girreser, D. Giuffrida, F. H. Kohnke, J. P. Mathias, F. M. Raymo, A. M. Z. Slawin, J. F. Stoddart, D. J. Williams, *J. Am. Chem. Soc.* **1993**, *115*, 5422–5429.

21 Y. Jin, C. Yu, R. J. Denman, W. Zhang, *Chem. Soc. Rev.* **2013**, *42*, 6634–6654.

22 S. J. Rowan, S. J. Cantrill, G. R. L. Cousins, J. K. M. Sanders, J. F. Stoddart, *Angew. Chem., Int. Ed.* **2002**, *41*, 898–952.

23 J. M. Lehn, *Chem. Eur. J.* **1999**, *5*, 2455–2463.

24 Q. Ji, R. C. Lirag, O. S. Miljanic, *Chem. Soc. Rev.* **2014**, *43*, 1873–1884.

25 S. L. Huang, G. X. Jin, H. K. Luo, T. S. A. Hor, *Chem-Asian J.* **2015**, *10*, 24–42.

26 Y. Jin, Q. Wang, P. Taynton, W. Zhang, *Acc. Chem. Res.* **2014**, *47*, 1575–1586.

27 Y. H. Jin, Y. L. Zhu, W. Zhang, *Cryst. Eng. Comm.* **2013**, *15*, 1484–1499.

28 G. Zhang, M. Mastalerz, *Chem. Soc. Rev.* **2014**, *43*, 1934–1947.

29 M. E. Belowich, J. F. Stoddart, *Chem. Soc. Rev.* **2012**, *41*, 2003–2024.

30 C. D. Meyer, C. S. Joiner, J. F. Stoddart, *Chem. Soc. Rev.* **2007**, *36*, 1705–1723.

31 M. L. C. Quan, C. B. Knobler, D. J. Cram, *Chem. Commun.* **1991**, 660–662.

32 Y. Liu, X. Liu, R. Warmuth, *Chem. Eur. J.* **2007**, *13*, 8953–8959.

33 T. Tozawa, J. T. Jones, S. I. Swamy, S. Jiang, D. J. Adams, S. Shakespeare, R. Clowes, D. Bradshaw, T. Hasell, S. Y. Chong, C. Tang, S. Thompson, J. Parker, A. Trewin, J. Bacsa, A. M. Slawin, A. Steiner, A. I. Cooper, *Nat. Mater.* **2009**, *8*, 973–978.

34 T. Hasell, X. F. Wu, J. T. A. Jones, J. Bacsa, A. Steiner, T. Mitra, A. Trewin, D. J. Adams, A. I. Cooper, *Nat. Chem.* **2010**, *2*, 750–755.

35 K. E. Jelfs, E. G. B. Eden, J. L. Culshaw, S. Shakespeare, E. O. Pyzer-Knapp, H. P. G. Thompson, J. Bacsa, G. M. Day, D. J. Adams, A. I. Cooper, *J. Am. Chem. Soc.* **2013**, *135*, 9307–9310.

36 M. E. Briggs, K. E. Jells, S. Y. Chong, C. Lester, M. Schmidtmann, D. J. Adams, A. I. Cooper, *Cryst. Growth Des.* **2013**, *13*, 4993–5000.

37 J. T. A. Jones, T. Hasell, X. F. Wu, J. Bacsa, K. E. Jelfs, M. Schmidtmann, S. Y. Chong, D. J. Adams, A. Trewin, F. Schiffman, F. Cora, B. Slater, A. Steiner, G. M. Day, A. I. Cooper, *Nature* **2011**, *474*, 367–371.

38 H. M. Ding, Y. H. Yang, B. J. Li, F. Pan, G. Z. Zhu, M. Zeller, D. Q. Yuan, C. Wang, *Chem. Commun.* **2015**, *51*, 1976–1979.

39 K. E. Jelfs, X. F. Wu, M. Schmidtmann, J. T. A. Jones, J. E. Warren, D. J. Adams, A. I. Cooper, *Angew. Chem., Int. Ed.* **2011**, *50*, 10653–10656.

40 P. Skowronek, B. Warzajtis, U. Rychlewska, J. Gawronski, *Chem. Commun.* **2013**, *49*, 2524–2526.

41 K. Acharyya, S. Mukherjee, P. S. Mukherjee, *J. Am. Chem. Soc.* **2013**, *135*, 554–557.

42 H. M. Ding, X. S. Meng, X. Cui, Y. H. Yang, T. L. Zhou, C. X. Wang, M. Zeller, C. Wang, *Chem. Commun.* **2014**, *50*, 11162–11164.

43 H. M. Ding, X. J. Wu, M. Zeller, Y. P. Xie, C. Wang, *J. Org. Chem.* **2015**, *80*, 9360–9364.

44 S. Hong, M. R. Rohman, J. Jia, Y. Kim, D. Moon, Y. Kim, Y. H. Ko, E. Lee, K. Kim, *Angew. Chem., Int. Ed.* **2015**, *54*, 13241–13244.

45 M. Mastalerz, *Chem. Commun.* **2008**, 4756–4758.

46 M. W. Schneider, H. J. S. Hauswald, R. Stoll, M. Mastalerz, *Chem. Commun.* **2012**, *48*, 9861–9863.

47 M. W. Schneider, I. M. Oppel, M. Mastalerz, *Chem. Eur. J.* **2012**, *18*, 4156–4160.

48 H. Takahagi, S. Fujibe, N. Iwasawa, *Chem. Eur. J.* **2009**, *15*, 13327–13330.

49 K. Kataoka, T. D. James, Y. Kubo, *J. Am. Chem. Soc.* **2007**, *129*, 15126–15127.

50 G. Zhang, O. Presly, F. White, I. M. Oppel, M. Mastalerz, *Angew. Chem., Int. Ed.* **2014**, *53*, 1516–1520.

51 G. Zhang, O. Presly, F. White, I. M. Oppel, M. Mastalerz, *Angew. Chem., Int. Ed.* **2014**, *53*, 5126–5130.

52 S. Klotzbach, T. Scherpf, F. Beuerle, *Chem. Commun.* **2014**, *50*, 12454–12457.

53 S. Klotzbach, F. Beuerle, *Angew. Chem., Int. Ed.* **2015**, *54*, 10356–10360.

54 K. Ono, K. Johmoto, N. Yasuda, H. Uekusa, S. Fujii, M. Kiguchi, N. Iwasawa, *J. Am. Chem. Soc.* **2015**, *137*, 7015–7018.

55 T. Inomata, K. Konishi, *Chem. Commun.* **2003**, 1282–1283.

56 J. Taesch, V. Heitz, F. Topic, K. Rissanen, *Chem. Commun.* **2012**, *48*, 5118–5120.

57 B. Zhu, H. X. Chen, W. Lin, Y. Ye, J. Wu, S. J. Li, *J. Am. Chem. Soc.* **2014**, *136*, 15126–15129.

58 C. X. Zhang, Q. Wang, H. Long, W. Zhang, *J. Am. Chem. Soc.* **2011**, *133*, 20995–21001.

59 Q. Wang, C. Yu, H. Long, Y. Du, Y. H. Jin, W. Zhang, *Angew. Chem., Int. Ed.* **2015**, *54*, 7550–7554.

60 Q. Wang, C. Yu, C. X. Zhang, H. Long, S. Azarnoush, Y. H. Jin, W. Zhang, *Chem. Sci.* **2016**, *7*, 3370–3376.

61 Q. Wang, C. X. Zhang, B. C. Noll, H. Long, Y. H. Jin, W. Zhang, *Angew. Chem., Int. Ed.* **2014**, *53*, 10663–10667.

62 S. Lee, A. Yang, T. P. Moneypenny, J. S. Moore, *J. Am. Chem. Soc.* **2016**, *138*, 2182–2185.

63 Y. C. Horng, T. L. Lin, C. Y. Tu, T. J. Sung, C. C. Hsieh, C. H. Hu, H. M. Lee, T. S. Kuo, *Eur. J. Org. Chem.* **2009**, 1511–1514.

64 A. R. Stefankiewicz, M. R. Sambrook, J. K. M. Sanders, *Chem. Sci.* **2012**, *3*, 2326–2329.

65 H. Li, H. C. Zhang, A. D. Lammer, M. Wang, X. P. Li, V. M. Lynch, J. L. Sessler, *Nat. Chem.* **2015**, *7*, 1003–1008.

66 M. Hutin, G. Bernardinelli, J. R. Nitschke, *Chem. Eur. J.* **2008**, *14*, 4585–4593.

67 B. Içli, N. Christinat, J. Tönnemann, C. Schüttler, R. Scopelliti, K. Severin, *J. Am. Chem. Soc.* **2009**, *131*, 3154–3155.

68 Y. H. Jin, A. Jin, R. McCaffrey, H. Long, W. Zhang, *J. Org. Chem.* **2012**, *77*, 7392–7400.

69 M. W. Schneider, I. M. Oppel, A. Griffin, M. Mastalerz, *Angew. Chem., Int. Ed.* **2013**, *52*, 3611–3615.

70 Y. Jin, B. A. Voss, A. Jin, H. Long, R. D. Noble, W. Zhang, *J. Am. Chem. Soc.* **2011**, *133*, 6650–6658.

71 M. Liu, M. A. Little, K. E. Jelfs, J. T. A. Jones, M. Schmidtmann, S. Y. Chong, T. Hasell, A. I. Cooper, *J. Am. Chem. Soc.* **2014**, *136*, 7583–7586.

72 J. L. Culshaw, G. Cheng, M. Schmidtmann, T. Hasell, M. Liu, D. J. Adams, A. I. Cooper, *J. Am. Chem. Soc.* **2013**, *135*, 10007–10010.

73 K. Acharyya, P. S. Mukherjee, *Chem. Eur. J.* **2015**, *21*, 6823–6831.

74 S. Jiang, J. T. A. Jones, T. Hasell, C. E. Blythe, D. J. Adams, A. Trewin, A. I. Cooper, *Nat. Commun.* **2011**, *2*.

75 P. Mateus, R. Delgado, P. Brandao, S. Carvalho, V. Felix, *Org. Biomol. Chem.* **2009**, *7*, 4661–4673.

76 J. Mosquera, S. Zarra, J. R. Nitschke, *Angew. Chem., Int. Ed.* **2014**, *53*, 1556–1559.

77 J. Lohrman, C. X. Zhang, W. Zhang, S. Q. Ren, *Chem. Commun.* **2012**, *48*, 8377–8379.

78 K. Tamaki, A. Ishigami, Y. Tanaka, M. Yamanaka, K. Kobayashi, *Chem. Eur. J.* **2015**, *21*, 13714–13722.

79 M. Brutschy, M. W. Schneider, M. Mastalerz, S. R. Waldvogel, *Adv. Mater.* **2012**, *24*, 6049–6052.

80 Z. H. Lin, J. L. Sun, B. Efremovska, R. Warmuth, *Chem. Eur. J.* **2012**, *18*, 12864–12872.

81 R. McCaffrey, H. Long, Y. Jin, A. Sanders, W. Park, W. Zhang, *J. Am. Chem. Soc.* **2014**, *136*, 1782–1785.

82 J. K. Sun, W. W. Zhan, T. Akita, Q. Xu, *J. Am. Chem. Soc.* **2015**, *137*, 7063–7066.

83 B. Mondal, K. Acharyya, P. Howlader, P. S. Mukherjee, *J. Am. Chem. Soc.* **2016**, *138*, 1709–1716.

84 T. Uemura, R. Nakanishi, S. Mochizuki, S. Kitagawa, M. Mizuno, *Angew. Chem., Int. Ed.* **2016**, *55*, 6443–6447.

85 T. Hasell, M. Schmidtmann, C. A. Stone, M. W. Smith, A. I. Cooper, *Chem. Commun.* **2012**, *48*, 4689–4691.

86 P. S. Huang, C. H. Kuo, C. C. Hsieh, Y. C. Horng, *Chem. Commun.* **2012**, *48*, 3227–3229.

87 Y. H. Jin, B. A. Voss, R. D. Noble, W. Zhang, *Angew. Chem., Int. Ed.* **2010**, *49*, 6348–6351.

88 L. Chen, P. S. Reiss, S. Y. Chong, D. Holden, K. E. Jelfs, T. Hasell, M. A. Little, A. Kewley, M. E. Briggs, A. Stephenson, K. M. Thomas, J. A. Armstrong, J. Bell, J. Busto, R. Noel, J. Liu, D. M. Strachan, P. K. Thallapally, A. I. Cooper, *Nat. Mater.* **2014**, *13*, 954–960.

89 T. Hasell, M. Miklitz, A. Stephenson, M. A. Little, S. Y. Chong, R. Clowes, L. J. Chen, D. Holden, G. A. Tribello, K. E. Jelfs, A. I. Cooper, *J. Am. Chem. Soc.* **2016**, *138*, 1653–1659.

90 T. Mitra, K. E. Jelfs, M. Schmidtmann, A. Ahmed, S. Y. Chong, D. J. Adams, A. I. Cooper, *Nat. Chem.* **2013**, *5*, 276–281.

91 J. H. Zhang, S. M. Xie, B. J. Wang, P. G. He, L. M. Yuan, J. Chromatogr. *A* **2015**, *1426*, 174–182.

92 A. Kewley, A. Stephenson, L. J. Chen, M. E. Briggs, T. Hasell, A. I. Cooper, *Chem. Mater.* **2015**, *27*, 3207–3210.

93 J. H. Zhang, S. M. Xie, L. Chen, B. J. Wang, P. G. He, L. M. Yuan, *Anal. Chem.* **2015**, *87*, 7817–7824.

94 T. Hasell, H. Zhang, A. I. Cooper, *Adv. Mater.* **2012**, *24*, 5732–5737.

95 A. F. Bushell, P. M. Budd, M. P. Attfield, J. T. A. Jones, T. Hasell, A. I. Cooper, P. Bernardo, F. Bazzarelli, G. Clarizia, J. C. Jansen, *Angew. Chem., Int. Ed.* **2013**, *52*, 1253–1256.

96 Q. L. Song, S. Jiang, T. Hasell, M. Liu, S. J. Sun, A. K. Cheetham, E. Sivaniah, A. I. Cooper, *Adv. Mater.* **2016**, *28*, 2629–2637.

97 N. O'Reilly, N. Giri, S. L. James, *Chem. Eur. J.* **2007**, *13*, 3020–3025.

98 N. Giri, C. E. Davidson, G. Melaugh, M. G. Del Popolo, J. T. A. Jones, T. Hasell, A. I. Cooper, P. N. Horton, M. B. Hursthouse, S. L. James, *Chem. Sci.* **2012**, *3*, 2153–2157.

99 G. Melaugh, N. Giri, C. E. Davidson, S. L. James, M. G. Del Popolo, *Phys. Chem. Chem. Phys.* **2014**, *16*, 9422–9431.

100 N. Giri, M. G. Del Popolo, G. Melaugh, R. L. Greenaway, K. Ratzke, T. Koschine, L. Pison, M. F. C. Gomes, A. I. Cooper, S. L. James, *Nature* **2015**, *527*, 216–220.

5

Orthogonal Dynamic Covalent and Non-covalent Reactions

Dan-Wei Zhang and Zhan-Ting Li

5.1 Introduction

Covalent synthesis is the basic route for the generation of organic molecules. Most covalent reactions are kinetically controlled, which means a designed product and possible by-products cannot be inter-converted. However, there are many covalent reactions which allow for the formation of one or more products that can convert into each other. For such dynamic covalent reactions that are under thermodynamic control, the distribution of the products relies on their relative stability and, at the equilibrium, the most thermodynamically stable product is produced in the highest yield. In supramolecular chemistry, chemists have always used non-covalent forces to investigate molecular recognition or assemble molecular building blocks into supramolecular entities. The processes involving non-covalent forces are typically reversible and thus the resulting supramolecular entities are labile and may not be separated as a stable "product" from solution, even though supramolecular structures can be observed routinely in the solid state by the X-ray crystal analysis. Thus, to discover new tools for creating dynamic yet stable structures and consequently new properties and functions, chemists have paid attention to dynamic covalent bonds.[1–3] The effort in this area has led to the new research field of dynamic covalent chemistry.

Research on dynamic covalent chemistry can be divided into two categories. The first category involves the construction of dynamic combinatorial libraries (DCLs),[4–14] from which synthetic receptors or sensors, catalytic systems, and ligands for biomolecules are expected to be obtained. In the second category, dynamic covalent bonds are utilized to selectively generate specific macrocycles, molecular cages, and polymeric and dendrite structures that may be used for molecular recognition and encapsulation,[15–22] self-healing, drug discovery, gelating, and sensing.[23–28] For the generation of macrocyclic and cage structures, the reversible feature of dynamic covalent bonds often enables high yielding of a single species.

The uniqueness of dynamic covalent bonds is that they combine the characteristics of covalent and non-covalent bonds. In addition, their reversibility can be controlled through changing the reaction conditions, for example a reversible bond can become strong and stable permanently under certain conditions. Typical examples of such bonds are disulfide and hydrazone bonds. The disulfide bond is stable under neutral

and acidic conditions, but exchanges quickly under basic or reductive conditions. Hydrazones are stable under neutral and basic conditions but can hydrolyze and exchange under acidic conditions in the presence of aldehydes, ketones or hydrazides. Thus, these two bonds are particularly useful for producing tunable combinatorial libraries. Besides disulfide and hydrazone bonds, imine, boronate ester and thioesters[5,16] as well as alkene and alkyne metathesis[21,22,26] have also been widely used for the research of dynamic covalent chemistry. Examples of using dynamic hemiacetal, thiohemiacetal or dithiane covalent bond have also been reported.[16]

In producing DCLs and molecular or polymeric dynamic covalent targets, multiple dynamic covalent bonds are usually formed in a one-pot manner. In some cases, two or more dynamic covalent bonds are used in one system. When different dynamic covalent bonds are used together, the orthogonal formation of respective covalent bonds is crucial. The orthogonality of non-covalent bonds is very common in life systems. The most representative example is the formation of the high-order structures of DNA and proteins. The self-assembly of DNA duplexes involves a combination of hydrogen bonding, aromatic stacking, hydrophobicity, and electrostatic interaction. The orthogonality of hydrogen-bonding interactions and hydrophobicity, which decreases and increases, respectively, with the increase in the medium polarity, plays an important role in the formation of DNA double helices. The secondary and tertiary structures of proteins are also stabilized by a combination of multiple orthogonal non-covalent/covalent interactions, including hydrogen bonding, hydrophobicity, coordination, salt bridges, and in many cases dynamic disulfide bonds. In artificial supramolecular self-assembly, orthogonal non-covalent interactions have also been widely used together for the generation of different kinds of advanced architectures.[29–37] In the past decade, considerable progress has been made in the use of orthogonal dynamic covalent bonds and their combination with non-covalent bonds for the construction of discrete supramolecular systems. The progress well illustrates the usefulness of these strategies in creating structural and functional diversity.

5.2 Orthogonal Dynamic Covalent Chemical Reactions

DCLs are formed by components that are reversibly assembled from a set of molecules. Orthogonal dynamic covalent bonds have been used to construct orthogonal DCLs, in which two or more reversible covalent bonds are activated under different conditions. The most successful reversible covalent reactions used for constructing orthogonal DCLs involve imine bond formation and exchange, the exchange of hydrazones, disulfides, and thioester groups. Studies on such orthogonal DCLs have considerably expanded the diversity and complexity of dynamic molecular libraries.

5.2.1 Imine and Disulfide Bonds

Among various reversible covalent reactions, imine formation by the condensation of aldehyde carbonyl groups with amines is of special importance, in view of its role in both biological and chemical processes. Imine bond formation and exchange is one of the most widely used reactions in the research of dynamic covalent chemistry.[15] The formation of multiple imine bonds is typically assisted by a template or additional
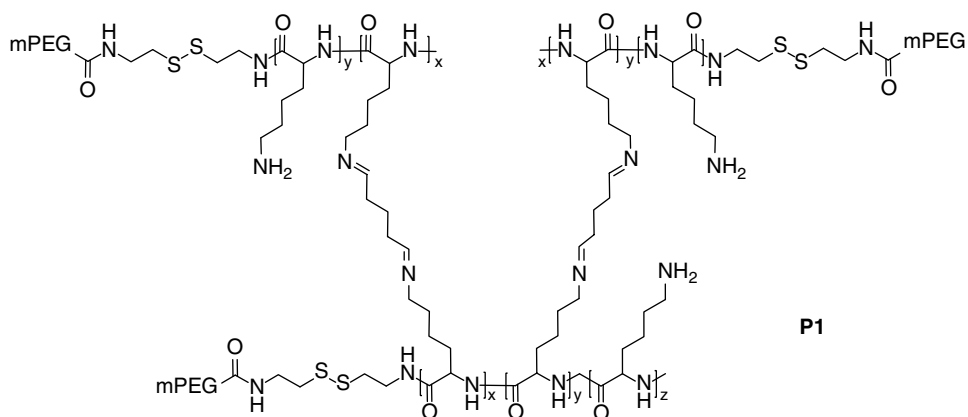
Figure 5.1 The structure of cationic polymer **P1**.

non-covalent interactions. Recently a combination of imine and disulfide bonds has been utilized by Shi and co-workers to build a dual stimulus-responsive cationic polymer **P1** for gene delivery (Figure 5.1).[38] The external PEG chains can be removed by redox-sensitive breaking of the disulfide bonds and the imine bonds can be dissociated by reducing the pH of the medium. The polymer shows high DNA binding affinity, allowing efficient complexation with DNA. Intracellular uptake of P1/DNA complex and release of DNA through dual stimulus-responsive degradation mechanisms have also been demonstrated, showing the potential of such polymer/DNA complex in future non-viral gene-delivery applications.

5.2.2   Imine and Boronate Ester Bonds

In 2014, Severin and co-workers reported a four-component organogel based on orthogonal chemical interactions involving the formation of imine and boronate ester bonds as well as s dative boron–nitrogen bonds.[39] Mixing components **2**, **3** and **4** in toluene gave rise to a library of compounds such as intermediate **6** by forming imine and boronate bonds. Further addition of a ligand **5** produced a network by forming N–B bonds. When the four components were added in the ratio of 1:1:2:1, most mixtures led to precipitates, whereas the mixtures of **2b**, **4a** and **5b** with **3a** or **3b** yielded gels, e.g. Gel 7 (Figure 5.2). One-step simultaneous mixing of all four components afforded similar results, supporting the view that the formation of imine and boronate ester bonds and N–B coordination are all reversible. When methanol, aniline or *N*-methylimidazole was added, the organogels were disrupted due to the dissociation of one of the three reversible interactions.

In 2008, Nitschke and co-workers reported the synthesis of macrocycle **8a** and molecular cage **8b** by orthogonal formation of imine and boronate bonds (Figure 5.3).[40] For the formation of **8a**, *p*-diaminobenzene, pentaerythritol, and *o*-formylphenylboronic acid were heated in DMF at 50 °C overnight to produce crystals of **8a** suitable for X-ray analysis. For the preparation of trigonal cage **8b**, cyclotricatechylene, *m*-xylylenediamine and *o*-formylphenylboronic acid were mixed in DMF at room temperature to give **8b** as the overwhelmingly major product, which well validated the use of iminoboronate
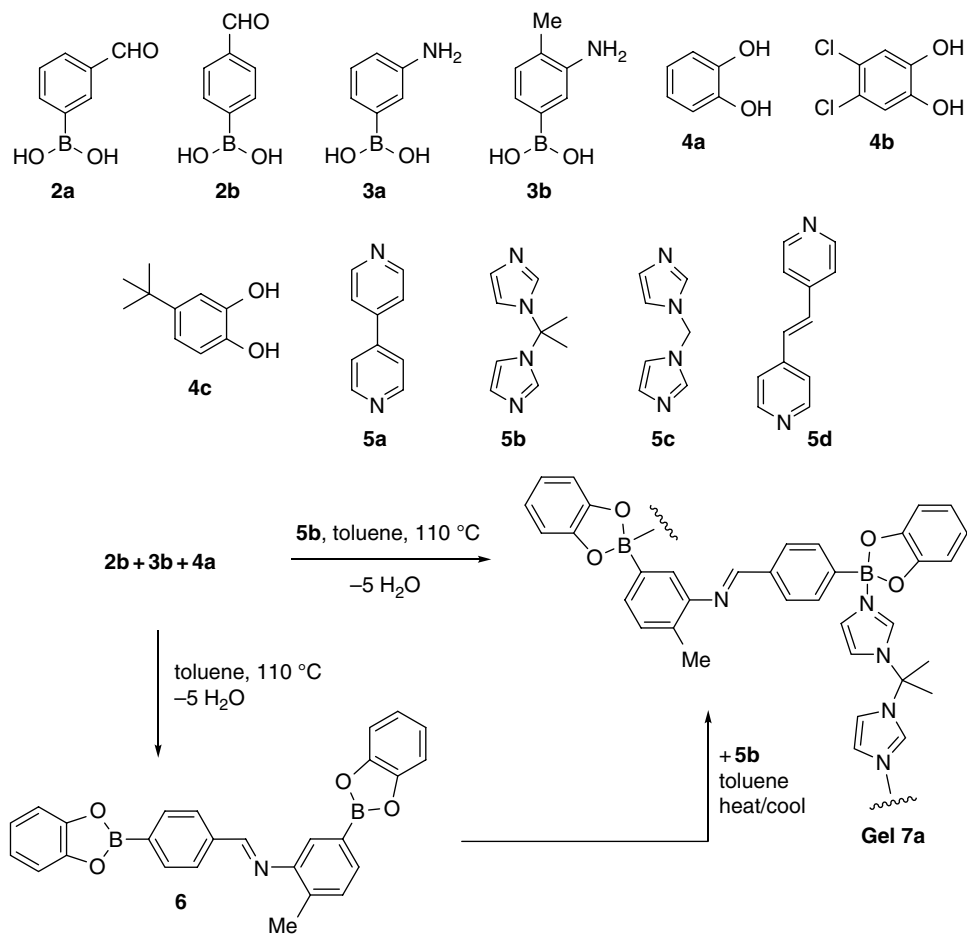
Figure 5.2 The formation of gel **7a** by a direct four-component reaction or by a two-step process involving the intermediate **6**.

subcomponent self-assembly to generate well-defined architectures. Using the same strategy, Severin and co-workers also constructed a number of macrocycles, including **9a–c** (Figure 5.3).[41–43]

5.2.3 Hydrazone and Disulfide Bonds

In 2008, Otto and co-workers reported a dynamic combinatorial library from four components **10a**, **10b**, **11a**, and **11b** by orthogonal use of hydrazone and disulfide bonds in aqueous solution (Figure 5.4).[44] The four components could form a library of a maximum of nine products (**12a–12i**). It was revealed that, in acidic solution, hydrazone exchange took place exclusively and in a mildly basic solution, disulfide exchange proceeded exclusively, whereas at intermediate pH, both reactions occurred simultaneously. Thus, by simply changing the pH of the solution, the activation or deactivation of two different covalent bonds could be controlled, which consequently led to the regulation of the product distributions.
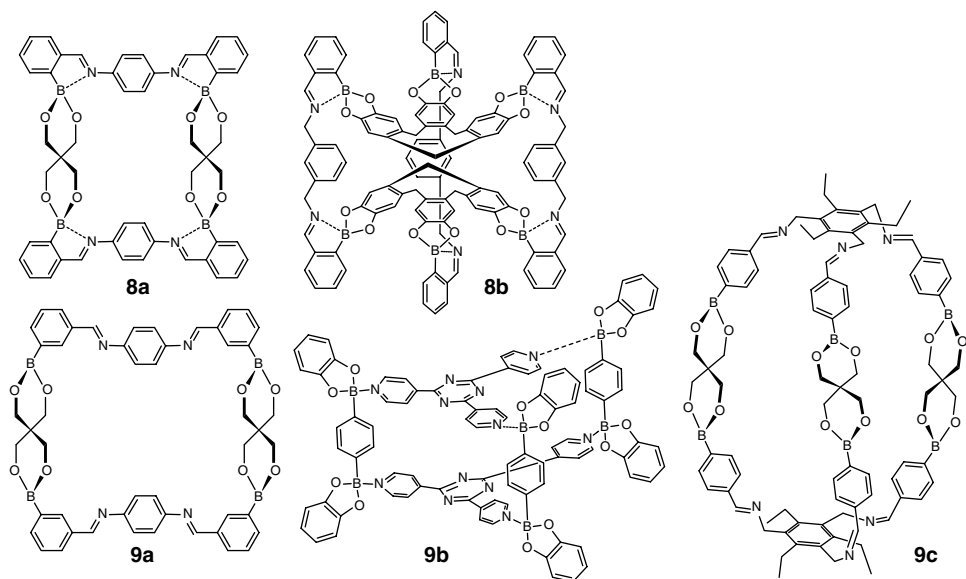
Figure 5.3 Structures of macrocycles and cages prepared through orthogonal formation of imine and boronate bonds.
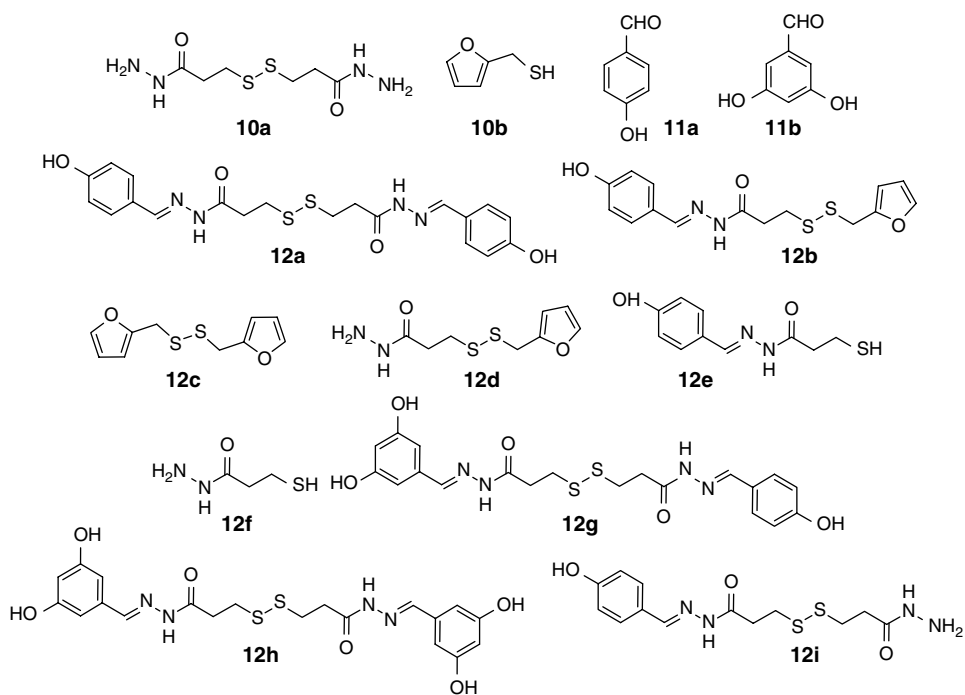
Figure 5.4 Components (12a–12i) of a dynamic combinatorial library obtained from 10a,b and 11a,b through the use of hydrazone and disulfide bonds.

In a study published back-to-back with this report, Furlan and co-workers showed that compounds **13–16** underwent similar exchange of the hydrazone and disulfide bonds (Figure 5.5).[45] Compounds **17a–17e** were detected in the libraries under different conditions. The hydrazones were exchanged by acid catalysis in the presence of disulfide and the thiol group did not interfere with the exchange. When the reaction medium was neutralized, the exchange of hydrazones was turned off, and the thiolate-disulfide exchange was activated. Such orthogonal hydrazone and disulfide exchanges have also been investigated by Miller and co-workers for constructing a three-component phase-segregated resin-bound DCL.[46] It was found that, compared to the solution phase reaction, the use of resin-bound immobilized monomers requires higher monomer concentration (10-fold higher) to form the trimeric products. Nevertheless, similar to the solution-phase system, exchange of hydrazone and disulfide bonds could proceed individually or simultaneously in the solid phase as well.

5.2.4 Disulfide and Thioester Bonds

In 2005, Otto and co-workers described a DCL from the orthogonal exchange of disulfide and thioester bonds.[47] In aqueous solution (pH = 6.9), compounds **18**, **19** and **20** underwent rapid thioester exchange (Scheme 5.1a). The thiol groups could be further oxidized by atmospheric oxygen to form disulfide bonds (Scheme 5.1b) which could further undergo exchange reactions (Scheme 5.1c). The three processes led to a library of eight oligomeric and macrocyclic products at the final equilibrium after 36 h, which were characterized by HPLC/ESI-MS (Figure 5.6).

By combining reversible hydrazone and disulfide bonds into one rationally designed molecule, Leigh and co-workers demonstrated the concept of a molecular walker.[48] Adding trifluoroacetic acid (TFA) and a small amount of water (5% v/v with respect to TFA) to a solution of **25** (0.1 mM) led to a steady-state distribution of two isomers (**25:26**) through hydrazone exchange (Scheme 5.2). No detectable amounts of oligomers or other side products were observed. For reversible disulfide exchange of **26** and **27** in chloroform, strong base (1,8-diazabicyclo-[5.4.0]undec-7-ene (DBU)), mild reducing agent (dithiothreitol (DTT)), and dimethyl 3,3′-disulfanediyldipropanoate ($(MeO_2CCH_2CH_2S)_2$) as the placeholder disulfide were added and the exchange led to the favorable formation of **27**. By repeating the acid and base conditions, the **27/28** and **28/25** exchanges could also be performed. The spacer length (*n* value) for the different walkers has a considerable effect on the ratio of positional isomers at the equilibrium, for example the ratio of **25:26** varies dramatically with different spacer length. Further introduction of a kinetically controlled step in the reaction sequence, that is, redox-mediated breaking and reforming of the disulfide linkages, can cause a directional bias in the distribution of the walker molecule on the track. This kind of molecular walker may be further developed to produce artificial, linear molecular motors that move directionally along polymeric tracks to transport cargoes and exhibit functions in a manner owned by biological motor proteins.[49]

5.2.5 Imine and Alkene Bonds

Heterosequenced and/or multifunctional macrocycles with site-specific substitution may be useful building blocks for complex interlocked molecular architectures and novel functional molecular devices. Zhang and co-workers explored a multicomponent
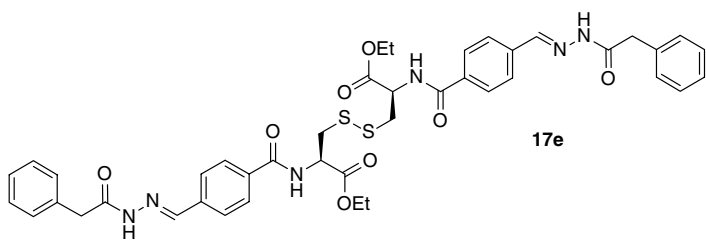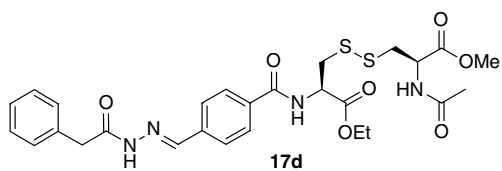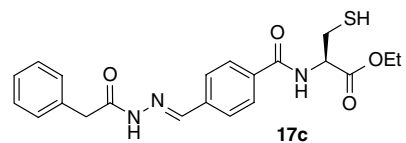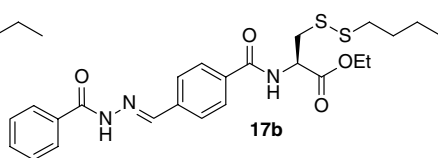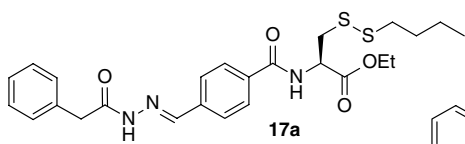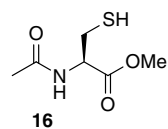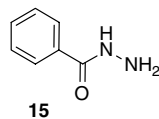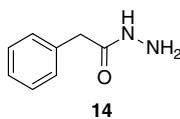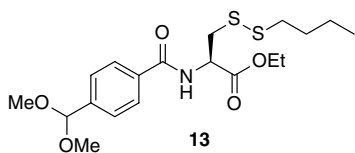
Figure 5.5 Hydrazones and thiol components (**13–16**) and the resulting DCL mixture (**17a–17e**).

(a)

(b)

(c)
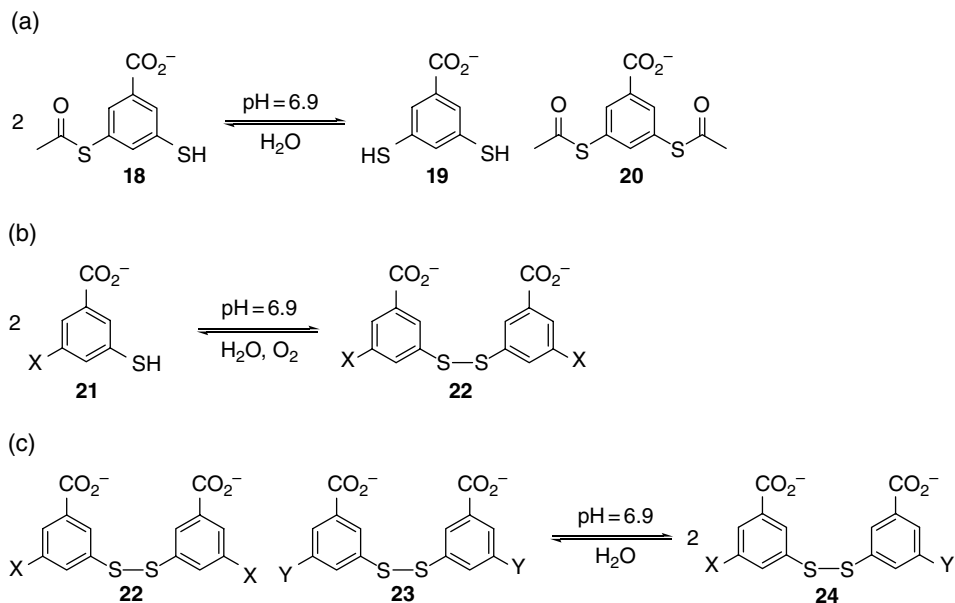
Scheme 5.1 Compounds **18**, **19** and **20** involved in thioester exchange (a) and their further disulfide formation and exchange (b and c).
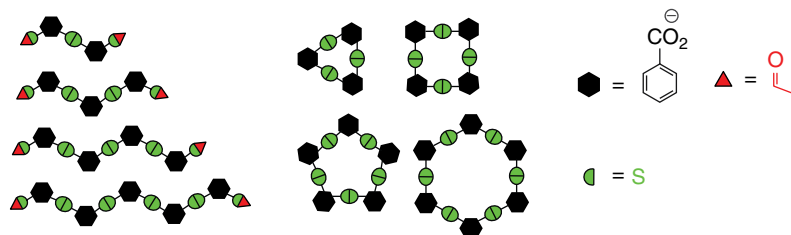
Figure 5.6 Linear and cyclic oligomers obtained at the final equilibrium of thioether and disulfide exchange between **18–20**.

orthogonal dynamic covalent chemistry method to prepare such macrocycles by performing imine coupling and alkene metathesis in one pot (Figure 5.7).[21] For example, compounds **29–31** were used to produce a series of macrocycles.[50] The metathesis reaction of **30** and **31** (1:1) under the catalysis of Grubbs' G2 catalyst afforded compounds **32–34** as a mixture. Treatment of the mixture of the three compounds with TFA produced macrocycles **35** and **36** as the predominant species. The two macrocycles could be separated using flash chromatography, but after the imines were reduced to amines, they became inseparable. Higher yielding of macrocycles **35** and **36** was observed when imine condensation of **29** and **31** was performed first to form **37** followed by the olefin metathesis in one pot. Since the TFA catalyst and water by-product involved in the imine condensation could diminish the catalytic activity of the Ru complex for olefin metathesis, removal of both compounds under vacuum is necessary for
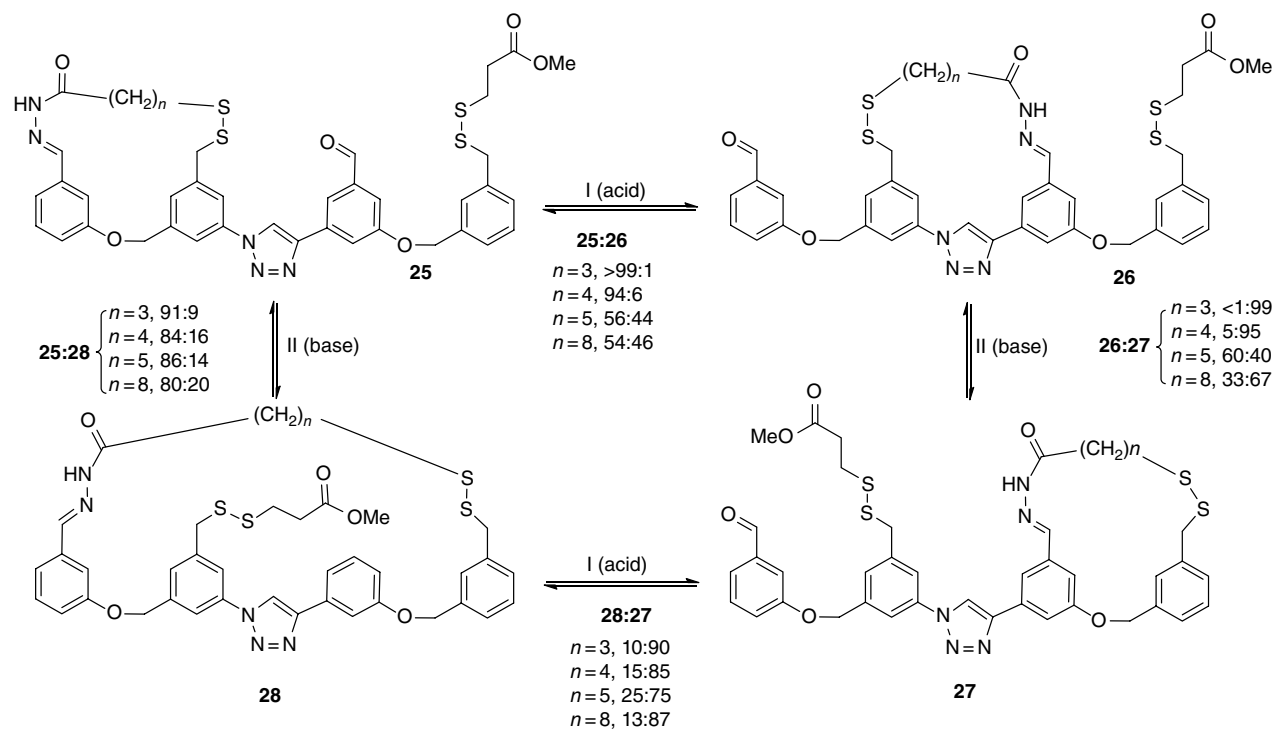
Scheme 5.2 Reversible reactions that connect four pairs of four positional isomers **25–28** under acid and base conditions.
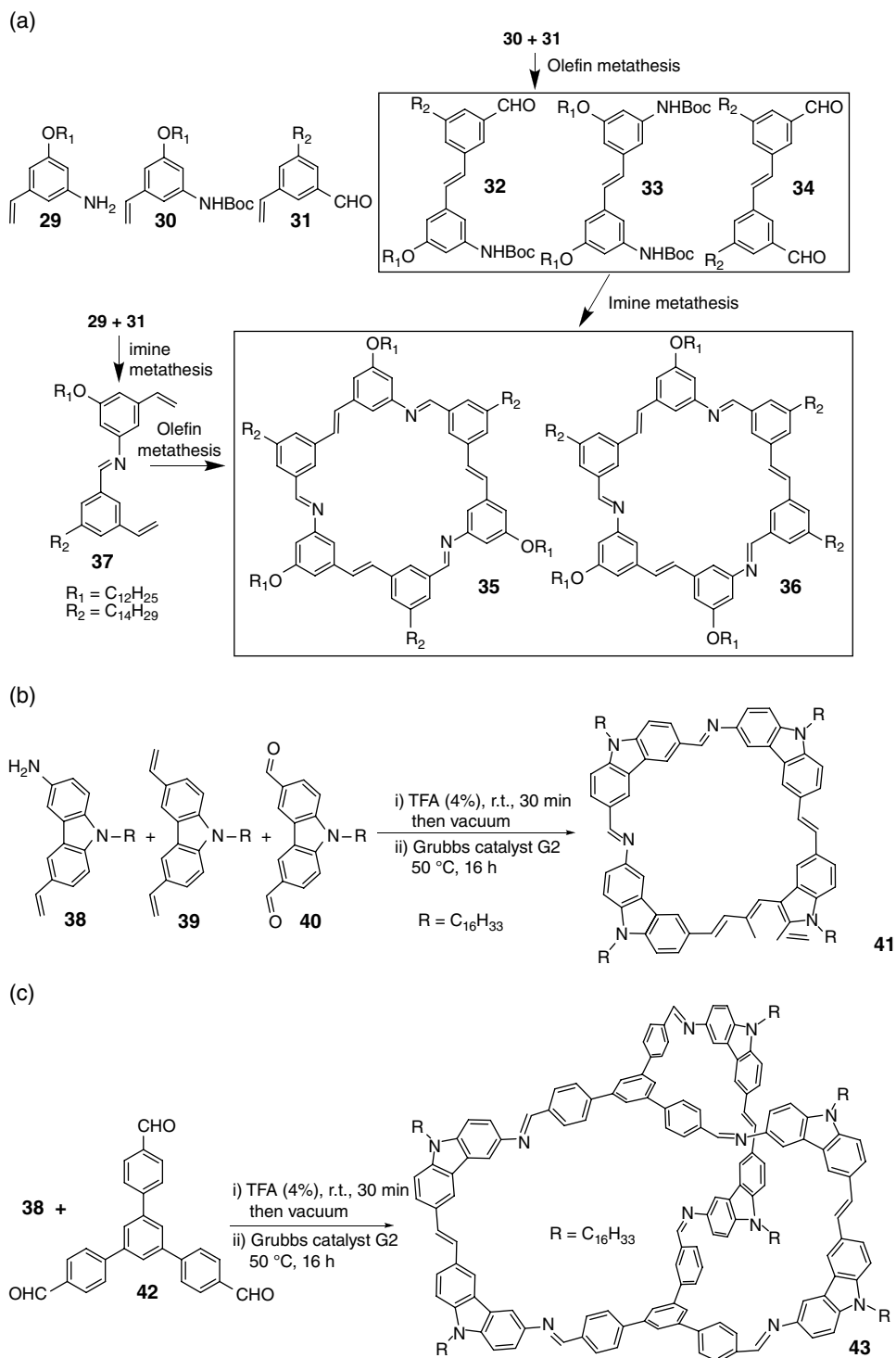
Figure 5.7 Synthesis of macrocycles (a and b) and a cage (c) through stepwise or one-pot imine condensation and olefin metathesis.

efficient synthesis of the macrocycles. Simultaneous imine condensation and olefin metathesis of **29** and **31** in the presence of TFA and Grubbs–Hoveyda second-generation catalyst proceeded with high conversion (>95%). However, even after 4 days the desired macrocyclic product was only obtained as a minor product.

Three-component cyclooligomerization was also achieved by treatment of compounds **38–40** with TFA and then Grubbs' second-generation catalyst (G2) to form macrocycle **41** as the predominant product (Figure 5.7), together with an arylenevinylene macrocycle made by four **39** monomers as a minor product.[51] From the reaction of **38** and **42** (6:2) under similar conditions, cage molecule **43** could be obtained in 51% yield.

5.2.6 Disulfide and Alkene Bonds

In 2014, Emrick and co-workers reported an example of orthogonal generation and degradation of polymers that contain the disulfide and alkene bonds.[52] Compounds **44** and **45a–d** underwent ring-opening metathesis polymerization (ROMP) in dichloromethane, which was catalyzed by Grubbs' G3 catalyst, to afford polymers **P46a–d** with nearly 30 mol% disulfide monomer in the backbone (Scheme 5.3). The disulfide bonds in the two monomers did not interfere with the polymerization process. Incorporation of disulfide groups into the polymer provided redox responsiveness of the polyolefin **P45**, which degrades in the presence of mild reducing agents, for example tri-*n*-butylphosphine, or under irradiation in the presence of photoinitiator (2,2-dimethoxy-2-phenylacetophenone). Adding thiols, for example 1-dodecanethiol, also caused degradative equilibrium exchange. In all these processes, the integrity of the C=C bonds in the backbone was not affected. This ROMP copolymerization strategy was further extended to polymer **P48** containing both disulfide and phosphoester groups to achieve selective and orthogonal degradation. **P48** was obtained from the reaction of compounds **44**, **45a** and **47** in dichloromethane (Scheme 5.3). This terpolymer undergoes orthogonal degradation: basic conditions (treatment with NaOMe) induce degradation of phosphoester groups with intact disulfides, whereas the addition of *n*-Bu$_3$P leads to disulfide cleavage with minimum impact on phosphoesters.

5.2.7 Disulfide, Thioester, and Hydrazone Bonds

On the basis of the study on DCLs using orthogonal disulfide and hydrazone bonds, Furlan and co-workers further developed a mixed strategy involving three simultaneous and orthogonal covalent reactions in one single system through the combination of the exchange of disulfides, thioesters, and hydrazones.[53] This DCL library consisted of five components, that is, compounds **13–15**, **49**, and **50** (Figure 5.8). The mixture was investigated in chloroform in the presence of an excess of piperidine and/or trifluoroacetic acid (TFA), which activate the disulfide and thioester exchange and hydrazone exchange, respectively. It was revealed that, by changing the order of addition of the reagents (piperidine and TFA), the hydrazone exchange products or the disulfide and thioester exchange products could be obtained selectively. Thus, biased DCLs could be obtained where the history of each DCL was manifested as a distinct distribution of products.

The Furlan group also investigated the orthogonal DCLs of compounds **51–53** (Figure 5.9).[54] Acid-catalyzed cyclization of compound **51** in chloroform and methanol (98:2, v/v) in the presence of TFA (30 mM) produced hydrazone-based macrocycles **54** and **55**. After 6 days at room temperature, the exchange reached equilibrium, with
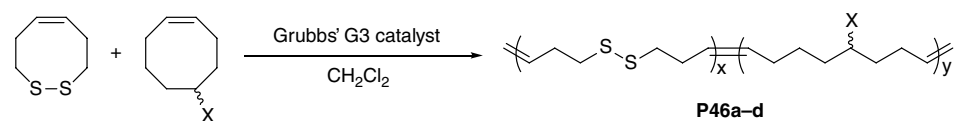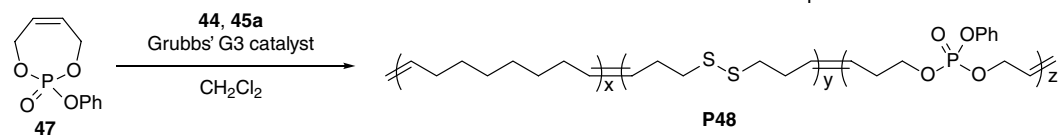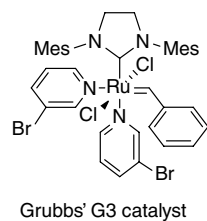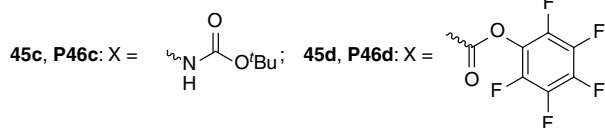
Scheme 5.3 The synthesis of disulfide-contained alkene polymers **P46a–d** and **P48** through ROMP.
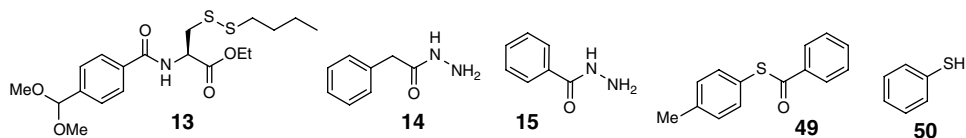
Figure 5.8 Components used in the formation of a DCL through orthogonal exchange of disulfides, thioesters, and hydrazones.

54: $n = 0$, $R_1 = R_2 = R_3 =$

55: $n = 1$, $R_1 = R_2 = R_3 =$

56: $n = 1$, $R_1 =$ ⸽⸽⸽ $R_2 = R_3 =$

57: $n = 0$, $R_1 = R_2 = R_3 =$
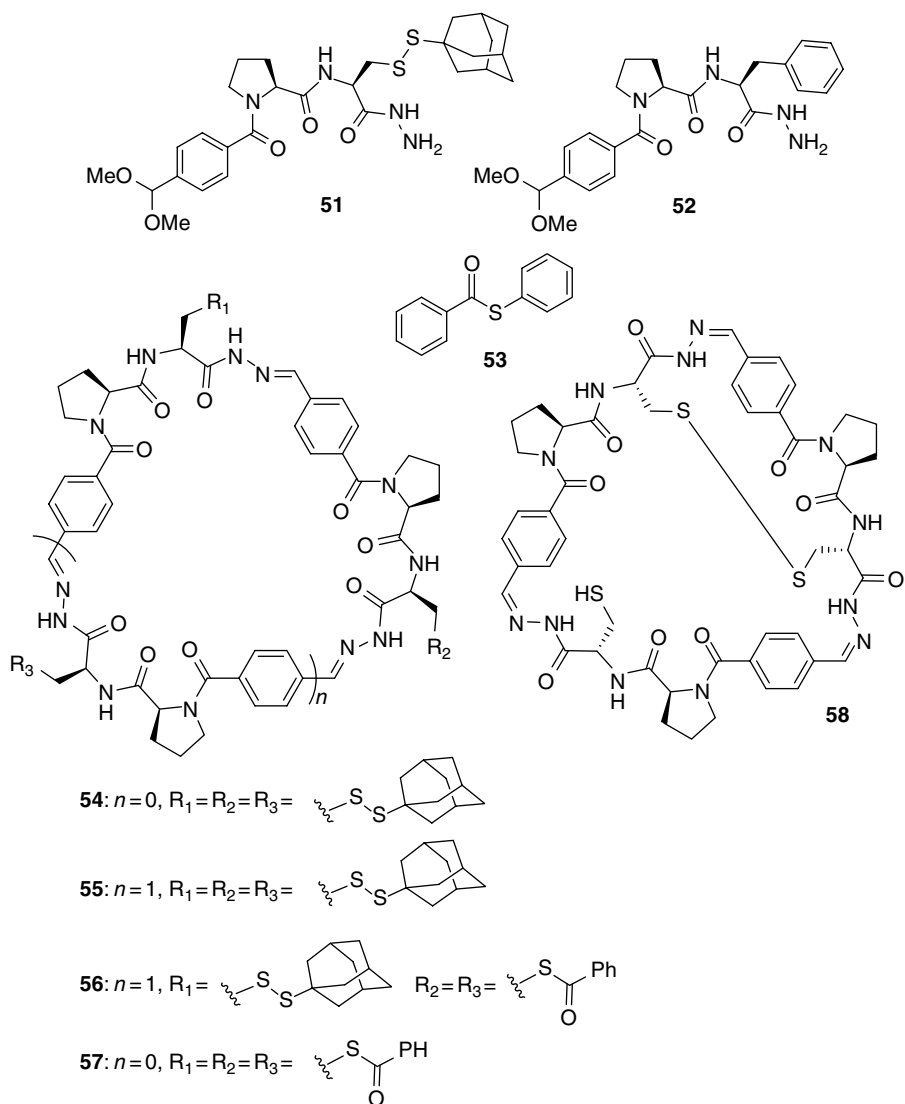
Figure 5.9 Macrocycles **54–58** obtained through the orthogonal exchange of disulfides, thioesters, and hydrazones from **51** to **53**.
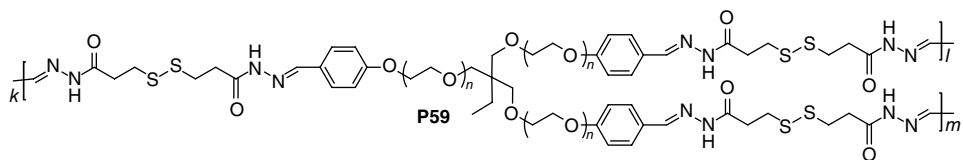
Figure 5.10 The structure of self-healing polymer network **P59**.

the yields of **54** and **55** being 41% and 59% (by HPLC peak area), respectively. In the presence of Li⁺ as a template ion (3.75 mM), trimer **55** could be obtained in 99% yield after 3 days.[55] By activating the disulfide and thioester exchange, the diversity of side chains in **55** was achieved without affecting the central scaffold. The activation was realized by 1,4-dithiothreitol in the presence of triethylamine and thioester **53** in chloroform and methanol (98:2, v/v). After 15 days, this DCL showed **55** was still the main component, and at least five new macrocycles bearing thioester, disulfide and thiol groups were formed, reflecting the exchange of the disulfide bonds of **55** and thioester **53**. Adding lithium bromide to the mixture led to a DCL of different composition. Clear amplification of macrocycles **56** (3.3-fold increase) and **57** (19-fold increase) containing two and three benzoyl thioester side chains was observed, respectively corresponding to 44% and 12% of the total area of the DCL chromatogram. These results showed the preference of lithium bromide for components that contained the benzoyl thioester groups, presumably due to the coordination of Li⁺ to carbonyls. Moreover, one previously undetected macrocycle **58** was also produced in the presence of the LiBr template.

In 2012, Chen and co-workers reported the generation of self-healing polymer network **P59** (Figure 5.10) from the reaction of disulfide-containing bishydrazones and trialdehydes.[56] This dynamic polymer formed hydrogels which underwent hydrazone and/or disulfide exchange to repair damage in acidic and basic media, respectively. In neutral environments where the hydrazone and disulfide exchange are kinetically impeded, the polymer still maintained its self-healing character when a catalytic amount of aniline was added as base during the formation of the polymer. As expected, the polymer displayed solution–gel transition in response to external stimuli. The hydrazone bonds were reversibly formed and broken by changing the pH, while the disulfide bonds underwent reversible formation and breakage by adding an oxidant and a reductant.

5.3 Dynamic Covalent Reactions and Hydrogen Bonding

Hydrogen bonding has been frequently utilized with dynamic covalent bonds to assemble complex molecular architectures. When monomers and target molecules or macromolecules contain groups such as amide, urea, thiourea, hydroxyl or carboxylic acid, the hydrogen bonding formed by these groups can impose an important effect on the formation of the dynamic covalent bonds and/or the properties of the target molecules or macromolecules.

5.3.1 Imine, Hydrazone, and Hydrogen Bonding

Lehn *et al.* reported several series of dynamic polymers by forming reversible covalent bonds. Such reversible polymers, named dynamers, allow for the generation of dynamic constitutional diversity.[57–59] For example, the polycondensation of dihydrazides **60a–c**
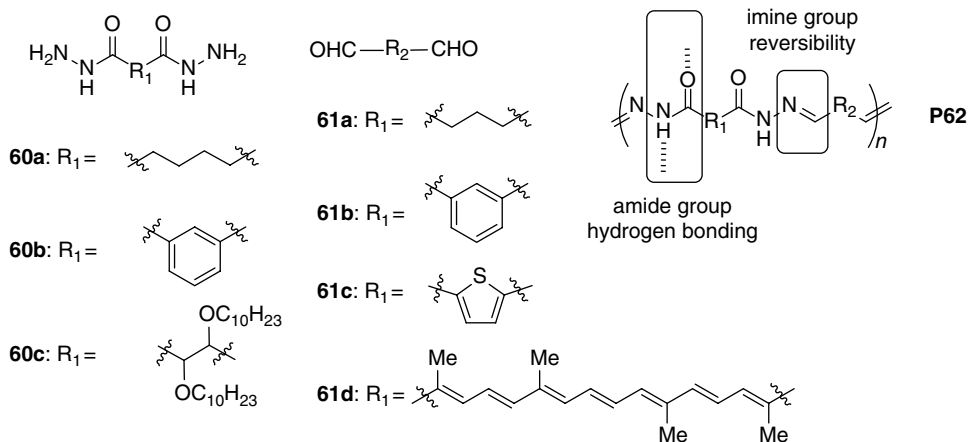
Figure 5.11 Dynamers **P62** prepared from various dihydrazides (**60a–60c**) and aldehydes (**61a–61d**).

with a dialdehyde **61a–d** produced various polyacylhydrazones **P62** (Figure 5.11). The acylhydrazone groups in these polymers formed intermolecular $C=O\cdots H-N$ hydrogen bonding. Although the hydrogen bonding seriously reduced the solubility of the polya-cylhydrazones in solvents of low polarity, orthogonality was observed for the hydrazone bond and the hydrogen bonding. This kind of polymer with double dynamicity has also been revealed to exhibit a self-healing function.[59] However, the healing process mainly involved the hydrogen-bonding motif.

There have been a number of examples of macrocycles generated through the formation of reversible imine bonds.[60,61] These macrocycles are good receptors for ammonium or hydrocarbon guests stabilized by intermolecular hydrogen bonding (Figure 5.12). Complexes **64 ⊂ 63** and **65 ⊂ 66** are recently reported examples. ^{1}H NMR in CDCl$_3$/CD$_3$CN (10:1) showed that macrocycle **63** complexed linear compound **64** by forming $C-H\cdots N=C$ hydrogen bonding.[60] The *syn* macrocycle **63** could convert to its *anti* conformer. The complexation for different guests could remarkably change the relative ratio of the two isomers. Trispyridinium **65** has also been used to template the formation of triply threaded pseudo[2]rotaxane **65 ⊂ 66** through imine-based dynamic reactions in CDCl$_3$ and CD$_3$CN.[61] Both ^{1}H NMR and single crystal X-ray analyses revealed that the two components formed intermolecular $C-H\cdots O$ hydrogen bonding, which, together with aromatic stacking, promoted the formation of the capsular compound **66**.

Similar hydrogen-bonded complex [2]rotaxanes **67 ⊂ 68a** and **67 ⊂ 68b** (Figure 5.12) have also been reported, which show excellent stability in solution.[62] The two imine bonds are stabilized by the intermolecular $N-H\cdots O$ hydrogen bonding. In the presence of excess of water, the imine bonds could be hydrolyzed to afford amine and aldehyde precursors. However, this process was markedly inhibited due to intermolecular $N-H\cdots O$ hydrogen bonding. Thus, it is proposed that the imine bonds and hydrogen bonding operate orthogonally and promote each other.

In 2008, Philp and co-workers reported an interesting example of self-replication by making use of orthogonal imine bonds and hydrogen bonding.[63] Imine **69** was pre-pared from the condensation of the corresponding amine and aldehyde precursors
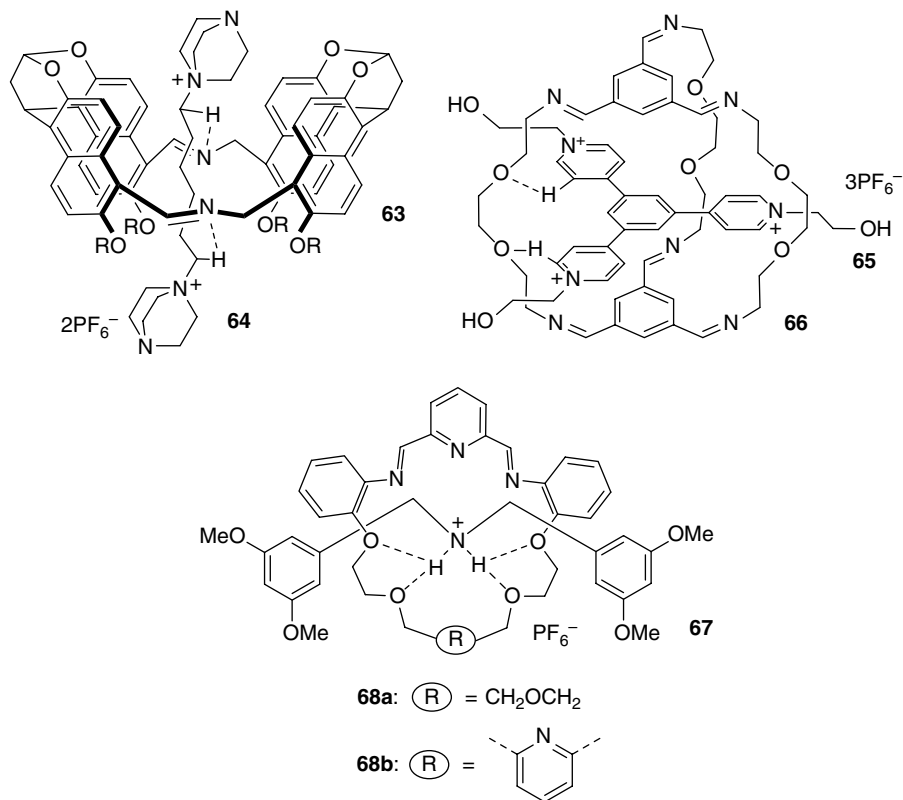
Figure 5.12 Structures of macrocycle-guest complexes stabilized by hydrogen bonding.
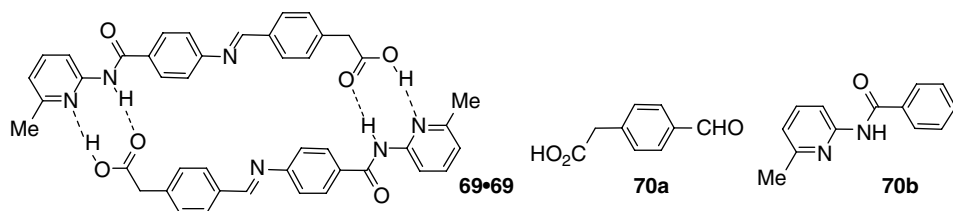
Figure 5.13 Self-replication system **69·69** formed through the use of imine and hydrogen bonds, and the structures of control compounds 70a,b.

(Figure 5.13). The association constant (K_a) of **69** for homodimerization in CDCl$_3$ was determined to be 65 000 M^{-1}. However, the K_a of the dimer of the control compounds **70a** and **70b** was only 50 M^{-1}. Clearly, the formation of the duplex **69–69** is significantly positively cooperative. The orthogonal imine bonds and hydrogen bonds stabilize each other.

In 2006, Stoddart and co-workers reported template-directed synthesis of mechanically interlocked molecular bundles using dynamic imine chemistry and hydrogen bonding (Figure 5.14).[64] Triangular compound **71** was used as a trisammonium ion template. ^{1}H NMR in CD$_3$NO$_2$ indicated that a mixture of **71** (13.8 mM) with 3 equivalents of **72** afforded kinetically stable complex **71·(72)$_3$** in 95% yield, which was stabilized by intermolecular N – H···O and N – H···N hydrogen bonding. ^{1}H NMR also
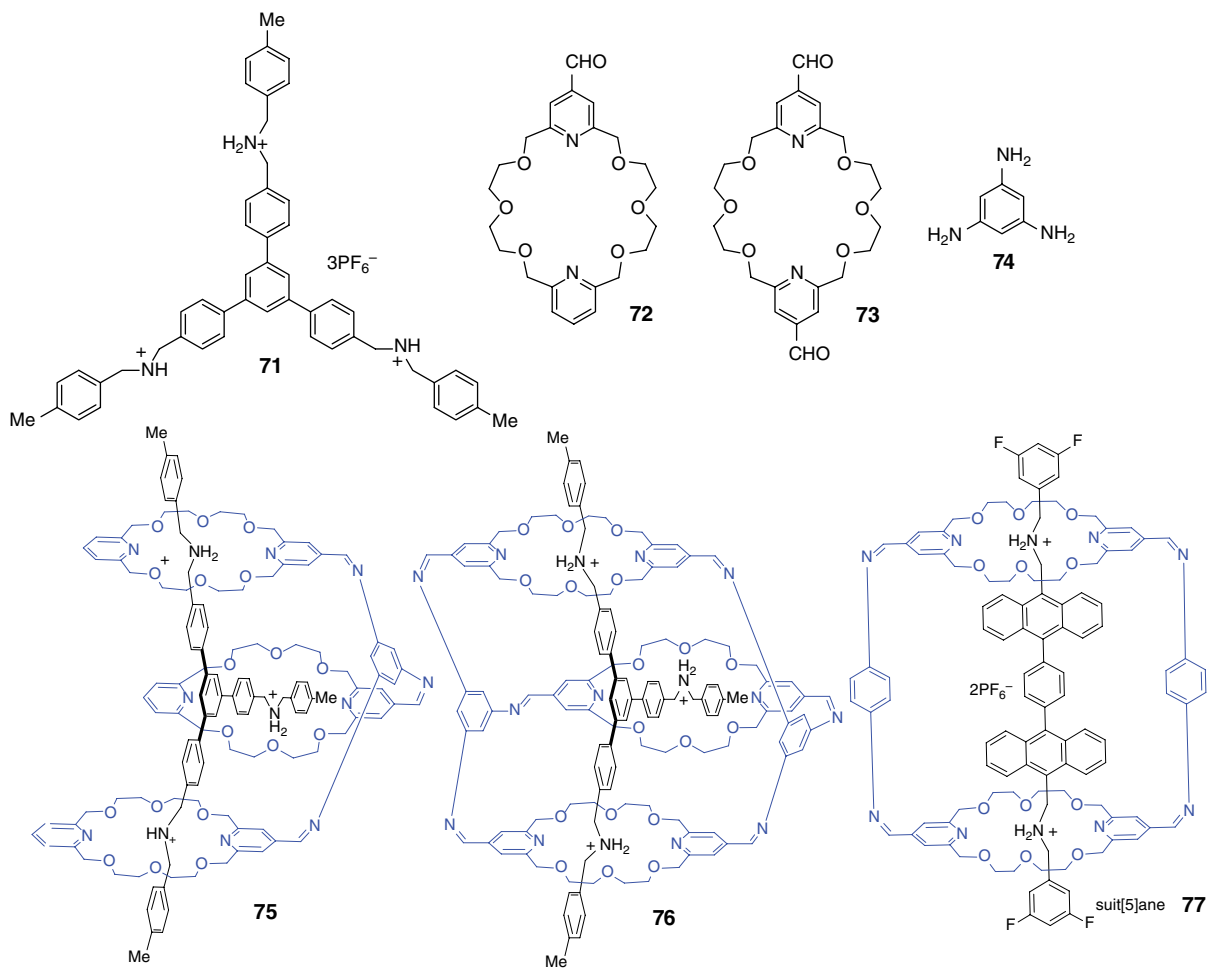
Figure 5.14 Mechanically interlocked molecular bundles (**75–77**) synthesized from **72–74** using **71** as the template through imine and hydrogen bond formation.

showed that adding 1 equivalents of **74** to the mixture led to the formation of a number of products initially. After 2 h, these kinetic intermediates converted to the most stable thermodynamic triimine product **75** with C_{3V} symmetry. Compounds **71** and **73** also afforded a 1:3 complex. The K_a for the complex of the ammonium subunit of **71** and **73** was determined to be 3520 M^{-1} in MeNO$_2$. Double capping of this complex was achieved by adding 2 equivalents of **74**. ^{1}H NMR in CD$_3$NO$_2$ showed that the most stable thermodynamically stable hexaimine mechanically interlocked molecular bundle **76** of D_{3h} symmetry was formed as the dominant product after 8 days. By using the same strategy of combining the reversible imine bonds and hydrogen bonding, Stoddart *et al.* have constructed a variety of dynamic interlocked supramolecular structures,[24] including the so-called supramolecular suit[5]ane **77**.[65]

In 2014, Mukherjee and co-workers reported an interesting supramolecular approach, which utilizes intramolecular hydrogen bonding as a driving force to accomplish exceptional self-sorting in the generation of imine-based organic cages.[66] A mixture of **78** and **79** in a ratio of 3:2 in chloroform produced organic cage **80** by forming six imine bonds (Scheme 5.4). Addition of 3 equivalents of **81** to the solution of **80** led to the formation of another cage **82**, which is stabilized by six intramolecular O – H···N hydrogen bonds, and the release of three molecules of **78**. When the three compounds **78**, **79** and **81** were mixed in a solution, cage **82** was also favorably formed, again indicating the higher stability of this hydrogen-bonded molecular cage.
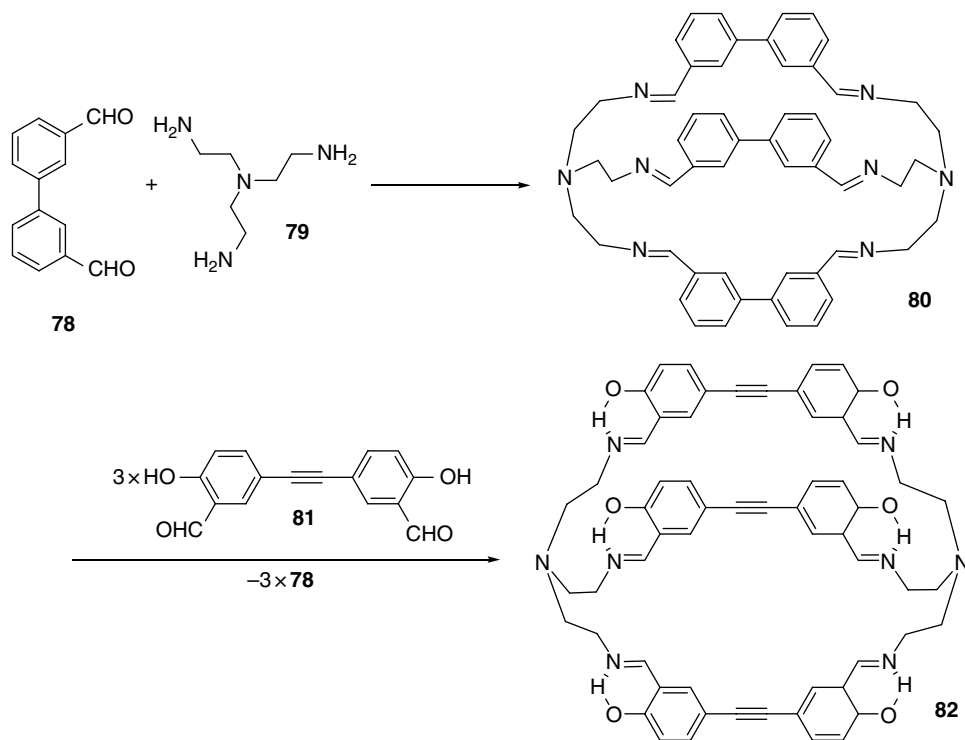
Scheme 5.4 The formation of organic **80** and its transformation to cage **82** with higher stability driven by the formation of six intramolecular hydrogen bonds.
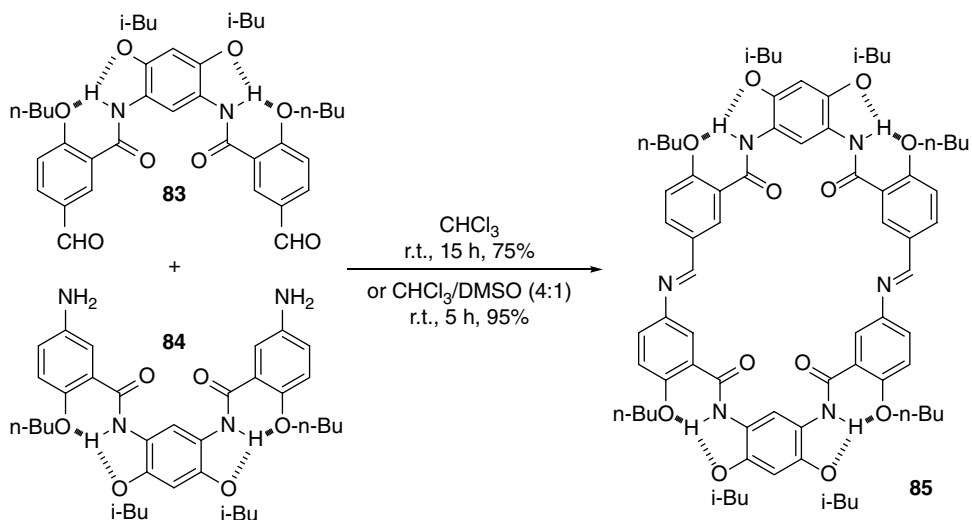
Scheme 5.5 Synthesis of diimine macrocycle **85**.

Li and co-workers utilized intramolecular hydrogen bonding to preorganize aromatic amide precursors to promote the formation of rigid aromatic macrocycles by imine or hydrazone bonds.[17,67] For example, U-shaped dialdehyde **83** and diamine **84** reacted in chloroform to give macrocycle **85** in 75% yield (Scheme 5.5).[68] When the reaction was carried out in chloroform/DMSO (4:1), the macrocycle could be formed in nearly quantitative yield.

By using the same approach, Li and co-workers also prepared many more complicated imine-based macrocycles, including **86** and **87**[68] and organic cages **88** and **89** (Figure 5.15).[69,70] Due to the hydrogen-bonding-induced preorganization of the precursors and probably the structural matching of the precursors, these products were formed exclusively at the equilibrium. The approach has also been extended to macrocycles by forming acylhydrazone bonds.[68,71] Both macrocycles **90** and **91** could be generated in nearly quantitative yield through the formation of three or six hydrazone bonds.

In 2011, Sanders and co-workers constructed a DCL from components **92–94** by making use of the dynamic hydrazone bonds and hydrogen bonding (Figure 5.16).[72] Unprecedented linear hydrazone-derived receptors for binding multiple $H_2PO_4^-$ ions were discovered. HPLC trace revealed that in chloroform/methanol (94:6, v/v), the library obtained from **92–94** contained four linear hydrazone derivatives and also four macrocyclic derivatives. When $H_2PO_4^-$ was added and the DCL was allowed to re-equilibrate, three linear receptors and two macrocyclic derivatives were amplified in the DCL at the expense of one macrocyclic species. Linear receptors containing as many as seven or nine building blocks were amplified. The preference of long linear receptors to competing macrocyclic host is remarkable, considering the entropic loss to the system. It was revealed that the linear tetrahydrazone oligomer **95** forms a helical receptor and cooperatively binds two $H_2PO_4^-$ ions, with $K_1K_2 = 800\,000\,M^{-2}$.

In 2013, Lehn and co-workers developed a novel approach to generate supramolecular polymers.[73] In this approach, a supramolecular component, **98·[99]₂** was prepared from a dynamic covalent library of hydrazone isomers obtained from cyclohexanedione
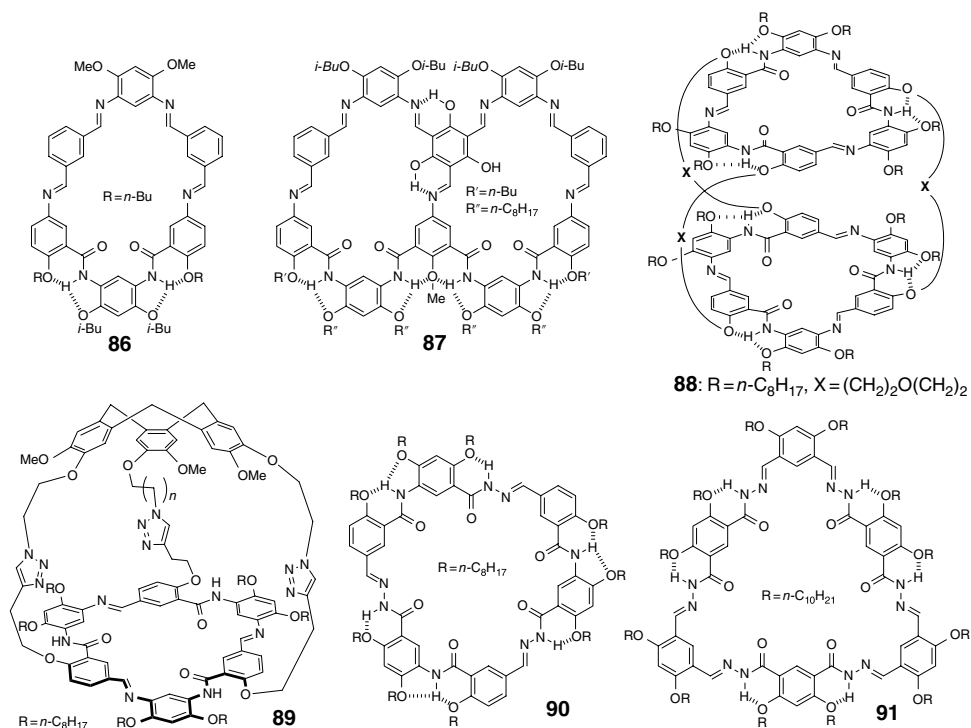
Figure 5.15 Imine- or hydrazine-linked macrocycles (**86**, **87**, **90**, and **91**) and cages (**88** and **89**) formed from precursors that are preorganized through hydrogen-bonding.
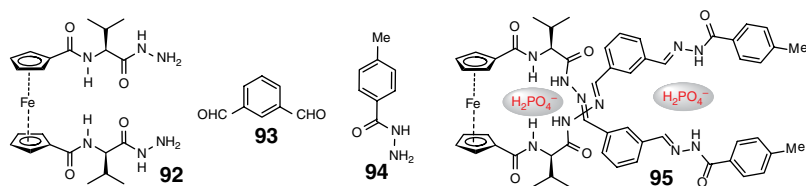
Figure 5.16 Linear oligomer **95** amplified in the presence of H^2PO^{4-} at the equilibrium of DCL obtained from **92–94**.

(**96**) and 2-hydrazino-pyridine (**97**) by target specific amplification of library constituent **99** in the presence of ditopic bis-cyanuric acid partner **98**. The formation of complementary hydrogen bonding between **99** and **98** is critical for the assembly of ditopic supramolecular component **98·[99]₂**. Covalent polymerization through oxidative formation of C–C linkages in chloroform in the presence of NEt_3 provided hydrogen-bonded supramolecular polymer **SP100** (Scheme 5.6).

The Lehn group also developed a reversible interconversion cycle by making use of the multiple dynamic properties (e.g., hydrogen bonding, metal coordination) of bisacylhydrazones **101a-d**.[74] These compounds form an intramolecular N–H···N hydrogen bond in the *E,Z* configuration in the solid state (Scheme 5.7), as revealed by the crystal structure. However, the ¹H NMR spectrum of **101a** in $CD_3CN/DMSO$-d₆ (3:1) indicates that it exists in *E,E* configuration in the solution phase. After 2 h of UV
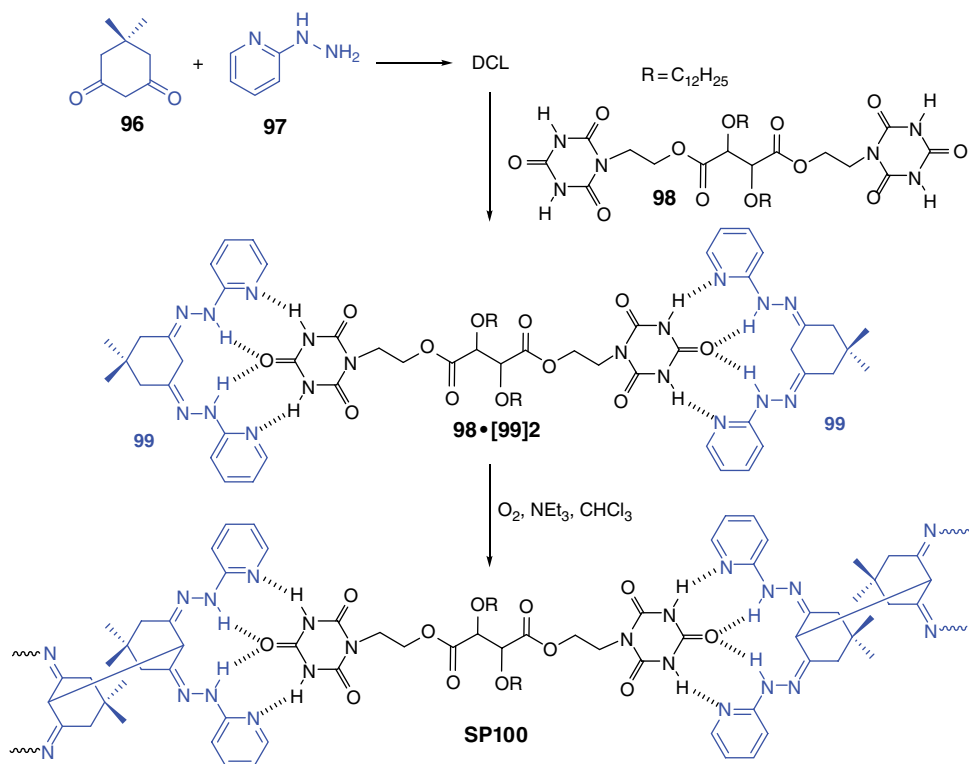
Scheme 5.6 The formation of main-chain hydrogen-bonded supramolecular polymer **SP100**.

101a: X = H
101b: X = OMe
101c: X = Cl
101d: X = NO$_2$

bisacylhydrazone
(W-shape)

EZ-**101a–d**
(S-shape)
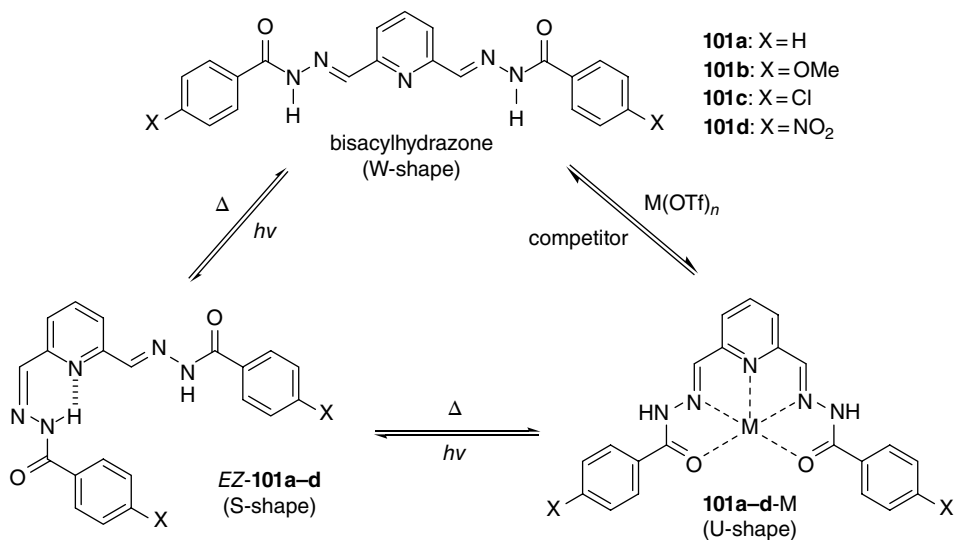
101a–d-M
(U-shape)

Scheme 5.7 Compounds **101a–d**, which undergo photo-, metallo- and thermo-induced configurational and conformational isomerizations.

irradiation, this *E,E* isomer converted into the *E,Z* isomer, which can convert back to the *E,E* isomer after heating at 80 °C overnight. The addition of Zn(OTf)$_2$ induced the isomerization of *E,E* or *E,Z* isomer to the *Z,Z* configuration due to the strong metal ion coordination effect. Adding a competing ligand tren tris(2-aminoethyl)amine) (tren) or irradiating the solution with UV light could cause the recovery of the *E,E* or *E,Z* configuration.

5.3.2 Disulfide and Hydrogen Bonding

In 2006, Gong and co-workers reported sequence-specific association of oligoamide strands using hydrogen boding and dynamic disulfide bond formation. Compounds **102** and **103** form a stable heterodimer stabilized by six intermolecular hydrogen bonds.[75] In dichoromethane, the addition of iodine (6 mM) to the mixture (0.5 mM) caused removal of the triphenylmethyl subunits at the two ends and the two molecules underwent cross-linking to produce disulfide-connected macrocycle **104** as the overwhelmingly major product. Self-dimers of the individual strand were not observed. In polar methanol and water-THF (90:10), **104** was also formed as the major product. However, when **102** or **103** alone was treated with iodine under the same conditions, they were self-cyclized into monomeric macrocycles through intramolecular disulfide bond formation. These observations suggested that in both less polar and highly polar solvents the intermolecular hydrogen bonds could promote the formation of the [1 + 1] macrocycle **104** (Figure 5.17). The reversibility of the disulfide bond and the hydrogen
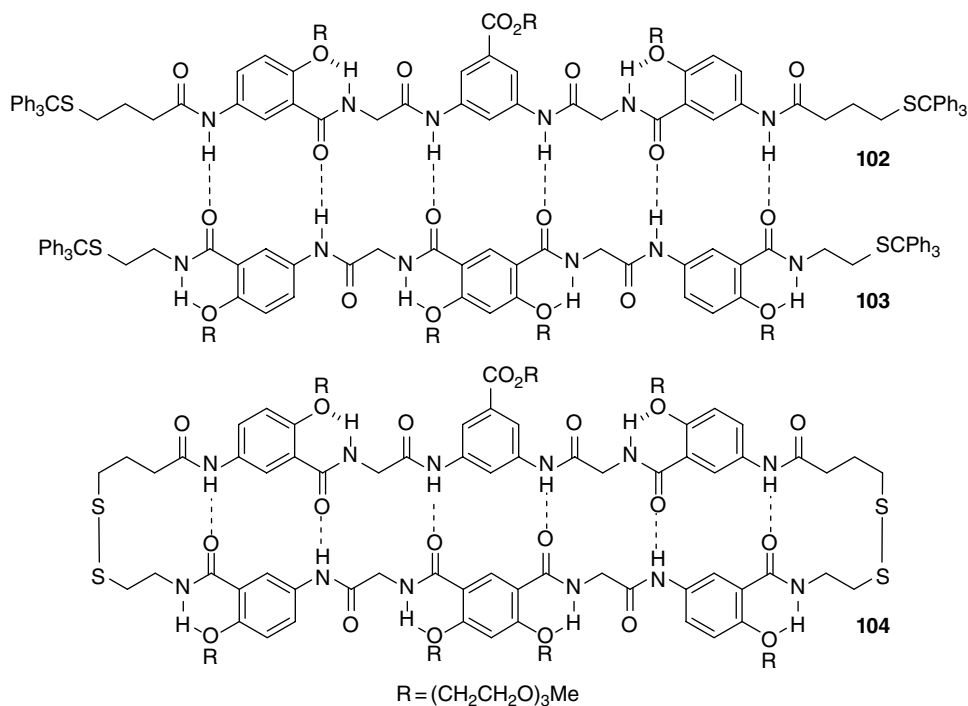
Figure 5.17 Macrocycle **104** formed from precursors **102** and **103** through disulfide and hydrogen bonding formation.

bond ensures the formation of thermodynamically stable dimer **104** over other mismatched combinations, such as self-dimers.

Later Gong and co-workers systematically investigated the sequence-specific cross-linking of oligoamides carrying various numbers and arrangement of hydrogen-bond donors and acceptors in both non-polar and aqueous media. Similar to the formation of **104** under redox conditions (I_2, CH_2Cl_2 or water/THF), compounds **105** and **106** formed quadruply hydrogen-bonded heterodimer **109** as the overwhelmingly major product (Figure 5.18).[76] It has been reported that as few as two hydrogen bonds are sufficient to form the sequence-specific dimer. For example, although doubly hydrogen-bonded heterodimer **107−108** had a low K_a ($25 \sim 50\,M^{-1}$) in chloroform, adding iodine to their solution in dichloromethane still afforded the $[1+1]$ macrocycle **110** as the dominant product and the self-coupled compounds were formed as minor products. The formation of hetero dimers **109** and **110** in polar medium (water–THF), where the intermolecular hydrogen bonding is quite weak, suggests even weak hydrogen bonds, when properly placed, can effectively direct and shift the equilibria towards the thermo-dynamically preferred product. Other products consisting of components that don't match in forming intramolecular hydrogen bonding are less preferred and converted to the stable dimers at equilibrium through reversible disulfide bond reactions.

The strategy to form sequence-specific duplex through the combination of hydrogen bonding and disulfide bonds has been applied to prepare dynamic covalent diblock poly-mers. Shen and co-workers prepared compounds **111** and **112a/b**, respectively, contain-ing hydrophilic (PEG) and hydrophobic (PLA) polymer chains (Scheme 5.8).[77] Following the principle developed by Gong, when the mixture of **111** and **112** in dichloromethane was treated with iodine, they efficiently coupled to produce sequence-specific macrocy-cles **P113a** and **P113b** with minimal formation of self-coupling product. The long hydrophilic poly(ethylene glycol) and hydrophobic polylactic acid blocks were thus com-bined to make the amphiphilic diblock copolymers. The resulting amphiphilic block copolymers self-assembled into long-lasting spherical micelles. Free thiols, such as dithi-othreitol (DTT), trigger the cleavage of the disulfide bonds, leading to the decomposition of the spherical micelles.

In 2005, Meijer and co-workers prepared 2-ureido-4[*1H*]-pyrimidone (Upy) deriva-tives (*R,R*)- and (*S,S*)-**114** (Figure 5.19).[78] Under conditions for disulfide exchange in chloroform in the presence of base and a catalytic amount of thiolate, the two isomers exchanged and equilibrated, resulting in the enrichment of *meso* (*R,S*) isomer. It was revealed that, at low concentrations, cyclic $[1+1]$ assemblies were the dominant products and the molecules themselves acted as templates for this binding mode. The *meso* diastereomers were formed preferentially, which had been attributed to a higher stability than the other diastereomers, although statistically they might also be favorable. At high concentrations, linear supramolecular polymeric aggregates became dominant. At all the used concentrations, the hydrogen bonding and disulfide bonds did not interfere with each other.

In aqueous solution, cyclic hexapeptides are able to complex anions to form sandwich complexes, which are stabilized by multiple hydrogen bonds. In 2003, Otto and Kubik prepared disulfide-linked biscyclopeptide **115**, which was mixed with dithiols **116−121** in water to afford a library of potential anion receptors.[79] This library contained com-pounds **122a−d** as the major products (Scheme 5.9). When the library was exposed to KI or K_2SO_4, pronounced amplification of receptors **122b−d** was observed owing to the
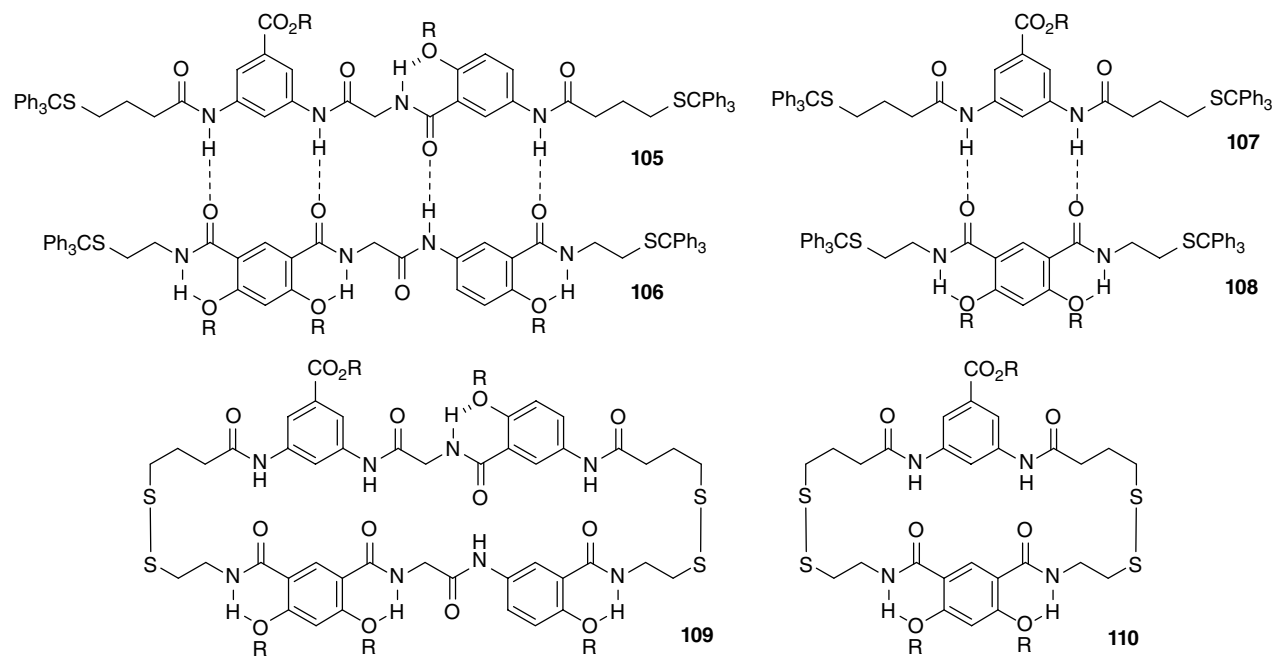
Figure 5.18 Cyclic hetero-dimers **109** and **110** formed from precursors **105–108**.
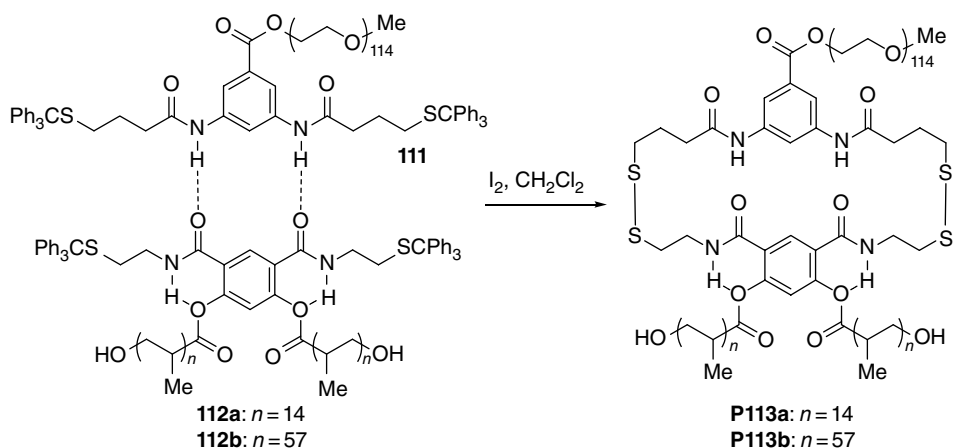
Scheme 5.8 Hydrogen bonding-assisted synthesis of amphiphilic copolymers **P113a** and **P113b**.
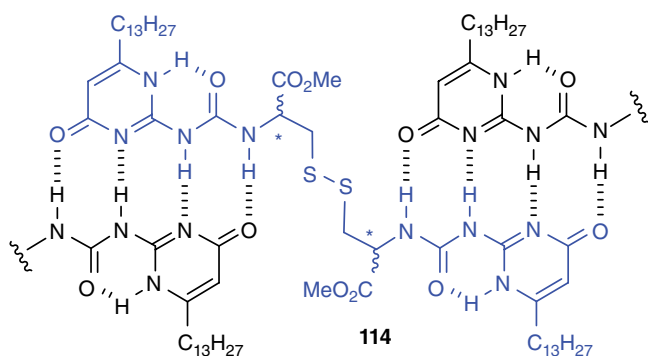
Figure 5.19 The structure segment of **114**.

templation effect. Receptors **122b** and **122c** were most strongly amplified by both ani-ons and could be isolated. Quantitative isothermal titration microcalorimetry (ITC) studies showed that they formed 1:1 complexes with anions.

In 2000, Ramström and Lehn designed a DCL of carbohydrate disulfides which was screened for affinity to the lectin-class protein concanavalin A.[80] The active site of concanavalin A recognizes carbohydrates through forming multiple hydrogen bonds with threonine and tyrosine hydroxy, aspartate carboxy and main-chain amide groups, whereas the natural substrate is a trimannose. Thus, a DCL of six different homodi-meric carbohydrate disulfides, including **123a** and **123b** (Figure 5.20), was used for the discovery of biologically active ligands. After reaching exchange equilibrium, the six carbohydrate disulfides could produce 21 possible distinct species. It was revealed that adding concanavalin A to the equilibrated mixture induced all mannose-containing species to be bound to the protein. These disulfides were thus amplified, but homo-mannose dimer **123b** was most strongly amplified through the best matching of the complementary hydrogen bonds formed between it and the protein template.
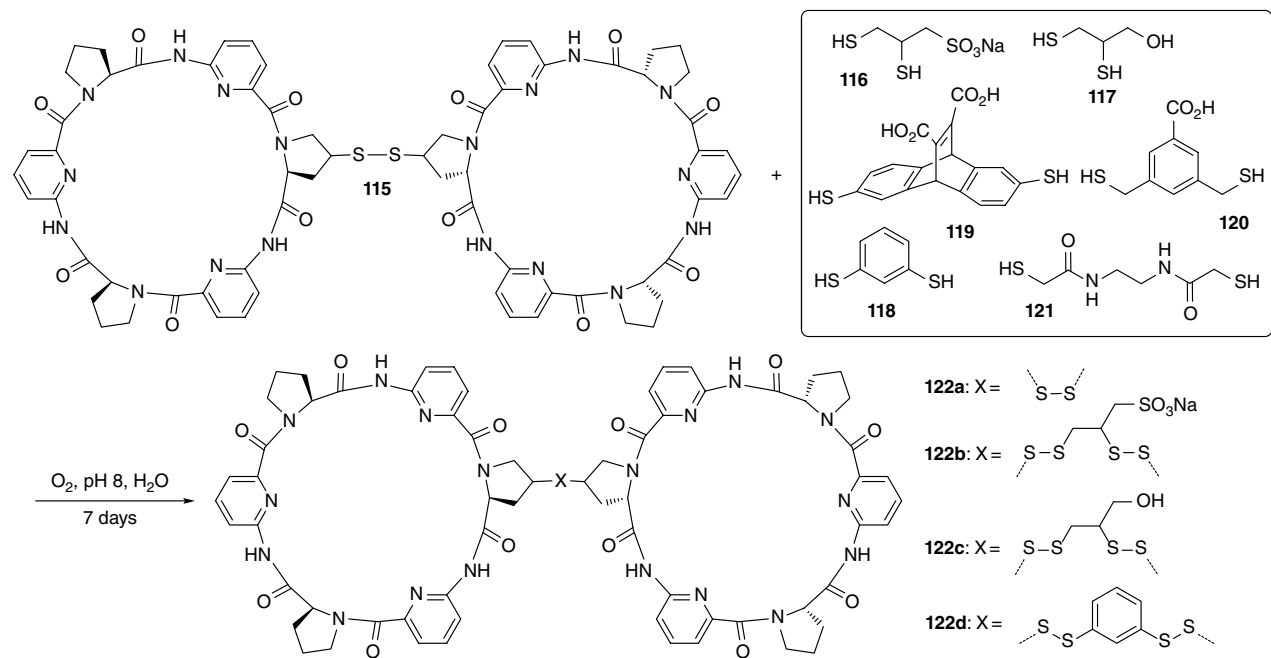
Scheme 5.9 Design of a diverse DCL of disulfide-linked biscyclopeptides which act as anion receptors amplified by anions in water.

Figure 5.20 The structures of homodimeric carbohydrate disulfides **123a** and **123b** used for the discovery of biologically active ligands.

123a   123b
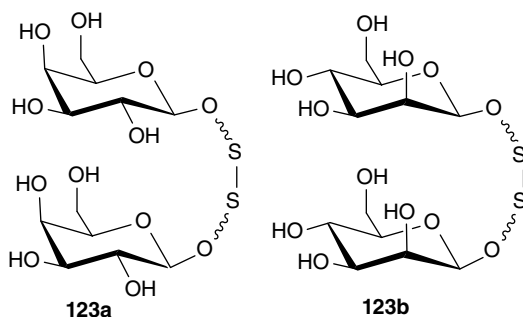
5.3.3 Alkene Metathesis and Hydrogen Bonding

In 2005, Gong further extended the quadruply hydrogen-bonded heterodimer motif by introducing an ethene group at the same end to prepare **124a–e** and **125a–e**.[81] These two ethylene groups were induced by the dimer backbone to approach each other in chloroform. In the presence of Grubbs' catalyst, the two molecules underwent alkene metathesis to afford compounds **126a–e** selectively (Scheme 5.10). When the tethered alkene units were orientated to the opposite sides, no similar cross-metathesis product was obtained. Clearly the hydrogen-bonded heterodimer acts as a template for the selective cross-metathesis of the two alkene groups.

In 2011, Yuan and Gong and co-workers found that, when the aromatic amide oligomers are tethered with two alkene units, their hydrogen-bonded dimers can induce the alkenes to undergo cross-metathesis to afford macrocyclic compounds.[82] By using this strategy, macrocycles **127a**, **127b** and **127c** have been prepared from the corresponding hydrogen-bonded dimers (2 mM) in dichloromethane in the presence of the Grubbs' catalyst (Figure 5.21). The yield of **127a** was quite low (<11%) and the metathesis reaction also produces self-coupled macrocycle **127d**. However, both **127b** and **127c** were obtained in nearly quantitative yield. Studies on model systems with two hydrogen bonds reveal that the length of the aliphatic chains connecting the tethered ethane units has an important effect on the macrocyclization.

5.4 Imine and Hydrazone, π-Stacking, and Donor–Acceptor Interaction

One important driving force for triply threaded pseudo[2]rotaxane **65 ⊂ 66** is the π-stacking between the benzene-1,3,5-triimine and the benzene-1,3,5-pyridinium units.[61] In 2009, Liu and co-workers further utilized the stacking between benzene-1,3,5-triimine and viologen units to construct [2]rotaxane **128** in nearly quantitative yield (Figure 5.22).[83] The viologen-incorporated linear molecules worked as a template in chloroform to template the formation of the cage component from the corresponding trialdehyde and diamine precursors. The rotaxane solution was yellow, with the absorption band centered around 420 nm, which indicates that charge transfer occurred between the two aromatic units. Similar to pseudo[2]rotaxane **65 ⊂ 66**, [2]rotaxane **128** was stabilized by across-component C–H···O hydrogen bonding between hydrogens of pyridinium units and oxygen atoms of the ethylene glycol loops. When using a
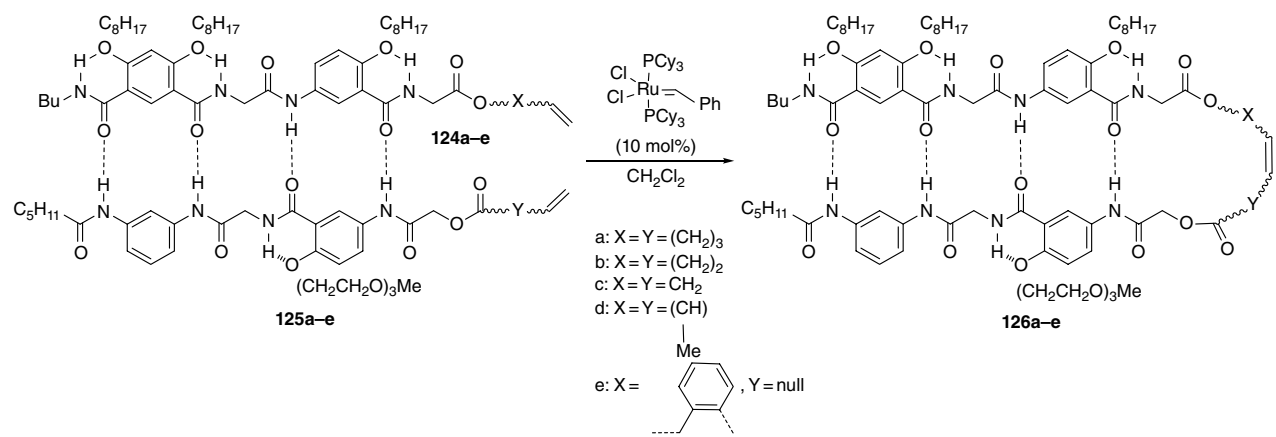
Scheme 5.10 Cross-metathesis of oligoamide-tethered olefins.
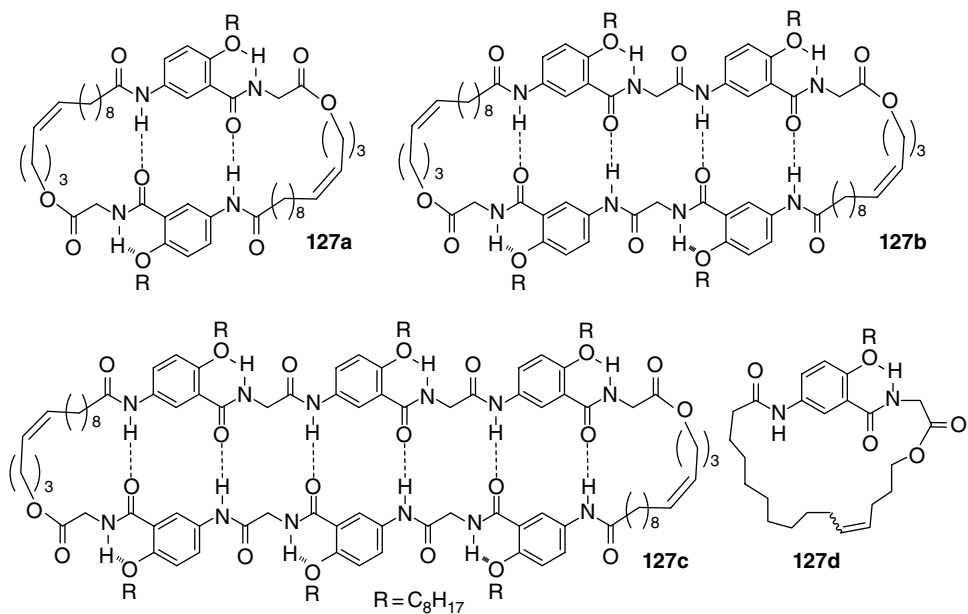
Figure 5.21 Macrocycles obtained through olefin metathesis with the aid of hydrogen-bonding between monomers.
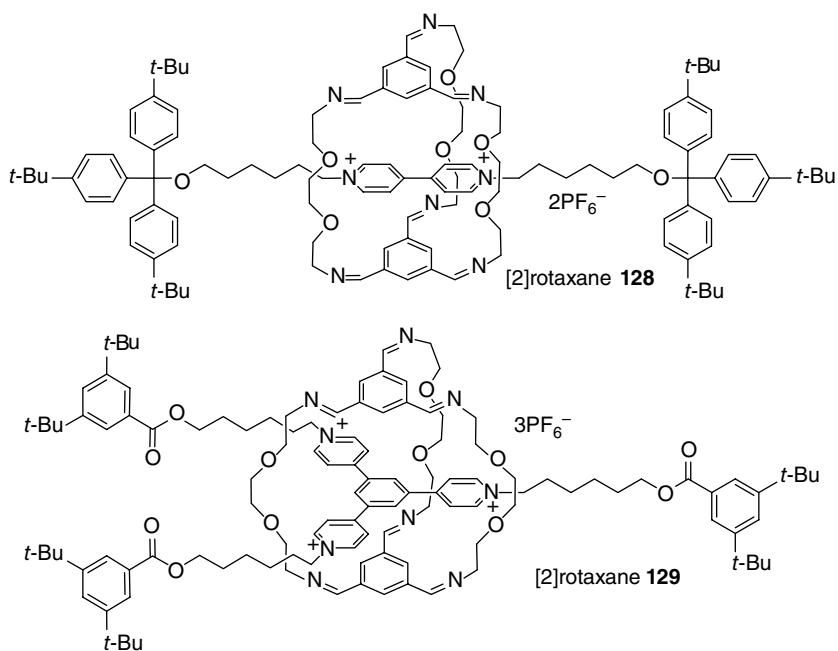
Figure 5.22 The structures of [2]rotaxane **128** and **129**.
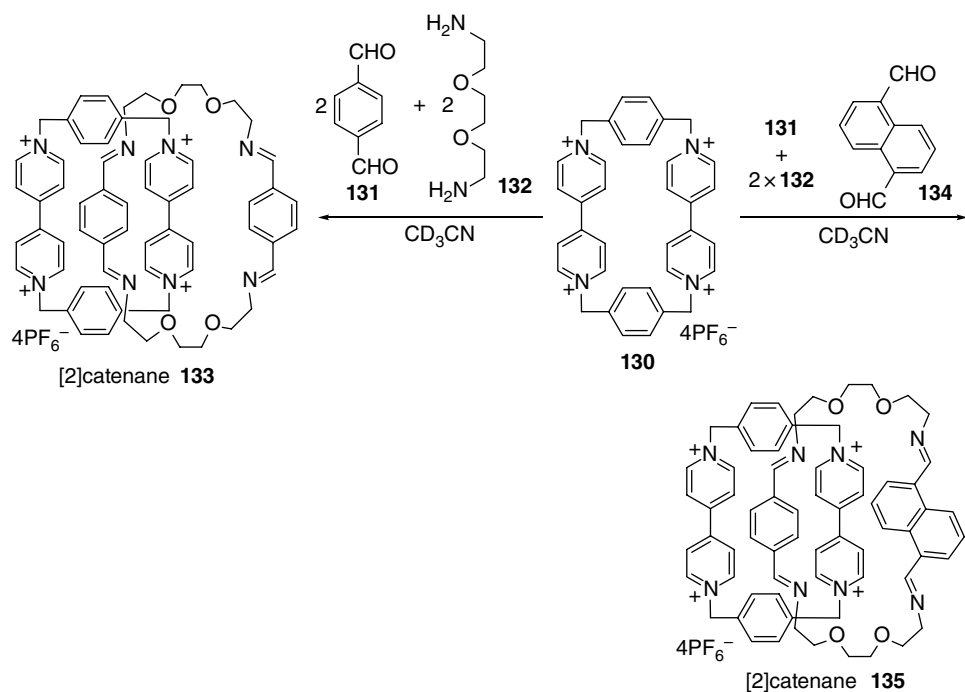
Scheme 5.11 The templated-synthesis of symmetric [2]catenane **133** and unsymmetrical [2]catenane **135** by forming four imine bonds.

triangular molecule as template, the same cage component was formed and [2]rotaxane **129** was obtained.[84] The exclusive formation of these rotaxanes is associated with the combination of π–π stacking interactions and hydrogen-bonding interactions, which lead to the thermodynamic stability of these complexes.

The aromatic stacking is also robust enough to drive the assembly of [2]catenanes. In this case, tetracationic cyclophane **130** was chosen as a template.[85] In acetonitrile, in the presence of 1 equivalents of **130**, dialdehyde **131**, and diamine **132** (1:1 molar ratio) coupled to afford [2]catenane **133** as a single species (Scheme 5.11). The three pairs of π-stacking stabilize the interlocked structure and endow the reaction high selectivity. Under the same conditions, using **130** as a template, the reaction of **131**, **132**, and **134** (1:2:1) afforded [2]catenane **135** as the overwhelmingly major product with **133** as a minor product (4%). The ^{1}H NMR spectrum and X-ray crystal structure showed that the benzene-1,4-diimine unit is located inside the cavity of the tetracationic cyclophane.

In 2015, Chen and co-workers prepared tetrathiafulvalene (TTF)/viologen-alternate polymers **P136a** and **P136b** by forming hydrazone bonds from the corresponding dialdehyde and di(acylhydrazine) precursors in acetonitrile (Figure 5.23).[86] These two hydrazone-based polymers have polymerization degrees of ca. 8 and 6, which were estimated using ^{1}H NMR spectra. Due to the donor–acceptor interaction between the adjacent electron-rich TTF and electron-deficient viologen units, the backbones adopted pleated folded conformation in acetonitrile as evidenced by UV-vis spectroscopy, which exhibits a strong concentration-independent charge-transfer absorption band. When the TTF units were oxidized to radical cation TTF[■+], the backbone of the polymer **P136a/b** existed in flexible conformations. In contrast, when the viologen
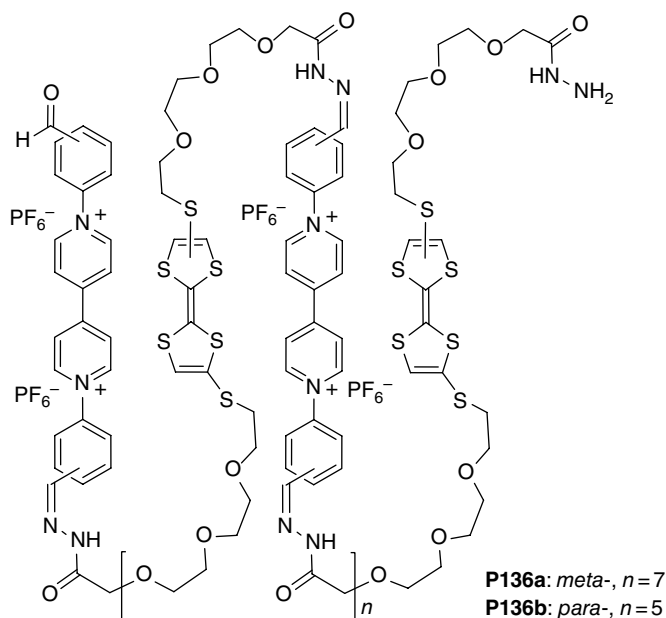
Figure 5.23 The structures of TTF/viologen-alternate polymers **P136a** and **P136b**.

units were reduced to radical cations, they underwent intramolecular stacking to induce the backbones to form another kind of pleated conformation.[87] Thus, by changing the redox state of the viologen units, the pleated folded conformation of the backbones can be tuned reversibly. It is noteworthy that for all the experiments performed, the hydrazone bonds were stable.

In 2015, Zhang and co-workers prepared polymers **P137a–d** through the condensation of **138** with the corresponding di(acylhydrazine) derivatives in acetonitrile (Figure 5.24).[88] The ^{1}H NMR spectra showed that these dynamic polymers all have a polymerization degree of ca. 10 and their backbones adopt flexible conformations. On reducing the viologen units to radical cations in acetonitrile, the radical cations in **P137b–d** underwent intramolecular stacking to induce the backbones to form pleated folded conformations. In contrast, the viologen radical cations of polymer **P137a** stacked intermolecularly. The apparent association constant for this stacking was markedly higher than that of monomer **138**, suggesting a positive cooperativity. Adding Li$^+$ cation induced the intramolecularly stacking in **P137a** to occur due to the folding of the oligo(ethylene glycol) chains through binding the metal cation. For **P137b–d**, Li$^+$ cations could also further strengthen their pleated conformations through binding to the oligo(ethylene glycol) chains.

5.5 Disulfide, π-Stacking, and/or Donor–Acceptor Interaction

In 2010, Sanders and co-workers utilized two dithiols **139** and **140**, which contain an electron-deficient naphthalenediimide (NDI) or an electron-rich dioxynaphthelene (DN) unit, respectively, to construct DCLs derived from donor–acceptor interactions
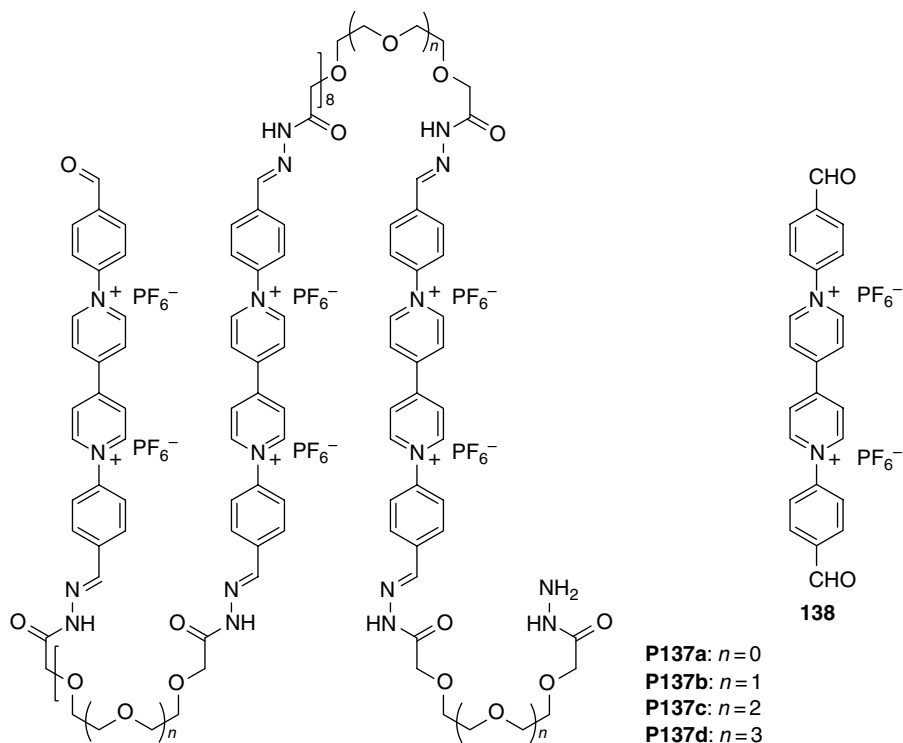
Figure 5.24 Viologen-containing polymer **137** formed from **138** through stacking interactions and hydrazine formation.

by using DN-derived **141** and NDI-derived **142** as the guest of the respective library (Figure 5.25).[89] The aqueous solution of **139** (5 mL) at pH = 8 was stirred in a capped vial to allow atmospheric oxidation of the thiol groups to produce disulfide-linked macrocyclic species. After 5 days, equilibrium was reached and the DCL solution contained the cyclic dimer **143**, trimer **144**, and tetramer **145** in proportions of ca. 50%, 35% and 15%. The addition of **141** to the DCL induced the solution to turn orange, indicating the formation of the charge-transfer complexation between the NDI and DN units of the two components. This donor–acceptor interaction induced shifting in the DCL composition. The cyclic tetramer **145** was amplified up to 6-fold, corresponding to 80% of the DCL materials,[90] at the expense of the cyclic dimer **143**. It was proposed that both cyclic tetramer **145** and trimer **144** were stabilized by **141** because the cavity of these two cyclic compounds could complex the DN guest through donor–acceptor interaction. Under the same conditions, the DCL formed from **140** contained cyclic monomer **146**, dimer **147**, and trimer **148** in proportions of 93%, 6% and <1%. The longer and more flexible side chains in **140** favored the formation of the cyclic monomer **146**, which is also the most entropically favorable species. The addition of **142** caused the re-equilibration, leading to a 4-fold increase in the proportions of both cyclic dimer **147** (23%) and trimer **148** (4%) at the expense of the cyclic monomer **146**.

The importance of the donor–acceptor interaction in the recognition of the DCL macrocycles evolved from **139** was also tested with electron-deficient templates **149–152** (Figure 5.25).[90] All the compounds **149**, **150**, and **151** amplified tetramer **145**, but had
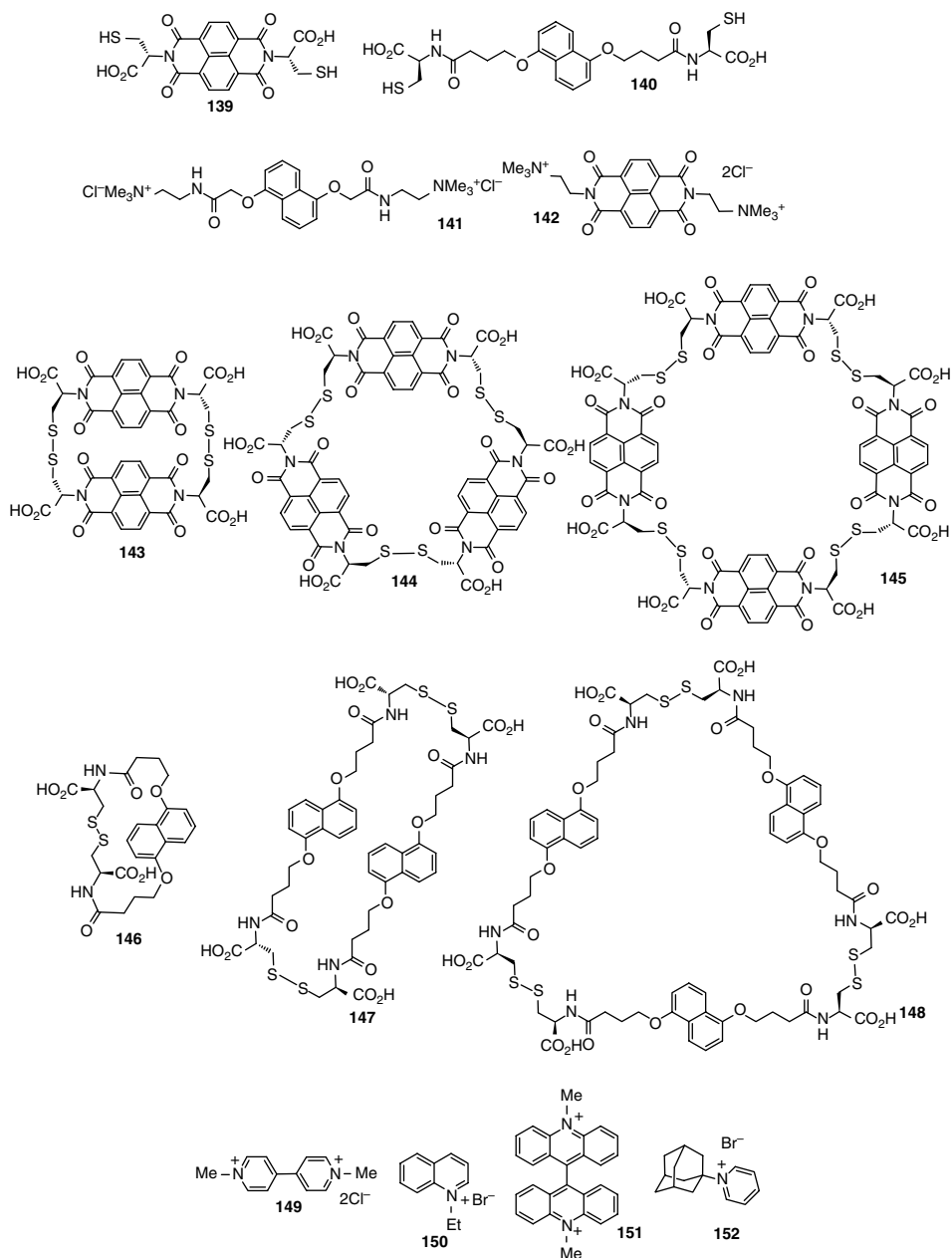
Figure 5.25 NDI or DN starting materials (**139–142**), the macrocycles (**143–148**) observed in the DCL and templates (**149–152**) that can amplify the formation of specific macrocycles.

an amplification factor that was significantly lower than that observed with compound **141** (4.4, 2.1, and 2.1, respectively vs. 5.7). The library distributions in the presence of **152** or **142** were very similar to that of the template-free DCL, suggesting that these two guests had no interactions with the macrocyclic species. In all the DCLs, the trimer **144** was minor and the trimer/tetramer (**144**/**145**) ratios ranged from 0.28 to 0.37,
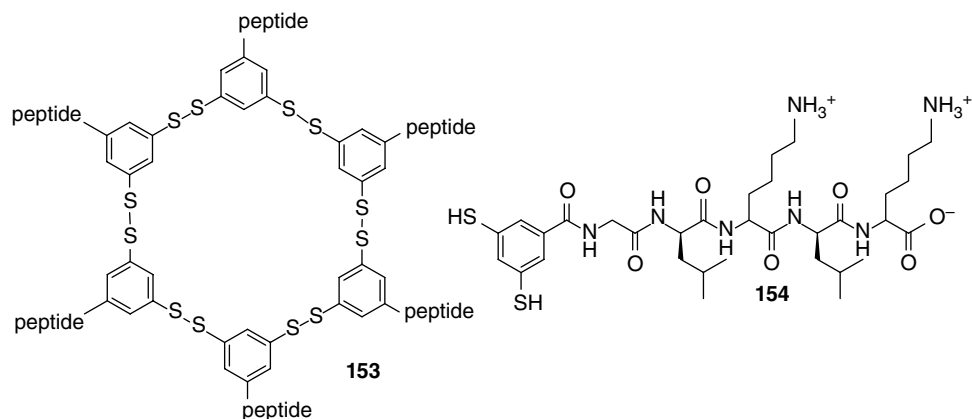
Figure 5.26 Macrocycle **153** formed from **154**.

indicating that **144** and **145** have comparable binding abilities towards all the studied templates. The above observations indicate that the donor–accepter interaction is necessary, but not sufficient to induce a large response in the DCLs made by **139**. The results also show that electrostatic and/or hydrophobic effects are unable to be independently responsible for the amplification of the tetramer because **142** and **152** or other cationic guests did not generate the templation effect on the DCLs of **139**. Thus, it was proposed that it was the combination of the donor–acceptor and electrostatic interactions that led to large amplification of the tetramer **145** in the presence of **141**. Other factors such as the relative size and structural matching of the host and the guest should also be important.

In 2010, Otto reported that mechanical forces (e.g., shaking) can act as a selection pressure in a DCL.[91] Hexameric disulfide macrocycle **153** (Figure 5.26) emerged on shaking a DCL made from dithiol **154**, which bears a short peptide sequence, predisposed to β-sheet formation by alternating hydrophobic and hydrophilic amino acid residues. In the absence of mechanical agitation, dithiol **154** mostly produced disulfide-linked macrocyclic trimer and tetramer that remained unchanged over a period of 7.5 months. However, by shaking the DCL solution, the self-assembly of cyclic hexamer **153**, one of the DCL species, occurred, resulting in the formation of fibers.[92] The self-assembly led to shifting of the product distribution in favor of **153**, that is, **153** was amplified by shaking. The self-assembly of **153** has been attributed to the one-dimensional stacking of the disulfide-linked macrocyclic backbone. Irradiating the self-assembled fibers broke the macrocycle and long disulfide-linked polymeric products were generated. The process was revealed to be reversible.

In 2012, Sanders and co-workers used linear precursors **155** and **156** as components to create a DCL strategy from which donor–acceptor [3]catenane can be obtained predominantly through template-induced amplification.[93] In the absence of salt or a template, their mixture afforded cyclic heterodimer of **155** and **156**, cyclic dimer of **156**, and cyclic tetramer of **155**, and a [2]catenane consisting of cyclic dimer of **156** and cyclic tetramer of **155** as important species. In the presence of 1 M NaNO$_3$ (one pot), [3]catenane **157**, the above [2]catenane, and cyclic tetramer were revealed to be the major species. In the presence of 0.5 mM spermine, [3]catenane **157** became the
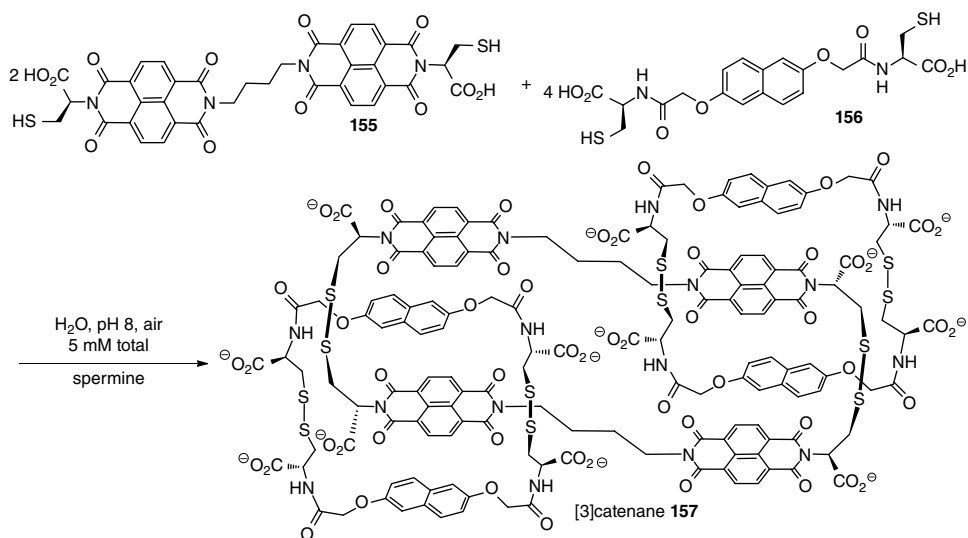
Scheme 5.12 Self-assembly of [3]catenane **157** from linear precursors **155** and **156** in water, templated by spermine.

overwhelmingly major species, together with the [2]catenane and cyclic tetramer as minor species (Scheme 5.12). The ^{1}H NMR showed that [3]catenane **157** bound spermine with a K_a of 110 000 M^{-1}. Because the aromatic moieties of the [3]catenane are too closely packed to accommodate a cavity large enough for spermine, it was proposed that the template was bound to the solvent accessible surface of the [3]catenane to interact with the arrayed carboxylate ions.

In 2012, Sanders and co-workers further investigated the DCLs made from compounds **158a–h** ($n = 2$–9) (Figure 5.27).[94] All the precursors underwent intramolecular disulfide bond formation in air at pH = 8 in the presence of 1 M NaNO$_3$ to produce cyclic monomers **159a–h** and cyclic dimers **160a–h**. For the DCLs made by **158f–h** whose two NDI units were connected by long aliphatic chains, all-acceptor [2]catenanes **161a–c** were also formed from the respective DCL. The yield of [2]catenane **161c** was significantly higher (in 60% proportion of the library composition). The formation of these all-acceptor [2]catenanes was attributed to the need of the assembled species to minimize the solvent-exposed hydrophobic surface area of their NDI units. The hydrophilic cysteine side chains of [2]catenane were proposed to be exposed to the solvent. For DCLs made by **158a–h** and **156**, macrocycles incorporating both precursors were produced. The electron-deficient NDI units of these hybrided macrocycles could form donor–acceptor interaction with the DN-incorporated cyclic dimer formed by **156** to produce different [2]catenanes of varying ring size.

In 2009, Sanders and co-workers also reported an investigation of the DCL made from compounds **139** and **156** (Scheme 5.13).[95] Compound **156** has two longer side chains and thus was able to form a cyclic monomer and dimer species, while **139** alone mainly forms the cyclic dimer. When these two species were mixed, cyclic heterodimer (**162**) was produced as a major species (60%), along with [2]catenanes **163a** (10%) and **163b** (<5%), and other cyclic heterotrimers and heterotetramers at the equilibrium.

158a–h (*n* = 2-9)

159a–h (*n* = 0-7)

160a–h (*n* = 2-9)

[2]catenane **161a**: *n* = 1
161b: *n* = 2
161c: *n* = 3
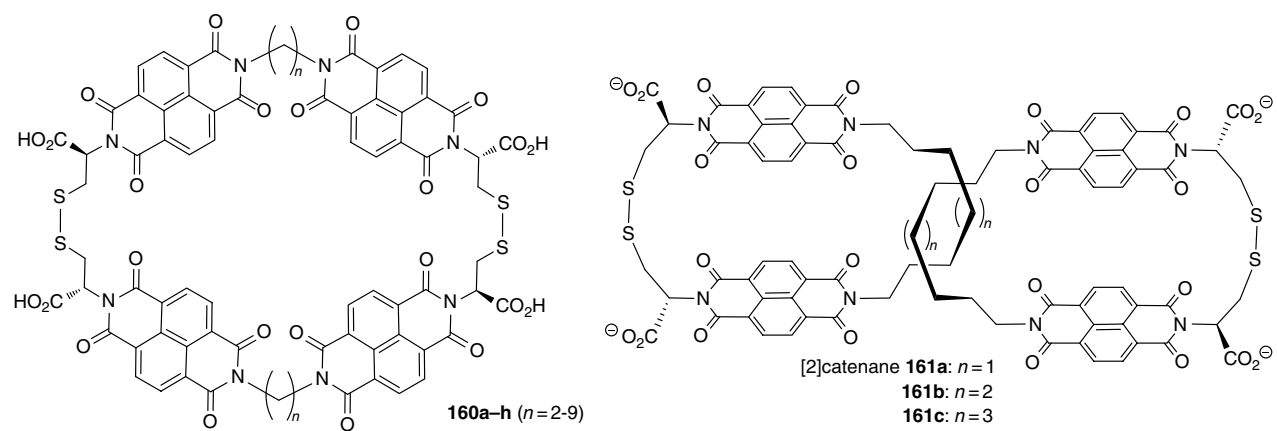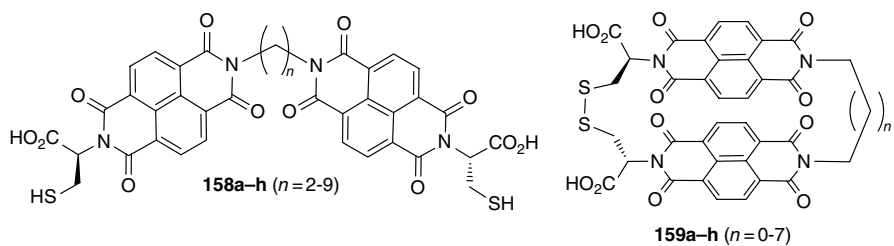
Figure 5.27 DCL made from compound **158**, which contains macrocycles **159–161**.
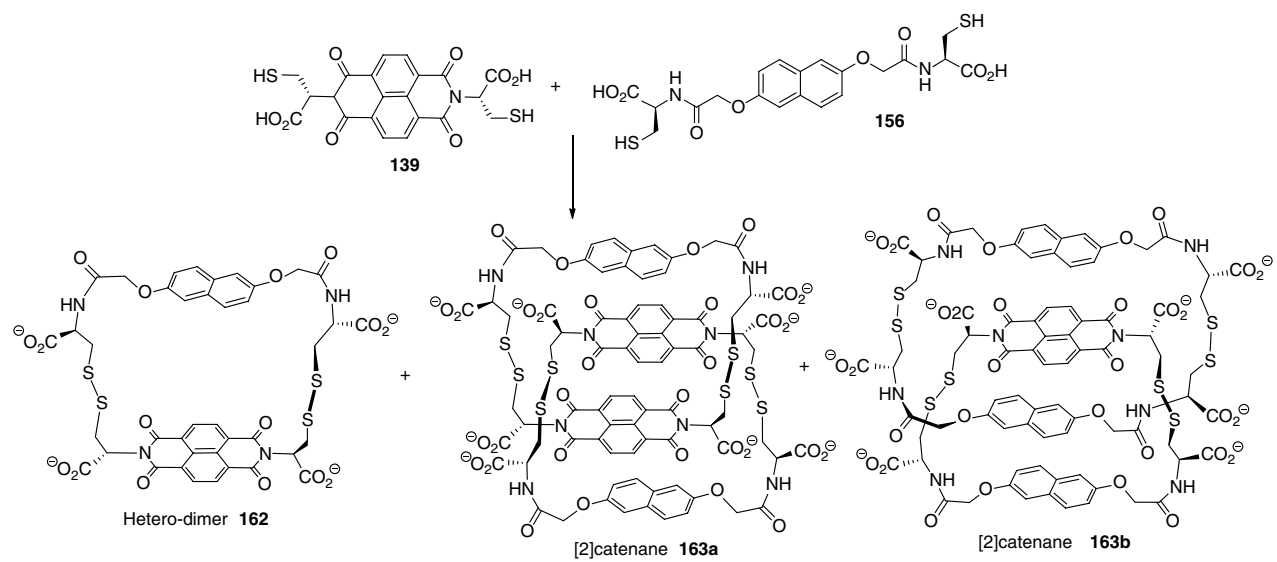
Scheme 5.13 Dimer **162** and catenanes **163a** and **163b** observed in DCL formed from compounds **139** and **156**.
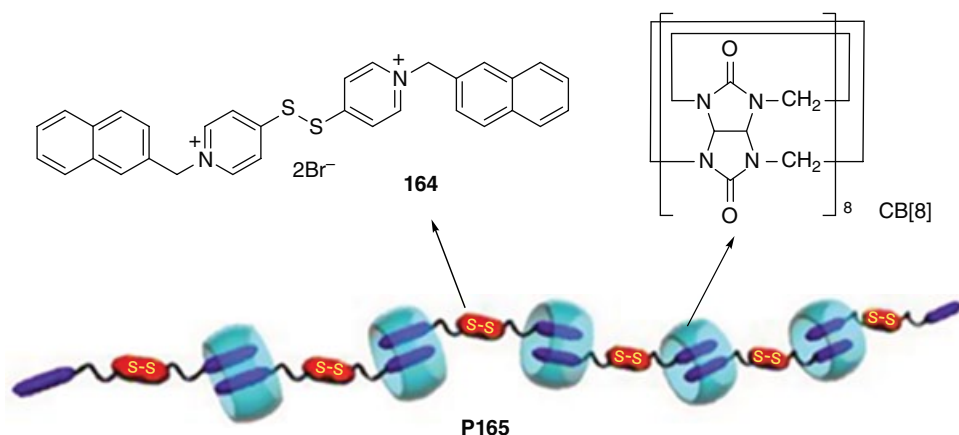
Figure 5.28 Supramolecular polymer **P165** formed through the interaction between cucurbit[8]uril (CB[8]) naphthalene units of monomer **164**.

Increasing the ionic strength of the medium facilitated the formation of [2]catenane **163a**, which was ascribed to its smallest average area of hydrophobic surface exposed to the polar solvent. In the presence of 1 M NaNO₃, [2]catenane **163a** was amplified to about 55% in proportion (5-fold increase), at the expense of the cyclic heterodimer (~10% vs. 60% initially). In the new DCL, [2]catenane **163b** was amplified to ~10%. In a low-salt DCL obtained from 1:3 ratio of **139** and **156**, [2]catenane **163b** became a significant component (~10%). Adding 1 M NaNO₃ further increased the abundance of **163b** to ~50%, making it the major component. At the 3:5 ratio of **139** and **156**, [2] catenanes **163a** and **163b** represented ~45% and ~30% of the total DCL proportions in the presence of 1 M NaNO₃, corresponding to an ~75% interlocking efficiency.

In 2014, Zhang and co-workers designed disulfide derivative **164** to construct a redox-tuned supramolecular polymer (Figure 5.28).[96] In water, two naphthalene units are located inside the cavity of cucurbit[8]uril (CB[8]), driven mainly by the hydrophobic effect. A supramolecular polymer **P165** was formed in water through the encapsulation of two naphthalene units of the neighboring two molecules of **164**. The addition of 1-adamantanamine hydrochloride caused depolymerization of the supramolecular polymer due to its high affinity to CB[8], resulting in the release of naphthalenes. The addition of glutathione reduced the disulfide group to two mercapto groups and again destroyed the supramolecular polymer.

In 2011, Sakai and Matile and co-workers reported a strategy of self-organizing surface-initiated polymerization (SOSIP) to create ordered and oriented functional systems on the transparent surface of indium tin oxide (ITO) (Figure 5.29).[97] The first step involved the attachment of **166** to the surface of ITO with two diphosphonate "feet". Reduction of the disulfides with DTT liberated the reactive thiolates. The reduced materials were then treated with **167** to propagate the molecular layer through intramolecular ring-opening disulfide exchange at both termini driven by the NDI stacking and cross-chain hydrogen bonding of the lysine, while at the same time active thiolates were released on the surface of the assembled architectures to allow for the next turn of
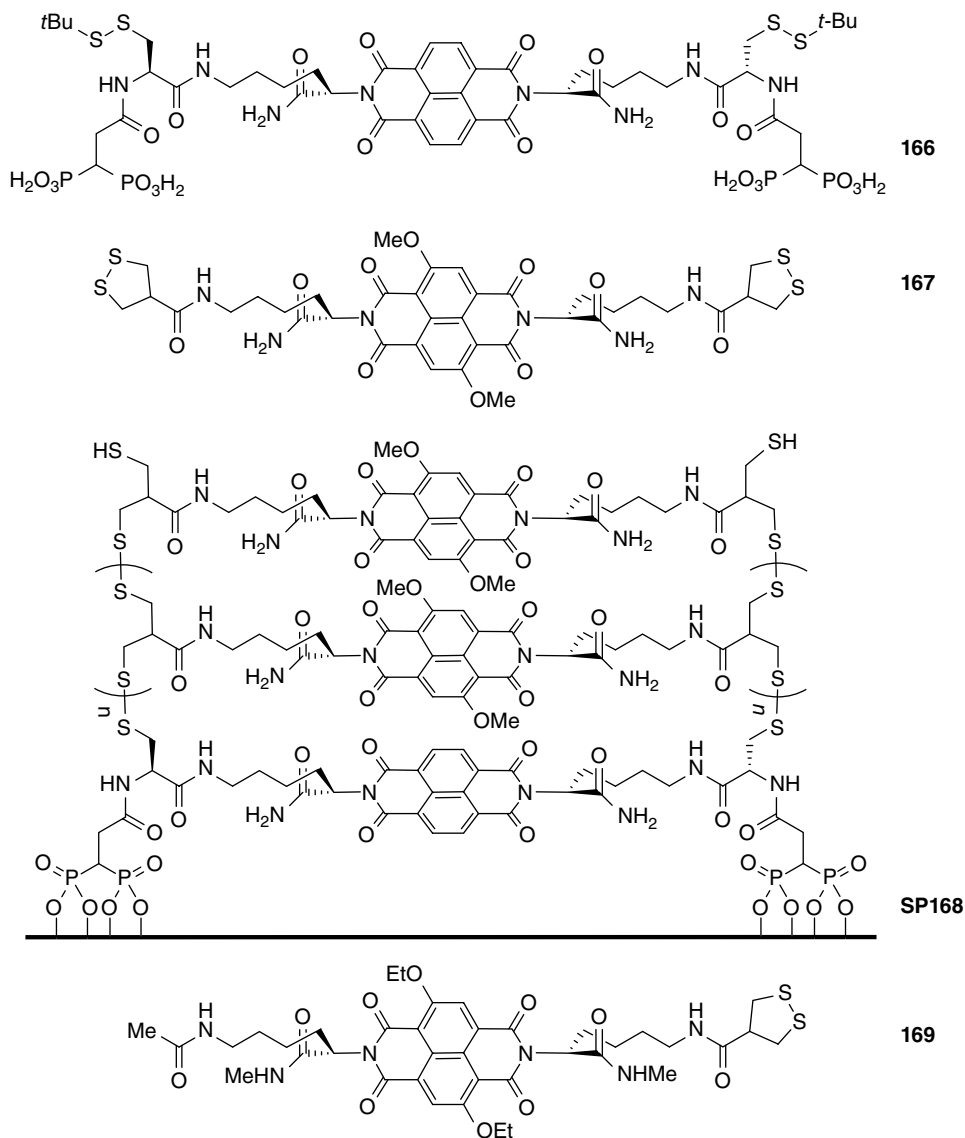
Figure 5.29 Surface-appended dynamic polymer **SP168** formed through the attachment of **166** to the surface followed by propogation. Structures of efficient propagator **167** and weak propagator **169** are also shown.

reversible disulfide exchange. By repeating this process, rapid access to surface-appended dynamic polymer **SP168** with controlled thickness and long-range order could be realized. The activity of SOSIP architectures for photocurrent generation was clearly better than that of disordered controls. The efficiency for the formation of **SP168** was strongly dependent on the nature and concentration of the propagators and the base catalyst. The

onset of competing polymerization of **167** in solution occurred at higher concentration and very weak polymerization was found with mono-asparagusyl propagator **169**, supporting the importance of surface-bound and preorganized dithiolates to template the polymerization.

5.6 Disulfide, Hydrazone, and π-Stacking Interaction

The SOSIP approach has been extended for the construction of other complicated self-assembled systems as photosynthesis models.[16] For example, for generating one series of covalent double-channel photosystems, **SP170a** was first prepared using the same approach (Figure 5.30).[98] The introduction of two NDI units to the first layer through two acylhydrazone bonds on the surface of ITO was expected to provide two additional aromatic moieties for the templation of the stacking of other tethered aromatic units. For **SP170a**, however, this stacking by the small benzene units was weak. Treatment of **SP170a** with hydroxylamine in water released the acylhydrazine and formed benzaldehyde oxime. The acylhydrazine-bearing precursors were then reacted with different
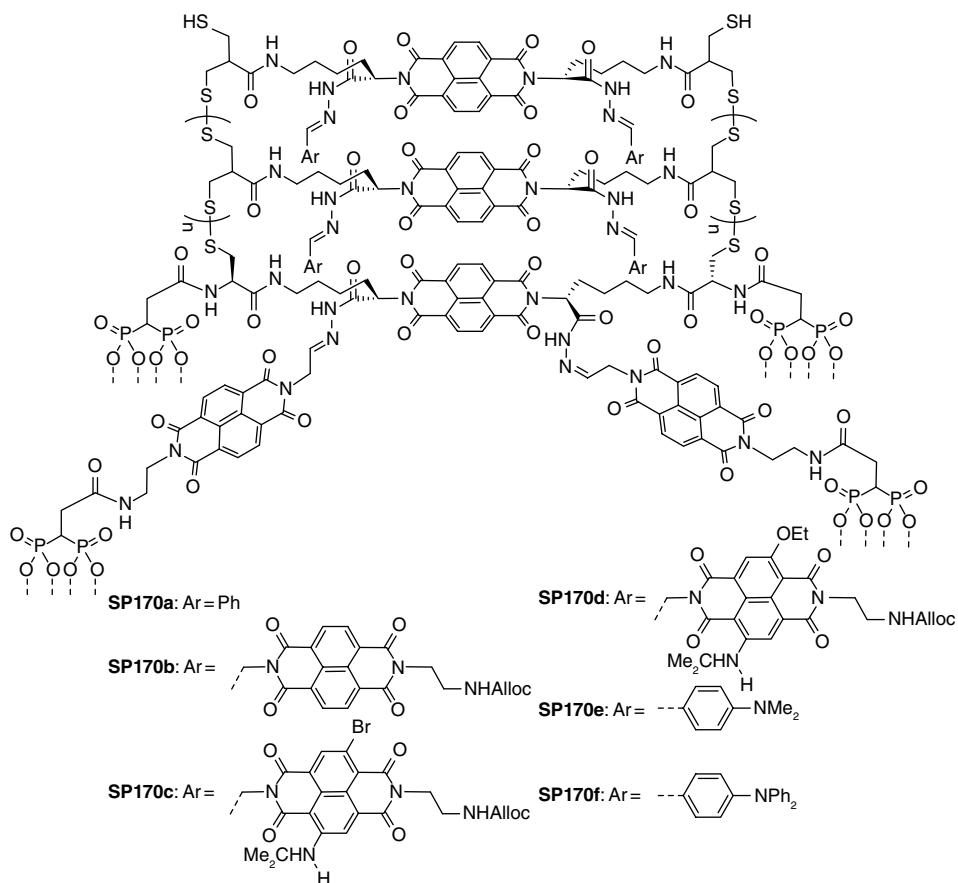
Figure 5.30 Surface-appended dynamic polymers **SP170**.

aldehydes to produce **SP170b–f**. The post-SOSIP stack exchange on the functional level was characterized by photocurrent generation on irradiation of the photosystem used as a working electrode in the presence of mobile triethanolamine hole acceptors, a Pt wire as a counter electrode, and Ag/AgCl as a reference electrode. The photocurrent after several on–off cycles of irradiation was unchanged, confirming the stability of the photosystems under the conditions used. The photocurrent generation of the stacks of the NDIs in photosystem **SP170c** was twice that of the unsubstituted NDIs in **SP170b**, while **SP170d–f** as photosystems were less active.

5.7 Hydrazone, Boronate, and π-Stacking Interaction

Matile and co-workers used orthogonal dynamic covalent bonds to design dynamic sensors for polyphenols (Figure 5.31).[99] The strategy was based on synthetic multi-functional pores that work in lipid bilayer membranes. The pores used are artificial β-barrels that bear aromatic moiety NDI and can quench the fluorescence of the anthracene unit of **171** through donor–acceptor interaction. To sense polyphenols, compound **172** was introduced to **171** to form **173** by a hydrazone bond. This compound can enter the designed pores and its fluorescence was weakened due to aromatic stacking of the anthracene group with the NDI units appended in the pores. The boronic acid group of **173** could form boronate with polyphenol such as **174** to produce **175**. This large hydrazone derivative could not enter the pores and thus exhibited fluorescence, indicating the binding to polyphenols. Using this strategy, boronic acid converters have been designed as reactive hydrazide amplifiers for sensing polyphenols in green tea also with synthetic pores.[100]

5.8 Concluding Remarks

Dynamic covalent bonds combine the robustness of covalent bonds with the reversibility of non-covalent bonds. The orthogonal combination of different dynamic covalent bonds allows for broader diversity of covalent self-assembled structures and thus provides the structural basis for exploring new functions and properties. Current effort has been mainly devoted to the construction of dynamic combinatorial libraries and complicated macrocycles, molecular cages, and interlocked systems. However, important advances have also been made in the generation of functional molecular systems, particularly for screening active molecules, sensing, and photosystems. Orthogonal combination of non-covalent interactions with dynamic covalent bonds endows chemists with more choices in creating new structures and exploring new functions. Such a combination should have a broadness that could be searchable using SciFinder because orthogonality is not described in many reported works even though non-covalent forces play a role in research of dynamic covalent chemistry. For research in the future, we believe that the creation of more complicated dynamic combinatorial libraries will certainly continue to receive attention. This will need the development of more sensitive techniques for quickly identifying the increased number of library components. Moreover, the application of the orthogonality concept in designing new smart and advanced materials remains largely underexplored.
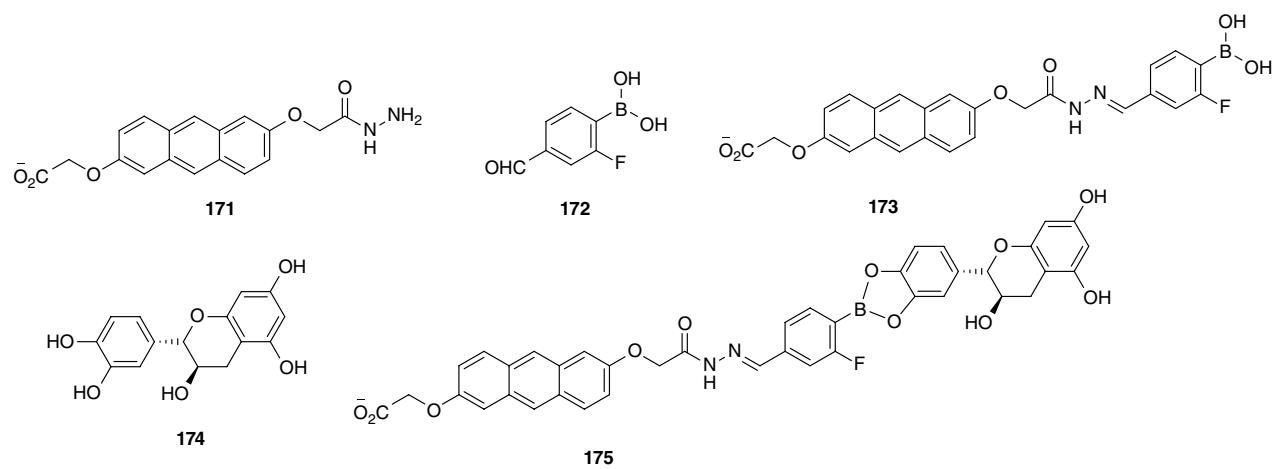
Figure 5.31 Dynamic sensor system involving boronate amplifier **173** obtained from **171** and **172** though hydrazone formation, which can sense a polyphenol such as **174** through the formation of a boronate, e.g. **175**.

References

1 J.-M. Lehn, *Chem. Eur. J.* **1999**, *5*, 2455–2463.

2 S. J. Rowan, S. J. Cantrill, G. R. L. Cousins, J. K. M. Sanders, J. F. Stoddart, *Angew. Chem., Int. Ed.* **2002**, *41*, 898–952.

3 Y. Jin, C. Yu, R. J. Denman, W. Zhang, *Chem. Soc. Rev.* **2013**, *42*, 6634–6654.

4 J. M. Lehn, A. V. Eliseev, *Science* **2001**, *291*, 2331–2332.

5 P. T. Corbett, J. Leclaire, L. Vial, K. R. West, J. L. Wietor, J. K. M. Sanders, S. Otto, *Chem. Rev.* **2006**, *106*, 3652–3711.

6 R. F. Ludlow, S. Otto, *Chem. Soc. Rev.* **2008**, *37*, 101–108.

7 G. Gasparini, M. Dal Molin, L. J. Prins, *Eur. J. Org. Chem.* **2010**, 2429–2440.

8 R. A. R. Hunta, S. Otto, *Chem. Commun.* **2011**, *47*, 847–858.

9 S. Otto, *Acc. Chem. Res.* **2012**, *45*, 2200–2210.

10 E. Moulin, G. Cormos, N. Giuseppone, *Chem. Soc. Rev.* **2012**, *41*, 1031–1049.

11 F. B. L. Cougnon, J. K. M. Sanders, *Acc. Chem. Res.* **2012**, *45*, 2211–2221.

12 J. Li, P. Nowak, S. Otto, *J. Am. Chem. Soc.* **2013**, *135*, 9222–9239.

13 A. Herrmann, *Chem. Soc. Rev.* **2014**, *43*, 1899–1933.

14 S. Ulrich, P. Dumy, *Chem. Commun.* **2014**, *50*, 5810–5825.

15 M. E. Belowich, J. F. Stoddart, *Chem. Soc. Rev.* **2012**, *41*, 2003–2024.

16 A. Wilson, G. Gasparini, S. Matile, *Chem. Soc. Rev.* **2014**, *43*, 1948–1962.

17 D. Zhang, Li. Zhanting, 32, 2009, *Chin. J. Org. Chem.* **2012**, *32*, 2009–2017.

18 Y. Liu, Z.-T. Li, *Aust. J. Chem.* **2013**, *66*, 9–22.

19 G. Zhang, M. Mastalerz, *Chem. Soc. Rev.* **2014**, *43*, 1934–1947.

20 S. P. Black, J. K. M. Sanders, A. R. Stefankiewicz, *Chem. Soc. Rev.* **2014**, *43*, 1861–1872.

21 Y. Jin, Q. Wang, P. Taynton, W. Zhang, *Acc. Chem. Res.* **2014**, *47*, 1575–1586.

22 C. Yu, Y. Jin, W. Zhang, *Chem. Rec.* **2015**, *15*, 97–106.

23 O. Ramstrom, J. M. Lehn, *Nature Rev. Drug Discov.* **2002**, *1*, 26–36.

24 C. D. Meyer, C. S. Joiner, J. F. Stoddart, *Chem. Soc. Rev.* **2007**, *36*, 1705–1723.

25 J. W. Sadownik, R. V. Ulijn, *Curr. Opin. Biotechnol.* **2010**, *21*, 401–411.

26 T.-Y. Luh, *Acc. Chem. Res.* **2013**, *46*, 378–389.

27 N. Giuseppone, *Acc. Chem. Res.* **2012**, *45*, 2178–2188.

28 N. Roy, B. Bruchmann, J. M. Lehn, *Chem. Soc. Rev.* **2015**, *44*, 3786–3807.

29 H. Hofmeier, U. S. Schubert, *Chem. Commun.* **2005**, 2423–2432.

30 R. Paulini, K. Muller, F. Diederich, *Angew. Chem., Int. Ed.* **2005**, *44*, 1788–1805.

31 M. D. Yilmaz, J. Huskens, *Soft Matter* **2012**, *8*, 11768–11780.

32 S.-L. Li, T. Xiao, C. Lin, L. Wang, *Chem. Soc. Rev.* **2012**, *41*, 5950–5968.

33 M. L. Saha, S. De, S. Pramanik, M. Schmittel, *Chem. Soc. Rev.* **2013**, *42*, 6860–6909.

34 C. H. Wong, S. C. Zimmerman, *Chem. Commun.* **2013**, *49*, 1679–1695.

35 E. Elacqua, D. S. Lye, M. Weck, *Acc. Chem. Res.* **2014**, *47*, 2405–2416.

36 X.-Y. Hu, T. Xiao, C. Lin, F. Huang, L. Wang, *Acc. Chem. Res.* **2014**, *47*, 2041–2051.

37 D. K. Kumar, J. W. Steed, *Chem. Soc. Rev.* **2014**, *43*, 2080–2088.

38 X. J. Cai, C. Y. Dong, H. Q. Dong, G. M. Wang, G. M. Pauletti, X. J. Pan, H. Y. Wen, I. Mehl, Y. Y. Li, D. L. Shi, *Biomacromolecules* **2012**, *13*, 1024–1034.

39 N. Luisier, K. Schenk, K. Severin, *Chem. Commun.* **2014**, *50*, 10233–10236.

40 M. Hutin, G. Bernardinelli, J. R. Nitschke, *Chem. Eur. J.* **2008**, *14*, 4585–4593.

41 N. Christinat, R. Scopelliti, K. Severin, *Angew. Chem., Int. Ed.* **2008**, *47*, 1848–1852.

42 B. Içli, N. Christinat, J. Tönnemann, C. Schüttler, R. Scopelliti, K. Severin, *J. Am. Chem. Soc.* **2009**, *131*, 3154–3155.

43 B. Icli, E. Solari, B. Kilbas, R. Scopelliti, K. Severin, *Chem. Eur. J.* **2012**, *18*, 14867–14874.

44 Z. Rodriguez-Docampo, S. Otto, *Chem. Commun.* **2008**, 5301–5303.

45 A. G. Orrillo, A. M. Escalante, R. L. E. Furlan, *Chem. Commun.* **2008**, 5298–5300.

46 A. V. Gromova, J. M. Ciszewski, B. L. Miller, *Chem. Commun.* **2012**, *48*, 2131–2133.

47 J. Leclaire, L. Vial, S. Otto, J. K. M. Sanders, *Chem. Commun.* **2005**, 1959–1961.

48 M. von Delius, E. M. Geertsema, D. A. Leigh, D. T. D. Tang, *J. Am. Chem. Soc.* **2010**, *132*, 16134–16145.

49 M. von Delius, E. M. Geertsema, D. A. Leigh, *Nat. Chem.* **2010**, *2*, 96–101.

50 K. D. Okochi, Y. H. Jin, W. Zhang, *Chem. Commun.* **2013**, *49*, 4418–4420.

51 K. D. Okochi, G. S. Han, I. M. Aldridge, Y. Liu, W. Zhang, *Org. Lett.* **2013**, *15*, 4296–4299.

52 C. C. Chang, T. Emrick, *Macromolecules* **2014**, *47*, 1344–1350.

53 A. M. Escalante, A. G. Orrillo, R. L. E. Furlan, *J. Comb. Chem.* **2010**, *12*, 410–413.

54 A. M. Escalante, A. G. Orrillo, I. Cabezudo, R. L. E. Furlan, *Org. Lett.* **2012**, *14*, 5816–5819.

55 R. L. E. Furlan, Y. F. Ng, S. Otto, J. K. M. Sanders, *J. Am. Chem. Soc.* **2001**, *123*, 8876–8877.

56 G. Deng, F. Li, H. Yu, F. Liu, C. Liu, W. Sun, H. Jiang, Y. Chen, *ACS Macro Lett.* **2012**, *1*, 275–279.

57 W. G. Skene, J. M. P. Lehn, *Proc. Natl. Acad. Sci. USA* **2004**, *101*, 8270–8275.

58 J. M. Lehn, *Aust. J. Chem.* **2010**, *63*, 611–623.

59 N. Roy, E. Buhler, J. M. Lehn, *Polym. Int.* **2014**, *63*, 1400–1405.

60 Z. He, G. Ye, W. Jiang, *Chem. Eur. J.* **2015**, *21*, 3005–3012.

61 A. B. Pun, K. J. Gagnon, L. M. Klivansky, S. J. Teat, Z. T. Li, Y. Liu, *Org. Chem. Front.* **2014**, *1*, 167–175.

62 K. C. F. Leung, W. Y. Wong, F. Arico, P. C. Haussmann, J. F. Stoddart, *Org. Biomol. Chem.* **2010**, *8*, 83–89.

63 V. del Amo, A. M. Z. Slawin, D. Philp, *Org. Lett.* **2008**, *10*, 4589–4592.

64 B. H. Northrop, F. Arico, N. Tangchiavang, J. D. Badjic, J. F. Stoddart, *Org. Lett.* **2006**, *8*, 3899–3902.

65 A. R. Williams, B. H. Northrop, T. Chang, J. F. Stoddart, A. J. P. White, D. J. Williams, *Angew. Chem., Int. Ed.* **2006**, *45*, 6665–6669.

66 K. Acharyya, P. S. Mukherjee, *Chem. Eur. J.* **2014**, *20*, 1646–1657.

67 D.-W. Zhang, X. Zhao, J.-L. Hou, Z.-T. Li, *Chem. Rev.* **2012**, *112*, 5271–5316.

68 J.-B. Lin, X.-N. Xu, X.-K. Jiang, Z.-T. Li, *J. Org. Chem.* **2008**, *73*, 9403–9410.

69 X.-N. Xu, L. Wang, G.-T. Wang, J.-B. Lin, G.-Y. Li, X.-K. Jiang, Z.-T. Li, *Chem. Eur. J.* **2009**, *15*, 5763–5774.

70 L. Wang, G.-T. Wang, X. Zhao, X.-K. Jiang, Z.-T. Li, *J. Org. Chem.* **2011**, *76*, 3531–3535.

71 B.-Y. Lu, G.-J. Sun, J.-B. Lin, X.-K. Jiang, X. Zhao, Z.-T. Li, *Tetrahedron Lett.* **2010**, *51*, 3830–3835.

72 S. R. Beeren, J. K. M. Sanders, *J. Am. Chem. Soc.* **2011**, *133*, 3804–3807.

73 N. Roy, E. Buhler, J. M. Lehn, *Polym. Chem.* **2013**, *4*, 2949–2957.

74 L. Ratjen, J. M. Lehn, *RSC Adv.* **2014**, *4*, 50554–50557.

75 M. F. Li, K. Yamato, J. S. Ferguson, B. Gong, *J. Am. Chem. Soc.* **2006**, *128*, 12628–12629.

76 M. F. Li, K. Yamato, J. S. Ferguson, K. K. Singarapu, T. Szyperski, B. Gong, *J. Am. Chem. Soc.* **2008**, *130*, 491–500.

77 Q. Yang, L. Bai, Y. Zhang, F. Zhu, Y. Xu, Z. Shao, Y.-M. Shen, B. Gong, *Macromolecules* **2014**, *47*, 7431–7441.

78 A. T. ten Cate, P. Y. W. Dankers, R. P. Sijbesma, E. W. Meijer, *J. Org. Chem.* **2005**, *70*, 5799–5803.

79 S. Otto, S. Kubik, *J. Am. Chem. Soc.* **2003**, *125*, 7804–7805.

80 O. Ramström, J.-M. Lehn, *Chembiochem* **2000**, *1*, 41–48.

81 X. W. Yang, B. Gong, *Angew. Chem., Int. Ed.* **2005**, *44*, 1352–1356.

82 J. S. Zeng, W. Wang, P. C. Deng, W. Feng, J. J. Zhou, Y. Y. Yang, L. H. Yuan, K. Yamato, B. Gong, *Org. Lett.* **2011**, *13*, 3798–3801.

83 L. M. Klivansky, G. Koshkakaryan, D. Cap, Y. Liu, *Angew. Chem., Int. Ed.* **2009**, *48*, 4185–4189.

84 A. Pun, D. A. Hanifi, G. Kiel, E. O'Brien, Y. Liu, *Angew. Chem., Int. Ed.* **2012**, *51*, 13119–13122.

85 G. Koshkakaryan, D. Cao, L. M. Klivansky, S. J. Teat, J. L. Tran, Y. Liu, *Org. Lett.* **2010**, *12*, 1528–1531.

86 L. Chen, H. Wang, D.-W. Zhang, Y. Zhou, Z.-T. Li, *Angew. Chem., Int. Ed.* **2015**, *54*, 4028–4031.

87 D.-W. Zhang, J. Tian, L. Chen, L. Zhang, Z.-T. Li, *Chem. Asian J.* **2015**, *10*, 56–68.

88 Y.-C. Zhang, D.-W. Zhang, H. Wang, Y. Zhou, Z.-T. Li, *Polym. Chem.* **2015**, *6*, 4404–4408.

89 H. Y. Au-Yeung, F. B. L. Cougnon, S. Otto, G. D. Pantos, J. K. M. Sanders, *Chem. Sci.* **2010**, *1*, 567–574.

90 H. Y. Au-Yeung, P. Pengo, G. D. Pantos, S. Otto, J. K. M. Sanders, *Chem. Commun.* **2009**, 419–421.

91 J. M. A. Carnall, C. A. Waudby, A. M. Belenguer, M. C. A. Stuart, J. J. P. Peyralans, S. Otto, *Science* **2010**, *327*, 1502–1506.

92 J. W. Li, J. M. A. Carnall, M. C. A. Stuart, S. Otto, *Angew. Chem., Int. Ed.* **2011**, *50*, 8384–8386.

93 F. B. L. Cougnon, N. A. Jenkins, G. D. Pantos, J. K. M. Sanders, *Angew. Chem., Int. Ed.* **2012**, *51*, 1443–1447.

94 F. B. L. Cougnon, N. Ponnuswamy, N. A. Jenkins, G. D. Pantos, J. K. M. Sanders, *J. Am. Chem. Soc.* **2012**, *134*, 19129–19135.

95 H. Y. Au-Yeung, G. D. Pantos, J. K. M. Sanders, *J. Am. Chem. Soc.* **2009**, *131*, 16030-+.

96 H. Yang, Y. Bai, B. Yu, Z. Wang, X. Zhang, *Polym. Chem.* **2014**, *5*, 6439–6443.

97 N. Sakai, M. Lista, O. Kel, S. Sakurai, D. Emery, J. Mareda, E. Vauthey, S. Matile, *J. Am. Chem. Soc.* **2011**, *133*, 15224–15227.

98 N. Sakai, S. Matile, *J. Am. Chem. Soc.* **2011**, *133*, 18542–18545.

99 S. Hagihara, H. Tanaka, S. Matile, *J. Am. Chem. Soc.* **2008**, *130*, 5656–5657.

100 S. Hagihara, H. Tanaka, S. Matile, *Org. Biomol. Chem.* **2008**, *6*, 2259–2262.

6

Self-sorting through Dynamic Covalent Chemistry

Chia-Wei Hsu and Ognjen Š. Miljanić

6.1 Definition of Self-sorting

The concept of *sorting* is intuitive to anyone who has ever dealt with a load of clean laundry. Starting with a messy pile of clothes, one organizes this complex and disordered system into a series of drawers, each containing a simpler, more ordered system: socks, shirts, underwear, etc. Indeed, *Webster's Third New International Dictionary* defines the verb "to sort" as "to put in a given place or rank according to kind, class, or nature".[1] Implicit in this definition is the operator, the "one who puts things into place". Could sorting of inanimate things in such a macroscopic context operate without an operator? In the case of laundry as we known it, the answer is unfortunately negative, but one could envision more sophisticated objects that could sort themselves in the absence of an intelligent operator. Imagine that all socks were less dense than all shirts, which in turn were less dense than all underwear. In such a scenario, a powerful enough air stream would effectively be able to sort this mixture. While the question of intelligent design still remains here (who turned on the air stream?), it is again intuitive that this sorting procedure would operate under a simple external stimulus, and that objects themselves would be endowed with a property that allows them to *self-sort*.

It is perhaps appropriate now to switch from socks and shirts to the microscopic world of molecules. The first part of the analogy is clear: our laundry pile is a complex mixture of many molecules, while our neat drawers approximate either isolated individual compounds, or – more conceptually – compounds that engage in reactivity without interference from each other. This analogy also highlights the potential importance of sorting in real life. Messy mixtures – often derived from naturally abundant sources – could be employed in industrial settings to produce multiple value-added chemicals in a single reactor without the need for tedious and expensive purification. The non-interfering reactivity of many molecules present in the same physical space is the basis of metabolism of complex organisms, and the undesirable interference of metabolic pathways is behind many pathological conditions. Finally, molecular recognition processes could be coordinated and scaled up to result in macroscopic self-sorting events.[2]

In a microscopic realm, an intelligent operator is severely constrained in their ability to manipulate objects directly: simple movement of individual molecules into separate

piles is both (currently) impossible and impractical for large-scale production. Thus, the operation is limited to the application of relatively rudimentary external stimuli – chemical reagents, supramolecular guests, solvents, heating, or cooling – and it is up to the properties of molecules to determine whether self-sorting will happen. In other words, we can never actively sort molecules; they will either self-sort under an externally applied stimulus, or will not sort at all.

Chemical self-sorting has been defined and reviewed previously. In a seminal 2003 paper, Wu and Isaacs defined self-sorting as the "high-fidelity recognition of self from non-self", and introduced the concepts of "thermodynamic self-sorting" and "kinetic self-sorting".[3] Thermodynamically self-sorting systems were defined as those which are self-sorted at their thermodynamic equilibrium state; all others were classified as kinetically self-sorting systems. In addition, the authors defined "narcissistic self-sorting" and "social self-sorting". The former was described as a situation where molecules of a given kind have a high affinity for themselves (Scheme 6.1, pathway B), while the latter referred to a situation where molecules have a high affinity for molecules of a different kind (Scheme 6.1, pathways A, C, and D).

In his 2015 review,[4] Schalley took a systems chemistry[5] approach to describing self-sorting systems by pointing out that self-sorting (or absence thereof) results from a network of competing recognition processes among the mixture components; these processes are controlled by the binding constants between all the possible pairs of those components. Schalley also introduced a distinction between the *integrative* and *non-integrative* self-sorting processes.[6,7] The latter were defined as those self-sorting events that just lead to the formation of a smaller than the maximum possible set of discrete complexes or adducts from the subunits present in the mixture (Scheme 6.1, pathways B–D). In contrast, integrative self-sorting was defined as a process which results in a single complex, in which more than two different subunits bind in two or more recognition events, with some positional control (Scheme 6.1, pathway A). The most comprehensive reviews of self-sorting were published by Würthner[8] in 2011, and Saha and Schmittel in 2012.[9] The former focused on self-sorting of systems through reversible non-covalent interactions (including metal–ligand bonds), while the latter centered on metal–organic systems, and endeavored to put self-sorting events on a quantitative footing, introducing the concept of a *degree of self-sorting.*
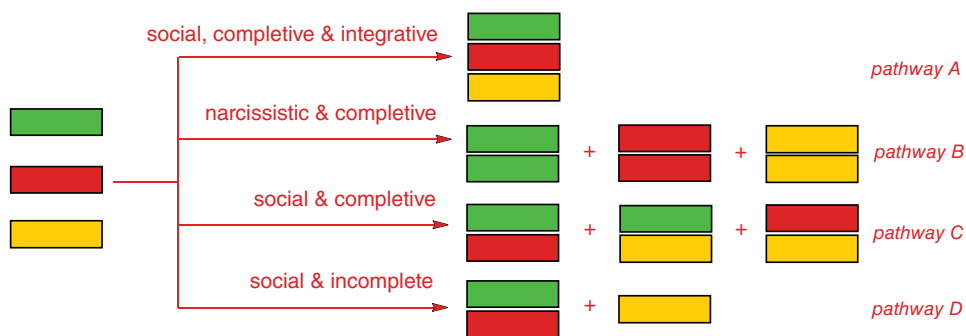
Scheme 6.1 Schematic representation of different kinds of self-sorting processes.

In our own previous reviews,[10,11] self-sorting was defined as the "spontaneous transformation of a low-order multicomponent system into several high-order sub-systems with fewer components". Implicit in this definition is a distinction between self-sorting and self-assembly. While both are ordering processes, and both commonly involve molecular recognition, self-sorting transforms a complex mixture into several ordered sub-systems, while self-assembly results in a single ordered assembly (but could leave a disordered and uninteresting mixture of products in the solution). This definition has some commonalities with Saha and Schmittel's distinction of *incomplete* and *completive self-sorting* events;[9,12] the latter are defined as processes that make quantitative use of all members of the library to produce one or several assemblies (Scheme 6.1, pathways A–C), while the former leave unused components (Scheme 6.1, pathway D).

Given this abundance of recent high-quality reviews of the field, we will not strive here to present a comprehensive, all-encompassing review. In fact, we hope that the reader will view our contribution as a personal account of our adventures – mostly in the realm of kinetic self-sorting – and will build their comprehensive image of self-sorting by consulting our and the other mentioned reviews. Our review will be limited to self-sorting processes in which interchange of components occurs through the formation and breakage of dynamic covalent bonds,[13–15] and thus many beautiful examples based on hydrogen bond exchange and other non-covalent interactions will not be covered. We will consider metal–ligand bonds as dynamic and covalent, but will only describe our subjective selection of the most illustrative ones; the reader is referred to accounts published by Schmittel,[9] Nitschke,[16] and Stang[17] for more comprehensive surveys. We will begin by reviewing thermodynamically controlled self-sorting, proceed to kinetically controlled phenomena, and close with a view on what future may hold for these systems.

6.2 Thermodynamically Controlled Self-sorting

6.2.1 Purely Organic Systems

One of the pioneering examples of self-sorting in an entirely organic chemistry context was demonstrated by Sanders.[18] Exposure of an equimolar mixture of **1** and **2** to a transesterification catalyst (MeOK/18-crown-6 in PhMe) resulted in dominant generation of a homotrimer of **1** (**3**) and homodimer of **2** (**4**), with minimal amounts of crossover products (Scheme 6.2). Thermodynamic control in this reaction was confirmed by control experiments in which separately prepared conjugates of **1** and **2** were subjected to transesterification conditions and found to again yield only a mixture of the trimer **3** and dimer **4**.

A mixture of two flexible cyclic dialdehydes (**5** and **6**) and two rigid aromatic amines (**7** and **8**) has been shown to self-sort at equilibrium into size-matched couples (Scheme 6.3).[19] While initially mismatched complexes formed, in which the larger macrocyclic dialdehyde **6** flexed and formed imines with both **7** and **8**, after equilibration the final composition revealed the two size-matched species **9** and **10** as the exclusive products.

Hafezi and Lehn constructed[20] a [2 × 2] imine DCL by combining equimolar amounts of one hydrophilic and one hydrophobic aldehyde with equimolar amounts of one
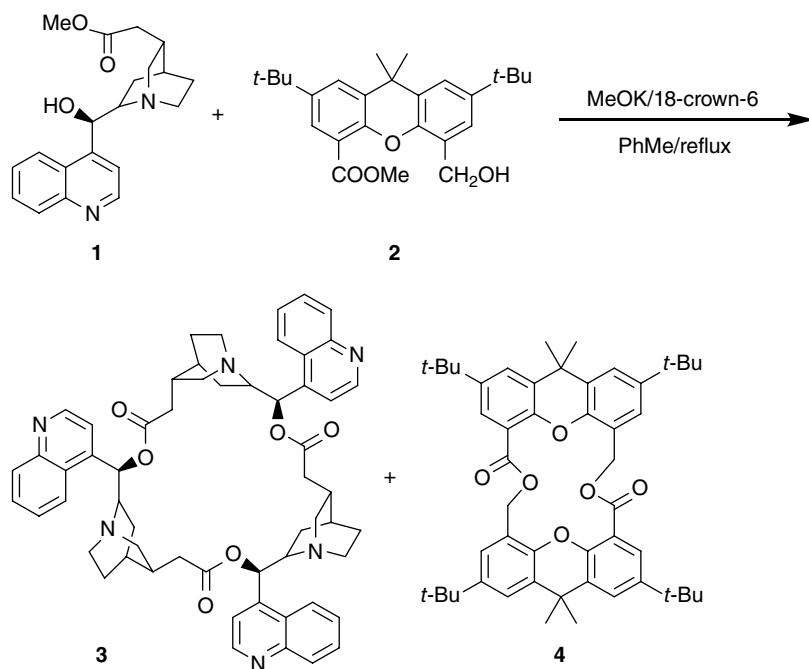
Scheme 6.2 Thermodynamically controlled self-sorting of an ester dynamic combinatorial library (DCL).

hydrophilic and one hydrophobic amine. In a mixed MeCN/H$_2$O solvent, all four possible imines were observed in roughly equimolar amounts. However, when the mixture was induced to phase separate by addition of NaCl or cooling, the mixture self-sorted to yield only two imines: the one composed of two hydrophobic constituents in the MeCN phase, and the one combining the two hydrophilic components in the aqueous phase. The self-sorting process was found to be reversible; upon phase reunification, the mixture returned to the original composition, with minor deviations explained as a consequence of imine hydrolysis. The same group later showed[21] that this self-sorting system can be rendered photoactive by replacing imines with a hydrazine, which is both prone to photoinduced *E/Z* isomerization and capable of binding Ca^{2+} in its *E* form. On irradiation, hydrazone is converted into a weakly cation-binding *Z* form, which releases free Ca^{2+}, causing phase separation.

Severin and coworkers have observed integrative self-sorting of DCLs with two operative exchange reactions: imine and boronic ester formation. Starting with 4-formylphenylboronic acid (**11**), triamine (**12**), and pentaerythritol (**13**, Scheme 6.4), ball-milling produced[22] a cage structure **14** in 94% yield; performing the same reaction in EtOH as a solvent resulted in isolation of **14** in lower 56% yield. Despite the potential competition between aldehydes and boronic acids for pentaerythitol as the resource, a single self-sorted structure was produced. Two-dimensional macrocycles could be produced analogously,[23] and this work was also extended to borasiloxane-[24] and borophosphate-based[25] cages and macrocycles.
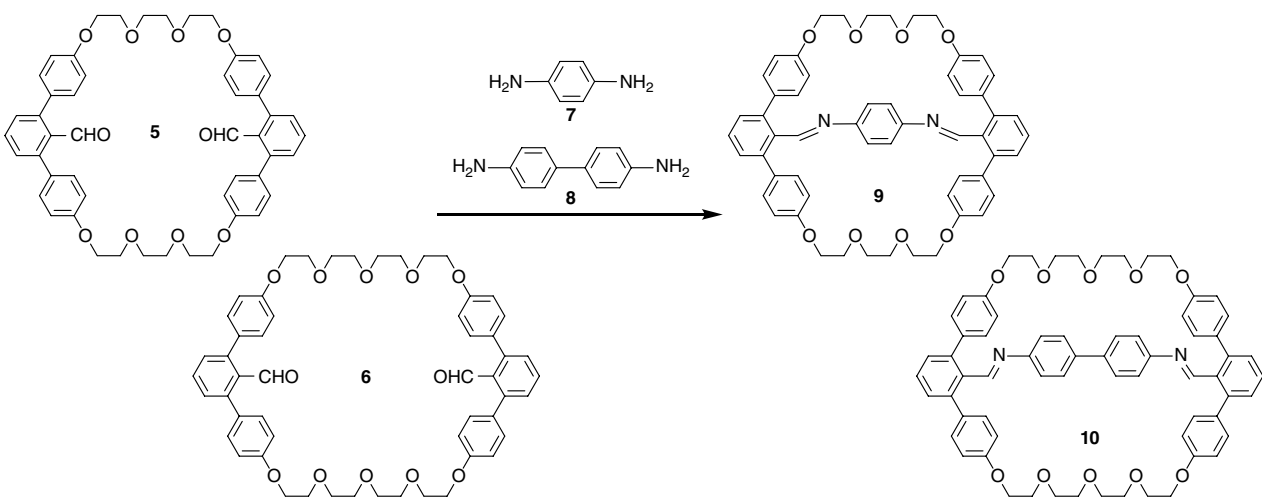
Scheme 6.3 Self-sorting of diamine/dialdehyde mixture during the course of formation of two size-matched imines.
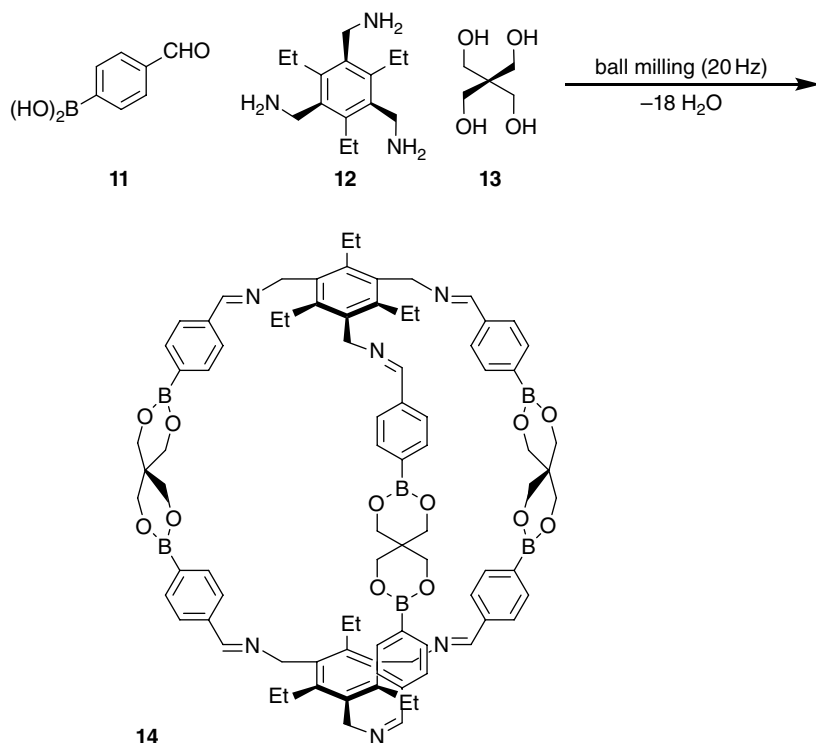
Scheme 6.4 Integrative self-sorting in the synthesis of a molecular cage (**14**) by Severin *et al.*

We have shown that self-sorting in DCLs can be achieved in systems with as many as four operational exchange reactions.[26] As a model system, we chose five reversible reactions, all of which are catalyzed by Brønsted acids: (*a*) imine formation from aldehydes and primary amines, (*b*) acetalization of aldehydes with alcohols, (*c*) boronic ester formation from alcohols and boronic acids, (*d*) alkene formation through intramolecular dehydration of alcohols, and (*e*) esterification of carboxylic acids and alcohols. If all five of these reactions were set to operate on a common set of starting materials, some significant interference between the five would be expected. For example, an aldehyde would have a choice of reaction with an amine or with an alcohol (pathways *a* and *b*), while an alcohol would have a choice of pathways *b*–*e*. However, an experiment has shown that not to be the case. In a reaction of aldehyde **15**, boronic acid **16**, amine **17**, diol **18**, alcohols **19** and **20**, and carboxylic acid **21**, only four products were observed (Scheme 6.5): imine **22** (formed from **15** and **17**, 93%), boronic ester **23** (from **16** and diol **18**), ester **24** (from **19** and **21**), and alkene **25** formed by dehydration of **20**. The mixture in effect self-sorted into a single imine, boronic acid, ester, and alkene product. The origins of this selectivity are unclear. While a thermodynamic argument for greater stability of the push–pull imine **22** could be made on resonance grounds, the attempted equilibration of a mixture of imine, ester, and acetal products was not observed, suggesting a kinetic preference.
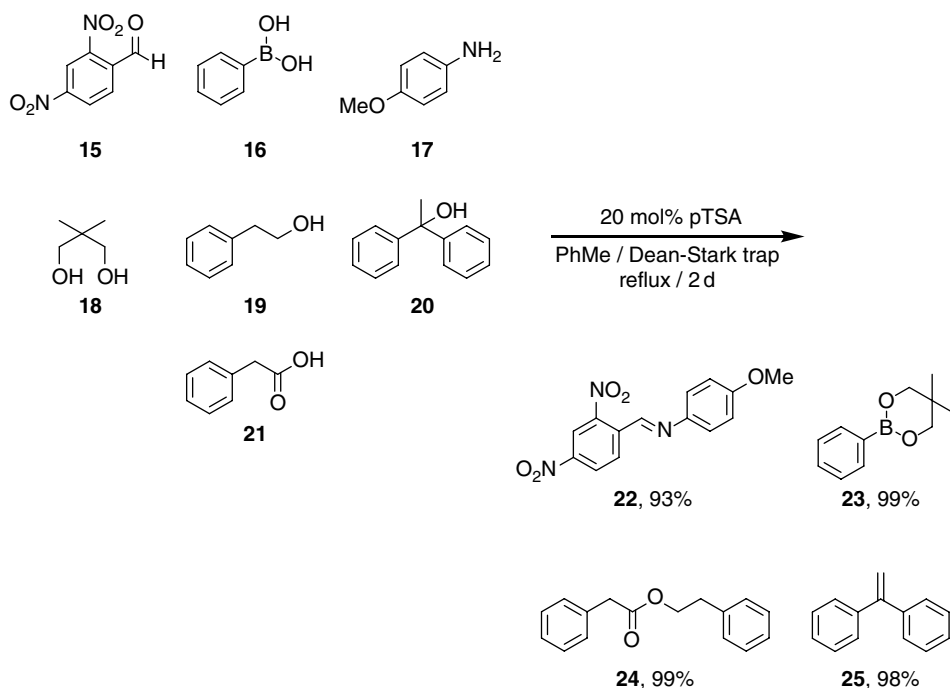
Scheme 6.5 Four dynamic reactions can proceed simultaneously and without interference to give four discrete products, despite the fact that other species are also possible products from the given pool of starting materials.

6.2.2 Metal–Organic Systems

Among the first observations of thermodynamically controlled self-sorting in metal–organic systems was Lehn's discovery of self-recognizing transition metal helicate complexes.[27] His previous work demonstrated that ligands such as **26** or **27** (Scheme 6.6), as well as their extended analogs with three or four bipyridine sites, will dimerize in the presence of Cu(I) to produce helical complexes in which Cu(I) coordinates in a tetrahedral geometry to two bipyridine units from two different molecules, causing a helical twist.[28] A more complex experiment probed the outcome of an experiment in which a mixture of these ligand precursors was exposed to a Cu(I) source, and it was found that mixed helicates are not formed despite their entropic favorability, instead the two exclusive products were $[\mathbf{26}_2Cu_2]^{2+}$ and $[\mathbf{27}_2Cu_3]^{3+}$ (Scheme 6.6). Similar self-sorting and exclusive formation of homomeric complexes was observed on exposure of more complex mixtures of bipyridine ligands to Cu(I).

In a further extension of this strategy, Lehn and coworkers have shown that Ni(II) will assemble with analogs of **26** and **27** (in which methyl groups were positioned *meta* relative to pyridine nitrogens, rather than *ortho*) into triple helicates, in which the octahedral environment around the metal results in the helical twist and coordination of three ligands.[29] Reaction of an equimolar mixture of Cu(I) and Ni(II) with a 3:2 mixture of **28** (Scheme 6.7) and **29** (unsubstituted analog of **27**) resulted in a double
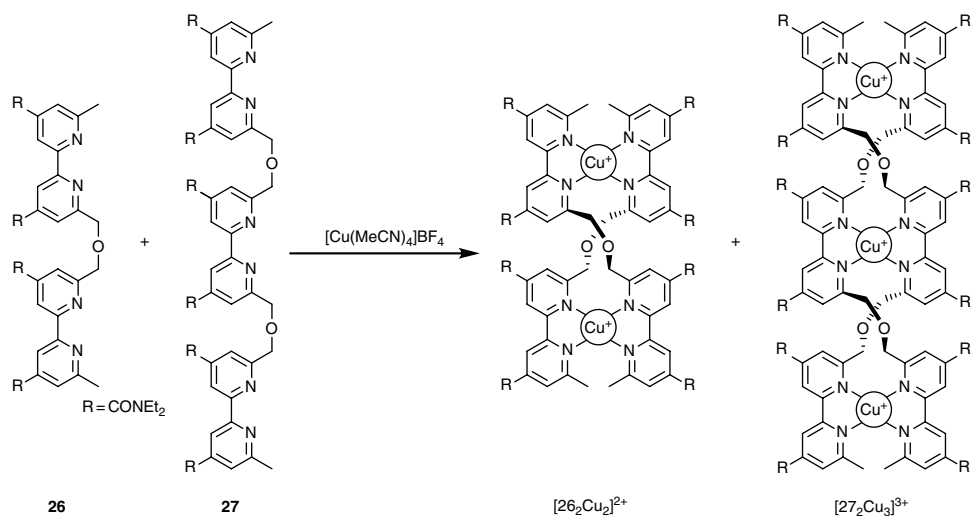
Scheme 6.6 Self-sorting of ligands **26** and **27** into two distinct helicates $[26_2Cu_2]^{2+}$ and $[27_2Cu_3]^{3+}$ in the presence of Cu(I).
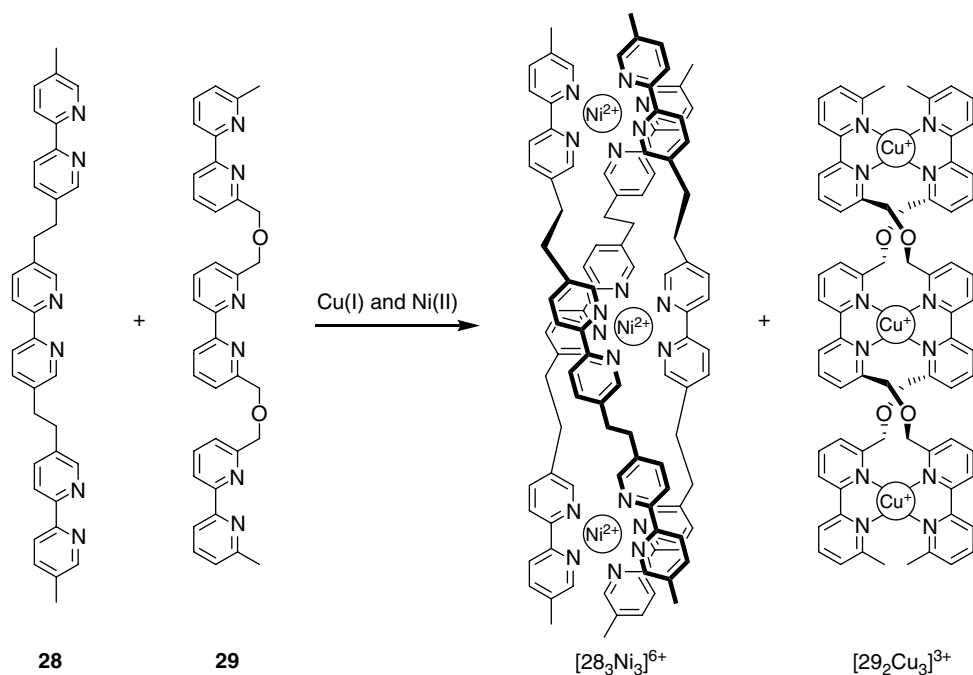
Scheme 6.7 Double self-sorting is observed in a mixture of **28**, **29**, Cu(I), and Ni(II); both ligands and both metals choose their preferred coordination partner, to produce a single double ($[29_2Cu_3]^{3+}$) and a single triple ($[28_3Ni_3]^{6+}$) helicate product.

recognition event, wherein the mixture components segregated into one double (out of three possible) and one triple (out of four possible) helix. The double helix contained only **29** and Cu(I), while the triple helix contained only **28** and Ni(II). This outcome was explained by the steric preference of the more crowded octahedral coordination environment around Ni(II) for the ligand with the more exposed bypiridine sites, that is, **28**.

Taylor and Anderson demonstrated length-dependent self-sorting of rigid oligoporphyrin/Zn(II) tapes into cooperatively assembled porphyrin ladders in the presence of 1,4-diazabicyclo[2.2.2]octane (DABCO), which coordinated to Zn(II) centers in adjacent strands.[30]

Nitschke and coworkers combined two dynamic reactions – imine exchange and ligand–metal coordination – in a series of papers aimed at utilizing imines as ligands for assemblies with transition metals in water. While imines typically quickly hydrolyze in water, binding to a transition metal stabilizes them; in some cases, that stabilization goes both ways, for example Cu(I) is stabilized against oxidation by coordination to an imine. One of their first forays in this area was the development of dynamic Cu(I) helicates,[31] similar in shape to those of Lehn, but different in that they require no ligand synthesis: Cu(I) simply amplifies the best-binding imine from the DCL created from multiple aldehydes and anilines (an example of a helicate structure is shown in Figure 6.1).

In a pioneering 2005 study,[32] Nitschke showed that a 4:2:3 mixture of **31**, **32**, and **33** produces just two discrete complexes ($[\mathbf{34}_2Cu]^{3-}$ and $[\mathbf{35}_2Cu_2]^{2+}$, Scheme 6.8) when mixed with CuBF$_4$, despite the possible existence of many potential mixed imine ligands.

In a more complex version of this experiment (Scheme 6.9), a mixture of two precursor aldehydes (**32** and **36**) and two amines (**37** and **38**) was treated with two
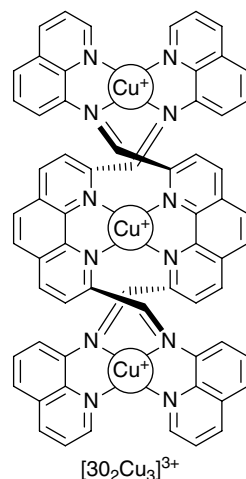
Figure 6.1 An example of a dynamic Cu(I) helicate prepared by Nitschke *et al.* through *in situ* formation of an imine ligand from precursor aldehyde and amines.

$[\mathbf{30}_2Cu_3]^{3+}$
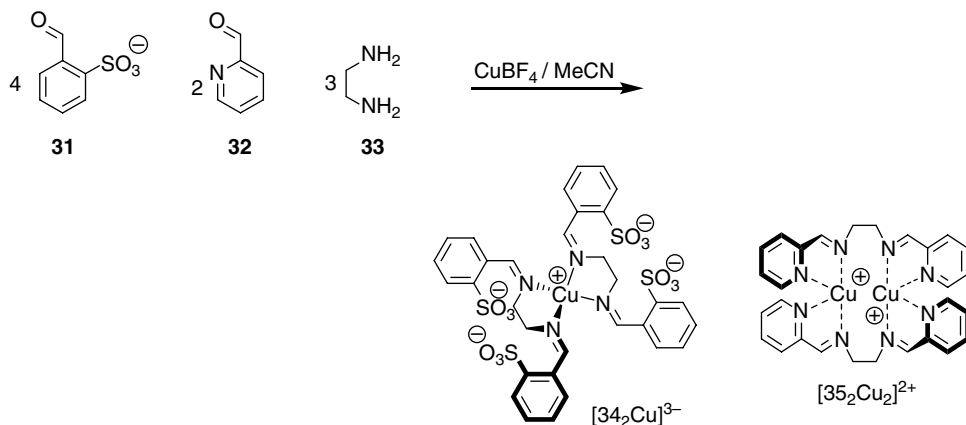
Scheme 6.8 Self-sorting of a mixture of three precursors into just two imine–Cu(I) complexes on exposure to Cu(I).
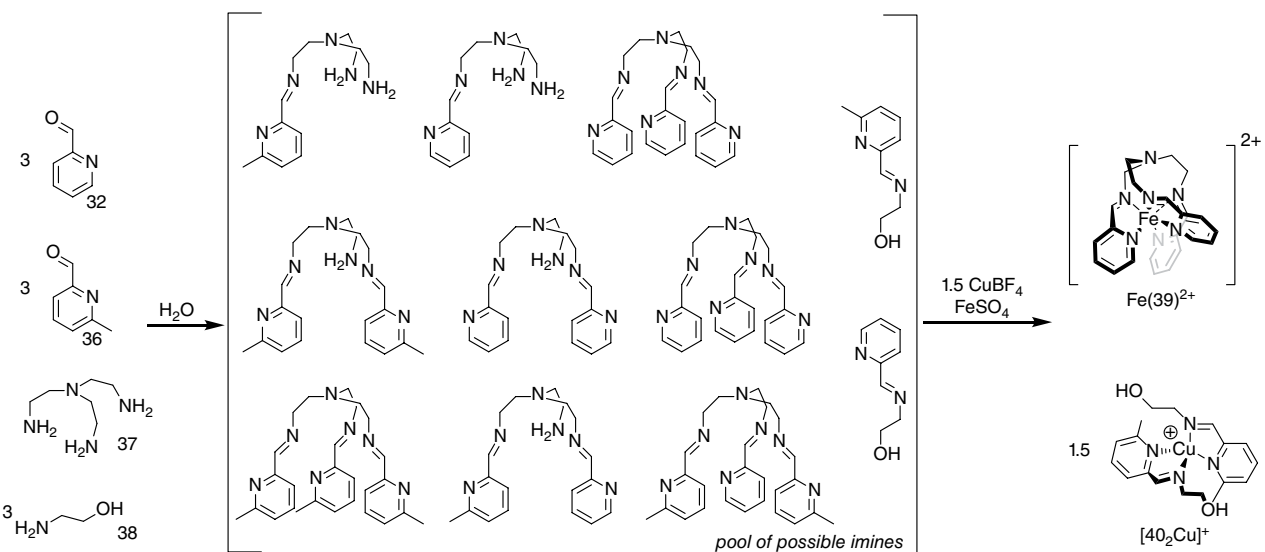
Scheme 6.9 Self-sorting of a mixture of four precursors into just two chelating ligand imines, which bind to Fe(II) and Cu(I) in octahedral and tetrahedral geometries, respectively.

metals: tetrahedral Cu(I) and octahedral Fe(II).[33] Eleven imine combinations could have possibly formed, but in the presence of the two metal sources this DCL collapsed in composition to just two imines that were the superior ligands for Fe(II) and Cu(I), thus only two imine/metal complexes were isolated: Fe(**39**)$^{2+}$ and [**40**$_2$Cu]$^+$. The high-fidelity self-sorting observed in this experiment was particularly noteworthy in light of its ability to distinguish between the structurally closely related aldehydes **32** and **36**, which differed only in the addition of a methyl group. Despite this minute difference, Cu(I) appeared to favor binding to imines derived from the methylated aldehyde (presumably on account of its more electron-rich nature), while Fe(II) in contrast avoided the methylated precursor, as it would lead to unfavorable steric clashes in the hexadentate imine complex.

In the realm of imine complexes that formed cage-like structures, Nitschke *et al.* have shown that a mixture of trisamines **41** and **42**, and diamine **8** (Scheme 6.10) produces three discrete tetrahedral cages when exposed to excess of 2-formylpyridine and Zn(II) at 70 °C.[34] Out of many possible combinations, only narcissistically self-sorted cages [**43**$_4$Zn$_4$]$^{8+}$, [**44**$_4$Zn$_4$]$^{8+}$, and [**45**$_6$Zn$_4$]$^{8+}$ were observed. This observation was rationalized as a consequence of different sizes of **41** and **42**, and different binding geometries in **41**/**42** (and their derivative imines **43**/**44**) on one hand, and **8** (and the derived **45**) on the other. These self-sorted structures then translated into distinct guest-binding functions, namely it was found that cages [**43**$_4$Zn$_4$]$^{8+}$ and [**45**$_6$Zn$_4$]$^{8+}$ both bind anions, but not neutral guests, while host [**44**$_4$Zn$_4$]$^{8+}$ binds small neutral guests such as *t*-BuOH or cyclohexane, but not anions. Furthermore, the larger cage [**45**$_6$Zn$_4$]$^{8+}$ was capable of binding the large PF$_6^-$ anion, while [**43**$_4$Zn$_4$]$^{8+}$ could not and was limited to smaller species like ClO$_4^-$, I$^-$, NO$_3^-$, and BF$_4^-$. This selectivity was capitalized on in an experiment where an equimolar mixture of the three cages was exposed to 40 equivalents of PF$_6^-$, 2 equivalents of NO$_3^-$, and 4 equivalents of cyclohexane. Only three complexes could be detected: [**45**$_6$Zn$_4$]$^{8+}$·PF$_6^-$, [**44**$_4$Zn$_4$]$^{8+}$·cyclohexane, and [**43**$_4$Zn$_4$]$^{8+}$·NO$_3^-$ (not shown in Scheme 6.10).

Differences in stability among the three cages could be used to selectively and sequentially release guests from their interior. Specifically, treating a mixture of host–guest complexes with 4-methoxyaniline – an amine that forms a more stable imine with 2-formylpyridine and thus destroys the imine constituents of the cages –resulted first in the decomposition of [**45**$_6$Zn$_4$]$^{8+}$ (and the release of PF$_6^-$), then [**44**$_4$Zn$_4$]$^{8+}$ (and the concomitant release of cyclohexane), and finally [**43**$_4$Zn$_4$]$^{8+}$ (which released the nitrate anion). This series of experiments was a powerful demonstration of the potential of self-sorting to produce sophisticated and functional assemblies. It was also conceptually expanded to include a cascade of chemical reactions, resulting in a "self-organizing chemical assembly line".[35]

Nitschke and co-workers also demonstrated[36] that a mixture of aminopyridine ligand **46** (Scheme 6.11), 2-formylpyridine, Fe(OTf)$_2$, and Pt(PhCN)$_2$Cl$_2$ will result in a single complex **47** formed through integrative self-sorting. In this thermodynamically controlled event, *in situ* formation of an imine between the free amino group of **46** and 2-formylpyridine creates a chelating ligand with two coordination sites. Three of these ligands bind to a single Fe(II) center, satisfying its octahedral geometry. The leftover pyridine moiety coordinates to Pt(II) in a 4:1 stoichiometry and square planar geometry, producing an overall cubic assembly in which Pt(II) resides at the center of each of the cube's six faces.
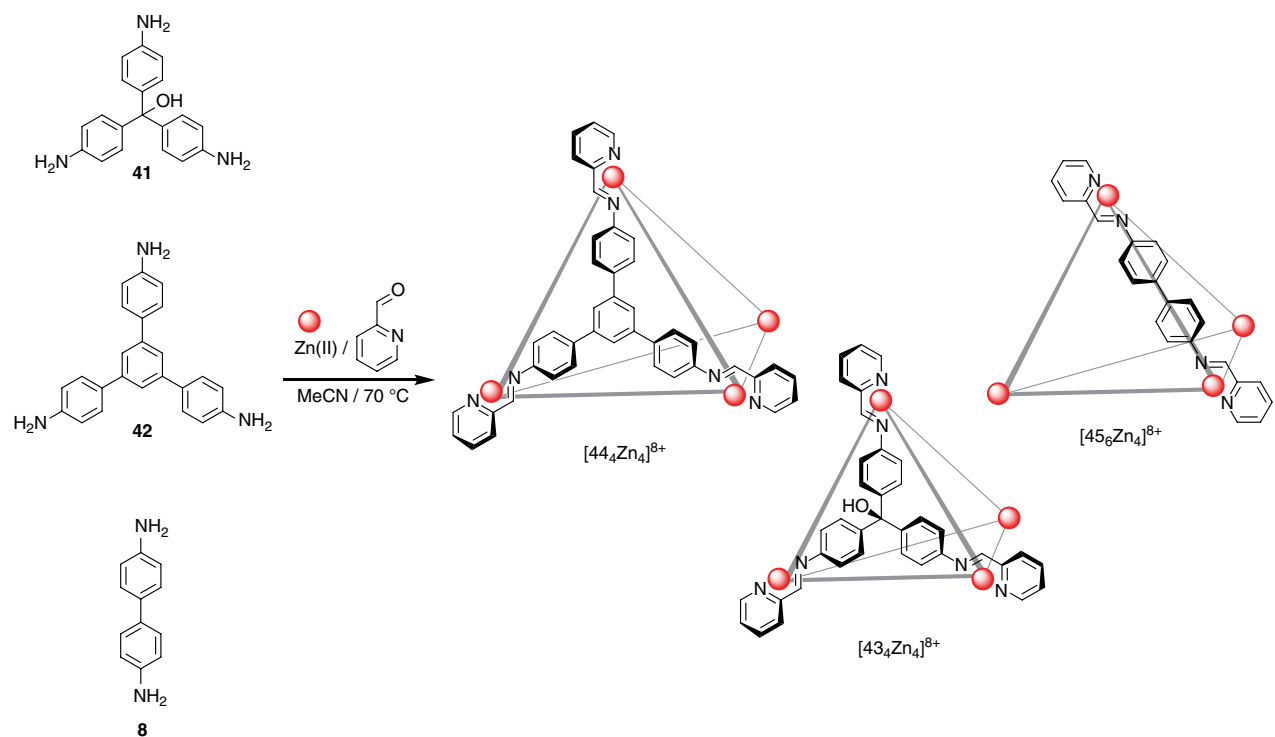
Scheme 6.10 Narcissistic self-sorting of three imine-based ligands on coordination to Zn(II) is caused by differences in their shape and size, and has been explored in the context of selective capture and release of anionic and neutral guests.
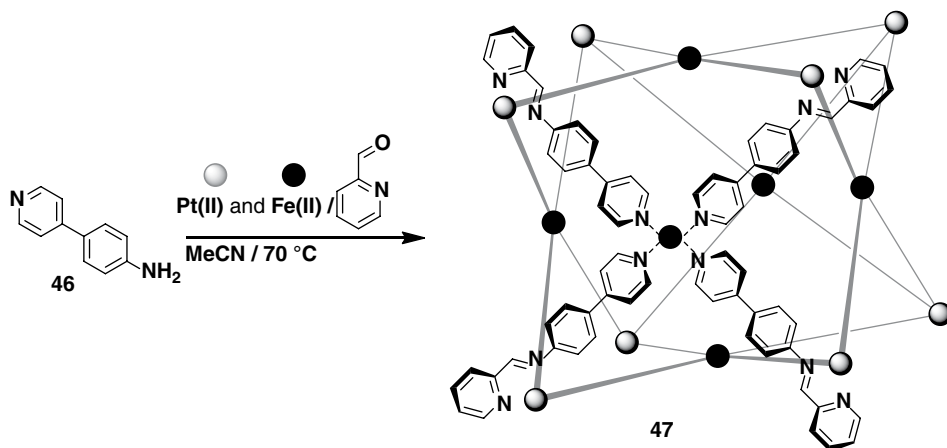
Scheme 6.11 Integrative self-sorting of a four-component mixture into a single metal–organic cube **47**.

Stang *et al.* described self-sorting in dynamic systems based on the exchange between multiple organoplatinum acceptors and pyridyl donors.[37] The high fidelity of this self-sorting process was achieved by using rigid precursors whose geometries and bonding angles dictated the formation of some and prohibited the formation of other assemblies. In the example shown in Scheme 6.12, anthracene-based diplatinum pincer compound **48** was exposed to an equimolar mixture of linear pyridyl-capped ligands **49** and **50** and trigonal **51**. It coordinated to all three offered ligands, but in a strictly sorted fashion, forming two rectangular complexes **52** and **53** (but no crossover product, which would be trapezoid in shape) and a double-decker trigonal prism in which **51** coordinated with **48** in 2:3 stoichiometry. Similar behavior was observed with diplatinum precursors in which the angle between the two available valences was 60°; these precursors favored triangular assemblies.[38] In fact, the rigidity of precursors in both the rectangular and triangular series resulted in self-sorting that was *shape-selective*, showing high preference for the formation of more symmetric structures, that is, equilateral vs. scalene triangles, rectangles vs. trapezoids. These shape requirements then also translated into *size selectivity*: ligands of different lengths always segregated into complexes which combined multiple copies of one ligand, excluding the shorter or longer analogs.[39] However, a linear ligand "connector" could not distinguish between the corners with 0° and 120° angles between the available valences, resulting in unselective formation of both rectangular and triangular assemblies if both corner subunits were present.[38]

The same group has also made forays in the area of directional self-sorting, wherein ligands orient in a precisely controlled arrangement in a complex structure. Specifically, using an unsymmetric bipyridine species **55** (Scheme 6.13),[40] in which one pyridine site was rendered less accessible than the other through double *ortho* substitution, only one of the four possible isomeric metallamacrocycles was created. In the exclusive product **56**, dipyridine substituents are oriented in a strict head-to-tail arrangement to avoid steric clashes between the *ortho*-methyl groups in the square planar geometry around Pt(II). When ligands with a less sterically crowded pyridine site were used (shown in an insert in Scheme 6.13), similar positional selectivity was not observed.
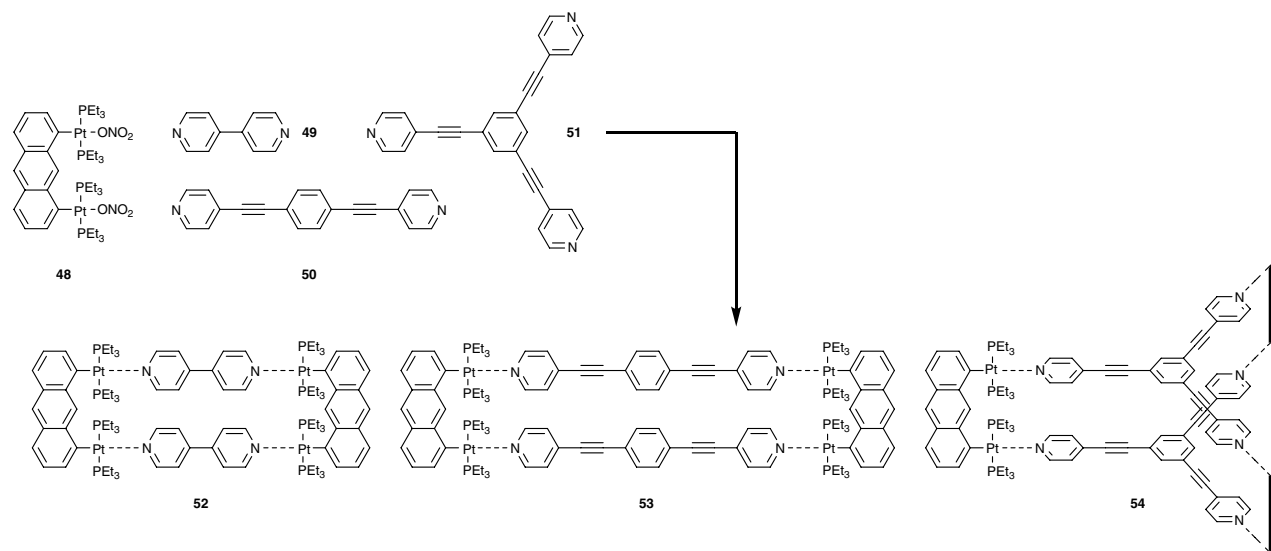
Scheme 6.12 Narcissistic self-sorting of a mixture of ligands **49–51** into three dimeric complexes **52–54** held together by anthracene-based diplatinum pincer **48**.
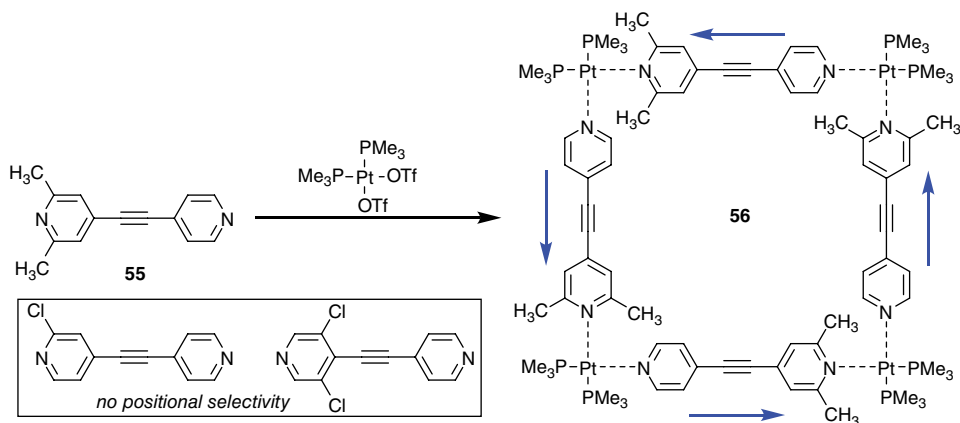
Scheme 6.13 Positional self-sorting in the assembly of a supramolecular square **56** from Pt(II) and unsymmetric dipyridine ligand **55**. Less sterically bulky ligands (insert) did not show similar selectivity.

Hooley's group at the University of California at Riverside has been active in the area of self-sorting of metal–organic capsules. Their initial studies showed that steric effects on substituents placed on the inside of the cluster play an important role in controlling the outcome of self-sorting of these clusters,[41] namely, bipyridine-based pincer ligands such as **57** (Scheme 6.14) have been shown to assemble into clusters with Pd(II), in which the stoichiometric ratio of ligand/Pd was 4:2. By substituting the central benzene ring of **57** between the two alkynyl substituents, functional groups could be placed in the interior of the resultant capsule. However, this ability for placement was not without limitations. Thus, Hooley found that combining **57** and its more bulky analog **58** in the presence of Pd(II) resulted in the exclusive formation of just two products: $[\mathbf{57}_4Pd_2]^{4+}$ and $[\mathbf{57}_3\mathbf{58}Pd_2]^{4+}$. Ligand **58** is simply too large to permit more than one copy of itself in the cluster and thus must surround itself with three copies of **57**. In parallel, ligand **57** forms a homotetrameric cluster $[\mathbf{57}_4Pd_2]^{4+}$, which has no similar steric qualms.

The same group has recently shown that sets of structurally remarkably similar imine ligands will narcissistically self-sort when exposed to $Fe(ClO_4)_2$.[42] In this experiment, four structurally similar amines were used: xanthone-derived **59** and **60–62**, which were derived from dibenzosuberone (Figure 6.2). In these compounds, the coordination angles between the two amino groups were determined to be 125.18°, 93.22°, 87.87°, and 86.75°. On exposure to 2 equivalents of 2-formylpyridine and 0.67 equivalents of $Fe(ClO_4)_2$ in MeCN, all four amines formed double imines, which then coordinated to Fe(II) in an overall 3:2 stoichiometry (an example of such a complex is shown in Figure 6.2, right). In more complex experiments where mixtures of proligands **60–62** were exposed to an excess of 2-formylpyridine and Fe(II), self-sorting behavior was observed, namely, each ligand narcissistically formed complexes with two more copies of itself, rather than engaging in mixed–ligand complexes. Furthermore, if the same set of proligands was exposed to just enough 2-formylpyridine and Fe(II) to form a single 3:2 complex, selectivity was observed. Ligand **60** reacted first, followed by **62**, followed by **61**, thus the self-sorting process could be controlled to yield three, two, or just one pure product. Interestingly, despite the large different coordination angle in **59**, its
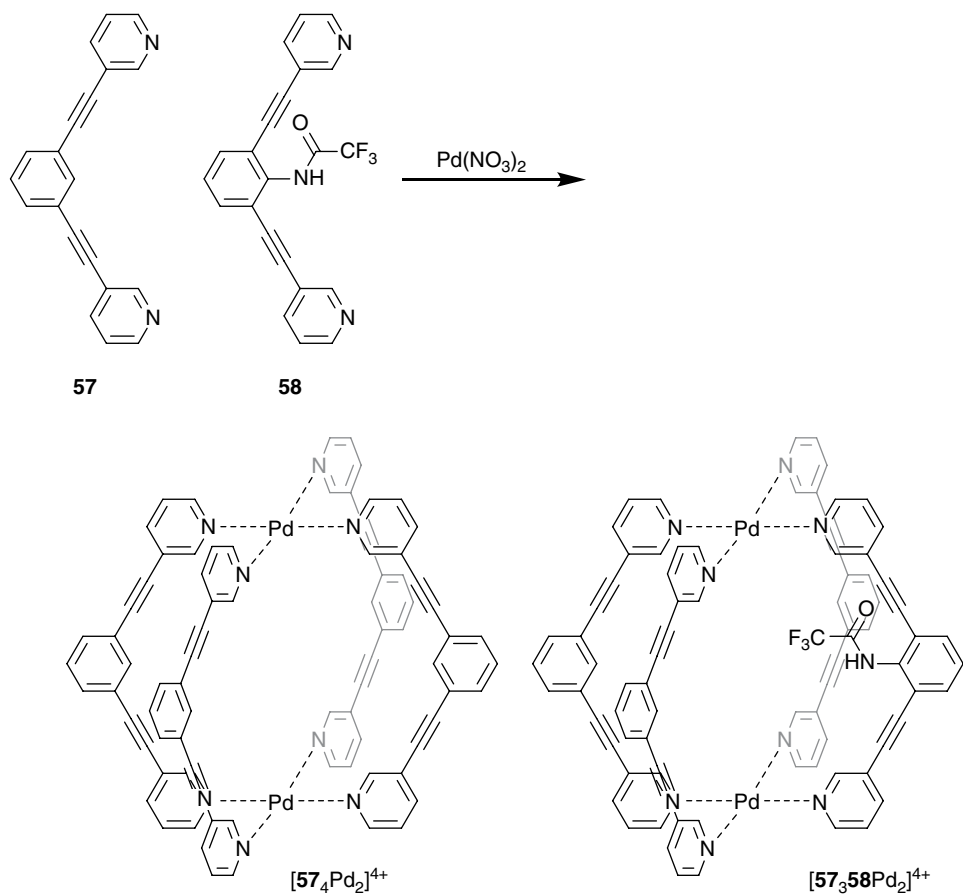
Scheme 6.14 Self-sorting of two pincer-shape bipyridine ligands **57** and **58** into 4:0 and 3:1 clusters $[\mathbf{57}_4\text{Pd}_2]^{4+}$ and $[\mathbf{57}_3\mathbf{58}\text{Pd}_2]^{4+}$, respectively.
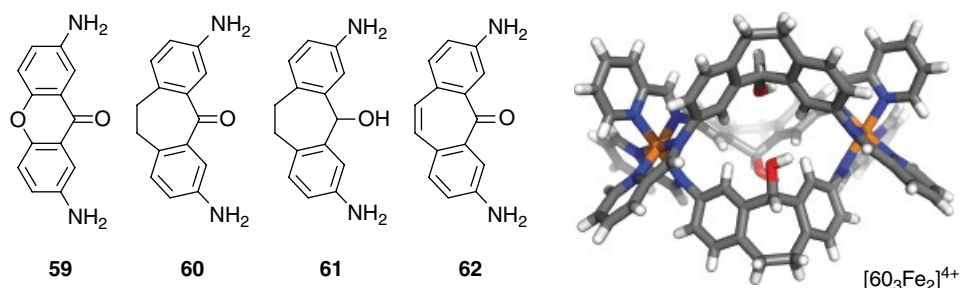
Figure 6.2 Structurally related diamine proligands **59–62** used by Hooley *et al.* in the synthesis of narcissistically self-sorting capsules. A crystal structure of an exemplary capsule, derived from **60**, is shown on the far right.

ability to discriminate among other ligands in Fe complexes was much worse, and heterocomplexes were routinely observed. The authors postulated that the very subtle differences in the structure of the original ligands are amplified when these ligands distort to form a complex; apparent avoidance of mismatching distortions was given as the putative reason for the observed self-sorting.

Continuing with the exploration of this process, Hooley's group designed a series of structurally related bis(salicylhydrazone) ligands with their salicylhydrazone moieties positioned at different angles. On exposure of this mixture to various lanthanide salts, only narcissistic assemblies were formed.[43] Hooley's group also showed that metal coordination, together with hydrogen bonding, can result in inducing chiral self-sorting of a prochiral imine ligand.[44]

While all of the above examples relied on homomeric self-sorting, wherein multiple copies of the same ligand "found" a metal and created a highly symmetric complex, Schmittel and coworkers focused their attention on the programmed preparation of low-symmetry complexes with irregular structures. This work was reviewed by Schmittel in 2012,[9] and we will therefore focus on key pre-2012 examples and most recent developments.

In 2010, Schmittel and co-workers reported an eight-component self-sorting process that resulted in a supramolecular scalene triangle.[45] Construction of this novel and highly challenging supramolecular macrocycle with a low-symmetry structure was a consequence of a well-developed self-sorting process that the same group previously established. Schmittel *et al.* have invested much time in developing electronically and sterically tuned ligands that would predictably form heteroleptic complexes with Cu(I) and Zn(II).[12,46] Thus, when an equimolar mixture of **63–68**, Zn(II), and Cu(I) (Scheme 6.15) was created, only three discrete complexes were formed: $[Zn(\mathbf{63})(\mathbf{64})]^{2+}$, $[Cu(\mathbf{66})(\mathbf{67})]^+$, and $\mathbf{65}\cdot\mathbf{68}$. Thermodynamic stability is behind the exclusive formation of these three species. Ligands **63** and **67** are too bulky to form homoleptic complexes; ligands **64** and **66** are not bulky, but still prefer to form heteroleptic complexes with **63** and **67** due to an additional $[\pi\cdots\pi]$ stacking stabilization coming from their pendant aryl groups. Finally, Zn-porphyrin **68** prohibits steric access to all ligands but 4-iodopyridine (**65**). The final piece of selectivity comes from the metal: Zn(II) coordinates to **63** and **64** to form a pentacoordinate metal center (a situation in which Cu(I) cannot find itself), with possible additional coordination from one of the four oxygens in methoxy groups. While isolated Cu(I) could form heteroleptic complexes with **63** and **66**, or with **67** and **66**, in the presence of Zn(II), which consumes all **63**, it forms only the latter, resulting in a self-sorted state.

With this self-sorting system well understood, the three supramolecular synthons could be relied on to form orthogonally even more complex architectures. Thus, in the extension of this study, Schmittel reported that precursors **69** (in which **65** and **67** are covalently linked), **70** (which combined **64** and **66**), and **71** (linking **63** and **68**) self-assembled in the presence of equimolar amounts of Cu(I) and Zn(II) into a scalene triangle (Scheme 6.16). The distances between the corners of the triangle were calculated to be 1.84, 1.60, and 1.44 nm.

In 2013, the same group applied a similar self-sorting strategy to the preparation of a low-symmetry scalene quadrilateral (Scheme 6.17).[47] Using a mixture of precursors **71–75**, and Zn(II) and Cu(I) in a precisely controlled 2:1 stoichiometry, a scalene
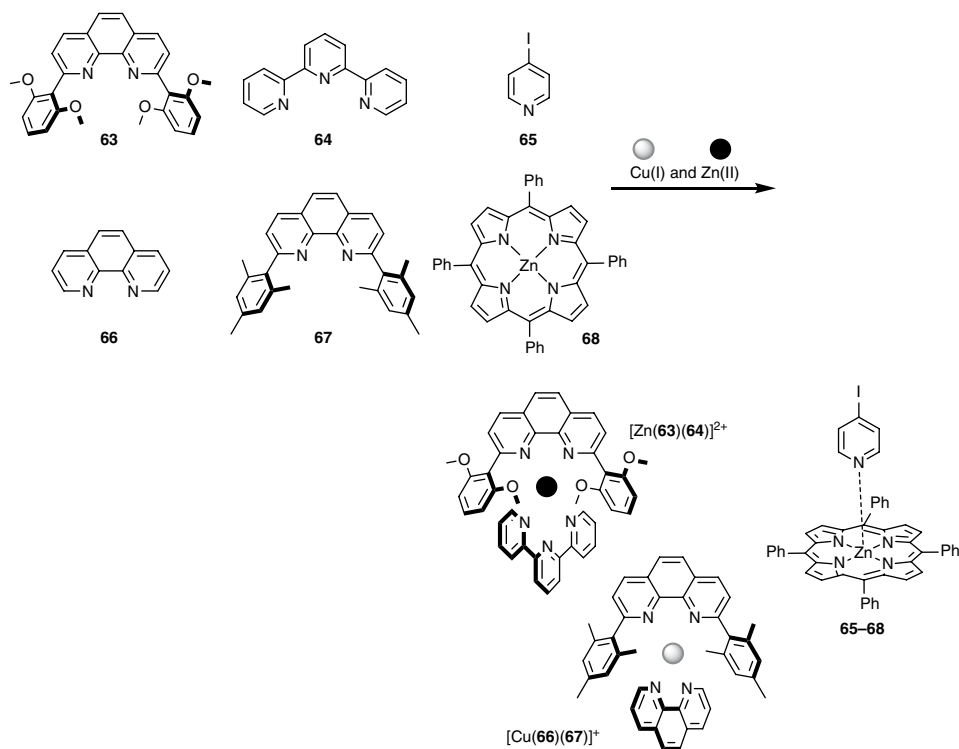
Scheme 6.15 Self-sorting of ligands **63–68** into three exclusive heteroleptic complexes in the presence of Cu(I) and Zn(II).

quadrilateral was formed with Zn(II) centers on two corners, Zn-porphyrin on one, and Cu(I) on the last corner. While the crystal structure of this macrocyclic compound could not be obtained, ^{1}H NMR spectroscopy and computations confirmed its low-symmetry structure: the distances between metal centers were calculated to be 1.98, 1.83, 1.60, and 1.50 nm. This remarkable and fully orthogonal assembly process presented an example of both integrative and completive self-sorting. A similar strategy was subsequently applied in the synthesis of a metallosupramolecular pentagon with sides of uneven length (1.76, 1.74, 1.74, 1.68, and 1.51 nm).[48]

Very recently, this group has reported a redox-dependent self-sorting process which operates a rotary switch between two stations.[49]

6.3 Kinetically Controlled Self-sorting

Kinetically controlled self-sorting processes are less common than their thermodynamic counterparts, but are arguably more relevant as models of biological systems that operate far from equilibrium.[50,51] Since 2010, our group has been very active in the area of kinetically controlled self-sorting of DCLs. We have developed a series of protocols that use an irreversible chemical or physical stimulus to reduce a DCL in
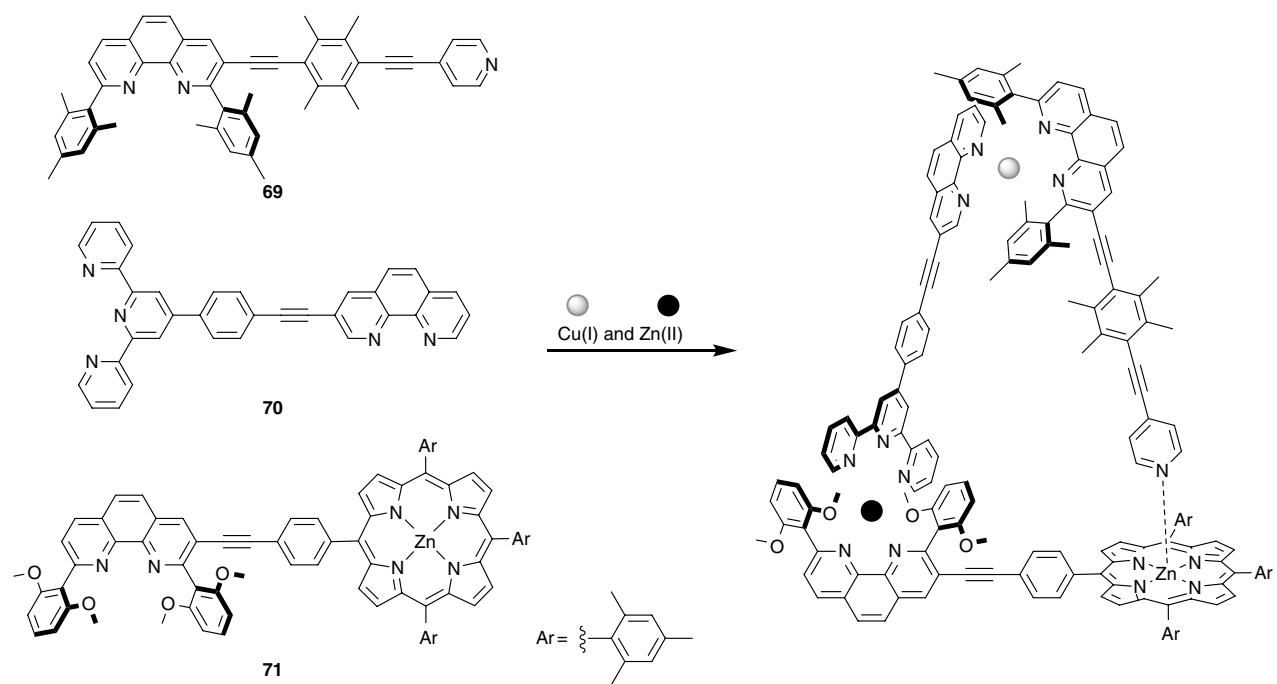
Scheme 6.16 Integrative and completive self-sorting of an equimolar mixture of **69**, **70**, and **71** in the presence of Cu(I) and Zn(II) results in the production of a scalene supramolecular triangle.
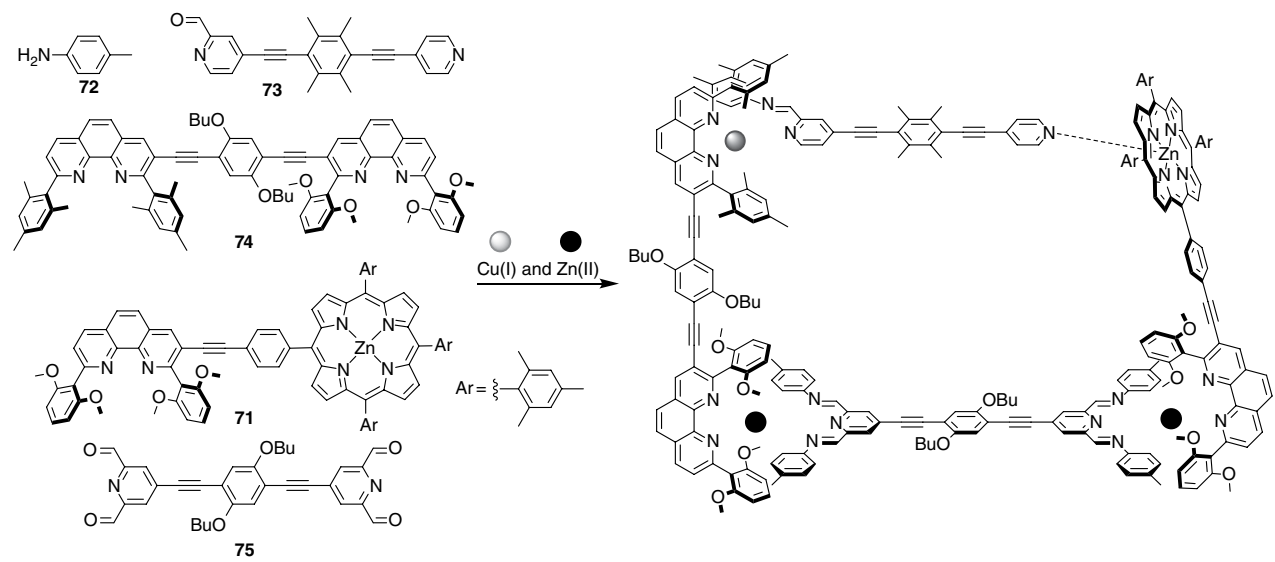
Scheme 6.17 Integrative and completive self-sorting of a seven-component mixture into a scalene quadrilateral.

complexity, typically from n^2 to n members. All of these protocols, which will be described in detail below, share some characteristics:

a) They operate in an open system which does not reach equilibrium until the self-sorting process is completed.
b) They do involve an equilibrating mixture of compounds that responds to disturbances in concentrations of individual components.
c) The external stimulus has to be selective enough to operate quickly on the fastest-responding component of the DCL, allowing other DCL components to produce more of the fast-responding member without responding to the stimulus themselves.
d) The external stimulus is iteratively ramped up in intensity to target more and more members of these libraries.

The operation of these protocols can be schematically represented using the matrices shown in Scheme 6.18.[52] Imagine a DCL constructed by a random reaction of five compounds of one kind (**A–E**) and five compounds of another kind (**76–80**), with the constraint that compounds of one kind do not react with the compounds of the same

	A	B	C	D	E
76	1.0	1.0	1.0	1.0	1.0
77	1.0	1.0	1.0	1.0	1.0
78	1.0	1.0	1.0	1.0	1.0
79	1.0	1.0	1.0	1.0	1.0
80	1.0	1.0	1.0	1.0	1.0

▶

	A	B	C	D	E
76	5.0	—	—	—	—
77	—	5.0	—	—	—
78	—	—	5.0	—	—
79	—	—	—	5.0	—
80	—	—	—	—	5.0

	A	B	C	D
76	1.0	1.0	1.0	1.0
77	1.0	1.0	1.0	1.0
78	1.0	1.0	1.0	1.0
79	1.0	1.0	1.0	1.0
80	1.0	1.0	1.0	1.0

▶

	A	B	C	D
76	4.0	—	—	—
77	1.0	3.0	—	—
78	—	2.0	2.0	—
79	—	—	3.0	1.0
80	—	—	—	4.0

	A	B	C	D	E
76	1.0	1.0	1.0	1.0	1.0
77	1.0	1.0	1.0	1.0	1.0
78	1.0	1.0	1.0	1.0	1.0
79	1.0	1.0	1.0	1.0	1.0
80	16.0	1.0	1.0	1.0	1.0

▶

	A	B	C	D	E
76	5.0	—	—	—	—
77	5.0	—	—	—	—
78	5.0	—	—	—	—
79	5.0	—	—	—	—
80	—	5.0	5.0	5.0	5.0

Scheme 6.18 DCLs can be viewed as matrices, and their self-sorting results in a redistribution of matrix components. Tables show the predicted outcome of self-sorting of an equimolar [5×5] DCL (top), an equimolar [4×5] DCL (center), and a non-equimolar [5×5] DCL (bottom).

kind, but can react with any compound of the other kind, and always in 1:1 stoichiometry. This system would then produce a [5 × 5] library of adducts, labeled **A76–E80**. Let us further assume that the responsiveness of components to a given stimulus drops off from **76** to **80** and **A** to **E**, and that the total responsiveness of adduct products is simply an additive combination of the responsivenesses of individual constituents of the adduct. Finally, let us assume that the unselective reaction between two strictly equimolar mixtures produces roughly equimolar amounts of all adducts **A76–E80**.

What happens when an external stimulus is selectively applied to this mixture? Compound **A76** will respond to the irreversible stimulus first and will be removed from the DCL (either physically or *de facto* chemically by being rendered unreactive). As **A76** is depleted from the DCL, all other library members that share either component **A** or component **76** with it (i.e., adducts **A77**, **A78**, **A79**, **A80**, **B76**, **C76**, **D76**, and **E76**) will react among themselves to replenish the consumed **A76**. If this process continues, it will eventually consume not just **A76** but also all eight other adducts that shared either of their constituents with **A76**. This irreversible stimulus would thus produce a five-fold excess of **A76** compared to the amount originally present in the DCL, while simultaneously reducing the DCL in complexity to a smaller [4 × 4] library. If the external stimulus is increased in intensity, it will then target the next most-responsive compound in the remaining DCL, namely **B77**. Its removal from the mixture will result in the subsequent disappearance of **B78**, **B79**, **B80**, **C77**, **D77**, and **E77** as these six compounds are sacrificed to make more of the rapidly depleting **B77**. A smaller [3 × 3] library will also be formed, from which **C78** could be isolated next, and so on, until the original 25-member DCL is reduced to just five pure compounds, **A76**, **B77**, **C78**, **D79**, and **E80**, all of which will be produced in five-fold excess compared to their original amounts. Conceptually, a square [*n* × *n*] equimolar matrix will result in the *n*-fold amplification of its diagonal members and disappearance of all others.

This general behavior is not limited to square matrices. In the case of an equimolar rectangular [*n* × *m*] matrix such as the one shown in Scheme 6.18, initial application of the irreversible stimulus will target **A76**, just like before. However, the matrix now cannot produce 5 equivalents of **A76** because it will run out of **76**, of which only 4 equivalents are present. Therefore, the first application of the stimulus creates 4 equivalents of **A76**, before it runs out of **76**. The self-sorting process then moves on to **A77**, of which 1 equivalent is generated (because we run out of **A**), and then zigzags its way down the diagonal, producing **B77** (3 equivalents, before we run out of **77**), **B78** (2 equivalents, before we run out of **B**), **C78** (2 equivalents, before we run out of **78**), and so on. While the overall simplification is not as dramatic as in the case of an equimolar square matrix, this experiment still amplifies well-defined DCL components in well-defined (and non-equimolar) stoichiometries, which will be important in cases where self-sorting processes need to produce very different amounts of desired products.

Finally, non-equimolar matrices are also supposed to undergo predictable simplification during a self-sorting event. The [5 × 5] matrix shown in Scheme 6.18 is equimolar with respect to all components except **A80**, which is present in a 16-fold excess. Application of a self-sorting stimulus to this DCL will produce 5 equivalents each of **A76**, **A77**, **A78**, and **A79** (before running out of **76**, **77**, **78**, and **79**, respectively). At that point, all 20 equivalents of **A** would have been consumed, and DCL would not have been able to produce any **A80**; instead, it would move on to producing 5 equivalents each of **B80**, **C80**, **D80**, and **E80**. In effect, an equimolar [*n* × *n*] DCL amplifies each of the diagonal members *n*-fold; if one DCL member is present in excess at the beginning

of a self-sorting process, self-sorting will simply "pull" this diagonal distribution toward the component present in excess. Similarly, deficit of one DCL member will "push" the diagonal distribution away from the component present in a lower amount than all the others.

In the next two subsections, this general principle will be illustrated for several procedures developed in our and other laboratories.

6.3.1 Self-sorting of Dynamic Libraries during Irreversible Chemical Reactions

Biological systems are capable of exerting exquisite spatiotemporal control over the chemoselectivity of numerous chemical reactions occurring within a typical cell. Components of metabolic pathways selectively recognize each other in this complex environment, and effectively sort into their respective pathways either under chemical (highly specific enzymatic catalysis) or physical (compartmentalization within cellular organelles) influences. An analogous ability to accomplish chemoselective reactivity in a fully synthetic mixture of compounds would have potential ramifications not only as a model for biology, but also as a platform for selective production of multiple value-added chemicals from complex ("messy") mixtures of precursors. This development could lead to dramatic savings in chemical industry, on account of eliminating the requirement for pristine starting materials.

In our original entry into the arena of kinetically controlled self-sorting, we used different oxidation rates of imine-based DCL members to effect self-sorting.[53] When a dynamic library of nine imines **81–89** (formed by an unselective reaction of three constituent aldehydes and three anilines**)** was subjected to mildly oxidative conditions, imine **83** oxidized first as it contained the most electron-rich aldehyde and aniline components (Scheme 6.19). As outline above, removal of **83** also resulted in the production of benzimidazole **90** and elimination of **81**, **82**, **86**, and **89** from the library, and the generation of a smaller four-compound reduced DCL. Increasing the temperature and resubjecting this smaller DCL to oxidation resulted in the oxidation of **85** into benzoxazole **91**, and left the oxidation-inert imine **87** as the residual compound. In effect, a [3 × 3] DCL was reduced into just three pure compounds, as DCL members traded their aldehyde and aniline constituents to eventually end up with pairs that could oxidize fastest under given circumstances.

In this protocol, control of the relative rates of oxidation and imine exchange was critical for the high fidelity of self-sorting. The rate of oxidation had to be kept significantly lower than that of imine exchange to allow the DCL enough time to re-equilibrate continuously during the process. This was achieved by using iodine as a weak oxidant; more potent oxidants such as 2,3-dichloro-5,6-dicyano-1,4-benzoquinone (DDQ) or chloranil, oxidized the mixture quickly and unselectively, effectively "freezing" the imine mixture composition and translating almost all imines in the DCL into their oxidized products. The second factor was the rate of iodine addition. By slowly adding iodine via a syringe pump, its concentration could be kept low, slowing the oxidation down while leaving the rate of imine exchange unchanged. This factor also had a profound influence on the product selectivity: slow addition resulted in a self-sorted state where electron-rich/electron-rich aldehyde/aniline combinations were dominant. In contrast, instantaneous addition of iodine resulted in a significantly lower selectivity of oxidation, but now electron-rich/electron-poor combinations dominated, as those imines were more stable at equilibrium.[54]
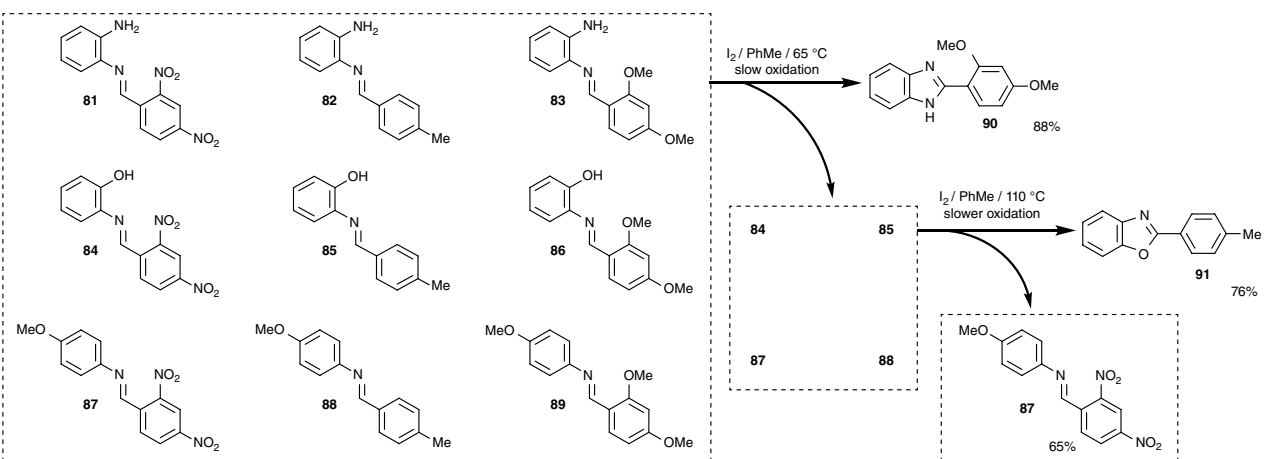
Scheme 6.19 Self-sorting of a dynamic [3×3] imine library during the course of an irreversible oxidation.

Kinetically controlled self-sorting can also be viewed as an iterative dynamic kinetic resolution of complex libraries. Ramström and co-workers have shown that a DCL composed of 10 nitroaldol adducts (formed by a random reaction of five aldehydes with 2-nitropropane) can be dynamically resolved during its reaction with *p*-chlorophenyl acetate in the presence of *Burkholderia cepacia* PS-C I lipase. Instead of 10 possible acetylation products, only two were observed in 53% and 33% yields and high enantiomeric purities. Relatively modest isolated yields would characterize these processes as low fidelity.[54] The same group subsequently demonstrated double kinetic resolution of a DCL composed of 24 Strecker adducts (formed by a reaction of TMSCN with a [3 × 4] imine DCL), wherein the lipase enzyme selected both the most reactive aldehyde and amine components in the acetylation reaction.[55]

Dynamic self-replication processes[56] are also a variant of self-sorting, in which components of a dynamic mixture sort into several systems, one of which is autocatalytic. These fascinating processes are of obvious interest in the theories of the origin of life.[57] Philp and co-workers have demonstrated self-replicating behavior in a DCL, wherein one component of an imine DCL catalyzed its own formation from precursor aldehydes and amines.[58] However, as this was an equilibrium process, self-replication could not change the overall distribution of DCL components, it only affected how quickly the equilibrium was established. To get around this thermodynamic limitation, Philp *et al.* introduced an irreversible final reaction that created a product which on one hand catalyzed its own formation, and on the other was no longer subject to equilibration.[59,60] This concept was practically realized in the mixed imine/nitrone DCL shown in Scheme 6.20. An equimolar mixture of aldehydes **92** and **93**, 4-fluoroaniline (**94**), and hydroxylamine **95** produced a DCL with two imines (**96** and **99**) and two nitrones (**97** and **98**). Exposure of this DCL to maleimide **100** resulted in an initially irreversible cycloaddition, wherein the two nitrones formed cycloadducts **101** and **102**, both present as mixtures of *cis* and *trans* isomers, but the imines did not react. Out of the four products, however, only *trans*-**101** could template its own formation by organizing into a ternary complex with its precursors **97** and **100**. Formation of this complex accelerated the rate of a selective cycloaddition between **97** and **100** approximately 100-fold; after 16 h, *trans*-**101** constituted about 80% of the product pool. The autocatalytic properties of *trans*-**101** were confirmed by kinetic studies and separate seeding control experiments.

Kinetic self-sorting is intimately guided by the Curtin–Hammett principle[61] as it operates best under fast equilibration conditions, wherein the chemoselectivity of the process is guided by the relative differences in the rates of (slow) irreversible reactions that remove material from equilibrium. Its applications are thus quite general, as any chemical process that satisfies these basic kinetic requirements should be expected to demonstrate self-sorting behavior. In fact, physical stimuli are equally well suited for the task, and the next section will review examples of self-sorting of DCLs under physical stimuli.

6.3.2 Self-sorting of Dynamic Libraries under Physical Stimuli

In 2011, we showed that complex imine-based DCLs could be reduced in complexity through distillative self-sorting.[62] The use of distillation to shift the chemical equilibrium has been amply precedented: it is the stuff of textbooks and is also the basis of a
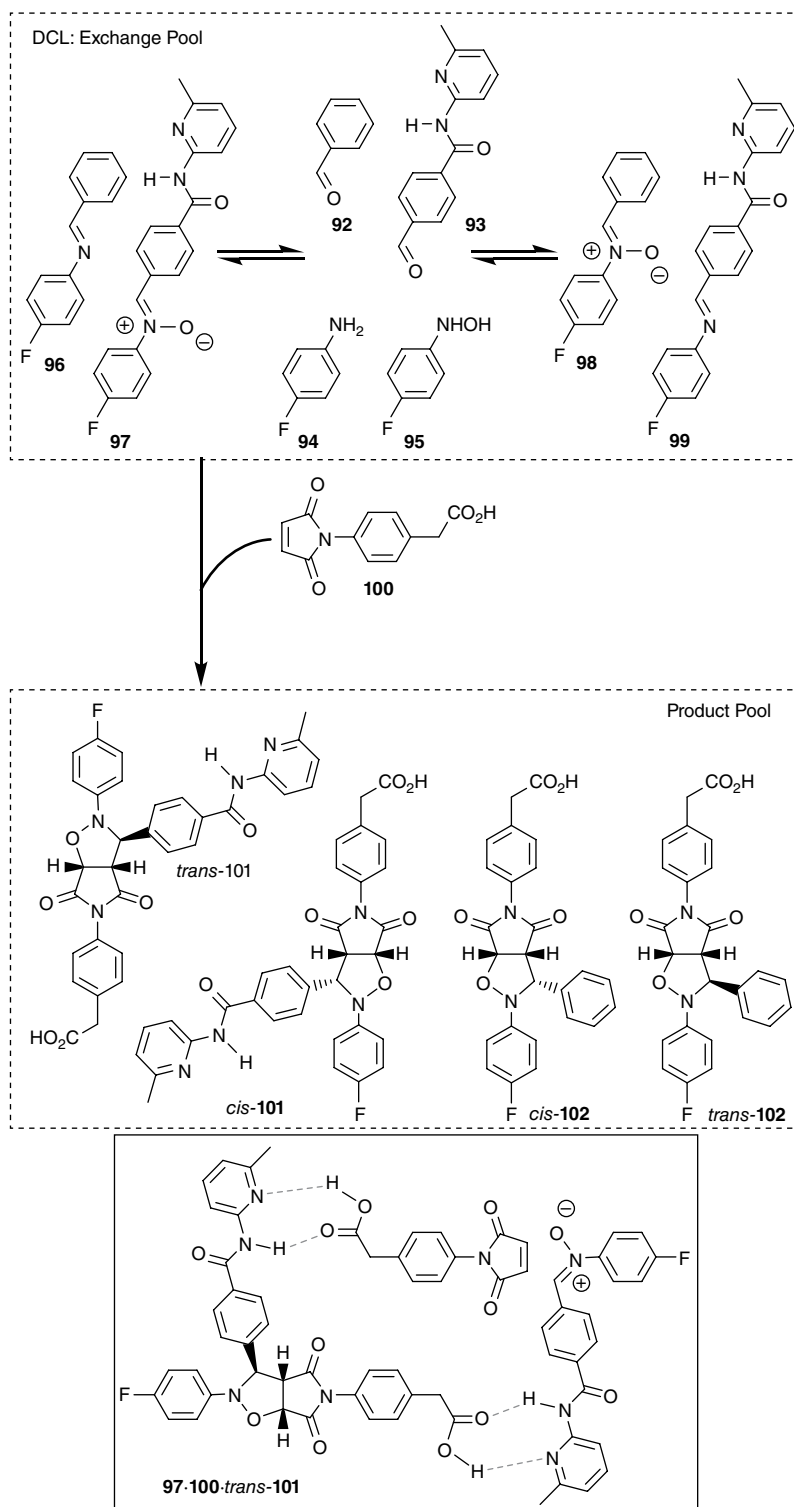
Scheme 6.20 Self-replication of the irreversibly produced cycloadduct *trans*-**101** from a DCL containing its precursor nitrone **97**. The insert at the bottom shows the ternary complex (**97·100·***trans*-**101**) that is the key operation species in the autocatalytic cycle.

number of industrial *reactive distillation* protocols wherein the chemical reactor doubles as a distillation still. Scheme 6.21 illustrates this distillative self-sorting of imines on an example of a [3 × 3] DCL. Starting from nine imines **103–111**, vacuum distillation (0.10 mmHg) first isolated the most volatile (and also lowest molecular mass) imine **105** (90%), eliminating imines **103**, **104**, **108**, and **111** from the library. The next distillation step proceeded at higher temperature (150 °C) and isolated imine **107** (94%), destroying imines **106** and **110** in the process, and leaving the least volatile **109** (99%) as the distillation residue. This protocol was extended to DCLs with as many as 25 imine components.

Distillation as a technique capitalizes on several features of kinetic self-sorting DCLs. First, it operates at high temperature and in the absence of solvent, ensuring that imine exchange is much faster than in solution. Second, it produces materials that are physically separated and isolated as pure compounds. Third, as a physical transformation, it does not suffer from side reactions and thus routinely gives products in >90% yields. Finally, as a technique commonly used in refining and chemical industry, it is the self-sorting method that is perhaps the closest to industrial applications. With all of these factors in mind, we next sought to expand distillative self-sorting to ester DCLs, which we assumed would be of greater industrial interest.[63] While imine DCLs exchanged in the absence of catalyst (presumably traces of water or leftover acid played that role), forcing esters to swap their acyl and alkoxy components required more substantial catalysts that we identified in the form of NaO*t*-Bu[64] and Ti(OBu)$_4$.[65] This ester self-sorting procedure was also used as the basis of an instructive experiment designed to teach undergraduate students about vacuum distillation and chemical equilibrium.[66] By taking the two cross-over esters **112** and **113** (Scheme 6.22) with fragrant odors (i.e., one with a light acyl and heavy alkoxy group, and another one with a light alkoxy and heavy acyl group), reactive distillation results in ester transmutation into the light/light combination **114** (found in the distillate) and heavy/heavy combination **115**, isolated in the residue. If starting and ending esters are chosen to have very different aromas, the outcome of this experiment can be qualitatively assessed by smelling, even by undergraduates, as this method is safe because the used esters are non-toxic, FDA-approved food additives. One example of such an experiment is shown in Scheme 6.22.

In 2015, we reported self-sorting of imine DCLs based on their differential adsorption on silica gel.[67] As adsorption affinities toward silica gel generally correlate to compound polarity, this procedure effectively sorts imines based on the polarity of their constituent aldehyde and amine components. Thus a DCL mixture disproportionates on the column into the most and the least polar components, completely sacrificing the cross-over products of intermediate polarity. Silica gel plays a dual role of adsorbent (which effects the self-sorting) and mild acid catalyst (which speeds up imine exchange). To accelerate imine exchange and make sure it is completed within 1–3 h (a typical length of a column chromatographic purification) the column was also heated to ~50 °C. In the example shown in Scheme 6.23, a starting library of four imines was analyzed before and after chromatographic purification. Initial molar ratio of imines **116:88:117:118** was 1.00:0.65:0.66:0.99. After chromatographic purification, the first fraction contained only imine **116** (85% yield), while the second fraction contained **117** (8%) and **118** (89%). Thus, during the course of a column chromatography, an initial unbiased DCL was transformed into two separate fractions which were strongly biased towards the least polar (**116**) and most polar (**118**) component of the original DCL.
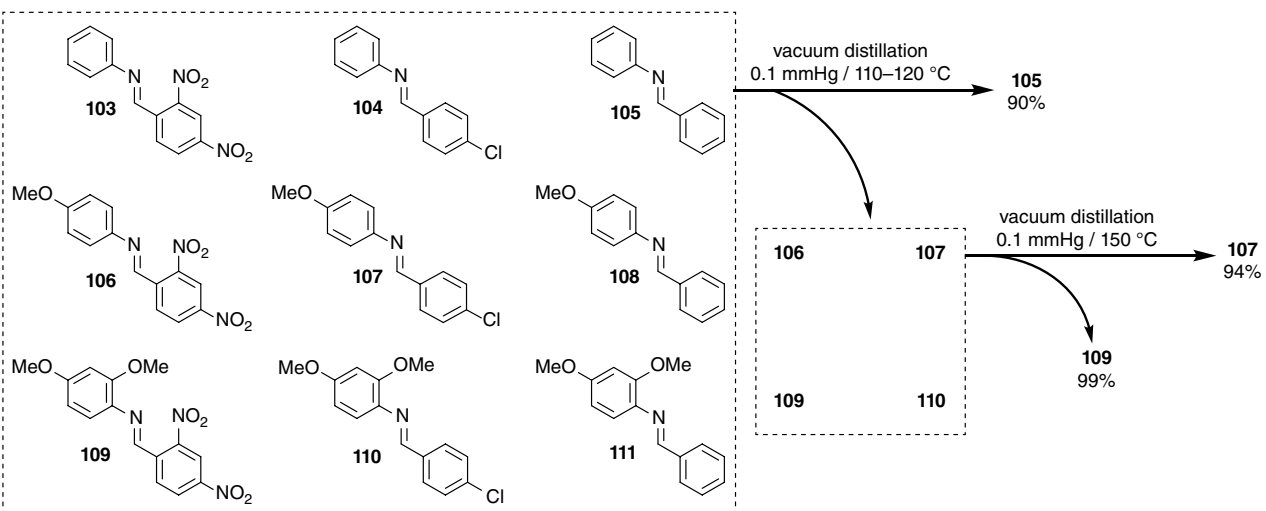
Scheme 6.21 Self-sorting of a dynamic [3×3] imine library during the course of a vacuum distillation.
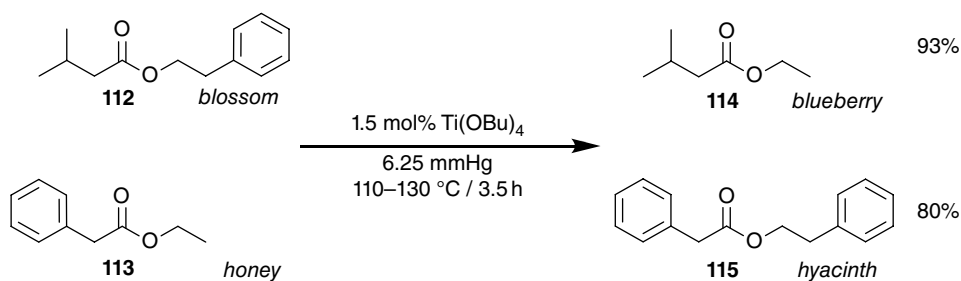
Scheme 6.22 Scent transmutation as a consequence of distillative self-sorting of an ester DCL. The fragrances of individual esters are given in italics below their structures.
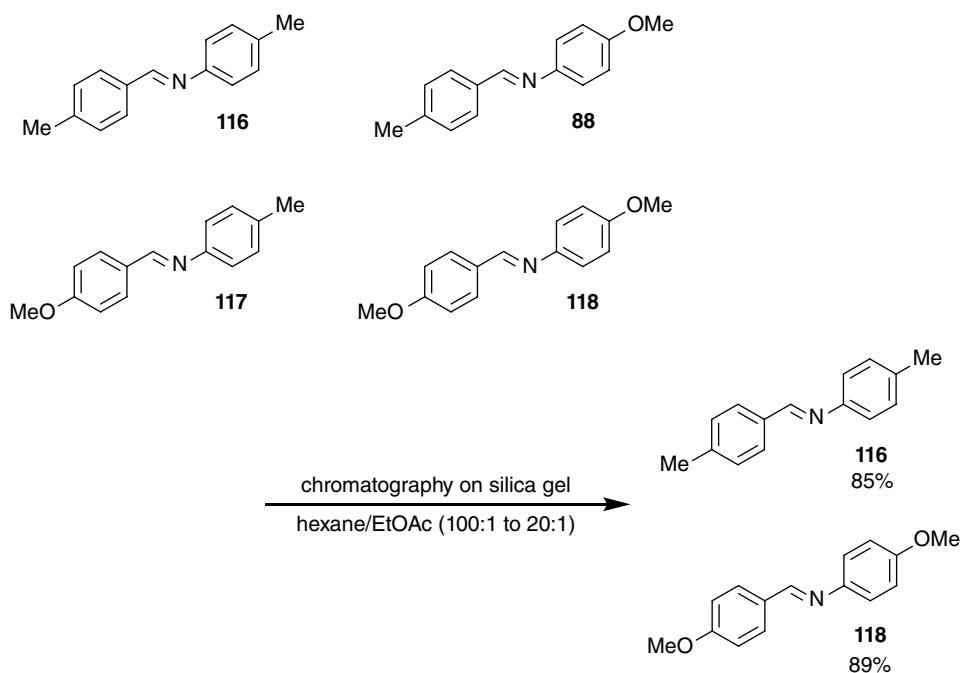
Scheme 6.23 An imine-based DCL amplifies its most and least polar components during the course of a column chromatography.

To ensure that this self-sorting is not thermodynamic in origin, we heated the initial DCL at reflux in the presence of silica gel. Although the imine distribution changed slightly, no significant biasing was observed, suggesting that, indeed, the open nature of the eluting system is essential to the self-sorting. Mixtures as high in complexity as [4 × 4] have been simplified into four pure products using this methodology.

One of the very commonly used strategies for shifting the position of a chemical equilibrium is selective precipitation of individual insoluble components. Those components are then amplified in the precipitate, as the equilibrium shifts to replenish the just-precipitated compound. If the same process is iteratively applied, multiple pure compounds can be obtained by sequential precipitation from the solution. While also
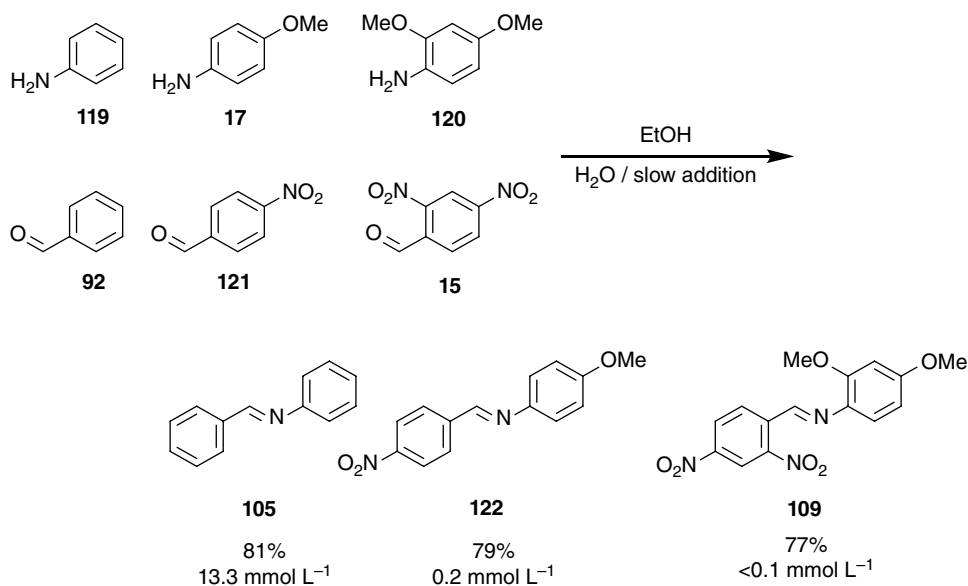
Scheme 6.24 Self-sorting of an imine DCL during the course of a slow precipitation. The number below the percentage yield indicates the solubilities of corresponding imines in EtOH/H$_2$O mixture (1:2.4, v/v).

physical in nature, precipitation as the self-sorting stimulus is quite different from the above discussed examples of distillation and adsorption. Both distillation and adsorption utilize quick equilibration of imine precursors (achieved by heating) and then sort the components based on their ability to irreversibly escape this quickly established equilibrium. In contrast, precipitation generally operates at low temperatures, so it has to rely on more significant differences in solubility that can be expressed even with a slow equilibration process.

We have studied the precipitative self-sorting of dynamic imine libraries,[68] and have found that the final composition of these mixtures is governed by the collective interplay of the solubilities of formed and potentially formed (virtual) products. For example, when an equimolar mixture of aldehydes **15**, **92**, and **121** and anilines **17**, **119**, and **120** (Scheme 6.24) was dissolved in EtOH and then subjected to slow addition of H$_2$O (which was intended to lower the solubility of imines), only three of the possible nine imines were formed: **105**, **122**, and **109**. This selectivity was driven by the extremely low solubilities of imines **109** and **122**, which sequestered all of their constituents from solution; this coprecipitation left only **119** and **92** in solution, which had no choice but to selectively form the soluble imine **105**.

Nitschke *et al*.[69] showed that a library of diastereomers of a helical imine/Cu(I) complex collapses into a single set of enantiomers on crystallization.

We have reported an example of a reaction that may present a case of precipitation-driven positional self-sorting. We revisited the benzoin condensation of isophthaldehyde (**123**) – despite literature precedent which mentions only polymeric products – and found that this reaction produces a cyclic trimer **124** of the starting material in 41% yield (Scheme 6.25).[70] We dubbed this compound cyclotribenzoin; it is not yet clear
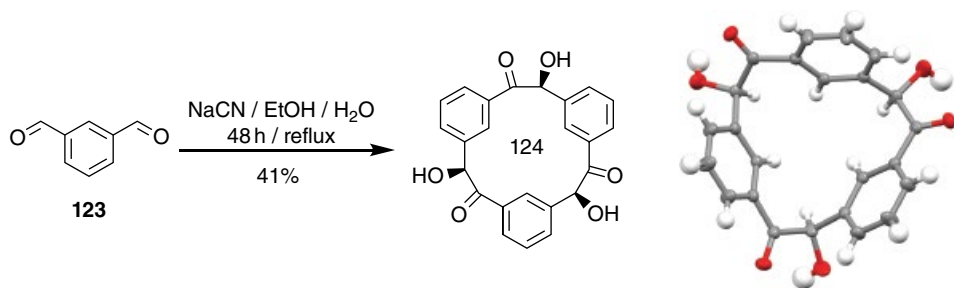
Scheme 6.25 Production of cyclotribenzoin **124** (crystal structure shown on the right) through a possible reversible benzoin condensation of isophthaldehyde: an example of precipitation-driven self-sorting?

whether this is an example of self-sorting, as our mechanistic investigations are undergoing. It may very well be one, as (i) benzoin condensation is in principle reversible, (ii) product is isolated by precipitation, and (iii) positional control is achieved as carbonyl and hydroxyl groups regioselectively alternate along the cyclic backbone (much like in Stang's example shown in Scheme 6.13). We have expanded these findings to the cyclic tetramer of terephthtaldehyde.[71]

6.4 Conclusions and Outlook

Self-sorting processes are intuitive and their expressions are found in many natural phenomena. During the past decade, a systematic study of these behaviors in synthetic systems has yielded many new insights, allowing the creation of a formalized and somewhat quantitative framework within which to study and classify self-sorting processes. It has been shown that a number of distinct physical and chemical stimuli can be employed to initiate self-sorting events, and these processes can yield highly sophisticated, low-symmetry assemblies.

In the domain of thermodynamic self-sorting, the work of Schmittel *et al*. has been truly pushing the envelope away from the beautiful and highly symmetric superstructures (which dominated the early days of supramolecular self-assembly) to low-symmetry but highly ordered structures where multiple different components find exactly the right place in a complex assembly. This clever utilization of integrative self-sorting processes is producing assemblies that are both more similar to naturally occurring systems and more likely to engage in sophisticated applications. As with other thermodynamically controlled processes, these are dominated by enthalpic considerations. It will be interesting to see what surprises lie in wait with structures that require assembly of numerous components and bring with them entropic challenges.

Kinetically controlled self-sorting has utilized many irreversible stimuli to target and amplify individual components in complex DCLs and engage them in useful reactivity. A proverbial "holy grail" in this area would be the ability to target literally any component of the DCL and express it. We are not there yet; as the matrices shown in Scheme 6.18 demonstrate, kinetic self-sorting is largely confined to the isolation of diagonal DCL members, with relatively limited flexibility. However, a DCL that responds

to two or more orthogonal stimuli (corresponding, in other words, to a matrix in which we could target both diagonals) under kinetic control could be used to, in principle, express any of its components by an appropriate combination of the two sorting factors. Given that kinetically controlled processes remove material from equilibrium and can yield well-defined and stable compounds that are no longer subject to equilibration, this procedure could quickly find applications in basic chemical industry.

In our view, the community is now perfectly positioned to take on the next grand challenge: self-sorting of naturally occurring mixtures. Cellular environments are perhaps still too complex to tackle, but many abundant and potentially useful naturally occurring mixtures could be explored in the context of self-sorting. These include natural lipids and oils (of relevance to the biofuel industry) or hydrolyzed lignin (which is an extremely abundant, but severely underutilized potential source of diverse aromatic structures).[72,73] Both of these mixtures are replete with compounds that can engage in dynamic combinatorial chemistry – esters, acetals, ketones, aldehydes, alkenes – and self-sorting could in principle be used to channel these mixtures into a handful of value-added products. Some attempts to engage these mixtures in dynamic covalent reactivity have already been made[74] and are highly encouraging.

References

1 *Webster's Third New International Dictionary and Seven Language Dictionary*, G. & C. Merriam Co, **1971**.

2 A. Harada, R. Kobayashi, Y. Takashima, A. Hashidzume, H. Yamaguchi, *Nat. Chem.* **2011**, *3*, 34–37.

3 A. Wu, L. Isaacs, *J. Am. Chem. Soc.* **2003**, *125*, 4831–4835.

4 Z. He, W. Jiang, C. A. Schalley, *Chem. Soc. Rev.* **2015**, *44*, 779–789.

5 R. F. Ludlow, S. Otto, *Chem. Soc. Rev.* **2008**, *37*, 101–108.

6 W. Jiang, H. D. Winkler, C. A. Schalley, *J. Am. Chem. Soc.* **2008**, *130*, 13852–13853.

7 W. Jiang, C. A. Schalley, *Proc. Natl. Acad. Sci.* **2009**, *106*, 10425–10429.

8 M. M. Safont-Sempere, G. Fernández, F. Würthner, *Chem. Rev.* **2011**, *111*, 5784–5814.

9 M. L. Saha, M. Schmittel, *Org. Biomol. Chem.* **2012**, *10*, 4651–4684.

10 K. Osowska, O. Š. Miljanić, *Synlett* **2011**, *2011*, 1643–1648.

11 Q. Ji, R. C. Lirag, O. Š. Miljanić, *Chem. Soc. Rev.* **2014**, *43*, 1873–1884.

12 K. Mahata, M. Schmittel, *J. Am. Chem. Soc.* **2009**, *131*, 16544–16554.

13 S. J. Rowan, S. J. Cantrill, G. R. Cousins, J. K. Sanders, J. F. Stoddart, *Angew. Chem., Int. Ed.* **2002**, *41*, 898–952.

14 P. T. Corbett, J. Leclaire, L. Vial, K. R. West, J.-L. Wietor, J. K. Sanders, S. Otto, *Chem. Rev.* **2006**, *106*, 3652–3711.

15 Y. H. Jin, C. Yu, R. J. Denman, W. Zhang, *Chem. Soc. Rev.* **2013**, *42*, 6634–6654.

16 J. R. Nitschke, *Acc. Chem. Res.* **2007**, *40*, 103–112.

17 B. H. Northrop, Y.-R. Zheng, K.-W. Chi, P. J. Stang, *Acc. Chem. Res.* **2009**, *42*, 1554–1563.

18 S. J. Rowan, D. G. Hamilton, P. A. Brady, J. K. Sanders, *J. Am. Chem. Soc.* **1997**, *119*, 2578–2579.

19 J. M. Han, J. L. Pan, T. Lei, C. Liu, J. Pei, *Chem. Eur. J.* **2010**, *16*, 13850–13861.

20 N. Hafezi, J.-M. Lehn, *J. Am. Chem. Soc.* **2012**, *134*, 12861–12868.

21 G. Vantomme, N. Hafezi, J.-M. Lehn, *Chem. Sci.* **2014**, *5*, 1475–1483.

22 B. Içli, N. Christinat, J. Tönnemann, C. Schüttler, R. Scopelliti, K. Severin, *J. Am. Chem. Soc.* **2009**, *131*, 3154–3155.

23 N. Christinat, R. Scopelliti, K. Severin, *Angew. Chem., Int. Ed.* **2008**, *47*, 1848–1852.

24 M. Pascu, A. Ruggi, R. Scopelliti, K. Severin, *Chem. Commun.* **2013**, *49*, 45–47.

25 J. Tönnemann, R. Scopelliti, K. Severin, *Eur. J. Inorg. Chem* **2013**, *2013*, 5071–5074.

26 R. C. Lirag, O. Š. Miljanić, *Chem. Commun.* **2014**, *50*, 9401–9404.

27 R. Kramer, J.-M. Lehn, A. Marquis-Rigault, *Proc. Natl. Acad. Sci.* **1993**, *90*, 5394–5398.

28 J.-M. Lehn, A. Rigault, J. Siegel, J. Harrowfield, B. Chevrier, D. Moras, *Proc. Natl. Acad. Sci.* **1987**, *84*, 2565–2569.

29 R. Krämer, J. M. Lehn, A. De Cian, J. Fischer, *Angew. Chem., Int. Ed.* **1993**, *32*, 703–706.

30 P. N. Taylor, H. L. Anderson, *J. Am. Chem. Soc.* **1999**, *121*, 11538–11545.

31 M. Hutin, R. Frantz, J. R. Nitschke, *Chem. Eur. J.* **2006**, *12*, 4077–4082.

32 D. Schultz, J. R. Nitschke, *Proc. Natl. Acad. Sci.* **2005**, *102*, 11191–11195.

33 D. Schultz, J. R. Nitschke, *Angew. Chem., Int. Ed.* **2006**, *45*, 2453–2456.

34 A. Jiménez, R. A. Bilbeisi, T. K. Ronson, S. Zarra, C. Woodhead, J. R. Nitschke, *Angew. Chem., Int. Ed.* **2014**, *53*, 4556–4560.

35 A. G. Salles Jr, S. Zarra, R. M. Turner, J. R. Nitschke, *J. Am. Chem. Soc.* **2013**, *135*, 19143–19146.

36 M. M. Smulders, A. Jiménez, J. R. Nitschke, *Angew. Chem., Int. Ed.* **2012**, *51*, 6681–6685.

37 Y. R. Zheng, H. B. Yang, K. Ghosh, L. Zhao, P. J. Stang, *Chem. Eur. J.* **2009**, *15*, 7203–7214.

38 C. Addicott, N. Das, P. J. Stang, *Inorg. Chem.* **2004**, *43*, 5335–5338.

39 Y.-R. Zheng, H.-B. Yang, B. H. Northrop, K. Ghosh, P. J. Stang, *Inorg. Chem.* **2008**, *47*, 4706–4711.

40 L. Zhao, B. H. Northrop, Y.-R. Zheng, H.-B. Yang, H. J. Lee, Y. M. Lee, J. Y. Park, K.-W. Chi, P. J. Stang, *J. Org. Chem.* **2008**, *73*, 6580–6586.

41 A. M. Johnson, R. J. Hooley, *Inorg. Chem.* **2011**, *50*, 4671–4673.

42 L. R. Holloway, M. C. Young, G. J. Beran, R. J. Hooley, *Chem. Sci.* **2015**, *6*, 4801–4806.

43 A. M. Johnson, C. A. Wiley, M. C. Young, X. Zhang, Y. Lyon, R. R. Julian, R. J. Hooley, *Angew. Chem., Int. Ed.* **2015**, *54*, 5641–5645.

44 M. C. Young, L. R. Holloway, A. M. Johnson, R. J. Hooley, *Angew. Chem., Int. Ed.* **2014**, *53*, 9832–9836.

45 K. Mahata, M. L. Saha, M. Schmittel, *J. Am. Chem. Soc.* **2010**, *132*, 15933–15935.

46 M. Schmittel, V. Kalsani, R. S. Kishore, H. Cölfen, J. W. Bats, *J. Am. Chem. Soc.* **2005**, *127*, 11544–11545.

47 M. L. Saha, M. Schmittel, *J. Am. Chem. Soc.* **2013**, *135*, 17743–17746.

48 M. L. Saha, N. Mittal, J. W. Bats, M. Schmittel, *Chem. Commun.* **2014**, *50*, 12189–12192.

49 M. Schmittel, S. De, S. Pramanik, *Org. Biomol. Chem.* **2015**, *13*, 8937–8944.

50 I. R. Epstein, J. A. Pojman, *An introduction to nonlinear chemical dynamics: oscillations, waves, patterns, and chaos*, Oxford University Press on Demand, **1998**.

51 D. D. Bonchev, D. Rouvray, *Complexity in chemistry, biology, and ecology*, Springer Science & Business Media, **2007**.

52 Q. Ji, O. S. Miljanić, *J. Org. Chem.* **2013**, *78*, 12710–12716.

53 K. Osowska, O. S. Miljanić, *J. Am. Chem. Soc.* **2010**, *133*, 724–727.

54 P. Vongvilai, M. Angelin, R. Larsson, O. Ramström, *Angew. Chem., Int. Ed.* **2007**, *46*, 948–950.

55 P. Vongvilai, O. Ramström, *J. Am. Chem. Soc.* **2009**, *131*, 14419–14425.

56 V. Patzke, G. von Kiedrowski, *Arkivoc* **2007**, *8*, 293–310.

57 P. Herdewijn, M. V. Kisakürek, *Origin of Life: Chemical Approach*, Wiley, **2008**.

58 V. del Amo, A. M. Slawin, D. Philp, *Org. Lett.* **2008**, *10*, 4589–4592.

59 V. C. Allen, C. C. Robertson, S. M. Turega, D. Philp, *Org. Lett.* **2010**, *12*, 1920–1923.

60 J. W. Sadownik, D. Philp, *Angew. Chem., Int. Ed.* **2008**, *47*, 9965–9970.

61 J. I. Seeman, *Chem. Rev.* **1983**, *83*, 83–134.

62 K. Osowska, O. Š. Miljanić, *Angew. Chem., Int. Ed.* **2011**, *50*, 8345–8349.

63 Q. Ji, O. Š. Miljanić, *J. Org. Chem.* **2013**, *78*, 12710–12716.

64 M. G. Stanton, C. B. Allen, R. M. Kissling, A. L. Lincoln, M. R. Gagné, *J. Am. Chem. Soc.* **1998**, *120*, 5981–5989.

65 P. Schnurrenberger, M. F. Züger, D. Seebach, *Helv. Chim. Acta* **1982**, *65*, 1197–1201.

66 Q. Ji, N. S. El-Hamdi, O. S. Miljanić, *J. Chem. Edu.* **2014**, *91*, 830–833.

67 C. W. Hsu, O. Š. Miljanić, *Angew. Chem., Int. Ed.* **2015**, *54*, 2219–2222.

68 R. C. Lirag, K. Osowska, O. Š. Miljanić, *Org. Biomol. Chem.* **2012**, *10*, 4847–4850.

69 M. Hutin, C. J. Cramer, L. Gagliardi, A. R. M. Shahi, G. Bernardinelli, R. Cerny, J. R. Nitschke, *J. Am. Chem. Soc.* **2007**, *129*, 8774–8780.

70 Q. Ji, L. H. Do, O. Š. Miljanić, *Synlett* **2015**, *26*, 1625–1627.

71 Q. Ji, H. Le, X. Wang, Y. S. Chen, T. Makarenko, A. J. Jacobson, O. Š. Miljanić, *Chem. Eur. J.* **2015**, *21*, 17205–17209.

72 J. Zakzeski, P. C. Bruijnincx, A. L. Jongerius, B. M. Weckhuysen, *Chem. Rev.* **2010**, *110*, 3552–3599.

73 A. J. Ragauskas, G. T. Beckham, M. J. Biddy, R. Chandra, F. Chen, M. F. Davis, B. H. Davison, R. A. Dixon, P. Gilna, M. Keller, *Science* **2014**, *344*, 1246843.

74 A. L. Korich, K. M. Clarke, D. Wallace, P. M. Iovine, *Macromolecules* **2009**, *42*, 5906–5908.

7

Dynamic Covalent Chemistry for Synthetic Molecular Machines

Yi Liu and Ken C.-F. Leung

7.1 Introduction

Driven by the need for miniaturization, research on molecular machines has received considerable attention as a concept transferred from the macroscopic world to the nanoscale.[1–4] Molecular machines are dynamic molecular systems, usually containing multiple movable components, the locations of which can be altered to generate motion-like conformational or configurational changes by external stimuli such as chemical, electrochemical or photochemical inputs. Each molecular machine represents a chemical device that can perform a specific function. Nature has evolved many kinds of biomolecular machines.[5] Recently synthetic molecular objects with increasing topological and functional complexity have been designed and synthesized, with the aim of rivalling those in living systems. Bistable mechanically interlocked molecules (MIMs),[4,6] such as [n]catenanes and [n]rotaxanes ($n > 1$), are among the most representative types of synthetic molecular machines (Figure 7.1), which refer to molecular systems with two ring components or one ring and one dumbbell component, respectively, interlocked with each other by mechanical bonds. The relative movement of the rings in [2]catenanes gives rise to circumrotary motion, while in the case of [2]rotaxanes, linear sliding motion can be generated from the relative movement between the ring and dumbbell component. In both cases, the relative ring-to-ring and ring-to-dumbbell locations are dictated at large by a variety of non-covalent bonding interactions.

The success of the development of versatile synthetic molecular machines essentially lies in the advancement of better understanding of strong and weak inter- and intramolecular interactions. Supramolecular chemistry,[7–9] which deals with non-covalent interactions such as hydrogen and halogen bonding interactions, π–π stacking interactions, electrostatic interactions, metal–ion binding, and solvent–solute interactions, has been utilized extensively to achieve pre-organization of molecular components for subsequent covalent linkage. Such a synthetic strategy that harnesses the power of molecular recognition and self-assembly is known as template-directed synthesis, which takes advantage of both thermodynamic and kinetic characteristics of classical non-covalent and covalent bonding interactions. Recently, dynamic covalent chemistry (DCvC),[10–13] which combines the thermodynamic reversibility of

(a)   (b)
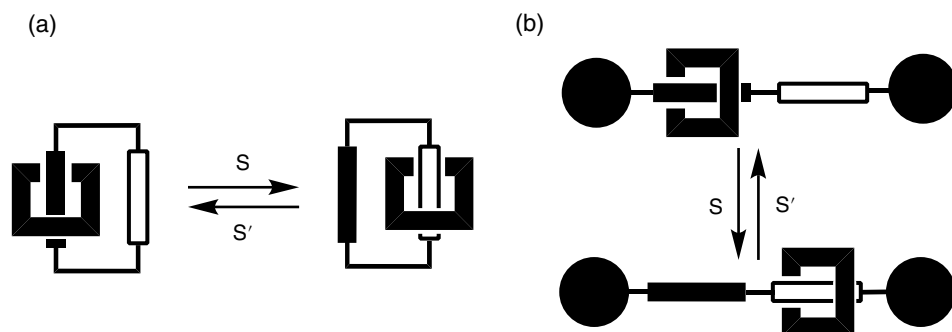
Figure 7.1 Molecular machines based on (a) a bistable [2]catenane and (b) a bistable [2]rotaxane.

non-covalent interactions and the kinetic stability of covalent interactions, has emerged as a powerful tool for target-oriented synthesis of topologically complex molecules[14,15] or diversity-oriented synthesis of dynamic constitutional libraries (DCLs).[16–18] When combining non-covalent templating with DCvC, the two levels of reversibility give rise to a remarkably versatile, equilibrium-based pathway towards high-yield syntheses of topologically interesting structures that are inaccessible by conventional covalent approaches. Various dynamic covalent reactions, such as imine chemistry, disulfide exchange, boronic ester linkage, and olefin metathesis, have been routinely exercised in the synthesis of sophisticated mechanically interlocked molecules, including those possessing bistability. The introduction of DCvC within bistable molecular machines also offers new opportunities for modulating the switching behavior between different states. In conventional molecular machines, the relative locations of different components are held by non-covalent interactions. When DCvC is used instead of non-covalent interactions, the covalent characteristics bring about more distinctive states as a result of larger energetic separations, implying more stable machine-like operations.[19]

In this chapter, we will summarize molecular machine-related DCvC in two categories: molecular machines that are assembled by DCvC and those that are operated by DCvC. In the first category, we will highlight some representative DCvC examples that have been recognized for their high efficacy and selectivity in the assembly of interlocked molecules, particularly these that can function as switchable systems. The general utilization of DCvC for interlocked molecules has been extensively reviewed and is not the focus of this chapter.[20] In this category we will also introduce several examples of DCvC-based non-interlocked molecular machines. The second category summarizes molecular machines that utilize dynamic bond formation and breakage to govern the switching between different states. In the final part of the chapter a perspective on DCvC and molecular machines is offered.

7.2 Molecular Machines Assembled by Dynamic Covalent Chemistry

In the following section, representative examples of switchable molecules are presented, including interlocked molecules and non-interlocked rotary molecular machines, all based on dynamic covalent bonds.

7.2.1 Mechanically Interlocked Molecular Machines

7.2.1.1 By Imine Chemistry

One of the most common strategies in applying DCvC for interlocked molecules is the so-called "clipping" method,[21] which involves the linkage of different partial macrocyclic components that are pre-organized around a template. This strategy has been extensively exercised in the imine-based synthesis of interlocked molecules. Stoddart and co-workers have pioneered the hydrogen-bonding mediated imine assembly from mixing bis(3,5-dimethoxybenzyl)ammonium hexafluorophosphate **1** with a solution of equimolar of 2,6-pyridinedicarboxaldehyde **2** and tetraethylene glycol bis(2-aminophenyl)ether **3** (Scheme 7.1a).[22] The desired [2]rotaxane **4** was obtained quantitatively in a few minutes. The high efficiency of the clipping reaction was the basis for the successful synthesis of monodisperse oligo[n]rotaxane **6** (Scheme 7.1b). Multiple dialkylammonium centers, such as those in **5**, were incorporated into the dumbbell component and subjected to clipping with dialdehyde **2** and diamine **3**. Monodisperse oligo[n]rotaxanes with n up to 15 were obtained in high yield when dibenzylammonium centers were used, thanks to positive cooperativity arising from extended π–π stacking interactions.[23,24]

The imine-based clipping reaction has been utilized by Tatay and co-workers in the synthesis of switchable copper-complexed interlocked systems.[25] Reacting dumbbell-shaped component **7** with diamine **8** and 2,6-diformylpyridine (**2**) in the presence of Cu(MeCN)$_4$PF$_6$, followed by reduction of the diimine gave rise to [2]rotaxane **9-Cu(I)** (Scheme 7.2). As evidenced by electron spin resonance spectroscopy and cyclic voltammetry, the introduction of such a pyridine bisamine moiety, which replaced the classical terpyridine terdentate unit, led to significant stabilization of the penta-coordinated Cu(I) site. On oxidation of Cu(I) to Cu(II), pirouetting of the macrocycle was activated to favor the formation of a tetra-coordinated Cu(II) complex between the two phenanthroline units. Such an electrochemical switching process took place at the millisecond timescale, which represented the fastest switching rotaxane in Cu-based interlocked dynamic systems. The DCvC incorporated here not only showcases the synthetic simplicity, but also has led to a bistable system with more distinct energetic separation between states and an acceleration of the reorganization processes.

A similar imine clipping reaction has also been employed in the synthesis of photoswitchable [2]catenanes **10**, one macrocyclic component of which contains an ammonium center for templated clipping of another macrocycle and a photoresponsive dithienylethene (DTE) unit (Scheme 7.3).[26] Good photochromic reversibility and excellent fatigue resistance were observed as a result of the formation of open and closed isomers of the DTE unit upon UV or visible light irradiation. The catenation of the imine-based macrocycle on the macrocyclic ammonium salt rendered enhanced photochromic properties compared to these of the ammonium salt containing macrocycles alone.

The facile imine bond formation also facilitates the synthesis of an anthracene-containing dynamic [2]rotaxane **AnthR-H·**PF$_6$, which behaves as an acid sensor as well as a molecular logic device based on the fluorescence response of the anthracene end group (Scheme 7.4).[27] The [2]rotaxane **AnthR-H·**PF$_6$ was prepared by the aforementioned "clipping" approach by reacting dialdehyde **2**, diamine **3**, and a dumbbell-shaped secondary dialkylammonium ion (**Anth-H·**PF$_6$ template). Owing to the
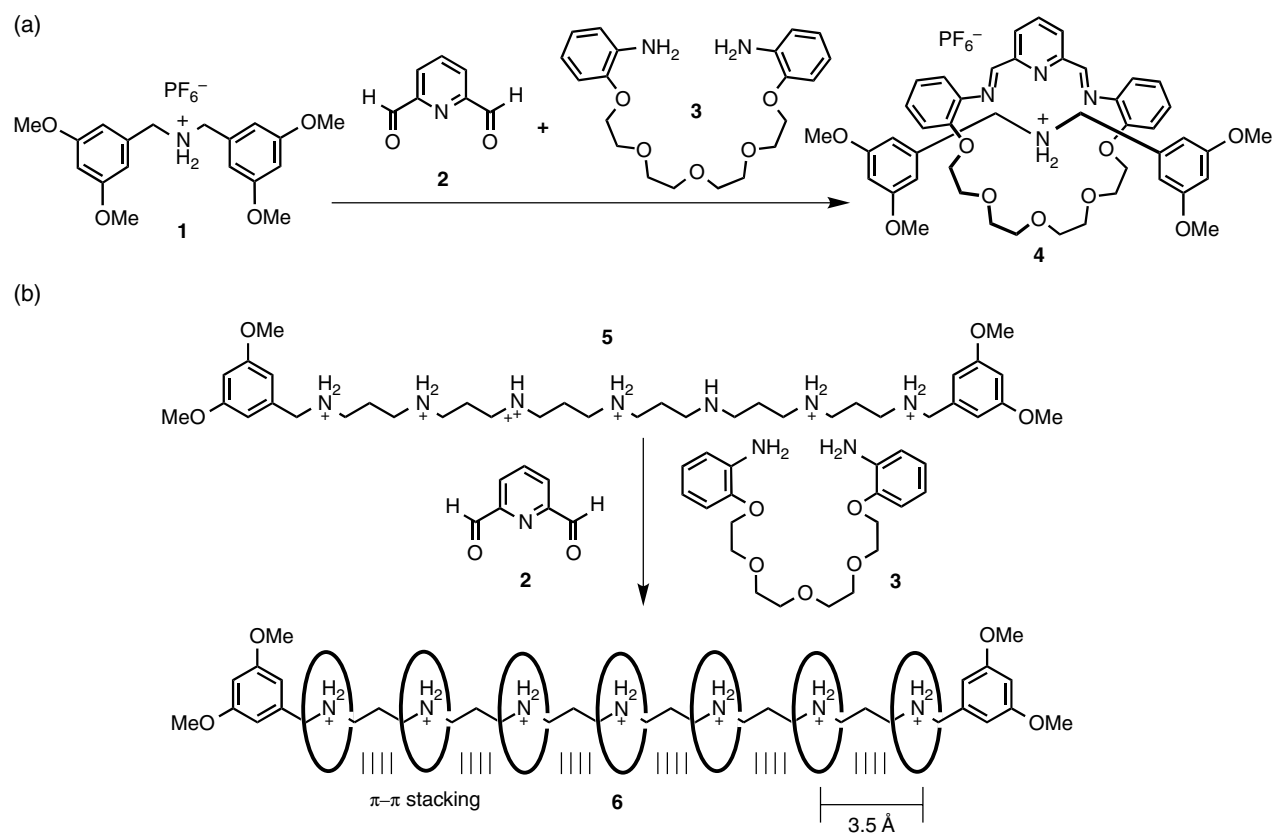
Scheme 7.1 The hydrogen-bonding templated clipping of (a) a [2]rotaxane and (b) [*n*]rotaxanes.
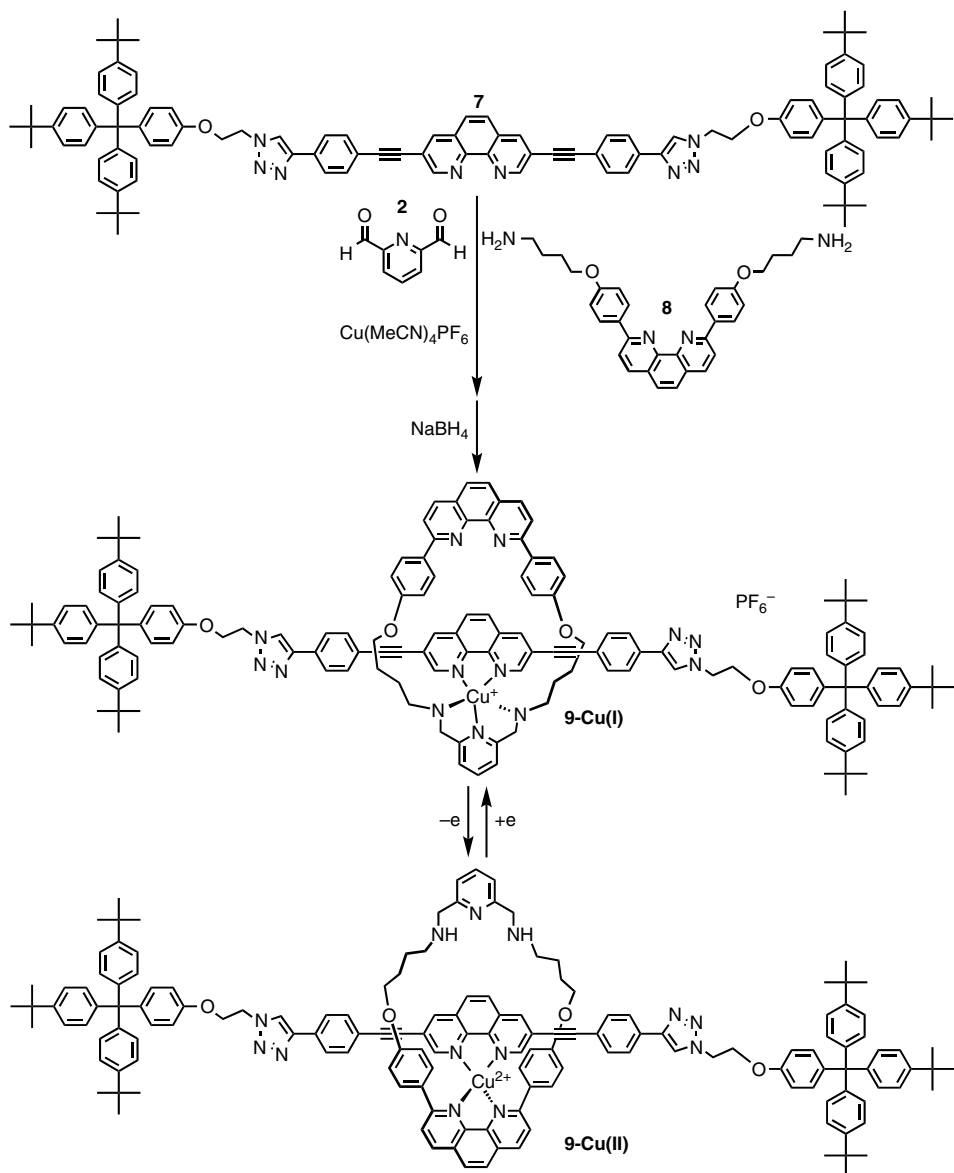
Scheme 7.2 A bistable [2]rotaxane synthesized by imine clipping reaction, and the related redox-activated switching between penta-coordinated and tetra-coordinated Cu centers.

complementary recognition associated with [N⁺H···O] and [N⁺CH···O] hydrogen bonds as well as electrostatic and π–π interaction between the macrocycle and dumbbell component, the thermodynamically stable dynamic [2]rotaxane was obtained in high yield (>90%), without formation of other higher-order macrocyclic homo-oligomers or acyclic oligomers. Furthermore, the anthracene fluorescence of the [2]rotaxane could be completely quenched by electron transfer from the imine and pyridine moieties in the macrocycle in close proximity. In addition, it is known
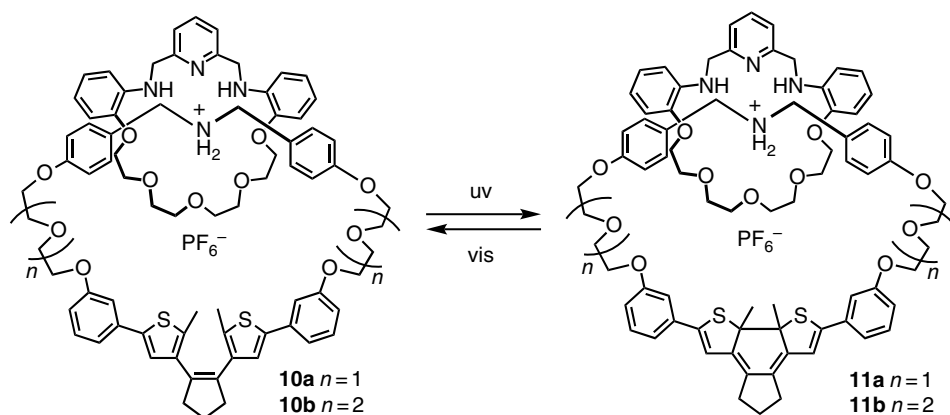
Scheme 7.3 Switchable [2]catenanes containing a photoresponsive dithienylethene unit.
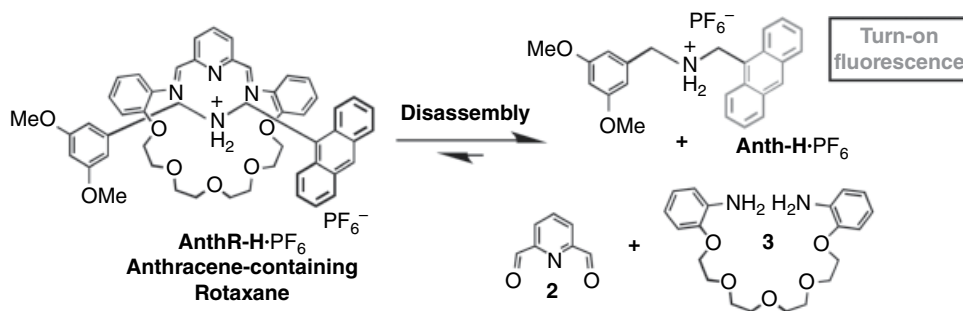
	Input				Output	
Entry	H_2O	H^+	KPF_6	Tol-NH_2	Anthracene fluorescence (418 nm, excitation = 290 nm)	Fluorescence at 330 nm (excitation = 290 nm)
A	0	0	0	0	0	1
B	1	0	0	0	0	1
C	0	1	0	0	(1)	(0)
D	0	0	1	0	0	1
E	0	0	0	1	0	1
F	1	1	0	0	1	0
G	1	0	1	0	0	1
H	1	0	0	1	0	1
I	0	1	1	0	(1)	(0)
J	0	1	0	1	(1)	(0)
K	0	0	1	1	0	1
L	1	1	1	0	1	0
M	1	1	0	1	1	0
N	1	0	1	1	0	1
O	0	1	1	1	(1)	(0)
P	1	1	1	1	1	0

Scheme 7.4 Dissociation of anthracene-containing rotaxane **AnthR-H·PF₆** with "turn-on" fluorescent properties and summary of the fluorescence output of the rotaxane **AnthR-H·PF₆** in the presence of four different additive inputs (H_2O, H^+, KPF_6, and Tol-NH_2). Input: "1" represents the presence of the additive while "0" represents the absence of the additive. Output: "1" represents observable fluorescence while "0" represents no observable fluorescence (fluorescence quenched). The output entries C, I, J, and O (parentheses) are somewhat uncertain since thoroughly dry conditions are difficult to realize.

that the imine bonds in macrocycles are responsive to the presence of water, acid, salt (KPF$_6$), and amine (*p*-toluidine). Two acid sensors (HCl/H$_2$O and HCl/Et$_2$O) have been identified with different modes of dimmer control, that is, logarithmic and linear. The use of a combination of stimuli for the [2]rotaxane is summarized in the table of Scheme 7.4, employing a binary notation with four different inputs and one output. Noticeably, the output entries C, I, J, and O are somewhat uncertain since it is difficult to reach thoroughly dry conditions. If the situation relating to the residual water molecules present in the solutions was overlooked, then the outputs could be interpolated (as the bracketed values). Since the fluorescence signal could be observed by various input or stimuli, different molecular logic was realized by rational selection of different combinations of input.

Other types of non-covalent interactions, such as donor–acceptor interactions, have also been utilized in the dynamic clipping of interlocked molecules. In the presence of an electron-deficient π-template, such as the bipyridinium (**BPY**)-containing dumbbell-shaped compound **12**, a six-component [2 + 3] clipping reaction that involves 2 equivalents of 1,3,5-benzenetrialdehyde (**13**) and 3 equivalents of 2,2′-(ethylenedioxy) diethylamine (**14**) (Scheme 7.5a) works efficiently to afford the desired [2]rotaxane **15** as the single product.[28] Weak interactions, the main one being π–π interactions between the **BPY** template and the macrobicycle, contribute to the overall stabilization of the threaded product, despite a symmetry mismatch between the host and the guest. Recently, c_3-symmetric trispyridinium (**TPY**) guests, such as **16** in Scheme 7.5b, have also been employed as an effective template for the formation of a triply-threaded [2] rotaxane **17**.[29]

The difference in templating power between **BPY** and **TPY** units renders an unconventional solvent-dependent switching between the two [2]rotaxanes **15** and **17** (Scheme 7.6).[30] In competition clipping experiments employing both **BPY** and **TPY** as the templates, exclusive formation of the **BPY**-based linear [2]rotaxane **15** could be achieved in pure CDCl$_3$, while in pure CD$_3$CN a 6.7:1 selectivity was achieved in favor of the **TPY**-based triply threaded [2]rotaxane **17**. Such an environmental responsive switching between different structures was related to the subtle differences of the aromatic–aromatic interactions that govern the templated formation of two [2]rotaxanes. The **BPY**-based clipping reaction was driven by electrostatic interactions between aromatic surfaces, while the **TPY**-based reaction was driven by solvophobic interactions. It is the difference in the collective non-covalent interactions that accounts for the opposite selectivity in different chemical environments, which can be essential for the design of complex molecular architecture, which rely on weak but cooperative non-covalent interactions.

The dynamic clipping approach combining π-templating and reversible imine chemistry has also been applied in the preparation of [2]catenanes (Scheme 7.7).[31] A mixing of terephthaldehyde (**18**), 2,2′-(ethylenedioxy)diethylamine (**14**), and the tetracationic cyclobisparaquat (**19**) (CBPQT^{4+}) in CD$_3$CN in 2:2:1 ratio resulted in the formation of a single species that corresponded to the [2]catenane **20**. No [2]catenane was formed when 1,5-diformylnaphthalene (**21**) was used instead of terephthaldehyde. Interestingly, when equimolar amounts of **18** and **21** were mixed with diamine **14** (2 equivalents) and cyclophane **19** (1 equivalent), an unsymmetrical [2]catenane **22** was formed selectively as the major product in 90% yield, together with ~5% of the symmetric [2]catenane **20**. Furthermore, only one translational isomer of **22** was observed both in solution and in
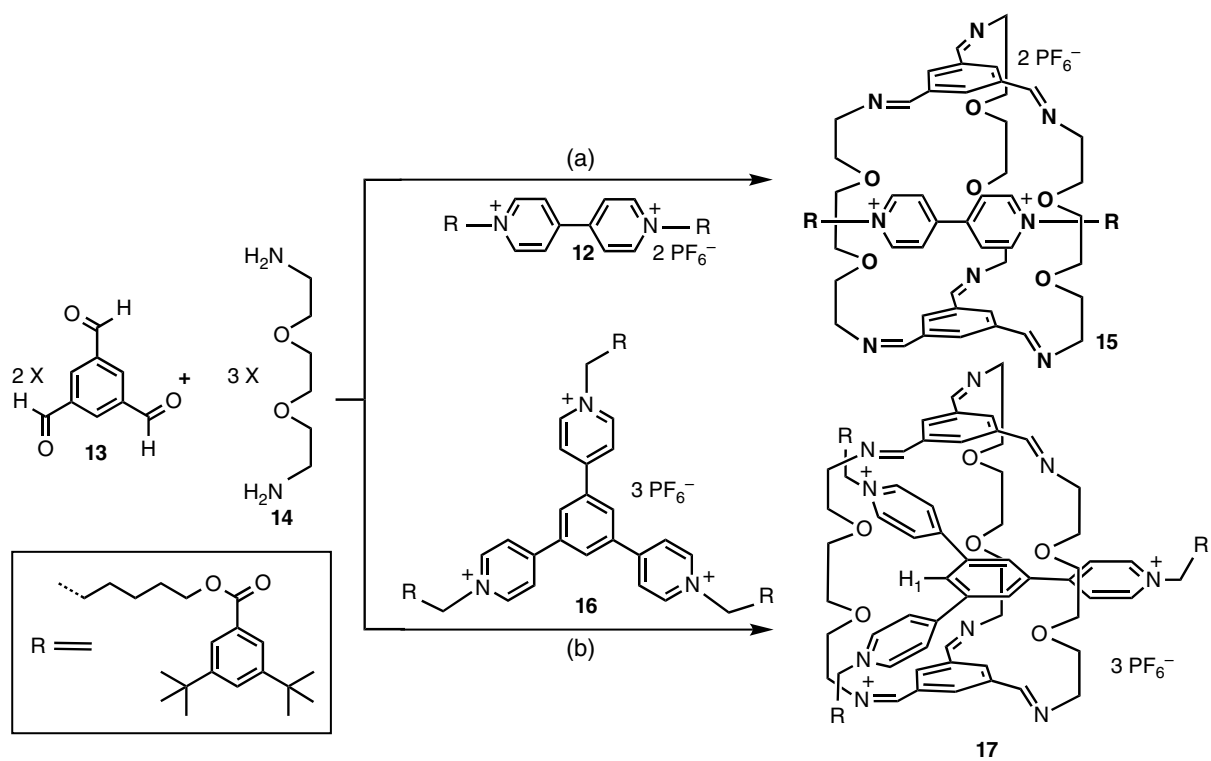
Scheme 7.5 Templated dynamic clipping for the formation of [2]rotaxanes by (a) a linear and (b) a c_3-symmetric template.
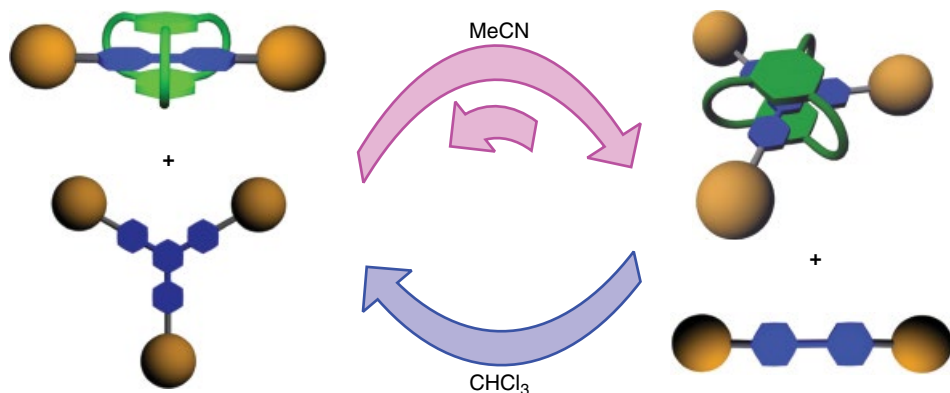
Scheme 7.6 Dynamic switching between a linear [2]rotaxane and a triply threaded [2]rotaxane in response to different solvent conditions.

the solid state, with the diiminobenzene ring system sitting inside the cavity of the tetracationic cyclophane and the diiminonaphthalene ring system sitting alongside. Steric effects, together with strong π–π interactions between the aromatic units and the collective [C-H···O] interactions in a molecular geometry with ideal preorganization, are responsible for the high selectivity expressed in the clipping reaction. This approach offers a thermodynamic pathway to desymmetrized [2]catenanes by installing different recognition units in one simple step in one of the macrocyclic components, which holds great promise for the construction of switchable molecules with multistability.

7.2.1.2 By Disulfide Bond Formation

Sanders and co-workers have detailed the construction of DCLs based on reversible S–S bond formation in aqueous solution,[32–37] from which donor–acceptor type [*n*] catenanes were identified and amplified.[33,37] For example, an aqueous disulfide DCL was derived from a mixture of an electron-accepting naphthalene diimide (NDI) derivative **23** and an electron-donating dioxynaphthalene (DNP) derivative **24** that was equilibrated under air oxidation (Scheme 7.8). It was found that the formation of donor–acceptor [2]catenane **25** was amplified by increasing the concentrations of each building block or under high ionic strength. [2]Catenane **25** consisted of two identical macrocyclic components, each containing one DNP and one NDI ring system, that were covalently linked by an S–S bond. Different from the conventional alternating donor–acceptor stacking geometry, it adopted a donor–acceptor–acceptor–donor stacking conformation, likely a consequence of enhanced hydrophobic interaction that compensated the diminished electrostatic interactions. The use of an electron-rich cationic template **26** could also amplify the formation of [2]catenane **25** by intercalating between the two electron-deficient NDI moieties, giving rise to a supramolecular assembly featuring five alternating donor and acceptor units. The construction of such an unusual donor–acceptor [2]catenane from acyclic precursors manifests the power of DCvC. A more detailed mechanistic study of the formation pathways of different donor–acceptor [2]catenanes,[38] as well as the formation of more complex [3] catenanes,[37] was reported based on similar constitutional DCLs.
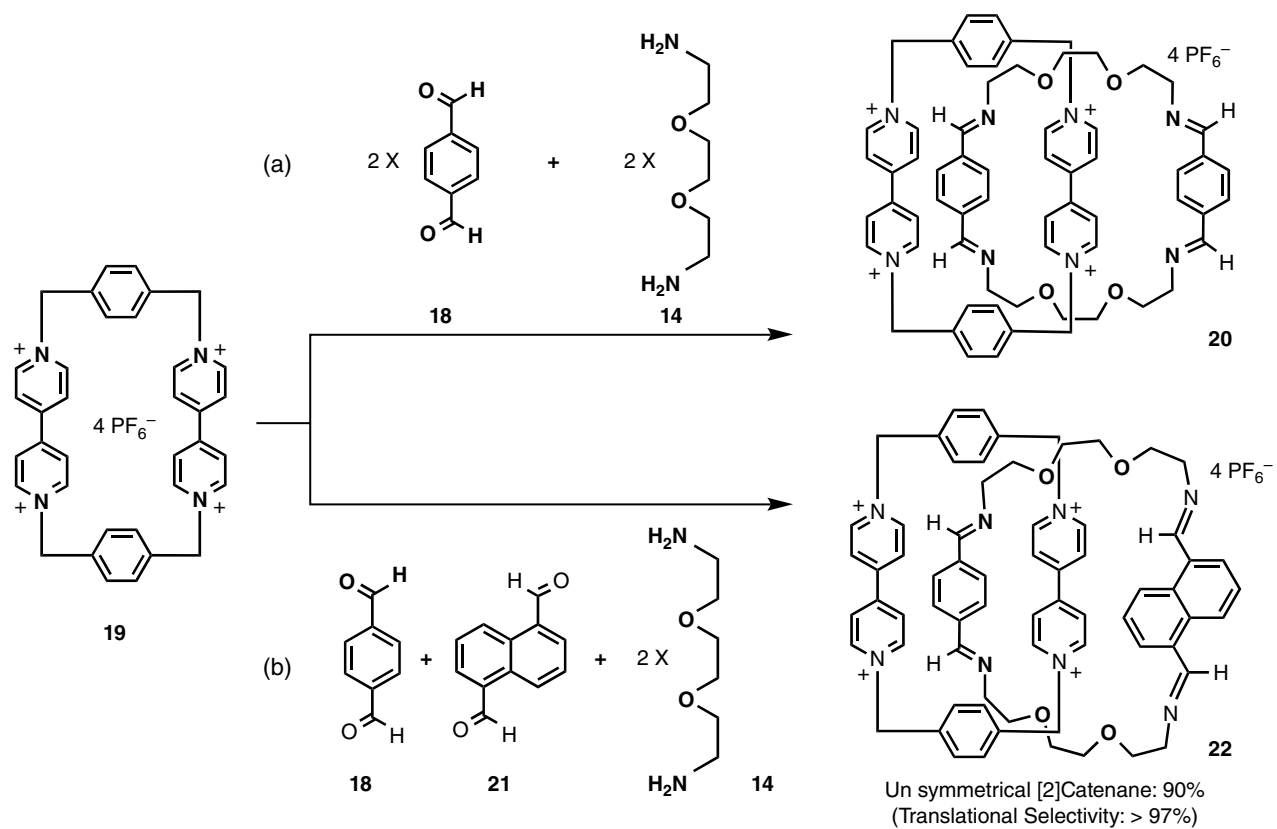
Scheme 7.7 Templated dynamic clipping for the selective formation of [2]catenanes.
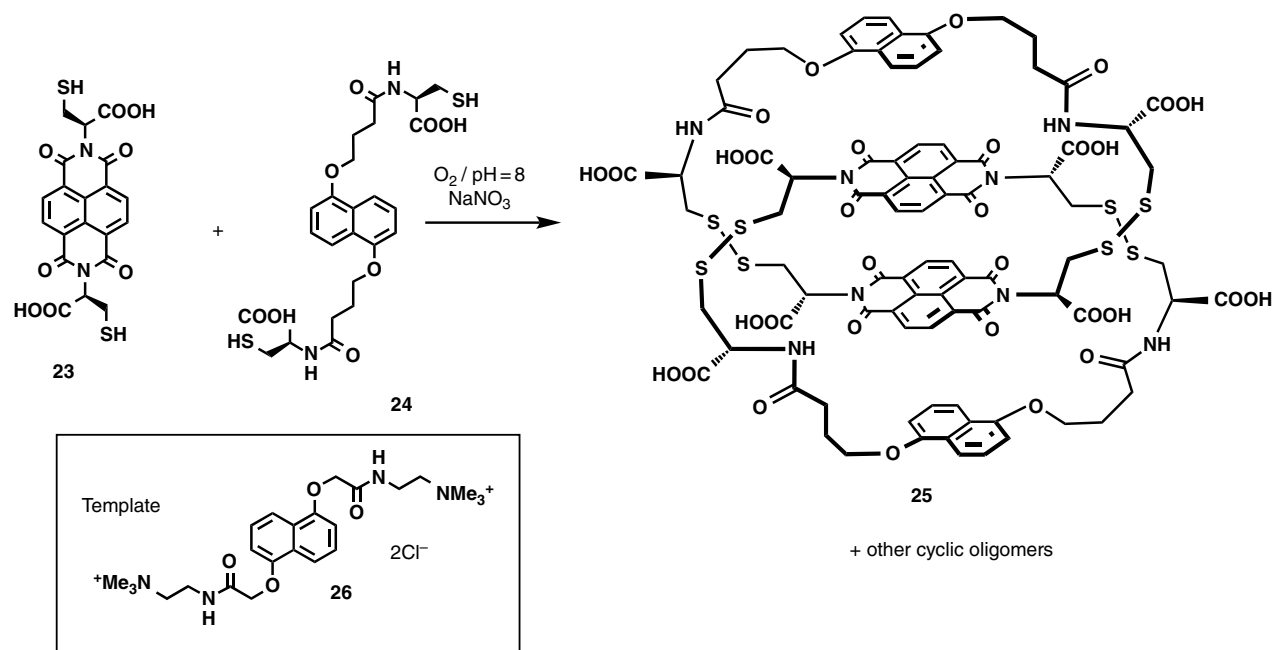
Scheme 7.8 Formation of a covalent donor–acceptor [2]catenane **25** from a dynamic covalent library with electron acceptor **23** and electron donor **24**. The structure of an electron-donating template **26** for product amplification is also illustrated.

(a)

(b)
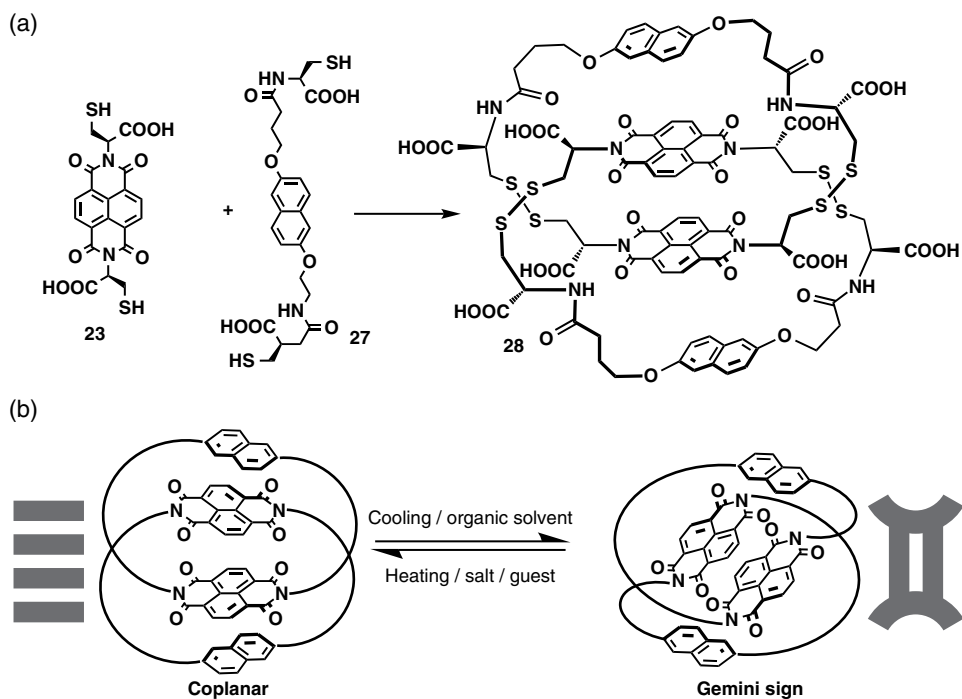
Scheme 7.9 (a) Synthesis of a donor–acceptor [2]catenane **28** that is able to (b) switch between a conventional parallel and an unconventional non-parallel conformation.

The power of DCvC also enabled the discovery of a conformationally switchable donor–acceptor [2]catenane **28** from a DCL. The reaction was carried out in water in a similar fashion to the synthesis of [2]catenane **25**, involving the same electron acceptor **23** and a slightly modified electron donor **27** (Scheme 7.9a), which differed from **24** by the substitution pattern on the DNP ring system (2,6- instead of 1,5-substitution).[35] Unlike [2]catenane **25**, two *co*-conformations were observed in the new [2]catenane **28**. While one of the conformations was the conventional coplanar donor–acceptor stack, the other one featured an unprecedented arrangement of the π systems, in which the flat NDI π surfaces were vertically stacked in parallel with each other to give a shape that is reminiscent of the astrological Gemini sign (Scheme 7.9b). Switching between the parallel and non-parallel conformations could be achieved by manipulating temperature or solvent polarity, or by the addition of the guest **26**. Raising the temperature or introduction of **26** favored the formation of the coplanar conformation, while decreasing the solvent polarity by adding acetone into water favored the formation of the Gemini conformation. The discovery of such an unconventional switchable system is another example that highlights the versatile role of DCvC in the discovery of compounds with unexpected structural features.

7.2.1.3 By Olefin Metathesis

The development of ruthenium–alkylidene complexes-catalyzed olefin metathesis has marked another major advance for the synthesis of interlocked molecules, including [2]rotaxanes,[39,40] [2]>catenanes,[41,42] and multiply threaded species.[43–46] For example,

ammonium binding has been utilized as the templating strategy to build triply threaded [2]rotaxanes[43] and [2]catenanes[44] in high yields after three-fold metathesis. As shown by Chen and co-workers, the D_{3h} symmetrical triptycene tris(crown ether) host **29** formed a complex with 3 equivalents of olefin-terminated dibenzylammonium (DBA) salt **30**, which, after olefin metathesis catalyzed by Grubbs' second-generation catalyst and subsequent hydrogenation, gave the triply threaded [2]catenane **31** in high yield (Scheme 7.10). Such multifold, templated metathesis has also been utilized in the synthesis of molecular trefoil knots,[47,48] and David's Star,[49] as pioneered by Sauvage and Leigh, respectively.

Chen and co-workers recently utilized the dynamic ring-closing olefin metathesis to build a triply interlocked [2]catenane **34** that could undergo stepwise rotary motion.[50]
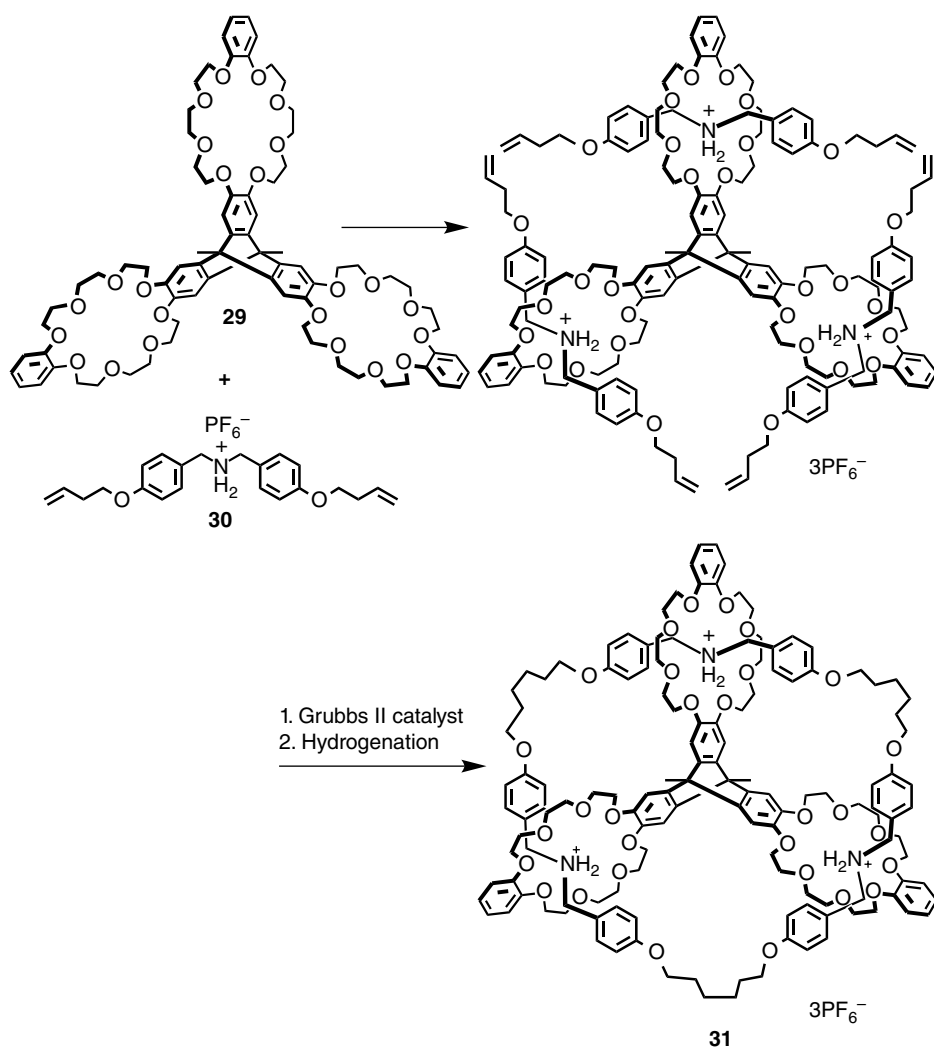
Scheme 7.10 Synthesis of a triply threaded [2]catenane by olefin metathesis.

Built on their earlier success on the synthesis of the D_{3h} symmetrical host **29**, they designed and synthesized a pyrazine-extended triptycene-derived tris(crown ether) **32** that had more free volume to accommodate three new recognition sites on the inner threading component (Scheme 7.11). The threading component **33** was constructed to contain three DBA and three methyltriazolium (MTA) recognition sites for dibenzo-24-crown-8 (DB24C8) and two alkenyl ends. Complexation between **32** and **33** occurred readily upon mixing, from which the [2]catenane **34** was obtained in 83% yield after treatment with a catalytic amount of Grubbs' second-generation catalyst and subsequent hydrogenation. The presence of multiple non-degenerative recognition sites in **34** rendered distinctive stepwise molecular motions during the acid–base triggered switching process, as all four *co*-conformations could be clearly identified by ^{1}H NMR titration experiment. Upon deprotonation with 1,8-diazabicyclo[5.4.0]undec-7-ene (DBU) of the first ammonium center in **34**, the surrounding crown ether left the DBA site to bind the nearest MTA site in the partially deprotonated **35** (Scheme 7.11b). The next deprotonation event of another DBA center activated the movement of the second DB24C8 arm to the nearby MTA site in **36**. Similar crown ether displacement was triggered during the final deprotonation of the third DBA center in **37**. All these processes could be reversed by the controlled addition of trifluoroacetic acid (TFA). It should be noted that the two MTA sites next to the same DBA site in the cyclic thread were spaced differently, which endowed unexpected selectivity due to the specific interlocked topology, with the one closer to the DBA site being the more favorable one after each protonation step. This study opens new windows for the design of artificial molecular machines with excellent mechanochemistry properties, the underlying motion mechanism of which could provide more insights into intricate biological molecular machines.

7.2.1.4 By Iodide-catalyzed DCvC

Stoddart and co-workers have employed an unusual thermodynamically controlled S_N2 reaction for the construction of switchable molecular motors by a magic-ring-like experiment. This was demonstrated in iodide-catalyzed catenation from two preformed covalent macrocycles, that is, an electron-deficient cyclobis(paraquat-*p*-phenylene) ring (**19**) and an electron-rich crown ether **38a** containing two dihydroquinone (HQ) units. Nucleophilic iodide attack of the benzylic carbons in **19** at 80 °C resulted in its ring opening (Scheme 7.12), leaving a linear molecule **39** that had less ring strain than the parent cyclophane. A pseudorotaxane was formed between **39** and the electron-rich crown ether by favorable host–guest interactions. Reverse S_N2 reaction between the free pyridine and the benzylic iodide regenerated the bisparaquat macrocycle, concurrent with formation of the interlocked [2]catenane **40a** in 46% isolated yield. The equilibrium was biased towards the side of [2]catenane because of the stabilizing π-donor–π-acceptor interactions between the two rings. The use of more electron-rich 1,5-dinaphtho[38]crown-10 (**38b**) proved advantageous, rendering the equilibrium virtually completely toward the [2]catenane side and a much higher isolated yield of 93%. This dynamic reaction was applied to the synthesis of bistable switchable [2]catenane **40c**[51] using this "magic ring" protocol. Under conditions identical to those used in the synthesis of **40a** and **40b**, **40c** was isolated in 60% yield, which was almost three times greater than that observed (23%) using conventional kinetically controlled reaction conditions.

(a)

1. Grubbs II catalyst
2. Hydrogenation

32 · 33

34

(b)

−H⁺

+H⁺

34

35

+H⁺   −H⁺

−H⁺

+H⁺

37

36
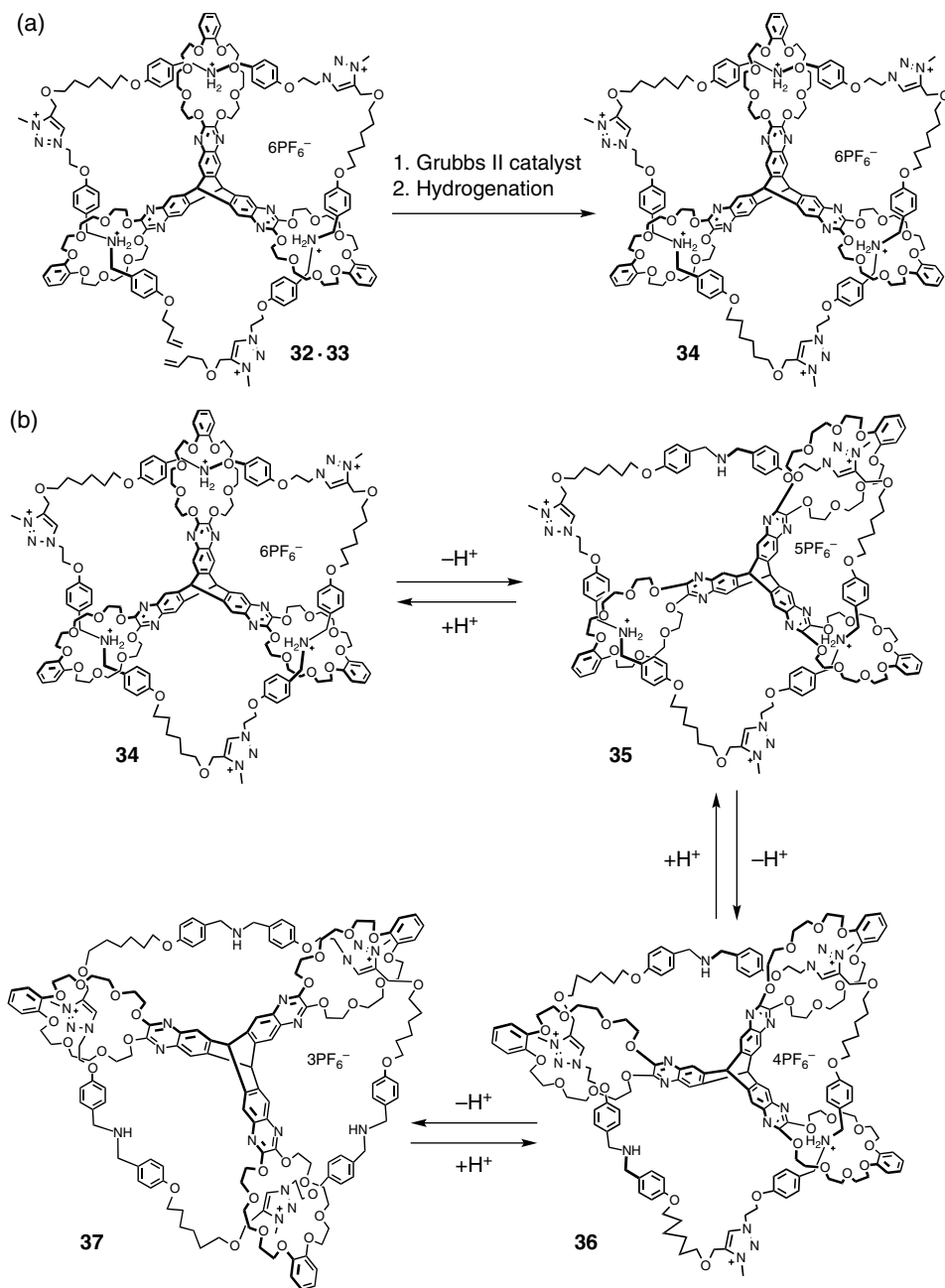
Scheme 7.11 (a) Synthesis of the triply interlocked [2]catenane **34** by olefin metathesis from the pseudorotaxane precursor **32·33**. (b) Illustration of the stepwise acid–base triggered switching process.
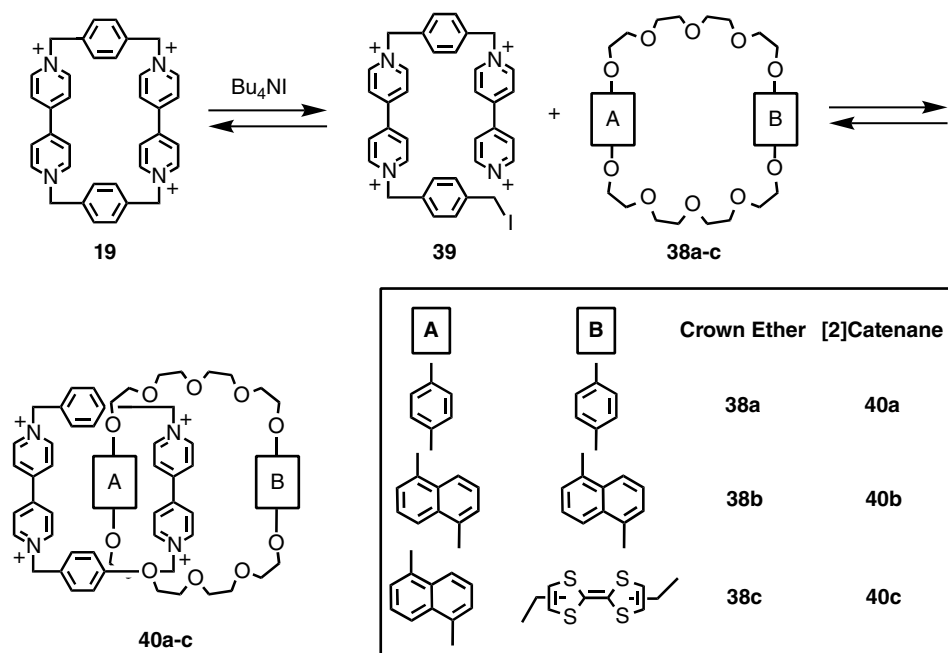
Scheme 7.12 Iodide-mediated ring-opening and ring-closing equilibrium that facilitate the formation of donor-acceptor [2]catenanes.

7.2.2 Non-interlocked Molecular Machines

Synthetic rotary molecular machines based on systems other than interlocked molecules can be accomplished by utilizing configurational isomerization of double bonds, such as *cis/trans* isomerization of the C = C bond demonstrated in chiral helical molecules.[52] The dynamic C = N double bond in imines and hydrazones could undergo similar isomerization and be utilized in a similar way to generate configurational and conformational changes through a sequence of chemical operations.

7.2.2.1 Imine-based Motors

As conjectured by Lehn,[53] imines and similar C = N-based classes of molecules can function as the simplest rotary motor. Two energetically biased processes are associated with configurational imine isomerization, namely, photochemically driven rotation and thermally activated "linear" inversion. The former process is based on a photochemical process that, on irradiation of the imine substrate, undergoes an "out-of-plane" rotation around the C = N bond via a perpendicular excited state PS_{rot}. When the two substituent groups are different (R_L and R_S represent larger and smaller substituents), such photochemical transformation may convert the thermodynamically more stable *anti* (*E*) form (R *trans* to R_L) to the less stable *syn* (*Z*) form (R *cis* to R_L). Following this photochemical process, the *syn* form can revert to the more favorable *anti* form through a thermally activated in-plane nitrogen inversion via a linear transition state TS_{inv}. Such photoinduced
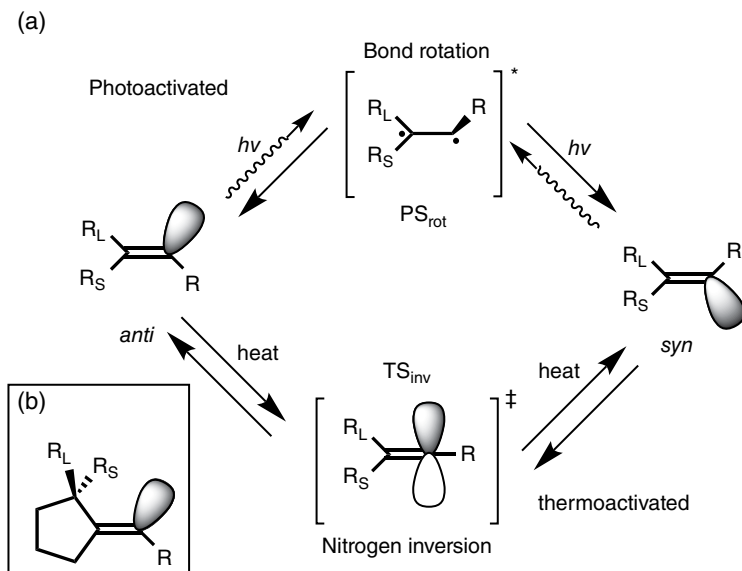
Scheme 7.13 (a) Two different pathways of configurational switching in imine through out-of-plane bond rotation (PS$_{rot}$) or in-plane nitrogen inversion (TS$_{inv}$). (b) A design of imine containing a symmetry-breaking chiral unit as a candidate for preferred unidirectional rotation. R$_L$ and R$_S$ represent larger and smaller substituents.

rotation of imines generates motor-like motions around the C–N axis with no directional selectivity. In order to incur unidirectional rotation, symmetry-breaking components, such as optically active cyclopentanone, which contains a chiral carbon center close to the imine group (Scheme 7.13b), was proposed to induce preferential rotation in one direction.

7.2.2.2 Imine-based Switches

Apart from the preparation of molecular motors, imine bonds can also be used for reversible switching control between the hydrophilic and hydrophobic surfaces of nanoparticles (Figure 7.2).[54] A hydrophilic, superparamagnetic iron oxide nanoparticle (SPIO-NH$_2$) with amine-functional groups can be condensed with hydrophobic, dendritic dialdehydes (Gn-CHO). From the wettability study, the SPIO-NH$_2$ demonstrates a water contact angle of 42° on a mica surface. On the other hand, the third-generation-dendronized SPIO (SPIO-G3) nanoparticles demonstrate a higher water contact angle of 85° on a mica surface. Thus, the dendronization of nanoparticles through imine bonds could result in a significant increase in the hydrophobicity. Actually, the hydrophobicity of the surface of the dendronized nanoparticles can be decreased by using different systems (Figure 7.2, inset graph) and tuned at different rates. The rate of decrease of the contact angle for SPIO-G3 is H$_2$O > 1% Co(OAc)$_2$/H$_2$O > DMF/H$_2$O (1:1), with rates of 4.0°, 2.9°, and 1.0° per minute, respectively. In particular, the use of a drop of 1% Co(OAc)$_2$/H$_2$O in the contact-angle measurement for SPIO-G3 gives a lower rate of decrease in the contact angle. This observation could be due to the
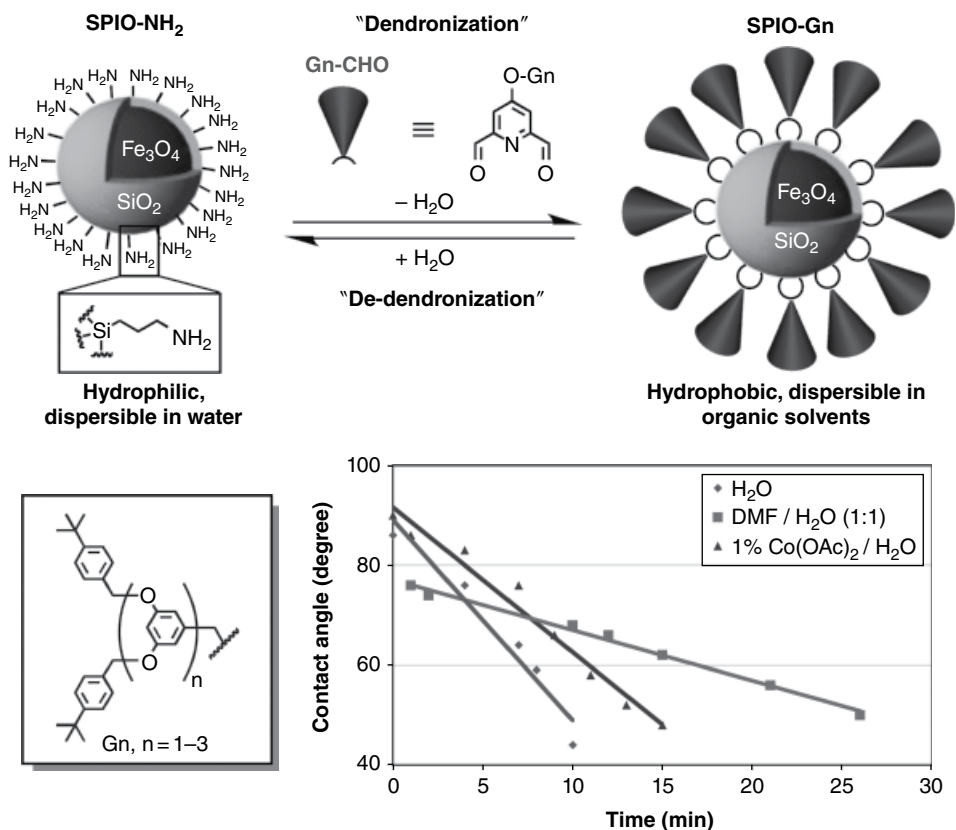
Figure 7.2 Graphical representation of the reversible control between hydrophilic SPIO-NH$_2$ nanoparticles and hydrophobic dendronized SPIO-Gn nanoparticles in the absence/presence of water. The graph is a plot of the contact angle (°) versus time (min), showing the wettability of SPIO-G3 nanoparticles using a drop of H$_2$O, DMF/H$_2$O (1:1), or 1% Co(OAc)$_2$/H$_2$O.

temporary templating process between the imine groups of SPIO-G3 and the Co^{2+} cations, which slows down the dissociation/hydrolysis process, revealing a larger final contact-angle value (48°) compared to the value using H$_2$O (44°). On the other hand, the use of a relatively less polar solvent system, DMF/H$_2$O (1:1), successfully reduces the dissociation rate of SPIO-G3 toward hydrolysis, with a 1.0°/min decrease in the contact angle. By removing the water molecules of the wetted SPIO-G3 nanoparticles, the surface of the nanoparticles becomes hydrophobic again, with an increased contact angle of >85°.

7.2.2.3 Hydrazone-based Switches

Aprahamian and co-workers reported the use of substituted aryl hydrazine derivatives as simple configurational rotary switches, in which the *E/Z* isomerization about the C=N bond was mediated by pH[55,56] and/or metal ion binding.[57,58] As shown in Scheme 7.14, hydrazones **41a/b** exist primarily as the *E* isomer at the equilibrium. On addition of trifluoroacetic acid, protonation of the pyridine moiety induces a
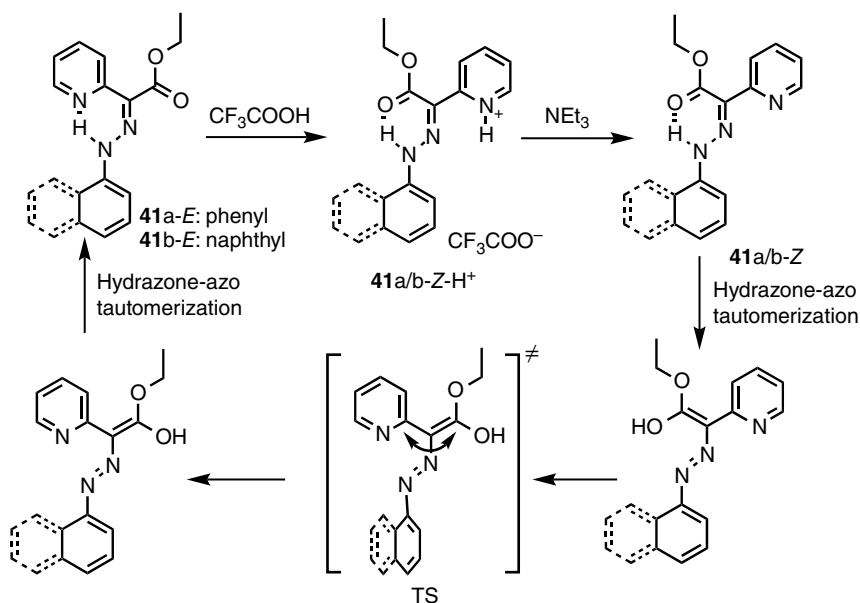
Scheme 7.14 Acid–base induced reversible switching of hydrazone **41a/b** and the proposed switching mechanism based on hydrazone-azo tautomerization.

rotation around the C=N double bond, corresponding to an *E* to *Z*-H⁺ switching. Such switching is reversible, as the *E* isomer can be reinstated by treatment with base. Combined kinetic studies and density functional theory calculations have shed light on the switching mechanism, which is a hydrazone-azo tautomerization followed by rotation around a C–N single bond, as opposed to the more common in-plane N–N inversion mechanism or the rotation mechanism around the C=N double bond.

When a quinoline ring system was used in **41c** to replace the naphthyl unit (Scheme 7.15a),[56] stepwise protonation of the pyridine and the quinoline units led to not only a similar rotation around the C=N double bond as these observed in **41a/b**, but also a conformational switching around the C–N single bond. The configurational and conformational switching occurred at each protonation event, and could be fully reverted to the ground state *E*-**41c** on treatment with NEt₃. In addition, it was found that **41c** also underwent *E/Z* isomerization on treatment with Zn²⁺ through a bioinspired coordination-coupled proton transfer mechanism (Scheme 7.15b).[58] In this process, coordination of Zn²⁺ with hydrazone led to both C=N bond rotation and a proton transfer from the hydrazone to pyridine. This process provides a new switching mechanism in which acid modulations can be applied without the addition of protons. Indeed, this metal ion coordination-induced proton transfer has proven to be a mild and neutral proton source that could be utilized to activate another hydrazone-based rotary switch as a tandem event.[57] Hydrazone **41d**, which is similar to **41c** but contains a methylimidazolyl group instead of a pyridyl one (Scheme 7.15c), can be switched to its Zn(**41d**-*Z*-H⁺) form by the addition of Zn(II) through the coordination-coupled deprotonation (CCD) mechanism. When this switching occurs in the presence of **41a**-*E*, a proton relay occurs, yielding Zn(**41d**-*Z*) and **41a**-*E*-H⁺. Such a process represents a
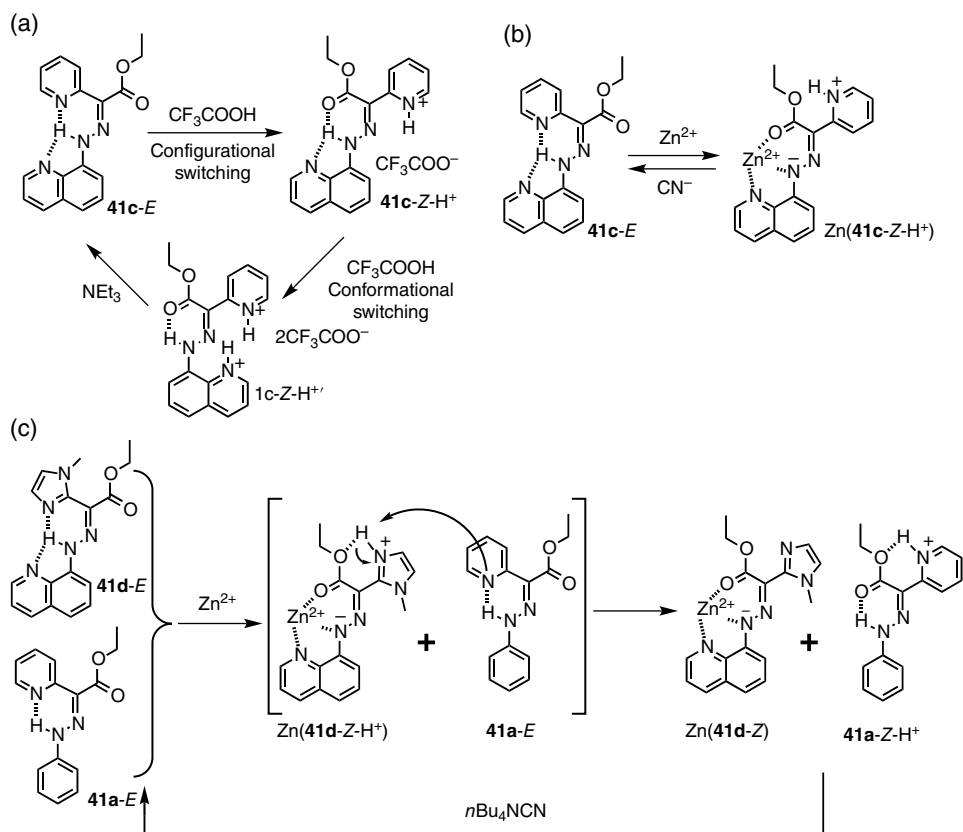
Scheme 7.15 Modified hydrazone switches: (a) a configurational and conformational switch activated by stepwise protonation, (b) a reversible switching activated by CCD mechanism, and (c) cascade switching based on the CCD mechanism.

novel switching cascade triggered by a single coordination event, which is reversible on addition of nBu$_4$NCN. The introduction of the methylimidazolyl group is critical for such a cascade switching, which does not proceed in the case of **41c**. The unusual acidity of the imidazolyl group over pyridine, which presumably is a result of a combination of electrostatic and conformational effects, is believed to be the key to the successive proton relay steps, the study of which might help elucidate the proton-coupled electron-transfer mechanism in photosynthetic bacteria.

7.3 Molecular Machines Operated by DCvC

Reversible covalent changes could be built within artificial molecular machines and utilized subsequently to direct controllable molecular motional changes, provided that the related covalent bonds can break and reform with high specificity under a mild chemical environment. The covalent characteristics should endow distinctive chemical
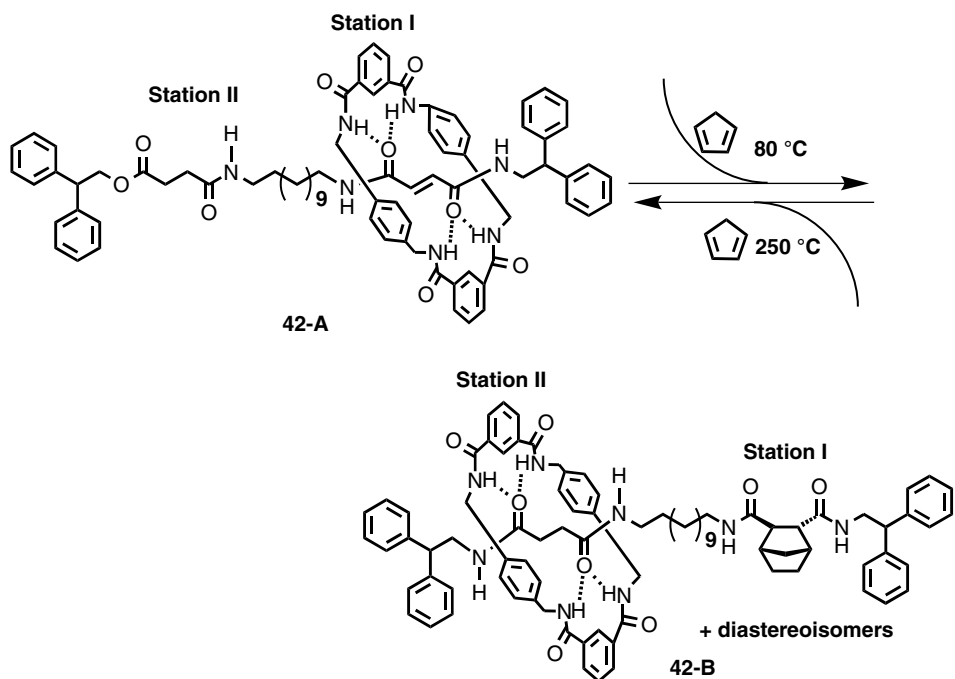
Scheme 7.16 Switching of molecular shuttle **42** by reversible Diels–Alder reaction.

states and thus bring high selectivity to their function. As summarized below, delicate design has led to great advancement of artificial molecular machines that are operated under reversible conditions.

7.3.1 Molecular Shuttles

Leigh and co-workers demonstrated an example of a bistable molecular shuttle that functioned through the formation and breaking of C–C bonds by virtue of the well-established reversible Diels–Alder reaction (Scheme 7.16).[59] The [2]rotaxane **42**-A was constructed to contain two stations, one diamide derived from fumaric acid (Station I) and one monoamide monoester derived from succinic acid (Station II), on the dumb-bell-shaped component. A tetraamide macrocycle was selectively located on Station I due to stronger hydrogen bonding interactions with fumaramide. Treating [2]rotaxane **42**-A with cyclopentadiene (CP) at 80 °C triggered its Diels–Alder cycloaddition to the double bond of Station I, resulting in shuttling of the tetraamide macrocycle from Station I to Station II. When the CP-appended [2]rotaxane **42**-B was heated at 250 °C under reduced pressure, retro-Diels–Alder reaction took place. The recovered Station I once again became the preferred recognition unit for the movable macrocycle, and the original state was restored.

Suzuki and co-workers have constructed bis-imine [2]rotaxanes **43a/b** that contain a macrocycle with two amino groups and a bisaldehyde dumbbell component (Figure 7.3a).[60] The macrocycle was affixed to the central bisaldehyde moiety due to the formation of imine bonds. When bis-imine rotaxane **43a** (A in Figure 7.3b) was

subjected to acidic hydrolysis conditions, stepwise imine dissociation was triggered. Corresponding aldehyde-ammonium-monoimine (B in Figure 7.3b) and dialdehyde-diammonium rotaxanes (C in Figure 7.3b) could be identified, the latter of which allowed the macrocycle shuttling between two identical p-OCH$_2$C$_6$H$_4$CH$_2$O spacers. The ratio of the dialdehyde-diammonium rotaxane increased on decreasing the temperature between 40 and -40 °C, suggesting that the imine hydrolysis is enthalpy driven while the imine bond formation is entropy driven. This example thus demonstrates that the submolecular mobility of the relative components could be controlled through temperature-dependent reversible imine formation.

Interestingly, when triethylene glycol spacers were used in **43b** as replacements for the p-OCH$_2$C$_6$H$_4$CH$_2$O ones in **43a**, the formation of intermediate aldehyde-ammonium-monoimine rotaxane was highly disfavored during hydrolysis.[61] Instead, the equilibrium was displaced towards the dialdehyde-diammonium rotaxane due to favorable hydrogen bonding between ammonium and the triethyleneglycol ether unit (Figure 7.3b). In contrast to [2]rotaxane **43a**, which behaves as a shuttle equilibrating between two identical states, in [2]rotaxane **43b** the shuttling is suppressed due to the
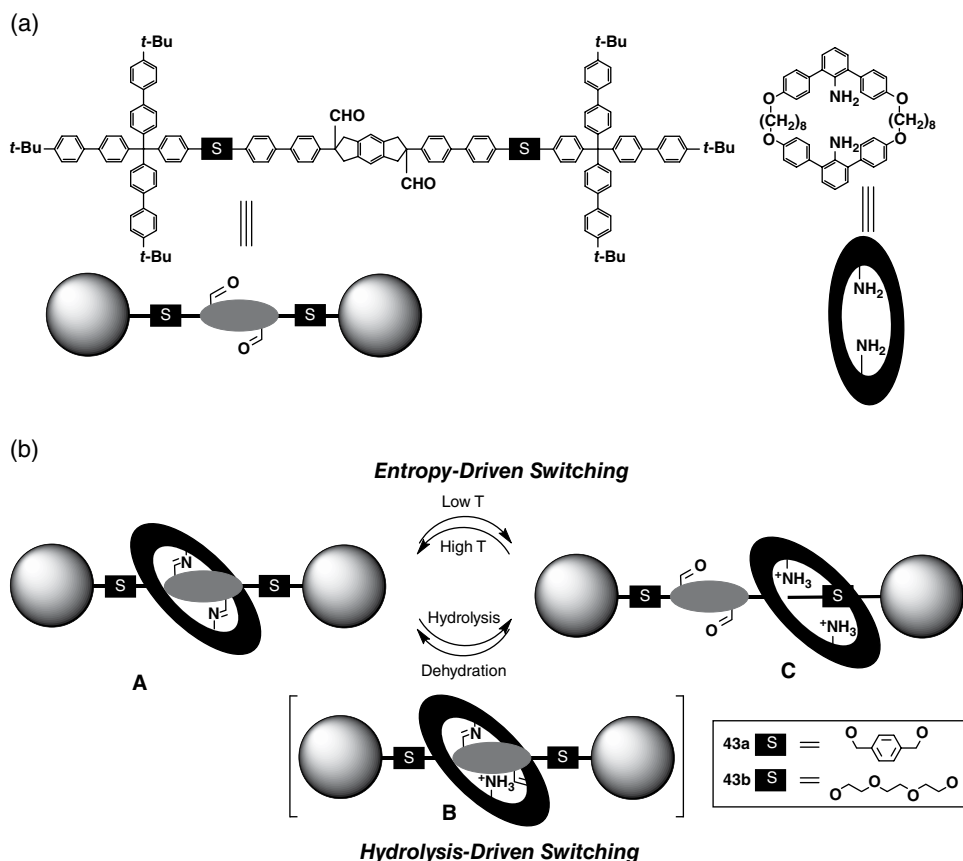
Figure 7.3 (a) Molecular structures of components of Suzuki's [2]rotaxanes **43a** and **43b**. (b) Acid- and temperature-dependent switching of the molecular shuttles.

same intramolecular hydrogen bonding interactions. The hydrating/dehydrating process could also be exercised by temperature control. At 100 °C under hydrolytic conditions, there was more than 95% bisimine [2]rotaxane, while at 0 °C there was 95% fully hydrolyzed [2]rotaxane, suggesting that this molecule could function as a molecular shuttle exhibiting entropy-driven translational isomerism with remarkable positional discrimination.

7.3.2 Molecular Walkers

Molecular walkers, which could be regarded as a special class of molecular motors, refer to the molecular systems where part of the molecules could move from one position to another after a series of chemical operations, similar to movements that walk along a track.[62] The first synthetic molecular walker was reported by Leigh and co-workers.[63] The molecule (**44**) consisted of a molecular track and a walker unit that was covalently linked by two different types of dynamic covalent bonds, namely, hydrazone and disulfide linkages (Scheme 7.17). The molecular track could be described as a four-station track, with two stations for hydrazone formation and two for disulfides, arranged alternately along the molecular backbone. Under acidic conditions, the macrocycle connecting stations **1** and **2** opened up at station **1** due to hydrazone hydrolysis. Under this equilibrating condition, hydrazone was formed at station **3** to give a new constitutional isomer, which corresponded to a first step moving of the walker along the track, with the other foot remaining locked on station **2** by a disulfide bond. The next walking step was activated by base, under which conditions the hydrazone foot at station **3** remained locked while the disulfide foot was unchained and allowed to complete the next step by reforming a new disulfide bond at station **4**. Such acid–base activation drove the walker to move from stations **1** and **2** to station **3** and **4**. All of the reactions employed in the operation of this walker track were equilibrium-based dynamic reactions, thus the walker unit moved back and forth along the track between chemically equivalent footholds, that is, the directionality was not well controlled. As a result, the final equilibrated systems consisted of a mixture of isomers, including 1,4-isomers and these intermediate walker-track systems, the ratio of which were related to the acid–base conditions. In an improved system,[64] the walker could be made to walk more preferentially in one direction by using an extra irreversible oxidation step to give rise to more of the completed walker-tracker 3,4-isomer in the equilibrated system.

The directionality, that is, the product distribution between the isomers, was further improved when an photoresponsive stilbene unit was incorporated in between two of the stations.[65] As shown in Scheme 7.18, in the initial state of molecular walker **45**, the stilbene unit adopted an *E* form. The directional migration of the walker unit from 1,2-isomer to 2,3-isomer was promoted by the following series of operations: after photochemical *E–Z* isomerization, the base activation step was applied to trigger the re-equilibrium of the walker between *Z*-1,2-**45** and *Z*-2,3-**45** with a ratio of 40:60. Subsequent photoisomerization of the *Z*-2,3-**45** walker gave the corresponding *E*-2,3-**45**, which also induced a strain within the walker macrocycle. The following acyl-hydrazone exchange could be activated by TFA hydrolysis to give *E*-3,4-**45**, which was greatly favored as driven by strain in *E*-2,3-**45**. This step was now furnished with a much enhanced selectivity (>95:5) towards the formation of *E*-3,4-**45**. The combined photoisomerization and acid–base activation steps could be used to reverse the walker-track migration sequence, thus rendering much improved processive and directional stepping.
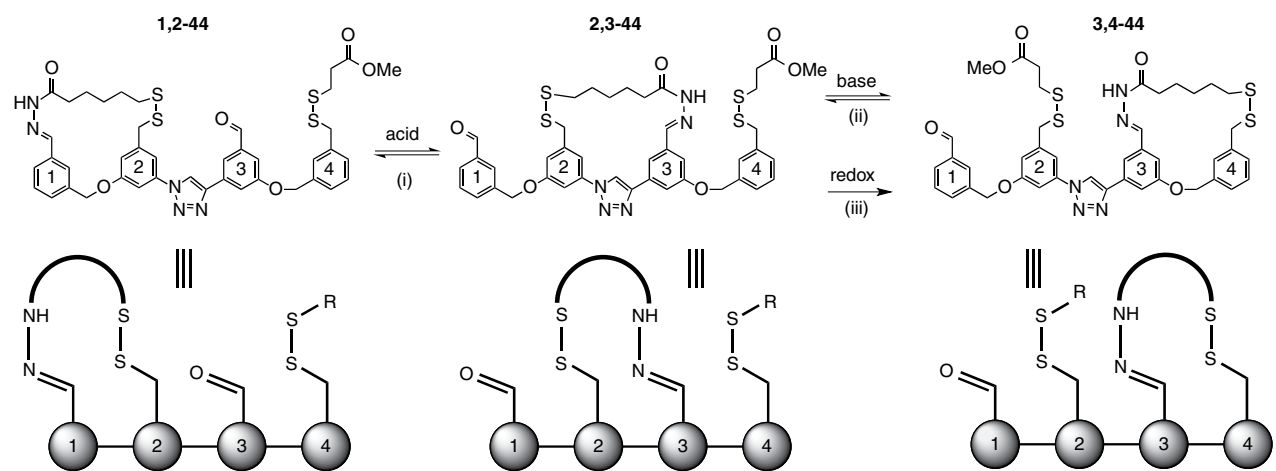
Scheme 7.17 The processive molecular walker **44** walking along the track via a series of dynamic covalent reactions.
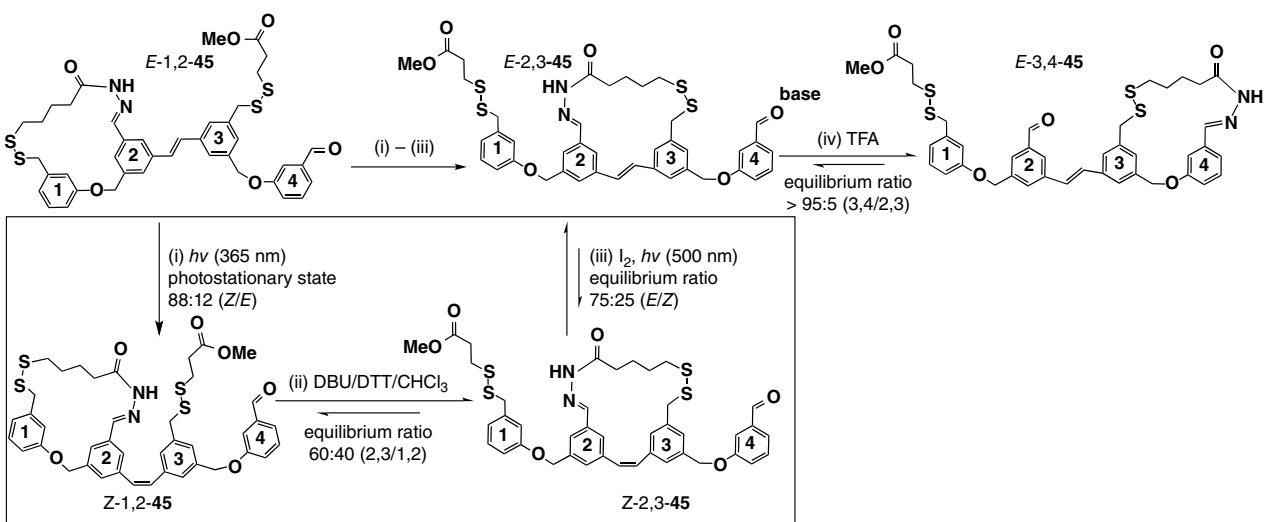
Scheme 7.18 A light-driven molecular walker **45**. The reactions highlighted in the box are breakdown steps for the formal walking steps from *E*-1,2-**45** to *E*-2,3-**45**.

Aside from these linear walkers, an elegant, biomimetic, interlocked molecular walker that also functions as a peptide synthesizer was recently reported by Leigh and co-workers,[66] which was reminiscent of ribosomal protein synthesis in biological systems. In this [2]rotaxane **46**, a macrocycle walker can move along a linear thread, which contains several amino acid-appended stations, while carrying a catalytic thiolate group. As the walker moves along the axial thread of the [2]rotaxane, it goes through several capture-rearrangement steps that ultimately lead to an autonomous peptide synthesis process in a sequence-specific manner (Scheme 7.19).

In [2]rotaxane **46**, the macrocyclic hydrazone walker was constructed to bear a cysteine unit with a trityl-protected thiolate group, and the axial component contained three different Boc-protected amino acid units that were separated from each other by rigid spacers. At the initial state, the macrocycle was located on the segments between the terminal stopper and the Boc-phenylalanine ester group. Activation of the walker was initiated by acid, which effectively liberated the free thiol and amino units after cleavage of trityl and Boc protecting groups to give **47** (step 1). On treatment with *N,N*-diisopropylethylamine, the thiol was deprotonated to become an active thiolate catalyst, which reacted with the nearby phenylalanine phenolic ester through transacylation reaction (step 2). The transferred phenylalanine unit was further relocated to the end of the macrocycle through an intramolecular 1,11-*S,N*-acyl transfer process (step 3), ending up with regeneration of the active thiolate site and elongation of the peptide sequence on the macrocycle. Once the first amino acid building block was removed, the macrocycle walker could move further along the track to reach the second amino acid building block. Another cycle of *O-S* transacylation and subsequent 1,14-*S,N*-acyl transfer steps (step 4) furnished the second peptide elongation process. Finally, one more repetitive sequential acyl transfer (step 5) completed the third elongation step. Dissociation of the macrocycle walker from the axial thread occurred after the removal of the last amino acid stopper, which, upon hydrazone hydrolysis, gave the sequence-specific hydrazide peptide **48b** (step 6). Remarkably, no starting material, deletions, or unexpected sequences were observed, highlighting the accuracy of the autonomous actions. Overall, a combination of transacylation reaction, thiolate regeneration and macrocycle walking was employed to generate a synthetic system that could function as an autonomous peptide synthesizer.

The above [2]rotaxane molecular walker was synthesized by a "final-step-threading" method, which relies on a key active template reaction as the last step of a long synthetic route. The low yield of the final threading limited its utility for longer peptide synthesis. This situation was significantly improved by utilizing a "rotaxane-capping" protocol, which involved attachment of a preformed [2]rotaxane synthon to the end of a fully formed strand of building blocks.[67] Threaded molecular machines with extended oligomeric, and potentially polymeric, tracks could be obtained following this protocol. Despite some limitations, such as slow kinetics and loss of the sequence information on the track during its working, such a molecular walker represents an important step towards the fabrication of artificial molecular machines that can perform complex work comparable to nature's biological machines.

Lehn and co-workers have described[68] a simple prototype of a system that displays relative motions of molecular moieties based on imine exchange within the reaction between salicylaldehyde (SALAL) and linear oligoamines (Scheme 7.20). For example, the 1:1 condensation product of SALAL and diethylene triamine gave **49**, in which
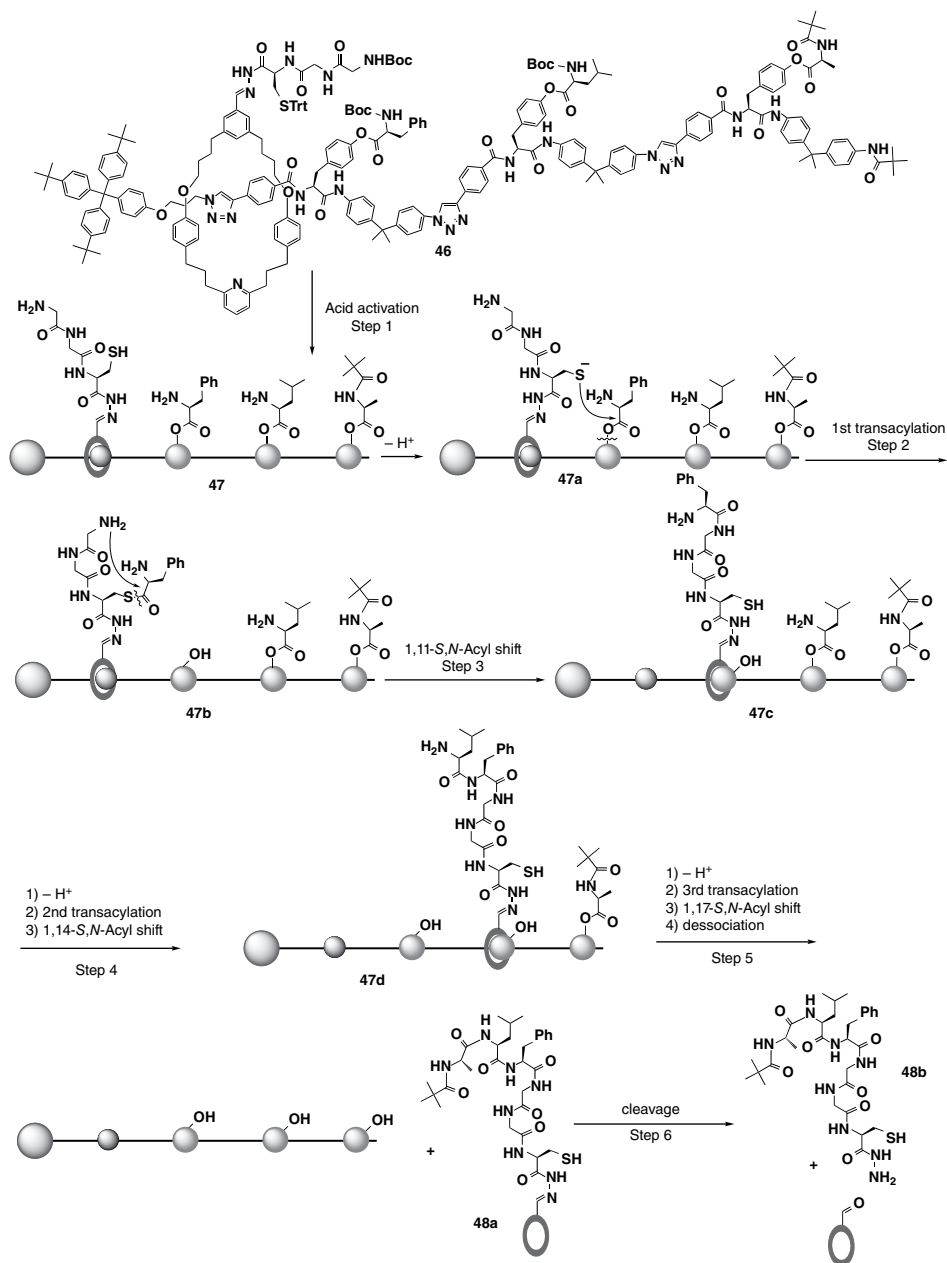
Scheme 7.19 A [2]rotaxane-based molecular walker **46** that synthesizes peptide **48b** after a sequence of capture-rearrangement steps.

non-directional displacement occurred as the aldehyde residue transferred along the polyamine chain by reversible covalent bond formation. As indicated in Scheme 7.20, cyclic aminal and iminium intermediates were formed during the intramolecular inch-worm-like movement of a salicylidene residue along the oligoamine chain, which was
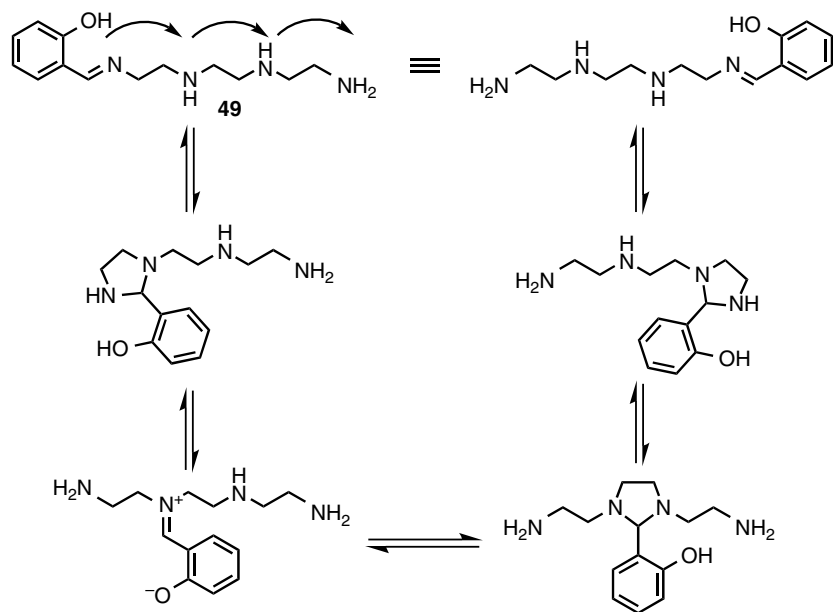
Scheme 7.20 Mechanism of the dynamic intramolecular inchworm-type walking of a salicylidene residue along an oligoamine chain.

processive since the two moieties remained attached along the way. Such motional processes take place without a change in molecular constitution, thus representing a novel category of dynamic covalent motions.

The above imine-based molecular walker showcases a simple prototype of processive machines, although the movement lacks directionality. In an improved design, controlled directional displacement of a molecular group has been achieved.[69] This was based on the reactions of *ortho*-carboxybenzaldehyde (CAXAL) with primary and secondary amines to give imines or amino lactones, respectively, depending on the acidity of the medium. When there was also a formyl group *ortho* to the hydroxyl, such as 2-formyl-3-hydroxybenzoic acid (SAXAL), it combined the structural benefits of both salicylaldehyde (SALAL), which preferred imine formation, and CAXAL, which preferred formation of lactone under acidic conditions. With the control of pH, the intramolecular walker **50** (Scheme 7.21) could thus be programmed to have the SAXAL unit walk along a non-symmetric polyamine chain, with an imine serving as the terminus under basic conditions on one end and a lactone formed on the other end under acidic conditions. In other words, the lactone **51** was formed quantitatively on reacting SAXAL under acidic conditions with the track in its free base form. Addition of 3 equivalents of base was required to shift the equilibrium to the imine form **50**. The displacement was fully reversible and addition of 3 equivalents of acid reverted the displacement completely to the starting lactone **51**. By utilizing the special reactivity of the *ortho*-carboxybenzaldehyde, this dynamic covalent motional system extends the DCvC of imines to secondary amines, and could open up new perspectives in this field.

In addition to imine chemistry, a molecular walker was constructed by Leigh and co-workers based on processive intramolecular Michael and retro-Michael reactions.[70]
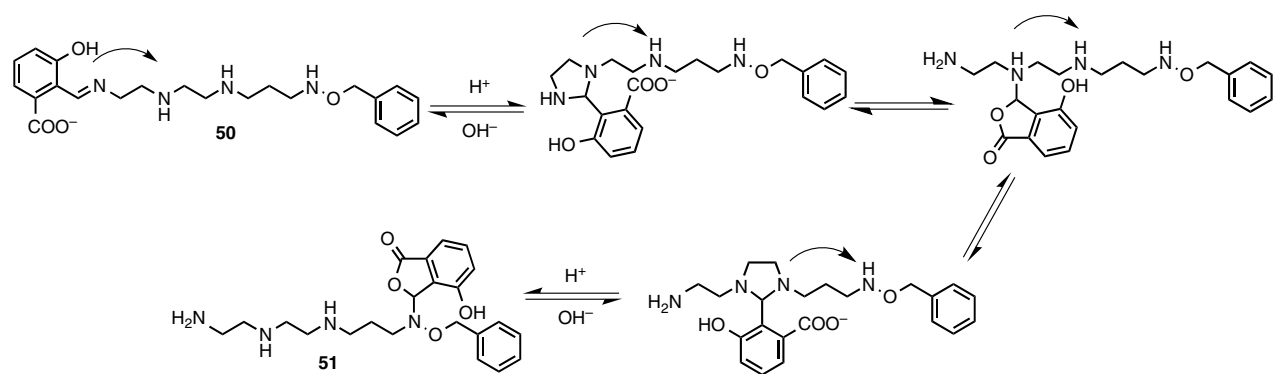
Scheme 7.21 Displacement of the SAXAL walker along the polyamine track bearing a primary amine as the imine-forming terminus and the benzoxyamine as the lactone terminus.
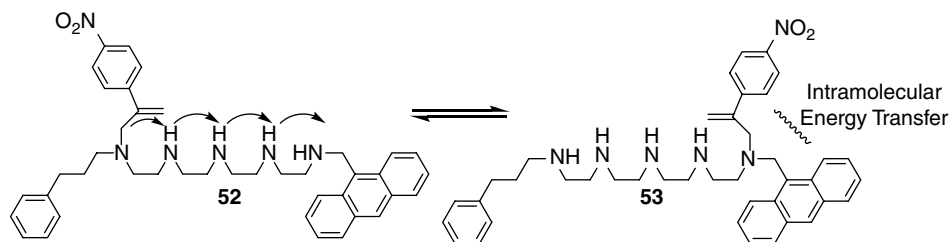
Scheme 7.22 A processive walker based on a Michael–retro-Michael addition mechanism that can perform a simple task, that is, quenching the fluorescence of the end anthracene group.

As shown in Scheme 7.22, a model walker-track conjugate **52** was designed to contain an α-methylene-4-nitrostyrene walking unit and an oligoethyleneimine track. The walking unit was initially linked to the first amine foothold of the track by one leg. Subsequent ring-closing intramolecular Michael addition reaction between the olefin bond of the styrene unit and the adjacent amine group of the track resulted in attachment of the walking unit to a neighboring foothold. Following a retro-Michael ring-opening rearrangement reaction, either of the legs of the walking unit was detached from the track, leaving a free, reactive olefin bond ready for repetitive foothold attachment and detachment sequences. Such a sequence allowed an α-methylene-4-nitrostyrene walker to travel through five footholds along the track step without external intervention. When an anthracene fluorophore was installed on the opposite end of the walker unit along the oligoethyleneimine track, 54% quenching of anthracene fluorescence was observed in **53** after a thermodynamic equilibrium was reached within 6.5 h, corresponding to an intramolecular static quenching effect imposed by the nitrostyrene walker that was closer in space after walking back and forth along the track. Recently, the α-methylene-4-nitrostyrene walker was shown to be able to walk along an oligoethyleneimine track with up to nine footholds with a naphthylmethylamine end.[71] Interestingly, naphthylmethylamine appeared to be the most favorable foothold for the walker, with the dynamics of the walker migration following the random walk of a Brownian particle in one dimension.

7.4 Concluding Remarks and Outlook

The marriage of DCvC and molecular machines has undoubtedly brought new opportunities to the field of artificial molecular machines. On one hand, design and synthesis of rather complex metastable molecular systems could benefit from the high selectivity and specificity aspects of DCvC. On the other hand, employment of DCvC opens the door to build molecular machineries with unconventional switching pathways that rely on constitutional changes in addition to *co*-conformational changes. Furthermore, operation of molecular machines by covalent bonding changes offers more distinctive states, implying more functions and controllability. Finally, as has been shown in synthetic molecular walkers, the use of orthogonal DCvC enables the fabrication of more sophisticated artificial molecular machines. These machines take advantage of the dynamic nature of reversible reactions, which is distinctive from those based on

non-covalent interactions. Most of the systems, however, rely on thermodynamically equilibrated systems. This leaves a lot of room for future studies of the kinetics of molecular machineries. Any chemical input, or input by other means that can affect the equilibrium, for example, kinetic fixation of a dynamic covalent bond, will be useful in enhancing the operation efficacy of such machines.

From a practical point of view, transforming molecular machines from chemical devices to mechanical devices that can accomplish real-world tasks is one of the most pressing tasks in contemporary nanoscience.[72] Scientists have made great strides in instating bistabilities in molecular systems, yet the integration of these switchable molecules into hierarchical and coherent suprastructures to perform work on their immediate environment across different length scales is still a grand challenge. On the single molecular level, how these machines respond to thermal fluctuation is fundamental to the understanding of basic molecular behavior. The fusion of DCvC and molecular machines naturally opens up a window to the discovery of biomimetic materials systems with controls that are on a par with or superior to nature's machines. The versatile features associated with synthetic molecular machines, which in many cases are inaccessible without the enabling DCvC, will continue to provide an informed search for more functional chemical devices and a pathway to real-world mechanical devices.

References

1 V. Balzani, A. Credi, M. Venturi, in *Molecular Devices and Machines – A Journey into the Nano World*, Wiley-VCH Verlag GmbH & Co. KGaA, **2004**.

2 E. R. Kay, D. A. Leigh, *Angew. Chem., Int. Ed.* **2015**, *54*, 10080–10088.

3 V. Balzani, A. Credi, F. M. Raymo, J. F. Stoddart, *Angew. Chem., Int. Ed.* **2000**, *39*, 3348–3391.

4 J.-P. Sauvage, *Acc. Chem. Res.* **1998**, *31*, 611–619.

5 C. Mavroidis, A. Dubey, M. Yarmush, *Annu. Rev. Biomed. Eng.* **2004**, *6*, 363–395.

6 J. F. Stoddart, *Angew. Chem., Int. Ed.* **2014**, *53*, 11102–11104.

7 J. M. Lehn, *Angew. Chem., Int. Ed.* **1990**, *29*, 1304–1319.

8 J. W. Steed, J. L. Atwood, *Supramolecular chemistry*, John Wiley & Sons, **2013**.

9 J.-M. Lehn, *Supramolecular chemistry, Vol. 1*, Vch, Weinheim, **1995**.

10 S. J. Rowan, S. J. Cantrill, G. R. L. Cousins, J. K. M. Sanders, J. F. Stoddart, *Angew. Chem., Int. Ed.* **2002**, *41*, 898–952.

11 J.-M. Lehn, *Chem. Soc. Rev.* **2007**, *36*, 151–160.

12 Y. Jin, C. Yu, R. J. Denman, W. Zhang, *Chem. Soc. Rev.* **2013**, *42*, 6634–6654.

13 A. Wilson, G. Gasparini, S. Matile, *Chem. Soc. Rev.* **2014**, *43*, 1948–1962.

14 N. M. Rue, J. Sun, R. Warmuth, *Isr. J. Chem.* **2011**, *51*, 743–768.

15 Y. Jin, Q. Wang, P. Taynton, W. Zhang, *Acc. Chem. Res.* **2014**, *47*, 1575–1586.

16 J. Li, P. Nowak, S. Otto, *J. Am. Chem. Soc.* **2013**, *135*, 9222–9239.

17 P. T. Corbett, J. Leclaire, L. Vial, K. R. West, J.-L. Wietor, J. K. M. Sanders, S. Otto, *Chem. Rev.* **2006**, *106*, 3652–3711.

18 S. Otto, K. Severin, *Topics Curr. Chem.* **2007**, *277*, 267–288.

19 A.-M. Stadler, J. Ramirez, *Topics Curr. Chem.* **2012**, *322*, 261–290.

20 Y. Liu, Z.-T. Li, *Aust. J. Chem.* **2013**, *66*, 9–22.

21 P. C. Haussmann, J. F. Stoddart, *Chem. Rec.* **2009**, *9*, 136–154.

22 P. T. Glink, A. I. Oliva, J. F. Stoddart, A. J. P. White, D. J. Williams, *Angew. Chem., Int. Ed.* **2001**, *40*, 1870–1875.

23 J. Wu, K. C.-F. Leung, J. F. Stoddart, *Proc. Natl. Acad. Sci. USA* **2007**, *104*, 17266–17271.

24 M. E. Belowich, C. Valente, R. A. Smaldone, D. C. Friedman, J. Thiel, L. Cronin, J. F. Stoddart, *J. Am. Chem. Soc.* **2012**, *134*, 5243–5261.

25 E. Coronado, P. Gavina, J. Ponce, S. Tatay, *Chem. Eur. J.* **2014**, *20*, 6939–6950.

26 Z. Li, F. Hu, G. Liu, W. Xue, X. Chen, S. H. Liu, J. Yin, *Org. Biomol. Chem.* **2014**, *12*, 7702–7711.

27 W.-Y. Wong, K. C.-F. Leung, J. F. Stoddart, *Org. Biomol. Chem.* **2010**, *8*, 2332–2343.

28 L. M. Klivansky, G. Koshkakaryan, D. Cao, Y. Liu, *Angew. Chem., Int. Ed.* **2009**, *48*, 4185–4189.

29 A. Pun, D. A. Hanifi, G. Kiel, E. O'Brien, Y. Liu, *Angew. Chem.* **2012**, *124*, 13296–13299.

30 A. B. Pun, K. J. Gagnon, L. M. Klivansky, S. J. Teat, Z.-T. Li, Y. Liu, *Org. Chem. Front.* **2014**, *1*, 167–175.

31 G. Koshkakaryan, D. Cao, L. M. Klivansky, S. J. Teat, J. L. Tran, Y. Liu, *Org. Lett.* **2010**, *12*, 1528–1531.

32 R. T. S. Lam, A. Belenguer, S. L. Roberts, C. Naumann, T. Jarrosson, S. Otto, J. K. M. Sanders, *Science* **2005**, *308*, 667–669.

33 H. Y. Au-Yeung, G. D. Pantos, J. K. M. Sanders, *J. Am. Chem. Soc.* **2009**, *131*, 16030–16031.

34 H. Y. Au-Yeung, G. D. Pantos, J. K. M. Sanders, *Proc. Natl. Acad. Sci. USA* **2009**, *106*, 10466–10470.

35 H. Y. Au-Yeung, G. D. Pantos, J. K. M. Sanders, *Angew. Chem., Int. Ed.* **2010**, *49*, 5331–5334.

36 S. P. Black, A. R. Stefankiewicz, M. M. J. Smulders, D. Sattler, C. A. Schalley, J. R. Nitschke, J. K. M. Sanders, *Angew. Chem., Int. Ed.* **2013**, *52*, 5749–5752.

37 F. B. L. Cougnon, N. A. Jenkins, G. D. Pantoş, J. K. M. Sanders, *Angew. Chem., Int. Ed.* **2012**, *51*, 1443–1447.

38 F. B. L. Cougnon, H. Y. Au-Yeung, G. D. Pantoş, J. K. M. Sanders, *J. Am. Chem. Soc.* **2011**, *133*, 3198–3207.

39 S. J. Cantrill, R. H. Grubbs, D. Lanari, K. C. F. Leung, A. Nelson, K. G. Poulin-Kerstien, S. P. Smidt, J. F. Stoddart, D. A. Tirrell, *Org. Lett.* **2005**, *7*, 4213–4216.

40 E. N. Guidry, J. Li, J. F. Stoddart, R. H. Grubbs, *J. Am. Chem. Soc.* **2007**, *129*, 8944–8945.

41 S. Li, M. Liu, B. Zheng, K. Zhu, F. Wang, N. Li, X.-L. Zhao, F. Huang, *Org. Lett.* **2009**, *11*, 3350–3353.

42 E. N. Guidry, S. J. Cantrill, J. F. Stoddart, R. H. Grubbs, *Org. Lett.* **2005**, *7*, 2129–2132.

43 J. D. Badjić, S. J. Cantrill, R. H. Grubbs, E. N. Guidry, R. Orenes, J. F. Stoddart, *Angew. Chem., Int. Ed.* **2004**, *43*, 3273–3278.

44 X.-Z. Zhu, C.-F. Chen, *J. Am. Chem. Soc.* **2005**, *127*, 13158–13159.

45 H. Hou, K. C. F. Leung, D. Lanari, A. Nelson, J. F. Stoddart, R. H. Grubbs, *J. Am. Chem. Soc.* **2006**, *128*, 15358–15359.

46 L. Wang, M. O. Vysotsky, A. Bogdan, M. Bolte, V. Böhmer, *Science* **2004**, *304*, 1312–1314.

47 C. Dietrich-Buchecker, G. Rapenne, *Chem. Commun.* **1997**, 2053–2054.

48 J.-F. Ayme, G. Gil-Ramírez, D. A. Leigh, J.-F. Lemonnier, A. Markevicius, C. A. Muryn, G. Zhang, *J. Am. Chem. Soc.* **2014**, *136*, 13142–13145.

49 D. A. Leigh, R. G. Pritchard, A. J. Stephens, *Nat. Chem.* **2014**, *6*, 978–982.

50 Z. Meng, Y. Han, L.-N. Wang, J.-F. Xiang, S.-G. He, C.-F. Chen, *J. Am. Chem. Soc.* **2015**, *137*.

51 M. Asakawa, P. R. Ashton, V. Balzani, A. Credi, C. Hamers, G. Mattersteig, M. Montalti, A. N. Shipway, N. Spencer, J. F. Stoddart, M. S. Tolley, M. Venturi, A. J. P. White, D. J. Williams, *Angew. Chem., Int. Ed.* **1998**, *37*, 333–337.

52 R. A. van Delden, M. K. J. ter Wiel, M. M. Pollard, J. Vicario, N. Koumura, B. L. Feringa, *Nature* **2005**, *437*, 1337–1340.

53 J.-M. Lehn, *Chem. Eur. J.* **2006**, *12*, 5910–5915.

54 K. C.-F. Leung, S. Xuan, C.-M. Lo, *ACS Appl. Mater. Inter.* **2009**, *1*, 2005–2012.

55 S. M. Landge, E. Tkatchouk, D. Benítez, D. A. Lanfranchi, M. Elhabiri, W. A. Goddard, I. Aprahamian, *J. Am. Chem. Soc.* **2011**, *133*, 9812–9823.

56 X. Su, I. Aprahamian, *Org. Lett.* **2011**, *13*, 30–33.

57 D. Ray, J. T. Foy, R. P. Hughes, I. Aprahamian, *Nat. Chem.* **2012**, *4*, 757–762.

58 X. Su, T. F. Robbins, I. Aprahamian, *Angew. Chem., Int. Ed.* **2011**, *50*, 1841–1844.

59 D. A. Leigh, E. M. Perez, *Chem. Commun.* **2004**, 2262–2263.

60 H. Kawai, T. Umehara, K. Fujiwara, T. Tsuji, T. Suzuki, *Angew. Chem., Int. Ed.* **2006**, *45*, 4281–4286.

61 T. Umehara, H. Kawai, K. Fujiwara, T. Suzuki, *J. Am. Chem. Soc.* **2008**, *130*, 13981–13988.

62 M. von Delius, D. A. Leigh, *Chem. Soc. Rev.* **2011**, *40*, 3656–3676.

63 M. von Delius, E. M. Geertsema, D. A. Leigh, *Nat. Chem.* **2010**, *2*, 96–101.

64 M. von Delius, E. M. Geertsema, D. A. Leigh, D.-T. D. Tang, *J. Am. Chem. Soc.* **2010**, *132*, 16134–16145.

65 M. J. Barrell, A. G. Campana, M. von Delius, E. M. Geertsema, D. A. Leigh, *Angew. Chem., Int. Ed.* **2011**, *50*, 285–290.

66 B. Lewandowski, G. De Bo, J. W. Ward, M. Papmeyer, S. Kuschel, M. J. Aldegunde, P. M. E. Gramlich, D. Heckmann, S. M. Goldup, D. M. D'Souza, A. E. Fernandes, D. A. Leigh, *Science* **2013**, *339*, 189–193.

67 G. De Bo, S. Kuschel, D. A. Leigh, B. Lewandowski, M. Papmeyer, J. W. Ward, *J. Am. Chem. Soc.* **2014**, *136*, 5811–5814.

68 P. Kovaříček, J.-M. Lehn, *J. Am. Chem. Soc.* **2012**, *134*, 9446–9455.

69 P. Kovaříček, J.-M. Lehn, *Chem. Eur. J.* **2015**, *21*, 9380–9384.

70 A. G. Campaña, A. Carlone, K. Chen, D. T. F. Dryden, D. A. Leigh, U. Lewandowska, K. M. Mullen, *Angew. Chem., Int. Ed.* **2012**, *51*, 5480–5483.

71 A. G. Campaña, D. A. Leigh, U. Lewandowska, *J. Am. Chem. Soc.* **2013**, *135*, 8639–8645.

72 A. Coskun, M. Banaszak, R. D. Astumian, J. F. Stoddart, B. A. Grzybowski, *Chem. Soc. Rev.* **2012**, *41*, 19–30.

8

Responsive Dynamic Covalent Polymers

Soma Mukherjee, Jessica J. Cash, and Brent S. Sumerlin

8.1 Introduction

Polymers have traditionally served as building blocks to prepare materials with enhanced mechanical, thermal, and electronic properties for specific applications. Incorporation of covalent crosslinking into the polymer matrix was used primarily to prevent degradation of the material and undesired change in the material's properties. Over the past few decades there has been a growing interest in preparing selectively tailored polymeric assemblies and interfaces having dynamic or reversible bonds, which can be broken and reformed by exposure to an appropriate stimulus, producing a macroscopic response.[1,2] Dynamic bonds encompass two broad categories: supramolecular or non-covalent interactions, and reversible-covalent or dynamic covalent interactions. Hydrogen bonding,[3,4] π–π stacking,[5] electrostatic interaction (ion–ion and ion–dipole),[6] and metal–ligand coordination[7,8] are some of the non-covalent interactions that have been utilized to construct reversible macromolecular architectures.[8–10] Non-covalent interactions are the basis of supramolecular chemistry, which has emerged spectacularly in the area of molecular recognition and recognition-based self-organization in the past few decades.[1] Cram, Lehn, and Pederson shared the Nobel Prize in chemistry in 1987 for their pioneering work in the area of molecular recognition, specifically for the discovery and investigation of cryptands, a family of synthetic bi- and polycyclic multidentate ligands for a variety of cations.[1,6] Their seminal works in the field of supramolecular chemistry laid the pathway for "dynamic covalent" chemistry, chemical reactions of reversible covalent bonds carried out under thermodynamic equilibrium conditions.[8] Some commonly explored dynamic covalent bonds are thermally cleavable alkoxyamines,[11,12] furan-maleimide Diels–Alder linkage,[13,14] esters,[15] disulfides,[16–21] boronic esters,[22] imines,[23] oximes,[24–27] and hydrazones (Scheme 8.1).[8]

Reversible change in the physical or chemical properties of a dynamic covalent polymer is generally caused by an external signal or stimulus. In many biopolymers in living organisms, exposure to a stimulus causes controlled responses. The similarity of this phenomena to systems based on synthetic reversible bonds has inspired many material designs in the scientific community.[28] The stimulus can originate from the change of

(a) Non-covalent interactions

H-bonding

Metal-ligand coordination

$$M(L_1)_n]^{m+} + nL_2 \rightleftharpoons M(L_2)_n]^{m+} + nL_1$$
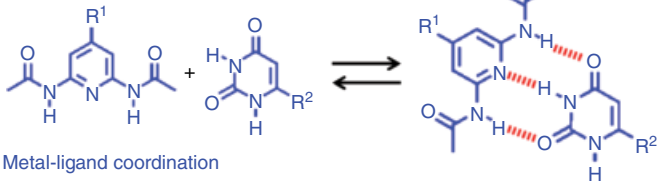
π-π stacking
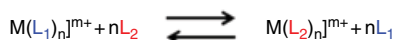
π acceptor π donor π-π stacking

Electrostatic interaction

$$R^1NH_3^+ + R^2COO^- \rightleftharpoons R^1NH_3^+ \cdots {}^-OOCR^2$$

(b) Dynamic-covalent bonds
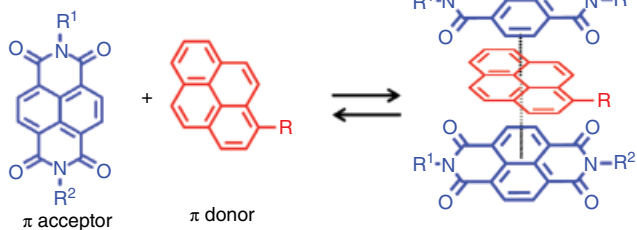
Alkoxyamines
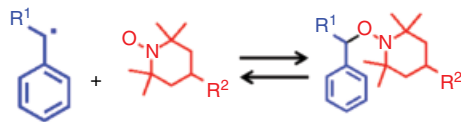
Diels-Alder linkages

Esters

$$R^1 \overset{O}{\underset{OH}{\wedge}} + R^2\text{-}OH \rightleftharpoons R^1 \overset{O}{\underset{O}{\wedge}} R^2 + H_2O$$
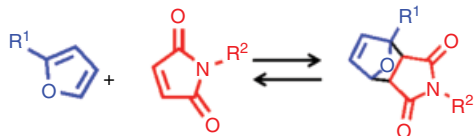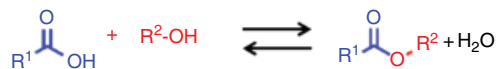
Imines, oximes, and hydrazones

$$R^1 \overset{O}{\underset{R^2}{\wedge}} + R^3\text{-}NH_2 \rightleftharpoons \overset{R^3}{\underset{R^1 \quad R^2}{N}} + H_2O$$

Disulfides

$$2\,R^1SH \rightleftharpoons R^1\text{-}S\text{-}S\text{-}R^1 + 2H^+ + 2e^-$$

Boronic esters

$$R^1\text{-B}\overset{OH}{\underset{OH}{}} + \overset{HO}{\underset{HO}{}}R^2 \rightleftharpoons R^1\text{-B}\overset{O}{\underset{O}{}}R^2 + 2H_2O$$
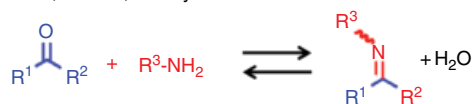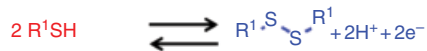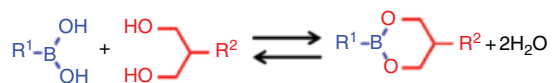
Scheme 8.1 Examples of (a) reversible non-covalent and (b) reversible covalent linkages for the preparation of dynamic polymeric materials.

the material's surrounding environment, such as changes in temperature, pH of the medium, applied mechanical force, light intensity, and the intensity of applied electric or magnetic field. The ability of dynamic polymers to adapt their structure and composition in response to the external stimuli has enabled the design of drug delivery devices, imaging agents, sensors, and smart surface coatings. The nature of the applied stimulus can be physical (e.g., change in temperature, light, electrical, magnetic, mechanical, and ultrasound), chemical (presence of solvent, chemical functionality, change in electrochemical potential, pH of the medium), or biological (presence of enzyme, receptors).[29,30] Depending on the applied stimulus the polymer may undergo conformational change (e.g., coil to globule transition), chemical changes (e.g., rearrangement, degradation and exchange of chemical functionality), or change in the non-covalent interactions (e.g., hydrogen bonding, solvent–solute interaction). Here we give an overview of stimuli-responsive polymers with reversible characteristics and their numerous applications, focusing on the recent developments in dynamic covalent polymers and briefly touching on dynamic solvent–solute interactions. Some excellent reviews have covered the development of stimuli-responsive materials with or without reversible bonds with emphasis on their prospective applications.[2,8,28,30–41]

8.2 Thermoresponsive Polymers

Temperature-responsive polymers have received a great deal of interest for various biomedical and bioengineering applications.[30] The ability of a polymeric material to respond to a change in temperature can arise due to either a volume phase transition at a critical solution temperature or the presence of a thermally labile linkage (e.g., nitroxide, reversible Diels–Alder linkages) in the polymer. We will present relevant examples of commonly employed thermoreversible linkages of both kinds in this section.

8.2.1 Polymers Possessing Critical Solution Temperatures

At critical solution temperature in aqueous media, the hydrophilic and hydrophobic interactions between the polymer and the solvent change abruptly, resulting in the collapse or expansion of the polymer chain in solution. Two kinds of critical solution temperatures have been observed: lower critical solution temperature (LCST) and upper critical solution temperature (UCST). The polymer solution appears monophasic below the LCST or above the UCST, and the polymer solution phase separates due to the collapse of the polymer chain above the LCST or below the UCST. Depending on the type of functional groups present on the polymer chain or the mechanism of polymer–solvent interaction, a polymer could have either a LCST or an UCST. The intermolecular interactions (hydrogen bonding and hydrophobic interactions) between polymer chains at critical solution temperatures have been utilized to induce reversible association and dissociation of biopolymers such as polypeptides, physically crosslinked hydrogels, and reverse micelles.[30,42] The potential utility of thermoresponsive polymers was envisioned in a number of different applications, such as delivery of therapeutics,[31,40,43–47] gene delivery,[48–55] filtration,[56–60] bioseparation,[61–63] and smart surfaces.[40,64–68] Some commonly explored polymers for thermoresponsive

behavior are poly (*N*-isopropylacrylamide),[30,31,38,69–81] poly(*N,N*-diethylacrylamide),[82] poly(ethylene glycol) and poly(propylene oxide),[31,83,84] poly(*N*-vinylcaprolactam),[85–88] poly(*N*-ethyl oxazoline),[89] poly[2-(dimethylamino)ethyl methacrylate],[90–92] poly-(methyl vinyl ether),[93–96] poly(acyl hydrazone),[97] and elastine-like oligo- and polypeptides.[38,98,99]

Synthetic polypeptides have been studied extensively for the possibility of creating functional biomaterials as their ordered secondary structures play crucial roles in many biological processes.[100–104] One of the key attributes of their secondary structure is the presence of non-covalent interactions such as hydrogen bonding, which can be reversibly dissociated to induce conformational change (e.g., random coil to β-spiral in an elastin-like polypeptide) in the polypeptide.[98] For example, thermoresponsive oligo(ethylene glycol) (OEG) units have been incorporated into polypeptides such as poly(L–lysine), poly(L–glutamate), and poly(L–cysteine) and the phase transition temperatures were shown to be modulated by changing the OEG length, comonomer ratio, and chirality of the polypeptide.[105,106] Specifically in recent work, Zhang *et al.* functionalized poly(L–lysine) with dendritic OEGs of varying length via imine formation. The author utilized the dynamic nature of imine bonds to show that the thermoresponsive behavior of the OEG polypeptides can be tuned by changing the hydrophilicity through functionalization with different OEGs via imine exchange. Moreover the author has also studied how external conditions (such as pH and temperature) affect the secondary structure of the polypeptide in an aqueous environment.[98] Likewise, Li *et al.* more recently prepared OEG containing another polypeptide (poly(L–glutamate)) by ring opening polymerization of α-amino acid *N*–carboxyanhydrides (NCA), and reported that the OEG chain length and sample history (e.g., method of purification, storage time) affected the secondary structure of the polymer and the thermoresponsive behavior.[100] In a contrasting result reported by Klok *et al.*, a copolymer with a similar polypeptide backbone was shown to retain secondary structure despite proceeding through a volume phase transition at its LCST. The authors used vapor deposition surface-initiated ring-opening polymerization to prepare thermoresponsive polyglutamate–*co*–oligo(ethylene glycol) brush (poly(EG$_x$–Glu), $x = 1$–3) (Scheme 8.2).[107] While all the polypeptides had volume phase transition temperatures, the highly ordered poly(L-EG$_x$–Glu) and poly(D-EG$_x$–Glu) had lower volume phase transition temperatures than poly(rac-EG$_x$–Glu) as the amide bonds on the backbone of poly(rac-EG$_x$–Glu) were available to undergo hydrogen bonding with the surrounding water.[107] Interestingly, these densely packed arrays of the
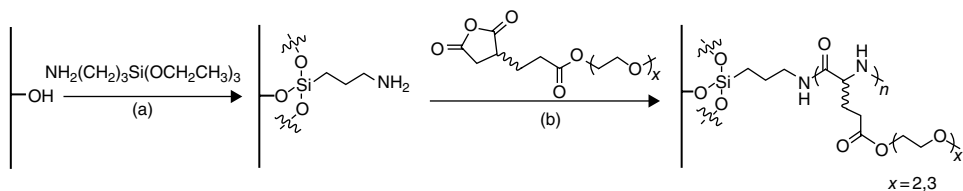
Scheme 8.2 Synthesis of polypeptide brushes via surface-initiated ring-opening polymerization:
(a) functionalization of the silicon wafer with (3-aminopropyl)triethoxysilane (APS) and
(b) ring-opening polymerization of NCA monomer to form poly(D-EG$_x$–Glu) brushes. Reprinted from *Macromolecules* **2015**, *48*, 2399. Copyright 2015 American Chemical Society.

surface-tethered helical peptides (poly(L-EG$_2$–Glu), poly(D-EG$_2$–Glu), and poly(L-EG$_3$–Glu)) retained their secondary structure on heating from 10 to 70 °C, which includes all phase transition temperatures. The author proposed that the dehydration of the brushes near their critical temperatures and the changes in the surface properties were due to the collapse of the OEG side chains while the retention of thickness was due to helical shape persistence.

The thermoresponsive behavior of polymers has also been utilized in reversible switching of different self-assembled morphologies and controlled release of a guest molecule from self-assembled structures (e.g., micelles and vesicles) close to the critical solution temperature. Ghose *et al.* prepared a random copolymer of *N*-hydroxy succinamide methacrylate ester and *n*-octyl methacrylate by reversible addition-fragmentation chain transfer (RAFT) polymerization, and functionalized the polymer with an amine-containing oligooxyethylene molecule to obtain a hydrophilic copolymer.[108] Self-assembly of the copolymers led to vesicular morphology ascertained by the encapsulation of a hydrophilic dye (Rhodamine 6G) in the core. The presence of characteristic absorption and emission peaks at 534 and 557 nm, respectively, in UV-vis spectra along with transmission electron microscopy (TEM) and dynamic light-scattering studies confirmed successful guest encapsulation. The author observed a unique morphological transition from vesicle to micelle on heating the aqueous solution of the polymer above 45 °C and the hydrodynamic diameter was reduced from 300 to 70 nm.

Physically crosslinked hydrogels have received considerable interest lately due to the possibility of easy reshaping of the material. One strategy to prepare physically crosslinked hydrogels is to heat an aqueous solution of a thermoresponsive polymer above its LCST. Debuigne *et al.* synthesized homopolymers and copolymers of *N*-vinylcaprolactam (VCL) and *N*-vinylpyrrolidone (NVP) [i.e., NVCL-*b*-P(NVCL-*stat*-NVP) and PNVCL-*b*-P(NVCL-*stat*-NVP)-*b*-PNVC], and studied their thermoresponsive behavior.[87] The di- and triblock copolymers possess double cloud points ranging from 25 to 70 °C, and gradual heating of the polymer solutions led to micelle formation above their first cloud points followed by complete dehydration and collapse of the polymer chains above their second cloud point, resulting in opaque gel. The gel prepared from triblock copolymers possessed a higher modulus than the gels prepared with diblock copolymer at the same concentration and stoichiometry. The authors attributed this result to the distinct micellar structure, which originated from the diblock and triblock copolymers. The colloidal gel that resulted from the diblock copolymers was found to be densely packed micellar structures, whereas the triblock copolymers gave rise to three-dimensional gels consisting of bridged micelles.

Thermoresponsive polymers have also been utilized in biomedical applications such as cell binding and growth, tissue engineering, reversible molecule absorption, and gene delivery.[109,110] Bradley *et al.* reported thermoresponsive hydrogels based on 2-(diethylamino)ethyl acrylate which support long-term human embryonic stem cell (hESC) growth and pluripotency over a period of 2–6 months.[109] Cell passaging of the hydrogels was simply carried out by transient modulation of the temperature from 37 to 15 °C for 30 min *in vitro*. The hydrogels (HG) were prepared with 2-(acryloyloxyethyl) trimethylammonium chloride (AEtMA-Cl) and 2-(diethylamino)ethyl acrylate (DEAEA) in varying ratios. The hydrogel (HG21, AEtMA-Cl:DEAEA = 3:1) allowed the attachment and growth of hESC at 37 °C, whereas at 15 °C HG21 became more hydrated, resulting in detachment of cell colonies. The author has also investigated capture or

release of proteins incorporated in HG21 in mTeSR1 (cell culture media for hESC) using similar thermoresponsive behavior. This is an excellent example of utilizing thermoresponsive behavior for cell culture or protein delivery without the need for any harsh chemicals.

8.2.2 Polymers Possessing Thermo-labile Chemical Linkages

Reversible characteristics in polymers can be imparted by incorporating thermo-labile bonds such as Diels–Alder linkages, alkoxyamine linkages, and disulfide bonds. A majority of the reports about thermally labile polymers relied on the Diels–Alder reaction and homolytic cleavage of nitroxides or alkoxyamines, whereas disulfides have been explored primarily to create redox-responsive polymers. Here we discuss more traditional examples of thermally responsive dynamic covalent materials.

8.2.2.1 Polymers Containing Alkoxyamine Linkages

The fundamental radical exchange reaction of 2,2,6,6-tetramethylpiperidine-1-oxy (TEMPO), as a radical scavenger during a free radical polymerization, led to the discovery of nitroxide-mediated polymerization (NMP), in which TEMPO acts as the reactive initiating radical and the stable mediating radical.[39,111–117]

The nitroxide radicals are stable at room temperature but at ~90 °C and above they undergo exchange with other nitroxides or hydrogen abstraction.[39] The exchange reaction between different nitroxides (Scheme 8.3) in two alkoxyamine-bearing polymers was first reported in 1996 by Hawker *et al.*[11] Later, Turro *et al.*[118] reported that the terminal nitroxide of the polystyrene prepared by NMP was capable of undergoing exchange with an excess amount of other nitroxides. Specifically, the authors functionalized the terminus of a polymeric alkoxyamine with a chromophore via nitroxide exchange with TEMPO-terminated polystyrene and a chromophore-bearing nitroxide. In an early attempt to synthesize dynamic covalent polymers by the nitroxide-exchange process, Takahara *et al.* mixed two different alkoxyamine-containing poly(methyl methacrylate)s and heated the reaction mixture to 100 °C to afford a crosslinked polymeric gel.[119] The de-crosslinking of the gel was carried out by heating the gel in the presence of alkoxyamine molecules like TEMPO or styryl-TEMPO. The same group has taken this concept further to prepare linear polymers having the alkoxyamine functionality in the polymer backbone by step growth polymerization of a nitroxide-containing diol and adipoyl chloride in dichloromethane.[120,121] The authors used nitroxide exchange to tune the molecular weights of the polymers by simply mixing (in anisole) equal quantities of two polymers having different molecular weights and heating the mixture at 100 °C for 12 h. A single peak was obtained for the resultant mixture in the size-exclusion chromatography (SEC) trace, confirming that the nitroxide exchange led to reorganization of the polymers.
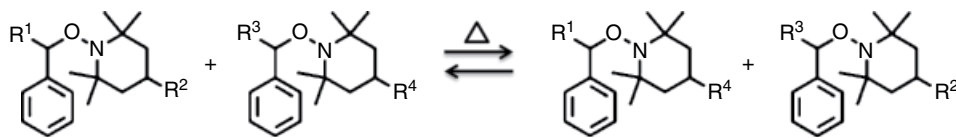
Scheme 8.3 Example of nitroxide exchange between two alkoxyamine molecules. R^1–R^4 = alkyl groups.

There are several other examples of incorporation of thermoreversible alkoxyamines in more complex macromolecular systems, such as brush copolymers to reversibly alternate silica surface properties,[122,123] core-crosslinked star polymers,[124–127] and cyclic polymers.[128] In a recent report, Otsuka and Takahara *et al.* synthesized poly(methyl methacrylate)-based brush copolymers containing exchangeable alkoxyamine units by surface-initiated atom transfer radical polymerization (ATRP).[123] The authors were able to reduce the surface free energy of the brush copolymer by grafting poly(2,3,4,5,6-pentafluorostyrene) (PPFS) (prepared by nitroxide-mediated polymerization) onto the brush copolymer by nitroxide exchange (Figure 8.1). The de-grafting of the PPFS from the brush surface was carried out with excess small alkoxyamine molecules via nitroxide exchange. Successful de-grafting was confirmed by contact angle measurements and X-ray photoelectron spectroscopy. This is a fundamental example of how exchangeability of dynamic bonds could lead to smart surfaces and reversible surface property control. The exciting findings of the above-mentioned research inspired the creation of more complex responsive surfaces and a new class of dynamic soft materials.[2] The mendability of nitroxide-bearing polymers in bulk was investigated. Zhang *et al.* prepared 4-(vinylbenzyl chloride)-based polymers having different pendent alkoxyamine groups to fabricate a two-component blend.[129] The blend of the different alkoxyamine-containing polymers was heated to cause the homolytic cleavage of C–ON bonds. Due to the hindered diffusion in the bulk state, an unwanted carbon-centered radical combination reaction was suppressed. The recombination of C–ON bonds was facilitated by the easier diffusion of the smaller nitroxide radical across the polymer matrix.

8.2.2.2 Polymers Containing Diels–Alder Linkages

Diels–Alder cycloaddition is another powerful synthetic technique for preparing mendable polymeric materials and is often referred to as "click chemistry".[130] The reaction does not require a catalyst, and the equilibrium can be tuned to favor the forward or reverse direction by changing the reaction temperature. The Diels–Alder reaction involves [2 + 4] cycloaddition of an electron-rich diene and an electron-poor dienophile (Scheme 8.1). Lehn and co-workers reported one of the first examples of the use of the Diels–Alder reaction between fulvene derivatives and cyanolefins to generate a dynamic library of Diels–Alder adducts that can exchange with each other reversibly between 25 and 50 °C.[131] Due to the inherent reversibility of some Diels–Alder adducts, for example furan-maleimide adducts, this reaction has been widely used to prepare smart healable materials. The first Diels–Alder self-healing systems were devised by Wudl *et al.*, who employed a tetra-furan molecule and a tri-maleimide compound as precursors to construct a crosslinked macromolecular network.[132] The authors prepared a thin film by casting a solution of the furan and maleimide derivatives, and heating the film to undergo Diels–Alder reaction. The specimen was used for repeatable self-healing experiments by a compact tension test. Healing was observed by scanning electron microscope (SEM), as a result of Diels–Alder reaction between de-bonded furan and maleimide moieties at 120–150 °C, with an average mending efficiency of 57%. These results were remarkable given that the healing was achieved without any additional component, and the mechanical properties (compression strength, compression modulus, and flexural strength) of the network film were comparable to those of a similar epoxy system (e.g., tensile strength as high as 68 MPa). In 2003, the authors addressed

Alkoxyamine-containing brush copolymers

PPFS-grafted brush copolymers
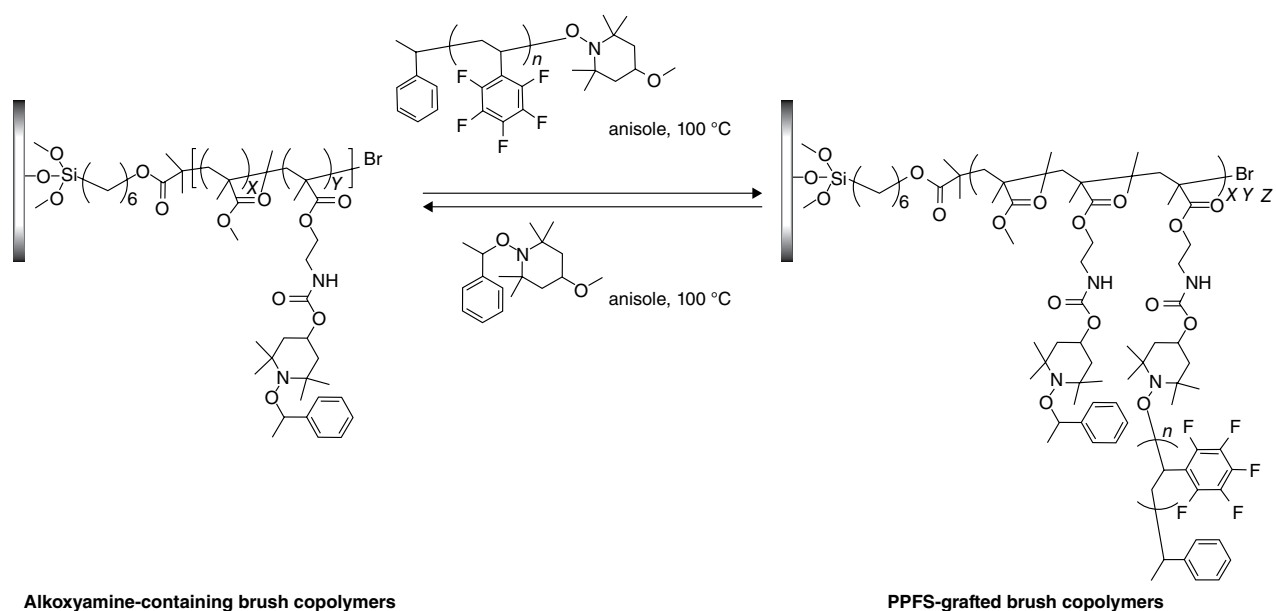
Figure 8.1 Brush copolymer-containing thermoreversible alkoxyamine units, prepared by surface-initiated atom transfer radical polymerization (ATRP). Poly(2,3,4,5,6-pentafluorostyrene) (PPFS) was grafted to the brush copolymer by nitroxide exchange at 100 °C and de-grafting was achieved by nitroxide exchange with excess small alkoxyamine molecules. Adapted from T. Sato, Y. Amamoto, H. Yamaguchi, T. Ohishi, A. Takahara and H. Otsuka, *Polym. Chem.*, 2012, **3**, 3077–3083, with permission from the Royal Society of Chemistry.

the limitation of healing efficiency by using a lower melting maleimide precursor to afford network formation in bulk.[133] Indeed, their new strategies led to higher healing efficiencies of 80% on average, and the healing by Diels–Alder and retro-Diels–Alder was repeatable multiple times, as evidenced by 78% healing efficiency in the second cycle.

Knowledge of the inherently reversible nature of Diels–Alder reaction led to much interesting work, such as thermo-responsive organic-inorganic hybrid optical polymers,[134] modular polymeric color switches employing a hetero Diels–Alder reaction,[135] rewritable surface coating,[136] self-healing films,[137] and polymeric thin-film for scanned-probed data storage and lithography applications.[138] Recently both Bowman *et al.*[139] and Goepferich *et al.*[140] demonstrated that poly(ethylene glycol) (PEG)-based hydrogels having furan-maleimide linkages could degrade at human body temperature by the retro-Diels–Alder reaction. Bowman *et al.* utilized a carboxyfluorescein-labelled 3-furan RGDS-peptide sequence (furan-RGDS) to create hydrogels by Diels–Alder reaction with the maleimide units in a PEG-based thiol-ene network (Figure 8.2). The thiol-ene Michael addition was performed with excess maleimide compound so that unreacted maleimide sites remained for subsequent Diels–Alder reaction with furan-RGDS. Creating the network with both permanent (thiol-ene) and reversible or labile (furan-maleimide link) bonds allowed control of the release rate of furan-RGDS by simply varying the available maleimide units for Diels–Alder reaction. The authors introduced cysteine, a monothiol, for capping the available maleimide functionality by thiol-ene reaction, to control the number of available maleimide groups, while maintaining a constant crosslink density. Exposing the hydrogel to different temperatures (37, 60, and 80 °C) resulted in a temperature-dependent release via a retro-Diels–Alder mechanism.

Recently, the Sumerlin group employed the Diels–Alder reaction to prepare core-crosslinked star polymers by an arm-first approach,[141] and segmented hyperbranched polymers by self-condensation vinyl polymerization.[142] For preparation of the core-crosslinked star polymers, well-defined block copolymers of styrene (S; polystyrene, PS) and maleic anhydride (MAn) [P(S-*alt*-MAn)-*b*-PS] were prepared via a one-pot cascade approach by RAFT polymerization. The maleic anhydride rings were opened with furfuryl amine to yield the functionalized polymer with the pendent furan groups, which were subsequently crosslinked with a bis-maleimide compound by Diels–Alder reaction to yield the core-crosslinked star polymers. Due to the reversible nature of the furan-maleimide links, the core-crosslinked polymers could degrade and reform over multiple cycles as demonstrated by the SEC and dynamic light-scattering (DLS) size distributions. Interestingly, the block copolymers could be self-assembled in a selective solvent (toluene) into micelles, and a dramatic increase in the rate of crosslinking was observed when the pendent furan molecules in the core of the micelles were allowed to react with bis-maleimide molecules. The strategy of preorientation of block copolymers in a selective solvent before crosslinking was also adopted by others to enhance the rate of star formation, as well as the yield and size dispersity of the resultant star polymers.[24,143]

The reversibility of the anthracene-maleimide Diels–Alder linkage was also explored but the retro-Diels–Alder reaction was found to be inefficient even at close to 200 °C. The authors attributed the low conversion of retro-Diels–Alder reaction to the competing forward Diels–Alder reaction.[144–146]
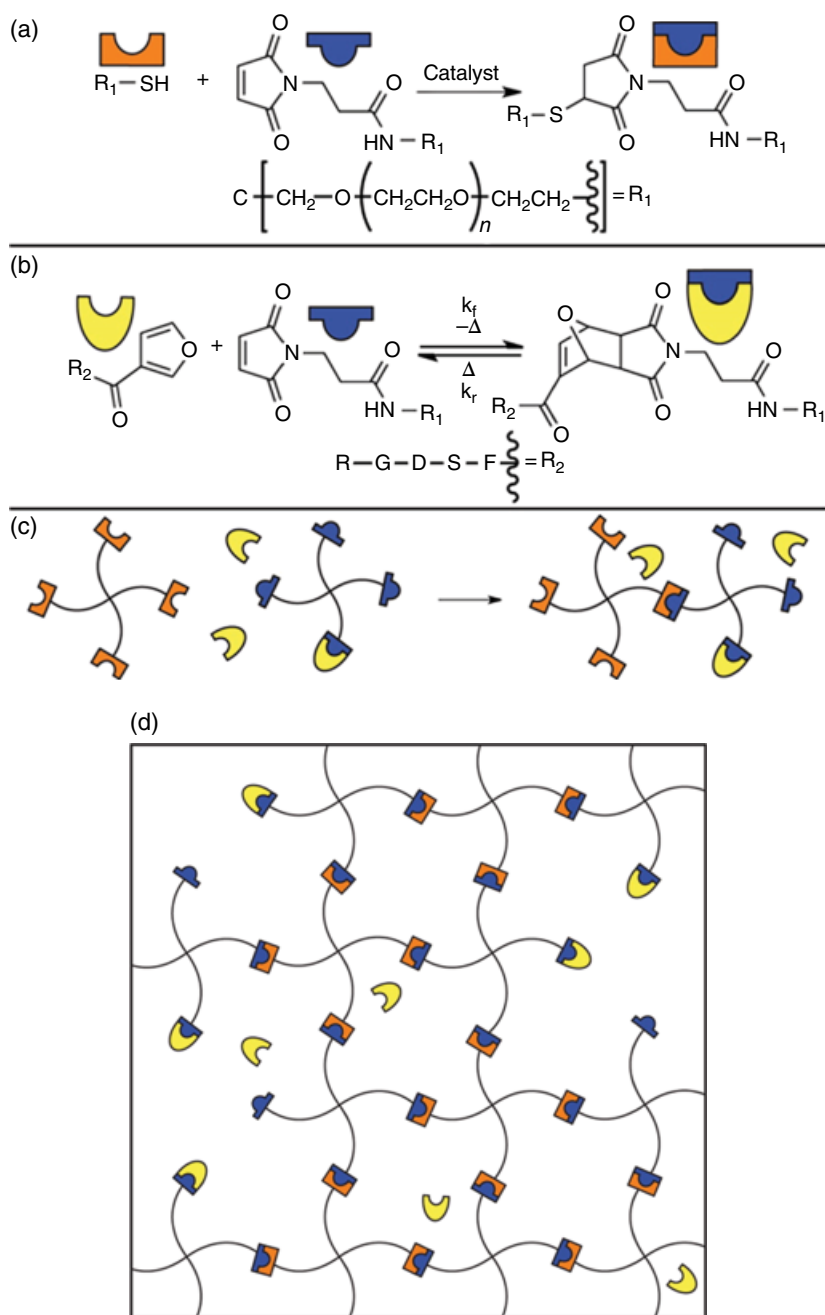
Figure 8.2 Synthesis of hydrogels by Diels–Alder cycloaddition of furan and maleimide derivatives. (a) Thiol-Michael addition reaction between a multifunctional maleimide (in excess) and thiol-PEG macromere. (b) Release of the furan-containing peptide sequence (furan-RGDS) by retro-Diels–Alder reaction. (c) Schematic representation of the thiol-Michael addition and Diels–Alder reaction employed to create the hydrogel. (d) Representation of the overall network obtained by thiol-Michael addition and Diels–Alder reaction. (e) Release study of furan-RGDS by retro-Diels–Alder reaction initially and (f) over a longer period of time, at 37 °C (circles), 60 °C (squares), and 80 °C (triangles). Adapted from K. C. Koehler, K. S. Anseth and C. N. Bowman, *Biomacromolecules*, **2013**, *14*, 538. Copyright 2013 American Chemical Society.

(e)

(f)
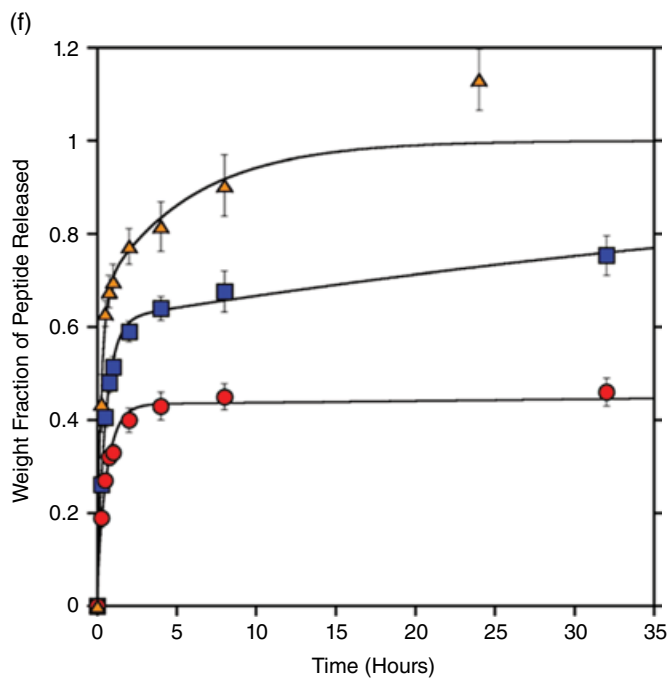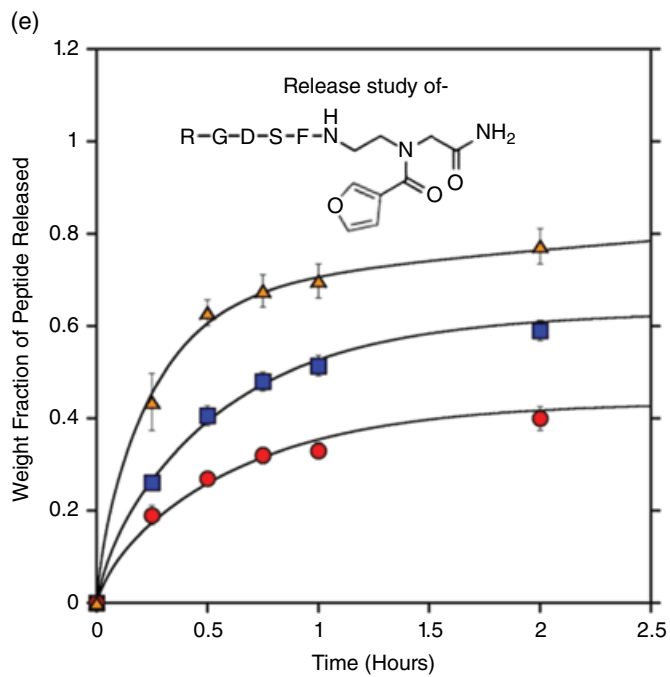
Figure 8.2 (Continued)

8.3 Photo-responsive Polymers

Light-sensitive linkages have been used to impart dynamic characteristic in polymeric materials. Light is an attractive source of stimulus as it eliminates the need for any chemical reagent and can operate in bulk with minimum side reaction, particularly in creating optically clear materials.[35] The ability to tune the response of photoresponsive materials by varying the light wavelength and intensity, duration, and location of exposure allows precise spatio-temporal control over system activation.[147] More significantly, the forward and reverse reactions often take place at different light wavelengths (λ), for example anthracene dimerizes at λ >350 nm whereas the reverse reaction is favored at λ <300 nm. Also the elimination of a chemical reagent allows multiple orthogonal functionalities in a single polymeric system. Functional groups capable of undergoing photo-induced pericyclic reaction, such as coumarin and anthracene, have been used to prepare polymeric materials.[148–150]

Takahara and co-workers reported the first example of a photoresponsive reorganizable linear polymer utilizing the radical exchange reaction between disulfides (disulfide metathesis).[151] The authors synthesized a disulfide-containing polyester (DSPES) by polycondensation of adipoyl chloride and 2-hydroxyethyldisulfide in dichloromethane in the presence of pyridine. Due to the presence of the disulfide links in the polymer backbone, the polymer was susceptible to disulfide exchange by UV irradiation. To test the hypothesis, two polyesters having different molecular weights (h-DSPES, $M_n = 60400$ g/mol, $M_w/M_n = 1.06$; l-DSPES $M_n = 8700$ g/mol, $M_w/M_n = 1.54$) were synthesized and mixed in equal quantities in solution to cast a film. The polymer film was irradiated with UV light (365 nm) and after 60 min the SEC traces of the two polymers were fused in one, confirming that the two polymers were reorganized via disulfide exchange.

Bowman *et al.* utilized the photoinduced sulfide-containing molecules to create polymeric materials possessing stress-relieving characteristics. In one of their seminal works the authors created a rubbery covalently crosslinked network via thiol-ene polymerization using pentaerythritoltetra(3-mercapto-propionate) (PETMP), triethyleneglycol divinylether (TEGDVE), a ring-opening monomer 2-methyl-7-methylene-1,5-dithiacyclooctane (MDTO) as a comonomer, and 1,6-hexanedithiol.[152] The presence of a residual amount of photoinitiator led to generation of radicals which could diffuse through the network via an addition-fragmentation chain-transfer process at the allyl sulfide moiety. This photo-induced reorganization led to rapid relief of any induced stress on the material. Higher incorporation of allyl sulfide bonds resulted in a higher degree of stress relaxation at a faster rate. The stress relaxation process was repeatable but needed the presence of radicals. The authors utilized a similar strategy to create a covalently adaptive network as a dental restorative resin via thiol-acrylate polymerization[153] and for permanent reconfiguration of surface patterns on covalently-adaptive networks by a UV-assisted nano-imprinting lithography process.[154]

In another interesting example, Yang *et al.* combined a reversible covalent and a non-covalent interaction to prepare a dynamic polymer.[155] The authors dimerized anthracene-functionalized pillar[5]arene on exposure to UV irradiation (350 nm). Pillar[5]arene-functionalized dimer was mixed with bisimidazole alkane via a host–guest interaction to yield a reversible polymer. The polymer was disintegrated through either an increase in temperature to dissociate the host–guest interaction, or exposure to UV

OX = Phosphates, Carboxylates, Sulfates, Amines, Carbonyls, Thiols etc.
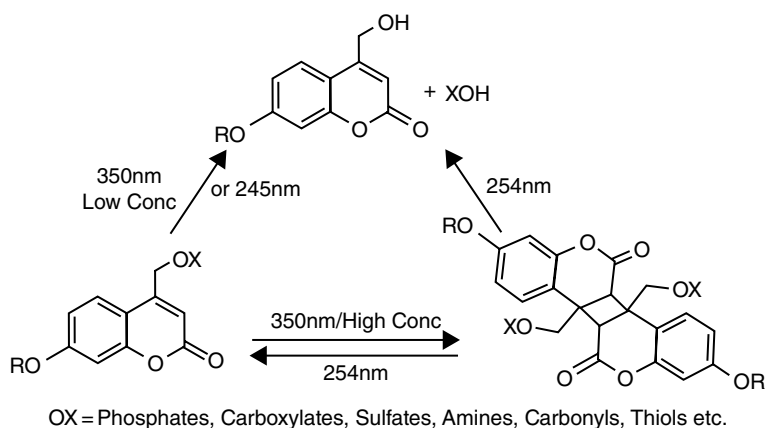
Scheme 8.4 Reversible photochemical reactions of coumarin compounds. Reprinted from *J. Mater. Chem. B* **2013**, *1*, 5942, with the permission from the Royal Society of Chemistry.

irradiation (<300 nm) to cleave the anthracene dimer. The reformation of the polymer was achieved by re-irradiating with UV light (>350 nm) to allow anthracene dimer formation, or cooling to 15 °C to allow host–guest interaction. This dynamic polymerization process was carried out over several cycles.

Coumarin-containing molecules have been investigated as protecting groups, therapeutics, and phototriggers for biological molecules.[148,156,157] Coumarin derivatives such as 7-methoxy coumarin undergo [2 + 2] cycloaddition at 350 nm to form dimerized cyclobutane in both solid and solution phase, and the reverse reaction occurs at a lower wavelength of ~254 nm (Scheme 8.4). Additionally some ester- or phosphate-substituted coumarins undergo hydrolysis on irradiation at 254 nm (Scheme 8.4). Joy *et al.* synthesized coumarin-based polyesters and created micropatterned substrates with the polymers.[158] The polymers and their photo-degradation products were found biocompatible and the cell viability with macrophage RAW 267.4 was comparable to the cell viability of poly(lactic acid–*co*–glycolic acid). In another recent work, Lu *et al.* synthesized a multifunctional amphiphilic copolymer of 7-(didodecylamino) coumarin-4-yl] methyl methacrylate, hydroxyethylacrylate, and folic acid modified *N*-(3-aminopropyl) methacrylamide hydrochloride by RAFT polymerization.[159] The copolymer was coated onto C18-modified hollow mesoporous silica nanoparticles for cell-imaging and selective cancer targeting. Doxorubicin was encapsulated in the polymer coated with silica nanoparticles. Irradiating the nanoparticles in the NIR region (800 nm) caused the removal of the photolabile coumarin units and subsequent release of >50% drug molecules.

8.4 Mechano-responsive Polymers

A range of physiological processes such as muscle contraction, sense of touch, hearing, and growth and reorganization of tissues and bones are enabled by mechanochemical transduction, which is the conversion of a mechanical stimulus into an electrical signal by cells.[160–162] Inspired by the role of mechanical force on biological systems, the

scientific community has been studying the influence of external mechanical force on the properties and stability of polymeric materials. Polymers can respond to mechanical stress by undergoing conformational change or bond-bending and bond-stretching deformation.[163] The response of synthetic polymeric material to mechanical force was first considered by Staudinger *et al.*[164–166] Initial studies in this area involved rational molecular design such that the mechanical force would alter the material's properties by breaking and reforming a reversible non-covalent or covalent linkages. Developments in polymers containing mechanoresponsive non-covalent linkages have made a significant progress in last few decades.[167–172] On exposure to an external mechanical force, the non-covalent interactions in a polymer are likely to break, relieving the stress on the polymer chain and preventing the cleavage of covalent bonds. If the interaction is reversible (such as hydrogen bonding), the removal of the stress will cause the process to go between bonded and debonded states and impart elasticity to the material.

The initial understanding of the effect of mechanical force on polymer properties was derived from research based on non-covalent interactions such as hydrogen bonding and metal–ligand coordination (Figure 8.3). For example, Guan *et al.* synthesized *titin* mimicking linear polymer containing a tandem array of cyclic ureido-pyrimidinone (UPy) dimers.[173] The UPy dimer was dissociated by a large strain with minimal increase in stress. The plastic deformation in the polymer was not permanent and the polymer was able to regain its original length and properties overnight at room temperature. Heating the sample to 80 °C led to the complete recovery of its dimension, stiffness, strength, and toughness in 30 s. In addition to the self-healing nature of the polymer the authors also observed shape memory behavior. Sijbesma *et al.* created a reversible coordination network by combining diphenylphosphinite telechelic polytetrahydrofuran with $[RhCl(COD)]_2$ or $[IrCl(COD)]_2$ in chloroform. The phosphine ligands attached to polytetrahydrofuran in the presence of Ir (I) or Rh (I) produced a network polymer and gel. On sonication, the gel turned into a sol, and removal of the mechanical force and sufficient equilibration time allowed the reformation of the gel. The authors suggested that the sonication-induced gel-to-sol transition was due to ligand exchange, which led to the change in topology and decrease in the total numbers of crosslinkable metal centers without changing the coordination chemistry. The process could be repeated without irreversible material degradation. Such reversible exchange of metal complexes could give rise to coordinatively unsaturated metal–ligand complexes, which can serve as catalysts for a multitude of reactions.

The majority of mechano-responsive polymers have been based on the spiropyran molecule, which has the potential to undergo a 6-π electrocyclic ring-opening reaction accompanied by a color change to yield planner merocyanine through C–O bond cleavage (Figure 8.3). Davis *et al.* synthesized polymers containing spiropyran as a mechanophore.[174] The authors used spiropyran-functionalized α-bromo esters to initiate single-electron transfer living radical polymerization of spiropyran-functionalized methacryloyl esters and methyl methacrylate in aqueous media. The colorless spiropyran-containing polymers experienced selective C–O bond scission during a tensile deformation and produced colored merocyanine. The material showed increased intensity of color with increasing tensile loading and produced the most intense color when the material failed. The design of mechano-responsive functionalities (or mechanophores) which change their color and fluorescence intensities under mechanical deformation has developed significantly over past few years, offering access to a
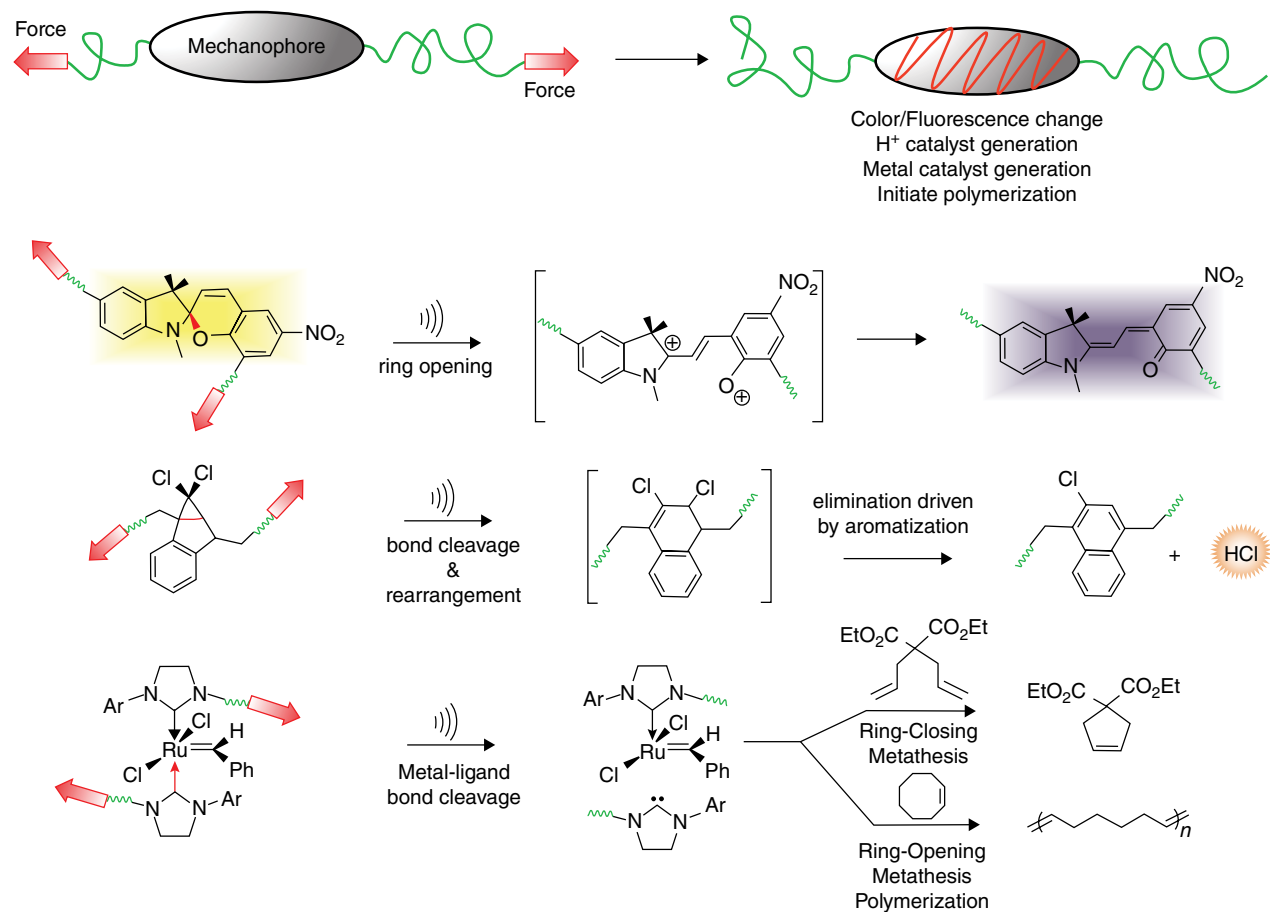
Figure 8.3 Mechanical stress-induced reactions. Reprinted with permission from DOI: 10.1021/acs.accounts.5b00184. Copyright 2015 American Chemical Society.

number of transformations, such as change in optical property (color or fluorescence),[174,175] isomerization,[176] release of small molecules,[177] generating proton catalyst,[178] and activating transition-metal catalyst (Figure 8.3).[179]

The mechanism of covalent bond scission under the influence of mechanical force and the specificity of the recombination reaction of generated radicals is yet to be fully understood. The understanding from the ongoing studies in this area will be a valuable platform to understand the mechanism of failure, fatigue, and degradation of polymeric material under stress, and to improve the toughness, durability, and lifetime of polymers, especially for protective coating and biomedical applications.[180–183]

8.5 pH- and Chemo-responsive Polymers

pH-responsive behavior in polymeric material could arise from the presence of ionizable weakly acidic or basic functional groups such as $-COOH$, $-NR_2$ or acid-/base-labile linkages such as acyl hydrazone and imines on the polymer backbone. At lower or higher pH, the weakly acidic or basic functional groups ionize and become soluble due to hydrogen bonding and/or electrostatic interaction. On the other hand, the acid-labile covalent bonds such as imines and hydrazone become susceptible to hydrolysis, leading to reversible cleavage of the bonds. Depending on the stability of a reversible link or the reaction environment, a reversible chemical reaction may need a catalyst, a competing chemical reagent, or a template to drive the reaction to a desired extent. Thus such an externally added reagent serves as chemical stimuli.

8.5.1 Polymers Containing Acyl Hydrazone Links

Acyl hydrazones ($-C=N-NH-(C=O)-$) have been widely used to construct dynamic combinatorial libraries and reversible polymeric materials.[6,41] Acyl hydrazones are formed by the reaction of a carbonyl compound and an acyl hydrazine molecule ($R^3CONHNH_2$, Scheme 8.5). Due to the reduced nucleophilicity of the $-NH_2$ group in the acyl hydrazine compound, the reaction often needs an acid catalyst, and the optimum rates of hydrolysis and exchange occur at pH 4.4. Lehn and co-workers demonstrated the utility of hydrazone exchange using trifluoroacetic acid (TFA) as a catalyst to prepare dynamic covalent polymers as well as "foldamers", which are discrete chain molecules or oligomers held by noncovalent interactions (e.g., hydrogen bonding) and able to fold into well-defined conformations, such as helices or β-sheets.[184–186]

In a seminal work, Fulton and co-workers prepared a polymer-scaffolded dynamic combinatorial library of acyl hydrazone functional polymers, and the authors showed that hydrazone exchange took place at acidic pH.[187] This polymer-based dynamic
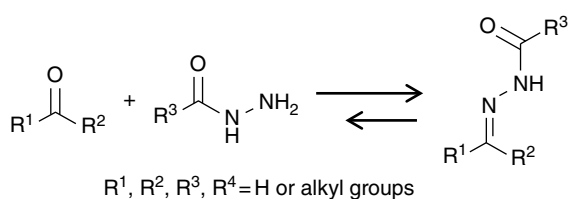
Scheme 8.5 Acyl hydrazone formation with a carbonyl compound (aldehyde or ketone) and an acyl hydrazine molecule.

R^1, R^2, R^3, $R^4 = H$ or alkyl groups

combinatorial library has generated considerable interest in the design of molecules that can mimic natural biomolecules and polymer-based receptors for small molecules or proteins. Later, the same group harnessed the reversibility of acyl hydrazone bonds along with the thermoresponsive behavior of a polymer to prepare single-chain nanoparticles (SCNPs) that can undergo reversible macroscopic transformation into a hydrogel network (Figure 8.4).[188] Specifically, oligoethylene glycol methacrylate (OEGMA$_{300}$) and *p*-(2-metharyloxyethoxy)benzaldehyde (MAEBA), which have similar molecular weights ($M_w = 37$–61 kDa), were copolymerized via RAFT polymerization. The linear polymers displayed thermoresponsive behavior due to their LCST ranging from 32 to 52 °C, depending on the OEGMA content in the polymers. The pendent aldehyde groups of the copolymers (polymer concentration = 0.1–1 wt % in AcOH/ AcONH$_4$ buffer) were intramolecularly crosslinked at pH 4.5 with a diacylhydrazine (or hydrazide) crosslinker by hydrazone formation. As the crosslinking progressed, the intramolecularly crosslinked polymer chains collapsed, leading to lower hydrodynamic volume, and the SEC trace of the copolymer was shifted to a higher elution time. On heating the crosslinked polymer solution above the LCST, the crosslinked SCNPs aggregated and the highly localized nanoparticle concentration resulted in
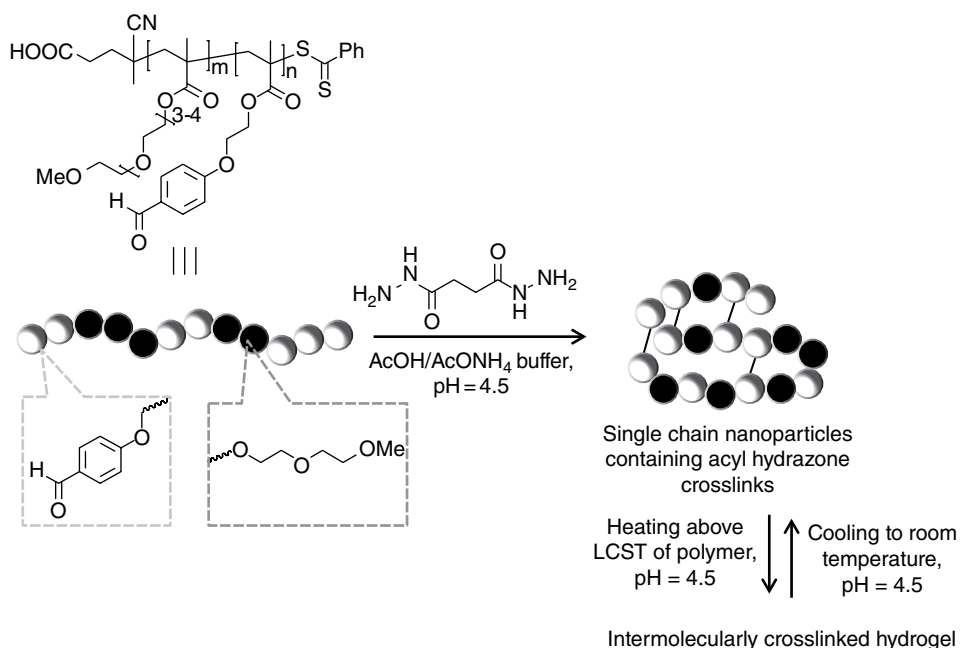
Figure 8.4 Formation of the single chain nanoparticles (SCNPs) via acyl hydrazone formation and the reversible transformation of the SCNPs to hydrogel. Aldehyde functionalized polymers (OEGMA-*co*-MAEBA) were intramolecularly crosslinked with a dihydrazide to yield SCNPs at pH 4.5. The black spheres in the polymer or crosslinked polymers in the scheme represent the OEGMA unit and white spheres indicate the aldehyde-functionalized MAEBA unit. The straight lines connecting the white spheres in the SCNP represent acyl hydrazone crosslinks (>C=N–NH–CO–). On heating the SCNP solution above the LCST of the corresponding polymer, hydrogel formation took place. The reverse transformation of the hydrogel to the SCNPs was carried out by cooling to 25 °C. Adopted from D. E. Whitaker, C. S. Mahon and D. A. Fulton, *Angew. Chem. Int. Ed.*, 2013, **52**, 956–959. Copyright 2013 Wiley.

intermolecular reorganization of the acyl hydrazone crosslinks at the molecular level. As a result, the intramolecular crosslinks were replaced by the interchain crosslinks, and the supramolecular interaction between the reorganized polymer chains induced hydrogel formation. The reverse transformation of the hydrogel to the SCNPs was triggered by cooling the hydrogel to 25 °C and equilibrating to the sol state over 0.5–20 days. The author's explanation of the reversible transformation was supported by the fact that with a decrease in the amount of crosslinking in the nanoparticles, the time required to equilibrate to the corresponding SCNPs also decreased.

In another example, Khan *et al.* combined the facile reversibility of acyl hydrazone linkages and the self-assembly of block copolymers to prepare a nanoporous membrane.[189] Nanoporous materials are useful in the areas of separation, water purification, catalysis, and fuel cell design.[190] The authors polymerized styrene (s) via ATRP using a PEG-macroinitiator containing a hydrazone linkage to yield a block copolymer PEG-*b*-PS. The block copolymer solution in benzene was spin coated onto a silicon surface to yield a 100 nm film. Solvent annealing and exposure to humidity (90%) resulted in a film in which the self-organized and hexagonal packed arrays of cylindrical PEG domains (25 nm) were dispersed in a continuous PS phase with a long-range lateral order. The film was immersed in a water–methanol mixture (2:1 vol/vol) or an acidic water bath (pH 4) to generate porosity by hydrolyzing the acyl hydrazone bonds connecting the styrene and ethylene glycol blocks, and simultaneously dissolving the PEG-hydrazide block. To confirm the removal of the PEG-hydrazide, the recovered porous thin film was exposed to the vapors of methylamine in methanol, and imine formation with the aldehyde groups in the PS matrix was confirmed by ^{1}H NMR spectroscopy. The mild conditions employed to prepare porous thin films offer a great opportunity to design highly ordered functional nanoporous materials.

Acyl hydrazone bonds were also utilized to form self-healing polymeric materials by others. Chen *et al.* carried out a detailed investigation of the reversible sol-to-gel transition and self-healing properties of organo-/hydrogels having acyl hydrazone bonds, and the authors reported the gelation kinetics and mechanical properties of acyl hydrazone-containing organogels.[191–193] The authors later combined the reversibility of acyl hydrazone bonds and disulfide linkages to prepare hydrogels capable of sol-to-gel transition on exposure to two different stimuli.[191] In another report Anseth *et al* showed that the temperature and pH of the reaction medium influences the reaction rate constant of acyl hydrazone formation, and the reverse reaction rate constant affects the stress relaxation characteristics of the acyl hydrazone-containing hydrogel.[194] The requirement of mild acidic conditions for hydrazone exchange offers tremendous possibilities for the design of self-mendable polymeric materials.

8.5.2 Polymers Containing Imine Linkages

The condensation reaction of an aldehyde or ketone with a primary amine results in an imine compound, often referred to as a Schiff base (Scheme 8.6).[195] The reaction equilibrium of imine formation is sensitive to environmental conditions such as pH, temperature, and reactant or product concentration. By careful selection of the electronic structures of the starting materials it is possible to control the optimum pH at which the reaction occurs.[34] Due to the facile reversibility of the imines, they are capable of exchanging partners in a multi-component mixture of imines via transimination,
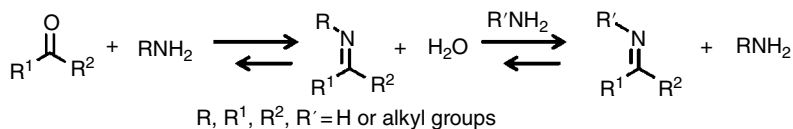
Scheme 8.6 The formation and exchange reactions of imines.

and this exchange reaction has been utilized extensively in creating libraries of constitutionally dynamic compounds (Scheme 8.6).[41,196,197]

Lehn and co-workers studied the equilibrium constant of the imine formation of various aldehyde and amine compounds in aqueous media and found that the equilibrium constant was higher for basic amines.[195] The same group also combined metal–ligand coordination with imine formation to construct a morphological switch involving metal-ion assisted interconversion between a polymer and macrocycles.[198] This example demonstrated that the dynamic exchange of reversible bonds could be a useful tool to induce morphological changes in macromolecular architecture.

Dynamic exchange of imines has also been widely used in preparing stimuli-responsive dynamic covalent polymeric materials. Recently, Zhang and co-workers reported crosslinked polyimine thermosets which can be reshaped, healed, and molded together simply using water under ambient conditions or under heat. They demonstrated that the polyimine network exhibits Arrhenius-like malleability in response to heat in the absence of any catalyst. Starting from powder form, robust coherent polymeric materials can be formed by the application of either heat or water in the absence of catalyst through multiple generations without losing mechanical properties.[199]

Recently, Fulton and co-workers constructed core-crosslinked star polymers and nanogel assemblies by the reaction of an aldehyde functional block copolymer with an amine-containing block copolymer.[200] The star polymers were able to dissociate into unimers reversibly via transimination with a small amine molecule in the presence of an acid catalyst. In another interesting work, Fulton *et al.* employed two orthogonal dynamic covalent bonds, imine and disulfide, to construct double-stimuli-responsive nanoparticles.[201] The crosslinking density in the core can be modulated by either maintaining pH 5.5 to cause hydrolysis of imine bonds or reducing the disulfide bonds with tris(2-carboxyethyl)phosphine (TCEP). With the dissociation of the imine and disulfide crosslinks, the nanoparticles disassembled, as indicated by the shift of the SEC trace to a higher elution time. They also demonstrated that Nile Red can be encapsulated in the nanoparticle, and the release of the Nile Red was afforded by simultaneous application of acidic pH (5.5) and reducing conditions. The release kinetics of Nile Red were monitored with fluorescence spectroscopy. This is an excellent example of a multifunctional system in which only specific functional groups respond to an external stimulus while others remain unaffected. This specificity of response depending on the environmental conditions could be useful for designing sensors and receptors.

A common approach to preparing nanoparticles for drug-delivery applications is the use of a crosslinked micelle as the drug carrier. Release of the drug is achieved by dissociation of the micelles only under a specific stimulus that is present in the targeted cellular environment. McCormick and co-workers utilized this concept to prepare shell-crosslinked micelles using a triblock copolymer containing amine groups in the middle block.[202] The authors synthesized poly(ethyleneglycol)-*b*-poly(3-aminopropyl

methacrylamide)-*b*-poly(*N*-isopropylacrylamide) (PEG-*b*-PAPMA-*b*-PNIPAM) via RAFT polymerization. The triblock copolymers self-assembled at higher temperature (50 °C, pH 9) as the PNIPAM blocks collapsed due to volume phase transition above the LCST. The shell containing the PAPMA and PEG blocks was crosslinked with terephthaldicarboxaldehyde (TAD) via imine formation. A model hydrophobic anti-inflammatory drug, prednisolone 21-acetate (PA), was encapsulated in the core of the shell-crosslinked micelles. A dialdehyde was used to crosslink the shell of the micelles via imine formation. The release of the hydrophobic drug was afforded by lowering the temperature to 25 °C, so that the PNIPAM core became hydrophilic, and lowering the pH (5.5) to hydrolyze the imine bonds in the micelle core. The release of the drug was monitored by UV-vis spectroscopy. The authors observed an enhanced rate of release of the hydrophobic drug at lower pH (5) irrespective of the temperature, confirming that the dissociation of the shell-crosslinked micelles was governed in large part by imine hydrolysis. The promising results of this study encouraged further development in the area of drug delivery using stimuli-responsive polymeric nanoparticles.

8.5.3 Polymers Containing Oxime Links

Oxime ligation has proven promising in the preparation of functionalized polymer scaffolds, surface modification of proteins, and cell surface engineering due to the high reaction efficiency, benign side product (i.e., water), and ambient reaction conditions.[26,203–209] The condensation reaction between an aldehyde or ketone and an alkoxyamine yields either an aldoxime or a ketoxime. Oxime formation was utilized by Maynard *et al.* to prepare micropatterned alkoxyamine-containing polymer films to conjugate an α-ketoamide protein by oxime formation using a photolithographic technique.[210] The authors also demonstrated immobilization of a site-selectively modified protein onto a gold surface by bio-orthogonal click reactions, including oxime formation.[211] In some other examples of protein conjugation, Francis *et al.* employed oxime ligation to synthesize thermoresponsive protein–polymer conjugates,[212] to construct protein functional hydrogels,[203] and to functionalize a polymer coating with an antifreeze protein for devices that operate at low temperature without ice build-up.[204]

The reversibility of oxime formation has received less attention, especially in the realm of polymer chemistry, possibly due to the greater hydrolytic stability of oximes compared to imines or hydrazones.[27] In fact, the enhanced hydrolytic stability of oxime renders the possibility of utilizing oxime formation to create functional materials needing superior aqueous stability. In contrast to hydrolytic stability, oxime bonds are suseptable to dynamic exchange with either an alkoxyamine molecule or a carbonyl compound in the presence of catalytic acid (Scheme 8.7). Eliseev and co-workers have studied the reaction kinetics and mechanism of imine/oxime exchange between different aliphatic or aryl alkoxyamine molecules, and the authors suggested the use of oxime exchange to create a library of oxime compounds capable of constitutional rearrangement under specific conditions.[26] Raines and co-workers reported a detailed study of the hydrolysis mechanism and the effects of the electronic structures of the carbonyl compounds and the alkoxyamines on the rates of hydrolysis and exchange.[27] Stoddart *et al.* utilized oxime ligation to functionalize mesoporous silica nanoparticles.[213] The authors synthesized an alkoxyamine silyl ether to decorate the silica nanoparticle surface and utilized the reversible oxime exchange reaction to reversibly attach various aldehyde and ketone compounds onto the nanoparticles.
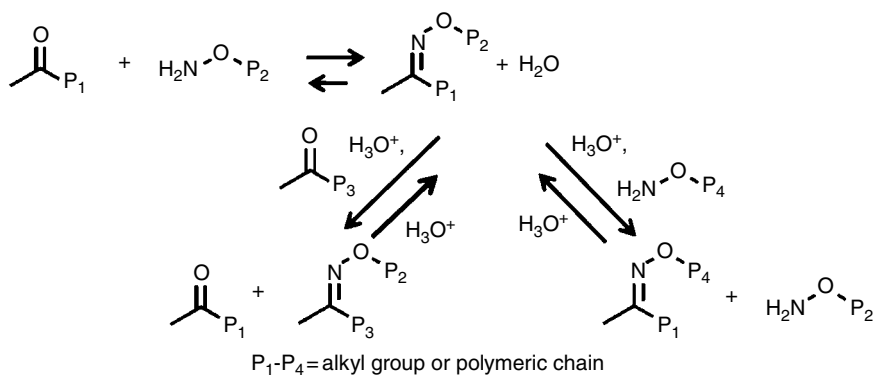
Scheme 8.7 Oxime formation between a carbonyl compound and an alkoxyamine. Dynamic oxime exchange (acid catalyzed) between oxime and alkoxyamine or carbonyl compounds.

The exchangeable nature of the oxime bond has recently started to receive interest with regard to preparing robust polymeric materials capable of bond reorganization at the molecular level. Sumerlin and co-workers have utilized the reversible oxime exchange to prepare core-crosslinked star polymers with a degradable oxime core.[24] Keto-functionalized block copolymers were synthesized by RAFT polymerization. The block copolymers [poly(dimethyl acrylamide)-*b*-poly(diacetone acrylamide)] were self-assembled in water and on addition of dialkoxyamine the polymers crosslinked to form core-crosslinked stars. The star polymers were dissociated by addition of excess mono-functional alkoxyamine, which competed for binding with the polymer-bound ketones in the presence of trifluroacetic acid catalyst. The reversible nature of oxime links was also utilized to form a self-healing hydrogel by the Sumerlin group.[214] Ketone-containing copolymers poly[(dimethyl acrylamide)-*stat-(*diacetone acrylamide)] were prepared with varying ketone content and the polymers were crosslinked with difunctional alkoxyamines to form hydrogel and organogel. The hydrogels were capable of self-healing after mechanical damage. The gel-to-sol transition of the hydrogels was induced by the addition of monofunctional alkoxyamine and trifluroacetic acid catalyst.

Recently the redox-responsive nature of oxime bonds was harnessed by Yousuf *et al.*, who employed a liposome-based methodology to functionalize cell surfaces with dynamic oxime links for application in stem-cell differentiation and tissue engineering.[25,215] The authors synthesized a hydroquinone (HQ) and aminoxy alkane or alkoxyamine (AO), and incorporated them into different liposomes.[25] The hydroquinone was transformed into an active quinone (Q) state by applying mild oxidation potential (either chemically or electrochemically) and was mixed with the AO-containing liposomes to react with the alkoxyamine to generate oxime via liposome–liposome fusion, as observed by transmission electron microscopy (TEM) images. This liposome–liposome fusion methodology was employed to tailor cell surfaces via oxime formation. An HQ-alkane was mixed with 1-palmitoyl-2-oleoylphosphatidylcholine (POPC) and DOTAP (a cationic lipid, 1,2-dioleoyl-3-trimethylammonium-propane) in a 10:88:2 ratio, and the AO was mixed with POPC and DOTAP in a 5:93:2 ratio. After their addition to the cells (Swiss 3T3T fibroblast (Fbs)) in culture, the liposome fused and delivered the chemical functionality to the cell surfaces. The oxime bonds were selectively cleaved by applying mild redox potential (−100 mV, 10 s, PBS, pH = 7.4) with the

working electrode, resulting in the release of ligands from the cell surface. This dynamic cycle was found to be non-toxic and, most importantly, could be performed *in situ* and under physiological conditions.

These reports clearly demonstrate that the inherent reversible exchangability of the oxime link can be a useful tool in the design of complex platforms for drug delivery, cell-surface modification, protein modification, and tissue engineering purposes.

8.5.4 Polymers Containing Disulfide Links

A redox stimulus causes change in the oxidation state of an element or a functional group by either cathodic/anodic[25,215] or chemical oxidation/reduction processes. Disulfides have been explored extensively as a redox-sentisitive functional group for different biomedical applications.[32,216] Some other redox-responsive moeities are ferrocene,[217] tetramethylpiperidine-1-oxyl (TEMPO),[218] dithienylethenes,[219] and metal-ligand complexes.[32,35] Disulfides are commonly found in natural systems and are known for their reversibility and exchange behavior. Disulfide bonds play an important role in biological systems, for example in the develoment of the secondary structure of proteins.[220] The disulfide links between the cysteine residues in proteins frequently undergo disulfide exchange to attain the lowest energy folded structure.[221] In most cases, the thiol-disulfide exchange process proceeds through the base-catalyzed pathway by generating a thiolate anion (Scheme 8.8).[151] The disulfide exchange, on the other hand, could occur via a radical pathway through generating a sulfenyl radical by photoirradiation.[222,223] Considerable work has been devoted to the preparation of reversible polymeric material using both routes.[1,224]

Matyjaszewski *et al.* synthesized self-healing polymeric materials by employing a redox-responsive thiol–disulfide exchange reaction.[225,226] In one of their reports, the authors made a multiarm star polymer precursor containing thiol groups, architecturally selected because of the favorable healing, which induces low intrinsic viscosity of the branched star polymers compared to their linear counterparts.[225]

The star polymers were synthesized by ATRP via a core-first approach, and subsequently the star polymers were chain-extended with a divinyl compound, bis(2-methacryloyloxyethyl disulfide) (DSDMA) to induce macroscopic crosslinking, which resulted in gel formation.[18] The disulfide links in the crosslinked gel were cleaved by reduction with tri-butyl phosphine, and the thiol-functionalized polymer was deposited on a silicon wafer to form a thin film. The thiol groups in the thin film were oxidized with either $FeCl_3$ or I_2 to obtain a disulfide crosslinked film, which was insoluble in chloroform and THF. The disulfide formation was confirmed by Raman spectroscopy. For control experiments, a thin film containing permanent crosslink was prepared by reacting the free thiol groups with 1,2,7,8-diepoxyoctane under basic conditions.

(a)

$R^1\text{-S-S-}R^2$ $\underset{\text{Oxidation}}{\overset{\text{Reduction}}{\rightleftarrows}}$ $R^1SH + R^2SH$
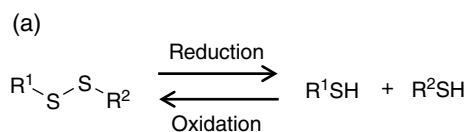
Scheme 8.8 (a) Reversible cleavage of disulfide bonds by reduction and recombination of thiols by oxidation and (b) thiol-disulfide exchange.

(b)

$R^1\text{-S-S-}R^2 + R^3SH \rightleftarrows R^1\text{-S-S-}R^3 + R^2SH$
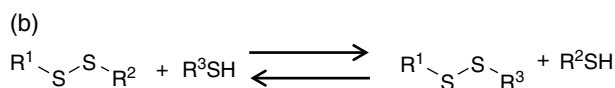
The self-healing study was performed by damaging the thin film with an atomic force microscope (AFM) tip or a penetrating cut by a microscratching method. The healing process was monitored by AFM and optical microscopy. The damaged film self-healed at room temperature with no external stimulus. The AFM study showed that damage at the center position was not fully healed after 70 min, but damage at the edge was completely healed after 70 min, suggesting that the healing was initiated from the bottom of the cut and the edge of the cut due to the accessibility of cut surfaces to each other. To bring about the contact of the damaged areas, the AFM tip was used to stroke the damaged surface in the direction perpendicular to the damaged area. Immediate smoothening of the damaged area was observed, and the Young's modulus (by HarmoniX tapping mode) of the healed area was found to be comparable to the modulus of the undamaged area. The healing capacity of the thin film was found to be dependent on the initial film thickness and the width of the damage. A thicker penetrating cut resulted in rapid healing, as observed by optical microscopy. No self-healing was observed in the control film sample due to the absence of any exchangeable links to cause healing. This study showed that reversible branched polymeric materials hold tremendous promise for self-healing applications due to their low viscosity and accessibility to higher functional groups.

In another example Thayumanavan *et al*. synthesized block copolymers composed of an acid-labile hydrophobic block, temperature-sensitive hydrophilic block, and a redox-responsive disulfide interface.[227] The block copolymers self-assembled into micelles and Nile Red was encapsulated in the micelle core in aqueous media. Release of Nile Red was facilitated by either lowering the pH of the medium or creating a reducing environment to cleave the disulfide linkages between two blocks. Based on the current results, the authors envisioned that combination of multiple stimuli-responsive units in polymeric drug-delivery systems could significantly accelerate the rate of drug release compared to a single-stimuli responsive polymeric system. Such a strategy could also be useful to design polymers for applications in the field of controlled release, catalysis, and separation. The reversibility of the disulfide link is currently a topic of intensive investigation to prepare drug-delivery vehicles due to the fact that disulfides can be reduced by glutathione, which is present in an intracellular environment at 3 mM concentration (which is 300 times greater than its concentration in blood). Polymeric nanoparticles have been used to encapsulate the drug and release it under a reducing environment in the presence of glutathione.[228,229]

Recently *Otto et al*. utilized the phototriggered homolytic cleavage of disulfide bonds to prepare a dynamic library of disulfide-containing macrocycles.[230] The authors prepared stacks of macrocycles from a peptide-containing dithiol building block with a β-sheet structure (Figure 8.5). Photoirradiation at 365 nm (using a 8 W UV lamp) resulted in oligomers, polymers, and gels (after prolonged irradiation for 3 days). The presence of excess dithiothreitol resulted in quantitative recovery of the starting material. The polymerization of self-assembled macrocycles combines kinetic (self-templating, aggregation-driven stabilization) and thermodynamic control to access polymers with well-defined folded structures.

8.5.5 Glucose-responsive Polymers

Glucose-responsive polymers have received a significant amount of interest because of their potential application in the sensing and delivery of insulin. Recent developments
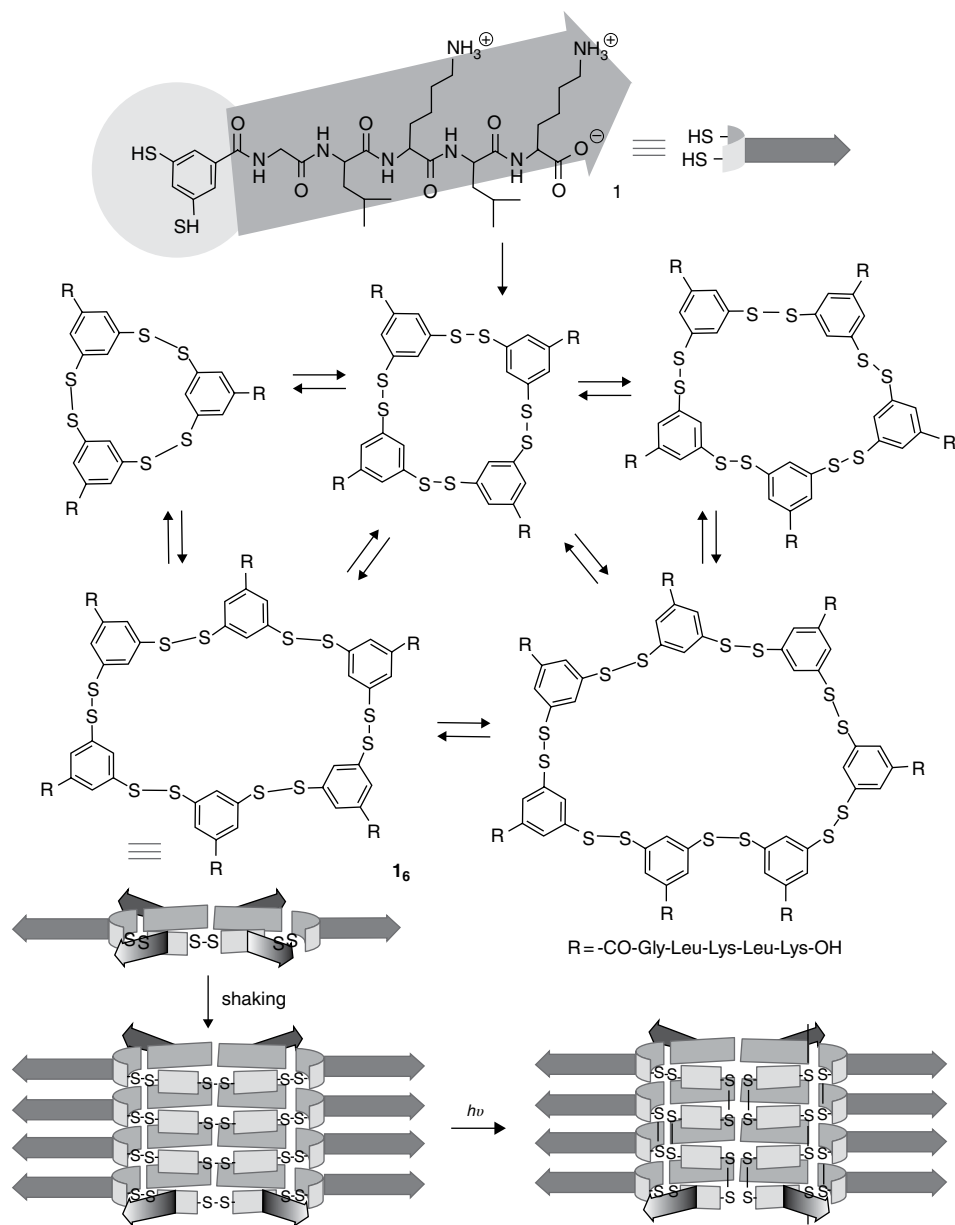
Figure 8.5 Preparation of stacks of disulfide macrocycles (1_6) from a dithiol building block (**1**) in borate buffer solution (pH 8.1). The disulfide macrocycles were covalently captured by photo-induced (365 nm) polymerization of the disulfide macrocycles. Adapted from *Angew. Chem. Int. Ed.* **2011**, *50*, 8384–8386. Copyright 2011 Wiley.

in designing polymers that specifically respond to sugar have opened up new possibilities to treat diabetes mellitus, which is defined as a group of metabolic disorders characterized by high blood sugar levels.[37,231] Treatment of diabetes generally involves regular monitoring of blood-sugar level and administration of insulin via

injection. This approach of self-administration of insulin lacks continuous control over the released dosage of insulin and reportedly only 20% of the insulin reaches the liver, which is the primary site of action.[232] A considerable amount of research has been dedicated to developing smart polymeric drug carriers that can release the payload in response to the increase in blood-glucose level.[30] The strategies for glucose-responsive delivery systems have relied on oxidation of glucose by glucose oxidase (GOx), binding of glucose with concanavalin A (Con A), and boronic acid-containing polymers which are capable of reversible bond formation with diols in carbohydrates.

The GOx catalyzed oxidation of glucose results in H_2O_2 and gluconic acid as byproducts. In the majority of the reports, pH-responsive polymers (e.g., polyacids or polybases) were loaded or conjugated with GOx and insulin, and then gluconic acid (the byproduct of the enzymatic oxidation of glucose) induced a pH response, resulting in swelling or deswelling of the polymeric systems and consecutive insulin release.[233–240]

Another kind of glucose-responsive delivery system utilizes the competitive binding of glucose and lectin, which is a carbohydrate-binding protein. A commonly employed lectin for insulin delivery is concanavalin A, which interacts with a diverse set of receptors, including mannose carbohydrate, blood group markers, and insulin-receptors.[30,37,241] Concovalin A-bound polymers and nano- or microgels were synthesized for recognition of glucose and insulin delivery.[239,242,243] The presence of glucose causes the complex of concovalin A and the carbohydrate-bearing polymer to dissociate and subsequently form glucose–concovalin A complex. This decomplexation–recomplexation process leds the release of insulin, encapsulated in the polymer or gel matrix.[37]

An alternative and more versatile approach is the use of boronic acid moieties, which can bind competitively with diols present in carbohydrates and other compounds and enable the release of insulin in a self-regulated manner. The ability of boronic acid compounds to reversibly bind to diols in sugars makes them an excellent candidate for glucose sensing applications and use as ligands during chromatography.[244] The solubility of boronic acids in aqueous media can be tuned by changing the pH of the media or the diol concentration. Boronic acids exist in equilibrium between the neutral trigonal form (**1**) and an anionic tetrahedral form (**2**) (Scheme 8.9).[245–249] The cyclic boronate esters formed by the reaction of neutral boronic acids (**1**) and diols are generally considered to be hydrolytically unstable in the presence of 1,2- or 1,3-diols, whereas the charged boronic acid (**2**) reversibly binds with 1,2- or 1,3-diols to form stable boronate ester (**3**), shifting the equilibria to the anionic forms **2** and **3**.[246,249] Additionally the neutral boronic acid-containing polymers are generally hydrophobic whereas the anionic boronate ester-containing polymers show hydrophilicity.[247] With increasing diol or sugar concentration, the anionic forms, **2** and **3**, dominate in solution. The equilibrium
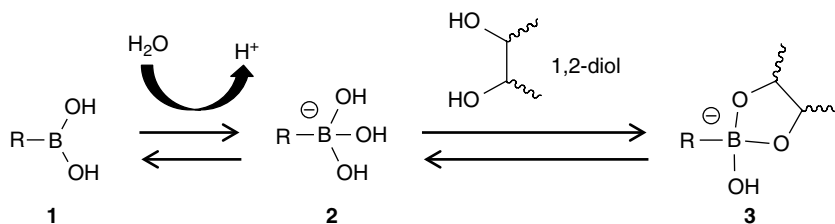
Scheme 8.9 Ionization equilibrium of boronic acid in aqueous environment. With increasing diol concentration the equilibria shifts towards the anionic boronate form (**3**).

between the hydrophobic neutral form (**1**) and the hydrophilic anionic forms (**2** and **3**) can be controlled by controlling the pH of the media and the concentration of sugar/diols, and this interesting transformation between **1** and **2** or **3** often leads to a diol-responsive behavior in boronic acid-containing polymers.

Most of the polymeric boronic acids reported in the literature are based on phenyl boronic acids with a pK_a between 6 and 9.[36,250–254] The solubility of boronic acids changes in aqueous media because of the apparent reduction in their pK_a in the presence of glucose. Some excellent reviews have covered the initial development and use of boronic acid-containing polymers from various perspectives.[36,254–259] Some recent examples are discussed in this section.

The majority of the boronic acid-based systems for carbohydrate sensing or insulin delivery have been based on hydrogels, which change their swelling behavior in the presence of glucose. One straightforward route to synthesize boronic acid-containing hydrogel is to employ boronic acid monomers such as 3-(acrylamido)-phenylboronic acid (3-AAPBA) and copolymerize with another water soluble monomer such as *N*-isoprpylacrylamide (NIPAM) or *N,N*-dimethylacrylamide (DMA) in the presence of a crosslinker, for example *N,N'*-methylenebis(acrylamide). Kataoka *et al.*[248,260] prepared glucose-responsive hydrogels by copolymerizing 3-AAPBA and NIPAM, and investigated the swelling kinetics of the hydrogel in the presence of glucose and the kinetics of the temperature-dependent hydrogel-shrinkage process. To utilize the glucose-responsive behavior of boronic acids for sensing application, Asher *et al.* incorporated a crystalline colloidal array, which diffracts visible light, into a polyacrylamide hydrogel.[261] The crystalline colloidal array embedded hydrogel was able to respond to glucose in low ionic strength solution by swelling and red-shifting its diffraction with increasing glucose concentration.

Another approach to synthesizing a boronate ester-containing hydrogel is to cross-link diol-containing polymers with borax or phenyl boronic acid-containing polymers.[262–264] However, the borax–diol complexation is known to happen at alkaline pH (≈9), which is not suitable for various biomedical applications. Furthermore, the crosslinking with boronic acid polymers has been found to be more efficient than the gelation reaction with borax due to the presence of multiple crosslinking sites on the boronic acid-containing polymer.[265,266] A considerable amount of research has been dedicated to reducing the pK_a of the boronic acids to physiological pH.[253,267] Engbersen *et al.* synthesized α,ω-phenylboronic acid-terminated poly(propylene oxide)-poly(ethylene oxide)-poly(propylene oxide) (PPO–PEO–PPO) to crosslink poly(vinyl alcohol) (Scheme 8.10).[264] The PPO–PEO–PPO spacer provided hydrophilicity and the secondary amine group in the *ortho* position of one of the crosslinkers reduced the pK_a of the boronic acid crosslinker by B–N coordination. The hydrogel showed frequency-dependent viscoelastic behavior and due to the dynamic nature of the boronate ester crosslinks, the hydrogel network could restructure itself at lower frequency during an oscillatory frequency sweep experiment.

A similar synthetic strategy has been used to prepare self-healing hydrogels. Messersmith *et al.* prepared pH-responsive self-healing hydrogel through complexation of branched catechol-functionalized poly(ethylene glycol) with 1,3-benzenediboronic acid.[268] The hydrogel exhibits higher stability at alkaline pH and lower stability under an acidic environment. Recently Sumerlin *et al.* employed poly(2-acrylamido)phenylboronic acid (2APBA) and poly(vinyl alcohol) or a catechol-functionalized polymer to
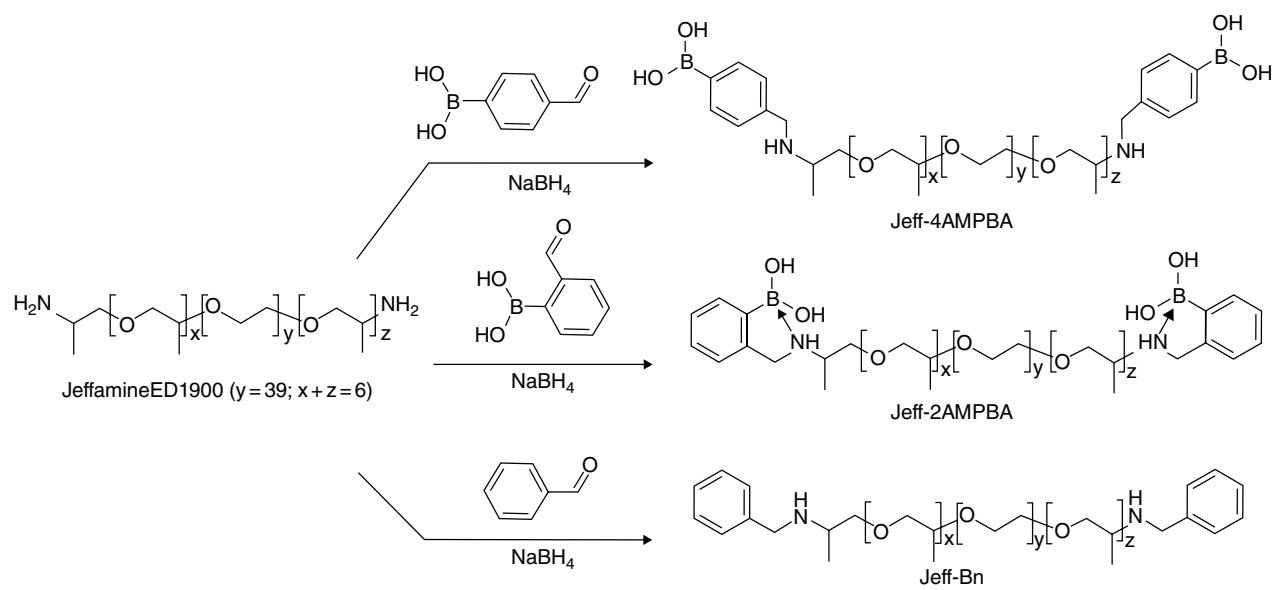
Scheme 8.10 Synthesis of boronic acid crosslinker (Jeff-AMPBA) by reductive amination of JeffamineED1900. Reprinted from *Soft Matt.* **2011**, *7*, 11111–11118, with permission from the Royal Society of Chemistry.

prepare hydrogel that can self-heal at acidic and neutral pH.[269] The intramolecular coordination between the carbonyl oxygen and boron allowed the gelation to happen at acidic and neutral pH. The authors also found that the oxidation of the dopamine moiety in catechol-functionalized polymer reduced the self-healing properties and minimized creep. The same group has recently prepared boronic ester-containing crosslinked bulk polymeric networks via a photoinitiated thiol-ene reaction that were capable of self-healing under humid conditions for several cycles.[270] Boronic acid-containing nanogel, microgels, and layer-by-layer assembled hydrogel films have also been prepared using boronic acid–diol complexation.[256,267]

Boronic acid-containing block copolymers and their self-assembled nanostructures have also received significant interest due to the possibility of employing self-assembled block copolymers as nanocarriers of insulin. Jäkle *et al.* utilized ATRP of styrene and pinacol-protected styrenic boronic acid or trimethyl-(4-vinyl-phenyl)-silane to prepare block copolymers.[271,272] Sumerlin *et al.* reported the first example of using RAFT polymerization of pinacol-protected phenyl boronic acid to synthesize water-soluble boronic acid-based polymers.[273] The amphiphilic block copolymers self-assembled in water and the pinacol boronate ester was deprotected by transesterification with another boronic acid. An alkaline environment was needed to cause glucose-responsive disassembly of the micelles. The authors also synthesized a glucose-responsive polymer by direct RAFT polymerization of unprotected and less hydrophobic boronic acid.[274] The polymers self-assembled in aqueous solution, and a micelle to unimer transition was induced in the presence of glucose. Sumerlin *et al.* later designed a boronic acid monomer with an acrylamide unit and electron-withdrawing substituents, which lowered the pK_a of the boronic acid moiety to 8.2.[275] The block copolymers showed pH-dependent self-assembly behavior. The block copolymers formed micelles at a pH less than the pK_a of individual block copolymers, and the size of the aggregates increased as the pH was raised from 7.4 to 8.2. On further increase in the pH of the solution to 8.5 (when pH > pK_a (=8.2)), the aggregates disassembled to form unimers. Addition of glucose to the aggregates at pH 7.4 led to reduction of their size in solution as the pendent boronic acid groups competitively bound to glucose and the aggregates transformed into water-soluble glucose-functionalized polymers. Self-assemblies of block copolymers containing boronic acid moieties have been utilized to encapsulate insulin for insulin delivery. Yang *et al.* prepared poly(ethylene glycol)–*block*–((2-phenylboronic esters-1,3-dioxane-5-ethyl) methylacrylate) by ATRP and the block copolymers were able to self-assembled in water.[276] Insulin was loaded in the micelle core and the release of insulin was triggered by the addition of glucose, which competitively bound with the pendent boronic acid groups in the polymer at alkaline pH. Sumerlin *et al.* also reported the synthesis of dynamic covalent star polymers by crosslinking boronic acid-containing block copolymers with multifunctional 1,2/1,3-diols.[22] The reversible nature of the boronic ester linkages allowed the disassembly of the star polymers in the presence of monofunctional diols. The findings of this research have inspired the polymer community to utilize the controlled exchange behavior of boronic esters to prepare more complex dynamic covalent architectures.[253,254,258,277]

Recently benzoxaborol compounds have received considerable interest for creating carbohydrate-responsive polymers due to their ability to bind to diols at physiological pH and to pyranose saccharides as well as sialic acid, both of which are abundant in glycocalyx in cancer cells.[277] Kim *et al.* synthesized benzoxaborol-containing block copolymers which self-assembled in water, and fluorescent-labelled insulin was

encapsulated in the micelles at pH 7.4.[278] The insulin was released in the presence of a monosaccharide which bound to the benzoxaborol under physiological pH. To incorporate the glucose-responsive behavior with reversible characteristic, Narain *et al.* utilized RAFT polymerization to synthesize copolymers of NIPAM and 5-methacrylamido-1,2-benzoxaborole, which were temperature, pH, and glucose responsive.[279] Two glycopolymers, poly(3-gluconamidopropyl methacrylamide) (PGAPMA) and poly(2-lactobionamidoethyl methacrylamide) (PLAEMA), were used to crosslink the benzoxaborol-containing polymers to form hydrogel. The gel-to-sol transition was induced by the addition of glucose at pH 7.4.

The unique characteristics of boronic acid polymers have encouraged the scientific community to construct a variety of responsive nanomaterials, including vesicles, nanoporous silica, polymersomes, and hollow nanospheres.[267] Even though more research in this area is emerging every day, the full potential of boronic acid-based polymers in biomedical research is yet to be realized.

8.6 Conclusion

The topics covered here are important both from a fundamental scientific standpoint and from a real-life applications perspective. The inspiration for creating stimuli-responsive polymers that can respond to environmental and biological stimuli has been provided by nature. Polymers with reversible characteristics are an ever-growing area of research as they are capable of responding to a stimulus by rearranging the structural components at a molecular level. Further progress in this area could greatly benefit research in the areas of therapeutics, sensors, coating for biomedical devices, artificial muscles, and actuators. The combination of reversibility and stimuli-responsiveness in a molecule was sought in many areas of polymer chemistry and the scope of such materials is yet to be fully understood. Greater challenges lie in developing complex dynamic covalent polymers without any undesirable changes in a material's property that are able to response to stimuli that are only present in trace amounts. The recyclability and long-term stability of such polymeric systems are other areas which need to be addressed in a judicial manner. Truly recyclable dynamic covalent polymers will not only add smart responsive behavior to a material but also provide a cost-effective alternative to an existing product. The combination of durability and dynamic behavior in polymers would also provide access to robust healable material. The access to different functionalization techniques, click chemistries, and controlled polymerization methods is critical in designing polymers that can respond to multiple stimuli in an orthogonal manner and may provide an accelerated response. Multi-stimuli responsive polymers adorned with reversibility can bring about enormous progress in life science research and also in information technology in the parallel writing of information or rewritable memory devices.

References

1 Y. Jin, C. Yu, R. J. Denman, W. Zhang, *Chem. Soc. Rev.* **2013**, *42*, 6634–6654.
2 M. A. C. Stuart, W. T. S. Huck, J. Genzer, M. Muller, C. Ober, M. Stamm, G. B. Sukhorukov, I. Szleifer, V. V. Tsukruk, M. Urban, F. Winnik, S. Zauscher, I. Luzinov, S. Minko, *Nat. Mater.* **2010**, *9*, 101–113.

3 G. Armstrong, M. Buggy, *J. Mater. Sci.* **2005**, *40*, 547–559.

4 F. Ouhib, M. Raynal, B. Jouvelet, B. Isare, L. Bouteiller, *Chem. Commun.* **2011**, *47*, 10683–10685.

5 S. Burattini, B. W. Greenland, D. H. Merino, W. Weng, J. Seppala, H. M. Colquhoun, W. Hayes, M. E. Mackay, I. W. Hamley, S. J. Rowan, *J. Am. Chem. Soc.* **2010**, *132*, 12051–12058.

6 J.-M. Lehn, *From Molecular to Supramolecular Chemistry*, in *Supramolecular Chemistry*, Wiley-VCH Verlag GmbH & Co. KGaA, **2006**, pp. 1–9.

7 A. Granzhan, T. Riis-Johannessen, R. Scopelliti, K. Severin, *Angew. Chem., Int. Ed.* **2010**, *49*, 5515–5518.

8 S. J. Rowan, S. J. Cantrill, G. R. L. Cousins, J. K. M. Sanders, J. F. Stoddart, *Angew. Chem., Int. Ed.* **2002**, *41*, 898–952.

9 A. Ciferri, *Supramolecular Polymers*, 2nd edn, CRC Group, Boca Raton, FL, **2005**.

10 R. J. Thibault, V. M. Rotello, A brief introduction to supramolecular chemistry in a polymer context, in *Molecular Recognition and Polymers*, John Wiley & Sons, Inc., **2008**, pp. 1–7.

11 C. J. Hawker, G. G. Barclay, J. Dao, *J. Am. Chem. Soc.* **1996**, *118*, 11467–11471.

12 H. Otsuka, K. Aotani, Y. Higaki, A. Takahara, *J. Am. Chem. Soc.* **2003**, *125*, 4064–4065.

13 H. Laita, S. Boufi, A. Gandini, *Eur. Polym. J.* **1997**, *33*, 1203–1211.

14 D. N. Amato, G. A. Strange, J. P. Swanson, A. D. Chavez, S. E. Roy, K. L. Varney, C. A. Machado, D. V. Amato, P. J. Costanzo, *Polym. Chem.* **2014**, *5*, 69–76.

15 A. M. Kotliar, *J. Polym. Sci.: Macromol. Rev.* **1981**, *16*, 367–395.

16 Q. Wang, L. Zhu, G. Li, C. Tu, Y. Pang, C. Jin, B. Zhu, X. Zhu, Y. Liu, *Macromol. Biosci.* **2011**, *11*, 1553–1562.

17 A. Sulistio, A. Blencowe, A. Widjaya, X. Zhang, G. Qiao, *Polym. Chem.* **2012**, *3*, 224–234.

18 J. Kamada, K. Koynov, C. Corten, A. Juhari, J. A. Yoon, M. W. Urban, A. C. Balazs, K. Matyjaszewski, *Macromolecules* **2010**, *43*, 4133–4139.

19 H. Gao, N. V. Tsarevsky, K. Matyjaszewski, *Macromolecules* **2005**, *38*, 5995–6004.

20 A. P. Bapat, J. G. Ray, D. A. Savin, B. S. Sumerlin, *Macromolecules* **2013**, *46*, 2188–2198.

21 J. A. Syrett, D. M. Haddleton, M. R. Whittaker, T. P. Davis, C. Boyer, *Chem. Commun.* **2011**, *47*, 1449–1451.

22 A. P. Bapat, D. Roy, J. G. Ray, D. A. Savin, B. S. Sumerlin, *J. Am. Chem. Soc.* **2011**, *133*, 19832–19838.

23 D. Zhao, J. S. Moore, *J. Am. Chem. Soc.* **2002**, *124*, 9996–9997.

24 S. Mukherjee, A. P. Bapat, M. R. Hill, B. S. Sumerlin, *Polym. Chem.* **2014**, *5*, 6923–6931.

25 A. Pulsipher, D. Dutta, W. Luo, M. N. Yousaf, *Angew. Chem., Int. Ed.* **2014**, *53*, 9487–9492.

26 V. A. Polyakov, M. I. Nelen, N. Nazarpack-Kandlousy, A. D. Ryabov, A. V. Eliseev, *J. Phys. Org. Chem.* **1999**, *12*, 357–363.

27 J. Kalia, R. T. Raines, *Angew. Chem., Int. Ed.* **2008**, *47*, 7523–7526.

28 E. Cabane, X. Zhang, K. Langowska, C. Palivan, W. Meier, *Biointerphases* **2012**, *7*, 1–27.

29 M. Delcea, H. Möhwald, A. G. Skirtach, *Adv. Drug Deliv. Rev.* **2011**, *63*, 730–747.

30 E. S. Gil, S. M. Hudson, *Prog. Polym. Sci.* **2004**, *29*, 1173–1222.

31 C. d. l. H. Alarcon, S. Pennadam, C. Alexander, *Chem. Soc. Rev.* **2005**, *34*, 276–285.

32 A. S. Hoffman, *Adv. Drug Deliv. Rev.* **2013**, *65*, 10–16.

33 J. A. Burdick, W. L. Murphy, *Nat. Commun.* **2012**, *3*, 1269.

34 A. W. Jackson, D. A. Fulton, *Polym. Chem.* **2013**, *4*, 31–45.

35 R. J. Wojtecki, M. A. Meador, S. J. Rowan, *Nat. Mater.* **2011**, *10*, 14–27.

36 J. N. Cambre, B. S. Sumerlin, *Polymer* **2011**, *52*, 4631–4643.

37 D. Roy, J. N. Cambre, B. S. Sumerlin, *Prog. Polym. Sci.* **2010**, *35*, 278–301.

38 D. Roy, W. L. A. Brooks, B. S. Sumerlin, *Chem. Soc. Rev.* **2013**, *42*, 7214–7243.

39 H. Otsuka, *Polym. J.* **2013**, *45*, 879–891.

40 N. Nath, A. Chilkoti, *Adv. Mater.* **2002**, *14*, 1243–1247.

41 J.-M. Lehn, *Prog. Polym. Sci.* **2005**, *30*, 814–831.

42 M.-C. Jones, P. Tewari, C. Blei, K. Hales, D. J. Pochan, J.-C. Leroux, *J. Am. Chem. Soc.* **2006**, *128*, 14599–14605.

43 A. K. Bajpai, S. K. Shukla, S. Bhanu, S. Kankane, *Prog. Polym. Sci.* **2008**, *33*, 1088–1118.

44 M. Hrubý, V. Šubr, J. Kučka, J. Kozempel, O. Lebeda, A. Sikora, *Appl. Radiat. Isot.* **2005**, *63*, 423–431.

45 J. E. Chung, T. E. Okano, Thermoresponsive polymeric micelles for double targeted drug delivery, in *Polymeric Drugs and Drug Delivery Systems*, CRC Press, **2000**.

46 M. Nakayama, T. Okano, T. Miyazaki, F. Kohori, K. Sakai, M. Yokoyama, *J. Control. Release* **2006**, *115*, 46–56.

47 W. Chen, L. Qu, D. Chang, L. Dai, S. Ganguli, A. Roy, *Chem. Commun.* **2008**, 163–165.

48 M. D. Lavigne, S. S. Pennadam, J. Ellis, L. L. Yates, C. Alexander, D. C. Górecki, *J. Gene Med.* **2007**, *9*, 44–54.

49 Z. Mao, L. Ma, J. Yan, M. Yan, C. Gao, J. Shen, *Biomaterials* **2007**, *28*, 4488–4500.

50 J. Yang, P. Zhang, L. Tang, P. Sun, W. Liu, P. Sun, A. Zuo, D. Liang, *Biomaterials* **2010**, *31*, 144–155.

51 N. Takeda, E. Nakamura, M. Yokoyama, T. Okano, *J. Control. Release* **2004**, *95*, 343–355.

52 M. Kurisawa, M. Yokoyama, T. Okano, *J. Control. Release* **2000**, *69*, 127–137.

53 B. R. Twaites, C. de las Heras Alarcón, D. Cunliffe, M. Lavigne, S. Pennadam, J. R. Smith, D. C. Górecki, C. Alexander, *J. Control. Release* **2004**, *97*, 551–566.

54 N. Cheng, W. Liu, Z. Cao, W. Ji, D. Liang, G. Guo, J. Zhang, *Biomaterials* **2006**, *27*, 4984–4992.

55 Y.-M. Zhou, A. Ishikawa, R. Okahashi, K. Uchida, Y. Nemoto, M. Nakayama, Y. Nakayama, *J. Control. Release* **2007**, *123*, 239–246.

56 I. Lokuge, X. Wang, P. W. Bohn, *Langmuir* **2007**, *23*, 305–311.

57 G. Wu, Y. Li, M. Han, X. Liu, *J. Membrane Sci.* **2006**, *283*, 13–20.

58 H. Kanazawa, Y. Matsushima, T. Okano, *Trends Anal. Chem.* **1998**, *17*, 435–440.

59 H. Kanazawa, *J. Separat. Sci.* **2007**, *30*, 1646–1656.

60 E. Ayano, H. Kanazawa, *J. Separat. Sci.* **2006**, *29*, 738–749.

61 A. S. Hoffman, P. S. Stayton, *Prog. Polym. Sci.* **2007**, *32*, 922–932.

62 Y. G. Takei, T. Aoki, K. Sanui, N. Ogata, T. Okano, Y. Sakurai, *Bioconjugate Chem.* **1993**, *4*, 341–346.

63 N. Shamim, L. Hong, K. Hidajat, M. S. Uddin, *Sep. Purif. Technol.* **2007**, *53*, 164–170.

64 R. M. P. da Silva, J. F. Mano, R. L. Reis, *Trends Biotechnol.* **2007**, *25*, 577–583.

65 H. Hatakeyama, A. Kikuchi, M. Yamato, T. Okano, *Biomaterials* **2007**, *28*, 3632–3643.

66 M. C. LeMieux, S. Peleshanko, K. D. Anderson, V. V. Tsukruk, *Langmuir* **2007**, *23*, 265–273.

67 K. Nagase, J. Kobayashi, T. Okano, *J. Roy. Soc. Interface* **2009**, *6*, Suppl 3, S293–S309.

68 D. Crespy, R. M. Rossi, *Polym. Int.* **2007**, *56*, 1461–1468.

69 A. P. Vogt, B. S. Sumerlin, *Macromolecules* **2008**, *41*, 7368–7373.

70 A. P. Vogt, B. S. Sumerlin, *Soft Matter* **2009**, *5*, 2347–2351.

71 H. Li, A. P. Bapat, M. Li, B. S. Sumerlin, *Polym. Chem.* **2011**, *2*, 323–327.

72 H. G. Schild, *Prog. Polym. Sci.* **1992**, *17*, 163–249.

73 D. Schmaljohann, *Adv. Drug Deliv. Rev.* **2006**, *58*, 1655–1670.

74 A. Kikuchi, T. Okano, *Prog. Polym. Sci.* **2002**, *27*, 1165–1193.

75 C. L. McCormick, B. S. Sumerlin, B. S. Lokitz, J. E. Stempka, *Soft Matter* **2008**, *4*, 1760–1773.

76 P. De, M. Li, S. R. Gondi, B. S. Sumerlin, *J. Am. Chem. Soc.* **2008**, *130*, 11288–11289.

77 P. De, S. R. Gondi, B. S. Sumerlin, *Biomacromolecules* **2008**, *9*, 1064–1070.

78 D. Roy, J. N. Cambre, B. S. Sumerlin, *Chem. Commun.* **2009**, 2106–2108.

79 X. Zhang, J. Li, W. Li, A. Zhang, *Biomacromolecules* **2007**, *8*, 3557–3567.

80 K. T. Oh, H. Yin, E. S. Lee, Y. H. Bae, *J. Mater. Chem.* **2007**, *17*, 3987–4001.

81 Z. M. O. Rzaev, S. Dinçer, E. Pişkin, *Prog. Polym. Sci.* **2007**, *32*, 534–595.

82 B. V. K. J. Schmidt, M. Hetzer, H. Ritter, C. Barner-Kowollik, *Macromol. Rapid Commun.* **2013**, *34*, 1306–1311.

83 S. Fusco, A. Borzacchiello, P. A. Netti, *J. Bioactive Compat. Polymers* **2006**, *21*, 149–164.

84 M. S. Kim, H. Hyun, K. S. Seo, Y. H. Cho, J. Won Lee, C. Rae Lee, G. Khang, H. B. Lee, *J. Polym. Sci. Part A: Polym. Chem.* **2006**, *44*, 5413–5423.

85 H. Vihola, A. Laukkanen, H. Tenhu, J. Hirvonen, *J. Pharm. Sci.* **2008**, *97*, 4783–4793.

86 H. Vihola, A.-K. Marttila, J. S. Pakkanen, M. Andersson, A. Laukkanen, A. M. Kaukonen, H. Tenhu, J. Hirvonen, *Int. J. Pharm.* **2007**, *343*, 238–246.

87 J.-M. Thomassin, K. Mathieu, A. Kermagoret, C.-A. Fustin, C. Jerome, A. Debuigne, *Polym. Chem.* **2015**, *6*, 1856–1864.

88 A. Gandhi, A. Paul, S. O. Sen, K. K. Sen, *Asian J. Pharm. Sci.* **2015**, *10*, 99–107.

89 L. T. T. Trinh, H. M. L. Lambermont-Thijs, U. S. Schubert, R. Hoogenboom, A.-L. Kjøniksen, *Macromolecules* **2012**, *45*, 4337–4345.

90 S. Kikuchi, Y. Chen, K. Fuchise, K. Takada, J. Kitakado, S.-i. Sato, T. Satoh, T. Kakuchi, *Polym. Chem.* **2014**, *5*, 4701–4709.

91 M. Zhang, W. Shen, Q. Xiong, H. Wang, Z. Zhou, W. Chen, Q. Zhang, *RSC Adv.* **2015**, *5*, 28133–28140.

92 F. L. Baines, S. P. Armes, N. C. Billingham, Z. Tuzar, *Macromolecules* **1996**, *29*, 8151–8159.

93 N. Bulychev, O. Confortini, P. Kopold, K. Dirnberger, T. Schauer, F. E. Du Prez, V. Zubov, C. D. Eisenbach, *Polymer* **2007**, *48*, 2636–2643.

94 O. Confortini, F. E. Du Prez, *Macromol. Chem. Phys.* **2007**, *208*, 1871–1882.

95 W. G. Reyntjens, L. E. Jonckheere, E. J. Goethals, *Macromol. Rapid Commun.* **2002**, *23*, 282–285.

96 N. Willet, S. Gabriel, C. Jerome, F. E. Du Prez, A.-S. Duwez, *Soft Matter* **2014**, *10*, 7256–7261.

97 J. F. Folmer-Andersen, J.-M. Lehn, *J. Am. Chem. Soc.* **2011**, *133*, 10966–10973.

98 J. Yan, K. Liu, X. Zhang, W. Li, A. Zhang, *J. Polym. Sci. Part A: Polym. Chem.* **2015**, *53*, 33–41.

99 M. A. Ward, T. K. Georgiou, *Polymers* **2011**, *3*, 1215.

100 C. Chen, Z. Wang, Z. Li, *Biomacromolecules* **2011**, *12*, 2859–2863.

101 H. Schlaad, Solution properties of polypeptide-based copolymers, in *Peptide Hybrid Polymers, Vol. 202* (eds H.-A. Klok, H. Schlaad), Springer Berlin Heidelberg, **2006**, pp. 53–73.

102 T. J. Deming, *Prog. Polym. Sci.* **2007**, *32*, 858–875.

103 H. R. Kricheldorf, *Angew. Chem., Int. Ed.* **2006**, *45*, 5752–5784.

104 J. R. Kramer, T. J. Deming, *J. Am. Chem. Soc.* **2010**, *132*, 15068–15071.

105 X. Fu, Y. Shen, W. Fu, Z. Li, *Macromolecules* **2013**, *46*, 3753–3760.

106 Y. Liao, C.-M. Dong, *J. Polym. Sci. Part A: Polym. Chem.* **2012**, *50*, 1834–1843.

107 Y. Shen, S. Desseaux, B. Aden, B. S. Lokitz, S. M. Kilbey, Z. Li, H.-A. Klok, *Macromolecules* **2015**, *48*, 2399–2406.

108 K. Dan, N. Bose, S. Ghosh, *Chem. Commun.* **2011**, *47*, 12491–12493.

109 R. Zhang, H. K. Mjoseng, M. A. Hoeve, N. G. Bauer, S. Pells, R. Besseling, S. Velugotla, G. Tourniaire, R. E. B. Kishen, Y. Tsenkina, C. Armit, C. R. E. Duffy, M. Helfen, F. Edenhofer, P. A. de Sousa, M. Bradley, *Nat. Commun.* **2013**, *4*, 1335.

110 T. Oya, T. Enoki, A. Y. Grosberg, S. Masamune, T. Sakiyama, Y. Takeoka, K. Tanaka, G. Wang, Y. Yilmaz, M. S. Feld, R. Dasari, T. Tanaka, *Science* **1999**, *286*, 1543–1545.

111 L. Tebben, A. Studer, *Angew. Chem., Int. Ed.* **2011**, *50*, 5034–5068.

112 A. Studer, T. Schulte, *Chem. Rec.* **2005**, *5*, 27–35.

113 R. Matsuno, K. Yamamoto, H. Otsuka, A. Takahara, *Chem. Mater.* **2003**, *15*, 3–5.

114 M. K. Georges, R. P. N. Veregin, P. M. Kazmaier, G. K. Hamer, *Macromolecules* **1993**, *26*, 2987–2988.

115 R. Matsuno, K. Yamamoto, H. Otsuka, A. Takahara, *Macromolecules* **2004**, *37*, 2203–2209.

116 H. Yukutake, M. Kobayashi, H. Otsuka, A. Takahara, *Polym. J.* **2009**, *41*, 555–561.

117 C. J. Hawker, *J. Am. Chem. Soc.* **1994**, *116*, 11185–11186.

118 N. J. Turro, G. Lem, I. S. Zavarine, *Macromolecules* **2000**, *33*, 9782–9785.

119 Y. Higaki, H. Otsuka, A. Takahara, *Macromolecules* **2006**, *39*, 2121–2125.

120 H. Otsuka, K. Aotani, Y. Higaki, A. Takahara, *Chem. Commun.* **2002**, 2838–2839.

121 H. Otsuka, K. Aotani, Y. Higaki, Y. Amamoto, A. Takahara, *Macromolecules* **2007**, *40*, 1429–1434.

122 T. Sato, Y. Amamoto, H. Yamaguchi, H. Otsuka, A. Takahara, *Chem. Lett.* **2010**, *39*, 1209–1211.

123 T. Sato, Y. Amamoto, H. Yamaguchi, T. Ohishi, A. Takahara, H. Otsuka, *Polym. Chem.* **2012**, *3*, 3077–3083.

124 Y. Amamoto, Y. Higaki, Y. Matsuda, H. Otsuka, A. Takahara, *J. Am. Chem. Soc.* **2007**, *129*, 13298–13304.

125 Y. Amamoto, Y. Higaki, Y. Matsuda, H. Otsuka, A. Takahara, *Chem. Lett.* **2007**, *36*, 774–775.

126 Y. Amamoto, M. Kikuchi, H. Masunaga, S. Sasaki, H. Otsuka, A. Takahara, *Macromolecules* **2010**, *43*, 1785–1791.

127 Y. Amamoto, M. Kikuchi, H. Otsuka, A. Takahara, *Macromolecules* **2010**, *43*, 5470–5473.

128 G. Yamaguchi, Y. Higaki, H. Otsuka, A. Takahara, *Macromolecules* **2005**, *38*, 6316–6320.

129 F. Wang, M. Z. Rong, M. Q. Zhang, *J. Mater. Chem.* **2012**, *22*, 13076–13084.

130 M. A. Tasdelen, *Polym. Chem.* **2011**, *2*, 2133–2145.

131 P. J. Boul, P. Reutenauer, J.-M. Lehn, *Org. Lett.* **2005**, *7*, 15–18.

132 X. Chen, M. A. Dam, K. Ono, A. Mal, H. Shen, S. R. Nutt, K. Sheran, F. Wudl, *Science* **2002**, *295*, 1698–1702.

133 X. Chen, F. Wudl, A. K. Mal, H. Shen, S. R. Nutt, *Macromolecules* **2003**, *36*, 1802–1807.

134 K. Adachi, A. K. Achimuthu, Y. Chujo, *Macromolecules* **2004**, *37*, 9793–9797.

135 T. Paulöhrl, A. J. Inglis, C. Barner-Kowollik, *Adv. Mater.* **2010**, *22*, 2788–2791.

136 T. N. Gevrek, R. N. Ozdeslik, G. S. Sahin, G. Yesilbag, S. Mutlu, A. Sanyal, *Macromol. Chem. Phys.* **2012**, *213*, 166–172.

137 Y.-L. Liu, T.-W. Chuo, *Polym. Chem.* **2013**, *4*, 2194–2205.

138 B. Gotsmann, U. Duerig, J. Frommer, C. J. Hawker, *Adv. Funct. Mater.* **2006**, *16*, 1499–1505.

139 K. C. Koehler, K. S. Anseth, C. N. Bowman, *Biomacromolecules* **2013**, *14*, 538–547.

140 S. Kirchhof, F. P. Brandl, N. Hammer, A. M. Goepferich, *J. Mater. Chem. B* **2013**, *1*, 4855–4864.

141 A. P. Bapat, J. G. Ray, D. A. Savin, E. A. Hoff, D. L. Patton, B. S. Sumerlin, *Polym. Chem.* **2012**, *3*, 3112–3120.

142 H. Sun, C. P. Kabb, B. S. Sumerlin, *Chem. Sci.* **2014**, *5*, 4646–4655.

143 J. Ferreira, J. Syrett, M. Whittaker, D. Haddleton, T. P. Davis, C. Boyer, *Polym. Chem.* **2011**, *2*, 1671–1677.

144 J. A. Syrett, G. Mantovani, W. R. S. Barton, D. Price, D. M. Haddleton, *Polym. Chem.* **2010**, *1*, 102–106.

145 J. R. Jones, C. L. Liotta, D. M. Collard, D. A. Schiraldi, *Macromolecules* **1999**, *32*, 5786–5792.

146 N. Yoshie, S. Saito, N. Oya, *Polymer* **2011**, *52*, 6074–6079.

147 V. B. Sutariya, Y. Pathak, *Biointeraction of Nanomaterials*, CRC Press, Taylor and Francis Group, New York, **2014**.

148 S. R. Trenor, A. R. Shultz, B. J. Love, T. E. Long, *Chem. Rev.* **2004**, *104*, 3059–3078.

149 Y. Zheng, M. Micic, S. V. Mello, M. Mabrouki, F. M. Andreopoulos, V. Konka, S. M. Pham, R. M. Leblanc, *Macromolecules* **2002**, *35*, 5228–5234.

150 Y. Chujo, K. Sada, R. Nomura, A. Naka, T. Saegusa, *Macromolecules* **1993**, *26*, 5611–5614.

151 H. Otsuka, S. Nagano, Y. Kobashi, T. Maeda, A. Takahara, *Chem. Commun.* **2010**, *46*, 1150–1152.

152 T. F. Scott, A. D. Schneider, W. D. Cook, C. N. Bowman, *Science* **2005**, *308*, 1615–1617.

153 H. Y. Park, C. J. Kloxin, T. F. Scott, C. N. Bowman, *Dent. Mater.* **2010**, *26*, 1010–1016.

154 L. M. Cox, Z. Li, N. Sowan, D. Nair, J. Xiao, C. N. Bowman, Y. Ding, *Polymer* **2014**, *55*, 5933–5937.

155 J.-F. Xu, Y.-Z. Chen, L.-Z. Wu, C.-H. Tung, Q.-Z. Yang, *Org. Lett.* **2013**, *15*, 6148–6151.

156 A. P. Pelliccioli, J. Wirz, *Photochem. Photobiol. Sci.* **2002**, *1*, 441–458.

157 T. Furuta, S. S. H. Wang, J. L. Dantzker, T. M. Dore, W. J. Bybee, E. M. Callaway, W. Denk, R. Y. Tsien, *Proc. Natl. Acad. Sci. USA* **1999**, *96*, 1193–1200.

158 M. V. S. N. Maddipatla, D. Wehrung, C. Tang, W. Fan, M. O. Oyewumi, T. Miyoshi, A. Joy, *Macromolecules* **2013**, *46*, 5133–5140.

159 W. Ji, N. Li, D. Chen, X. Qi, W. Sha, Y. Jiao, Q. Xu, J. Lu, *J. Mater. Chem. B* **2013**, *1*, 5942–5949.

160 A. S. French, *Ann. Rev. Physiol.* **1992**, *54*, 135–152.

161 A. W. Orr, B. P. Helmke, B. R. Blackman, M. A. Schwartz, *Developmental Cell* **2006**, *10*, 11–20.

162 P. G. Gillespie, R. G. Walker, *Nature* **2001**, *413*, 194–202.

163 J. Li, C. Nagamani, J. S. Moore, *Acc. Chem. Res.* **2015**.

164 H. Staudinger, H. F. Bondy, *Berichte der deutschen chemischen Gesellschaft (A and B Series)* **1930**, *63*, 734–736.

165 H. Staudinger, E. O. Leupold, *Berichte der deutschen chemischen Gesellschaft (A and B Series)* **1930**, *63*, 730–733.

166 H. Staudinger, W. Heuer, *Berichte der deutschen chemischen Gesellschaft (A and B Series)* **1934**, *67*, 1159–1164.

167 C. Löwe, C. Weder, *Adv. Mater.* **2002**, *14*, 1625–1629.

168 R. A. Nallicheri, M. F. Rubner, *Macromolecules* **1991**, *24*, 517–525.

169 S. H. Foulger, P. Jiang, A. C. Lattam, D. W. Smith, J. Ballato, *Langmuir* **2001**, *17*, 6023–6026.

170 J. E. Comrie, W. T. S. Huck, *Macromol. Rapid Commun.* **2008**, *29*, 539–546.

171 O. Azzaroni, B. Trappmann, P. van Rijn, F. Zhou, B. Kong, W. T. S. Huck, *Angew. Chem., Int. Ed.* **2006**, *45*, 7440–7443.

172 M. M. Caruso, D. A. Davis, Q. Shen, S. A. Odom, N. R. Sottos, S. R. White, J. S. Moore, *Chem. Rev.* **2009**, *109*, 5755–5798.

173 A. M. Kushner, J. D. Vossler, G. A. Williams, Z. Guan, *J. Am. Chem. Soc.* **2009**, *131*, 8766–8768.

174 D. A. Davis, A. Hamilton, J. Yang, L. D. Cremar, D. Van Gough, S. L. Potisek, M. T. Ong, P. V. Braun, T. J. Martinez, S. R. White, J. S. Moore, N. R. Sottos, *Nature* **2009**, *459*, 68–72.

175 Y. Chen, A. J. H. Spiering, Karthikeyan S, G. W. M. Peters, E. W. Meijer, R. P. Sijbesma, *Nat. Chem.* **2012**, *4*, 559–562.

176 J. M. Lenhardt, M. T. Ong, R. Choe, C. R. Evenhuis, T. J. Martinez, S. L. Craig, *Science* **2010**, *329*, 1057–1060.

177 M. B. Larsen, A. J. Boydston, *J. Am. Chem. Soc.* **2013**, *135*, 8189–8192.

178 C. E. Diesendruck, B. D. Steinberg, N. Sugai, M. N. Silberstein, N. R. Sottos, S. R. White, P. V. Braun, J. S. Moore, *J. Am. Chem. Soc.* **2012**, *134*, 12446–12449.

179 A. Piermattei, S. Karthikeyan, R. P. Sijbesma, *Nat. Chem.* **2009**, *1*, 133–137.

180 K. Imato, A. Irie, T. Kosuge, T. Ohishi, M. Nishihara, A. Takahara, H. Otsuka, *Angew. Chem., Int. Ed.* **2015**, *54*, 6168–6172.

181 R. Groote, B. M. Szyja, F. A. Leibfarth, C. J. Hawker, N. L. Doltsinis, R. P. Sijbesma, *Macromolecules* **2014**, *47*, 1187–1192.

182 J. Wang, I. Piskun, S. L. Craig, *ACS Macro Letters* **2015**, 834–837.

183 K. R. Fitch, A. P. Goodwin, *Chem. Mater.* **2014**, *26*, 6771–6776.

184 W. G. Skene, J.-M. P. Lehn, *Proc. Natl. Acad. Sci. USA* **2004**, *101*, 8270–8275.

185 T. Ono, T. Nobori, J.-M. Lehn, *Chem. Commun.* **2005**, 1522–1524.

186 E. Kolomiets, J.-M. Lehn, *Chem. Commun.* **2005**, 1519–1521.

187 D. A. Fulton, *Org. Lett.* **2008**, *10*, 3291–3294.

188 D. E. Whitaker, C. S. Mahon, D. A. Fulton, *Angew. Chem., Int. Ed.* **2013**, *52*, 956–959.

189 J. Rao, A. Khan, *Polym. Chem.* **2013**, *4*, 2691–2695.

190 M. Ulbricht, *Polymer* **2006**, *47*, 2217–2262.

191 G. Deng, F. Li, H. Yu, F. Liu, C. Liu, W. Sun, H. Jiang, Y. Chen, *ACS Macro Lett.* **2012**, *1*, 275–279.

192 G. Deng, C. Tang, F. Li, H. Jiang, Y. Chen, *Macromolecules* **2010**, *43*, 1191–1194.

193 F. Liu, F. Li, G. Deng, Y. Chen, B. Zhang, J. Zhang, C.-Y. Liu, *Macromolecules* **2012**, *45*, 1636–1645.

194 D. D. McKinnon, D. W. Domaille, J. N. Cha, K. S. Anseth, *Chem. Mater.* **2014**, *26*, 2382–2387.

195 C. Godoy-Alcántar, A. K. Yatsimirsky, J. M. Lehn, *J. Phys. Org. Chem.* **2005**, *18*, 979–985.

196 B. Buchs, G. Godin, A. Trachsel, J.-Y. de Saint Laumer, J.-M. Lehn, A. Herrmann, *Eur. J. Org. Chem.* **2011**, *2011*, 681–695.

197 N. Giuseppone, G. Fuks, J.-M. Lehn, *Chem. Eur. J.* **2006**, *12*, 1723–1735.

198 S. Ulrich, E. Buhler, J.-M. Lehn, *New J. Chem.* **2009**, *33*, 271–292.

199 P. Taynton, K. Yu, R. K. Shoemaker, Y. H. Jin, H. J. Qi, W. Zhang, *Adv. Mater.* **2014**, *26*, 3938–3942.

200 A. W. Jackson, C. Stakes, D. A. Fulton, *Polym. Chem.* **2011**, *2*, 2500–2511.

201 A. W. Jackson, D. A. Fulton, *Macromolecules* **2012**, *45*, 2699–2708.

202 X. Xu, J. D. Flores, C. L. McCormick, *Macromolecules* **2011**, *44*, 1327–1334.

203 A. P. Esser-Kahn, M. B. Francis, *Angew. Chem., Int. Ed.* **2008**, *47*, 3751–3754.

204 A. P. Esser-Kahn, V. Trang, M. B. Francis, *J. Am. Chem. Soc.* **2010**, *132*, 13264–13269.

205 L. S. Witus, C. Netirojjanakul, K. S. Palla, E. M. Muehl, C.-H. Weng, A. T. Iavarone, M. B. Francis, *J. Am. Chem. Soc.* **2013**, *135*, 17223–17229.

206 J. G. Hardy, P. Lin, C. E. Schmidt, *J. Biomater. Sci., Polym. Ed.* **2015**, *26*, 143–161.

207 M. R. Hill, S. Mukherjee, P. J. Costanzo, B. S. Sumerlin, *Polym. Chem.* **2012**, *3*, 1758–1762.

208 F. Lin, J. Yu, W. Tang, J. Zheng, A. Defante, K. Guo, C. Wesdemiotis, M. L. Becker, *Biomacromolecules* **2013**, *14*, 3749–3758.

209 G. N. Grover, R. L. Braden, K. L. Christman, *Adv. Mater.* **2013**, *25*, 2937–2942.

210 K. L. Christman, R. M. Broyer, Z. P. Tolstyka, H. D. Maynard, *J. Mater. Chem.* **2007**, *17*, 2021–2027.

211 Z. P. Tolstyka, W. Richardson, E. Bat, C. J. Stevens, D. P. Parra, J. K. Dozier, M. D. Distefano, B. Dunn, H. D. Maynard, *Chembiochem.* **2013**, *14*, 2464–2471.

212 K. J. Mackenzie, M. B. Francis, *J. Am. Chem. Soc.* **2012**, *135*, 293–300.

213 D. P. Ferris, P. R. McGonigal, L. S. Witus, T. Kawaji, M. M. Algaradah, A. R. Alnajadah, M. S. Nassar, J. F. Stoddart, *Org. Lett.* **2015**, *17*, 2146–2149.

214 S. Mukherjee, M. R. Hill, B. S. Sumerlin, *Soft Matter* **2015**, *11*, 6152–6161.

215 S. Park, N. P. Westcott, W. Luo, D. Dutta, M. N. Yousaf, *Bioconjugate Chem.* **2014**, *25*, 543–551.

216 D. J. Phillips, M. I. Gibson, *Chem. Commun.* **2012**, *48*, 1054–1056.

217 M. Mazurowski, M. Gallei, J. Li, H. Didzoleit, B. Stühn, M. Rehahn, *Macromolecules* **2012**, *45*, 8970–8981.

218 K. Oyaizu, H. Nishide, *Adv. Mater.* **2009**, *21*, 2339–2344.

219 H. Logtenberg, W. R. Browne, *Org. Biomol. Chem.* **2013**, *11*, 233–243.

220 N. E. Zhou, C. M. Kay, R. S. Hodges, *Biochemistry – US* **1993**, *32*, 3178–3187.

221 C. S. Sevier, C. A. Kaiser, *Nature Reviews Molecular Cell Biol.* **2002**, *3*, 836–847.

222 E. Banchereau, S. Lacombe, J. Ollivier, *Tetrahedron Lett.* **1995**, *36*, 8197–8200.

223 P. S. Surdhar, D. A. Armstrong, *J. Phys. Chem.* **1987**, *91*, 6532–6537.

224 S. P. Black, J. K. M. Sanders, A. R. Stefankiewicz, *Chem. Soc. Rev.* **2014**, *43*, 1861–1872.

225 J. A. Yoon, J. Kamada, K. Koynov, J. Mohin, R. Nicolaÿ, Y. Zhang, A. C. Balazs, T. Kowalewski, K. Matyjaszewski, *Macromolecules* **2012**, *45*, 142–149.

226 Y. Amamoto, H. Otsuka, A. Takahara, K. Matyjaszewski, *Adv. Mater.* **2012**, *24*, 3975–3980.

227 A. Klaikherd, C. Nagamani, S. Thayumanavan, *J. Am. Chem. Soc.* **2009**, *131*, 4830–4838.

228 J. Dai, S. Lin, D. Cheng, S. Zou, X. Shuai, *Angew. Chem., Int. Ed.* **2011**, *50*, 9404–9408.

229 A. N. Koo, H. J. Lee, S. E. Kim, J. H. Chang, C. Park, C. Kim, J. H. Park, S. C. Lee, *Chem. Commun.* **2008**, 6570–6572.

230 J. Li, J. M. A. Carnall, M. C. A. Stuart, S. Otto, *Angew. Chem., Int. Ed.* **2011**, *50*, 8384–8386.

231 O. Veiseh, B. C. Tang, K. A. Whitehead, D. G. Anderson, R. Langer, *Nature Rev. Drug Discov.* **2015**, *14*, 45–57.

232 C. Foged, H. M. Nielsen, *Expert Opin. Drug Deliv.* **2008**, *5*, 105–117.

233 C. M. Hassan, F. J. Doyle, N. A. Peppas, *Macromolecules* **1997**, *30*, 6166–6173.

234 Y. Ito, M. Casolaro, K. Kono, Y. Imanishi, *J. Control. Release* **1989**, *10*, 195–203.

235 H. Huang, J. Shaw, C. Yip, X. Wu, *Pharm. Res.* **2008**, *25*, 1150–1157.

236 S. I. Kang, Y. H. Bae, *J. Control. Release* **2003**, *86*, 115–121.

237 K. Podual, F. J. Doyle Iii, N. A. Peppas, *Polymer* **2000**, *41*, 3975–3983.

238 T. Traitel, Y. Cohen, J. Kost, *Biomaterials* **2000**, *21*, 1679–1687.

239 V. Ravaine, C. Ancla, B. Catargi, *J. Control. Release* **2008**, *132*, 2–11.

240 N. Kashyap, B. Viswanad, G. Sharma, V. Bhardwaj, P. Ramarao, M. N. V. Ravi Kumar, *Biomaterials* **2007**, *28*, 2051–2060.

241 P. Cuatrecasas, G. P. E. Tell, *Proc. Natl. Acad. Sci. USA* **1973**, *70*, 485–489.

242 T. Miyata, A. Jikihara, K. Nakamae, A. S. Hoffman, *J. Biomater. Sci., Polymer Ed.* **2004**, *15*, 1085–1098.

243 T. Ye, S. Yan, Y. Hu, L. Ding, W. Wu, *Polym. Chem.* **2014**, *5*, 186–194.

244 T. James, S. Shinkai, *Artificial Receptors as Chemosensors for Carbohydrates, Vol. 218*, Springer Berlin Heidelberg, **2002**.

245 T. Miyata, T. Uragami, K. Nakamae, *Adv. Drug Deliv. Rev.* **2002**, *54*, 79–98.

246 J. P. Lorand, J. O. Edwards, *J. Org. Chem.* **1959**, *24*, 769–774.

247 K. Kataoka, H. Miyazaki, T. Okano, Y. Sakurai, *Macromolecules* **1994**, *27*, 1061–1062.

248 K. Kataoka, H. Miyazaki, M. Bunya, T. Okano, Y. Sakurai, *J. Am. Chem. Soc.* **1998**, *120*, 12694–12695.

249 G. Springsteen, B. Wang, *Tetrahedron* **2002**, *58*, 5291–5300.

250 W. Yang, X. Gao, B. Wang, *Biological and Medicinal Applications of Boronic Acids*, in *Boronic Acids*, Wiley-VCH Verlag GmbH & Co. KGaA, **2006**, pp. 481–512.

251 X.-C. Liu, J. L. Hubbard, W. H. Scouten, *J. Organomet. Chem.* **1995**, *493*, 91–94.

252 J. Yan, G. Springsteen, S. Deeter, B. Wang, *Tetrahedron* **2004**, *60*, 11205–11209.

253 A. L. Korich, P. M. Iovine, *Dalton Trans.* **2010**, *39*, 1423–1431.

254 F. Cheng, F. Jakle, *Polym. Chem.* **2011**, *2*, 2122–2132.

255 A. R. Martin, J.-J. Vasseur, M. Smietana, *Chem. Soc. Rev.* **2013**, *42*, 5684–5713.

256 Y. Guan, Y. Zhang, *Chem. Soc. Rev.* **2013**, *42*, 8106–8121.

257 Q. Wu, L. Wang, H. Yu, J. Wang, Z. Chen, *Chem. Rev.* **2011**, *111*, 7855–7875.

258 N. Fujita, S. Shinkai, T. D. James, *Chem. Asian J.* **2008**, *3*, 1076–1091.

259 W. Wu, S. Zhou, *Macromolecular Biosci.* **2013**, *13*, 1464–1477.

260 A. Matsumoto, R. Yoshida, K. Kataoka, *Biomacromolecules* **2004**, *5*, 1038–1045.

261 S. A. Asher, V. L. Alexeev, A. V. Goponenko, A. C. Sharma, I. K. Lednev, C. S. Wilcox, D. N. Finegold, *J. Am. Chem. Soc.* **2003**, *125*, 3322–3329.

262 A. Kikuchi, K. Suzuki, O. Okabayashi, H. Hoshino, K. Kataoka, Y. Sakurai, T. Okano, *Anal. Chem.* **1996**, *68*, 823–828.

263 I. D. Robb, J. B. A. F. Smeulders, *Polymer* **1997**, *38*, 2165–2169.

264 M. Piest, X. Zhang, J. Trinidad, J. F. J. Engbersen, *Soft Matter* **2011**, *7*, 11111–11118.

265 A. E. Ivanov, H. Larsson, I. Y. Galaev, B. Mattiasson, *Polymer* **2004**, *45*, 2495–2505.

266 S. Kitano, K. Kataoka, Y. Koyama, T. Okano, Y. Sakurai, *Die Makromolekulare Chemie, Rapid Commun.* **1991**, *12*, 227–233.

267 R. Ma, L. Shi, *Polym. Chem.* **2014**, *5*, 1503–1518.

268 L. He, D. E. Fullenkamp, J. G. Rivera, P. B. Messersmith, *Chem. Commun.* **2011**, *47*, 7497–7499.

269 C. C. Deng, W. L. A. Brooks, K. A. Abboud, B. S. Sumerlin, *ACS Macro Lett.* **2015**, *4*, 220–224.

270 J. J. Cash, T. Kubo, A. P. Bapat, B. S. Sumerlin, *Macromolecules* **2015**, *48*, 2098–2106.

271 Y. Qin, V. Sukul, D. Pagakos, C. Cui, F. Jäkle, *Macromolecules* **2005**, *38*, 8987–8990.

272 Y. Qin, G. Cheng, A. Sundararaman, F. Jäkle, *J. Am. Chem. Soc.* **2002**, *124*, 12672–12673.

273 J. N. Cambre, D. Roy, S. R. Gondi, B. S. Sumerlin, *J. Am. Chem. Soc.* **2007**, *129*, 10348–10349.

274 D. Roy, J. N. Cambre, B. S. Sumerlin, *Chem. Commun.* **2008**, 2477–2479.

275 D. Roy, B. S. Sumerlin, *ACS Macro Letters* **2012**, *1*, 529–532.

276 Y. Yao, X. Wang, T. Tan, J. Yang, *Soft Matter* **2011**, *7*, 7948–7951.

277 G. A. Ellis, M. J. Palte, R. T. Raines, *J. Am. Chem. Soc.* **2012**, *134*, 3631–3634.

278 H. Kim, Y. J. Kang, S. Kang, K. T. Kim, *J. Am. Chem. Soc.* **2012**, *134*, 4030–4033.

279 Y. Kotsuchibashi, R. V. C. Agustin, J.-Y. Lu, D. G. Hall, R. Narain, *ACS Macro Lett.* **2013**, *2*, 260–264.

9

Self-healing Polymers through Dynamic Covalent Chemistry

Keiichi Imato and Hideyuki Otsuka

9.1 Introduction

Dynamic covalent bonds can selectively undergo reversible breaking and re-formation under equilibrium conditions without irreversible side reactions, generally on exposure to certain environmental factors, as detailed in other chapters. Incorporation of dynamic covalent bonds into polymer architectures produces structurally dynamic polymers that exhibit unique macroscopic functionalities in response to external stimuli.[1] The materials' stimuli-responsive properties originate from the reversible chemistry of the dynamic bonds at the molecular level. One of the most fascinating abilities of dynamic polymers is to repair damage inflicted on them and restore their structural integrity without manual intervention, which is referred to as a "self-healing" property. Although polymeric materials have been widely used with tremendous success in engineering fields due to their advantages, such as light weight, processability, and flexibility, and are indispensable for our daily lives, they are susceptible to external factors, which infrequently result in undesirable reduction in their physical properties, irreparable damage, and ultimately failure. Self-healing can remove these limitations through the restoration of damage and recovery of the materials' mechanical strength, leading to improved lifetimes, durability, and reliability of the materials as well as waste reduction (Figure 9.1a,b). Therefore, it is undeniable that self-healing polymeric materials would offer numerous possibilities, in particular for applications such as artificial organ and space development purposes, where there is little scope for intervention and assisted repair, and where long-term reliability is imperative. While nature possesses this healing ability, previous manmade materials generally did not. Instead, all current engineering materials have been developed on the basis of a passive "damage prevention" paradigm, with which every effort is made to prevent the breakage of irreversible covalent bonds and focus on enhancing the mechanical, thermal, or electronic properties of the materials for desired applications. This is in contrast to an active "damage management" concept, where the damage to the materials cannot be avoided but can be detected and repaired before the material fails, as in the human body. Self-healing is one such unique active concept inspired by nature.

(a)

(b)

(c)
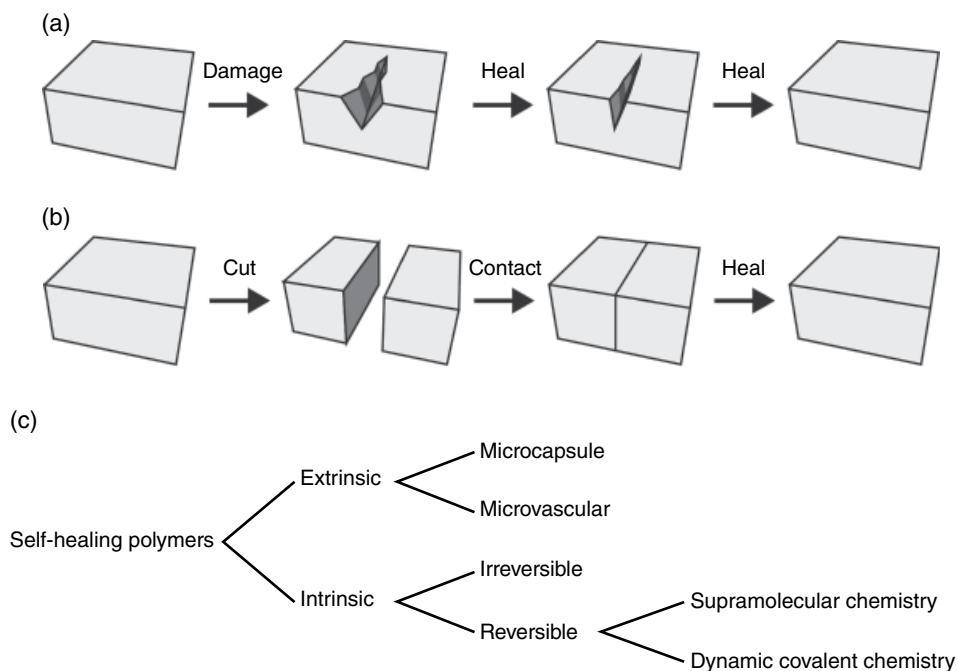
Figure 9.1 Schematic representation of self-healing materials: (a) healing of damaged surface and (b) healing of cut materials by bringing the pieces together. (c) Classification of approaches to self-healing polymeric materials.

Self-healing can be regarded as the ability of a material to repair damage autonomously or automatically without external intervention. However, healing triggered by an external stimulus such as heating, light irradiation, or with the aid of a chemical agent has also been often regarded as self-healing. Thus, we herein define self-healing as healing with or without an external trigger. To date, self-healing in polymeric materials has been achieved by various approaches (Figure 9.1c). One approach is extrinsic self-healing systems such as monomer (healing agent) delivery to a damaged area and subsequent polymerization (microcapsule and microvascular systems).[2–4] The other is intrinsic systems using unique entropic elasticity of slide-ring networks,[5] topological interaction of dangling chains in polymer networks,[6] pseudo-metabolic reactions,[7,8] and irreversible chemical reactions.[9–12] However, each system has a drawback, for example a limited number of healing times, inability to repair damage at the molecular level, and extremely low material mechanical strength. Therefore, another approach incorporating dynamic bonds or interactions into polymer networks has attracted much attention due to the advantages of an unlimited number of healing times and damage repair at the molecular level, in principle, fully restoring the materials' original properties. The healing mechanism involves reversible chemistry of the dynamic bonds or interactions, that is, cleavage when damaged and re-formation after damage (Figure 9.2). The reversibility also induces exchange reactions between the dynamic bonds or interactions and rearrangements of the polymer networks, which regenerate chain entanglements and produce healing. This is also an intrinsic approach based on

(a)

Dynamic bonds or interactions

(b)

Damage

Healing
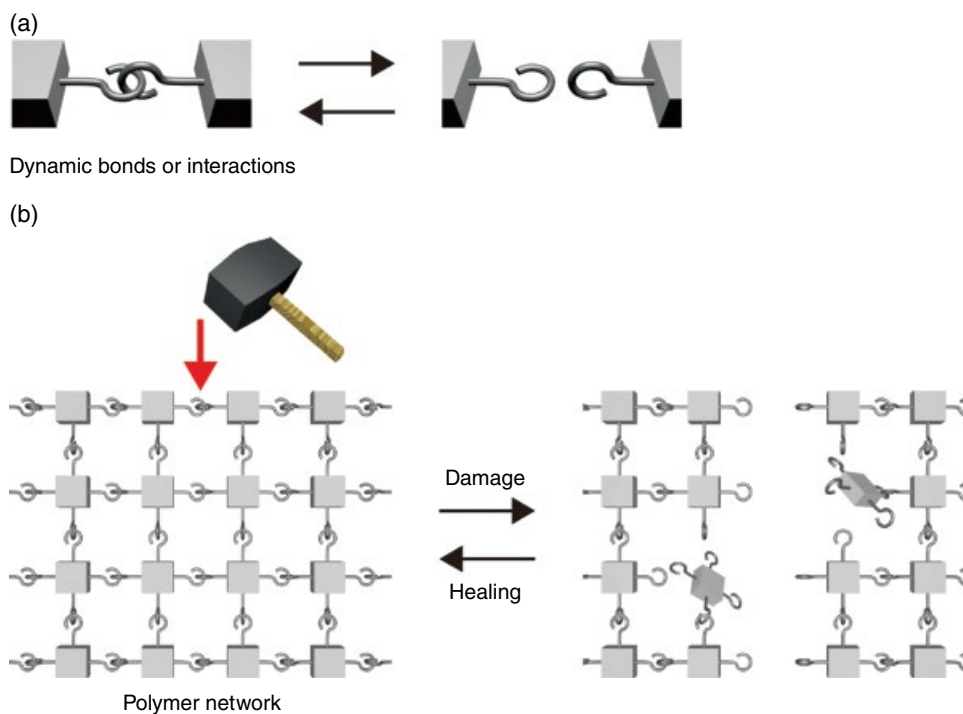
Polymer network

Figure 9.2 Schematic representation of self-healing by dynamic bonding systems: (a) dissociation and re-formation of dynamic bonds or interactions and (b) healing of a polymer network with dynamic linkages.

either supramolecular chemistry[13] or dynamic covalent chemistry.[14–16] There are some differences between them, and which should be used depends on the intended purpose. In general, supramolecular chemistry is controlled by molecular polarity. Thus, supramolecular interactions are sensitive to external chemical factors as represented by water, but they are in continuous equilibrium under ambient conditions. Various types of reactions for self-healing through supramolecular chemistry have been reported, including hydrogen bonding,[17] π–π stacking interactions,[18] ionic bonds,[19–21] coordination bonds,[22] and host–guest interactions.[23,24] On the other hand, dynamic covalent chemistry is based on reversible covalent chemical reactions. Dynamic covalent bonds are generally stable under ambient conditions and behave like robust traditional covalent bonds, but reversibility can be accessed by an external stimulus. Numerous reactions of dynamic covalent bonds have been exploited for self-healing in polymers. The reported systems can be categorized into five types with respect to the reaction mechanisms, as shown in Figure 9.3. Reversible condensation reactions include reversible cleavage and re-formation of acylhydrazone bonds,[25] imine bonds,[26,27] boronate ester linkages,[28] and hemiaminal linkages.[29] Diels–Alder/retro-Diels–Alder reactions, which are the most famous among self-healing systems through reversible covalent bonds[30] as well as urea bonds, can fall into reversible addition reactions.[31] Transesterification,[32] olefin metathesis,[33] and siloxane chemistry[34] are considered to be chain exchangeable reactions in the presence of the respective,

Reversible condensation reactions

Acylhydrazone bonds
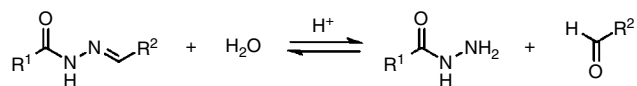
Imine bonds
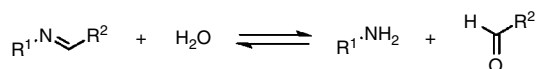
Boronate ester linkages
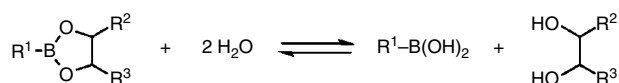
Hemiaminal linkages
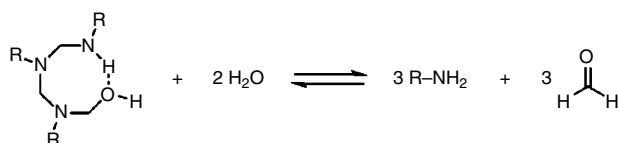
Catalyzed chain exchange reactions

Transesterification
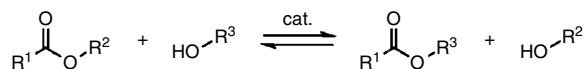
Olefin metathesis
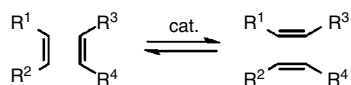
Siloxane chemistry
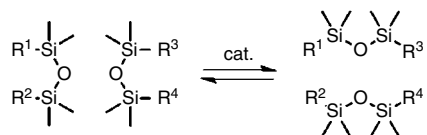
Figure 9.3 Dynamic covalent systems available for self-healing polymeric materials.

Reversible addition reactions

Diels–Alder/retro-Diels–Alder reactions
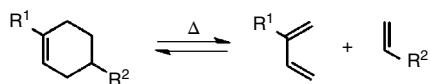
Urea bonds
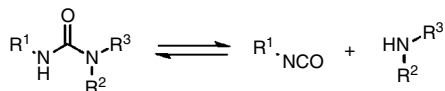
Radical transfer and crossover reactions

Disulfide bonds
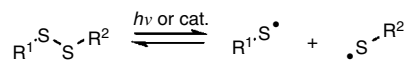
Thiuram disulfide bonds
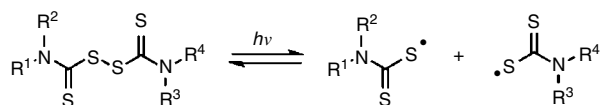
Trithiocarbonate linkages
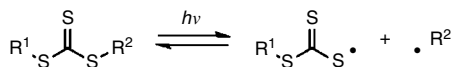
Homolytic bond cleavage and re-formation

Alkoxyamine linkages
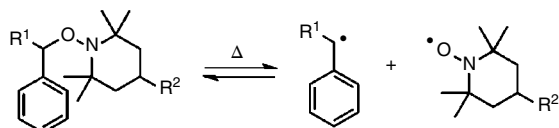
Diarylbibenzofuranone linkages
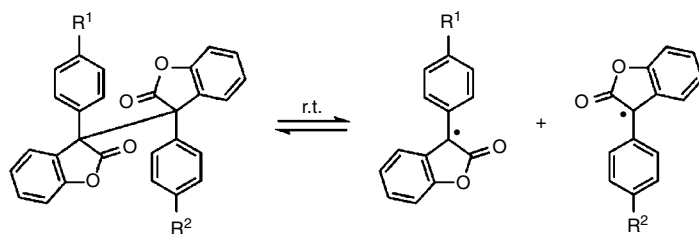
Figure 9.3 (Continued)

proper catalysts. Disulfide bonds[35,36] and related linkages[37] are well known to undergo radical transfer and crossover reactions in response to light irradiation. Finally, homolytic bond cleavage and re-formation represented by alkoxyamine linkages[38] and diarylbibenzofuranone linkages[39] have also been used to impart self-healing abilities to polymeric materials.

These dynamic covalent systems can exert their dynamic nature only under suitable conditions, where self-healing is required, therefore every system is promising for practical use. To utilize the self-healing reactions appropriately, we must understand the features of each system. The following sections review each healing system in detail, and this chapter provides important insight into the rapidly expanding area of self-healing polymeric materials through dynamic covalent chemistry.

9.2 Reversible Condensation Reactions

The reversibility of condensation reactions is typically controlled by varying pH. As a result, the reactions are often used in aqueous solutions and hydrogels. Numerous self-healing hydrogels and organogels utilizing reversible condensation reactions have been reported. Since the hydrogels are soft materials with physical properties similar to soft tissues and reversible condensation reactions are highly sensitive to water (moisture), they do not have great potential for engineering purposes, although they can be used in biomedical applications.

9.2.1 Acylhydrazone Bonds

One of the well-known reversible condensation reactions exploitable for self-healing is the condensation of acylhydrazine and aldehyde. This reaction forms water and an acylhydrazone bond, which is stable under neutral and basic conditions. The reaction can be drastically accelerated by a catalytic amount of acid. Cleavage of the acylhydrazone bond occurs at the same time, and the reversible reaction reaches an equilibrium under acid catalysis as well.[40] Hydrazone bonds without an electron-withdrawing group are considered to be inert under acidic conditions even with water. When acylhydrazone bonds were incorporated in a polymer network, the polymer gel showed reversible sol–gel transitions and possessed self-healing properties based on the reversible breaking and regenerating of acylhydrazone bonds by adjusting the acidity of the swelling solvent (Figure 9.4).[25] Two pieces of cracked acylhydrazone gels containing a mild acid catalyst (acetic acid) can be autonomously merged into a whole piece by simply situating them next to each other and maintaining the contact for several hours at ambient temperature, without any external intervention. The joint between the two pieces is strong enough to sustain a vigorous squeeze by tweezers, and the mechanical properties of the healed samples recovered to nearly the same as those of the original sample after a day, even at room temperature.[41] This self-healing could be observed repeatedly, and the gels were remoldable and recyclable. The fast gelation of the reaction and capacity of gelling a wide range of organic liquids have been utilized for constructing a self-supporting viscoelastic scaffold to restore large-scale damage.[4]

Because acylhydrazone bonds are reversible under acidic conditions, combination with a complementary linkage, which is reversible under basic conditions, is a
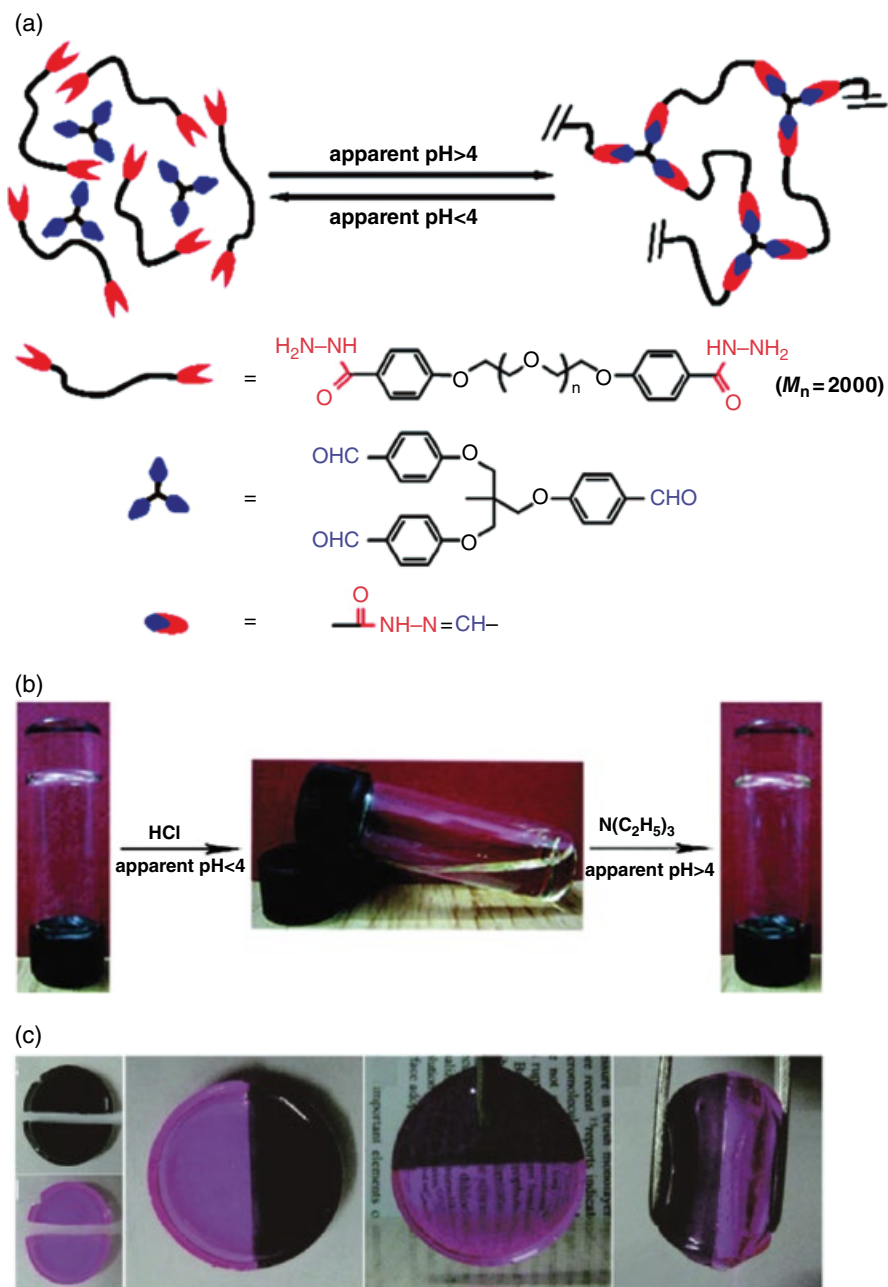
Figure 9.4 Dynamic covalent gel based on reversible acylhydrazone bonds: (a) polymer network crosslinked by acylhydrazone linkages, (b) reversible sol–gel transitions, and (c) self-healing of acylhydrazone gels. Reproduced with permission.[25] Copyright 2010, ACS Publications.

functional and interesting strategy. Hydrogels with acylhydrazone bonds and disulfide bonds showed self-healing under both acidic and basic conditions.[42]

9.2.2 Imine Bonds

Reversible imine chemistry is also available for self-healing in polymers.[43] Imine bonds, which are formed from amines and aldehydes (or ketones) with generation of water, exhibit three distinct reversible processes similar to hydrazones (Scheme 9.1): bond formation/hydrolysis, where an equilibrium is set up between the imine/water and the amine/aldehyde, exchange reaction (transimination), where the imine reacts directly with an amine, and metathesis, where the imine undergoes exchange reaction with another imine. The reversibility can be accessed even at neutral conditions and more easily under acidic conditions. Therefore, imine bonds are considered to be more dynamic than (acyl) hydrazone bonds as a result of the mesomeric effect of hydrazone bonds, which decreases the electrophilicity of the $C = N$ bond.[43,44] Some self-healable polymer networks based on imine chemistry have been prepared and studied as biocompatible hydrogels.[26,45–47] Malleable polyimines that behave like a classic thermoset at ambient conditions can be reprocessed and repaired by application of either heat or water in the absence of any catalyst has also been reported.[27] Such polyimine thermosets have successfully been used in fully recyclable woven carbon fiber composites as well as ultrathin solid-state Li-ion electrolyte membranes.[48,49] A similar crosslinked polymer with aromatic imine bonds has also been reported to exhibit self-healing behavior in air at room temperature in the absence of a catalyst.[50]

9.2.3 Boronate Ester Linkages

Some self-healable gels have been prepared that utilize reversible boronate esters, which are formed from complexation of certain diols and boronic acid.[28,51–54] The complexation mechanism is quite complex, and the optimal pH for the complexation is affected by many factors, such as solvent, buffer, sterics, and hydrogen bonding.[55,56] Complexation of 1,3-benzenediboronic acid with a branched catechol derivatized

Hydrolysis and bond re-formation
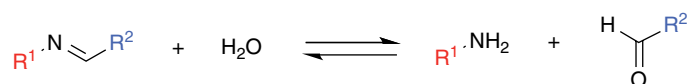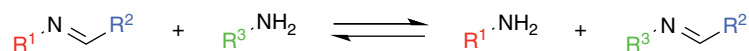
Exchange reaction

Metathesis
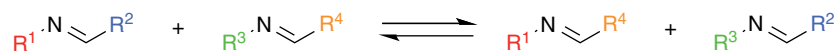
Scheme 9.1 Three types of reversible imine reactions: hydrolysis and bond re-formation, exchange reaction, and metathesis.

poly(ethylene glycol) under basic aqueous conditions (pH 9.0) formed tetrahedral boronate esters, giving rise to a three-dimensional polymeric network and gel formation.[28] The storage modulus of the hydrogel was greater than the loss modulus across a wide frequency range and changed little with frequency, indicative of a covalently crosslinked gel. The ester linkages dissociated on decrease of the pH to 3.0, forming a liquid. This gel-to-sol transition was confirmed by a color change from red to yellow, which was attributed to dissociation of the boronate–catechol complex. As a result of its dynamic nature, the hydrogel possessed self-healing ability. The gel was cut into two pieces and then simply placed into contact at the fractured surfaces. Thirty seconds after fusion, no obvious border was observed between the connected gels and the joint between the two parts was strong enough to be manually stretched without fracturing. This self-healing was effective and repeatable, regardless of where the gel was cut or fused. Such self-healing hydrogels using reversible boronate ester linkages have the potential to be applied to biomedical materials[57] due to the low tissue inflammatory response, like imine bonds.

The kinetics of boronate ester transesterification is known to be tunable over many orders of magnitude, simply by changing a neighboring group.[58] The neighboring group effect on the kinetics enables crosslinked polymers with boronate ester linkages to heal completely in the bulk state at 50 °C without any solvents and catalysts.[59]

9.2.4 Hemiaminal Linkages

Hemiaminal linkages formed by the condensation of amines and formaldehyde at ambient temperatures are reversible in the presence of water.[29] Organogels crosslinked by hemiaminal linkages exhibited self-healing abilities. The linkages could be transformed into hexahydrotriazines by further heating to 200 °C, resulting in much stiffer but irreversible polymer networks. Despite these unique properties, there is only one example demonstrating self-healing based on reversible hemiaminal linkages.[29] An organogel with hemiaminal linkages formed from diamine-terminated poly(ethylene glycol) (4.6 kDa) and paraformaldehyde showed self-healing within seconds of placing two gel pieces in contact with each other.

9.3 Reversible Addition Reactions
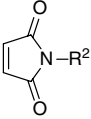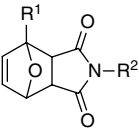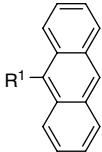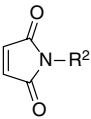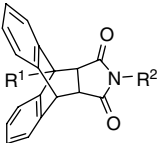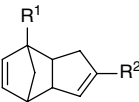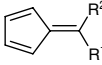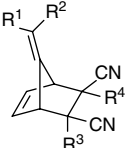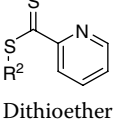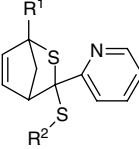
Unlike condensation reactions, addition reactions do not involve elimination of molecules, therefore the reversible systems are more straightforward and easily controllable by chemical and physical factors. In these systems, the dissociated components are stable under the usage condition, but they remain highly and selectively reactive with each other. To date, a very few reversible addition reactions are known to be exploitable for self-healing.

9.3.1 Diels–Alder Reaction

The combination of Diels–Alder (DA) reaction, [4 + 2] cycloaddition of a conjugated diene and a dienophile, and retro-Diels–Alder (retro-DA) reaction, thermally induced [4 + 2] cycloreversion of the product, is the most studied system of self-healing through

reversible covalent chemistry.[60] The DA reaction is among the most important reactions in organic chemistry because of the ability to form C–C bonds in high yields and good stereochemistry. Various reaction partners and reaction conditions of reversible DA reactions are available for the preparation of thermally healable polymers (Table 9.1), therefore one can utilize the reversible nature of such dynamic materials by careful selection of a diene and a dienophile. Cyclic dienes, like furan and cyclopentadiene, are exceptionally good reagents for DA reactions, since the conjugated dienes are always locked in the desired *cis* conformation. Because the involved orbitals in a DA reaction are normally the HOMO of a diene and the LUMO of a dienophile, it is preferable if the energy levels of these two orbitals are similar. An electron-donating group at the 1-position of a diene increases the HOMO energy level, and therefore furan can undergo a more rapid DA reaction at lower temperatures than cyclopentadiene. On the

Table 9.1 Well-known Diels–Alder reaction partners and corresponding reaction conditions.

Diene	Dienophile	Adduct	Conditions
Furan	Maleimide		DA: between rt and 120 °C Retro-DA: >120 °C Several hours to days
Anthracene			DA: > 100 °C Retro-DA: >200 °C Several hours to days
Cyclopentadiene			DA: between 80 and 120 °C Retro-DA: >120 °C or >180 °C Several hours to days
Fulvene	Dicyanoethylene		DA: < rt Retro-DA: > rt Minutes to hours
	Dithioether		Hetero-DA: between rt and 80 °C Retro-hetero-DA: >80 °C Minutes (catalyst trifluoroacetic acid)

rt, room temperature.
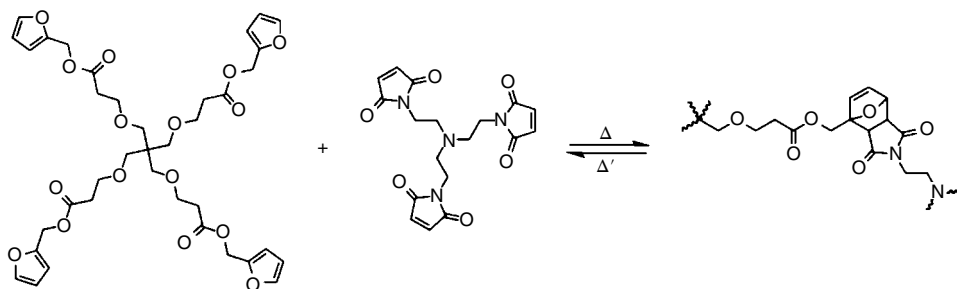
Scheme 9.2 Diels–Alder reaction between the tetrafunctional furan and trifunctional maleimide to produce a healable highly crosslinked material.

other hand, conjugation of a dienophile decreases the LUMO energy level. Thus, maleimide is a good dienophile and cyclopentadiene can be both a diene and a dienophile for DA reactions, although simple alkenes have relatively high-energy LUMOs and do not react well with dienes.

A report on thermally remendable polymers through a reversible DA reaction between furan and maleimide was a trigger to initiate a global interest in self-healing polymers.[30,61] A tetrafunctional furan and trifunctional maleimide formed a highly crosslinked polymeric material, which had similar mechanical properties to those of commercially available epoxy resins but also had an additional property of healing by heating (Scheme 9.2). After a structural fracture of the material, a thermal treatment above 120 °C allowed disconnection of 30% of the crosslinking, which reconnected upon cooling and mended the crack with a significant recovery of the material's mechanical properties (approximately 50%). This healing can be repeated multiple times, although the healing efficiency was slightly reduced for each cycle. This concept has also been used in better known engineering materials such as epoxy resins,[62–64] polyketones,[65] polyesters,[66] polyamides,[67] and poly(methylmethacrylate)s,[68] which have advantageous characteristics, including solvent and chemical resistance, thermal and electrical properties, and good adherence.

To shift the reaction and healing temperature to a higher range and use the polymers under severe conditions, anthracene–maleimide crosslinks were incorporated into the polymer networks.[69] The DA reaction made it possible to generate crosslinked materials at higher temperatures (>100 °C) and heal sustained damage at even higher temperatures (>200 °C).

A simplified DA system using a single component, a cyclic monomer containing dicyclopentadiene, has been developed for self-healing polymers.[70] Because cyclopentadiene can act as a diene and a dienophile, the system showed a unique feature that none of the other DA reactions exhibited. Upon heating (120 °C), the cyclic monomer underwent a retro-DA reaction and opened, producing a linear monomer with two reactive cyclopentadienes at the chain ends (Scheme 9.3). The cyclopentadienes then dimerized intermolecularly to form a linear polymer and subsequently underwent trimerization to form crosslinks, constructing a network with a high elastic modulus. This material was able to thermally re-heal the damage, achieving 40–60% recovery of the material's fracture strength by thermal healing.
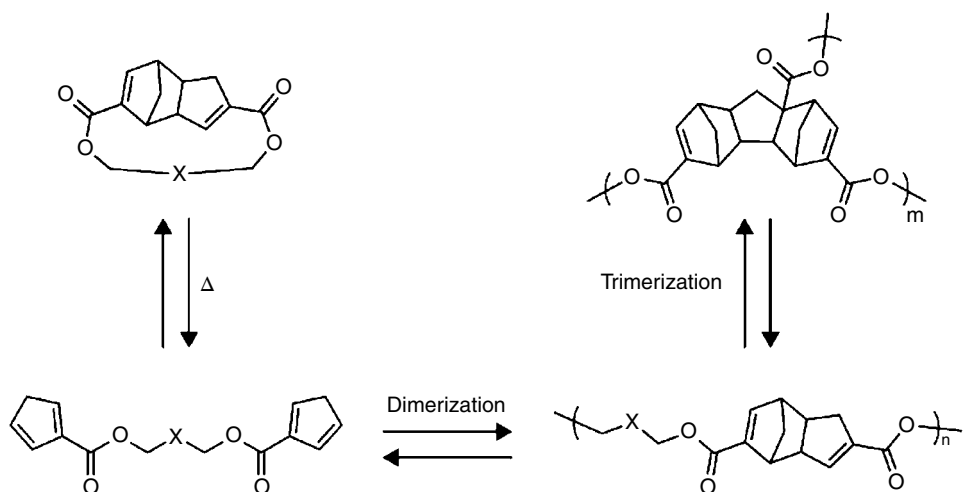
Scheme 9.3 Diels–Alder and retro-Diels–Alder reactions of a cyclic monomer containing dicyclopentadiene to form a re-healable polymer network. The process involves reversible ring opening, dimerization (polymerization), and trimerization (crosslinking).

Many reversible DA reactions used in self-healing polymers need heating not only to enhance the mobility of the reactive groups at the crack plane, but also to accelerate both the DA and retro-DA reactions. The high mending temperature has restricted the application area. In addition, there are very few reversible DA reactions available for self-healing features, which allow fast crosslinking or polymerization. Generally, reaction times of several days are required for DA reactions in the bulk of a polymer, therefore more rapid reversible DA reactions at lower temperatures have been sought for self-healing. It was reported that functionalized fulvenes and dicyanoethylenes can react rapidly and reversibly at temperatures below room temperature.[71,72] This system produced room-temperature healable materials, and only 10 s after pressing two pieces of film together they could no longer be separated by pulling them apart.[73] It is important to note that the film constantly creates new chain ends and forms new connections at room temperature, but it is not adhering to anything other than itself.

DA reactions form not only carbon–carbon bonds but also carbon–heteroatom bonds, and these reactions are widely used synthetically as a type of click chemistry.[74,75] Cyclic dienes and dithioesters with electron-withdrawing groups react very rapidly below room temperature, even in bulk, especially when the reaction is catalyzed by a Lewis acid or trifluoroacetic acid. A difuran-functionalized oligomer and trifunctional thioester could be crosslinked in the bulk state at room temperature within minutes and de-crosslinked at temperatures above 80 °C within minutes.[76] This system has great potential to be applied to self-healing polymers, although the small window of temperatures, relatively high costs, and instability at higher temperatures limiting the number of healing cycles are disadvantages for this application.

Because *endo*/*exo* stereoisomers of DA adducts might influence the thermal reversibility and hence thermal remendability of polymer networks (Scheme 9.4), a number of model compounds containing DA adducts formed from furan and maleimide derivatives were characterized.[77] It was established that the *endo* and *exo* DA stereoisomers
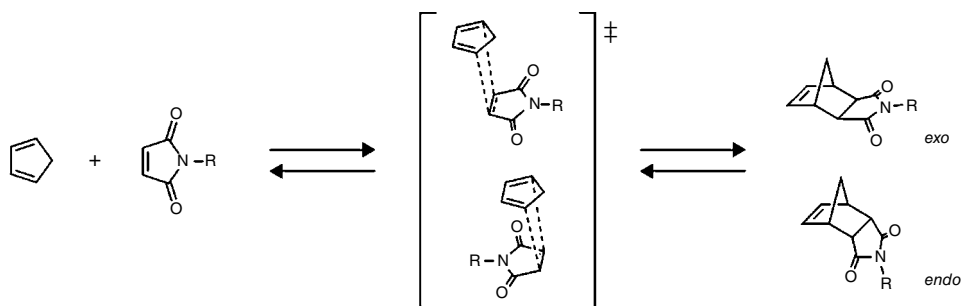
Scheme 9.4 Schematic Diels–Alder/retro-Diels–Alder reactions between a diene and a dienophile. There are two possible six-centered transition states, providing the kinetically favored *endo* product and thermodynamically favored *exo* product.

show significantly different thermal responses: the retro-DA reaction of the *endo* adducts typically takes place at temperatures 20–40 °C lower than that of the corresponding *exo* adducts in all cases, with the exception of some aromatic maleimides.

9.3.2 Urea Bonds

An amine and an isocyanate react to form a urea bond, which is stable and generally irreversible due to conjugation between the lone electron pair on the nitrogen atom and the π electrons on the carbonyl *p* orbital. The inverse reaction requires harsh conditions, for example highly acidic or basic solutions at high temperature or in the presence of a special catalyst such as an enzyme. However, it has been reported that introducing bulky substituents to a urea nitrogen atom weakens the urea bond, allowing the inverse reaction to occur under mild conditions.[78,79] The addition of a bulky group is believed to disturb the orbital co-planarity of the urea bond, which diminishes the conjugation effect and thus weakens the carbonyl–amine interaction. Indeed, polymers crosslinked by urea linkages bearing a bulky substituent on the nitrogen atom exhibit relatively fast self-healing at ambient temperatures and body temperature (Figure 9.5).[31,80] An almost complete recovery of the mechanical properties (87% of the initial strain) was achieved by healing at 37 °C for 12 h. The free isocyanate groups present at low quantities in the crosslinked polymers are susceptible to hydrolysis in air and irreversibly transform to amine groups after decarboxylation. These can react with free isocyanate groups to form irreversible non-dynamic urea bonds without a bulky group. Therefore, the self-healing ability is expected to be lost gradually with time and healing cycles.

Amide bonds also have the potential to act as a reversible addition reaction like urea bonds, but the dissociated intermediate from amidolysis (ketene) would be too reactive to show reversible formation, preventing this type of chemistry from being applied to a system for self-healing.

9.4 Catalyzed Exchange Reactions

Some robust covalent bonds can exchange partners simply by using appropriate catalysts, rather than by chemical modification. Utilization of such systems (i.e., catalyzed chain exchange reactions) can impart self-healing ability as well as processability and
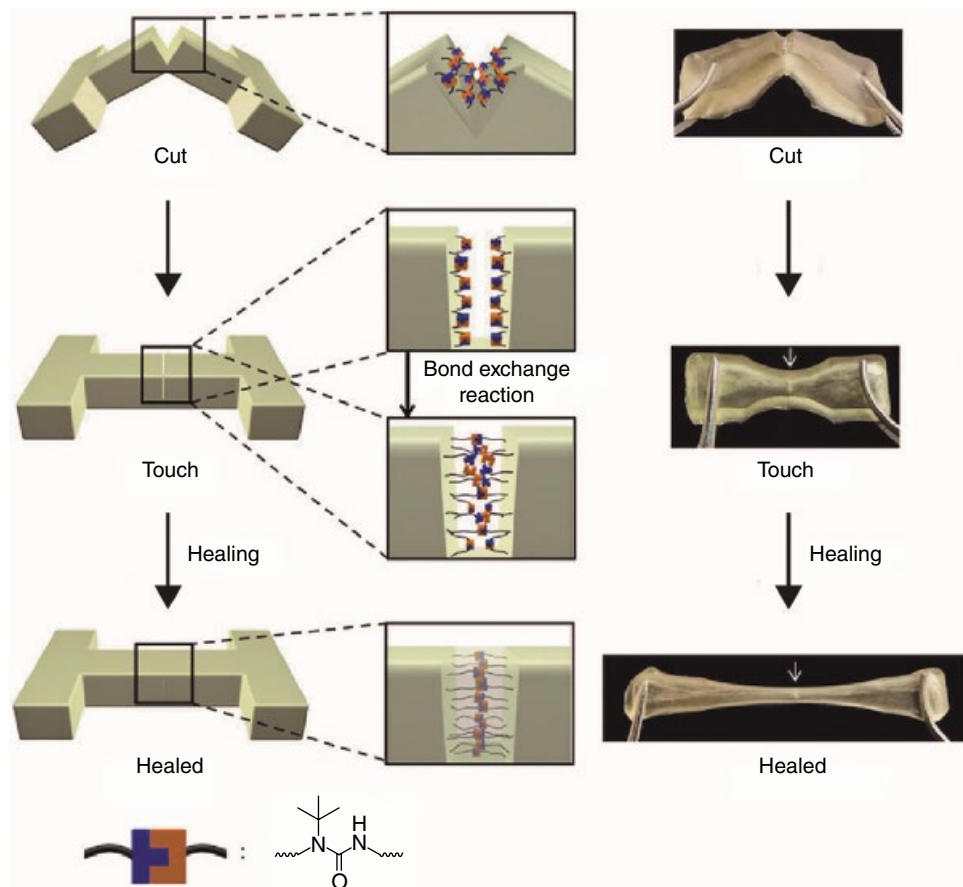
Figure 9.5 Illustration and snapshots of the self-healing process of polymers crosslinked by urea linkages bearing a bulky group. Reproduced with permission.[31] Copyright 2014, NPG.

recyclability to numerous existing crosslinked polymeric materials that have outstanding mechanical, thermal, and environmental resistance, therefore this chemistry is versatile, requiring readily available ingredients and no special equipment. The catalyzed reversible chain exchange reactions do not depolymerize the network, unlike DA reactions, and they do not cause an abrupt decrease in viscosity in a narrow temperature range. Rather, they rearrange the network topology while keeping the total number of links and the average functionality of crosslinks constant. The viscosity gradually decreases with increasing temperature. The kinetics can be controlled by the type and amount of catalyst used.[81]

9.4.1 Transesterification

Transesterification, a process whereby one ester is transformed into another through exchange of the alkoxy moieties, is one of the classical and well-established organic reactions. Essentially, this reaction occurs by simply mixing the two components, an ester and an alcohol. However, this reaction proceeds very slowly, and a proper catalyst is required to accelerate the rate of the reaction.[82]
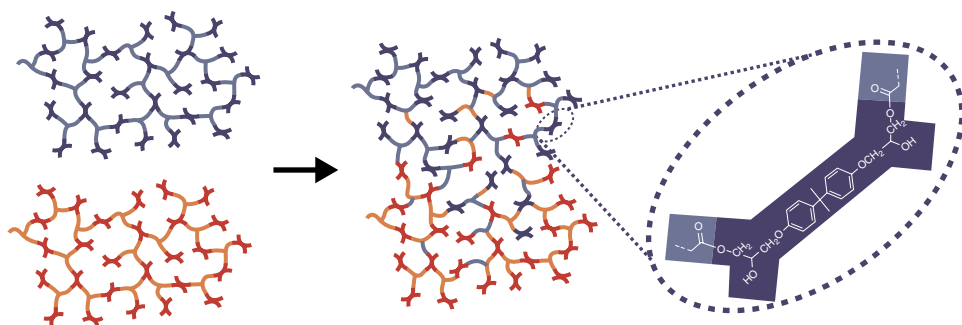
Figure 9.6 Schematic view of epoxy (hydroxy-ester) networks with transesterification exchange processes that preserve the total number of links and average functionality of crosslinks and do not cause depolymerization. Reproduced with permission.[32] Copyright 2012, ACS Publications. (*See insert for colour representation of the figure.*)

It has been reported that embedding zinc acetate (catalyst) into a classical and widely available epoxy resin produces a silica-like malleable polymeric material (Figure 9.6).[83] The material behaves like a hard epoxy resin at room temperature and does not dissolve in any good solvents, even after immersion at high temperatures for a long period of time. However, in contrast to classical epoxy resins, transesterification exchange reactions and the resulting topological rearrangements enable stress relaxation and malleability at high temperatures. Indeed, broken or ground resin could be reprocessed and reshaped by compression molding at 240 °C for 3 min, and the recycled object has essentially the same mechanical properties and insolubility as the original.

Transesterification has also been applied to self-healing materials.[32] A soft epoxy network with good elastomeric properties at room temperature demonstrated self-healing behavior dependent on healing time, temperature, and concentration of the transesterification catalyst. The mechanical properties of a sample catalyzed by 5 mol% zinc acetate were fully recovered after welding for several hours at 150 °C. When the healed sample was elongated, the rupture was cohesive and occurred in the bulk material far from the welded interface.

9.4.2 Olefin Metathesis

Olefin metathesis is a transition-metal-catalyzed organic reaction that involves the redistribution of fragments of alkenes (olefins) by the scission and regeneration of strong carbon–carbon double bonds. Although numerous catalysts for this reaction have been developed, the Grubbs' Ru metathesis catalysts made the reaction a powerful tool for synthetic organic and polymer chemists because of the tolerance for many functional groups, water, and oxygen.[84]

Similar to the products obtained by transesterification, the networks obtained by introducing a Grubbs' catalyst into olefin containing crosslinked polymers become malleable, processable, adaptable, and self-healable while retaining dimensional stability and solvent resistance (Figure 9.7).[33,85] The Ru-catalyzed rapid exchange and resulting rearrangement of the network topology occur at room temperature using extremely low catalyst loading (less than 0.01% relative to the molarity of olefin in the networks). Because olefin-containing polymers, including crosslinked polybutadiene, polyisoprene, and polynorbornenes, are large-volume materials with important commercial
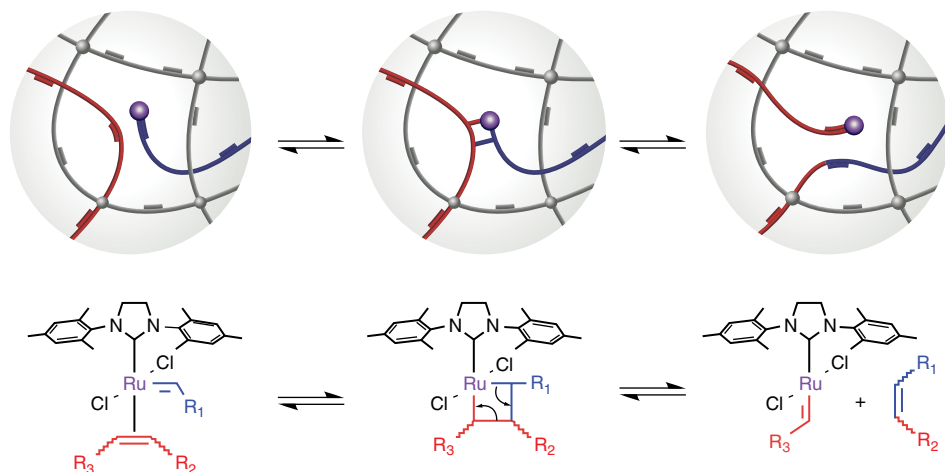
Figure 9.7 Concept of using olefin metathesis to make cross-linked polymers malleable and self-healable. Reproduced with permission.[85] Copyright 2012, ACS Publications.

applications, olefin metathesis can be used as a simple and practical method for developing self-healing polymeric materials.

9.4.3 Siloxane Chemistry

The anionic equilibration of crosslinked poly(dimethylsiloxane) prepared through tetramethylammonium silanate-initiated ring-opening copolymerization of octamethylcyclotetrasiloxane and bis(heptamethylcyclotetrasiloxanyl)-ethane has been known for more than 60 years (Figure 9.8).[86,87] The tetramethylammonium dimethylsilanolate termini in the network are "living" propagating species, which are not neutralized by ambient atmosphere exposure (stable toward water, oxygen, and carbon dioxide), and promote thermally activated equilibration among different network isomers and cyclic oligomers. Therefore, siloxane chemistry can be utilized in development of self-healing materials[34,88] Indeed, the sample of poly(dimethylsiloxane) network with active ends, which was cut into two pieces, can be re-healed via siloxane equilibration to restore the original mechanical strength when heated at 90 °C for 24 h.[34] The healed sample broke at a different location when bent, rather than at the initial cut, indicating complete mechanical healing. Although the living chain ends are deactivated at 150 °C, producing volatile trimethylamine, the addition of basic catalysts like tetramethylammonium silanate can, essentially, convert any crosslinked dimethylsilicone elastomers to living ones. Hence, this system has great potential for use in a variety of self-healable networks.

9.5 Radical Transfer and Crossover Reactions

Radical transfer and crossover reactions are typically initiated by photoirradiation and only become dynamic on exposure to a specific wavelength. Pioneering research on unique polymers utilizing such a system includes the development of crosslinked

(a)

(b)
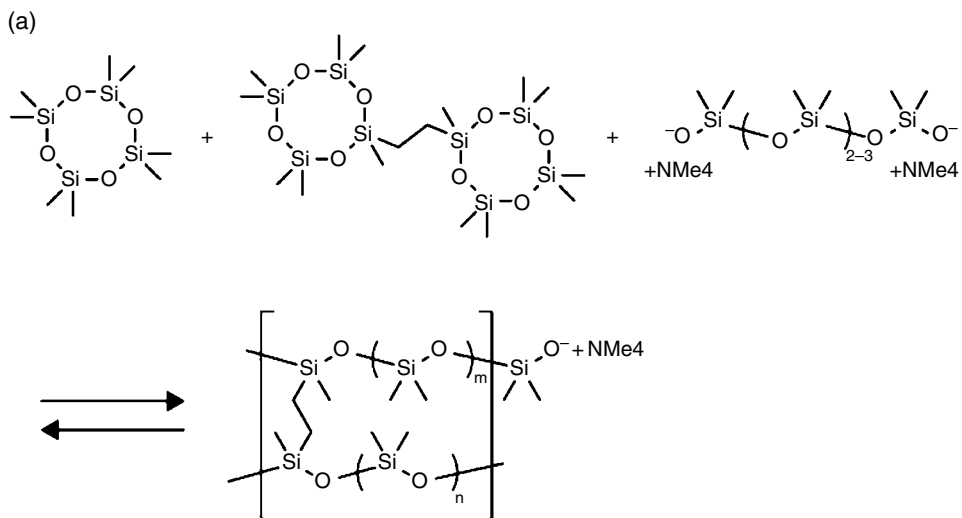
Figure 9.8 (a) Equilibrium between cyclic monomers and a crosslinked polymer in anionic polymerization. (b) Photographs of the self-healing process of a crosslinked polymer with living chain ends. Reproduced with permission.[34] Copyright 2012, ACS Publications.

polymers with photoinduced plasticity.[89] A covalently crosslinked polymer with allyl sulfide linkages can undergo photomediated reversible cleavage of the backbone and chain rearrangement, allowing rapid stress relief at ambient conditions, without diminishing mechanical properties. The reversible backbone cleavage originates from addition-fragmentation chain transfer through a sulfur radical mechanism, which is initiated by homolytic photolysis of residual photoinitiator in the polymer matrix (Scheme 9.5). This addition-fragmentation process can alter the network topology with the network connectivity (the number of allyl sulfide groups) unchanged. Radical transfer and
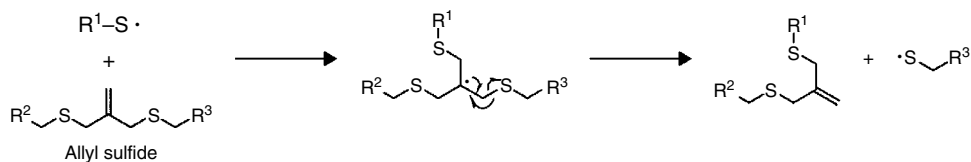
Scheme 9.5 Reaction mechanism for the addition-fragmentation chain transfer of allyl sulfides incorporated into polymer backbones.

crossover reactions have been used to fabricate self-healing polymeric materials in which light can be applied locally to a damaged site. Hence, objects can, in principle, be healed even under load using such reactions.

9.5.1 Disulfide and Diselenide Bonds

Similar to allyl sulfide linkages, disulfide and diselenide bonds can undergo radical transfer and crossover reactions on exposure to UV light[90] and visible light, respectively.[91] They have been used to develop self-healing polymeric materials.[35,92,93] Thiyl and selenol radicals formed from photoinduced homolytic cleavage of disulfide and diselenide bonds or other radical species such as carbon- and phosphorus-centered radicals[35] are able to initiate multiple fragmentation and exchange reactions (Scheme 9.6a). In particular, crosslinked polymers with disulfide bonds are known to exhibit photodegradation, photoadaptation, and photohealing under ambient conditions, which originate from the fragmentation reactions of disulfide bonds.

In addition to the radical mechanism, disulfide bonds exhibit dynamic behavior also through a thiol–disulfide exchange mechanism in the presence of thiols and a proper catalyst.[94,95] This mechanism is not related to radical transfer and crossover reactions, but has been utilized for self-healing catalyzed by amine with[96–98] or without heating,[99] catalyzed by phosphine,[100] and under basic conditions.[42] In these systems, thiolates are formed by the deprotonation of thiols and subsequently attack disulfide bonds as nucleophiles, initiating thiol–disulfide exchange reactions (Scheme 9.6b), therefore the healing systems are highly pH dependent and need base catalysts or basic
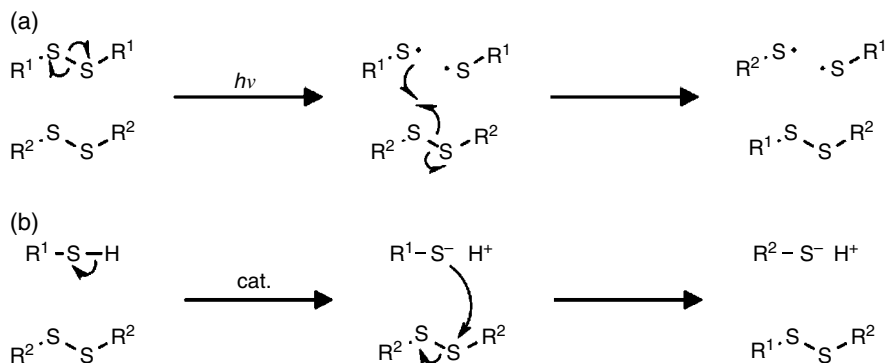
Scheme 9.6 (a) Disulfide exchange through a photoinduced radical mechanism and (b) thiol–disulfide exchange involving thiolate generation by a catalyst or under basic conditions.

conditions to form thiolates. However, the conditions that promote thiol–disulfide exchange also promote thiol–thiol oxidative coupling, reducing the thiol concentration and changing the material's mechanical properties.

9.5.2 Thiuram Disulfide Bonds

The S–S bonds incorporated in thiuram disulfide units are known to homolytically dissociate at relatively low temperatures (>70 °C) or in visible light, which is available from natural sources and is less harmful than UV light, and act as "iniferter" units.[101] It has been demonstrated that the radical transfer and crossover reactions of thiuram disulfide linkages in crosslinked polymers enable network reorganization, resulting in self-healing in air at room temperature on exposure to visible light.[36] When the polymer was damaged, healing in air under visible light gradually recovered the mechanical properties with the exposure time and almost completely after 12 h. Because the dithiocarbamyl radicals generated in the polymer by exposure to visible light remain for a relatively long time, the healing proceeds even in the dark after the exposure. However, while the radicals are insensitive to oxygen, they can participate in some side reactions when exposed to air for a long time. Healing of the surfaces cut and left for 4 or 24 h was less efficient than fragments placed in close contact immediately after cut. This seems to result from migration of the dithiocarbamyl radicals to the interior of the polymer by continuous reorganization of the surfaces or through loss of CS_2, reducing the concentration of the radicals at the surface. Incorporation of a similar dithiocarbamate iniferter unit into a polymer network also enabled UV-light-triggered healing[101]

9.5.3 Trithiocarbonate Linkages

Trithiocarbonate units are able to act as photoinitiators in reversible addition-fragmentation chain transfer polymerizations similar to the allyl sulfide moiety described above,[102,103] and therefore undergo photostimulated reshuffling reactions. Indeed, crosslinked polymers with trithiocarbonate linkages could heal damage by UV light irradiation (Figure 9.9).[37] This healing was achieved under a nitrogen atmosphere at room temperature with the help of mild pressure to facilitate tight contact of the damaged surfaces and/or solvent to increase the chain mobility. In the gel state, the mechanical properties were fully restored by healing for 12 h, but in the bulk state a small crack remained on the surface, even after healing for 48 h, due to limited chain mobility. It was also reported that network reorganization through trithiocarbonate reshuffling reactions can be initiated by other radical species or a Cu(I) catalyst.[104] Although these self-healing processes were successfully repeated multiple times, the carbon radical intermediates formed from photoinduced cleavage of trithiocarbonate linkages are reactive with oxygen, which limits the applications of the linkages.

9.6 Homolytic Bond Cleavage and Re-formation

Some covalent bonds can undergo homolytic bond cleavage in response to an appropriate stimulus and selectively reform in the absence of the stimulus. The radicals generated by the cleavage should be stable or otherwise cause side-reactions little through selective coupling under usage conditions. Such bonds are considered to produce

(a)
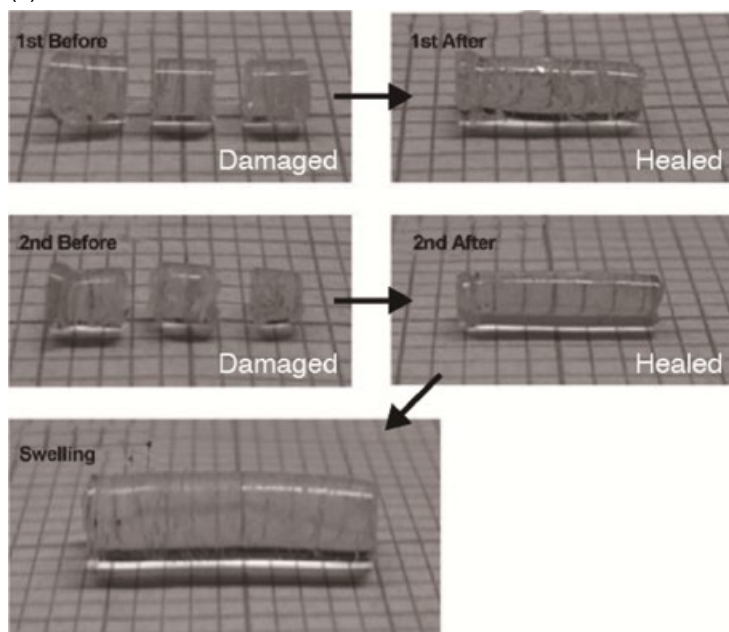
(b)
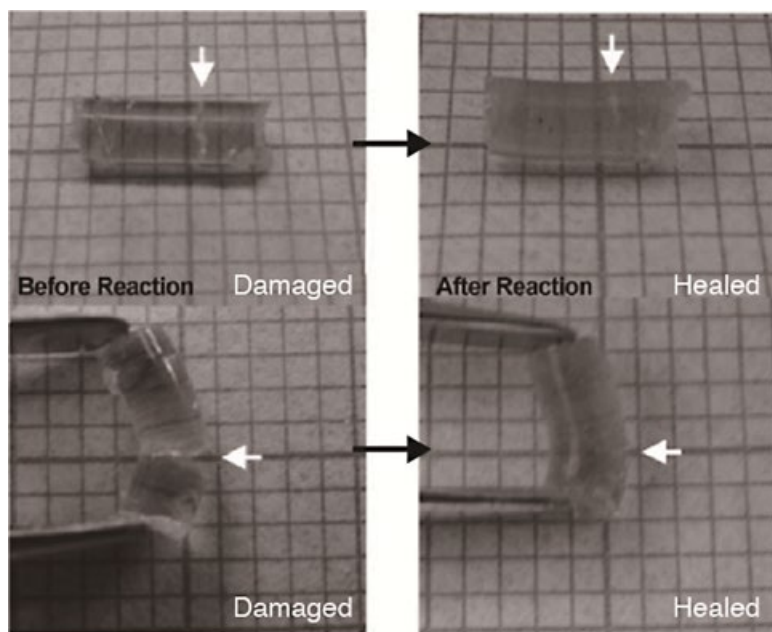
Figure 9.9 Photographs of crosslinked polymers with trithiocarbonate linkages (a) in repetitive self-healing under UV light irradiation in acetonitrile (in the gel state) and (b) in self-healing under UV light irradiation in the bulk state. Reproduced with permission.[37] Copyright 2011, Wiley Publications.

exchange reactions, where the dissociated radicals react with complementary radicals, but hardly attack another bond and do not initiate radical transfer and fragmentation reactions. Therefore, the mechanism is different from the transfer and fragmentation reactions described above for catalyzed exchange reactions and disulfide bonds. Crosslinked polymers with this system can exhibit network rearrangements, which originate from the exchange reactions and result in self-healing.

9.6.1 Alkoxyamine Linkages

Alkoxyamine derivatives containing 2,2,6,6-tetramethylpiperidine-1-oxy (TEMPO) are known to dissociate homolytically to carbon- and nitroxide-centered radicals by means of heating and are used as initiators for nitroxide-mediated living radical polymerization, where the growing polymer chain ends are reversibly capped by the nitroxide radicals.[105,106] In the absence of monomer, alkoxyamine units dissociate and associate reversibly and exchange their bonds on heating (>60 °C).[107,108] In this system, coupling (termination) reactions between carbon radicals occur during the early stage, but rarely occur after a small increase in the overall concentration of nitroxide radicals relative to carbon radicals because of the persistent nature of the nitroxide radicals (nitroxide radicals do not react with each other), which is termed as the persistent radical effect.[109,110] Thus, alkoxyamine units can work as dynamic linkages in polymers through the radical mechanism.

It has been demonstrated that the incorporation of alkoxyamine linkages into crosslinked polymers enables healing of damage in a wide range of polymeric materials, from soft elastomers to hard epoxy resins, by heating to >125 °C[38,111] or >80 °C[112,113] (the difference in healing temperature depends on the chemical structures of the alkoxyamines and the polymer chain mobility) (Figure 9.10) or by UV light irradiation.[114] Because carbon-centered radicals generated from alkoxyamine linkages generally react with oxygen and form peroxyl radicals, which lead to irreversible side reactions, healing should be carried out in an inert gas atmosphere, otherwise it cannot be repeatedly observed.

It is known that the healing temperature is significantly affected by the chemical and steric effects of substituents on alkoxyamines.[115–117] Modification of nitrile on alkoxyamines stabilizes dissociated carbon radicals and reduces the homolysis temperature because of the strong capability of nitrile to adsorb electrons (Figure 9.11). In addition, the oxygen resistance of the carbon radicals can also be improved by this modification, therefore thermoplastic polyurethanes and crosslinked epoxy elastomers with nitrile-modified alkoxyamine linkages exhibit repeated self-healing in air at room temperature or even below.

The reversible reaction of alkoxyamines is evaluable by electron paramagnetic resonance (EPR) spectroscopy, which can detect unpaired electrons, including radicals. Although it is difficult to evaluate other reversible reactions incorporated into polymer networks, the radical mechanism and EPR examination enable easy access to *in situ* evaluation of the equilibrium states of alkoxyamines.

9.6.2 Diarylbibenzofuranone Linkages

While alkoxyamine is composed of an unstable carbon radical and a stable nitroxide radical, diarylbibenzofuranone is formed from the reaction between two stable carbon

(a)

| Virgin | Cut | Healed | | 3rd Healed |

(b)

| Virgin | Broken | Healed |
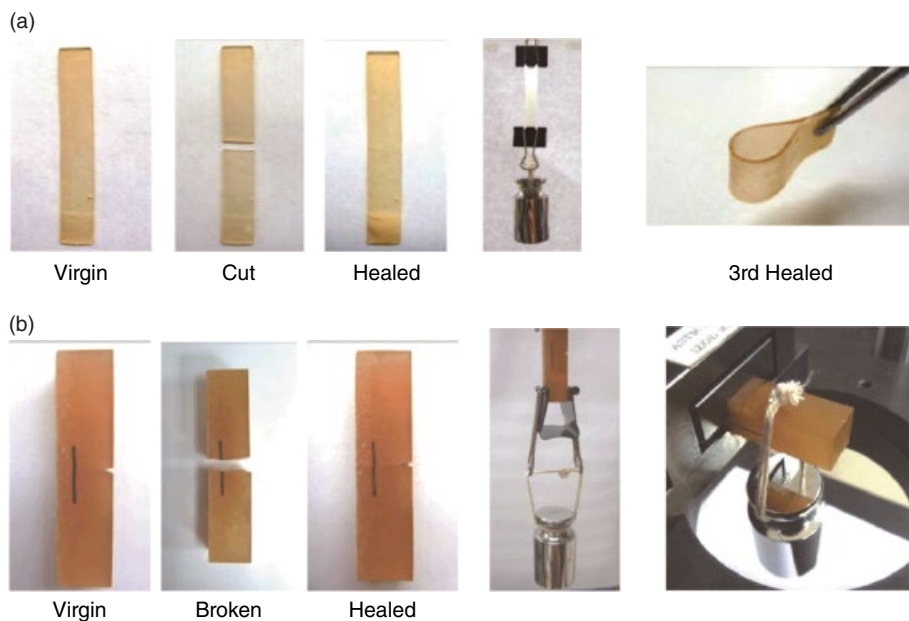
Figure 9.10 (a) Self-healing behavior of a soft polyurethane elastomer with alkoxyamine linkages. Reproduced with permission.[112] Copyright 2014, Elsevier. (b) Self-healing behavior of a hard epoxy resin with alkoxyamine linkages. Reproduced with permission.[113] Copyright 2014, Royal Society of Chemistry.
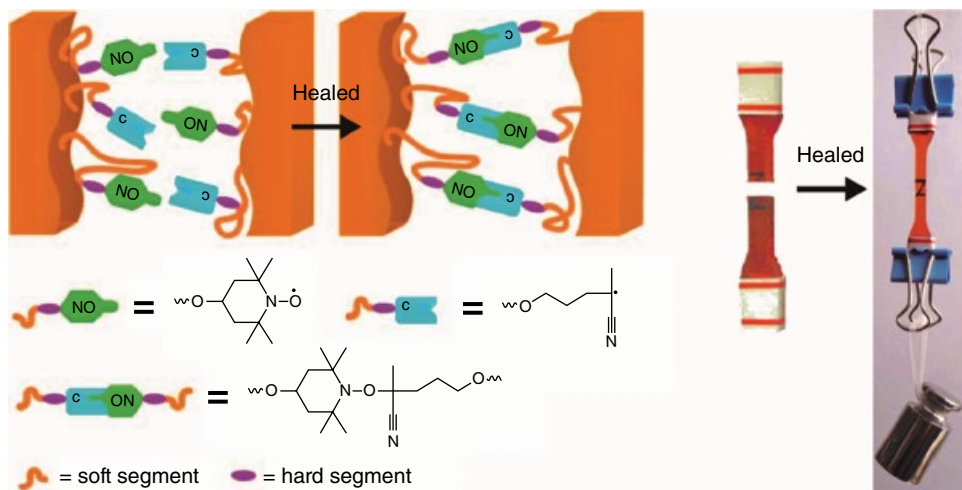
Figure 9.11 Schematic diagram of the healing reaction and photographs of the healing behavior of polymeric materials with nitrile-modified alkoxyamine linkages. Reproduced with permission.[115] Copyright 2013, Royal Society of Chemistry. Reproduced with permission.[116] Copyright 2014, Elsevier.
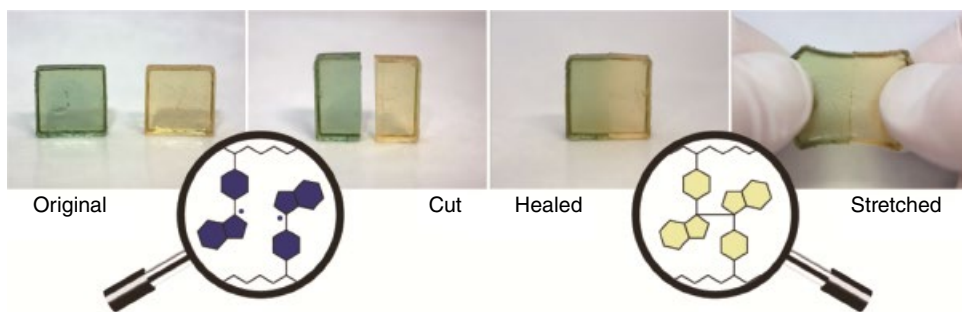
Figure 9.12 The self-healing behavior of gels crosslinked by diarylbibenzofuranone linkages.

radicals. Diarylbibenzofuranone is known to be in an equilibrium state between the combined dimer and dissociated radicals, even at room temperature.[118] The carbon-centered radicals are tolerant of oxygen and also unreactive with other chemicals, except for unstable radicals.[119–123] Because of these unique properties, diarylbibenzo-furanone acts as a better antioxidant compared to 3,5-di-*tert*-butyl-4-hydroxyanisole, a well-known and much-used antioxidant.[124,125]

Introduction of diarylbibenzofuranone into polymer networks enables reorganization of the networks and self-healing of damage in air at ambient temperature without any stimulation.[39,126–129] Gels crosslinked by diarylbibenzofuranone linkages fully restored the mechanical properties by healing for 24 h after being cut into two pieces and pressed together tightly (Figure 9.12).[39] The scars had almost disappeared and the healed samples were broken at random positions, including the cut position, when elongated.

The equilibrium of diarylbibenzofuranone was also evaluated by *in situ* EPR measurements.[130–134] Since all radicals formed from the cleavage of diarylbibenzofuranone are stable, even quantitative estimation of the amount of radicals generated in polymer matrices was possible, which clarified the relationship between the self-healing behavior and the equilibrium.

9.7 Conclusions

As shown in this chapter, numerous types of reversible systems based on dynamic covalent chemistry have been exploited for self-healing properties in polymeric materials. Meanwhile, some reactions that do not involve thermodynamic equilibrium but involve reversible covalent bond cleavage and re-formation under different stimuli are also known to be capable of developing self-healing polymeric materials. For example, photochemical [2 + 2] cycloaddition of cinnamoyl groups to form cyclobutane structures and reversion of the cyclobutane in response to damage enabled healing with the aid of a light source (Scheme 9.7).[135,136] Similarly, photoreversible reactions (dimerization and dissociation) of anthracenes and coumarins have been used for self-healing.[137–139] A system involving thermal [2 + 2] cycloaddition of trifluorovinylethers and reversion of the resulting perfluorocyclobutane is also a candidate for self-healing.[140] While thermal decomposition of perfluorocyclobutane is an irreversible reaction, pure
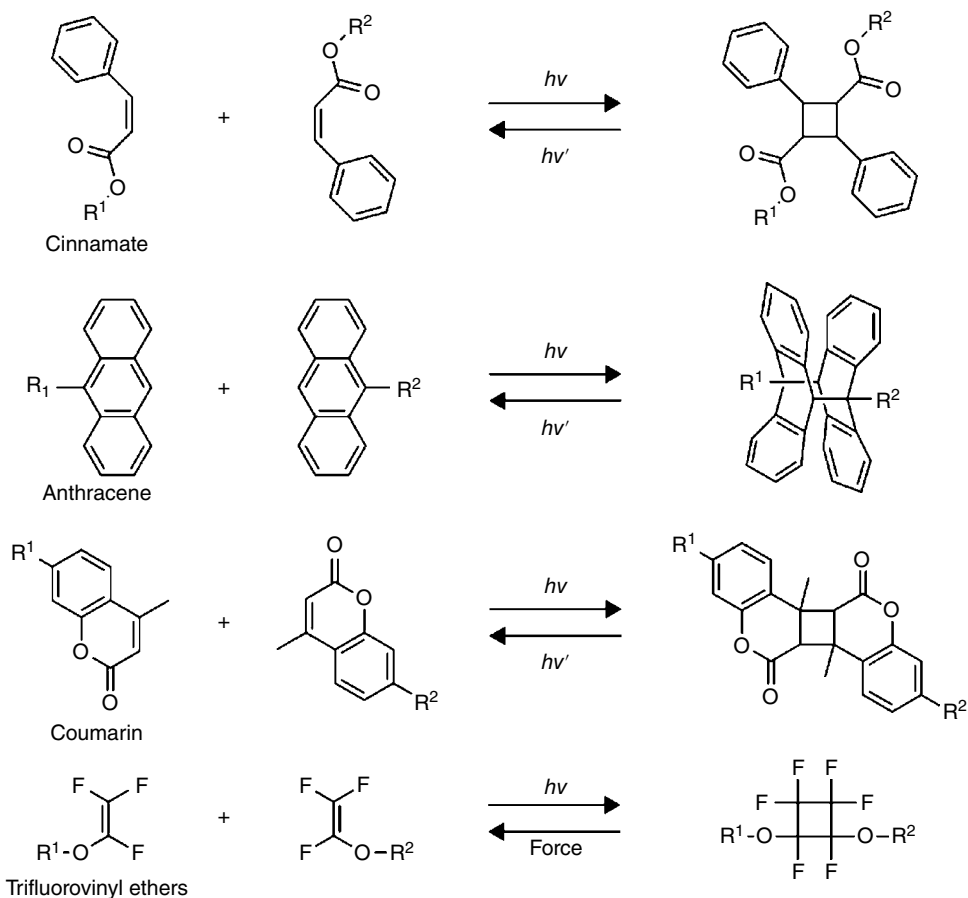
Scheme 9.7 Other chemical reactions available for self-healing.

mechanical decomposition results in a cycloreversion to thermally remendable trifluorovinylether units through a diradical mechanism. These systems are not as well studied as dynamic covalent and supramolecular systems, but introduction of these systems into polymers is a promising approach to impart self-healing ability.

The development of self-healing materials through dynamic bonds or interactions to more practical ones faces a big challenge: simultaneous pursuit of high self-healing ability and good mechanical properties to generate "tough polymers". High self-healing ability involves strenuous molecular motion of dynamic units, while good mechanical properties need to restrain the mobility of polymer chains. To overcome this difficulty, various approaches have been examined, including hard–soft phase separation, where dynamic units are incorporated in the soft phase,[141–144] introduction of crystalline components,[89,145] composites with nanomaterials,[146–150] and utilization of sacrificial bonds.[151] Efficient self-healing was achieved in these systems, and other research has focused on their practical use.[152–155] However, more precise macromolecular design that results in much better mechanical properties and healing efficiency will be necessary.

Self-healing polymers have become reality in material science, and a number of such polymers are currently available on the market. However, there are still unresolved technical issues related to cost, energy supply, and stability that must be solved to enable an accelerated industrial breakthrough. In addition, the chemistry of healing has matured, and thus a new transformative concept is required to move to the next stage. Multidisciplinary studies ranging from molecular chemistry to material physics and occasionally biology are required to accomplish these goals.

References

1 R. J. Wojtecki, M. A. Meador, S. J. Rowan, *Nat. Mater.* **2011**, *10*, 14–27.
2 S. R. White, N. R. Sottos, P. H. Geubelle, J. S. Moore, M. R. Kessler, S. R. Sriram, E. N. Brown, S. Viswanathan, *Nature* **2001**, *409*, 794–797.
3 K. S. Toohey, N. R. Sottos, J. A. Lewis, J. S. Moore, S. R. White, *Nat. Mater.* **2007**, *6*, 581–585.
4 S. R. White, J. S. Moore, N. R. Sottos, B. P. Krull, W. A. S. Cruz, R. C. R. Gergely, *Science* **2014**, *344*, 620–623.
5 Y. Noda, Y. Hayashi, K. Ito, *J. Appl. Polym. Sci.* **2014**, *131*, DOI: 10.1002/APP.40509.
6 M. Yamaguchi, S. Ono, M. Terano, *Mater. Lett.* **2007**, *61*, 1396–1399.
7 K. Takeda, M. Tanahashi, H. Unno, *Sci. Technol. Adv. Mat.* **2003**, *4*, 435–444.
8 K. Takeda, H. Unno, M. Zhang, *J. Appl. Polym. Sci.* **2004**, *93*, 920–926.
9 B. Ghosh, M. W. Urban, *Science* **2009**, *323*, 1458–1460.
10 S. Billiet, W. Van Camp, X. K. D. Hillewaere, H. Rahier, F. E. Du Prez, *Polymer* **2012**, *53*, 2320–2326.
11 Q. Wei, J. Wang, X. Y. Shen, X. A. Zhang, J. Z. Sun, A. J. Qin, B. Z. Tang, *Sci. Rep.* **2013**, *3*, DOI: 10.1038/Srep01093.
12 O. S. Taskin, B. Kiskan, Y. Yagci, *Macromolecules* **2013**, *46*, 8773–8778.
13 L. Brunsveld, B. J. B. Folmer, E. W. Meijer, R. P. Sijbesma, *Chem. Rev.* **2001**, *101*, 4071–4097.
14 S. J. Rowan, S. J. Cantrill, G. R. L. Cousins, J. K. M. Sanders, J. F. Stoddart, *Angew. Chem., Int. Ed.* **2002**, *41*, 898–952.
15 T. Maeda, H. Otsuka, A. Takahara, *Prog. Polym. Sci.* **2009**, *34*, 581–604.
16 Y. Jin, C. Yu, R. J. Denman, W. Zhang, *Chem. Soc. Rev.* **2013**, *42*, 6634–6654.
17 P. Cordier, F. Tournilhac, C. Soulie-Ziakovic, L. Leibler, *Nature* **2008**, *451*, 977–980.
18 S. Burattini, H. M. Colquhoun, J. D. Fox, D. Friedmann, B. W. Greenland, P. J. F. Harris, W. Hayes, M. E. Mackay, S. J. Rowan, *Chem. Commun.* **2009**, 6717–6719.
19 Q. Wang, J. L. Mynar, M. Yoshida, E. Lee, M. Lee, K. Okuro, K. Kinbara, T. Aida, *Nature* **2010**, *463*, 339–343.
20 K. Haraguchi, K. Uyama, H. Tanimoto, *Macromol. Rapid Commun.* **2011**, *32*, 1253–1258.
21 T. L. Sun, T. Kurokawa, S. Kuroda, A. Bin Ihsan, T. Akasaki, K. Sato, M. A. Haque, T. Nakajima, J. P. Gong, *Nat. Mater.* **2013**, *12*, 932–937.
22 M. Burnworth, L. M. Tang, J. R. Kumpfer, A. J. Duncan, F. L. Beyer, G. L. Fiore, S. J. Rowan, C. Weder, *Nature* **2011**, *472*, 334–U230.
23 M. Nakahata, Y. Takashima, H. Yamaguchi, A. Harada, *Nat. Commun.* **2011**, *2*, DOI: 10.1038/Ncomms1521.

24 T. Kakuta, Y. Takashima, M. Nakahata, M. Otsubo, H. Yamaguchi, A. Harada, *Adv. Mater.* **2013**, *25*, 2849–2853.

25 G. H. Deng, C. M. Tang, F. Y. Li, H. F. Jiang, Y. M. Chen, *Macromolecules* **2010**, *43*, 1191–1194.

26 Y. L. Zhang, L. Tao, S. X. Li, Y. Wei, *Biomacromolecules* **2011**, *12*, 2894–2901.

27 P. J. Taynton, K. Yu, R. K. Shoemaker, Y. Jin, H. J. Qi, W. Zhang, *Adv. Mater.* **2014**, *26*, 3938–3942.

28 L. H. He, D. E. Fullenkamp, J. G. Rivera, P. B. Messersmith, *Chem. Commun.* **2011**, *47*, 7497–7499.

29 J. M. Garcia, *et al. Science* **2014**, *344*, 732–735.

30 X. X. Chen, M. A. Dam, K. Ono, A. Mal, H. B. Shen, S. R. Nutt, K. Sheran, F. Wudl, *Science* **2002**, *295*, 1698–1702.

31 H. Z. Ying, Y. F. Zhang, J. J. Cheng, *Nat. Commun.* **2014**, *5*, DOI: 10.1038/Ncomms4218.

32 M. Capelot, D. Montarnal, F. Tournilhac, L. Leibler, *J. Am. Chem. Soc.* **2012**, *134*, 7664–7667.

33 Y. X. Lu, Z. B. Guan, *J. Am. Chem. Soc.* **2012**, *134*, 14226–14231.

34 P. W. Zheng, T. J. McCarthy, *J. Am. Chem. Soc.* **2012**, *134*, 2024–2027.

35 B. D. Fairbanks, S. P. Singh, C. N. Bowman, K. S. Anseth, *Macromolecules* **2011**, *44*, 2444–2450.

36 Y. Amamoto, H. Otsuka, A. Takahara, K. Matyjaszewski, *Adv. Mater.* **2012**, *24*, 3975–3980.

37 Y. Amamoto, J. Kamada, H. Otsuka, A. Takahara, K. Matyjaszewski, *Angew. Chem., Int. Ed.* **2011**, *50*, 1660–1663.

38 C. Yuan, M. Z. Rong, M. Q. Zhang, Z. P. Zhang, Y. C. Yuan, *Chem. Mater.* **2011**, *23*, 5076–5081.

39 K. Imato, M. Nishihara, T. Kanehara, Y. Amamoto, A. Takahara, H. Otsuka, *Angew. Chem., Int. Ed.* **2012**, *51*, 1138–1142.

40 W. G. Skene, J. M. P. Lehn, *Proc. Natl. Acad. Sci. USA* **2004**, *101*, 8270–8275.

41 F. Y. Liu, F. Y. Li, G. H. Deng, Y. M. Chen, B. Q. Zhang, J. Zhang, C. Y. Liu, *Macromolecules* **2012**, *45*, 1636–1645.

42 G. H. Deng, F. Y. Li, H. X. Yu, F. Y. Liu, C. Y. Liu, W. X. Sun, H. F. Jiang, Y. M. Chen, *ACS Macro Lett.* **2012**, *1*, 275–279.

43 M. E. Belowich, J. F. Stoddart, *Chem. Soc. Rev.* **2012**, *41*, 2003–2024.

44 J. B. Conant, P. D. Bartlett, *J. Am. Chem. Soc.* **1932**, *54*, 2881–2899.

45 Y. L. Zhang, B. Yang, X. Y. Zhang, L. X. Xu, L. Tao, S. X. Li, Y. Wei, *Chem. Commun.* **2012**, *48*, 9305–9307.

46 Y. Z. Gao, Q. Luo, S. P. Qiao, L. Wang, Z. Y. Dong, J. Y. Xu, J. Q. Liu, *Angew. Chem., Int. Ed.* **2014**, *53*, 9343–9346.

47 Z. Wei, J. H. Yang, Z. Q. Liu, F. Xu, J. X. Zhou, M. Zrinyi, Y. Osada, Y. M. Chen, *Adv. Funct. Mater.* **2015**, *25*, 1352–1359.

48 P. Taynton, H. G. Ni, C. P. Zhu, K. Yu, S. Loob, Y. H. Jin, H. J. Qi, W. Zhang, *Adv. Mater.* **2016**, *28*, 2904–2909.

49 J. M. Whiteley, P. Taynton, W. Zhang, S. H. Lee, *Adv. Mater.* **2015**, *27*, 6922–6927.

50 Z. Q. Lei, P. Xie, M. Z. Rong, M. Q. Zhang, *J. Mater. Chem. A* **2015**, *3*, 19662–19668.

51 J. Xu, D. G. Yang, W. J. Li, Y. Gao, H. B. Chen, H. M. Li, *Polymer* **2011**, *52*, 4268–4276.

52 C. C. Deng, W. L. A. Brooks, K. A. Abboud, B. S. Sumerlin, *ACS Macro Lett.* **2015**, *4*, 220–224.

53 L. R. He, D. Szopinski, Y. Wu, G. A. Luinstra, P. Theato, *ACS Macro Lett.* **2015**, *4*, 673–678.

54 J. J. Cash, T. Kubo, A. P. Bapat, B. S. Sumerlin, *Macromolecules* **2015**, *48*, 2098–2106.

55 G. Springsteen, B. H. Wang, *Tetrahedron* **2002**, *58*, 5291–5300.

56 J. Yan, G. Springsteen, S. Deeter, B. H. Wang, *Tetrahedron* **2004**, *60*, 11205–11209.

57 T. D. James, K. R. A. S. Sandanayake, S. Shinkai, *Angew. Chem., Int. Ed.* **1996**, *35*, 1910–1922.

58 G. Wulff, M. Lauer, H. Bohnke, *Angew. Chem., Int. Ed.* **1984**, *23*, 741–742.

59 O. R. Cromwell, J. Chung, Z. B. Guan, *J. Am. Chem. Soc.* **2015**, *137*, 6492–6495.

60 H. Kwart, K. King, *Chem. Rev.* **1968**, *68*, 415–447.

61 X. X. Chen, F. Wudl, A. K. Mal, H. B. Shen, S. R. Nutt, *Macromolecules* **2003**, *36*, 1802–1807.

62 Y. L. Liu, C. Y. Hsieh, *J. Polym. Sci., Part A: Polym. Chem.* **2006**, *44*, 905–913.

63 Q. Tian, Y. C. Yuan, M. Z. Rong, M. Q. Zhang, *J. Mater. Chem.* **2009**, *19*, 1289–1296.

64 Q. A. Tian, M. Z. Rong, M. Q. Zhang, Y. C. Yuan, *Polym. Int.* **2010**, *59*, 1339–1345.

65 Y. Zhang, A. A. Broekhuis, F. Picchioni, *Macromolecules* **2009**, *42*, 1906–1912.

66 N. Yoshie, M. Watanabe, H. Araki, K. Ishida, *Polym. Degrad. Stabil.* **2010**, *95*, 826–829.

67 Y. L. Liu, Y. W. Chen, *Macromol. Chem. Phys.* **2007**, *208*, 224–232.

68 A. A. Kavitha, N. K. Singha, *ACS Appl. Mater. Inter.* **2009**, *1*, 1427–1436.

69 N. Yoshie, S. Saito, N. Oya, *Polymer* **2011**, *52*, 6074–6079.

70 E. B. Murphy, E. Bolanos, C. Schaffner-Hamann, F. Wudl, S. R. Nutt, M. L. Auad, *Macromolecules* **2008**, *41*, 5203–5209.

71 M. H. Howard, V. Alexander, W. J. Marshall, D. C. Roe, Y. J. Zheng, *J. Org. Chem.* **2003**, *68*, 120–129.

72 P. J. Boul, P. Reutenauer, J. M. Lehn, *Org. Lett.* **2005**, *7*, 15–18.

73 P. Reutenauer, E. Buhler, P. J. Boul, S. J. Candau, J. M. Lehn, *Chem. Eur. J.* **2009**, *15*, 1893–1900.

74 A. J. Inglis, S. Sinnwell, M. H. Stenzel, C. Barner-Kowollik, *Angew. Chem., Int. Ed.* **2009**, *48*, 2411–2414.

75 M. A. Tasdelen, *Polym. Chem.* **2011**, *2*, 2133–2145.

76 A. J. Inglis, L. Nebhani, O. Altintas, F. G. Schmidt, C. Barner-Kowollik, *Macromolecules* **2010**, *43*, 5515–5520.

77 J. Canadell, H. Fischer, G. De With, R. A. T. M. Van Benthem, *J. Polym. Sci., Part A: Polym. Chem.* **2010**, *48*, 3456–3467.

78 J. C. Stowell, Padegima.Sj, *J. Org. Chem.* **1974**, *39*, 2448–2449.

79 M. Hutchby, C. E. Houlden, J. G. Ford, S. N. G. Tyler, M. R. Gagne, G. C. Lloyd-Jones, K. I. Booker-Milburn, *Angew. Chem., Int. Ed.* **2009**, *48*, 8721–8724.

80 Y. Zhang, *et al. Adv. Mater.* **2016**, *28*, 7646–7651.

81 M. Capelot, M. M. Unterlass, F. Tournilhac, L. Leibler, *ACS Macro Letters* **2012**, *1*, 789–792.

82 J. Otera, *Chem. Rev.* **1993**, *93*, 1449–1470.

83 D. Montarnal, M. Capelot, F. Tournilhac, L. Leibler, *Science* **2011**, *334*, 965–968.

84 R. H. Grubbs, *Tetrahedron* **2004**, *60*, 7117–7140.

85 Y. X. Lu, F. Tournilhac, L. Leibler, Z. B. Guan, *J. Am. Chem. Soc.* **2012**, *134*, 8424–8427.

86 R. C. Osthoff, A. M. Bueche, W. T. Grubb, *J. Am. Chem. Soc.* **1954**, *76*, 4659–4663.

87 S. W. Kantor, W. T. Grubb, R. C. Osthoff, *J. Am. Chem. Soc.* **1954**, *76*, 5190–5197.

88 W. Schmolke, N. Perner, S. Seiffert, *Macromolecules* **2015**, *48*, 8781–8788.

89 T. F. Scott, A. D. Schneider, W. D. Cook, C. N. Bowman, *Science* **2005**, *308*, 1615–1617.

90 E. Banchereau, S. Lacombe, J. Ollivier, *Tetrahedron Lett.* **1995**, *36*, 8197–8200.

91 S. Ji, W. Cao, Y. Yu, H. Xu, *Angew. Chem., Int. Ed.* **2014**, *53*, 6781–6785.

92 B. T. Michal, C. A. Jaye, E. J. Spencer, S. J. Rowan, *ACS Macro Lett.* **2013**, *2*, 694–699.

93 S. Ji, W. Cao, Y. Yu, H. Xu, *Adv. Mater.* **2015**, *27*, 7740–7745.

94 M. Arisawa, M. Yamaguchi, *J. Am. Chem. Soc.* **2003**, *125*, 6624–6625.

95 R. Caraballo, M. Rahm, P. Vongvilai, T. Brinck, O. Ramstrom, *Chem. Commun.* **2008**, 6603–6605.

96 J. Canadell, H. Goossens, B. Klumperman, *Macromolecules* **2011**, *44*, 2536–2541.

97 U. Lafont, H. van Zeijl, S. van der Zwaag, *ACS Appl. Mater. Inter.* **2012**, *4*, 6280–6288.

98 M. Pepels, I. Filot, B. Klumperman, H. Goossens, *Polym Chem – UK* **2013**, *4*, 4955–4965.

99 A. Rekondo, R. Martin, A. R. de Luzuriaga, G. Cabanero, H. J. Grande, I. Odriozola, *Materials Horizons* **2014**, *1*, 237–240.

100 Z. Q. Lei, H. P. Xiang, Y. J. Yuan, M. Z. Rong, M. Q. Zhang, *Chem. Mater.* **2014**, *26*, 2038–2046.

101 T. Otsu, *J. Polym. Sci., Part A: Polym. Chem.* **2000**, *38*, 2121–2136.

102 Y. Z. You, C. Y. Hong, R. K. Bai, C. Y. Pan, J. Wang, *Macromol. Chem. Phys.* **2002**, *203*, 477–483.

103 R. Ran, Y. Yu, T. Wan, *J. Appl. Polym. Sci.* **2007**, *105*, 398–404.

104 R. Nicolay, J. Kamada, A. Van Wassen, K. Matyjaszewski, *Macromolecules* **2010**, *43*, 4355–4361.

105 C. J. Hawker, *J. Am. Chem. Soc.* **1994**, *116*, 11185–11186.

106 C. J. Hawker, A. W. Bosman, E. Harth, *Chem. Rev.* **2001**, *101*, 3661–3688.

107 H. Otsuka, K. Aotani, Y. Higaki, A. Takahara, *Chem. Commun.* **2002**, 2838–2839.

108 H. Otsuka, *Polym. J.* **2013**, *45*, 879–891.

109 H. Fischer, *Macromolecules* **1997**, *30*, 5666–5672.

110 H. Fischer, *J. Polym. Sci., Part A: Polym. Chem.* **1999**, *37*, 1885–1901.

111 F. Wang, M. Z. Rong, M. Q. Zhang, *J. Mater. Chem.* **2012**, *22*, 13076–13084.

112 C. E. Yuan, M. Z. Rong, M. Q. Zhang, *Polymer* **2014**, *55*, 1782–1791.

113 C. E. Yuan, M. Q. Zhang, M. Z. Rong, *J. Mater. Chem. A* **2014**, *2*, 6558–6566.

114 S. Telitel, Y. Amamoto, J. Poly, F. Morlet-Savary, O. Soppera, J. Lalevee, K. Matyjaszewski, *Polym. Chem.* **2014**, *5*, 921–930.

115 Z. P. Zhang, M. Z. Rong, M. Q. Zhang, C. E. Yuan, *Polym. Chem.* **2013**, *4*, 4648–4654.

116 Z. P. Zhang, M. Z. Rong, M. Q. Zhang, *Polymer* **2014**, *55*, 3936–3943.

117 Z. P. Zhang, Y. Lu, M. Z. Rong, M. Q. Zhang, *RSC Adv.* **2016**, *6*, 6350–6357.

118 M. Frenette, C. Aliaga, E. Font-Sanchis, J. C. Scaiano, *Org. Lett.* **2004**, *6*, 2579–2582.

119 J. C. Scaiano, A. Martin, G. P. A. Yap, K. U. Ingold, *Org. Lett.* **2000**, *2*, 899–901.

120 E. V. Bejan, E. Font-Sanchis, J. C. Scaiano, *Org. Lett.* **2001**, *3*, 4059–4062.

121 E. Font-Sanchis, C. Aliaga, K. S. Focsaneanu, J. C. Scaiano, *Chem. Commun.* **2002**, 1576–1577.

122 E. Font-Sanchis, C. Aliaga, E. V. Bejan, R. Cornejo, J. C. Scaiano, *J. Org. Chem.* **2003**, *68*, 3199–3204.

123 E. Font-Sanchis, C. Aliaga, R. Cornejo, J. C. Scaiano, *Org. Lett.* **2003**, *5*, 1515–1518.

124 M. Frenette, P. D. MacLean, L. R. C. Barclay, J. C. Scaiano, *J. Am. Chem. Soc.* **2006**, *128*, 16432–16433.

125 V. Filippenko, M. Frenette, J. C. Scaiano, *Org. Lett.* **2009**, *11*, 3634–3637.

126 M. Nishihara, K. Imato, A. Irie, T. Kanehara, A. Kano, A. Maruyama, A. Takahara, H. Otsuka, *Chem. Lett.* **2013**, *42*, 377–379.

127 K. Imato, A. Takahara, H. Otsuka, *Macromolecules* **2015**, *48*, 5632–5639.

128 K. Imato, T. Ohishi, M. Nishihara, A. Takahara, H. Otsuka, *J. Am. Chem. Soc.* **2014**, *136*, 11839–11845.

129 K. Imato, M. Nishihara, A. Irie, A. Takahara, H. Otsuka, *Gels* **2015**, *1*, 58.

130 K. Imato, A. Irie, T. Kosuge, T. Ohishi, M. Nishihara, A. Takahara, H. Otsuka, *Angew. Chem., Int. Ed.* **2015**, *54*, 6168–6172.

131 K. Imato, T. Kanehara, T. Ohishi, M. Nishihara, H. Yajima, M. Ito, A. Takahara, H. Otsuka, *ACS Macro Lett.* **2015**, *4*, 1307–1311.

132 K. Imato, T. Kanehara, S. Nojima, T. Ohishi, Y. Higaki, A. Takahara, H. Otsuka, *Chem. Commun.* **2016**, *52*, 10482–10485.

133 T. Kosuge, K. Imato, R. Goseki, H. Otsuka, *Macromolecules* **2016**, *49*, 5903–5911.

134 H. Oka, K. Imato, T. Sato, T. Ohishi, R. Goseki, H. Otsuka, *ACS Macro Lett.* **2016**, 1124–1127.

135 C. M. Chung, Y. S. Roh, S. Y. Cho, J. G. Kim, *Chem. Mater.* **2004**, *16*, 3982–3984.

136 L. Hu, X. J. Cheng, A. Q. Zhang, *J. Mater. Sci.* **2015**, *50*, 2239–2246.

137 P. Froimowicz, H. Frey, K. Landfester, *Macromol. Rapid Commun.* **2011**, *32*, 468–473.

138 J. Ling, M. Z. Rong, M. Q. Zhang, *Polymer* **2012**, *53*, 2691–2698.

139 S. Banerjee, R. Tripathy, D. Cozzens, T. Nagy, S. Keki, M. Zsuga, R. Faust, *ACS Appl. Mater. Inter.* **2015**, *7*, 2064–2072.

140 H. M. Klukovich, Z. S. Kean, S. T. Iacono, S. L. Craig, *J. Am. Chem. Soc.* **2011**, *133*, 17882–17888.

141 Y. L. Chen, A. M. Kushner, G. A. Williams, Z. B. Guan, *Nat. Chem.* **2012**, *4*, 467–472.

142 J. Hentschel, A. M. Kushner, J. Ziller, Z. B. Guan, *Angew. Chem., Int. Ed.* **2012**, *51*, 10561–10565.

143 Y. L. Chen, Z. B. Guan, *Chem. Commun.* **2014**, *50*, 10868–10870.

144 D. Mozhdehi, S. Ayala, O. R. Cromwell, Z. B. Guan, *J. Am. Chem. Soc.* **2014**, *136*, 16128–16131.

145 N. Oya, T. Ikezaki, N. Yoshie, *Polym. J.* **2013**, *45*, 955–961.

146 J. Fox, J. J. Wie, B. W. Greenland, S. Burattini, W. Hayes, H. M. Colquhoun, M. E. Mackay, S. J. Rowan, *J. Am. Chem. Soc.* **2012**, *134*, 5362–5368.

147 M. V. Biyani, E. J. Foster, C. Weder, *ACS Macro Lett.* **2013**, *2*, 236–240.

148 Y. L. Chen, Z. B. Guan, *Polym. Chem.* **2013**, *4*, 4885–4889.

149 S. Coulibaly, A. Roulin, S. Balog, M. V. Biyani, E. J. Foster, S. J. Rowan, G. L. Fiore, C. Weder, *Macromolecules* **2014**, *47*, 152–160.

150 C. Wang, N. Liu, R. Allen, J. B. H. Tok, Y. P. Wu, F. Zhang, Y. S. Chen, Z. N. Bao, *Adv. Mater.* **2013**, *25*, 5785–5790.

151 J. A. Neal, D. Mozhdehi, Z. B. Guan, *J. Am. Chem. Soc.* **2015**, *137*, 4846–4850.

152 B. C. K. Tee, C. Wang, R. Allen, Z. N. Bao, *Nat. Nanotechnol.* **2012**, *7*, 825–832.

153 C. Wang, H. Wu, Z. Chen, M. T. McDowell, Y. Cui, Z. A. Bao, *Nat. Chem.* **2013**, *5*, 1042–1048.

154 C. K. Gong, J. J. Liang, W. Hu, X. F. Niu, S. W. Ma, H. T. Hahn, Q. B. Pei, *Adv. Mater.* **2013**, *25*, 4186–4191.

155 H. Wang, B. W. Zhu, W. C. Jiang, Y. Yang, W. R. Leow, H. Wang, X. D. Chen, *Adv. Mater.* **2014**, *26*, 3638–3643.

10

Emerging Applications of Dynamic Covalent Chemistry from Macro- to Nanoscopic Length Scales

Joseph C. Furgal, Megan Dunn, Tao Wei, and Timothy F. Scott

10.1   Introduction

Dynamic covalent chemistry (DCvC), involving a class of covalent bond-forming reactions whose products can be rearranged or reverted back to the constituent reactants under particular reaction conditions, has many emerging applications ranging from organic electronics to molecular separations to drug delivery systems. This chapter builds on the techniques discussed in the preceding chapters by giving an overview of the use of DCvC in applications developed over the past several years across length scales from the macroscopic to the nanoscopic. In the first part of this chapter, we examine large-scale applications involving self-healing and stimuli-responsive materials, followed by applications employing nanoscale assemblies in biomedical-related fields, and the other fields where desirable attributes emerge from the well-defined, robust nanoscale structures generated by DCvC, including organic electronics, gas storage, catalysis, and separations. Finally, potential new areas of DCvC in nanotechnology are explored.

10.2   Rearrangeable Polymer Networks

Rearranging the covalent bond connectivity in crosslinked polymeric networks can afford several unique attributes that are unattainable from permanently crosslinked materials, including stress-relaxation,[1–3] shape and topography modification,[2,4] and reversible, autonomic crack-healing.[5–9] Tremendous research attention has been devoted towards achieving this third attribute (i.e., healing) in covalently crosslinked polymers in recent years owing to the potential for successful implementations to yield tremendous improvements in the longevity and reliability of structural materials. To date, crack-healing approaches in crosslinked polymers have typically utilized liquid-filled inclusions, such as capsules or channels, whose contents flow upon rupture and polymerize *in situ* to bridge the flaw interfaces,[10–12] or bond rearrangement[13–15] or transient depolymerization reactions.[16–18] These latter approaches often rely on the incorporation of dynamic covalent bonds in the backbone of these polymeric matrices

whereby network strand exchange or reorganization proceeds on activation of reversible chemical reactions. Thus, such polymeric matrices are able to respond to physical stimuli and/or chemical effectors and behave as adaptive materials.[8] Several classes of dynamic covalent bonds, including imines,[19] disulfides,[5] boronate esters,[6,7,20] and Diels–Alder (DA) cycloadditions,[16–18] have been incorporated in the network strands of crosslinked polymers to afford "dynamicity". Indeed, owing to their capacity for reversion or rearrangement, dynamic materials provide an intriguing avenue for the development of adaptive polymers which allow for reversible exchange, reorganization, or self-healing in response to physical or chemical stimuli.[8] In this section, we examine dynamic, crosslinked polymers incorporating dynamic covalent functional groups in their network strands that display responsive/adaptive and/or self-healing attributes and discuss their current limitations and how such deficiencies might be addressed.

10.2.1 Stress Relaxation and Shape Modification

Several approaches have been explored to effect stress relaxation and equilibrium, post-polymerization shape modifications in crosslinked polymers. Early work by Scott *et al.* incorporated functional groups that are able to undergo addition-fragmentation chain transfer (AFCT) in the backbone of crosslinked polymeric elastomers such that, on introduction of radical species, the network connectivity was rearranged, affording a mechanism for stress relaxation (Figure 10.1a).[1,21] Interestingly, this network rearrangement and concomitant stress relaxation only proceeded in the presence of radicals which could be introduced by photocleavage of an incorporated photoinitiator, enabling photopatterning of the stress relaxation and, in turn, the equilibrium shape of the material (Figure 10.1b–d). Moreover, as the introduced radicals recombined rapidly in the absence of irradiation, the process could be switched on and off.

Fairbanks *et al.* incorporated a water-soluble photoinitiator (lithium acylphosphinate) into a covalently crosslinked hydrogel generated by the oxidation of thiol-functionalized, four-armed poly(ethylene glycol) (PEG) to fabricate a photo-responsive hydrogel where, on irradiation, radicals generated by cleavage of the photoinitiator could break and rearrange the disulfide bonds in the network strands of the gel (Figure 10.2).[4] Overcoming the common challenges of light attenuation and low quantum yield that often hamper photoadaptable polymers, they were able to generate relief patterns in these materials by applying a normal force to the gel and irradiating it with 10 mW/cm^2 of 365 nm UV light through a photomask. On subsequent removal of the normal force, the unexposed regions recovered their original dimensions whereas the regions exposed to light remained in their deformed state, that is, the generated features were recessed relative to the rest of the gel. They also demonstrated the self-healing abilities of the hydrogel by manipulating the photoinitiator concentration to control the number of radicals formed in the sample. Moreover, if the concentration of sulfur radicals was on the same order of magnitude as the carbon and phosphorus radicals formed from the photoinitiator, the gel would break up into PEG groups. If there were considerably more sulfur radicals in the sample, disulfide exchange would occur, allowing for self-healing.

10.2.2 Reversible Self-healing

One class of dynamic covalent bond that has found recent application in self-healable polymers to rearrange the connectivity is hindered urea bonds (HUBs). Here, urea

Figure 10.1 Stress relaxation in crosslinked polymers by addition-fragmentation chain transfer. (a) The allyl sulfide group incorporated in the polymer backbone facilitates bond rearrangement via radical-mediated AFCT. (b) Schematic diagram of the mechanophotopatterning of a uniaxially deformed sample, where the AFCT-based material is stretched and irradiated through a photomask. (c) After irradiation, the material exhibits a pattern that is consistent with the pattern of the mask (scale bar = 1 mm). (d) Stylus profilometry reveals an excellent correspondence between the mask and the topographical features on the surface of the sample.[21] Reprinted with permission. Copyright 2011 John Wiley and Sons. (*See insert for colour representation of the figure.*)
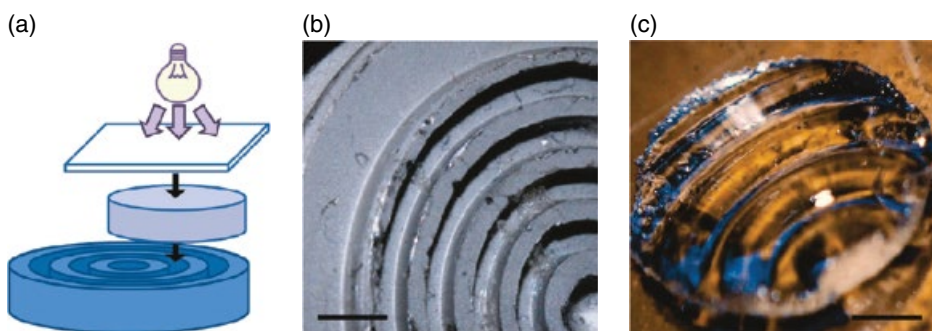
Figure 10.2 Rearranging the covalent connectivity of a disulfide-based hydrogel. (a) Schematic showing the formation of a pattern into the photoadaptable hydrogel. (b) The patterned surface, scale bar = 1.5 mm. (c) The resulting patterned hydrogel, scale bar = 1.5 mm.[4] Reprinted with permission.

groups bearing a bulky substituent on the nitrogen atom are able to reversibly dissociate into isocyanate and amine (Figure 10.3a).[9,22] Having examined several HUBs with different substituents to evaluate their binding and reaction rate constants, Ying *et al.*[9] determined that the intermediately sized 1-(*tert*-butyl)-1-ethylurea (TBEU) moiety
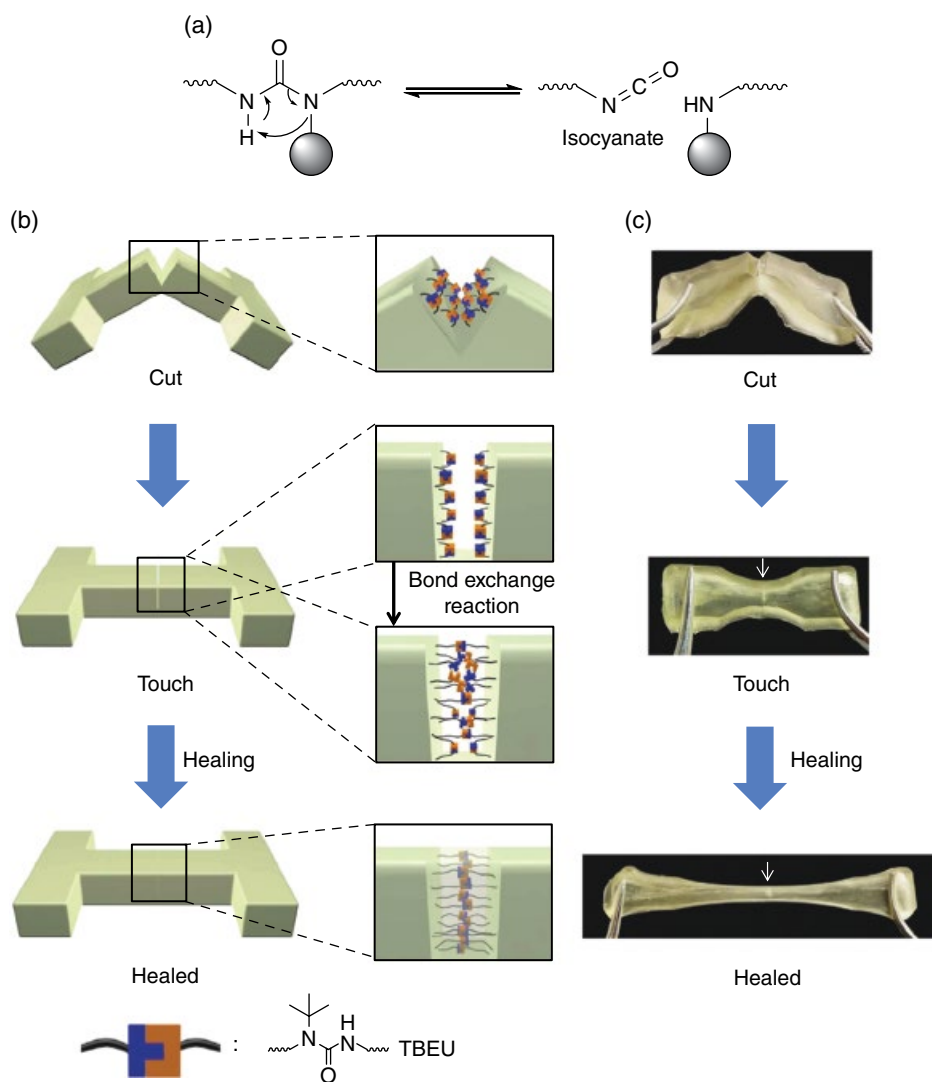
Figure 10.3 Self-healing of HUB-based materials. (a) A sterically hindered urea bond (i.e., HUB, a urea bond that has a bulky substituent affixed to one of its nitrogens) is able to dissociate to an isocyanate and a secondary amine group that are stable at low temperature but are able to co-react to reform the HUB. (b) The self-healing process of a polymer network incorporating 1-(*tert*-butyl)-1-ethylurea (TBEU) functional groups in its backbone. (c) Selected snapshots during the course of the self-healing experiment of TBEU-based poly(urethane-urea).[9] Reprinted with permission. Copyright 2014 Nature Publishing Group.

exhibited a good compromise between high binding constant and rapid forward and reverse reaction rates. Subsequently, crosslinked poly(urethane-urea)s incorporating HUBs with different *N*-substituents were prepared which exhibited elastic behavior with good mechanical strength and thermal stability, although they were susceptible to creep. The self-healing properties of these materials were further investigated and

TBEU-based materials showed particular promise owing to their advantageous balance of dynamicity and urea bond strength. These TBEU-bearing materials were able to self-heal at room temperature and recover 50% of breaking strain after 12 h of contact between the cleaved surfaces. Although more bulky *N*-substituents in HUBs afforded increased bond exchange rates, the weak bond strengths that accompanied these functional groups were undesirable for self-healing applications. HUBs provide a novel platform to synthesize catalyst-free dynamic and self-healing materials with tunable properties under mild conditions.

Another common dynamic covalent reaction used to generate self-healing materials is the condensation reaction between boronic acids and diols that affords boronic esters. Cash *et al.* incorporated dynamic boronic esters into crosslinked polymer networks and developed self-healing materials prepared via the radical-mediated thiol–ene addition reaction (Figure 10.4).[6] By simply adding a few drops of water to the freshly cut surfaces, the equilibrium of surface-exposed boronic ester groups shifted toward the dissociated state, thus generating free boronic acid and diol groups, and allowing the formation of new bridges via boronic esters along the damaged interface, enabling healing of the resultant materials to proceed at room temperature. The reversibility and dynamic exchange of boronic esters in the presence of water allowed these materials to covalently repair damage over multiple cycles at room temperature, but, much like the HUB-based materials, the reversibility of the crosslinks led to creep.

The boronate ester bond has a high bond dissociation energy (B–O bond, 124 kcal/mol) and its transesterification rate can be tuned over many orders of magnitude using simple neighboring group effects, ranging from effectively inert to extremely fast, which could be further incorporated into bulk polymer network and utilized to tune its properties. Cromwell *et al.* demonstrated the utilization of the transesterification rates of boronic esters to tune the malleability and self-healing efficiencies of bulk materials.[20] They employed two telechelic diboronic ester small molecules with variable transesterification kinetics to dynamically crosslink 1,2-diol-containing polymer backbones (Figure 10.5). The material crosslinked with fast-exchanging diboronic ester demonstrated improved malleability and enhanced healing compared to the slow-exchanging variant under the same conditions. This approach could provide materials with a variety of applications, ranging from robust self-healing elastomers to processable thermosets.

Canadell *et al.* developed self-healing materials by incorporating disulfide linkages into a covalently crosslinked rubber via a thiol–epoxy copolymerization.[5] Dynamic exchange of disulfide bonds facilitates the renewal of crosslinks across the damaged surfaces. As a result, the obtained rubber was able to achieve autonomous healing at the damaged surfaces and fully restore its mechanical properties under moderate temperature, which could be repeated for multiple iterations (Figure 10.6). Their reported approach was versatile and could be applied to enable self-healing in rubberized materials.

Pyun *et al.* reported the synthesis of stimuli-responsive, dynamic covalent copolymers via a process they coined "inverse vulcanization", where labile sulfur–sulfur (S–S) bonds were incorporated into polymer networks by the direct copolymerization of elemental sulfur (S_8) and 1,3-diisopropenylbenzene (DIB) (Figure 10.7a).[23,24] The S–S bonds in these poly(sulfur-*random*-(1,3-diisopropenylbenzene)) (poly(S-*r*-DIB)) copolymers could be reversibly cleaved by external thermomechanical stimuli (i.e., both heat and shear), as illustrated in Figure 10.7b, and the self-healing dynamics were controlled
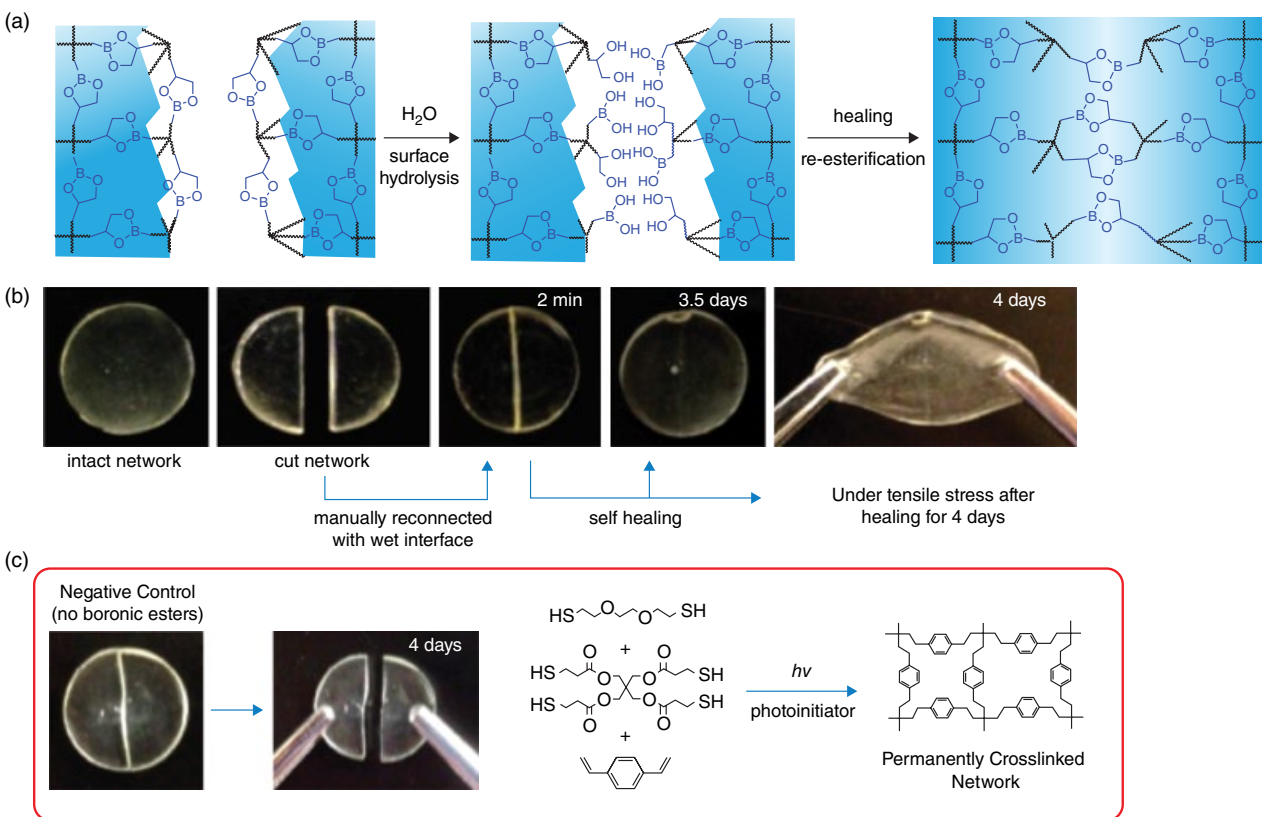
Figure 10.4 Self-healing of polymer networks incorporating boronic ester-based backbones. (a) The proposed mechanism of healing, whereby hydrolysis of surface-bound boronic esters reveals free boronic acid and vicinal diol functionalities which, on contact of the two surfaces, participate in condensation reactions to regenerate the boronic ester backbone, bridging the interface between the surfaces and thus healing the material. Note that, although the middle image suggests complete hydrolysis of the boronic esters at the surface, there may also be intact boronic esters that participate in the healing process via transesterification. (b) Photographic images of the self-healing of a boronic ester-based network formulated with a divinyl boronate ester in conjunction with a mixture of multifunctional thiol monomers. (c) Control experiment demonstrating attempted healing of a network formulated with a mixture of multifunctional thiol monomers and divinylbenzene to afford a permanently crosslinked polymer.[6] Reprinted with permission. Copyright 2015 American Chemical Society.

(a)

(b)

Fast exchange crosslinker   Slow exchange crosslinker

(c)

= Telechelic Boronic Ester   = 1,2-diol
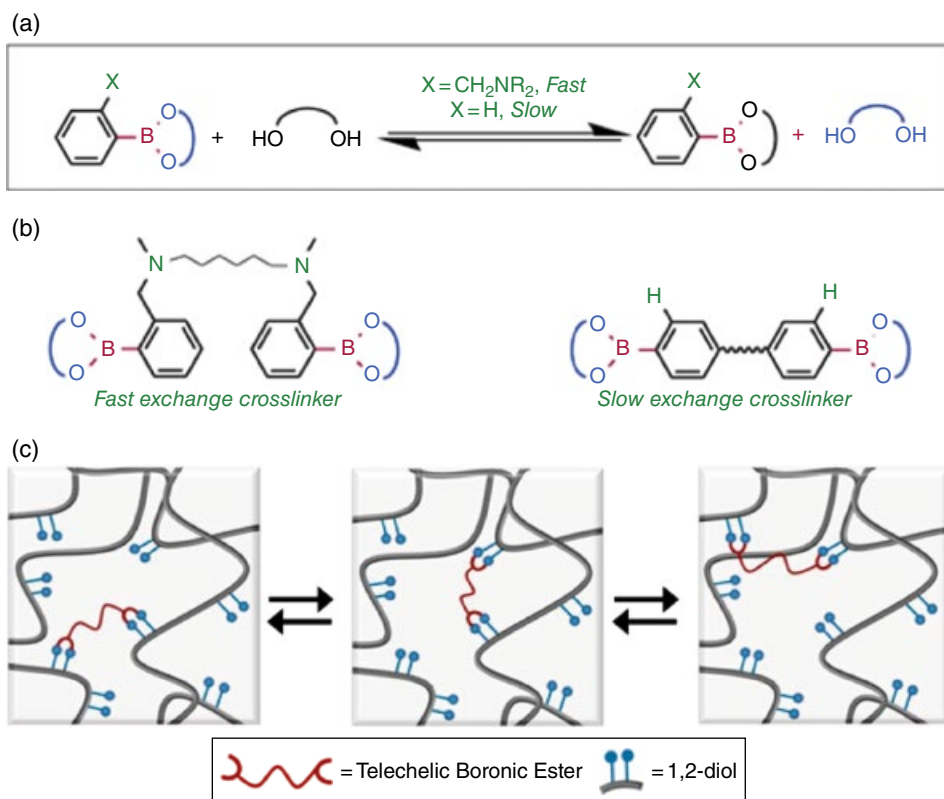
Figure 10.5 Connectivity rearrangement in a tunable, crosslinked, boronate ester-based polymer network. (a) Tuning the neighboring group to control the exchange kinetics of boronate ester. (b) Design of diboronate ester crosslinkers with tunable exchange kinetics. (c) Dynamic exchange of boronate ester crosslinkers affords dynamic materials.[20] Reprinted with permission. Copyright 2015 American Chemical Society.

(a)   (b)
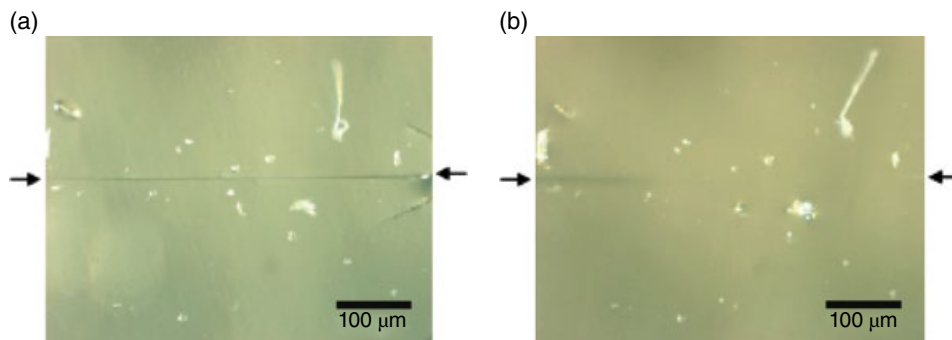
Figure 10.6 Optical microscope images of a covalently crosslinked, self-healing thiol–epoxy polymer (a) before and (b) after the healing process.[5] Reprinted with permission. Copyright 2011 American Chemical Society.
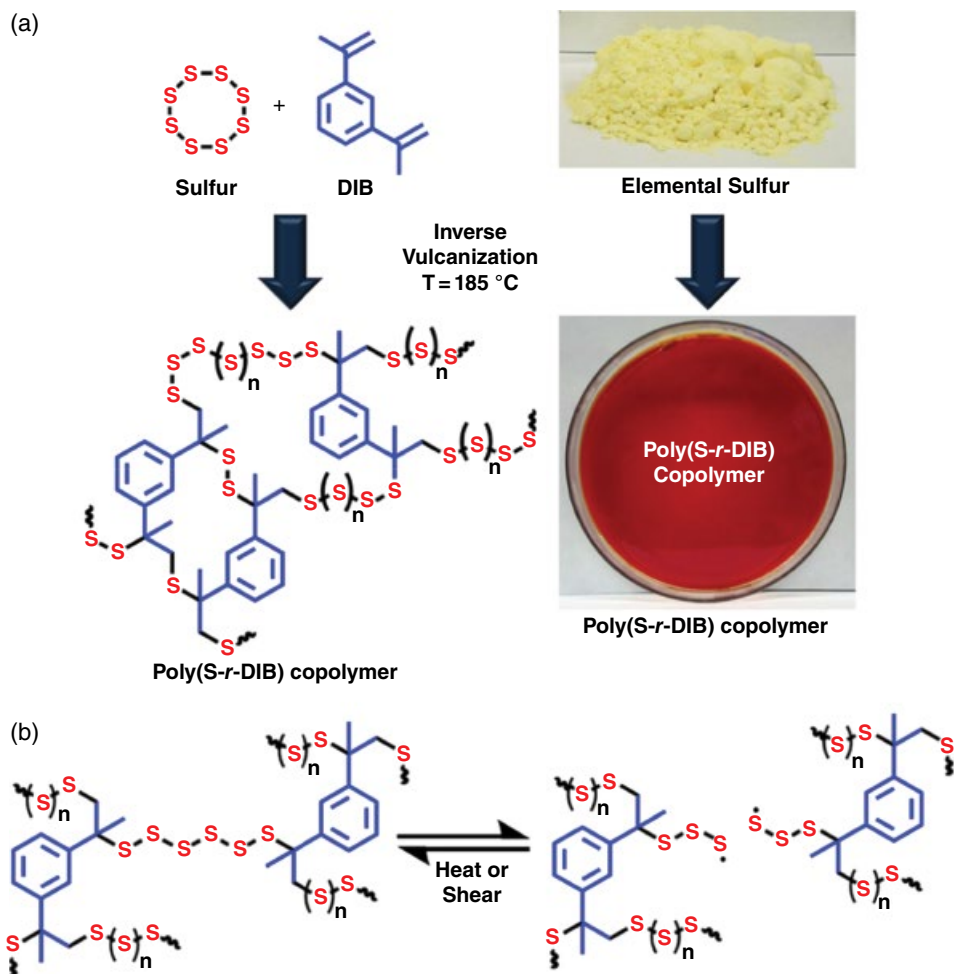
Figure 10.7 (a) Preparation of poly(sulfur-*random*-1,3-diisopropenylbenzene) (poly(S-*r*-DIB)) copolymers utilizing the inverse vulcanization process. (b) Representation of dynamic behavior under thermomechanical stimuli.[24] Reprinted with permission. Copyright 2014 American Chemical Society.

by simply varying the co-monomer feed ratios used in the copolymerization. Sulfur-rich copolymer compositions exhibited more facile reversible bond scission upon exposure to either heat or mechanical stimuli, attributable to the lower bond dissociation energies of S−S bonds in longer S−S chains, as observed in copolymer systems with well-defined polysulfide materials. The dynamic behavior in poly(S-*r*-DIB) copolymers as a function of dynamic S−S bond content was investigated in the solid state using both electron paramagnetic resonance (EPR) spectroscopy and *in situ* rheological measurements, which demonstrated a compositional dependence of the healing behavior in the copolymers with the highest sulfur content (80 wt% sulfur) affording the most rapid dynamic response and recovery of rheological properties. Furthermore, a high content of S−S bonds yielded materials with novel electrochemical and optical properties that

could be employed for high-capacity lithium–sulfur (Li–S) batteries and high refractive index polymers for infrared optics. The reported materials thus represented a new class of self-healing materials that exploited the unique properties of S–S bonds.

10.2.3 Overcoming the Limitations of Dynamic Covalent Healable Materials

Notably, all of the above approaches utilize materials with significant chain mobility and associated segmental diffusion to achieve mass transport and reaction at the damage site. A recent commentary recognized that self-healing mechanisms based on reversible, dynamic intermolecular interactions necessitate sufficient chain dynamics attainable only above T_g, and asked whether hard autonomous self-healing (supramolecular) materials might be a contradiction in terms.[25] Indeed, the example of a relatively hard self-healing thermoplastic elastomer,[25] reported by Guan *et al.*, exhibited a modulus of 38 MPa,[26] well below that of vitrified, crosslinked polymers, which typically exhibit moduli of ~1–3 GPa,[27] or even up to ~10–14 GPa for poly(hexahydrotriazine)s.[28] Of course, significant mobility is not necessary in all materials to achieve crack healing; under ultra-high vacuum conditions, and in the absence of an oxide layer the hard surfaces of some metals and other materials are able to simply adhere on contact as "there is no way for the atoms to 'know' that they are in different pieces of [metal]".[29] Although certainly attainable in elastomeric materials, despite each atom already being covalently bound to neighboring atoms, achieving analogous sub-T_g cold welding behavior in thermosets, where chain mobility is severely limited, remains an intractable problem.

As suggested above, one approach to achieve healing in rigid crosslinked polymeric materials is to simply heat the material above its T_g to afford sufficient chain mobility and effect transient and reversible depolymerization. Many examples of healable, crosslinked materials employing thermally reversible Diels–Alder cycloaddition have been developed,[16,30–32] although care to avoid irreversible side reactions from proceeding at raised temperatures should be taken with these systems.[33] Alternatively, the incorporation of thermally cleavable alkoxyamine groups in crosslinked polymers has also been examined as a route to achieve temperature-mediated healing.[34–36] Here, the C–O bonds of alkoxyamine derivatives are stable under ambient conditions but homolytically dissociate into styryl and nitroxyl radicals, and rapidly recombine on heating (see Scheme 10.1a). This temperature-mediated dynamic equilibrium facilitates alkoxyamine moieties to exchange their units intermolecularly via radical crossover reactions.[34,36,37] Yuan *et al.*[36] utilized the dynamic reversible feature of C–O bonds in alkoxyamines and developed a thermally reversible polymer with crack remendability by incorporating alkoxyamine linkages into crosslinked polystyrene as crosslinkers, which could cleave and reconnect on heating (Scheme 10.1b). The concurrent breakage of alkoxyamine linkers and recombination of resultant radicals prevent the crosslinked networks from complete disruption. As a result, the polymer network is able to retain its integrity and load-bearing capacity whenever the cracked parts are repaired.

Su *et al.* similarly examined the reversible crosslinking of alkoxyamine-bearing polymers with initially low T_g values.[38] Using a radical copolymerization of 2-ethylhexyl acrylate and two kinds of alkoxyamine-containing acrylate monomers, linear polymers bearing alkoxyamine pendant groups were successfully prepared (Scheme 10.2). On heating to 100 °C, radical exchange reactions between alkoxyamine units resulted in

(a)

Alkoxyamine

(b)
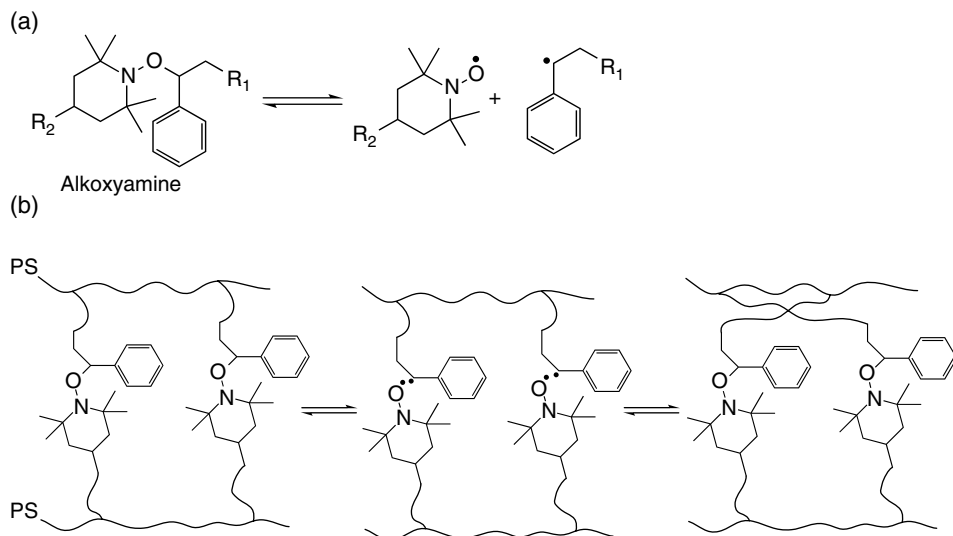
Scheme 10.1 (a) Alkoxyamines reversibly dissociate into styryl and nitroxyl radicals on heating. (b) Dynamic de-crosslinking, crossover, crosslinking, or exchange reactions of an alkoxyamine-functionalized polystyrene (PS).[36] Reprinted with permission. Copyright 2011 American Chemical Society.
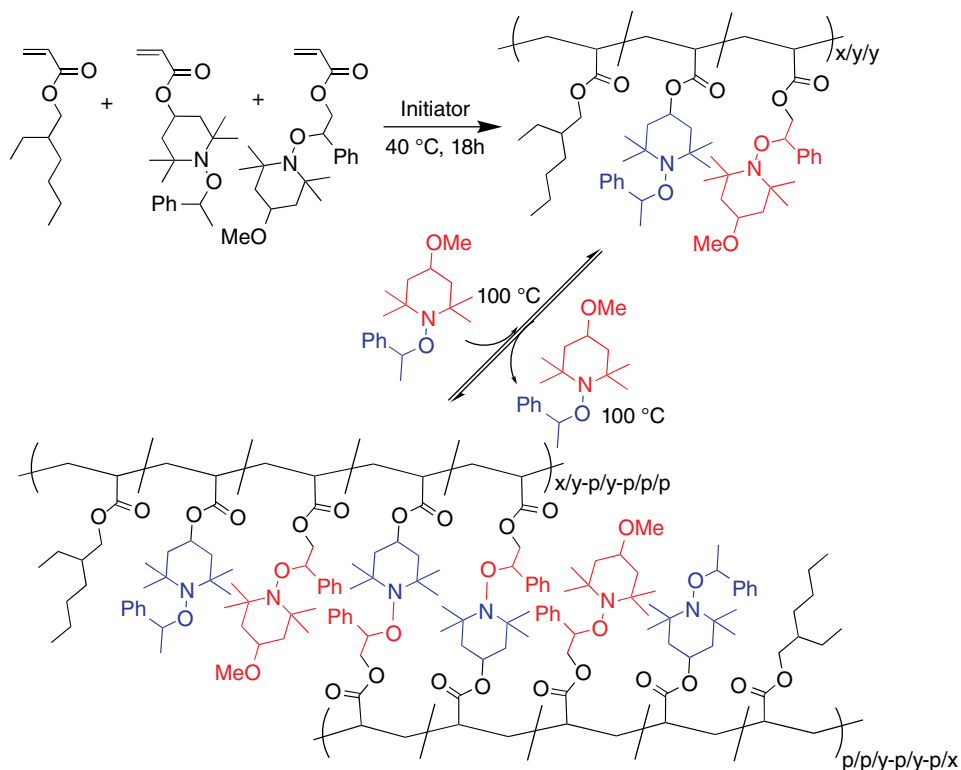
Scheme 10.2 Crosslinking and de-crosslinking reactions of alkoxyamine-appended polymers with low glass transition temperature under bulk conditions.[38]
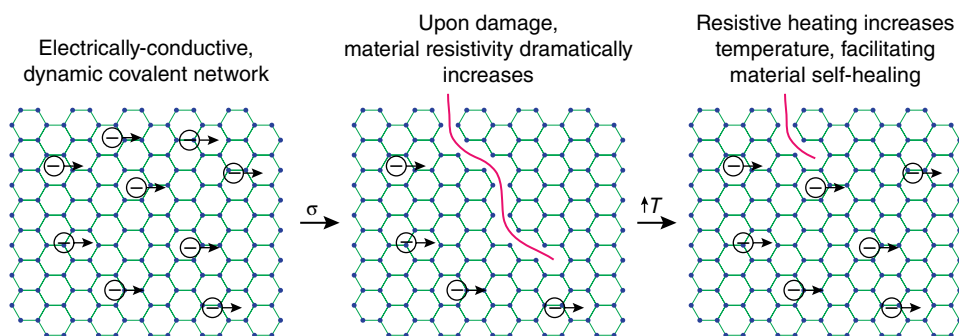
Figure 10.8 Proposed operation of an electrically conductive dynamic covalent polymeric network undergoing damage and subsequent self-healing owing to resistive heating.[39]

significant crosslinking such that the material underwent a transition from a liquid-like flowable polymer to a rubber-like polymer. Subsequent de-crosslinking was readily achieved by further radical exchange reactions between the crosslinked polymers and either an alkoxyamine-containing small molecule or stable nitroxyl radical, resulting in a transition to a liquid-like polymer. Given that radical reactions are tolerant of many functional groups, this reaction could be applied to generate stimuli-responsive smart materials, including solvent-free PSAs and thermoplastics.

Unfortunately, the above examples describing the healing of rigid crosslinked polymers necessarily require externally applied heat to heal the material on fracture, precluding autonomous healing. In contrast, Bielawski *et al.* proposed a particularly clever approach to address this deficiency of temperature-mendable polymers by running an electric current through a dynamic covalent conducting polymer (Figure 10.8).[39] Here, bond cleavage within the polymeric network owing to damage would yield an increase in electrical resistivity, resulting in significant, localized resistive heating. Sufficient heating within the material would then lead to an increase in mobility and rearrangement of the polymer connectivity, whereupon the recovery of the electrical conductivity of the now-healed polymer would reduce the resistive heating, allowing the material to cool. Although this concept has yet to be implemented, dynamic covalent conducting polymers that provide potentially useful starting points for such a self-healing system are discussed in further detail below; indeed, approaches to achieve wholly autonomous healing in rigid polymeric materials are certain to be intensively investigated over the coming years.

Another serious issue impeding the broader adoption of self-healing, dynamic covalent polymers is the network connectivity rearrangement, necessary to affect the healing behavior, which is typically accompanied by a susceptibility to creep.[6,9] A recent attempt to address this deficiency employed a hybrid polymeric network composed of Diels–Alder- and polyurethane-based components.[32] Here, the polyurethane acted as a permanent, irreversibly crosslinked scaffold while the Diels–Alder network effects self-healing upon heating. Although this successfully achieved the goal of a thermally remendable polymer network that retained its shape on heating, the fracture toughness of the healed materials typically approached 80% of that of the virgin materials.

10.3 Biotechnological Applications

The utilization of DCvC to rearrange the covalent connectivity of crosslinked polymers is typically for applications such as stress relaxation or self-healing where the structure of the polymeric materials is essentially amorphous. In contrast, DCvC is often employed to generate well-defined, nanoscopic molecular structures for biotechnological applications, a length scale necessary for the structures to interact with cells and cellular components, via dynamic covalent self-assembly. The term "self-assembly" describes processes in which pre-existing components spontaneously aggregate to form ordered structures or patterns owing to the local interactions amongst the components themselves.[40,41] Many important examples of self-assembly can be found throughout chemistry, materials science, and biology, such as the formation of molecular crystals,[42] phase-separated polymers,[43] self-assembled monolayers[44] and lipid bilayers,[45] polypeptide folding,[46] and nucleic acid hybridization.[47] Self-assembly mechanisms necessarily utilize kinetically labile molecular interactions, where a rapid equilibrium exists between the initial reactants and the potential products.[41] This characteristic affords a mechanism for error correction during the assembly process, allowing for the formation of the most thermodynamically stable product by minimization of the Gibbs energy. Thus, these self-assembly reactions effect the arrangement of components into the final desired structure via an iterative, "trial-and-error" exploration of the potential alternative configurations.

The self-assembly processes observed in biological systems are often based on weak intermolecular interactions such as hydrogen bonding, π stacking, or van der Waals interactions.[48] One consequence of the relative weakness of these transient interactions is that the assembled structures are often fragile and susceptible to mechanical degradation. Covalent bonds typically exhibit bond energies that are over an order of magnitude higher than those for hydrogen bonds[49] and could conceivably provide a route for the fabrication of far more mechanically robust assemblies. However, the creation of exquisite nanostructures by self-assembly and the toughness imparted by covalent bonds are generally perceived as mutually exclusive owing to the prevalent irreversibility of covalent bond-generating reactions. Fortunately, dynamic covalent interactions are known to be reversible under particular reaction conditions,[50–52] enabling the error correction mechanism that is essential for the selective fabrication of supramolecular structures. As a result of the enormously greater strength and directionality offered by covalent bonds in comparison to the weaker interactions observed in biology, DCvC offers an elegant approach to nanostructure assembly that combines complexity and toughness. In this section we examine the utilization of DCvC in biotechnological applications, from the direct interaction of dynamic covalent reactants with biomolecules to the generation of self-assembled nanostructures and finally to the rearrangement of macroscopic hydrogels.

10.3.1 Kinase Inhibitors

Despite its relatively low abundance in proteins, the amino acid cysteine can often be found at or near key functional sites, making it a particularly interesting residue for examining various cellular mechanisms. Importantly, cysteine is present in the active binding pocket of over 200 protein kinases, enzymes that play a regulatory role in

multiple cellular pathways. Inhibition of these cysteine-bearing kinases has proven to be a promising therapeutic method for treating different types of cancer owing to the role kinases play in the progression of various diseases.[53] This has led to the development of kinase inhibitors that form irreversible covalent bonds between acrylamide-based Michael acceptors and the active cysteine.[54] Unfortunately, these inhibitors often lack specificity, encouraging the incorporation of reversible covalent bonds that retain potency while limiting the chance of off-target interactions.[55]

Serafimova *et al.* developed a method for reversibly targeting kinases with an exposed cysteine residue in close proximity to the active site.[55] By modifying irreversible Michael acceptors with a nitrile group, they were able to elicit a reversible interaction with greater specificity for non-catalytic cysteines than the current acrylamide-based kinase inhibitors used in clinical trials. Moreover, they reported that *N*-isopropyl cyanoacrylamide was able to elicit a faster and stronger potency and the same selective inhibition of RSK1 and RSK2, two kinases with exposed cysteines involved in the pathway of regulation in MDA-MB-231 breast cancer cells, when compared to an existing irreversible inhibitor FMK.

This same group expanded on their previous study by using a fragment-based ligand design to determine the first known inhibitor for MSK1-CTD, a key activator in the pathway of various cancers.[56] They likewise utilized a reversible bond between thiol groups on cysteine residues and cyanoacrylamides as the basis for their system to produce an efficient and selective binding of the exposed cysteine in the active site of the kinase, effectively inhibiting its activity. In contrast to their earlier work, this kinase had no known inhibitor, prompting the group to synthesize a library of cyanoacrylamides that led them to the discovery of a successful inhibitor. The potency of the inhibitor was not solely dependent on the reversible covalent bond between the nitrile and the thiol, but also other specific molecular interactions necessary to inhibit the kinase. Thus, the effectiveness of the inhibitor concurrently relies on non-covalent interactions that affect the structure of the different cyanoacrylamides.

10.3.2 Micelles

Micelles have demonstrated utility in drug delivery systems largely owing to their nanoscale size range and their ability to encapsulate hydrophobic therapeutic agents.[57] Micelles can be formed by the aggregation of traditional surfactants or by the self-assembly of larger block copolymers. Amphiphilic surfactants typically comprise a hydrophilic head and hydrophobic tail, and self-assemble into micelles at concentrations of surfactants exceeding the so-called critical micelle concentration (cmc). Polymeric micelles are assembled from amphiphilic block copolymers where one block is a hydrophilic group that forms the outer shell of the micelle in an aqueous environment and the other block forms the hydrophobic core of the micelle. In addition to their size and ability to encapsulate water-insoluble drugs, micelles can be built from a large range of block copolymers that utilize different chemistries, allowing for the fabrication of polymeric micelles that can be tailored for their intended applications.[58] Dynamic covalent chemistry has been introduced to both surfactant and polymeric micelles as a method of mediating the assembly.

Minkenberg *et al.*[59] converted a non-amphiphilic surfactant comprising a polar head group with an aromatic aldehyde into an amphiphile by exposing the surfactant to an
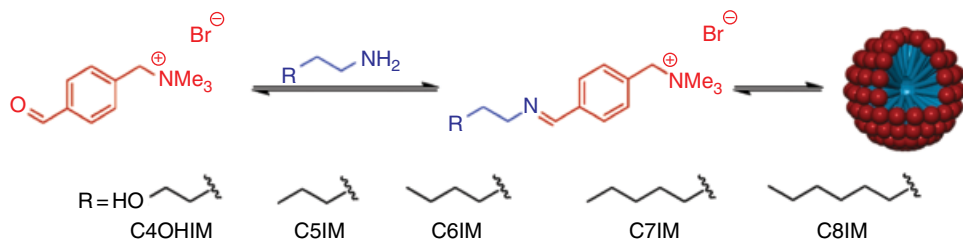
Scheme 10.3 The controlled formation of micellar aggregates from the aromatic aldehyde polar head group reversibly reacting with various amines to form an amphiphilic surfactant that can self-assemble into micelles.[59] Reprinted with permission. Copyright 2009 American Chemical Society. (*See insert for colour representation of the figure.*)

aliphatic amine that, on reversible imine bond formation by the condensation reaction between an aldehyde and an amine, left an apolar tail that could self-assemble into pH-controllable micelles (see Scheme 10.3). This allowed them to control the micelle formation by switching between the assembled amphiphilic structure to the disassembled non-amphiphilic state by manipulating the pH, shifting the equilibrium towards the reactants and thus reversing the formed imine bond. They also showed the potential utility of this technology in drug delivery systems by controlling the uptake and release of Nile Red, a hydrophobic organic dye.

Building on this work, Minkenberg *et al.* subsequently combined two water-soluble dynamic covalent surfactants containing either aldehyde or amine functional groups to generate vesicles composed of reversible imine bonds.[60] These vesicles clustered to form vesicle networks that led to pH-reversible gels, shown in Scheme 10.4, which potentially could be used as self-healing materials or as vehicles for drug delivery systems. Such self-assembling hydrogels might also serve as promising mimics for biological support structures such as the cytoskeleton and extracellular matrix.

Minkenberg *et al.*[61] continued this work by utilizing the same amine/aldehyde reaction to fabricate gemini surfactants then used those surfactants to make wormlike micelles, as shown in Scheme 10.5. Gemini surfactants are characterized by having multiple amphiphilic functional groups on each short strand. This is the first evidence of a reversible aggregation of gemini surfactants to form wormlike micelles; these so-called gemini surfactants have shown great potential in both biological applications such as gene transfection and industrial applications as viscoelastic additives for cosmetics. They formed the surfactants from aliphatic amines of various lengths and a bis-aldehyde-functionalized quaternary ammonium head group.

In contrast to the surfactant-based assembly shown above, Jackson and Fulton used reversible addition-fragmentation chain transfer (i.e., RAFT) polymerization to fabricate polymeric building blocks with aldehyde- and alkoxyamine-functionalized end groups.[35] RAFT polymerization, a controlled radical polymerization technique useful for synthesizing low-dispersity linear polymers,[62] uses a chain transfer agent (CTA) that in this case was functionalized to incorporate the dynamic covalent functional groups. The authors then used the monomers styrene, isoprene, and methyl methacrylate, and the functionalized CTAs to form polymers that they connected through a reversible bond between the aldehyde and alkoxyamine to produce a block copolymer. They further leveraged the reversibility of this reaction to control the assembly and
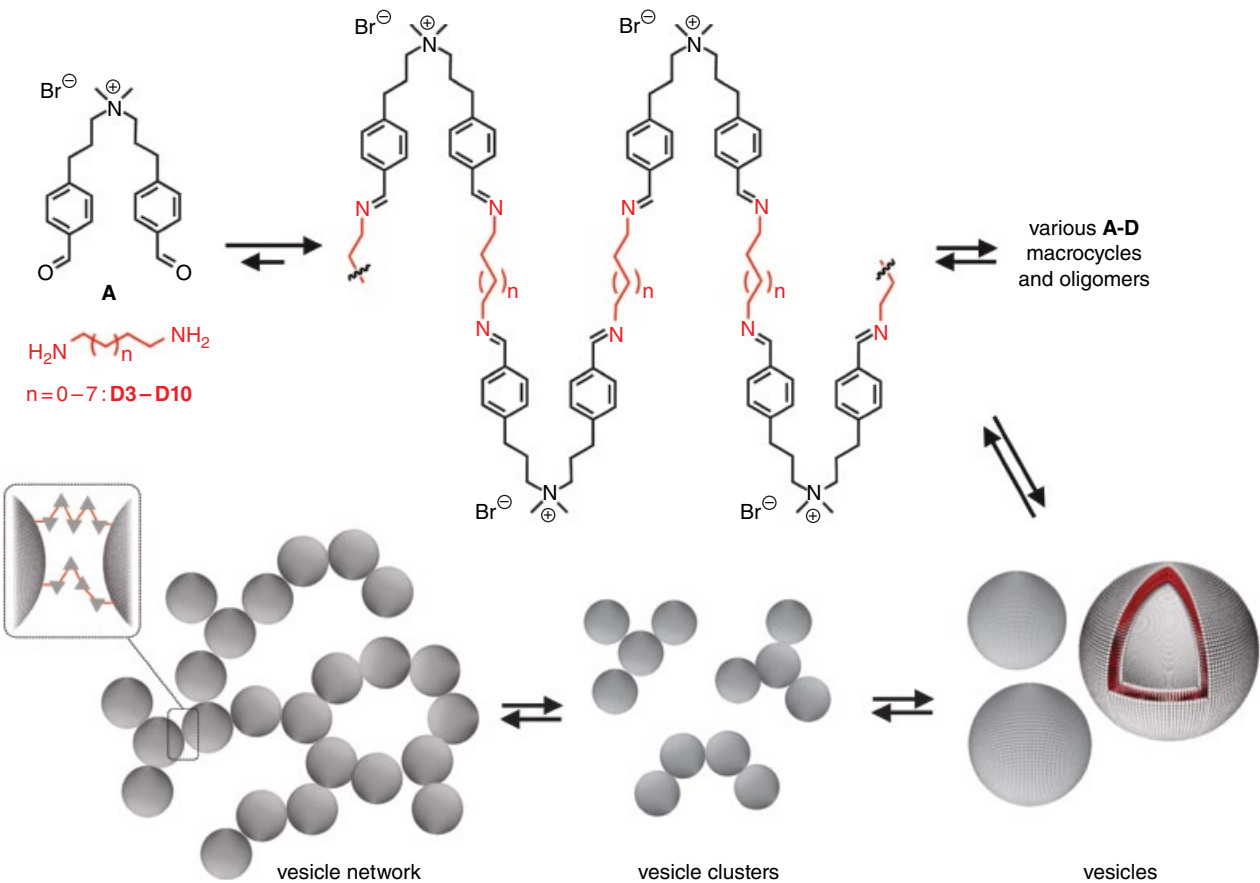
Scheme 10.4 The formation of imine bonds from difunctionalized aldehydes and aliphatic amines to form macrocycles and oligomers leading to the vesicles, clusters, and ultimately networks capable of forming pH-reversible hydrogels.[60] Reprinted with permission. Copyright 2012 Royal Society of Chemistry.
(*See insert for colour representation of the figure.*)
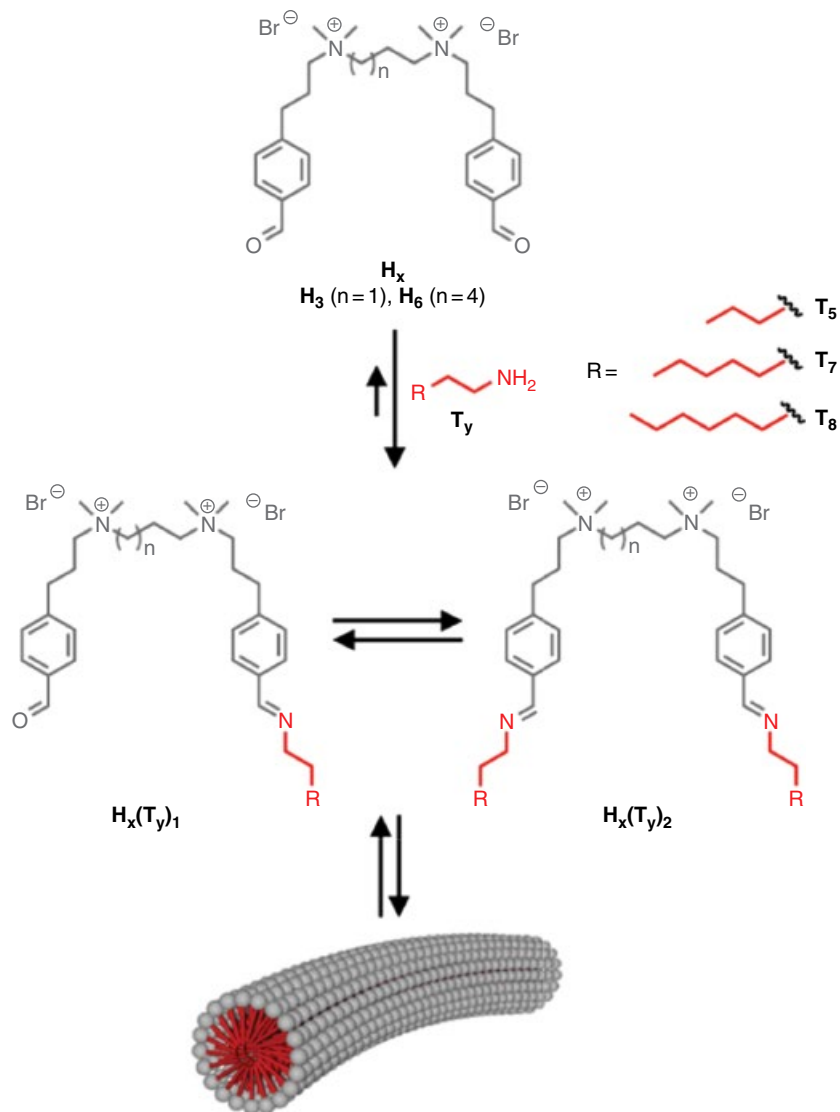
Scheme 10.5 The formation of wormlike micelles from gemini surfactants comprising a bis-aldehyde head group and amine tail groups.[61] Reprinted with permission. Copyright 2012 American Chemical Society. (*See insert for colour representation of the figure.*)

disassembly of micelles. The block copolymer that was used had blocks of polyisoprene and polystyrene that assembled micelles in organic solvents based on the solubility of the individual blocks in a given solvent. Using DMF as the solvent, they were able to form micelles that had a shell of polystyrene and core of polyisoprene. Furthermore, the micelles would disassemble by reversing the equilibrium to the aldehyde and alkoxy-amine that were used to assemble the block copolymers.

Li *et al.* used reversible disulfide chemistry to fabricate responsive crosslinked micelles that were loaded with paclitaxel (PTX), an antineoplastic agent, for controlled release at
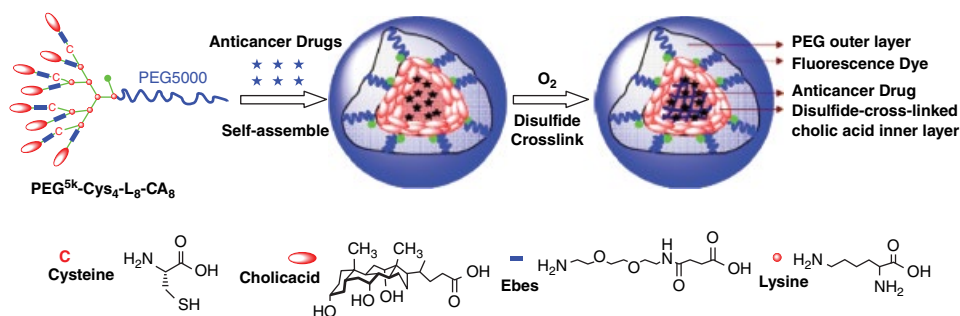
Figure 10.9 The formation of PTX-loaded micelles through disulfide bond formation.[63] Reprinted with permission. Copyright 2011 Elsevier Ltd.

tumor sites, as shown in Figure 10.9.[63] They introduced cysteine into a linear-dendritic system of polyethylene glycol (PEG) and cholic acid that was subsequently oxidized to form disulfide bonds in the core of the micelle. This crosslinked micelle had increased stability and a lower cmc than analogous non-crosslinked micelles, but the crosslinked micelles had a slower release of PTX. The authors demonstrated control over the release of the PTX by altering the amount of cellular glutathione. In animal studies, they found that the crosslinked micelles more efficiently collected and released at an ovarian cancer tumor site in mice.

10.3.3 Targeting and Transport

Dynamic combinatorial libraries (DCLs), generated from simple precursor molecules bearing dynamic covalent moieties that can react to form various larger structures through reversible bonding, are useful devices for discovering a wide range of functionalities and have proven to be appropriate for determining synthetic receptors and biological ligands.[64] Hamieh *et al.* used a DCL to determine a receptor for nicotine, a somewhat hydrophilic moiety, in water at a neutral pH.[65] The building blocks of the receptor were capable of undergoing reversible thiol–disulfide exchange and contained functional groups capable of binding with nicotine. They used these building blocks to assemble multiple structures to find a suitable receptor. Nicotine has shown potential as a therapeutic agent for different diseases; the receptor could act as a carrier where the disulfide bond could be reduced in the body.

Bhat *et al.*[66] demonstrated how DCLs have been successfully applied to biological systems using disulfide–thiol exchange reactions, but there have been limited studies showing the utility of other types of DCvC. They created a DCL with amine and aldehyde building blocks to show the utility of the reaction in binding proteins. In contrast to the *in situ* reduction methods typically used in amine/aldehyde systems, this group used aniline as a nucleophilic catalyst in the formation of stable acylhydrazones, allowing the reaction to be carried out at a biologically relevant pH.

Several membrane proteins contain glycan structures that bind to different amino acids; these saccharides are expressed differently in cancerous cells, making them ideal screening targets for early detection. Bicker *et al.*[67] incorporated boronic acid moieties into a synthetic lectin library owing to the ability of the boronic acids to reversibly react

with the diols found on the saccharides. They used this library to determine boronic acid-functionalized synthetic lectins that specifically bind with glycoproteins.

Wu *et al.*[68] developed a transport system for moving amino acids across the lipid bilayer by combining DCvC in the form of an aldehyde reacting with the amine group of a glycine residue to form a hemiaminal or imine linkage with hydrogen bonding of a carboxylate group of the amino acid to squaramide.

10.3.4 Dynamic Covalent Gels: Self-healing and Drug Delivery/Transport

Most water-soluble, functionalized nanoparticles are formed by an inverse microemulsion method that is based on lipophilic solvents yielding gels that are not suitable to encapsulate hydrophobic molecules. Ryu *et al.*[69] developed a non-emulsion method for fabrication of these nanoparticles that were incorporated into nanogels; this method allowed for the encapsulation of hydrophobic groups, as shown in Figure 10.10. They added a stimuli-responsive disulfide bond to form inter/intrastrand crosslinking in the gel formation, making this material potentially useful in drug delivery applications
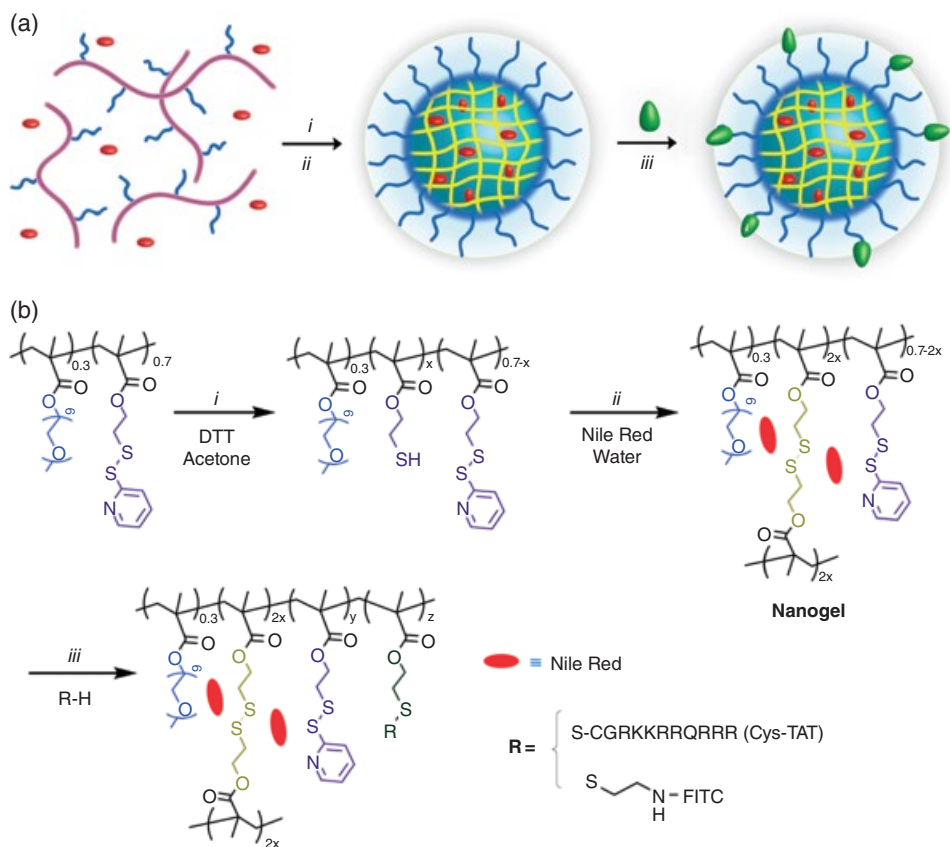
Figure 10.10 (a) The formation of a nanogel from functionalized nanoparticles and (b) structures of the nanogel, including the disulfide chemistry.[69] (i) Cleavage of specific amount of a pyridyl disulfide (PDS) group by dithiothreitol (DTT). (ii) Nanogel formation by inter/intrachain cross-linking. (iii) Surface modification of nanogels with thiolmodified Tat peptide or fluorescein isothiocyanate (FITC). Reprinted with permission. Copyright 2010 American Chemical Society. (*See insert for colour representation of the figure.*)
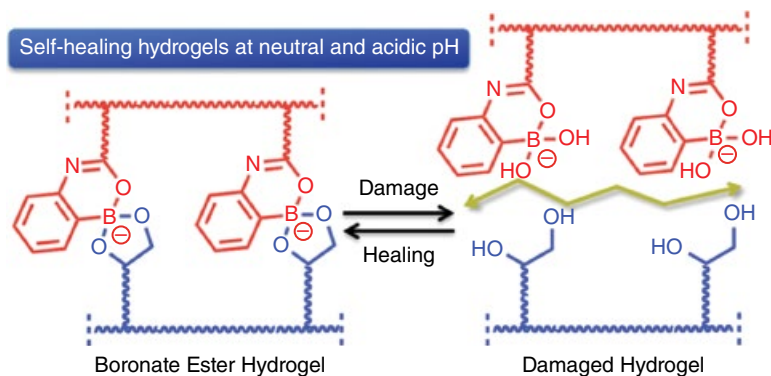
Figure 10.11 Self-healing, boronate ester-based hydrogels at neutral and acidic pH.[7] Reprinted with permission. Copyright 2015 American Chemical Society.

where the body could reduce the disulfide bond, leading to the disassembly of the nanogel and release of the encapsulated hydrophobic moiety.

Deng *et al.*[7] reported the synthesis and characterization of boronate ester crosslinked hydrogels capable of self-healing under a wide pH range from acidic to neutral (Figure 10.11). This was achieved by introducing an intramolecular coordinating boronic acid monomer, 2-acrylamidophenylboronic acid (2APBA), where the internal coordination between carbonyl oxygen and boron helped to stabilize crosslinks formed at acidic and neutral pH. Two different types of hydrogels were prepared by a 2APBA copolymer crosslinked with either poly(vinyl alcohol) (PVOH) or a catechol-functionalized copolymer. The self-healing ability of the obtained hydrogels was examined through physical and rheological studies. Rheometry indicated little dependence of pH on the strength of hydrogels and PVOH-crosslinked materials displayed greater strength as a result of higher crosslinking density. Furthermore, reduced self-healing properties, decreased stress relaxation, and minimalized creep were observed in catechol crosslinked hydrogel because of the sensitivity of the dopamine moieties to oxidation, potentially leading to gradual changes in hydrogel properties. The broader pH range at which healing can occur facilitates the potential applications of boronate ester hydrogels as biological materials. With the additional stability at lower pH, the boronate ester hydrogels are likely advantageous in acidic environments such as the gastrointestinal tract.

Acylhydrazone formation exhibits reversibility under mild conditions with acid catalysis, regenerating the starting reagents. This reversibility can be employed in the presence of additional aldehydes or hydrazides to generate new acylhydrazones owing to aldehyde or hydrazide exchange promoted by acid catalysis and/or heat.[70] Consequently, Deng *et al.* demonstrated the synthesis of a reversible polymer gel network with acylhydrazone bonds as crosslinks by condensation of acylhydrazines at two ends of a poly(ethylene oxide) (PEO) (A_2) with aldehyde groups in tris[(4-formylphenoxy)methyl]ethane (B_3) (Figure 10.12).[71] This polymer gel displays reversible sol–gel phase transition subjected to pH change in the system. On lowering the pH, the polymer gel transformed to starting polymer (monomer) solution, whereas it turned back to the gelled state on addition of base, a sol–gel transition that could be reversibly performed
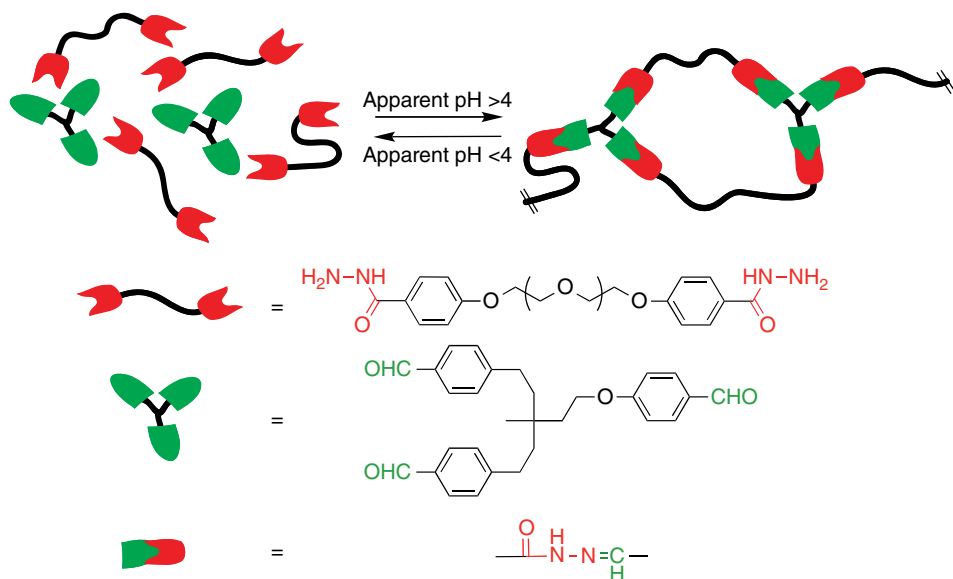
Figure 10.12 Construction of covalent crosslinked polymer gel based on reversible covalent acylhydrazone bonds.[71]

for several cycles. Additionally, this polymer gel displayed self-healing properties attributable to the dynamic and reversible breakage and regeneration of acylhydrazone bonds.

Deng *et al.*[72] further developed dynamic hydrogels with an environmental adaptive self-healing ability and dual responsive sol–gel transitions by combining acylhydrazone and disulfide linkage together in the same polymer network (Figure 10.13a). This hydrogel could spontaneously repair damage under both acidic (pH 3 and 6) and basic (pH 9) conditions via either acylhydrazone or disulfide exchange (Figure 10.13b). Nonetheless, the hydrogel was not able to self-heal at pH 7 because both bonds were kinetically locked, whereas the self-healing ability could be improved by accelerating acylhydrazone exchange with a catalytic amount of aniline. The self-healing processes of this hydrogel were proven to be effective and robust without external stimuli under room temperature. The hydrogel also illustrated unique reversible sol–gel transitions in response to both pH (HCl/triethylamine) and redox (dithiothreitol/H_2O_2) triggers. This work represents an example of incorporating additional orthogonal dynamic bonds to achieve complex and multi-responsive systems. These multi-responsive hydrogels could be applied as smart soft materials that could be used in organ repair and stimuli-responsive drug delivery.

Haldar *et al.* demonstrated the construction of self-healing gels from diblock copolymers of hydroxyethylmethacrylate functionalized with primary amine-bearing leucine pendant groups and polyisobutylene (PIB) ((P(H_2N-Leu-HEMA)-*b*-PIB)) in the presence of a PIB-based, dialdehyde-functionalized crosslinker (HOC-PIB-CHO) through imine bond formation without the help of any external stimuli (Figure 10.14).[19] These hydrogels were prepared by varying the gelator concentration, [H_2N]/[CHO] ratios, and molecular weight of the block segments in 1,4-dioxane at ambient temperature.
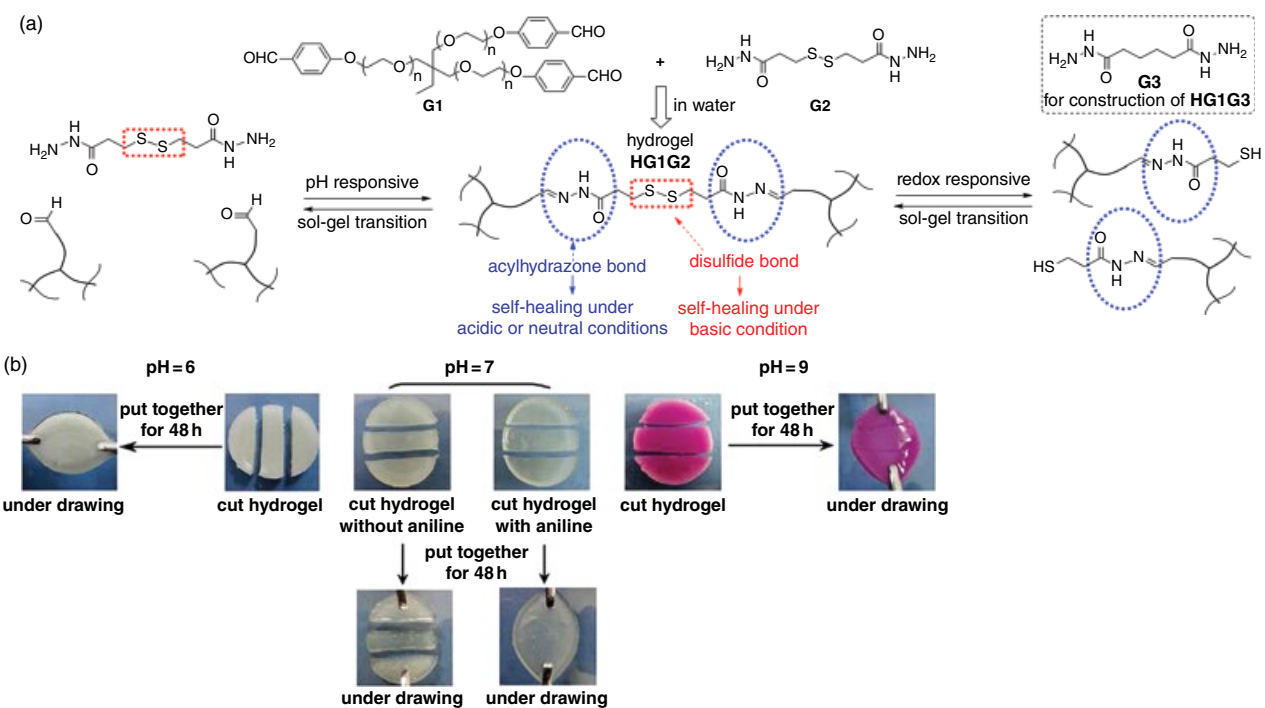
Figure 10.13 (a) Strategy for constructing a dynamic hydrogel with an environmental adaptive self-healing ability and dual responsive sol–gel transitions based on acylhydrazone and disulfide chemistry. (b) Environmental adaptive self-healing of a dynamic hydrogel.[72] Reprinted with permission. Copyright 2012 American Chemical Society. (*See insert for colour representation of the figure.*)
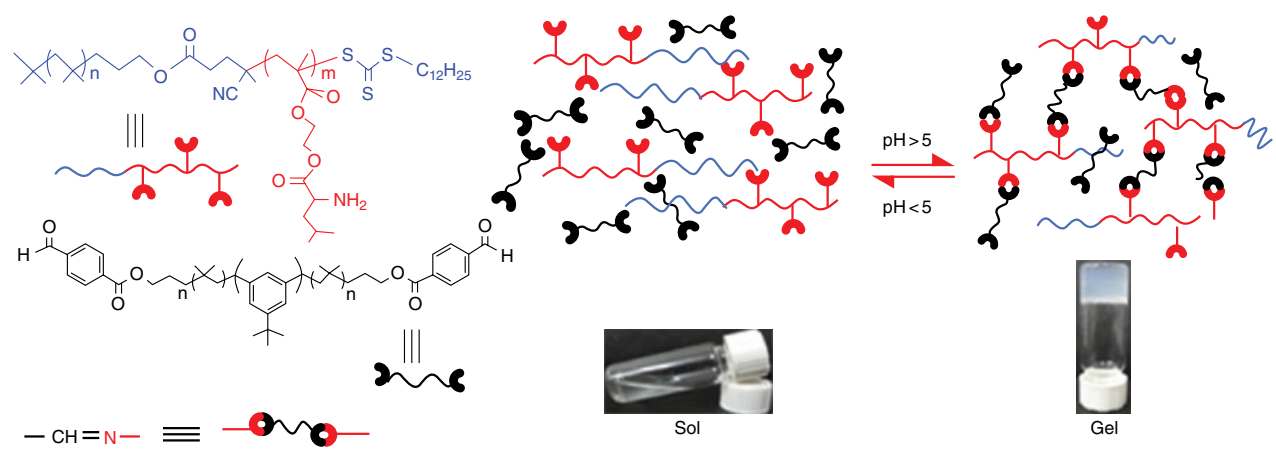
Figure 10.14 Dynamic covalently crosslinked polymeric gel synthesis from PIB-**b**-P(NH$_2$-Leu-HEMA) and HOC-PIB-CHO in 1,4-dioxane at room temperature and responsiveness toward pH.[19] Reprinted with permission. Copyright 2015 American Chemical Society.

The mechanical properties of the gels were characterized by rheological measurements. The polymeric gel network exhibited reversible sol–gel transition for several cycles by adjusting the pH of the medium on exposure to hydrochloric acid (HCl) and triethyamine (Et_3N) triggers. FT-IR spectroscopy indicated the formation of imine bonds in the gel network. The poor swelling ability of the gels implied highly interconnected networks formed during gelation, which was further confirmed by field emission-scanning electron microscopy (FE-SEM). Such pH-responsive, dynamic covalently crosslinked gels with reasonable mechanical stability provide avenues to develop smart soft materials for organ repair and pH-triggered delivery of biologically relevant materials.

10.3.5   Nucleic Acid Probes

Synthetic nucleic acid probes serve as essential tools in understanding the biological role of nucleic acids by using base pair chemistry to target particular nucleic acid sequences. Vieregg *et al*. developed a successful probe referred to as a shielded covalent probe that possesses selectivity for the desired target in the presence of competing sequences, a strong affinity towards the desired target, and robustness when employed in harsh conditions.[73] They incorporated 3-cyanovinylcarbazole, a light-activated reversible crosslinker, through solid phase synthesis into the backbone of the probe sequence such that it was shielded in a duplex allowing for complementary hybridization of the base pairs. The 3-cyanovinylcarbazole was activated with UV-A light to bind with a pyrimidine base on the target strand, a covalent linking that was reversible on exposure to UV-B light.

10.4   Other Applications

As noted above, DCvC can be employed both on macroscopic systems to rearrange the covalent connectivity of amorphous materials, enabling stress relaxation or self-healing processes, and on nanoscopic systems to generate robust, self-assembled molecular nanostructures. Of course, self-assembly is not necessarily limited to the fabrication of nanoparticulate constructs; rather, tremendously interesting and useful properties can emerge from the assembly of macroscopic structures with long-range order on the nanoscale. Here, we examine the utilization of DCvC in a variety of applications that benefit from such emergent properties, from organic electronic materials where molecular alignment is necessary for efficient charge transfer, to molecular storage, capture, and separation where well-defined porosity enables materials to discriminate between even very similar molecular species, to surface science and other applications where the reconfiguration of the covalent bond connectivity in ordered materials offers unique and useful attributes.

10.4.1   Organic Electronics

The field of organic electronic materials has rapidly adopted DCvC owing to the facile self-assembly processing and the error correction mechanisms it inherently provides. These materials range from one-dimensional graphene derived sheets to three-dimensional covalent organic framework (COF) structures, and employ many of the

usual dynamic coupling strategies, including amine/aldehyde and boronic acid/catechol condensations, as well as some novel variants and hybrids of the two. Conjugated COF-based materials have been found to exhibit relatively high electron mobilities owing to their ordered/low defect structures, approaching 10 cm^2 V^{-1} s^{-1}, ideal for molecular nanowires. Moreover, the light-harvesting potential of these materials shouldn't be overlooked, although low efficiencies, compared to more mature linear conjugated polymers, of >0.9% have been achieved. DCvC-based materials that exhibit high ionic and electronic conductivities have also been fabricated. Here we give a brief background of some of the recent developments in this application area.

Wan *et al*. reported the first example of a luminescent and semiconducting COF, consisting of a belt shape made from pyrene and triphenylene derivatives linked in a hexagonal mesoporous skeleton.[74] Their topological design was developed by condensing trifunctional monomers (hexahydroxytriphenylene) on the corners with difunctional monomers (pyrene-2,7-diboronic acid) on the edges of the hexagons. The belts were of uniform dimension throughout, with a width of ~300 nm and thickness ~100 nm. The resultant material exhibited a broad absorption over the UV and visible regions, with a single blue emission band at 474 nm resulting from the pyrene subunit by intramolecular charge transfer. Furthermore, strong fluorescence anisotropic effects were observed, suggesting that the material mediated energy transfer between components and also facilitated energy migration over the crystalline belt. On/off switching in conductivity was observed depending on the voltage bias (i.e., conductive with an electric current of 4.3 nA under a 2 V bias). This relatively high current was likely related to the highly ordered structure, and even doping with iodine increased the electric current, suggesting *p*-type semiconducting character.

Calik *et al*. developed two-dimensional COF-based materials for integrated heterojunction organic photovoltaics, allowing for a single photoactive layer.[75] Their strategy combined boronic acid/catechol-based coupling to incorporate the electron-donating ability of 2,3,6,7,10,11-hexahydroxyltriphenylene and the electron-accepting potential of 5,15-bis(4-boronophenyl)porphyrin into a single system. The two components were combined in a 2:3 ratio to form hexagonal pores within the two-dimensional network with a narrow pore size distribution, which could further stack through π–π interactions to form hexagonal columns. This material offered external quantum efficiencies of ~30% and a HOMO (−5.42 eV) to LUMO (−3.46 eV) gap of 1.96 eV, but charge recombination remained a major barrier for implementation.

Similarly, Spitler and Dichtel developed a Lewis acid-catalyzed, phthalocyanine-based COF derived from the boronic acid/catechol dynamic coupling strategy.[76] Their strategy employed the use of a phthalocyanine tetra-acetonide coupled to a 1,4-bisphenylboronic acid using BF$_3$.OEt as a Lewis acid catalyst. A square prism of alternating phthalocyanine macrocycles that then stack in an eclipsed fashion to form 2.3 nm pores parallel to the stacked chromophores was obtained. The thermal and mechanical stability, self-correcting nature by DCvC, broad-spectrum absorption over the range of 250–1200 nm with strong J-aggregates, and anticipated high photocurrent make this a promising material for organic photovoltaic devices.

Ding and co-workers developed a COF-type panchromatic material based on the co-condensation of a Ni-based metallophthalocyanine with an electron-deficient benzothiadiazole.[77] The resulting material (coined 2D-NiPc-BTDA COF) adopted a square shape with ordered π-stacking controlling the two-dimensional orientation of multiple

sheets. The addition of benzothiadizole to corners of metallophthalocyanine caused the normally hole-transporting skeleton to become an electron-transporting network. The stacked material showed broad-spectrum absorption and photoconductivity up to 1000 nm, and high sensitivity in the infrared and electron mobilities as high as 0.6 $cm^2 V^{-1} s^{-1}$.

Yaghi *et al.* also designed COFs, based on two different methodologies, with high charge carrier mobilities for electronics applications.[78] The first (COF-366) employed an amine/aldehyde Schiff base formation between tetra(aminophenyl)porphyrin and terephthaldehyde to afford square lattice materials with 20 Å hollow channels. The second (COF-66) employed the boronic acid/catechol condensation to couple tetra(boronic acid-phenyl)porphyrin with tetrahydroxyanthracene to form a square lattice of porphyrins containing anthracene spacers with 23 Å hollow channels. These materials also stacked in the AA stacking sequence or fully eclipsed, with the distances between layers being 5.64 and 3.81 Å, respectively, allowing for effective π–π interactions. The number of photo-induced charge carriers was determined by integrating the time-of-flight transient at different bias voltages, whereby it was determined that both COFs were hole carriers (p-type semiconductors) with mobilities of 8.1 and 3.0 $cm^2 V^{-1} s^{-1}$. The lifetimes of the charge carriers was ~80 μs, suggesting impressive charge separation ability which is dependent on the charge carrier mobility lifetime. For comparison, the carrier mobility of amorphous silicon is ~1 $cm^2 V^{-1} s^{-1}$, demonstrative of the impressive mobilities attainable by materials fabricated by DCvC.

Chandra *et al.* described the development of covalent organic nanosheets via mechanical delamination for a wide variety of energy applications, including conducting sheets and light harvesting.[79] This method employed solvothermal amine/aldehyde condensation reactions to form two-dimensional networks from 1,3,5-trihydroxy-tribenzaldehyde and various diamines. Although specific conduction and light harvesting studies were not investigated, the mechanical delamination procedure through grinding was effective at producing monolayer sheets by breaking up π–π interactions, ideal for large-scale processing. Furthermore, the Tyndall effect was observed for these materials in solution, showing the small particle sizes obtained were analogous to colloidal dispersions.

A stable, highly ordered, and π-delocalized COF (CS-COF) material capable of solar energy harvesting, with power conversion efficiencies of up to 0.9% under unoptimized conditions, was developed by Guo and co-workers.[80] Their methodology took advantage of a Schiff base formation between an amine (C_3-symmetric triphenylene hexamine (TPHA)) and a ketone (C_2-symmetric *tert*-butylpyrene tetraone (PT)), rather than the more typical aldehyde, allowing for the formation of conjugated heterocycles. With a Brunauer–Emmett–Teller (BET) surface area of 776 $m^2 g^{-1}$ and pore volume of 0.34 $cm^3 g^{-1}$, this material exhibited a hydrogen uptake of 1.94 wt% at 77 K and 10 bar. Although hydrogen uptake is a reasonable goal, the energy harvesting potential of this CS-COF is even more intriguing as it exhibited a hole mobility of 4.2 $cm^2 V^{-1} s^{-1}$, making it among the best hole-transporting organic semiconductors. For solar cell devices, C_{60} fullerenes were incorporated into the COF pores via a sublimation process, dispersing them evenly throughout the network, and analyzed under air mass 1.5 conditions for their solar performance (Figure 10.15). Interest in thiophene-based COF materials has also been growing owing to the known excellent hole-transport properties of thiophene-based polymers. Such thiophene-based COFs were fabricated by Bertrand *et al.* based on the condensation of thiophenediboronic acids and
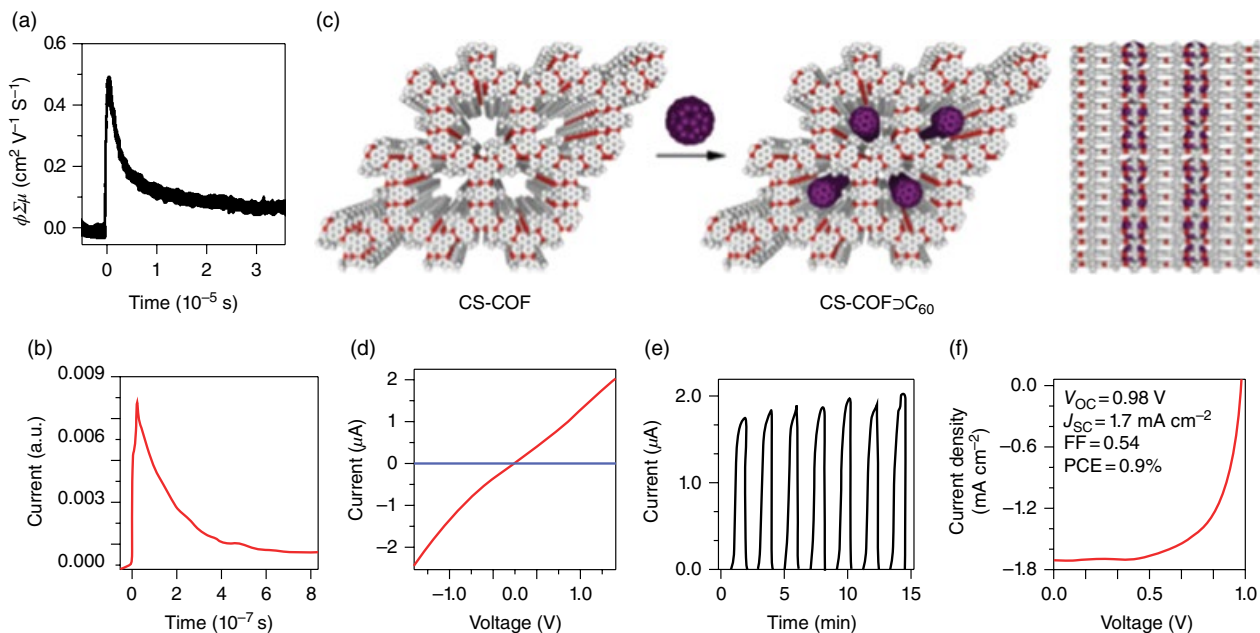
Figure 10.15 Carrier mobility and photoelectric properties of CS-COF. (a) Conductivity transient using flash photolysis time-resolved microwave conductivity methods with excitation by a 355-nm laser pulse. (b) Time-of-flight transient current integration for CS-COF with a 355-nm laser pulse at a power of 34 mJ cm^{-2} per pulse. (c) Schematic representation of synthesis of CS-COF⊃C$_{60}$ by sublimed crystallization of fullerenes in the open one-dimensional channels. A side view of CS-COF⊃C$_{60}$ is also shown. (d) I–V curve of a 50-nm thick CS-COF⊃C$_{60}$/poly(methyl methacrylate (PMMA) film sandwiched between Al and Au electrodes at bias voltages ranging from −1.5 to 1.5 V in air at 25 °C. (e) Photocurrent switching at a bias voltage of 1.5 V in air at 25 °C, with repetitive light on–off actions on the 50-nm-thick CS-COF⊃C$_{60}$/PMMA film. (f) J–V curve of the photovoltaic cell under irradiation with air mass 1.5 conditions (V_{OC} 1⁄4 0.98 V, J_{SC} 1⁄4 1.7 mA cm^{-2}, FF 1⁄4 0.54).[80] Reprinted with permission. Copyright 2013 Nature Publishing Group.

2,3,6,7,10,11-hexahydroxytriphenylene.[81] These materials were found to be prone to defects with structural variation under different synthetic conditions, but the generated structures exhibited unique charge transfer complexes, suggesting their potential for integration into organic electronic devices with appropriate redox partners.

Tanoue *et al.* developed a method of making conjugated covalent self-assembled nanoarchitectures in aqueous solutions.[82] They used a combination of amine and aldehyde units (shown in Figure 10.16) to make Schiff base macromolecular nanoarchitectures. These π-conjugated assemblies are candidate systems for molecular nanowires in nanoelectronics, as reported by Frisbie *et al.*, who examined growing conjugated Schiff base polymers from gold supports and analyzed their current flow (up to 10^{-5} A) and resistivities (up to 10^{11} ohm).[83] The authors found that the use of iodine-modified Au(111) surfaces was necessary to couple the monomers in aqueous solution, comparable to putting the monomers in an organic solvent. Dynamic, real-time imaging of covalent bond breakage and formation was achieved with high-resolution imaging, showing the clear reversibility of the process as it occurred at a solid–liquid interface rather than in solution. Ikegami *et al.* explored a similar approach using self-assembled azobenzene derivatives attached through reversible covalent siloxane chemistry to conductive surfaces for the development of reversible, optically manipulatable, superconductive materials.[84] Interest in these types of materials is for optical memory and switching applications, since they behave in an analogous way to field effect transistors (FET). The materials developed here gave control of the surface resistance by alternating between *cis* and *trans* conformations of the azobenzene derivatives, 0.50 and 0.21 ohm respectively. The reason for the change in resistance is attributed to the change in dipole on switching between *cis* and *trans* derivatives, with the *trans* derivative showing a lower overall HOMO energy level containing a lower overall interface dipole. The change in dipole due to photoisomerization changes the electron density in illuminated areas of the material. The simplicity of these methods demonstrates easy "bottom up" solid supported self-assembly of supramolecular nanoarchitectures with design on demand.

De Hatten *et al.* [85] described the approach of subcomponent self-assembly to synthesize a liner polymer capable of modulated responses to multiple stimuli. They utilized the condensation between linear diamine and dialdehyde subcomponents around a copper(I) template (Figure 10.17a) in the presence of bulky trioctylphosphine ancillary ligands and afforded a linear, conjugated polymeric material in DMSO solution. Interestingly, this polymer solution underwent sol-to-gel transition when the temperature was raised to 140 °C (Figure 10.17b), contradictory to the behavior of most gel-forming polymers, which do this on cooling. The sol-to-gel transition was attributable to the formation of $Cu^{I}N_4$ crosslinks as the equilibrium for the reaction $2[Cu^{I}N_2P_2] \rightleftharpoons [Cu^{I}N_4] + [CuP_n]^+ + (4-n)P$ favors the right-hand side at raised temperature. The direct linkage of Cu^{I} ions to conjugated polymer backbones enables enhanced electrical conductivity owing to orbital overlap. Therefore, this material also exhibited thermochromism and photoluminescence, with the color and intensity of both absorption and emission showing temperature dependence. Furthermore, this polymer demonstrated both dynamic covalent and metallo-supramolecular nature and was able to respond differently to combinations of stimuli as the application of one stimulus (thermal) modulates the material's response to another (light). This material could be potentially used for more complex and useful optoelectronic applications in the domains of electroluminescent materials and photovoltaics.
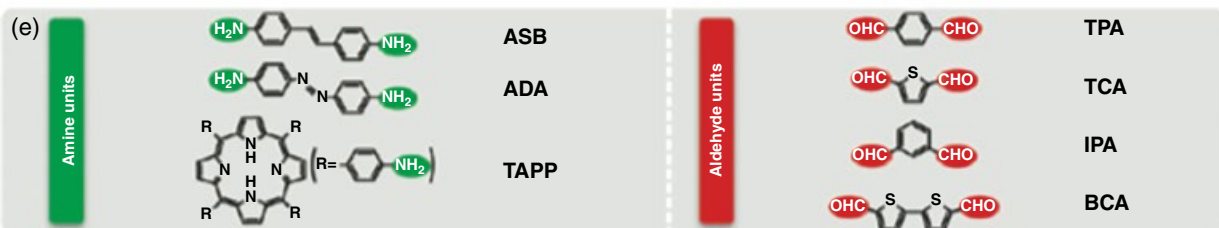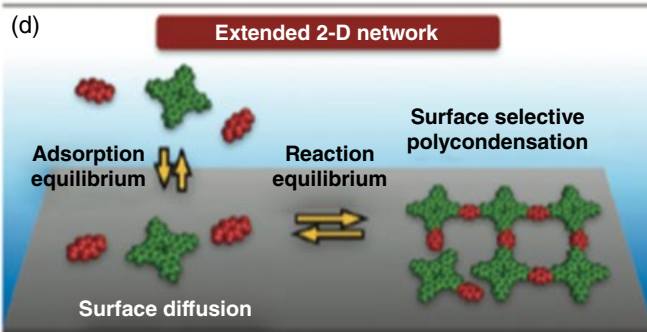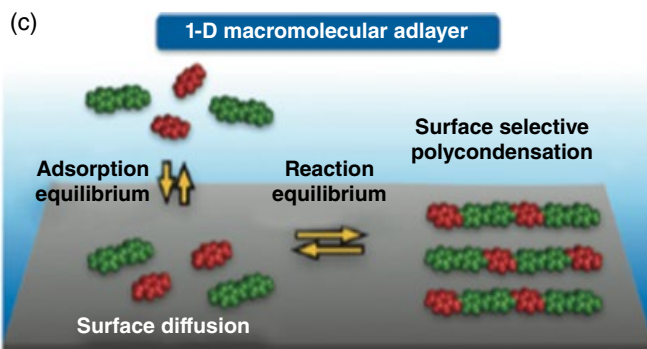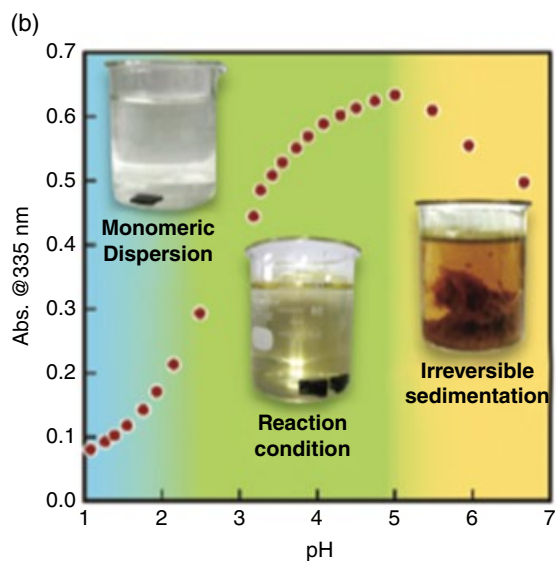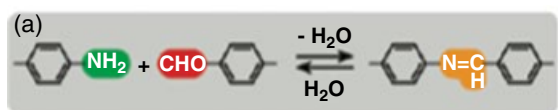
Figure 10.16 Surface templating in reversible conjugated COF systems.[82] Reprinted with permission. Copyright 2011 American Chemical Society.
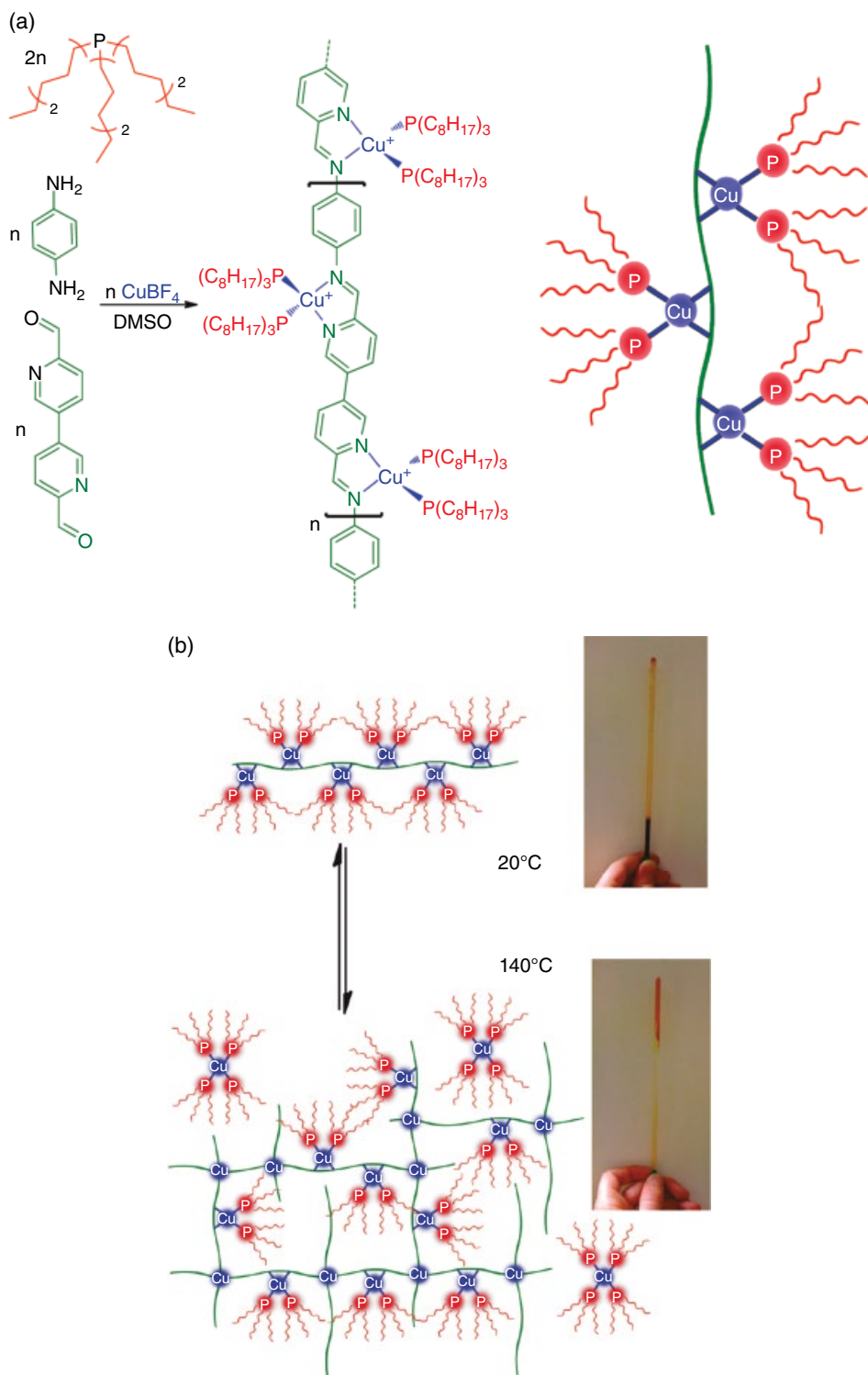
Figure 10.17 (a) The preparation of a conjugated metal–organic polymer from subcomponents (left) and its cartoon representation (right). (b) Schematic representation of the gelation mechanism (left); photographs of inverted NMR tubes showing the polymer in solution (top right) and following the sol–gel transition (bottom right).[85] Reprinted with permission. Copyright 2011 American Chemical Society. (*See insert for colour representation of the figure.*)

Xu and co-workers developed a two-dimensional COF material based on the reaction of 1,3,5-tricarbaldehyde benzene in conjunction with various diamines on a pyrolytic graphite surface template.[86] The graphite template allowed for ordering of the aromatic starting materials on the surface to form uniform, planar sheets. With templating and dynamic Schiff base chemistry, materials were made that show few defects by STM and had tunable pore sizes from ~1.7 to 3.5 nm depending on the length of the aromatic diamine backbone. The authors made an interesting observation that in some cases only two out of three aldehyde groups appeared to react owing to the spatial constraints in material growth. They also found that the growth mechanism was not clearly stepwise and instead growth happened simultaneously at separate sites, leaving the potential for defect formation on trapping. These materials appeared analogous to their graphite structure and offer potential applications in organic electronics and as nanoreactors.

In a clever approach, Bielawski *et al.* derived a series of reversible, covalent, conjugated polymers based on *N*-heterocyclic carbenes (NHCs) and bis(isothiocyanates) (see Scheme 10.6).[87] NHC-type derivatives are appealing because they allow for conservation of conjugated linkages and react with many reagents in a reversible fashion. Polymers of up to 18 kDa (PDI = 2.9) were obtained in the isothiocyanate system, while
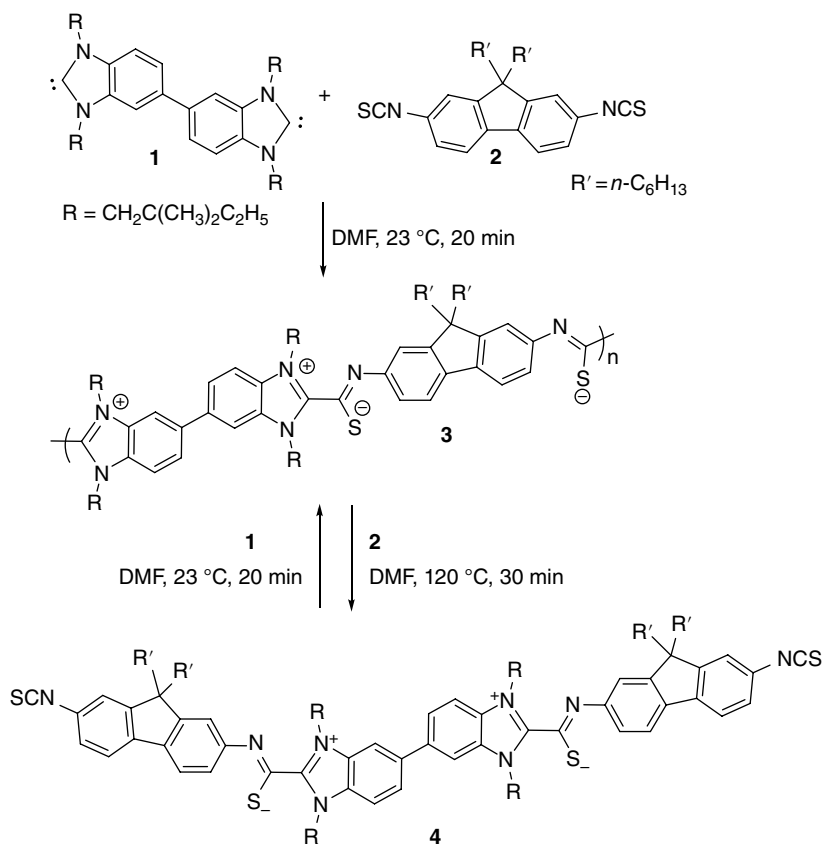
Scheme 10.6 Reversible coupling of a *N*-heterocyclic carbene/bis(isothiocyanate).[87]

addition of a thiocyanate monomer caused the polymer to rearrange, decreasing the molecular weight by more than 4 kDa, demonstrating the dynamic nature of the material. Whereas the initial polymer was not electrically conductive (10^{-10} S/cm), the electrical conductivity increased to 1.7 mS/cm on doping with iodine vapor. This series represents a novel method of making conjugated polymers by retaining the conjugation of initial monomer units, an ideal characteristic for organic-based electronics.

Ionic conductivity is also of interest in the field of organic electronics for applications in polymer membranes in ion batteries. Wei *et al.* developed a recyclable, high ionic conductivity gel using dynamic disulfide bond crosslinking.[88] A triblock copolymer was prepared in a stepwise fashion: first, RAFT polymerization was used to copolymerize styrene and 4-vinylbenzyl chloride into a triblock copolymer, then the chloride groups were replaced by azides and finally the azide groups were functionalized with *O*-ethyl-*S*-prop-2-ynyl to form sites for disulfide bridge crosslinking. The disulfide bridges could be broken up by using a mild reducing agent, and reform the ionic gel after solvent removal and oxidation of the thiol groups. Ionic conductivity measurements were measured by AC impedance over the frequency range $1–10^5$ Hz and 10 mV, and conductivities of ~7 ms/cm were achieved after an averaging of two reduction and oxidation cycles. Zhang *et al.* also developed ion-conducting COFs through ionic spiroborate formation. The polymer enabled the transportation of lithium ions with room temperature lithium ion conductivity of 3.05×10^{-5} S·cm^{-1} and an average Li$^+$ transference number value of 0.80 ± 0.02.[89]

10.4.2 Gas Storage/Capture

Network polymeric materials such as COFs have been gaining attention in the area of gas storage and capture owing to their high surface areas, low defects, tunable pore sizes, and affinities for many common and industrially relevant gases, including hydrogen, methane, and carbon dioxide. These materials can then find uses in energy storage and capturing CO_2 for storage or conversion to useful products from fossil fuel combustion. The introduction of DCvC methods into the development of COF materials has allowed for further reduction of defects, assembly/disassembly by altering material environment, and the ability for captured gases such as CO_2 to be directly attached/detached from the COF surfaces through covalent interactions.[90,91]

Yaghi *et al.* have developed a series of COF networks that show promise as hydrogen storage materials.[92] These materials are based on boronic acid/catechol dynamic covalent chemistries by combining tetra-boronic acid phenyl methane/silane (TBPM/TBPS), di-boronic acid benzene (BDBA), and 2,3,6,7,10,11-hexahydroxytriphenylene (HHTP). Hydrogen uptakes of up to 10 wt% were achieved with both TBPM/HHTP and TBPS/HHTP systems, and the best volumetric uptake was 40.4 g/L for TBPM boroxanes. In another example, Furukawa and Yaghi developed a series of COF materials, as shown in Figure 10.18.[93] These materials were based on two distinct dynamic bonding motifs to synthesize materials in two and three dimensions. They found that group 3 COF materials with three-dimensional structure have the best overall behavior for gas storage. For example, COF-102 offered gas uptake at 35 bar of 72 mg/g of hydrogen at 77 K, 187 mg/g at 298 K for methane, and 1180 mg/g at 298 K for carbon dioxide, placing these COF materials into a gas storage capacity class similar to that of metal organic frameworks (MOFs) and among the best adsorbents for hydrogen, methane, and carbon dioxide.
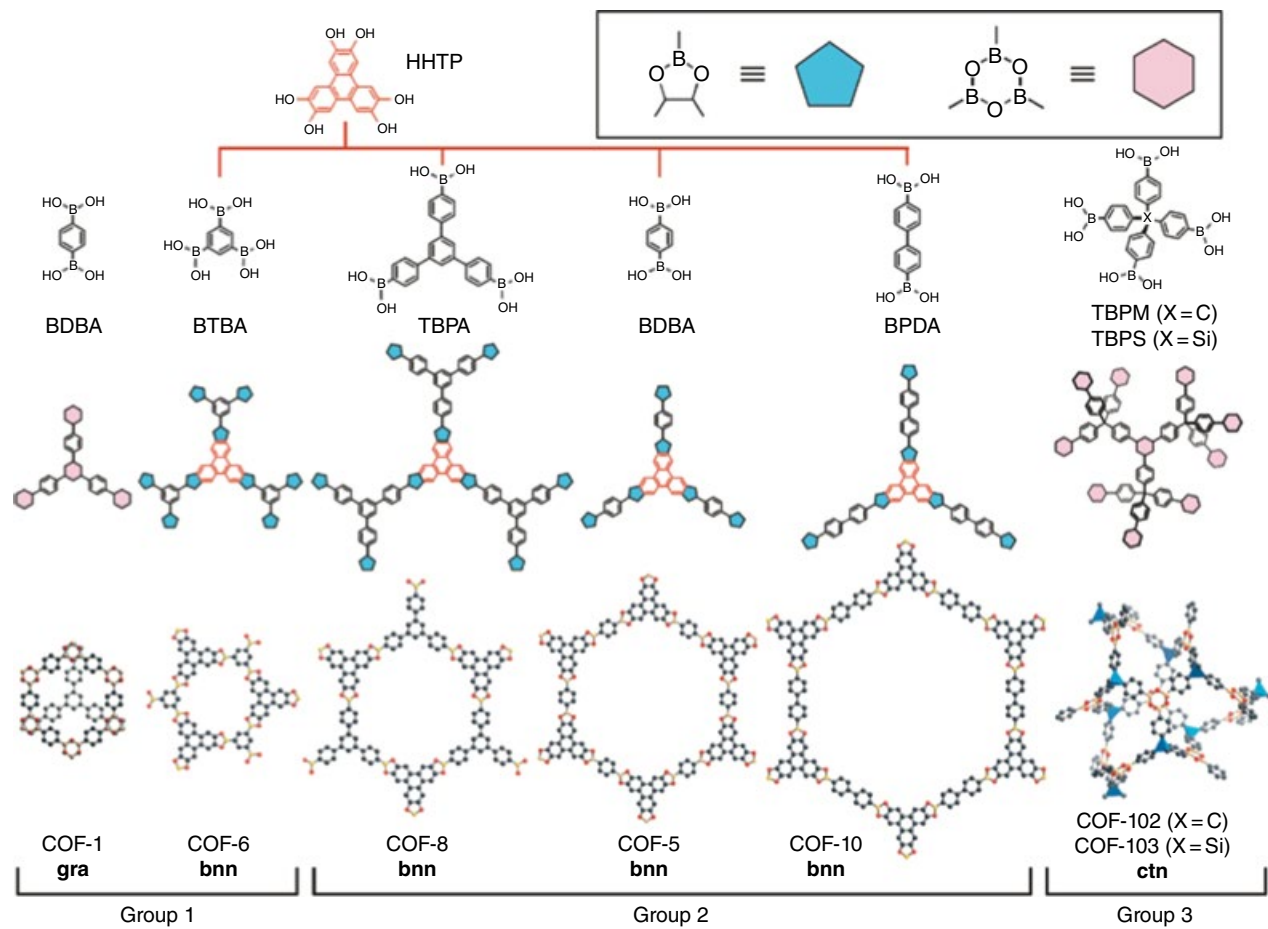
Figure 10.18 COF systems synthesized by implementation of boronic acid/catechol coupling strategies.[93] Reprinted with permission. Copyright 2009 American Chemical Society.

Building on the work of the Yaghi group, Goddard *et al.* designed a group of methane storage materials based on the COF-102 and COF-103 backbones with varying side chain functional group alterations to adjust pore sizes and gas molecule "solubility" parameters.[94] They used theoretical Monte Carlo and molecular dynamics simulations to study the methane uptake of various proposed materials, finding that COF-102-Ant, COF-102-Eth-trans, and COF-103 Eth-trans all exceed the US Department of Energy methane storage mandate of 180 v/v at room temperature and 35 bar.

A series of two-dimensional mesoporous COF materials based on imine Schiff base formation for high-pressure gas storage have been developed.[95–97] For example, El-Kaderi used the co-condensation of 1,3,6,8-tetrakis(*p*-formylphenyl)pyrene and *p*-phenylenediamine to form a two-dimensional network with hydrogen uptake at 35 bar at up to 24 mmol/g, 29 mmol/g for CO_2 and 10 mmol/g for methane. Again building on the work of Yaghi and El-Kaderi *et al.*, Zeng *et al.* developed a COF system using two different types of dynamic covalent chemistries through an orthogonal reaction approach (boronic acid/catechol and Schiff base imine) to synthesize high-porosity materials with high H_2 adsorption capacity.[98] Using 4-formylphenylboronic acid (FPBA), 1,3,5-tris(4-aminophenyl)-benzene (TAPB), and 2,3,6,7,10,11-hexadyhydroxytriphenylene (HHTP), they were able to control the condensation procedure to favor particular reaction sequences to obtain different shapes and sizes of two-dimensional COF materials. One material, NTU-COF-2, achieved a surface area of 1619 m^2/g with a pore volume of 0.86 cm^3/g. Gas storage uptake measurements on this material revealed 1.55 wt% or 174 cm^3/g at 1 bar and 77 K for hydrogen and 10.2 wt% (51.8 cm^3/g) of CO_2 at 273 K and 1 bar.

In a variation of bonding, a series of borazine-linked, COF-based materials were synthesized for gas storage using the thermal decomposition of 1,3,5-(*p*-aminophenyl)-benzene-borane to generate materials with surface areas of 1178 m^2/g, thermal stabilities at temperatures exceeding 400 °C, and hydrogen uptake of up to 2.4 wt% at 77 K and 15 bar.[99]

10.4.3 Catalysis

Catalysis is an ever-growing area of chemistry, from developing new reactions to making known reactions more efficient. One of the key methods for making catalysts more efficient is by reducing the entropy component in the reaction by binding the catalyst and substrate within close proximity to each other, thus reducing the overall reaction energy requirement.[100] One of the methods is to introduce reversible covalent interactions between substrate and catalysts, inducing intramolecularity and thus increasing reaction rates. Some of the common systems involved in reversible covalent bonds are those of *N*-heterocyclic carbenes, iminium and enamine, carbonyl, boron, various organometallic and enzyme catalysts. Our focus here will be on developments of organic-based reversible catalytic systems.

One particularly interesting class of reversible catalysis is that incorporating boron, since boronic acids easily undergo rapid exchange under protic conditions. Hall *et al.* have reported that 2-iodophenyl boronic acid is a highly effective catalyst for the amidation of carboxylic acids under ambient conditions.[101] More importantly, boron catalysis has the ability to catalyze the formation of C–C bonds. Hall and co-workers also developed a strategy to catalyze a variety of Diels–Alder type cycloaddition reactions containing acrylic acid derivatives.[102,103] For example, they found that acrylic
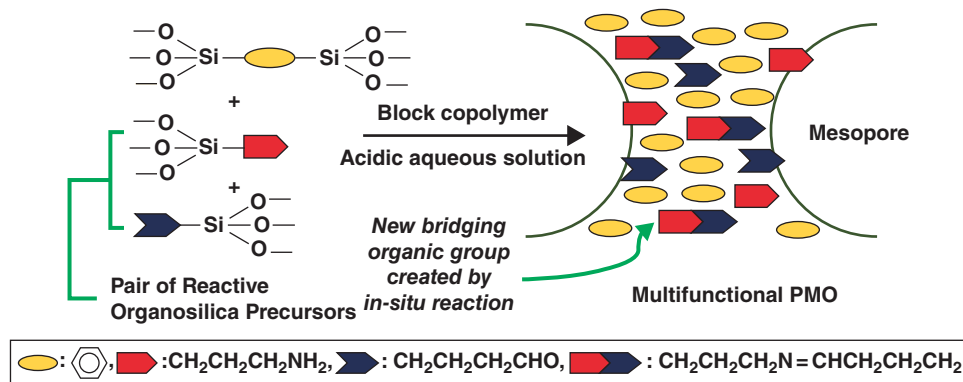
Figure 10.19 Synthesis of mesoporous organosilicas by Schiff base formation.[107] Reprinted with permission. Copyright 2010 Royal Society of Chemistry.

acid reacts selectively with diene substrates over the corresponding esters. The covalent bonds made between the boron catalyst (2-iodophenyl boronic acid) and the carboxylic acid led to the formation of a Brønsted activated intermediate, which caused an increase in the reaction rate of the Diels–Alder reaction.[101] Tandem Diels–Alder and amidation reactions have also been observed. Taylor and Whiting have shown that 2-iodophenyl or diphenyl boronic acid are effective at catalyzing direct aldol additions.[104,105]

Silica nanoparticles are easily functionalized with high potential for molecular separation and/or immobilization of various biological molecules, such as enzyme-based catalysts.[106] As an example, Karimi *et al.* used 50 nm amine functionalized silica nanoparticles modified with a di-aldehyde to reversibly immobilize inulinase, a key enzyme in the catalytic hydrolysis of insulin and the production of high-fructose corn syrup, through Schiff base formation. By attaching the enzyme to the nanoparticle substrate, the enzyme showed higher thermal stability than the free enzyme and retained up to 80% of the activity of the free enzyme after attachment. The optimum temperature of operation of the bound enzyme increased by 15 °C over the unbound enzyme, with the fully crosslinked system giving the best overall cycle performance. This increase in operating temperature and crosslinking ability makes this catalyst system better suited for industrial use.

Cho *et al.* described the synthesis of periodic mesoporous organosilicas (PMO) bridged by Schiff base formation (Figure 10.19).[107] These materials were synthesized using PEO-poly(lactic acid-*co*-glycolic acid)-PEO as a template under acid hydrolysis conditions to form PMOs from 3-aminopropyltriethoxysilane (APTES) as the amine source and triethoxysilyl butyraldehyde (TEBA) as the aldehyde source. Surface areas of up to 790 m^2/g and accessible pores of ~8 nm were achieved. Bifunctional PMOs containing converted acid (–COOH) and base (–NH$_2$/NH$_3^+$) groups within the mesopore walls were prepared by post-synthetic oxidation with potential applications in cooperative catalysis (e.g., for asymmetric synthesis).

10.4.4 Molecular Separations

One of the persistent challenges for the chemical industry is the ability to effectively separate materials on large scales or those that possess very similar properties with only a difference in chirality. Many methods have been developed for these types of

separation, namely intramolecular interactions, but few have effectively used dynamic covalent chemistries to aid in high-quality and high-purity separation. Siegel *et al.* have been pioneers in this field, developing a series of separation techniques using reversible boronic ester formation, thiol–disulfide exchange, and reversible hydrazone formation for targeting groups such as diols (i.e., sugars, catechols), thiols (cysteinyl), and carbonyls.[108] Some DCvC-based techniques and separation materials are discussed below.

One of the growing areas in molecular separations is in chiral separation materials. Xu *et al.* developed a method of synthesizing a chiral nanocube by edge-directed DCvC.[109] Their method relied on Schiff base formation between 1,4-diamino benzene, used as a bridge, and C_3-trialkoxy-triformylcyclobenzylene, forming chiral corner caps, in a 3:2 ratio to afford chiral nanocubes. The chirality of these materials gives them potential for uses as chiral separation materials based on both intramolecular interactions as well as a molecular encapsulant.

Efficient carbon dioxide capture/separation is an ongoing societal challenge. To address this challenge, Leclaire *et al.* proposed a dynamically crosslinked material based on amine/aldehyde Schiff base formation which relied on the disruption of the imide bond and interaction of the free amine with CO_2 to form ammonium carbamate derivatives at room temperature, and the ability to release CO_2 from the material on heating.[110] They found that up to 20% by mass CO_2 was incorporated into the material as a guest compound. Furthermore, besides CO_2 capture, the authors suggested that CO_2 could be used as an efficient building block in DCvC methods, and as an auxiliary for the purification of polyamine and polyaldehydes from homologous mixtures. Using a similar methodology, Corriu *et al.* employed the reversible binding potential of CO_2 as an assembly agent for amine functionalized organosilicas.[111] Although the application described in the paper for the CO_2 capture was for a coupling agent, the strategy described could be implemented as a reversible process for capturing CO_2 by forming carbamate salts and the subsequent release of trapped CO_2 upon heating.

Dendritic polymers are attractive materials for molecular separations due to their spherical shape and high number of terminal functional groups. Polikarpov *et al.* developed a maltose-modified hyperbranched poly(ethylene imine) (PEI-Mal) as a dynamic covalent coating and pseudo-stationary phase for capillary electrophoresis separation methods.[112] Four proteins (albumin, lysozyme, myoglobin, and insulin) were investigated against the effects of pH, polymer concentration, and density of the maltose shell on separation, with pH affecting the protonation of the polymer and thus the overall separation ability, and density changing the electrophoretic mobility. High repeatability and improved separation were achieved in separating proteins with PEI-Mal as a dynamic coating. For concentrating proteins, PEI-Mal was covalently coated and used in conjunction with large-volume sample stacking (LVSS) and field-enhanced sample injection (FESI) to concentrate proteins with up to a 1320-fold enhancement. The low detection limit (100–500 ng/ml) allowed for the analysis of albumin levels in blood and urine directly.

10.4.5 Surface Science

Surface immobilization of proteins is a key component to better understand many biomedical and biotechnological problems. A major challenge in this field is maintaining site-specific spatial control over the immobilization. Yang *et al.* were able to control the immobilization of proteins on a surface by functionalizing a ferrocene with a cysteine

group and then coupling that species to a thioester-functionalized yellow fluorescent protein.[113] The protein was added site-specifically to a β-cyclodextrin self-assembled monolayer (βCD SAM) on a gold slide. Initially, they utilized monovalent variants comprising the functionalized protein that had a weak binding to the βCD SAM, but the introduction of disulfide chemistry to create a divalent variant increased the binding affinity. This study resulted in the immobilization of proteins with a uniform thickness of one protein.

Thongsomboon *et al.* developed a method for nanoprinting patterns into films that utilized a thermally reversible Diels–Alder reaction between a maleimide and furan as a crosslinker.[114] They incorporated furan-protected maleimide and furanyl groups into cyclic carbonates that underwent an alcohol-initiated ring-opening polymerization to form random copolymers. They spin-coated the polymer onto silicon wafers to produce a film capable of thermal crosslinking. The crosslinking proceeded by first removing the furan protection, leaving the exposed maleimide by heating the film for 1 h at high temperature (130 °C) and then lowering the temperature (90 °C) to allow the Diels–Alder adduct to form. They used the reversibility of the crosslinking reaction to form patterns on the film from a master template by raising the temperature to break the crosslinking and lowering the temperature to reform the adduct in the desired shape (see Figure 10.20a); atomic force microscopy was used to image the imprinted patterns on the films (Figure 10.20b–e). These biodegradable films could find utility in applications in biomedical surface coatings where the carbonate group could be functionalized for specific cellular interactions.

To overcome the limitations of non-reversible covalent bonding strategies to afford self-assembled monolayers (SAMs), Tauk *et al.* demonstrated the possibility of tailoring the functionalization of surfaces with a DCvC-based selection processes by controlling the molecular composition of SAMs in space and time from a set of dynamic constituents that can be anchored selectively through pH modulation.[115] This was demonstrated with a model system where either a quartz plate or silicon wafer, silanized with a triethoxysilane aldehyde to afford an aldehyde-coated surface, was immersed in a solution of compounds bearing different types of primary amine functionalities (i.e., aromatic or aliphatic) (see Figure 10.21). Subsequently, the plate (or wafer) was slowly withdrawn from the immersate solution while the solution pH was varied by controlled addition of acid or base. Owing to the variation in pK_a of the primary amines, this approach successfully yielded dynamic covalent SAMs, termed "DynaSAMs" by the authors, with gradient chemical compositions. Approaches such as this one will certainly lead to the design of active surfaces and interfaces able to reconfigure their chemical constituents in response to environmental parameters.

Photolithography is an important area of interest due to the ever-decreasing size and increasing efficiencies of electronic devices, and improvements in this area have allowed for the development of sub-10 nm features on advanced microchips. The use of DCvC methods allows for efficient assembly and disassembly on a given stimuli. Kudo *et al.* developed a soluble, calixarene-based ladder polymer via the one-pot condensation of resorcinol and 1,4-butanedial under thermodynamic control.[116] The refractive index and photoinduced deprotection was explored for the resulting *tert*-butyloxycarbonyl (BOC) protected polymer (all free hydroxyls protected). Protection of the initial polymer allowed for a photo-deprotectable material to be developed for photolithographic purposes in the presence of a photoacid generator in
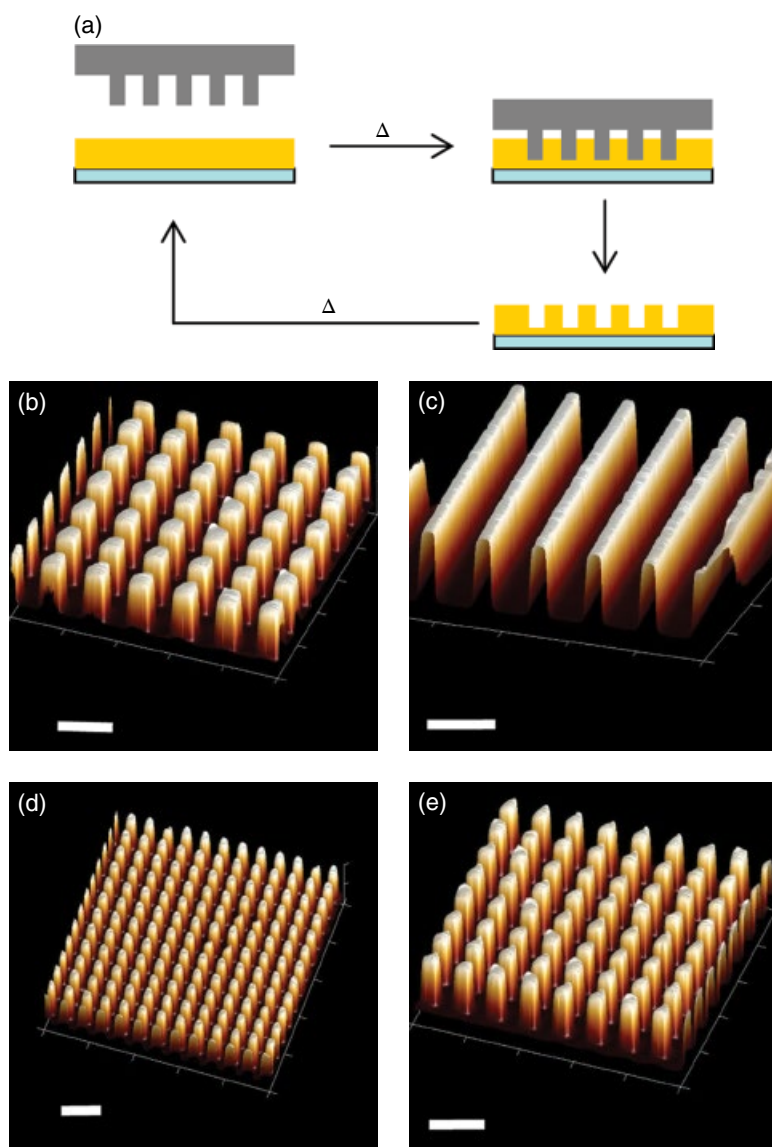
Figure 10.20 (a) The fabrication of a patterned film from a template using a Diels–Alder cycloaddition reaction. (b)–(e) AFM images of the different shapes and scales made from different templates (scale bar 1 μm).[114] Reprinted with permission. Copyright 2013 American Chemical Society.

thin films, releasing isobutylene and CO_2. The BOC-protected material also had a lower refractive index owing to the cavities contained within the polymer.

10.4.6 Color-changing Materials

Shape recovery in conjunction with mechanophore activation would provide access to a variety of applications, including the ability to introduce mechanochemical function
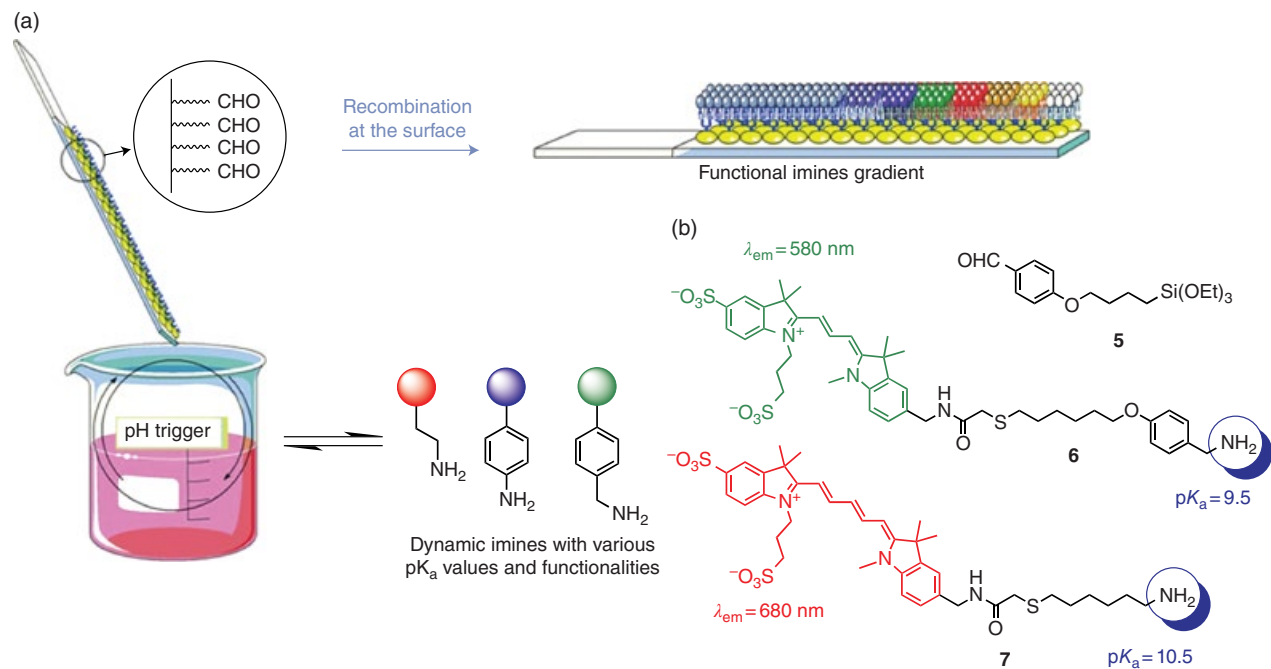
Figure 10.21 The fabrication of dynamic, self-assembled monolayers (DynaSAMs) and the formation of chemical gradients. (a) An aldehyde-functionalized surface is withdrawn from a solution of amines with various pK_a values as the pH is varied. Each amine is affixed with a functional group associated with a unique physical property (colored dots) for a given pK_a, which thus leads to a gradient of functional imines. (b) Chemical structures used for a model DynaSAM system: triethoxysilane aldehyde (**5**), Cy3 benzylamine (**6**), and Cy5 alkylamine (**7**).[115] Reprinted with permission. Copyright 2009 Nature Publishing Group. (*See insert for colour representation of the figure.*)
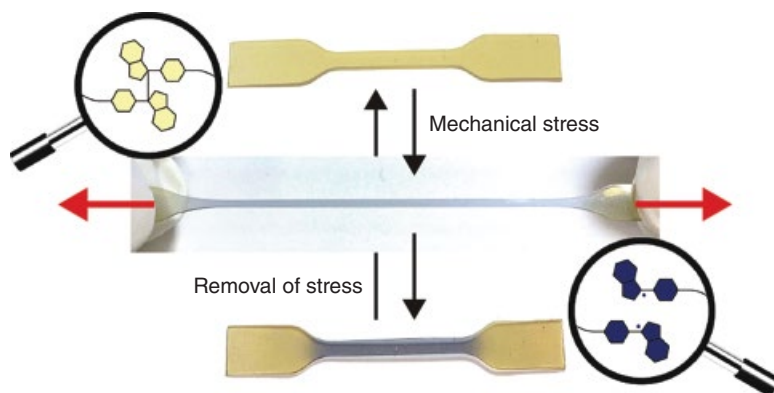
Figure 10.22 A mechanically-activated film is blue under stress owing to mechanically induced homolytic cleavage of diarylbibenzofuranone moieties incorporated in the network backbone to yield blue-colored radicals. Subsequent unloading allows radical recombination, resulting in loss of the blue coloration.[117] Reprinted with permission. Copyright 2015 American Chemical Society. (*See insert for colour representation of the figure*.)

to soft, active devices. Imato *et al*. reported the utilization of diarylbibenzofuranone (DABBF)-based dynamic covalent mechanophores embedded into an elastomeric polyurethane network to afford covalent bond activation under macroscopically reversible deformations (Figure 10.22).[117] The DABBF moiety is a dimeric dynamic covalent functional group that is able to act as a colorimetric mechanophore by undergoing force-induced homolytic cleavage on exposure to mechanical stimuli, resulting in the generation of colored radical species, allowing for direct spatial and temporal visualization of stress accumulation. Thus, by employing the colorimetric DABBF mechanophore, Imato *et al*. demonstrated that bond activation proceeded on application of a mechanical stress while removal of the stress allowed recombination of the generated radicals. The polyurethane-DABBF films displayed a distinct blue color when tension was applied, whereas they returned to their original yellow coloration when the stress was removed, a change that could be quantified spectroscopically. Macroscopically reversible activation promotes the future pursuit of reversible molecular responses and function beyond the color change provided by DABBF.

Nanofabric COF materials comprise another intriguing application area for DCvC. Huang *et al*. used a mixture of 2,6-dihydroxynaphthalene-1,5-dicarbaldehyde and 2,4,6-tris(4-aminophenyl)-pyridine to develop a self-tautomerizing COF through solvothermal synthesis.[118] They observed that the material underwent a morphological transformation from microspheres to nanofibers by implementing a unique dissolution−recrystallization mechanism, possibly attributable to the reversible nature of the dynamic imine bonds. The nanofibers were capable of growing on an aramid fiber surface to make nanofiber composites and offered reversible colorimetric humidity-responsive behavior (see Figure 10.23). These types of materials offer applications as sensors and catalyst surfaces.

10.4.7 Food Chemistry

DCvC has been applied to a specific application in the food industry; hydroxymethyl-furfural (HMF) is a common product of the Maillard reaction that originates from
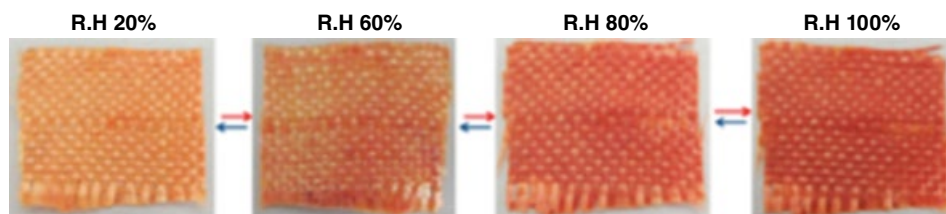
Figure 10.23 Reversible, humidity-responsive color change in COF/aramid hybrid fabrics.[118] Reprinted with permission. Copyright 2013 American Chemical Society. (*See insert for colour representation of the figure.*)
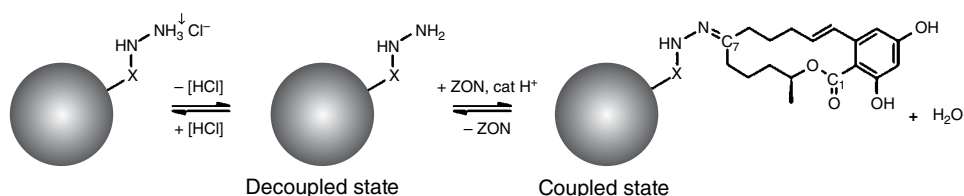
Scheme 10.7 Separation of ZON from edible oils with hydrazine bound to polystyrene resins.[120] Reprinted with permission. Copyright 2010 Elsevier B.V.

sucrose and fructose, but there is a lack of understanding for what happens to HMF after formation. HMF, occurring in a variety of foods such that the average person consumes 150 mg/day, has been found to be weakly toxic and has the ability to break DNA strands, encouraging the authors to do an extensive study on the binding abilities of HMF with different amino acids to further assess its reactivity. Nikolov *et al.*[119] compared the degradation products of Schiff base adducts formed from HMF and the amino acids.

In an interesting utilization of DCvC-mediated molecular separations, Siegel *et al.* used hydrazine chemistry to extract toxins from edible oils.[120] Here, the target of interest was the *Fusarium* mycotoxin zearalenone (ZON), a compound often found in cereals, nuts, spices, and corn that has been shown in animal studies to be teratogenic, hyperestrogenic, and carcinogenic at daily intakes higher than 0.0005 mg/kg of body weight. Although ZON is readily removed from many food products by organic solvent extraction owing to its hydrophobicity, its removal from oils has proven far more challenging. Thus, the authors used hydrazine groups anchored to a polystyrene resin as the stationary support phase in an HPLC separation method (Scheme 10.7). The carbonyl group on ZON reacted with the hydrazine to form a hydrazone species, allowing for separation of the remaining materials. ZON was then able to be released from the stationary phase by hydrolysis to regenerate the hydrazine.

10.4.8 Fluoride-catalyzed Silsesquioxane Bond Rearrangement

The fluoride-catalyzed rearrangement of silsesquioxanes has not historically been described as a dynamic covalent reaction, but it certainly exhibits all of the hallmarks of DCvC. Furgal *et al.* recently demonstrated the control of silsesquioxane cage size by dynamic exchange of siloxane bonds in different solvents.[121] Solvent choice, reactant
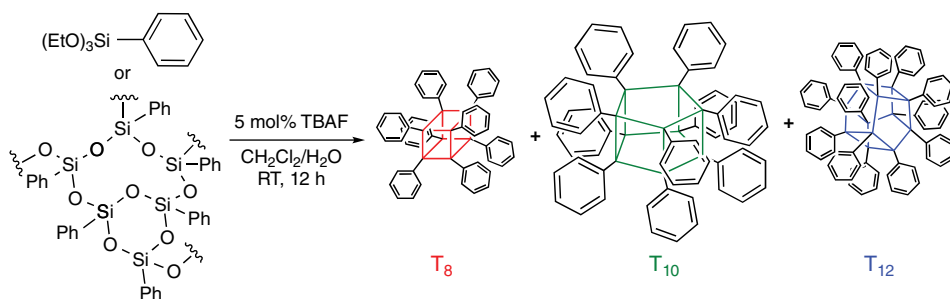
Scheme 10.8 Fluoride-catalyzed rearrangement of $PhSiO_{1.5}$ favoring the $[PhSiO_{1.5}]_{10}$ product.[121]

concentration and amount of catalyst were shown to have the largest influence on controlling the cage size obtained, typically of 8, 10, and 12 silicons. This work described the synthesis of $[PhSiO_{1.5}]$ derivatives, where the cage equilibrium was shifted to favor the 10-silicon cage (Scheme 10.8). Furthermore, mixed functional silsesquioxanes have also been developed by this fluoride-catalyzed equilibration method, making mixed vinyl/phenyl and vinyl/methyl cage systems and equilibrated polymeric materials.[122,123] These dynamic methods may be useful in developing new fluoride-equilibrated hybrid materials and surface functionalization.

10.5 Conclusion

Since its inception, DCvC has found use in a diverse variety of applications across many length scales, from polymer science to biomedicine to molecular separations, but DCvC as a field has yet to mature. For example, although stress relaxation and self-healing in crosslinked polymers have been extensively demonstrated in elastomers, the frontiers of research in these materials will involve rigid systems that are not susceptible to creep, attributes that will likely necessitate novel DCvC approaches. Additionally, nanoparticulate assemblies with improved targeting for selective drug delivery are certain to continue to find use in biomedical applications. Applications requiring robust materials with molecular alignment or well-defined, nanoscale porosity will similarly benefit from continued work in the DCvC arena. Finally, the range of reactions that fall under the DCvC umbrella continues to expand, with each new example bringing with it unique properties otherwise unattainable using conventional, irreversible covalent bond-forming reactions. Given these and other emergent applications, DCvC is certain to have a bright research future over the coming decades.

References

1 T. F. Scott, A. D. Schneider, W. D. Cook, C. N. Bowman, *Science* **2005**, *308*, 1615–1617.

2 T. F. Scott, R. B. Draughon, C. N. Bowman, *Adv. Mater.* **2006**, *18*, 2128–2132.

3 C. J. Kloxin, T. F. Scott, C. N. Bowman, *Macromolecules* **2009**, *42*, 2551–2556.

4 B. D. Fairbanks, S. P. Singh, C. N. Bowman, K. S. Anseth, *Macromolecules* **2011**, *44*, 2444–2450.

5 J. Canadell, H. Goossens, B. Klumperman, *Macromolecules* **2011**, *44*, 2536–2541.

6 J. J. Cash, T. Kubo, A. P. Bapat, B. S. Sumerlin, *Macromolecules* **2015**, *48*, 2098–2106.

7 C. C. Deng, W. L. A. Brooks, K. A. Abboud, B. S. Sumerlin, *ACS Macro Lett.* **2015**, *4*, 220–224.

8 N. Roy, B. Bruchmann, J. M. Lehn, *Chem. Soc. Rev.* **2015**, *44*, 3786–3807.

9 H. Z. Ying, Y. F. Zhang, J. J. Cheng, *Nat. Commun.* **2014**, *5*.

10 S. R. White, N. R. Sottos, P. H. Geubelle, J. S. Moore, M. R. Kessler, S. R. Sriram, E. N. Brown, S. Viswanathan, *Nature* **2001**, *409*, 794–797.

11 E. N. Brown, S. R. White, N. R. Sottos, *J. Mater. Sci.* **2004**, *39*, 1703–1710.

12 K. S. Toohey, N. R. Sottos, J. A. Lewis, J. S. Moore, S. R. White, *Nat. Mater.* **2007**, *6*, 581–585.

13 Y. Amamoto, J. Kamada, H. Otsuka, A. Takahara, K. Matyjaszewski, *Angew. Chem., Int. Ed.* **2011**, *50*, 1660–1663.

14 Y. Amamoto, H. Otsuka, A. Takahara, K. Matyjaszewski, *ACS Macro Lett.* **2012**, *1*, 478–481.

15 Y. Amamoto, H. Otsuka, A. Takahara, K. Matyjaszewski, *Adv. Mater.* **2012**, *24*, 3975–3980.

16 X. X. Chen, F. Wudl, A. K. Mal, H. B. Shen, S. R. Nutt, *Macromolecules* **2003**, *36*, 1802–1807.

17 E. B. Murphy, E. Bolanos, C. Schaffner-Hamann, F. Wudl, S. R. Nutt, M. L. Auad, *Macromolecules* **2008**, *41*, 5203–5209.

18 B. J. Adzima, C. J. Kloxin, C. N. Bowman, *Adv. Mater.* **2010**, *22*, 2784–2787.

19 U. Haldar, K. Bauri, R. Li, R. Faust, P. De, *ACS Appl. Mater. Inter.* **2015**, *7*, 8779–8788.

20 O. R. Cromwell, J. Chung, Z. B. Guan, *J. Am. Chem. Soc.* **2015**, *137*, 6492–6495.

21 C. J. Kloxin, T. F. Scott, H. Y. Park, C. N. Bowman, *Adv. Mater.* **2011**, *23*, 1977–1981.

22 M. Hutchby, C. E. Houlden, J. G. Ford, S. N. G. Tyler, M. R. Gagne, G. C. Lloyd-Jones, K. I. Booker-Milburn, *Angew. Chem., Int. Ed.* **2009**, *48*, 8721–8724.

23 W. J. Chung, J. J. Griebel, E. T. Kim, H. Yoon, A. G. Simmonds, H. J. Ji, P. T. Dirlam, R. S. Glass, J. J. Wie, N. A. Nguyen, B. W. Guralnick, J. Park, A. Somogyi, P. Theato, M. E. Mackay, Y. E. Sung, K. Char, J. Pyun, *Nat. Chem.* **2013**, *5*, 518–524.

24 J. J. Griebel, N. A. Nguyen, A. V. Astashkin, R. S. Glass, M. E. Mackay, K. Char, J. Pyun, *ACS Macro Lett.* **2014**, *3*, 1258–1261.

25 R. Hoogenboom, *Angew. Chem., Int. Ed.* **2012**, *51*, 11942–11944.

26 Y. L. Chen, A. M. Kushner, G. A. Williams, Z. B. Guan, *Nat. Chem.* **2012**, *4*, 467–472.

27 W. D. Cook, T. F. Scott, S. Quay-Thevenon, J. S. Forsythe, *J. Appl. Polym. Sci.* **2004**, *93*, 1348–1359.

28 J. M. Garcia, G. O. Jones, K. Virwani, B. D. McCloskey, D. J. Boday, G. M. ter Huurne, H. W. Horn, D. J. Coady, A. M. Bintaleb, A. M. S. Alabdulrahman, F. Alsewailem, H. A. A. Almegren, J. L. Hedrick, *Science* **2014**, *344*, 732–735.

29 R. P. Feynman, R. B. Leighton, M. Sands, *Friction*, in *The Feynman Lectures on Physics, Vol. I*, **2011**.

30 Q. Tian, Y. C. Yuan, M. Z. Rong, M. Q. Zhang, *J. Mater. Chem.* **2009**, *19*, 1289–1296.

31 P. Reutenauer, E. Buhler, P. J. Boul, S. J. Candau, J. M. Lehn, *Chem. Eur. J.* **2009**, *15*, 1893–1900.

32 G. B. Lyon, A. Baranek, C. N. Bowman, *Adv. Funct. Mater.* **2016**, *26*, 1477–1485.

33 B. J. Adzima, H. A. Aguirre, C. J. Kloxin, T. F. Scott, C. N. Bowman, *Macromolecules* **2008**, *41*, 9112–9117.

34 Y. Higaki, H. Otsuka, A. Takahara, *Macromolecules* **2004**, *37*, 1696–1701.

35 A. W. Jackson, D. A. Fulton, *Macromolecules* **2010**, *43*, 1069–1075.

36 C. Yuan, M. Z. Rong, M. Q. Zhang, Z. P. Zhang, Y. C. Yuan, *Chem. Mater.* **2011**, *23*, 5076–5081.

37 Y. Amamoto, M. Kikuchi, H. Masunaga, S. Sasaki, H. Otsuka, A. Takahara, *Macromolecules* **2009**, *42*, 8733–8738.

38 J. Su, Y. Amamoto, T. Sato, M. Kume, T. Inada, T. Ohishi, Y. Higaki, A. Takahara, H. Otsuka, *Polymer* **2014**, *55*, 1474–1480.

39 K. A. Williams, A. J. Boydston, C. W. Bielawski, *J. Roy. Soc. Interface* **2007**, *4*, 359–362.

40 G. M. Whitesides, J. P. Mathias, C. T. Seto, *Science* **1991**, *254*, 1312–1319.

41 G. M. Whitesides, M. Boncheva, *Proc. Natl. Acad. Sci. USA* **2002**, *99*, 4769–4774.

42 A. J. Blake, N. R. Champness, P. Hubberstey, W. S. Li, M. A. Withersby, M. Schroder, *Coord. Chem. Rev.* **1999**, *183*, 117–138.

43 E. L. Thomas, *Science* **1999**, *286*, 1307–1307.

44 A. Ulman, *Chem. Rev.* **1996**, *96*, 1533–1554.

45 J. M. Schnur, *Science* **1993**, *262*, 1669–1676.

46 M. J. Gething, J. Sambrook, *Nature* **1992**, *355*, 33–45.

47 M. Zuker, *Nucleic Acids Res.* **2003**, *31*, 3406–3415.

48 S. G. Zhang, *Nat. Biotechnol.* **2003**, *21*, 1171–1178.

49 M. B. Smith, J. March, *March's Advanced Organic Chemistry – Reactions, Mechanisms, and Structure*, 6th edn, John Wiley & Sons, Hoboken, New Jersey, **2007**.

50 S. J. Rowan, S. J. Cantrill, G. R. L. Cousins, J. K. M. Sanders, J. F. Stoddart, *Angew. Chem., Int. Ed.* **2002**, *41*, 898–952.

51 C. J. Kloxin, T. F. Scott, B. J. Adzima, C. N. Bowman, *Macromolecules* **2010**, *43*, 2643–2653.

52 Y. H. Jin, C. Yu, R. J. Denman, W. Zhang, *Chem. Soc. Rev.* **2013**, *42*, 6634–6654.

53 N. J. Pace, E. Weerapana, *ACS Chem. Biol.* **2013**, *8*, 283–296.

54 D. W. Fry, A. J. Bridges, W. A. Denny, A. Doherty, K. D. Greis, J. L. Hicks, K. E. Hook, P. R. Keller, W. R. Leopold, J. A. Loo, D. J. McNamara, J. M. Nelson, V. Sherwood, J. B. Smaill, S. Trumpp-Kallmeyer, E. M. Dobrusin, *Proc. Natl. Acad. Sci. USA* **1998**, *95*, 12022–12027.

55 I. M. Serafimova, M. A. Pufall, S. Krishnan, K. Duda, M. S. Cohen, R. L. Maglathlin, J. M. McFarland, R. M. Miller, M. Frodin, J. Taunton, *Nat. Chem. Biol.* **2012**, *8*, 471–476.

56 R. M. Miller, V. O. Paavilainen, S. Krishnan, I. M. Serafimova, J. Taunton, *J. Am. Chem. Soc.* **2013**, *135*, 5298–5301.

57 K. Kataoka, A. Harada, Y. Nagasaki, *Adv. Drug Deliv. Rev.* **2001**, *47*, 113–131.

58 K. Miyata, R. J. Christie, K. Kataoka, *React. Funct. Polymers* **2011**, *71*, 227–234.

59 C. B. Minkenberg, L. Florusse, R. Eelkema, G. J. M. Koper, J. H. van Esch, *J. Am. Chem. Soc.* **2009**, *131*, 11274–11275.

60 C. B. Minkenberg, W. E. Hendriksen, F. Li, E. Mendes, R. Eelkema, J. H. van Esch, *Chem. Commun.* **2012**, *48*, 9837–9839.

61 C. B. Minkenberg, B. Homan, J. Boekhoven, B. Norder, G. J. M. Koper, R. Eelkema, J. H. van Esch, *Langmuir* **2012**, *28*, 13570–13576.

62 G. Moad, E. Rizzardo, S. H. Thang, *Polymer* **2008**, *49*, 1079–1131.

63 Y. P. Li, K. Xiao, J. T. Luo, W. W. Xiao, J. S. Lee, A. M. Gonik, J. Kato, T. A. Dong, K. S. Lam, *Biomaterials* **2011**, *32*, 6633–6645.

64 J. Li, P. Nowak, S. Otto, *J. Am. Chem. Soc.* **2013**, *135*, 9222–9239.

65 S. Hamieh, R. F. Ludlow, O. Perraud, K. R. West, E. Mattia, S. Otto, *Org. Lett.* **2012**, *14*, 5404–5407.

66 V. T. Bhat, A. M. Caniard, T. Luksch, R. Brenk, D. J. Campopiano, M. F. Greaney, *Nat. Chem.* **2010**, *2*, 490–497.

67 K. L. Bicker, J. Sun, J. J. Lavigne, P. R. Thompson, *ACS Combinatorial Sci.* **2011**, *13*, 232–243.

68 X. Wu, N. Busschaert, N. J. Wells, Y. B. Jiang, P. A. Gale, *J. Am. Chem. Soc.* **2015**, *137*, 1476–1484.

69 J. H. Ryu, S. Jiwpanich, R. Chacko, S. Bickerton, S. Thayumanavan, *J. Am. Chem. Soc.* **2010**, *132*, 8246–8247.

70 J. M. Lehn, *Prog. Polym. Sci.* **2005**, *30*, 814–831.

71 G. H. Deng, C. M. Tang, F. Y. Li, H. F. Jiang, Y. M. Chen, *Macromolecules* **2010**, *43*, 1191–1194.

72 G. H. Deng, F. Y. Li, H. X. Yu, F. Y. Liu, C. Y. Liu, W. X. Sun, H. F. Jiang, Y. M. Chen, *ACS Macro Lett.* **2012**, *1*, 275–279.

73 J. R. Vieregg, H. M. Nelson, B. M. Stoltz, N. A. Pierce, *J. Am. Chem. Soc.* **2013**, *135*, 9691–9699.

74 S. Wan, J. Guo, J. Kim, H. Ihee, D. Jiang, *Angew. Chem., Int. Ed.* **2008**, *47*, 8826–8830.

75 M. Calik, F. Auras, L. M. Salonen, K. Bader, I. Grill, M. Handloser, D. D. Medina, M. Dogru, F. Lo, D. Trauner, A. Hartschuh, T. Bein, **2014**.

76 E. L. Spitler, W. R. Dichtel, *Nat. Chem.* **2010**, *2*, 672–677.

77 X. Ding, L. Chen, Y. Honsho, X. Feng, O. Saengsawang, J. Guo, A. Saeki, S. Seki, S. Irle, S. Nagase, V. Parasuk, D. Jiang, *J. Am. Chem. Soc.* **2011**, *133*, 14510–14513.

78 S. Wan, F. Gándara, A. Asano, H. Furukawa, A. Saeki, S. K. Dey, L. Liao, M. W. Ambrogio, Y. Y. Botros, X. Duan, S. Seki, J. F. Stoddart, O. M. Yaghi, *Chem. Mater.* **2011**, *23*, 4094–4097.

79 S. Chandra, S. Kandambeth, B. P. Biswal, B. Lukose, S. M. Kunjir, M. Chaudhary, R. Babarao, T. Heine, R. Banerjee, *J. Am. Chem. Soc.* **2013**, *135*, 17853–17861.

80 J. Guo, Y. Xu, S. Jin, L. Chen, T. Kaji, Y. Honsho, M. A. Addicoat, J. Kim, A. Saeki, H. Ihee, S. Seki, S. Irle, M. Hiramoto, J. Gao, D. Jiang, *Nat. Commun.* **2013**, *4*, doi: 10.1038/ncomms3736.

81 G. H. V. Bertrand, V. K. Michaelis, T.-C. Ong, R. G. Griffin, M. Dinca, *Proc. Nat. Acad. Sci.* **2013**, *110*, 4923–4928.

82 R. Tanoue, R. Higuchi, N. Enoki, Y. Miyasato, S. Uemura, N. Kimizuka, A. Z. Stieg, J. K. Gimzewski, M. Kunitake, *ACS Nano* **2011**, *5*, 3923–3929.

83 S. Ho Choi, B. Kim, C. D. Frisbie, *Science* **2008**, *320*, 1482–1486.

84 A. Ikegami, M. Suda, T. Watanabe, Y. Einaga, *Angew. Chem., Int. Ed.* **2010**, *49*, 372–374.

85 X. de Hatten, N. Bell, N. Yufa, G. Christmann, J. R. Nitschke, *J. Am. Chem. Soc.* **2011**, *133*, 3158–3164.

86 Z. Xu, P. Zhao, Y. Chen, G. Deng, *Polymer* **2013**, *54*, 2647–2651.

87 A. G. Tennyson, B. Norris, C. W. Bielawski, *Macromolecules* **2010**, *43*, 6923–6935.

88 C. Wei, M. Chen, D. Liu, W. Zhou, M. Khan, X. Wu, N. Huang, L. Li, *RSC Adv.* **2015**, *5*, 22638–22646.

89 Y. Du, H. S. Yang, J. M. Whiteley, S. Wan, Y. H. Jin, S. H. Lee, W. Zhang, *Angew. Chem., Int. Ed.* **2016**, *55*, 1737–1741.

90 X. Feng, X. Ding, D. Jiang, *Chem. Soc. Rev.* **2012**, *41*, 6010–6022.

91 S. Y. Ding, W. Wang, *Chem. Soc. Rev.* **2013**, *42*, 548–568.

92 S. S. Han, H. Furukawa, O. M. Yaghi, W. A. Goddard, *J Am Chem Soc* **2008**, *130*, 11580–11581.

93 H. Furukawa, O. M. Yaghi, *J. Am. Chem. Soc.* **2009**, *131*, 8875–8883.

94 J. L. Mendoza-Cortes, T. A. Pascal, W. A. Goddard, J. Phys. *Chem. A* **2011**, *115*, 13852–13857.

95 M. G. Rabbani, A. K. Sekizkardes, Z. Kahveci, T. E. Reich, R. Ding, H. M. El-Kaderi, *Chem. Eur. J.* **2013**, *19*, 3324–3328.

96 Y. H. Jin, Y. L. Zhu, W. Zhang, *Cryst. Eng. Comm.* **2013**, *15*, 1484–1499.

97 Y. L. Zhu, W. Zhang, *Chem. Sci.* **2014**, *5*, 4957–4961.

98 Y. Zeng, R. Zou, Z. Luo, H. Zhang, X. Yao, X. Ma, R. Zou, Y. Zhao, *J. Am. Chem. Soc.* **2015**, *137*, 1020–1023.

99 K. T. Jackson, T. E. Reich, H. M. El-Kaderi, *Chem. Commun.* **2012**, *48*, 8823.

100 K. L. Tan, *ACS Catal.* **2011**, *1*, 877–886.

101 R. M. Al-Zoubi, O. Marion, D. G. Hall, *Angew. Chem., Int. Ed.* **2008**, *47*, 2876–2879.

102 H. Zheng, R. McDonald, D. G. Hall, *Chem. Eur. J.* **2010**, *16*, 5454–5460.

103 H. Zheng, D. G. Hall, *Tetrahedron Lett.* **2010**, *51*, 3561–3564.

104 D. Lee, S. G. Newman, M. S. Taylor, *Org. Lett.* **2009**, *11*, 5486–5489.

105 K. Aelvoet, A. S. Batsanov, A. J. Blatch, C. Grosjean, L. G. F. Patrick, C. A. Smethurst, A. Whiting, *Angew. Chem., Int. Ed.* **2008**, *47*, 768–770.

106 M. Karimi, I. Chaudhury, C. Jianjun, M. Safari, R. Sadeghi, M. Habibi-Rezaei, J. Kokini, *J. Molec. Catal. B: Enzymatic* **2014**, *104*, 48–55.

107 E.-B. Cho, O. H. Han, S. Kim, D. Kim, M. Jaroniec, *Chem. Commun.* **2010**, *46*, 4568–4570.

108 D. Siegel, *Analyst* **2012**, *137*, 5457–5482.

109 D. Xu, R. Warmuth, *J. Am. Chem. Soc.* **2008**, *130*, 7520–7521.

110 J. Leclaire, G. Husson, N. Devaux, V. Delorme, L. Charles, F. Ziarelli, P. Desbols, A. Chaumonnot, M. Jacquin, F. Fotiadu, G. Buono, *J. Am. Chem. Soc.* **2010**, *132*, 3582–3593.

111 J. Alauzun, E. Besson, A. Mehdi, C. Reyé, R. J. P. Corriu, *Chem. Mater.* **2008**, *20*, 503–513.

112 N. Polikarpov, V. Potolytsyna, E. Bessonova, S. Tripp, D. Appelhans, B. Voit, L. Kartsova, *J. Chromatogr. A* **2015**, *1378*, 65–73.

113 L. T. Yang, A. Gomez-Casado, J. F. Young, H. D. Nguyen, J. Cabanas-Danes, J. Huskens, L. Brunsveld, P. Jonkheijm, *J. Am. Chem. Soc.* **2012**, *134*, 19199–19206.

114 W. Thongsomboon, M. Sherwood, N. Arellano, A. Nelson, *ACS Macro Lett.* **2013**, *2*, 19–22.

115 L. Tauk, A. P. Schroder, G. Decher, N. Giuseppone, *Nat. Chem.* **2009**, *1*, 649–656.

116 H. Kudo, K. Shigematsu, K. Mitani, T. Nishikubo, N. C. Kasuga, H. Uekusa, Y. Ohashi, *Macromolecules* **2008**, *41*, 2030–2036.

117 K. Imato, T. Kanehara, T. Ohishi, M. Nishihara, H. Yajima, M. Ito, A. Takahara, H. Otsuka, *ACS Macro Lett.* **2015**, *4*, 1307–1311.

118 W. Huang, Y. Jiang, X. Li, X. Li, J. Wang, Q. Wu, X. Liu, *ACS Appl. Mater. Inter.* **2013**, *5*, 8845–8849.

119 P. Y. Nikolov, V. A. Yaylayan, *J. Agric. Food Chem.* **2011**, *59*, 6099–6107.

120 D. Siegel, K. Andrae, M. Proske, C. Kochan, M. Koch, M. Weber, I. Nehls, *J. Chromatogr. A* **2010**, *1217*, 2206–2215.

121 J. C. Furgal, T. Goodson III, R. M. Laine, *Dalton Trans.* **2016**, *45*, 1025.

122 M. Ronchi, S. Sulaiman, N. R. Boston, R. M. Laine, *Appl. Organometal. Chem.* **2009**, *24*, 551–557.

123 J. C. Furgal, J. H. Jung, S. Clark, T. Goodson, R. M. Laine, *Macromolecules* **2013**, *46*, 7591–7604.

Index

Figure 2.10 A DCL of competing peptide self-replicators based on coiled-coil formation. (a) Peptide sequence of the bulding blocks and the replicators. (b) The topology of replication. Electrophilic (**35–37**) and nucleophilic (**38** and **38a**) building blocks react to form peptides **39–41** and **39a–41a**. These can form homo-or heteromeric coiled-coil trimers, which themselves serve as template for the monomer formation from the building blocks. The kinetic profiles of replicator concentrations of systems starting from 150 μM building block concentration are shown in the presence of (c) excess RSH (d) 1 M NaClO$_4$ and (e) 45 μM **42** (which templates the formation of **41**).

Figure 2.12 (a) The reaction of FeCl$_2$ and diamine **48** with dialdehyde **49** or **50** gives rise to the Solomon link **51** (left) or the pentafoil knot **52** (right), respectively. (b) Mixing the four subcomponents gives rise to a library of mixed pentafoil knots, while the two knotted species do not undergo subcomponent exchange.

Figure 2.17 A DCL of charged hydrophobic aldehydes and hydrophilic amines can be controlled with pH. At high pH, imines with short hydrophilic tails are formed, assembling into spherical aggregates. Upon increase of pH, imines with long hydrophilic tails are selected, changing the shape of the amphiphiles and causing core-shell inversion of the micelles. The inverted micelles may, depending on their surface interactions, aggregate into larger mesophases.

Figure 2.23 A comparison of a static DNA encoded chemical library (top) with a dynamic one (bottom). The dynamic library has shorter DNA complementary domains, allowing for amplification of the best binding dimers by the target protein.
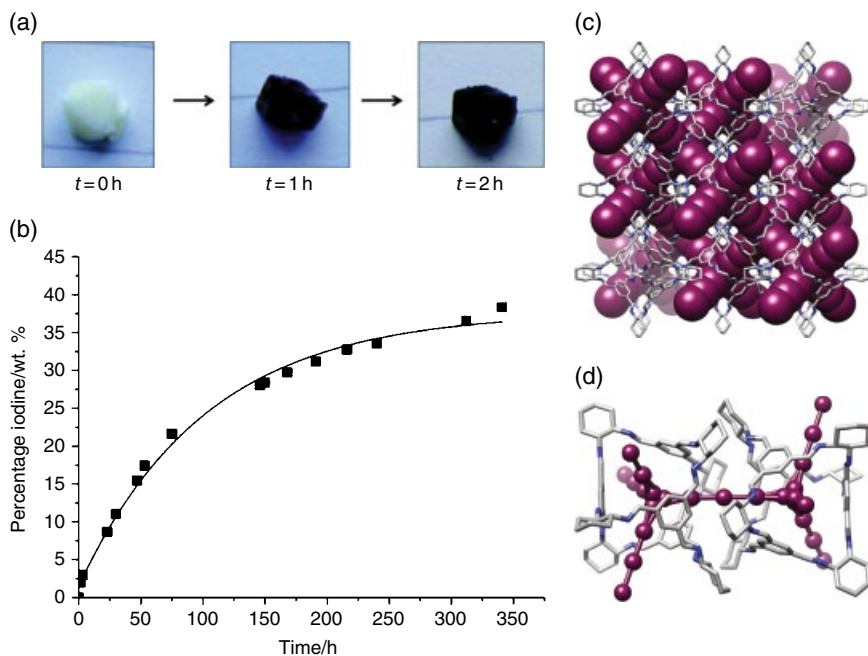
Figure 4.1 (a) The color change when a single crystal of **C4** was exposed to iodine vapor. (b) Gravimetric uptake of iodine as a function of time. (c) Packing diagram for **I@C4.** (d) One possible conformation of I_5^- species in neighboring cage molecules.
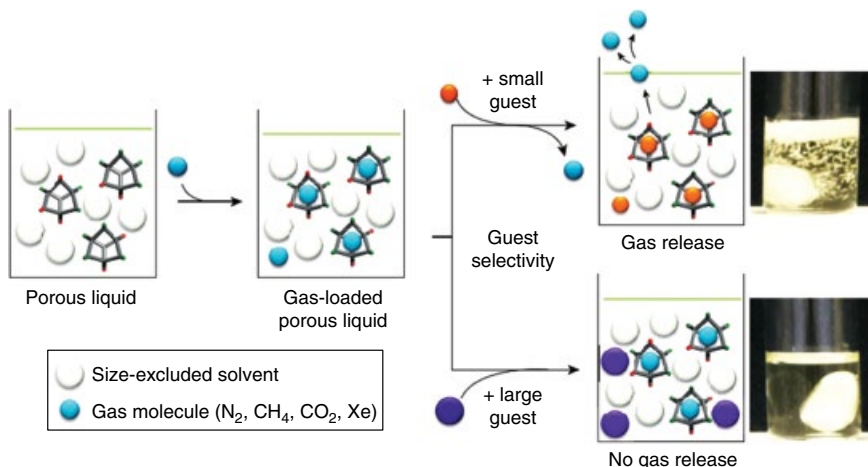
Figure 4.3 The gas-release behavior of porous liquids.
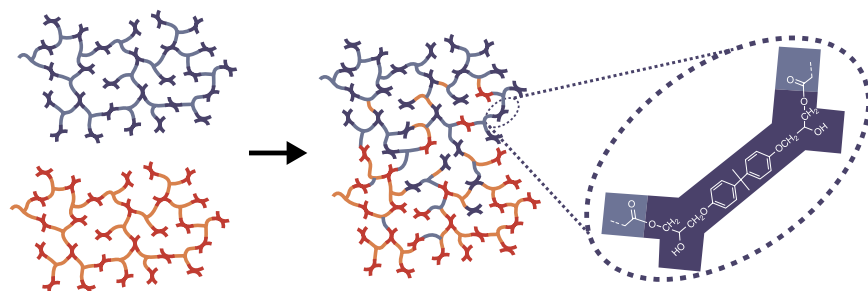
Figure 9.6 Schematic view of epoxy (hydroxy-ester) networks with transesterification exchange processes that preserve the total number of links and average functionality of crosslinks and do not cause depolymerization. Reproduced with permission.[32] Copyright 2012, ACS Publications.

Figure 10.1 Stress relaxation in crosslinked polymers by addition-fragmentation chain transfer. (a) The allyl sulfide group incorporated in the polymer backbone facilitates bond rearrangement via radical-mediated AFCT. (b) Schematic diagram of the mechanophotopatterning of a uniaxially deformed sample, where the AFCT-based material is stretched and irradiated through a photomask. (c) After irradiation, the material exhibits a pattern that is consistent with the pattern of the mask (scale bar = 1 mm). (d) Stylus profilometry reveals an excellent correspondence between the mask and the topographical features on the surface of the sample.[21] Reprinted with permission. Copyright 2011 John Wiley and Sons.

Scheme 10.3 The controlled formation of micellar aggregates from the aromatic aldehyde polar head group reversibly reacting with various amines to form an amphiphilic surfactant that can self-assemble into micelles.[59] Reprinted with permission. Copyright 2009 American Chemical Society.
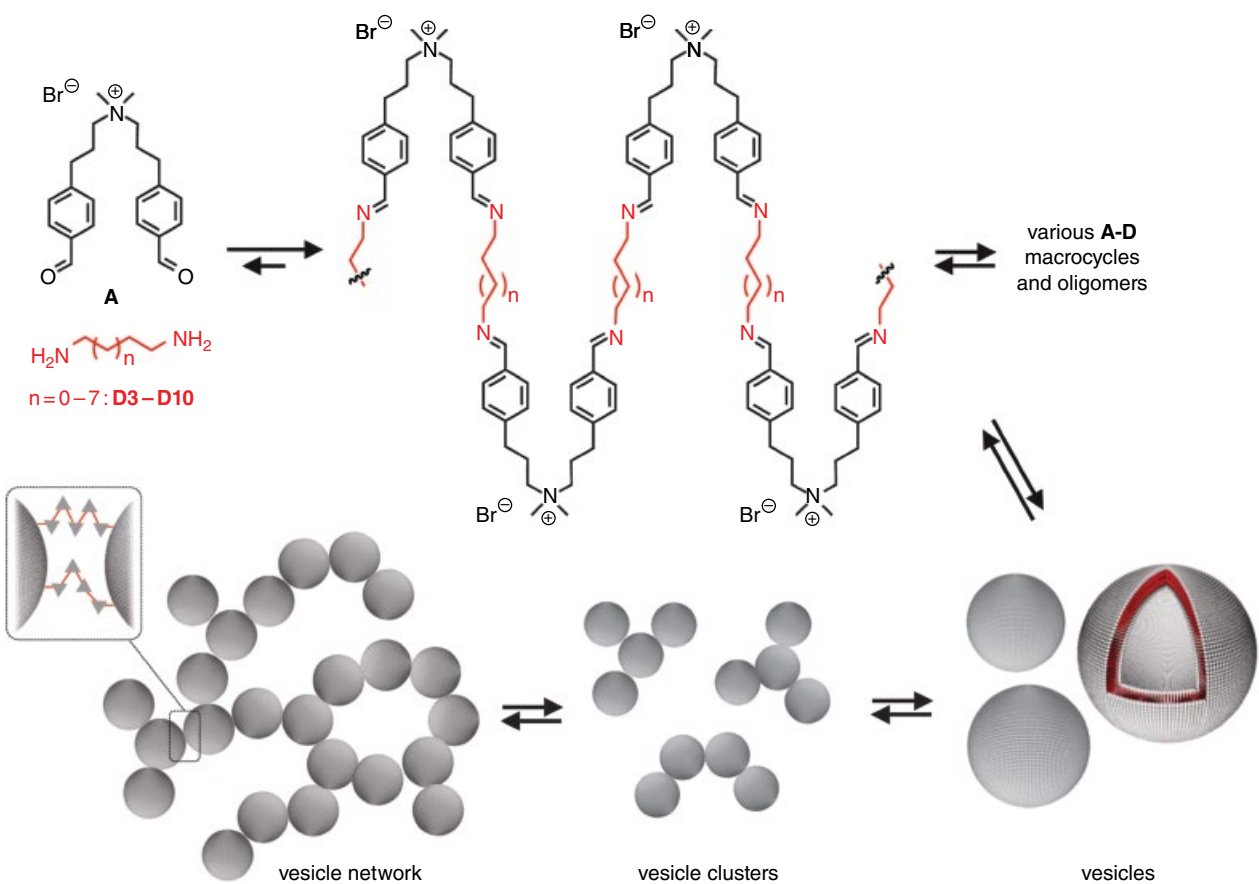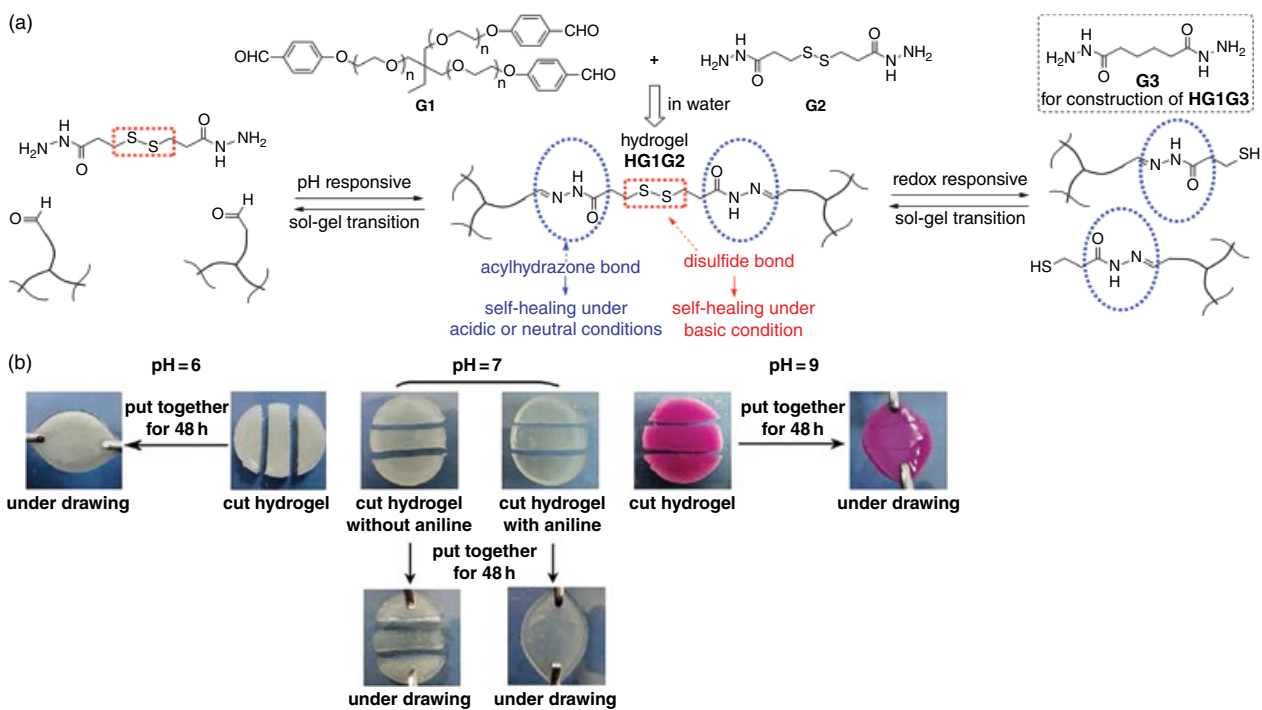
Scheme 10.4 The formation of imine bonds from difunctionalized aldehydes and aliphatic amines to form macrocycles and oligomers leading to the vesicles, clusters, and ultimately networks capable of forming pH-reversible hydrogels.[60] Reprinted with permission. Copyright 2012 Royal Society of Chemistry.
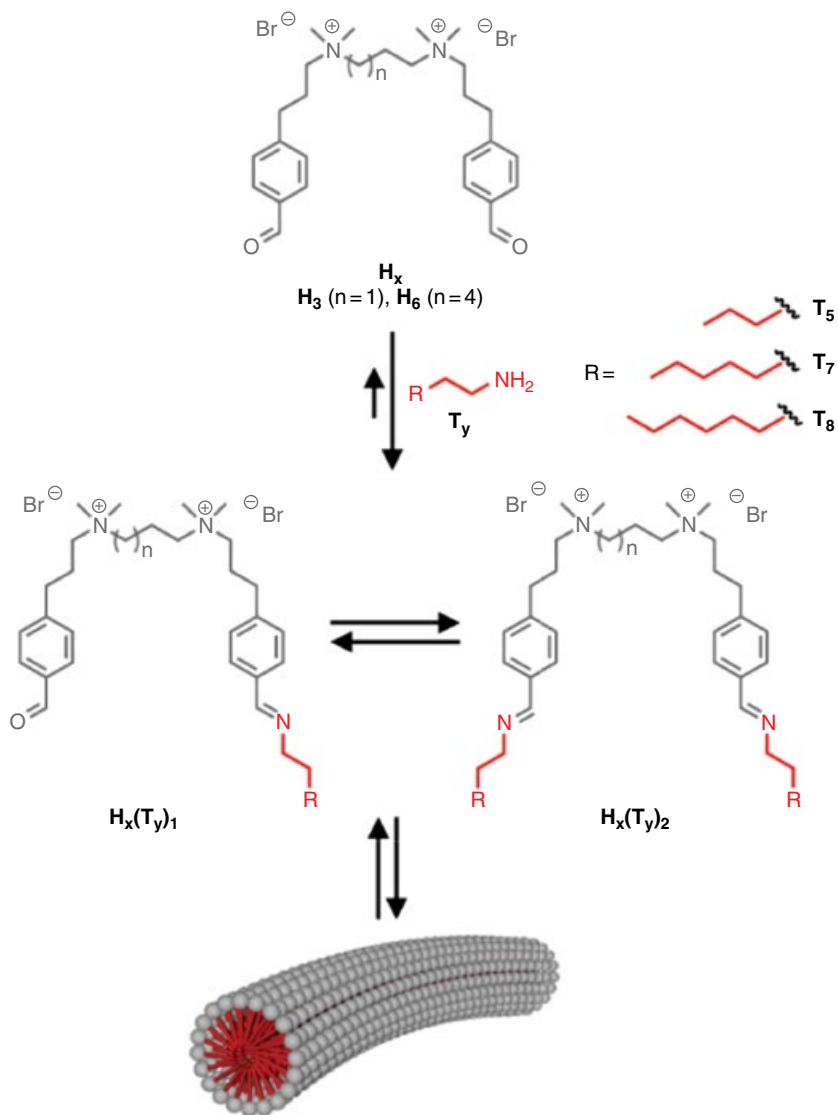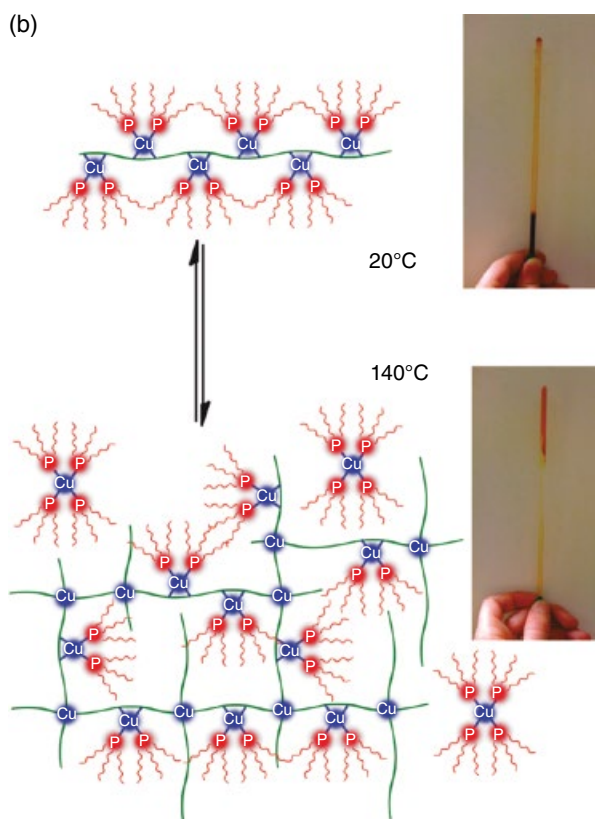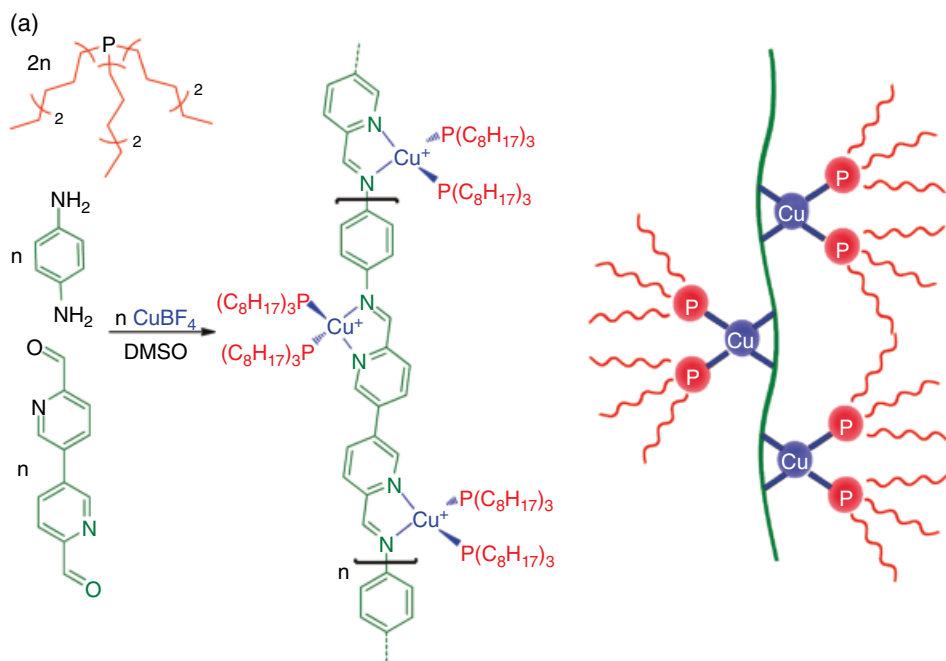
Scheme 10.5 The formation of wormlike micelles from gemini surfactants comprising a bis-aldehyde head group and amine tail groups.[61] Reprinted with permission. Copyright 2012 American Chemical Society.
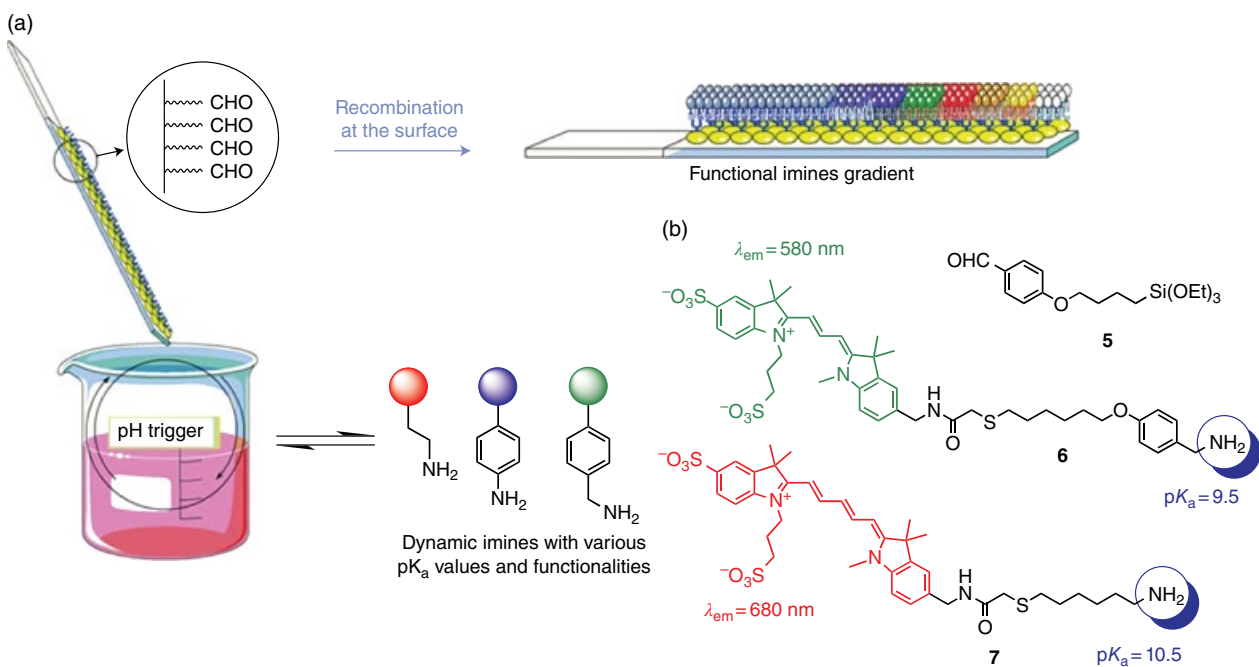
Figure 10.10 (a) The formation of a nanogel from functionalized nanoparticles and (b) structures of the nanogel, including the disulfide chemistry.[69] (i) Cleavage of specific amount of a pyridyl disulfide (PDS) group by dithiothreitol (DTT). (ii) Nanogel formation by inter/intrachain cross-linking. (iii) Surface modification of nanogels with thiolmodified Tat peptide or fluorescein isothiocyanate (FITC). Reprinted with permission. Copyright 2010 American Chemical Society.

Figure 10.13 (a) Strategy for constructing a dynamic hydrogel with an environmental adaptive self-healing ability and dual responsive sol–gel transitions based on acylhydrazone and disulfide chemistry. (b) Environmental adaptive self-healing of a dynamic hydrogel.[72] Reprinted with permission. Copyright 2012 American Chemical Society.
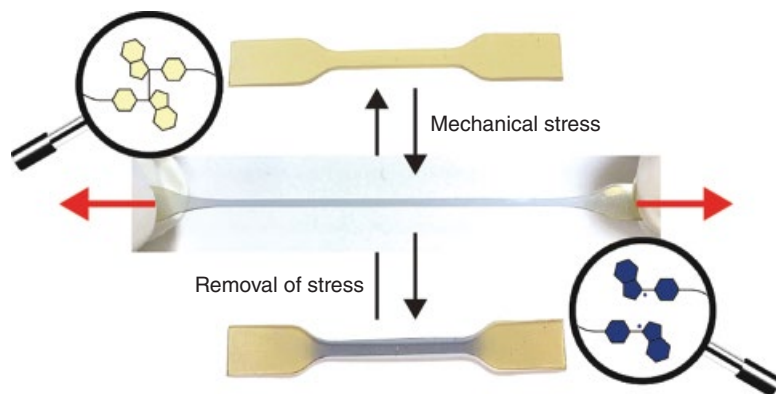
Figure 10.17 (a) The preparation of a conjugated metal–organic polymer from subcomponents (left) and its cartoon representation (right). (b) Schematic representation of the gelation mechanism (left); photographs of inverted NMR tubes showing the polymer in solution (top right) and following the sol–gel transition (bottom right).[85] Reprinted with permission. Copyright 2011 American Chemical Society.
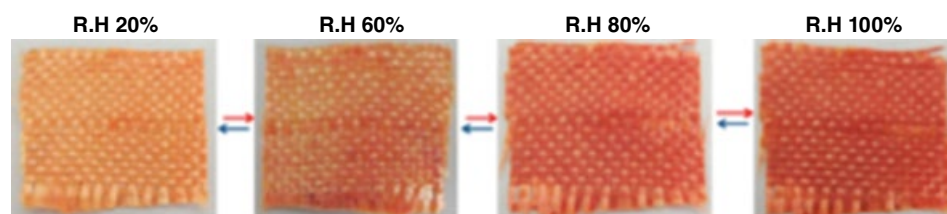
Figure 10.21 The fabrication of dynamic, self-assembled monolayers (DynaSAMs) and the formation of chemical gradients. (a) An aldehyde-functionalized surface is withdrawn from a solution of amines with various pK_a values as the pH is varied. Each amine is affixed with a functional group associated with a unique physical property (colored dots) for a given pK_a, which thus leads to a gradient of functional imines. (b) Chemical structures used for a model DynaSAM system: triethoxysilane aldehyde (**5**), Cy3 benzylamine (**6**), and Cy5 alkylamine (**7**).[115] Reprinted with permission. Copyright 2009 Nature Publishing Group.

Figure 10.22 A mechanically-activated film is blue under stress owing to mechanically induced homolytic cleavage of diarylbibenzofuranone moieties incorporated in the network backbone to yield blue-colored radicals. Subsequent unloading allows radical recombination, resulting in loss of the blue coloration.[117] Reprinted with permission. Copyright 2015 American Chemical Society.

Figure 10.23 Reversible, humidity-responsive color change in COF/aramid hybrid fabrics.[118] Reprinted with permission. Copyright 2013 American Chemical Society.